University of Alberta

The synthesis and use of *tetrakis*[2-hydroxyphenyl]ethene in Ziegler-Natta catalysis.

by

Udo H. Verkerk ©

A thesis submitted to the Faculty of Graduate Studies and Research in partial fulfillment of the requirements for the degree of Doctor of Philosophy.

Department of Chemistry

Edmonton, Alberta
Fall 2001

National Library
of Canada

Acquisitions and
Bibliographic Services

395 Wellington Street
Ottawa ON K1A 0N4
Canada

Bibliothèque nationale
du Canada

Acquisitions et
services bibliographiques

395, rue Wellington
Ottawa ON K1A 0N4
Canada

Your file Votre référence

Our file Notre référence

The author has granted a non-exclusive licence allowing the National Library of Canada to reproduce, loan, distribute or sell copies of this thesis in microform, paper or electronic formats.

L'auteur a accordé une licence non exclusive permettant à la Bibliothèque nationale du Canada de reproduire, prêter, distribuer ou vendre des copies de cette thèse sous la forme de microfiche/film, de reproduction sur papier ou sur format électronique.

The author retains ownership of the copyright in this thesis. Neither the thesis nor substantial extracts from it may be printed or otherwise reproduced without the author's permission.

L'auteur conserve la propriété du droit d'auteur qui protège cette thèse. Ni la thèse ni des extraits substantiels de celle-ci ne doivent être imprimés ou autrement reproduits sans son autorisation.

0-612-69009-1

Canada

University of Alberta

Library Release Form

Name of Author: Udo H. Verkerk

Title of Thesis: The synthesis and use of *tetrakis*[2-hydroxyphenyl]ethene in Ziegler-Natta catalysis.

Degree: Doctor of Philosophy

Year this Degree Granted: 2001

Permission is hereby granted to the University of Alberta Library to reproduce single copies of this thesis and to lend or sell such copies for private, scholarly, or scientific research purposes only.

The author reserves all other publication and other rights in association with the copyright in the thesis, and except as hereinbefore provided, neither the thesis nor any substantial portion thereof may be printed or otherwise reproduced in any material form whatever without the author's prior written permission.

UHVerkerk

#407-11012-82nd Avenue,
Edmonton, AB T6G 2P6

2/10/2001

University of Alberta

Faculty of Graduate Studies and Research

The undersigned certify that they have read, and recommended to the Faculty of Graduate Studies and Research for acceptance, a thesis entitled **The synthesis and use of *tetrakis*[2-hydroxyphenyl]ethene in Ziegler-Natta catalysis** submitted by Udo H. Verkerk in partial fulfillment of the requirements for the degree of Doctor of Philosophy.

Dr. Jeffrey M. Stryker (Supervisor)

Dr. Joseph Takats

Martin Cowie

Dr. Martin Cowie

Sieghard Wanke

Dr. Sieghard E. Wanke

Dr. Karl Kopecky

M.C.

Dr. Michael McGlinchey
(External Examiner)

24/9/2001

Voor mijn ouders.

Abstract

In this thesis a high yield synthetic route was developed into a calix[4]arene analog, *tetrakis*[2-hydroxyphenyl]ethene, the key step of which consists of an acid catalyzed dimerization of bis(2-methoxyphenyl)diazomethane. Due to the change in topology, compared to a calix[4]arene four positions *ortho* to the OH groups have become available for introducing steric bulk near the polar pocket making the molecule an ideal oxo-surface for building discrete Ziegler-Natta catalysts.

Although assumed on the basis of the geometrical arrangement of four phenol groups, the actual similarity between calix[4]arenes and the *tetrakis*[2-hydroxyphenyl]ethene turned out to be limited. The results of variable-temperature ^{1}H-NMR spectroscopic studies showed that, at room temperature, the aryl rings of these compounds had free rotational mobility. Because of the unhindered correlated rotation of the aryl rings, the reaction of *tetrakis*[2-hydroxyphenyl]ethene with triethylaluminum was expected to give a mixture of products. Instead an unprecedented "crown-like" compound was obtained in non-Lewis basic solvents. Unfortunately the use of this compound as an anion abstracting agent, which would have made an attractive Ziegler-Natta cocatalyst, was compromised by its low Lewis acidity. The obtained compound underwent ligand redistribution when dissolved in THF or acetonitrile to give an "aluminum-sandwich" in between two tetraarylethene ligands. A similar structure is formed by calix[4]arenes.

In order to create a model of a supported Ziegler-Natta catalyst, the magnesium salt of *tetrakis*[2-hydroxyphenyl]ethene was prepared. After addition of $TiCl_4$ to this compound, suspended in toluene, an active catalyst was formed with triethylaluminum. The in situ formation of $MgCl_2$ is proposed to form

supported titaniumphenoxides. Based on literature reports and the actual measured polydispersity of the produced PE the involvement of oxygen near to the active catalyst center is suggested.

In this thesis some of the problems encountered in practical Ziegler-Natta catalysis research were addressed. In order to have a continuous and safe supply of toluene, an automated solvent purification system was designed, made and used. A descending well reactor was designed, built and tested as a potential solution for the contamination problems encountered in small scale polymerization runs, but according to the results major improvements of the basic design are required.

Acknowledgments

A thesis is never a "stand-alone" achievement of a single individual, but rather the result of a multitude of interactions within a Chemistry Department. As such these contributions need to be emphasized simply because this thesis could not have grown in the present final form without these contributions.

First of all I would like to thank my doctoral committee for bearing with me for, among other things, 324 (boring ?) pages (excluding the appendix) of this thesis, and, more important criticizing the work. There is no intellectual growth without criticism.

I would like to thank the technical staff in the Chemistry Department and Chemical Engineering Department for their assistance, and sharing their practical knowledge with me, an "outsider." Without their combined contributions no thesis could have been written.

In particular I would like to mention Roman Lipiecki (who built the hardware) and Larry Coulson (who designed and built the electronics) whom I will miss as valuable teachers and without whom Chapter 5 could not have been written. Although not a member of the technical staff of the Chemistry Department in relation to Chapter 5 Ron Greidanus should be mentioned for making the technical drawings.

All crystal structures were resolved and refined by Dr. Bob McDonald of the X-ray crystallographic laboratory of the Department of Chemistry. Crystallographic details can be obtained by contacting Dr. McDonald (e-mail: bob.mcdonald@ualberta.ca) using the SDL/XCL code of the appropriate appendix.

Administration: Ilona Baker, Vi Craige, Marie Labbe, Mary-Lou Lee, Jeannette Loiselle, Selina Mah, Anne Morris, Christine Otter.

Chemical Engineering: Anne Hearn, Long Wu.

Chemical exchange: Pat Doran, Dr. W. Hunter.

Chemical Storerooms: John Crerar, Tyler Fitzgerald, Dr. R. Gosavi, Bernie Hippel, Ken Jorgensen, Andrew Yeung.

Computer Services: Larry Coulson, Scott Dellinger, Ron Gardner, Shannon Qualie.

Electronic Services: Allan Chilton, Ed Feschuk, Kim Nguy-Do.
Elemental Analysis Services: Andrea Dunn, Darlene Mahlow.
Glassblowers Services: Todd Carter, Murray Connors, Gerald Streefkerk, John Toonen.
"Get me out of here:" Dr. Neil Branda, Dr. F. Cantwell, Dr. M. Cowie, Dr. Karl Kopecky, Dr. R.E.D. McClung, Dr. P. Steffler, Dr. Jeff Stryker, Dr. J. Takats, Dr. M. McGlinchey, Dr. S.E. Wanke.
Group members: Jignesh Bulsara, Dr. Charles Carter, Dr. Jianxin Chen, Dr. Trevor Dzwiniel, Sara Eisler, Molla Endeshaw, Megumi Fujita, Dr. Grace Greidanus, Jason Norman, Dr. Christina Older, Dr. Sensuke Ogoshi, Andy Skauge, James Sochan, Dan St.Cyr, Paul Tiege, Ross Witherall, Brian Wong, Dr. Makoto Yasuda, Dr. Guizhong Qi, Xin Qui.
Machine shop: Randy Benson, Paul Crothers, Hubert Hofmann, Roman Lipiecki, Kevin Rolston, Dieter Starke, Henry Stolk, Richard Tomski.
Mass Spectrometry Services: Larry Harrower, Dr. Alan Hogg, Dr. Angelina Morales-Izquierdo, Don Morgan, Dr. Randy Whittal.
NMR Spectroscopy Services: Gerdy Aarts, Tom Brisbane, Glenn Bigham, Lai Kong, Dr. Tom Nakashima.
Polymer Analysis, Chemical Engineering: Mrs. Bu
Spectroscopic Services: Dianne Formanski, Jim Hoyle, Bob Swindlehurst.
X-ray Crystallographic Services: Dr. Bob McDonald.

I would like to acknowledge and thank the current and former group members for many pleasant moments around the dining table and in the lab.

Finally, I would like to thank Hisako and my family for their continuous support and encouragement in difficult times.

Table of Contents

page

Chapter 1: Ziegler-Natta Catalysis: an introduction 1
- 1.1 Ziegler-Natta catalyst prehistory 4
- 1.2 Catalyst evolution 6
  - 1.2.1 Supported catalysts 6
  - 1.2.2 On the active site in supported catalysts 9
- 1.3 Metallocene catalysts 12
  - 1.3.1 On the active site in metallocene catalysts 14
  - 1.3.2 The escape from metallocene catalysts 21
- 1.4 The cocatalyst evolution 25
  - 1.4.1 Trialkylaluminum 25
  - 1.4.2 The MAO cocatalyst 25
  - 1.4.3 Weaker coordinating anions: boron and beyond 29
- 1.5 Building an active site 30
  - 1.5.1 Prior art 32
  - 1.5.2 Organizing elements: polydentate ligands 35
  - 1.5.3 Calix[4]arenes 38
  - 1.5.4 Breaking the ring: tetraarylethene 39
- 1.6 Project goals 41
- 1.7 Notes and references 42

Chapter 2: The preorganization of four phenol groups 61
- 2.1 Introduction 61
- 2.2 Results 64
- 2.3 Discussion 72
  - 2.3.1 Static stereochemistry of the obtained tetraarylethenes 73

2.3.2 Dynamic stereochemistry of the obtained tetraarylethenes 81

2.3.3 On the formation of dihydro-dibenzo[b,e]oxepin 88

2.4 Experimental 94

2.5 Notes and references 119

Chapter 3: Coordination studies of *tetrakis*[2-hydroxyphenyl]ethene with alkylaluminum compounds **126**

3.1 Introduction 126

3.2 Results 127

3.3 Discussion 135

3.3.1 The crystal structure of compound **1** 135

3.3.2 Comparison with other aluminum complexes of phenol-based tetradentate ligands 143

3.3.3 The crystal structure of compound **2** 146

3.3.4 The crystal structure of compound **4** 151

3.3.5 The structure of compound **1** in solution 155

3.3.6 The disproportionation of compound **1** 166

3.4 Experimental 184

3.5 Notes and references 191

Chapter 4: The use of the *tetrakis*[2-hydroxyphenyl]ethene oxo-surface in Ziegler-Natta catalysis **196**

4.1 Introduction 196

4.2 Results 197

4.2.0 Caveat 197

4.2.1 Attempts to synthesize discrete compounds 198

4.2.2 Synthesis of supported Magnesium salts 198

4.2.3 Probing the precatalyst homogeneity 202

4.2.4 Optimization of the Ti/ligand magnesium salt ratio 207

4.2.5 The effect of added hydrogen 207
4.3 Discussion 209
4.3.1 The crystal structure of compound **1** 209
4.3.2 The crystal structure of compound **2** 216
4.3.3 On the formation of compound **1** and **2** 219
4.4 The Ziegler-Natta catalysis results 223
4.5 Experimental 234
4.6 Notes and references 271
Chapter 5: Development of new instrumentation 276
5.1 Introduction 276
5.2 The solvent purification unit. 276
5.2.1 Theory of functioning 280
5.2.2 Detailed description: electronic part 286
5.2.3 Detailed description: hardware 288
5.2.4 Detailed description: starting the solvent purification unit 291
5.2.5 Discussion 294
5.2.6 Safety considerations 296
5.3 The descending well reactor 297
5.3.1 Theory of operation 298
5.3.2 Assembly and testing of the descending well reactor 303
5.4 Notes and references 308
Chapter 6: General discussion and conclusions 309
Appendices 325
A, Chapter 2, section 2.3.1 325
B, Chapter 2, section 2.3.1 331
C, Chapter 2, section 2.2 337
D, Chapter 3, section 3.3.1 345

E, Chapter 3, section 3.3.3 357

F, Chapter 3, section 3.3.4 363

G, Chapter 4, section 4.3.1 371

H, Chapter 4, section 4.3.2 385

I, Chapter 5, section 5.2.2 392

J, Chapter 5, section 5.2.3 399

List of Tables

page

Chapter 1: Ziegler-Natta Catalysis: an introduction **1**

Table 1.1 Ziegler-Natta catalyst comparison 7

Chapter 2: The preorganization of four phenol groups **61**

Table 2.1 Isomers of *ortho* substituted tetraarylethenes, assuming a static perpendicular conformation 75

Table 2.2 Selected crystallographic data for tetraarylethenes 80

Table 2.3 ^{1}H-NMR chemical shifts of hydroxy groups of tetradentate ligands 87

Table 2.4 ^{13}C-NMR chemical shifts of methoxy groups: the buttressing effect 89

Table 2.5 The yield of oxepine as a function of the reaction conditions ... 104

Chapter 3: Coordination studies of *tetrakis*[2-hydroxyphenyl]ethene with alkylaluminum compounds **126**

Table 3.1 Nuclear Overhauser effect observed on saturating specific ^{1}H-NMR signals of compound **1** 129

Table 3.2 THF titration of a 0.02 M solution of compound **1** in toluene-d_8 at room temperature 130

Table 3.3 Crotonaldehyde complexation of compound **1** compared to other Lewis acids 130

Table 3.4 Non-bonding distances around the oxygen atoms of compound **1** 141

Table 3.5 Comparison of the solid state structural features of In, Ga, Al containing eight membered rings 142
Table 3.6. Calculated ring shielding contribution arising from one benzene ring for the equatorial methylene groups in compound **1** 158
Table 3.7 Calculated ratio of the NOE effect between aromatic hydrogens and equatorial CH_2 groups in compound **1** 162

Chapter 4: The use of the *tetrakis*[2-hydroxyphenyl]ethene oxo-surface in Ziegler-Natta catalysis **196**
Table 4.1 Ligand distribution over the precipitate and supernatant layers, using excess $TiCl_4$ 206
Table 4.2 The effect of hydrogen on the M_w and polydispersity of the precatalyst combination $TiCl_4$/magnesium chloride salt of 2,2'-thiobis[4,6-(1,1-dimethylethyl)]phenol 209
Table 4.3 The influence of the supported titanium compound on the catalyst activity 225
Table 4.4 The influence of $MgCl_2$ on the PE polydispersity of $Ti(OR)_4$ based Ziegler-Natta catalysts 226
Table 4.5 Polymerization study: homogeneity of $TiCl_4$/ magnesium salt of *tetrakis*[2-hydroxyphenyl]ethene 244
Table 4.6 Polymerization study: influence of the ratio $TiCl_4$/ magnesium salt of *tetrakis*[2-hydroxyphenyl]ethene 248
Table 4.7 Polymerization study: homogeneity of $TiCl_4$/ magnesium salt of *tetrakis*[5-(1,1-dimethylethyl)-2-hydroxyphenyl]ethene 253
Table 4.8 Polymerization study: influence of the ratio$TiCl_4$/ magnesium salt of 2,2'-thiobis[4,6-bis(1,1-dimethylethyl)] phenol........ 259

Table 4.9 Polymerization study: homogeneity of $TiCl_4$/ magnesium salt of *tetrakis*[2-hydroxyphenyl]ethene 263

Table 4.10 Polymerization study: influence of hydrogen on the oligomer content of $TiCl_4$/ magnesium salt of 2,2'-thiobis[4,6-bis(1,1-dimethylethyl)]-phenol 268

Table 4.11 Polymerization study: influence of hydrogen on the molecular weight of PE 269

Table 4.12 Polymerization study: oligomer analysis using GCMS 270

Chapter 5: Development of new instrumentation 276

Table 5.1 Situation/state action table 281

Table 5.2 Testing the descending well reactor 305

List of Figures

page

Chapter 1: Ziegler-Natta Catalysis: an introduction **1**

Figure 1.1 Stereochemistry of Polypropylene 5

Figure 1.2 The Breslow-Newburg mechanism 14

Figure 1.3 Activation of electrophiles through association according to Negishi 30

Figure 1.4 Phenol based ligands in Ziegler-Natta catalysis 37

Figure 1.5 Calix[4]arene conformations 38

Figure 1.6 Helicity in tetraarylethenes 40

Figure 1.7 Substituted *tetrakis*[2-hydroxyphenyl]ethenes 41

Chapter 2:The preorganization of four phenol groups **61**

Figure 2.1 Oxo-surfaces 61

Figure 2.2 Perspective view of *tetrakis*[2-hydroxyphenyl]ethene 76

Figure 2.3 Perspective view of *tetrakis*[3-bromo-(1,1-dimethylethyl)-2-hydroxyphenyl]ethene 78

Figure 2.4 Variable temperature ^{1}H-NMR spectroscopy of *tetrakis*[2-methoxyphenyl]ethene 84

Chapter 3: Coordination studies of *tetrakis*[2-hydroxyphenyl]-ethene with alkylaluminum compounds **126**

Figure 3.1 ^{1}H-NMR chemical shifts for compound **1** 127

Figure 3.2 Assignment of the protons of Crotonaldehyde/THF.................. 131

Figure 3.3 Perspective view of compound **1** 136

Figure 3.4 Perspective view of compound **2** 147

Figure 3.5 Perspective view of compound **4** 152

Figure 3.6 Proposed assignment of the ^{1}H-NMR signals of compound **1** 156

Figure 3.7 Ring numbering and positions of equatorial methylene groups in compound **1** 157

Figure 3.8 Proposed assignment of the ^{1}H-NMR signals of equatorial ethyl groups in compound **1** 159

Figure 3.9 Intramolecular nonbonding H-H distances in compound **1** 160

Figure 3.10 Measured NOE effects for equatorial ethyl groups of compound **1** 163

Figure 3.11 Measured NOE effects for the aromatic protons of compound **1** 164

Figure 3.12 Measured "relay effects" in compound **1** 164

Figure 3.13 Measured NOE effects for axial ethyl groups in compound **1** 165

Figure 3.14 Tentative assignment of the ^{1}H-NMR signals of the equatorial and axial ethyl groups in compound **1** 166

Figure 3.15 Non-bonding distances in compound **1** 170

Chapter 4: The use of the *tetrakis*[2-hydroxyphenyl]ethene oxo-surface in Ziegler-Natta catalysis **196**

Figure 4.1 Polymerization activity of the precipitate and supernatant of the magnesium chloride salt of *tetrakis*[2-hydroxyphenyl] ethene 204

Figure 4.2 Polymerization activity of the precipitate and supernatant of the magnesium chloride salt of *tetrakis*[5-(1,1-dimethyl ethyl)-2-hydroxyphenyl]ethene.. 204

Figure 4.3 Polymerization activity of the precipitate and supernatant of the magnesium chloride salt of 4-*tert*-butylphenol 205
Figure 4.4 Variation of the polymerization activity as a function of the mixing time of the magnesium chloride salt of *tetrakis*[5-(1,1-dimethylethyl)-2-hydroxyphenyl]ethene and $TiCl_4$ 208
Figure 4.5 Variation of the polymerization activity as a function of the mixing time of the magnesium chloride salt of 2,2'-thio bis[4,6-(1,1-dimethylethyl)]phenol and $TiCl_4$ 208
Figure 4.6 Perspective view of compound **1** 211
Figure 4.7 Perspective view of compound **2** 217
Figure 4.8 The activity of $MgCl_2$ supported $Ti(OEt)_4$ and the polydispersity of the obtained PE 227
Figure 4.9 The activity of $MgCl_2$ supported $Ti(OR)_2X_2$ 227
Figure 4.10 $Ti(OAr)_4$ as an oligomerization catalyst 230

Chapter 5: Development of new instrumentation 276
Figure 5.1 The solvent purification according to Grubbs, et al 278
Figure 5.2 The modified solvent purification unit 279
Figure 5.3 Full section view of the descending well reactor 299
Figure 5.4 Isometric half section of the descending well reactor 300
Figure 5.5 Exploded view of the descending well reactor 306

List of Schemes

page

Chapter 1: Ziegler-Natta Catalysis: an introduction **1**

Scheme 1.1 Proposed metallocene insertion mechanisms 17

Scheme 1.2 Proposed chain termination steps for metallocene based Ziegler-Natta catalysts 18

Chapter 2: The preorganization of four phenol groups **61**

Scheme 2.1 Proposed synthesis of *tetrakis*[2-alkoxyphenyl]ethene 63

Scheme 2.2 Isomerization scheme for *ortho* substituted tetraphenylethenes, based on a 180° rotation of a single ring 82

Scheme 2.3 Proposed mechanism for oxepine formation 91

Scheme 2.4 Ceraulo's double rearrangement as observed under mass spectrometry conditions 93

Chapter 3: Coordination studies of *tetrakis*[2-hydroxyphenyl]ethene with alkylaluminum compounds **126**

Scheme 3.1 Proposed averaging process of the ethyl groups of compound **1** in THF 172

Scheme 3.2 Stereoisomers of calix[4]arenes and *tetrakis*[2-hydroxy phenyl]ethenes 175

Scheme 3.3 First stage of the proposed disproportionation mechanism of compound **1** in THF........................ 177

Scheme 3.4 Proposed intermediate interconversion 178

Scheme 3.5 Proposed disproportionation mechanism of compound **1**: transfer of ethyl group from central aluminum........................ 180

Scheme 3.6 Dimerisation of the intermediates to form compound **2** 181
Scheme 3.7 Overall disproportionation reaction 182

Chapter 4: The use of the *tetrakis*[2-hydroxyphenyl]ethene oxo-surface in Ziegler-Natta catalysis **196**
Scheme 4.1 Proposed reaction mechanism leading to active supported and non supported Ziegler-Natta catalysts 229

Chapter 5: Development of new instrumentation **276**
Scheme 5.1 State diagram of the "solvent take off" situation 281
Scheme 5.2 State diagram of the "solvent reservoir empty" situation 282
Scheme 5.3 State diagram of the solvent purification unit 284

List of Abbreviations

A	Ampere
ACN	acetonitrile
AES	atomic emission spectroscopy
AIBN	2,2'-azobisisobutyronitrile
Alt.	alternating
Ar	aryl
atm	atmosphere
av	average
Bu	butyl
c.a.	common anode
CI	chemical ionization
Cp	η^5-cyclopentadienyl
d	depth
dB	decibel
DC	direct current
DDQ	2,3-dichloro-5,6-dicyano-1,4-benzoquinone
deg.	degrees
DMSO	dimethylsulphoxide
EA	elemental analysis
EPR	electron paramagnetic resonance
eq.	equivalent
ES	electrospray
Et	ethyl
EI	electron impact
g	gram

GC	gas chromatography
η	hapticity
h	height
HDPE	high density polyethylene
HRMS	high resolution mass spectrometry
Hz	Hertz
IC	integrated circuit
ICP	ion conductive plasma
IR	infrared
KΩ	kiloOhm
L	liter
LDPE	low density polyethylene
LLDPE	linear low density polyethylene
LED	light emitting diode
mA	milliampere
MAO	methylaluminoxane
Me	methyl
mL	milliliter
mom.	momentary
MS	mass spectrometry
NBS	N-bromosuccinimide
NMR	nuclear magnetic resonance
n.o.	normally open
NOESY	nuclear overhauser effect spectroscopy
Ω	Ohm
osc.	oscillator
PE	polyethylene

Ph	phenyl
pp	peak to peak
ppm	parts per million
Pr	propyl
psig	pounds per square inch gauge pressure
spst	single pole, single throw
R	alkyl group
RT	room temperature
scfh	standard cubic feet per hour
slpm	standard liters per minute
S S	stainless steel
tert	tertiary
THF	tetrahydrofuran
TLC	thin layer chromatography
TMEDA	N,N,N',N'-tetramethylethanediamide
TMS	trimethylsilyl
TREF	temperature rising elution fractionation
T-ROESY	transmitter rotating frame Overhauser enhanced spectroscopy
Triflic	trifluoromethanesulfonic
TsOH	*para*-toluenesulphonic acid
µ	micron
µF	microfarad
µL	microliter
URL	underwriters laboratories
UV	ultraviolet
V	Volt

w	width
W	Watt
wt	weight
$W_{1/2}$	peak width at half the peak height
X	halide
xs	excess

1. Ziegler-Natta Catalysis: an introduction

Forty years of intense research efforts cannot be compressed in an introduction of 41 pages without harming the so-treated material. On the other hand the research described in this thesis has to be placed in the context of past research and present knowledge. Because of this friction the introduction is a limited subjective selection of the existing literature, with an emphasis on the use of titanium in Ziegler-Natta ethene polymerization. The literature selection is *not* up-to-date, as important scientific contributions seem to appear on an almost weekly basis at the time of writing. Patent literature in general has not been taken into consideration, because scientific standards do not necessarily apply and because there is too much patent literature to be managed by a single person. This does imply that some parts of the introduction are 1 to 2 years behind the current state of development in industry.

Certain definitions and technical terms are unavoidable, but the treated topic is so broad that occasionally reference will be made to introductory texts.

Ziegler-Natta catalysis refers to a metal-based catalytic process whereby an olefin is converted into different forms of polyolefins: a more narrow definition seems hazardous considering the pace of development at the moment. Different forms of the Ziegler-Natta catalysts often are described as first, second or higher generation catalysts. Unfortunately the subsequent numbering of the generations of polypropylene and polyethylene catalysts is different, while the actual numbering seems to be related to author, employer, polymer yield, catalyst composition or a combination of these. At the point of writing the development of new catalysts is so fast that it is unclear at which catalyst generation we are. Catalyst generation numbers will therefore not be used. In Ziegler-Natta catalysis considerable uncertainty surrounds the proposed chemical entity performing the catalysis. This can be a single chemical species consisting of one or more metal atoms, or a multitude of chemically different polymetallic aggregates.

A precatalyst in this thesis is a species that has to react with a cocatalyst in order to form the actual active catalyst (eq. 1.1). By itself a precatalyst is assumed to have no catalytic activity. Both in the literature and in this thesis the word "catalyst" is sometimes used where "precatalyst" should be used.

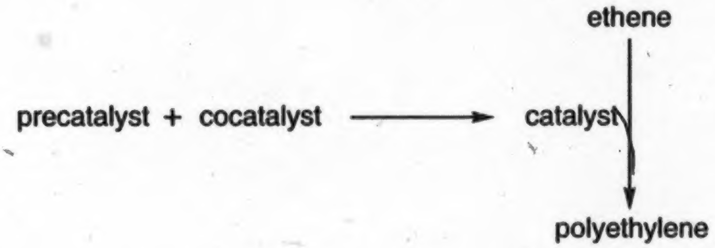

eq. 1.1

In the literature *soluble* catalysts are called *"homogeneous"* which is true at the start of the polymerization, while an *insoluble* catalyst is called *"heterogeneous"*. During polymer formation the homogeneous catalyst can become heterogeneous (polyethylene) or stay homogeneous (polypropylene) depending on the polymer solubility under the reaction conditions. In this thesis "homogeneous catalysts" are catalysts that *initially* are in solution. In the literature *experimental* proof of the "homogeneous" claim of either precatalyst or catalyst is in general absent. With regard to the reported catalyst activities in the literature, the "Gibson Health Warning" applies.[1] Comparing catalyst activities reported by different groups of researchers is hazardous because often information is missing on the kinetic profile of the catalytic species. Some catalysts are only active for a short period of time so that polymerization runs of 1 minute give a high catalyst activity, while a 1 hour run using the same catalyst under the same conditions would give a much lower activity. In addition, experimentally determined catalyst activities are highly dependent on the reaction conditions; for a spectacular example see section 1.4.2 (page 25).

In this thesis a polymer is a single chain of n repeating ("mer") units, with $n > 100$, *as well as* a heterogeneous mixture of polymer chains with different chain lengths ($n \geq 2$) and sidechain branching. An oligomer is a chain with $2 \geq n > 100$ repeating units. Because of the polymer heterogeneity, physical methods like end-group analysis, light-scattering measurements or osmometry when applied to measure the molecular weight of such a polymer will give an *average* of the molar masses of the polymer molecules that make up a sample. Depending on the technique used to determine the "molecular weight" of the polymer sample *different* molecular weight *averages* will be determined. If the physical method determines the *number* of polymer molecules in a sample of known weight (for example; end-group analysis) the average of the obtained molecular weight is the number average M_n. If instead a technique is used in which the obtained signal is based on the *size* or *weight* of the individual polymer molecules (for example; light-scattering experiments) the weight average molecular weight M_w of the polymer sample is obtained. A single M_n or M_w does not indicate the width of the chain length distribution of a polymer sample, but by itself represents the ratio of the propagation and termination rate constants. To get an indication to what extent the polymer sample deviates from the number average molecular weight M_n, the ratio of M_w/M_n, the polydispersity of the polymer sample, is often cited. The polydispersity of "a polymer" is actually related to the standard deviation[2] of the number-average molecular weight, it represents the chain length distribution that makes up a polymer sample and is one of the characteristic "fingerprints" of the active catalyst. The interest goes beyond the statistical part. The polydispersity is one of the factors determining the physical properties of the formed polymer mixture. Notice that different catalysts do not necessarily form the same polyethylene. Some catalysts form linear polyethylene with no side branches, the so-called High Density PolyEthylene (HDPE), while others form polyethylene with a few side branches (Linear Low Density PE, LLDPE) or multiple side branches in the polyethylene chain (Low Density PE, LDPE). Information on the polymer chain structure is not present in the M_n or M_w and has to be determined by ^{13}C-NMR, IR and/or Temperature Rising Elution Fractionation (TREF, see page 11). Side chain branching (and the side chain distribution within the polyethylene chain) represents another characteristic fingerprint of the used catalyst.

1.1 Ziegler-Natta Catalyst Prehistory.

The development of Ziegler-Natta catalysts started from a failed experiment in the Ziegler laboratories in 1953[3] that revealed the possibility that transition metals could act as catalysts. This initiated a systematic search to discover other metals that might show similar activities. The breakthrough came with $TiCl_4$ (the "precatalyst"), which produced catalysts that polymerized ethene at room temperature and atmospheric pressure when mixed with trialkylaluminum (the "cocatalyst") compounds.[3]

The next step originated from Natta's insight. In Natta's opinion, the monomer insertion between the growing chain and a metal atom should permit far better stereochemical control of the polymerization process.[4] This led Natta to investigate the polymerization of propene using the Ziegler catalysts, resulting (after fractionation) in the isolation of isotactic polypropylene (Fig. 1.1, page 5). If the structure of the Ziegler catalyst did influence the stereoselectivity of the insertion process, and the experimental results indicated this, then a regular crystalline surface might show even better results. Instead of using liquid $TiCl_4$, crystalline $TiCl_3$ was tried. An impressive increase in the yield of isotactic polypropylene was the result.[4]

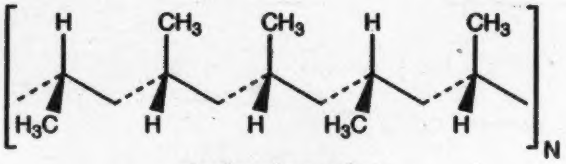
H
CH3
CH3
H
CH3
H3C
H
H
H3C
H
N

atactic polypropylene

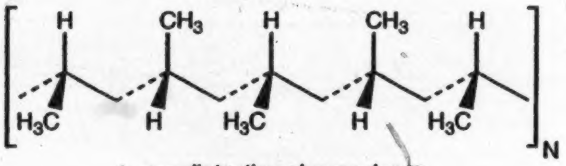
H
CH3
H
CH3
H
H3C
H
H3C
H
H3C
N

syndiotactic polypropylene

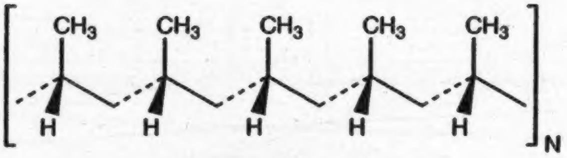
CH3
CH3
CH3
CH3
CH3
H
H
H
H
H
N

isotactic polypropylene

Figure 1.1

Further improvement was achieved by other groups leading to a catalyst consisting of finely milled $AlCl_3$ and a specific crystalline form of $TiCl_3$ to give catalysts of higher activity (for ethene) and selectivity (for propene).[5]

These developments formed the core of both novel chemistry and a new industry for which Ziegler and Natta were awarded the Nobel prize in 1963.

1.2 Catalyst Evolution.

1.2.1 Supported Catalysts.

The activity of the existing $TiCl_3/AlCl_3$ based catalysts was insufficient (Table 1.1, page 7), leading to a substantial catalyst residue in the formed polymer. This residue had a detrimental influence on polymer properties like color, corrosion and light stability, making the removal of catalyst residues ("deashing") by extraction and chemical treatment necessary. To bring the amount of catalyst residues in the final product below a certain limit in order to avoid the additional extraction, a higher activity catalyst was required by industry. In addition, the existing catalysts did not have sufficient flexibility with regard to the adjustment of the molecular weight distribution of the formed polyethylene. These were the main factors pushing the development towards higher activity catalysts.[6]

The assumption that magnesium rather than aluminum in the $TiCl_3$ lattice might yield higher catalyst activity[7] guided the direction of the development towards magnesium. The existence of the successful Solvay catalysts using HOMgCl as a solid support for $TiCl_4$ also must have contributed significantly to focus research.[8] In the following period basically every conceivable combination of magnesium and titanium was patented,[9] for examples outside the patent literature see references 14-18. The most active catalysts discovered were based on $MgCl_2$ with a disordered crystalline structure,[5] so called "active" $MgCl_2$, combined with $TiCl_4$. As the amount of $MgCl_2$, in general, is in huge excess to the amount of $TiCl_4$ used, these catalysts are called "supported catalysts." To achieve the formation of active $MgCl_2$ several procedures have been described in the open and patent literature.[10] A mechanical and a chemical route can be distinguished.[11]

Table 1.1: Ziegler-Natta catalyst comparison

$TiCl_3 \cdot 1/3\ AlCl_3$	Activity: 20 Kg PE/mol Ti·hr·atm Al/Ti ratio: 50 Pressure: 1 atm Solvent: kerosene Runtime: 60 min. Temperature: 80 °C Reference: 14
$TiCl_4$ / ball milled $MgCl_2$	Activity: 1.7 ton PE/mol Ti·hr·atm (1.7 ton = $1.7 \cdot 10^3$ Kg) Al/Ti ratio: 25 (Et_3Al) Pressure: 1 atm Solvent: kerosene Runtime: 60 min. Temperature: 80 °C Reference: 14
$TiCl_4 \cdot 11.9\ MgCl_2 \cdot 22\ THF$	Activity: 8.5 ton PE/mol Ti·hr·atm Al/Ti ratio: 128 (Et_3Al) Pressure: 3 atm Solvent: hexane Runtime: 30 min. Temperature:70 °C Reference: 98
Cp_2ZrCl_2	Activity: 654 Kg PE/mol Zr·hr·atm Al/Ti ratio: 500 (MAO) Pressure: 1 atm Solvent: toluene Runtime: 10 min. Temperature: RT Reference: 39
$Cp_2Zr(CH_3)_2$	Activity: 59 ton PE/mol Zr·hr·atm Al/Ti ratio: 148000 (MAO) Pressure: 8 bar Solvent: toluene Runtime: 60 min. Temperature:70 °C Reference: 39

The goal of all approaches is the formation of micro crystalline $MgCl_2$ clusters on which a monolayer of $TiCl_4$ can be attached.[12] Accordingly the highest polymerization activity is achieved by methods that generate high surface area particles of small crystallite size and suitable morphology.[10, 19]

In the mechanical procedure (Table 1.1, page 7) the catalyst components are mixed together in suitable ratios (a Lewis base is generally added), and ball milled for several hours.[10] The use of ultrasonic radiation to reduce the $MgCl_2$ crystal size,[13] and the generation and condensation of gaseous[10] $MgCl_2$ have also been reported to achieve the formation of high surface area $MgCl_2$.

Chemical routes generate amorphous "active $MgCl_2$" by forming $MgCl_2$ clusters starting from $MgCl_2$ molecules (Table 1.1, page 7). Several routes to form active $MgCl_2$ have been described in the literature and are in general characterized by treatment of $Mg(OR)_2$, $Mg(OR)Cl$ or MgR_2[18] as a solid (the Grignard reagents can also be dispersed on silica gel, alumina or other carriers, see reference 17) or solution with an excess chlorinating agent, often at increased temperatures.[14,15] Dissolving $MgCl_2$ in a suitable solvent, followed by removal of this solvent is another chemical route into active $MgCl_2$. The so obtained active $MgCl_2$ can subsequently be loaded with $TiCl_4$ to form the precatalyst. To eliminate possible byproducts like $Ti(OR)_nCl_{(4-n)}$ compounds subsequent washings with solvents or $TiCl_4$ are incorporated into the procedure. This is an important step because these byproducts can be polymerization or oligomerization catalysts,[16] diminishing the catalyst and product reproducibility.

In the early stages in the development of supported catalysts, the mechanical treatment was preferred owing to the relative simplicity of the method and low cost. The disadvantage of ball-milling is that there is a limit to the smallest crystal size that can be obtained. Continued milling beyond a due to crystal annealing caused by the high local temperatures generated in the process.[9] The mechanical route is therefore less suitable in generating high activity catalysts.

Subsequently, chemical routes have been preferred as a more flexible route into catalyst supports based on small $MgCl_2$ clusters.[19]

1.2.2 On the active site in supported catalysts.

In spite of 48 years of research very little is known about the actual catalytic species in heterogeneous Ziegler-Natta catalysts. There are several reasons for this.[20] First of all, the number of slightly different catalyst systems is very large. Secondly, the analytical tools are not available to investigate active species present in low concentrations in heterogeneous materials at the start of the reaction, and deeply buried and finely dispersed in the polymer at the end of the reaction.[20] Thirdly, the experimental observations are often difficult to reproduce due to the extreme sensitivity of the actual active species to catalyst poisons like water and oxygen. The situation is not improved by the large number of published speculations, which in general do not reveal to what extent these speculations are based on experimental facts.

In order to obtain insight into the catalytic activity, experimental observations on model compounds and theoretical calculations have been used, the results of which depend on the model on which the calculations are made.[21] The relation of the model to reality is known because by necessity the model reduces the information content of the process it mirrors. What is unknown is to what extent essential information has been lost in the reduction process. The same can be stated for model reactions. The following list is a compilation of the established and commonly accepted experimental facts with regard to heterogeneous $MgCl_2$- supported Ziegler-Natta catalysts.[4,5]

1) The $TiCl_4/MgCl_2$ combination by itself is inactive for polymerization of olefins. Et_3Al by itself will form oligomers with olefins at higher temperatures through the "Aufbaureaktion".[3]

2) When the "precatalyst" $TiCl_4/MgCl_2$ mixture is combined with the "cocatalyst" Et_3Al an active catalyst for olefin polymerization is formed. Extensive reduction of titanium takes place.[5,22] Radiolabelling experiments indicate the incorporation of the alkyl derived from the trialkyl aluminum in the polymer chain. The relation between the oxidation state of the titanium and the catalyst activity is unclear, in part due to the limited number of publications on this topic.[5,22]

3) The active catalyst seems located at specific, disordered, sites on the $MgCl_2$ crystals as shown by electron microscopy studies and the correlation found between catalyst activity and structural disorder of the $MgCl_2$ support.[23] The active catalyst is stabilized by $MgCl_2$ interactions and is temperature sensitive.[23]

4) The exact number of catalytic sites is unknown, and is not a constant.[24] Depending on the catalyst mix, an increasing, decreasing, or a more or less constant polymerization activity is observed.

5) At least one of the catalytic centers must be a stereogenic center. This is based on the observation of isotactic polypropylene formation.[4]

6) There are several kinds of catalytic centers. When polypropylene is fractionated syndiotactic, isotactic and atactic polypropylene (Fig. 1.1, page 5) can be isolated: different catalytic centers exist with different stereoselectivities.

The precatalyst centers, that presumably correspond to these catalytic centers, have different tendencies to complex with optically active Lewis bases.[25] EPR studies on supported catalysts also support the presence of several chemically different titanium species.[25] On the basis of these experiments up to seven different classes of active sites have been proposed to exist on the $MgCl_2$ surface.[5]

7. The olefin monomer repeatedly inserts in a metal-carbon bond contained in the catalyst. The carrier of the propagating chain is unknown and could be either Al, Mg or Ti. Aluminum based polymerization catalysts have been published, see section 1.3.2 (page 21). Model compounds containing Mg as an active polymerization catalyst have not yet been reported, but polyethylene formation with $MgEt_2$ has been reported.[29] It is unknown if the actual catalyst is charged[30] or neutral.[4]

8. The monomer insertion is occasionally interrupted by termination of the polymerization under release of the formed polyethylene. The termination is mainly through chain transfer to the incoming ethene molecule.[5,31] Chain transfer to aluminum and β-H elimination are minor termination processes. The statistical nature of both termination and initiation processes gives rise to the chain length distribution of the polymer sample as expressed in the polydispersity.

It is generally believed that the molecular-weight distribution closely reflects the chemical heterogeneity of the catalytic sites.[26] Temperature Rising Elution Fractionation (a polymer fractionation technique whereby side chain branching determines when a polymer chain elutes off the column as a function of solvent/column temperature) results actually have been interpreted to reflect the number of different active sites on the $MgCl_2$ surface.[27] However, the theory that the molecular-weight distribution reflects the number of chemically different active sites has not been proven. It is assumed that the presence of a limited number of chemically different active centers is able to explain all the observed molecular weight distributions. Each "single-site" member of these families supposedly produces an identical statistical distribution of polymer chain lengths which corresponds to the Schulz-Flory most probable distribution[28] with a polydispersity of 2. Summation over all chemically different sites produces the envelope which represents the actual observed molecular weight distribution.

This is convenient in its simplicity, but not necessarily reflecting reality, as the observed molecular weight distribution can also be theoretically derived by assuming a continuum of chemically different active sites.[28] There are several indications in the literature that the assumption of a limited number of chemically different active sites to explain the molecular weight distribution is questionable if not erroneous.[27,28] Given the observation that the active sites are located on disordered sites, this should not come as a surprise. On the basis of this review, a discussion of the many proposed active site models does not seem appropriate. For completeness, the reader is referred to reference 31 for a discussion of these models.

1.3 Metallocene Catalysts.

Natta originally assumed that the heterogeneity of the Ziegler-Natta catalysts was responsible for the catalyst activity, but experiments by Natta[32] and others[33] using titanocene dichloride and triethylaluminum showed that soluble catalysts could also form polyethylene. Other presumably homogeneous systems (tetrabenzyl- and tetraallyl-titanium and zirconium)[35] were also under scrutiny but the activities of all these homogeneous catalysts never could reach the activities or stereoselectivity of heterogeneous supported catalysts and were soon abandoned. Because these soluble metallocene catalysts did polymerize ethene they were considered valuable models for heterogeneous Ziegler-Natta catalysts.[36]

The torpid activity in the field of homogeneous Ziegler-Natta catalysis changed dramatically with the discovery by Ewen/Kaminsky/Brintzinger[37] that *ansa*-bridged metallocenes (eq. 1.8, page 21) were able to rival the stereoselectivity of heterogeneous catalysts, and the simultaneous[38] discovery by Sinn and Kaminsky[39] that water dramatically increased the activity of metallocene catalysts by converting the trialkylaluminum cocatalyst into a more active methylaluminoxane, MAO (eq. 1.2), see section 1.4.2 (page 25).

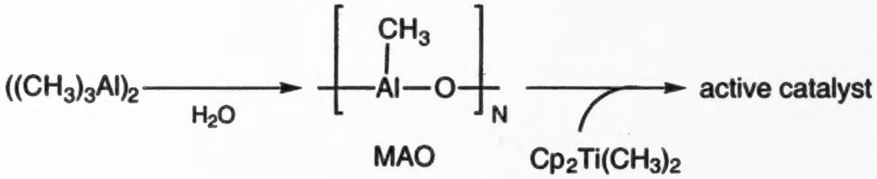

Activity: 3 ton PE/mol Ti·hr·atm
Al/Ti ratio: 10811
Pressure: 8 bar
Solvent: toluene
Runtime: 90 min.
Temperature: RT
Reference: 39

eq. 1.2

With polymerization activities in the 4 ton of isotactic polypropylene/ mol catalyst·hr·atm range and narrow polydispersities, industry became interested, resulting in an avalanche of patents and publications as well as novel chemistry.[40]

Thanks to the solubility of the catalyst, significant progress was made in understanding the actual active species yielding new ways into active catalysts.

1.3.1 On the Active Site in Metallocene catalysts.

The Breslow-Newburg paper[33] in 1959 contained proposals for the ethene polymerization mechanism of titanocene/alkylaluminum catalysts that seemed to be confirmed in the following thirty years.

In the original paper the function of the aluminum compound was clearly described: "the function of the aluminum would therefore be first to alkylate the titanium and then to put a formal or potential positive charge on the titanium and increase its complexing ability" (for the olefin, Figure 1.2). Independently Shilov postulated a titanocene cation as the active center, while Dyachkovski obtained indications through elegant electrodialysis experiments that this indeed was the case.[41]

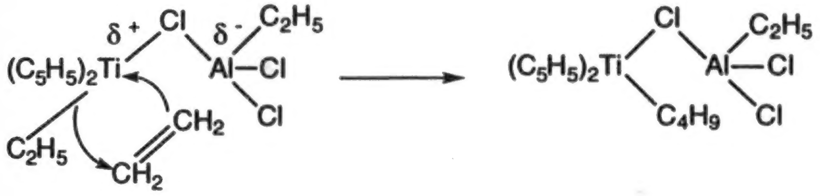

Figure 1.2

If the reaction of Kaminsky and Sinn can be taken as a model for acceptance of these ideas, skepticism prevailed.[42] More convincing evidence came with the isolation of an insertion product by Eisch, et al.,[43] and the synthesis of isolable cationic 14 electron d^0 titanocene and zirconocene species by Jordan, Bochmann and others,[44,45] heralding a more detailed understanding of the homogeneous Ziegler-Natta catalysts.

The following picture of the catalytic process emerged, although the criticism of Möhring and Coville with regard to experimental data should be kept in mind: there are very few comparative studies.[53]

1) The precatalyst is a group 4 dialkyl or alkylhalo-metallocene formed in situ by the alkylaluminum cocatalyst (eq. 1.3).

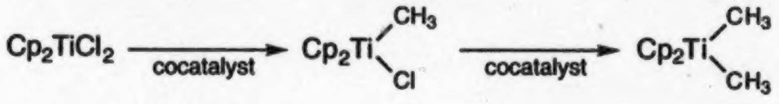

eq. 1.3

2) An active catalyst is characterized by the formation of a cationic 14-electron d^0 titano/zirconocene species. All evidence, like electrodialysis,[41] transition metal NMR,[54] different synthetic ways to arrive at an active catalyst[44,45] and the influence of solvent polarity[43] and counter anion on the polymerization activity[55] points in this direction. Several routes into the proposed cationic species, like one-electron oxidation, alkyl/hydride abstraction, and protonolysis have been developed,[44,45] giving rise to active homogeneous ethene polymerization catalysts (eq. 1.4, page 16).

3) On the basis of the observed increase of catalytic activity with monomer concentration it is generally believed that the incoming olefin forms a complex with the cationic metal center under reversible displacement of the counter anion (eq. 1.5, page 16). This step has not experimentally been observed, but has been modeled by Jordan,[56] Brintzinger,[52] and others.[34]

At this point the emerging picture starts to become less clear. Although the ion pair separation is considered critical for the activity of the formed catalyst, the relative concentrations of solvent separated and associated ion pairs as well as their contributions to the measured overall activity of the catalyst are unknown. It is unknown if the olefin can coordinate to the cationic metal without ion pair dissociation. Reliable comparative measurements of the ion-pair effect are few, and fraught with difficulties.[55] If the model of Brintzinger,[56] who uses reversible complexation of the zirconocene cation with trimethylphosphine as an "ethene" molecule, has any validity for the real catalyst, the olefin insertion is much faster than the recombination of the separated ion pair.

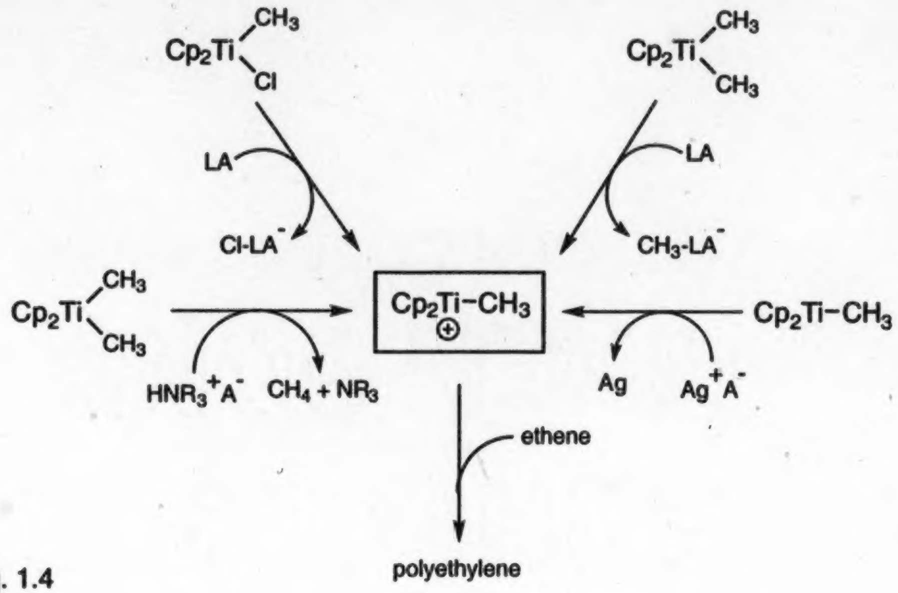

Cp2Ti(CH3)Cl
LA
Cl-LA⁻
Cp2Ti(CH3)2
LA
CH3-LA⁻
Cp2Ti(CH3)2
HNR3⁺A⁻
CH4 + NR3
Cp2Ti-CH3 ⊕
Cp2Ti-CH3
Ag
Ag⁺A⁻
ethene
polyethylene

eq. 1.4

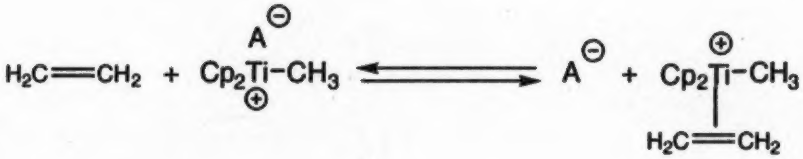

H2C=CH2
A⊖
Cp2Ti-CH3 ⊕
H2C=CH2

eq. 1.5

4) Ethene insertion into the metal-alkyl bond takes place. Several mechanisms have been proposed with varying amounts of α-agostic assistance in the insertion step, see Scheme 1.1 (page 17). Such α-agostic interactions are proposed to orient the polymer chain in such a way as to minimize interactions between alkyl substituents of the incoming monomer (for example propene) and the ligand/polymer array during the insertion. Agostic assistance[58] has been measured for a number of systems. However the effect is not always measurable or present, leaving open the possibility of other

mechanisms (like the Cossee-Arlman mechanism, no α-agostic interactions in ground- or transition-state) operating.[58] Unfortunately, as remarked by Brintzinger in relation to the validity of extended Hückel calculations,[57] whenever the electron deficiency of the reaction complex is relieved by some external ligand species like the counter anion, the agostic reaction mode would lose most of its advantage. More data on α-agostic effects are therefore needed, especially with regard to possible counter anion effects in cationic species.[59]

Scheme 1.1: Proposed Metallocene insertion mechanisms.

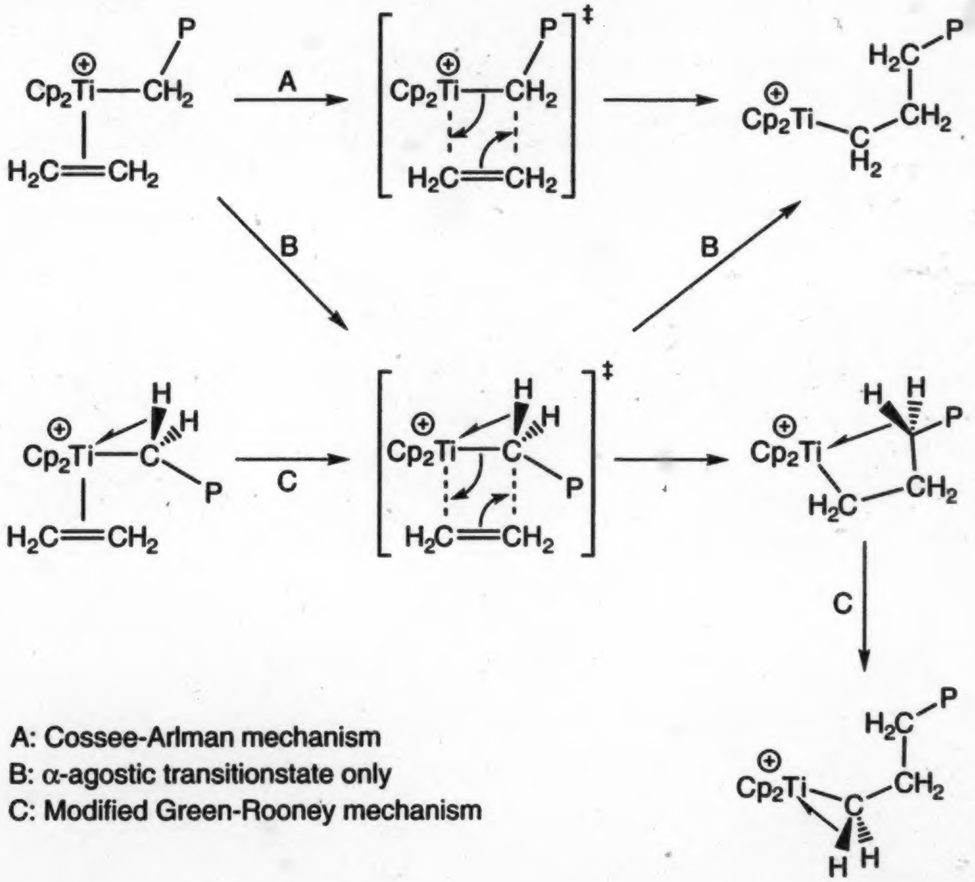
Cp₂Ti
CH₂
P
H₂C=CH₂
A
B
B
C
C
‡
‡
A: Cossee-Arlman mechanism
B: α-agostic transitionstate only
C: Modified Green-Rooney mechanism

5) The repeated coordination and insertion of the olefin is occasionally interrupted by chain termination. Different chain termination processes have been experimentally determined by detailed polymer-product analysis.[60] Transfer of a β-H can take place to the monomer (B in Scheme 1.2) or to the cationic metal at room temperature (C in Scheme 1.2). The ratio of these two β-H transfer processes is strongly metallocene structure dependent. In addition, polymer chain transfer to aluminum (A in Scheme 1.2) can take place.[60]

Scheme 1.2: proposed chain termination steps for metallocene based Ziegler-Natta catalysts.

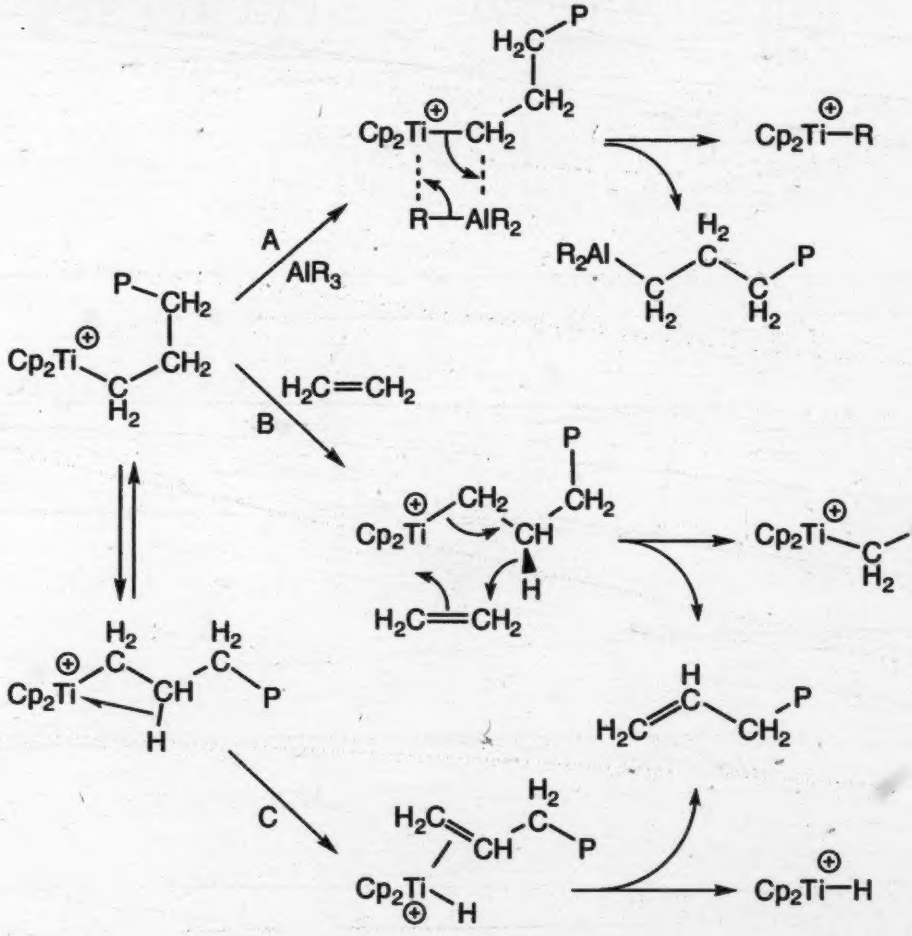

This mechanism only becomes competitive at low temperatures or high concentrations of the aluminum cocatalyst.

The reason *why* cationic metallocenes are able to sustain repeated insertions without β-H elimination interruption to obtain a long linear polymer is unclear. Jordan, et al., cite bond strength effects.[61] The alkyl metal bond, according to Jordan, et al., is selectively strengthened compared to the metal hydrogen bond when the metal center is in the *cationic* form. This would disfavor β-H elimination. Resconi, et al.,[60] propose a decrease in β-H elimination with decreasing metal Lewis acidity, and support this argument with the experimental observation that replacement of the Cp ring in a cationic zirconocene complex with a more electron donating pentamethyl-Cp increases the molecular weight of the formed polypropylene. Although this might be masked by steric effects preventing the formation of a β-H transfer transition state, a study by Bercaw, et al.,[62] on a *neutral* permethylscandocene complex is cited wherein a positive charge buildup is found for the transition state leading to β-H elimination. Such a transition state would be disfavored by electron donating Cp rings.

6) The principle of microscopic reversibility seems to apply for the olefin-insertion step, as shown by Basset, et al.[63] This is an important result with regard to the environmental impact of polyolefins and how to handle that problem.

In the last five years it has become clear that this mechanistic picture is too simple. Several groups reported on the formation of dimers of cationic metallocenes and unreacted dialkyl metallocenes.[46,47] Apparently neutral dialkylmetallocenes stabilize the formed metallocene cation more effectively than solvent molecule or anion coordination (eq. 1.6, page 20).

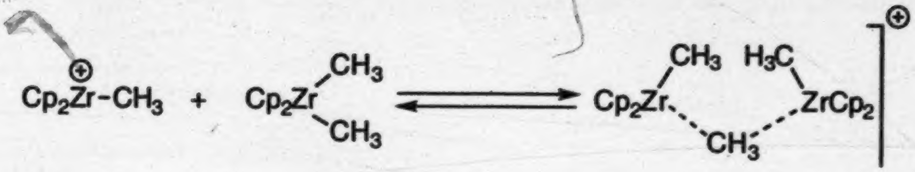

eq. 1.6

Brintzinger has questioned the existence of the proposed metallocene ion pairs (in absence of excess dialkylmetallocenes or Lewis acidic cocatalysts) focusing the attention instead on the behavior of ion pairs in apolar solutions: diffusion measurements indicate the presence of ion-pair *dimers* and *higher aggregates* in solution (eq. 1.7).[51]

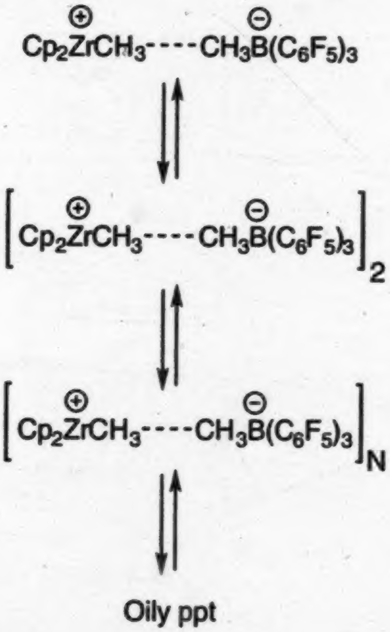

eq. 1.7

Depending on the concentration, a colloidal microphase containing ion-pair clusters is possible. Oily deposits formed in reactions of metallocenes with cocatalysts have appeared regularly (and ignored with the same frequency) in the literature in the past.[52]

If instead an excess of the Lewis acidic cocatalyst is present, "dicationic" species can be formed that recently have been shown to be highly active polymerization catalysts (eq. 1.8).[49]

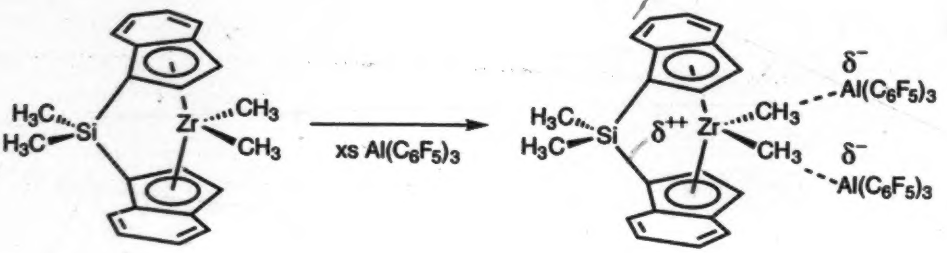

eq. 1.8

Of course none of this would matter, except that it has become unclear if the originally proposed metallocene cation really is the (sole ?) active species, and to what extent all these equilibria and aggregation states exist and influence the outcome of the catalysis. Unfortunately, depending on the concentration of the ion pairs, the studied system seems to approach yet another *heterogeneous* system.

1.3.2 Escape from metallocene catalysts.

The metallocene complexes of the early transition metals have turned out to be highly flexible and successful Ziegler-Natta catalyst precursors, as expressed by industry in the form of extensive patent coverage of this family of catalysts. It was therefore not surprising to see the impetus of research in this field shift in the direction of non-metallocene ligands,[1,64] with truly amazing results in the last 5 years. In a 1995 review, Brintzinger, et al.,[65] noted that a "living" polymerization, where the formed polymer chains permanently stay attached to the metal center on which they simultaneously start to grow (leading to a polymer polydispersity of 1), had not been observed for either heterogeneous Ziegler-Natta catalysts or for zirconocene-based catalysts for α-olefin polymerizations. A year later McConville, et al.,[66] reported the living polymerization of 1-octene using a chelating diamide complex of titanium with high activity (eq. 1.9). The polymerization activity for ethene was reported at the same time using a similar diamide ligand by Tinkler, et al.,[67] and turned out to be disappointing. It is unknown if any living character in the ethene polymerization was observed.

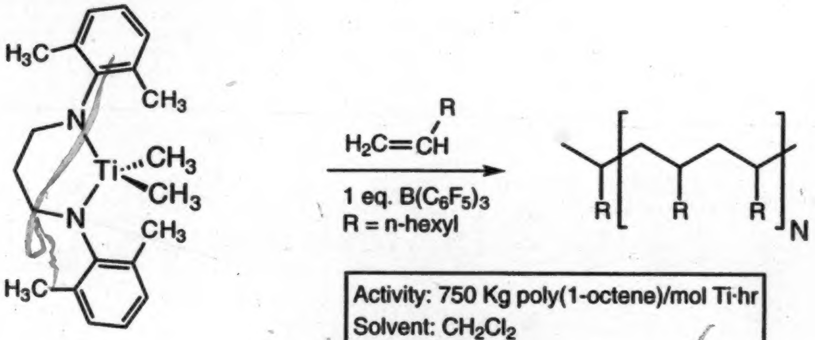

eq. 1.9

Activity: 750 Kg poly(1-octene)/mol Ti·hr
Solvent: CH_2Cl_2
Runtime: 10 min.
Temperature: 23 °C
Reference: 66
Polydispersity: 1.07

In relation to the discussion of heterogeneous supported catalysts, the publications of Jordan and Coles[68] and Gibson et al.[68] should be noted. Using an amidinate ligand, cationic aluminum alkyl complexes could be induced to produce polyethylene (see eq. 1.10, page 23).

The outline of a new breakthrough[69] in Ziegler-Natta catalysis became clear in 1998 with the publication of iron-based catalysts by Gibson, et al.,[70] (eq. 1.11, page 23) and Brookhart, et al.[71] Using bulky tridentate pyridinebisimine ligands, extremely high ethene polymerization activity was reported. The Brookhart group[71] reported 330 tons of polyethylene/mol Fe·hr at 60 °C and 600 psig, indicating that higher temperatures and pressures are possible with

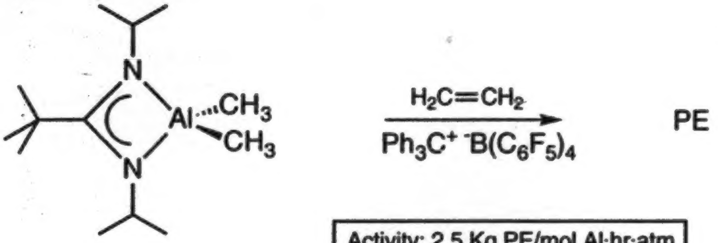
N
N
Al
CH_3
CH_3
$H_2C{=}CH_2$
$Ph_3C^+ \, ^-B(C_6F_5)_4$
PE

Activity: 2.5 Kg PE/mol Al·hr·atm
Pressure: 2 atm
Solvent: toluene
Runtime: 1 hr.
Temperature: 60 °C
Reference: 68
Polydispersity: 3.30

eq. 1.10

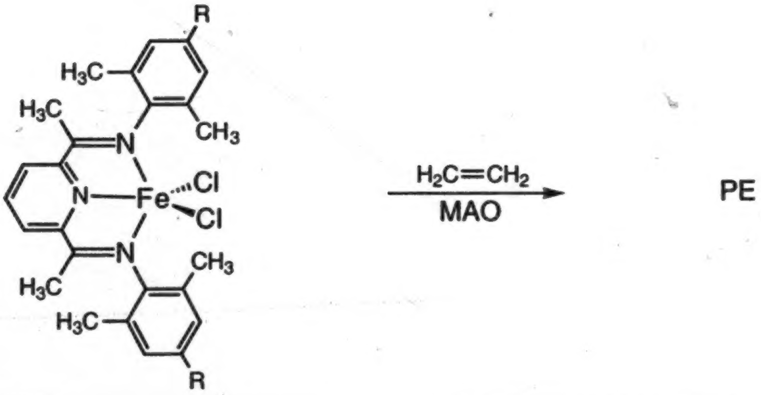
R
H_3C
H_3C
CH_3
N
N
Fe
Cl
Cl
N
CH_3
H_3C
H_3C
R
$H_2C{=}CH_2$
MAO
PE

R = CH_3
Activity: 21 ton PE/mol Fe·hr·atm
Al/Fe ratio: 1000
Pressure: 10 bar
Solvent: isobutane
Runtime: 1 hr.
Temperature: 35 °C
Reference: 70
Polydispersity: 10.7

R = H
Activity: 8.1 ton PE/mol Fe·hr·atm
Al/Fe ratio: ≥ 300
Pressure: 600 psig
Solvent: toluene
Runtime: 10 min.
Temperature: 60 °C
Reference: 71

eq. 1.11

this robust system. All indications are that these systems are able to compete with, or surpass existing metallocene based Ziegler-Natta catalysts. These catalysts still need highly purified, and therefore expensive, feedstock (solvent, ethene) and a huge excess of cocatalyst (MAO, 1000 equivalents).

This problem was addressed in 2000 by Grubbs et al.[72] in another landmark paper for Ziegler-Natta catalysis (eq. 1.12). In an extension of the work of Keim, et al.,[73] by using a salicylaldimine ligand a nickel based polymerization catalyst was obtained with a reported activity of 3.7 tons of polyethylene/mol Ni·hr at 100 psig ethene and narrow PE polydispersity (1.5-3.0).

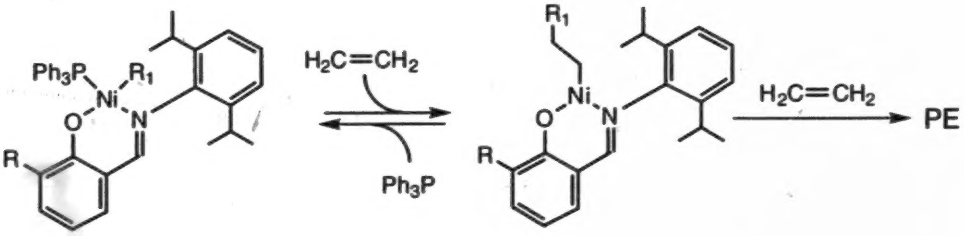

R_1 = Phenyl
R = 9-anthracene

Activity: 940 Kg PE/mol Ni·hr·atm
Pressure: 100 psig
Solvent: toluene
Runtime: 1-2 hrs.
Temperature: 45-50 °C
Reference: 72

eq. 1.12

More important, the catalyst maintained high activity in the presence of polar species like water, ethers, ketones and esters, promising less stringent purity requirements for Ziegler-Natta catalysis.

These are highlights of the last couple of years, indicating the tremendous pace of research in this area: a lot of details are unknown or unpublished at this point. At the same time it should be realized that gradual improvement of existing catalysts and increases in our mechanistic understanding are still taking place (albeit at a slower pace) amidst the fireworks of new breakthroughs.

1.4 The Cocatalyst Evolution.

1.4.1 Trialkylaluminum.

Optimization of catalyst behavior by adjustment of the cocatalyst took place right from the beginning of Ziegler-Natta catalyst development. Although other alkyl-metal compounds also showed precatalyst activation, the lower activity of the obtained catalysts combined with the low cost of the trialkylaluminum cocatalyst prevented practical use.[5] Experiments using dialkylaluminum chloride and alkylaluminum dichloride indicated that too high a Lewis acidity of the cocatalyst would force the formation of an oligomerization catalyst[31] and lower the yield of polyethylene,[30,74] and were therefore abandoned. No further evolution of the cocatalyst took place because no gain in the polymerization activity of heterogeneous supported catalysts could be achieved by modification of the cocatalyst. Cocatalyst modifications did have an effect on the polydispersity of the formed polymers[26] and the stereospecificity of the catalyst.[11] The field remained stagnant until the discovery of MAO cocatalysts.

1.4.2 The MAO cocatalyst.

During investigations using a titanocene dichloride/dimethylaluminum chloride polymerization catalyst, Breslow and Long found, according to their report in 1975,[39] that the results became *less* reproducible when impurities were *removed* from the polymerization reaction. When water (in the form of wet toluene) was deliberately added to an otherwise clean reaction, the polymerization activity of the titanocene catalyst increased by a factor 40. Similar results had been reported by Reichert and Meyer.[39] No quantitative measurements were reported in the article.[39] A year later, Sinn and Kaminsky isolated the partial hydrolysis product of trimethylaluminum (eq. 1.2, page 13) and used this product as a cocatalyst.[39,75] A tremendous increase in metallocene polymerization activity was reported, but only when the cocatalyst was used in huge excess (10000 equivalents) compared to the metallocene compound (Table 1.1, page 7).

The material formed by partial hydrolysis was a methylaluminoxane, which in subsequent investigations turned out to be a complicated heterogeneous mixture of interconverting oligomers as well as residual trimethylaluminum,[76] hindering if not preventing the understanding of the functioning of this cocatalyst. The structure of the formed aluminoxanes has been proposed to be linear,[76] cyclic,[6,76] cluster-like[80] or cage-like.[81,82]

Mechanistic studies showed that the first step in the catalyst generation by this cocatalyst is the formation of a mono- or bis-alkylated titano/zirconocene by ligand exchange with the MAO or residual trimethylaluminum.[77] The subsequent step, removal of an alkyl anion from the metallocene to form a metallocene cation, originally was thought to occur through protonolysis (eq. 1.13, page 27) by residual OH groups in the MAO.[78] However the isolation of catalytically inactive methylaluminoxane/ dimethylzirconocene models[78] seemed incompatible with this hypothesis (eq. 1.14, page 28). Instead MAO is assumed to abstract the alkyl/chloride anion from the metallocene as indicated by ^{13}C NMR[77] and conductivity measurements of the formed metallocene cation.[79] The actual alkyl/chloride abstracting species is unknown and theresulting anion has not been isolated but the resulting "MAO-anion" is assumed to have unusually low coordinating capability. This is speculated to be

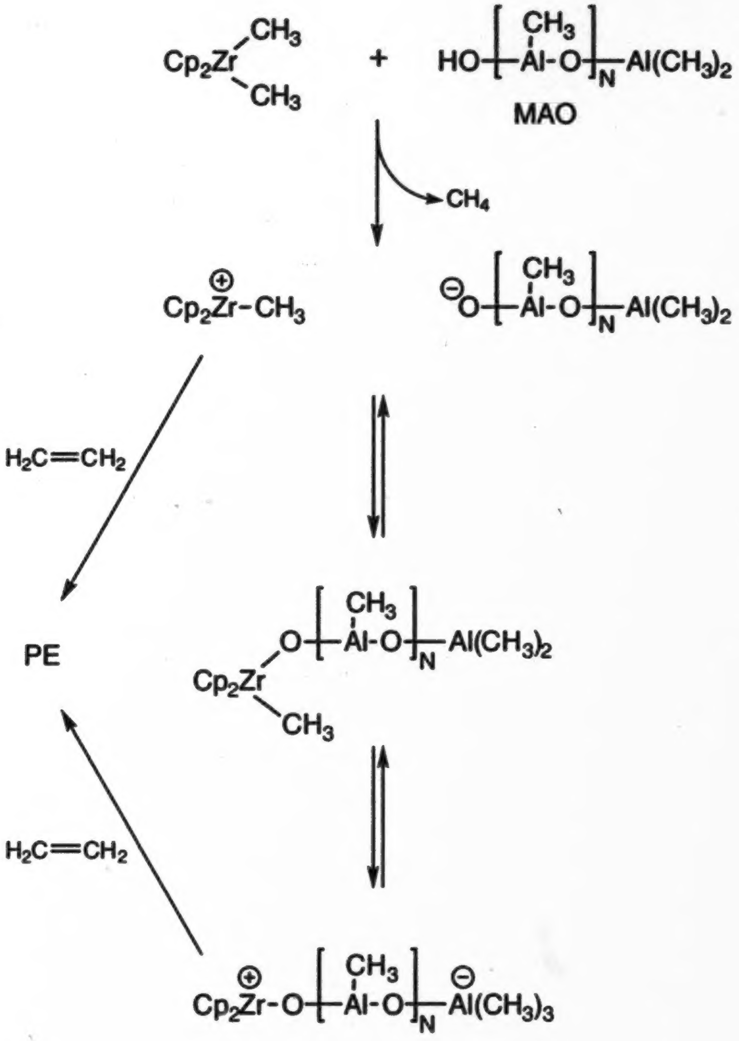

eq. 1.13

due to delocalization of the negative charge over the large MAO cluster surface (eq. 1.15, page 28), effectively forming a large delocalized counteranion.[80]

Three dimensional cages have been proposed to be present in MAO.[83] Such cages have been isolated by Barron, et al., by controlled hydrolysis of tri-*tert*-butylaluminum.[82] The products isolated by Barron, et al., generate active polymerization catalysts in the presence of dimethylzirconocenes. Due to strain incorporated in the hydrolysis products, the aluminoxane cages can break open by heterolytic bond cleavage to generate a stronger Lewis acidic site (eq. 1.16, page 29).

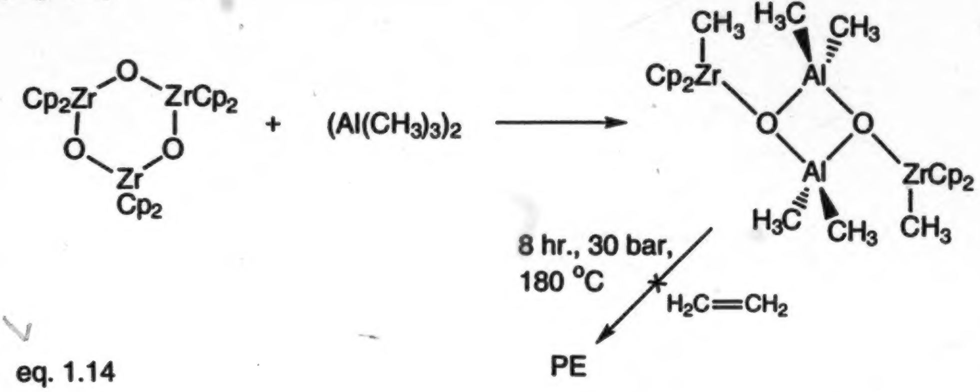
Cp2Zr
ZrCp2
Zr
Cp2
O
+
(Al(CH3)3)2
CH3
H3C
Al
ZrCp2
8 hr., 30 bar,
180 °C
H2C=CH2
PE

eq. 1.14

This phenomenon has been coined "latent Lewis acidity". Although the products, isolated by Barron, et al.,[82] seem to have limited value as cocatalysts due to the inherent steric hinderance, alkyl exchange of the isolated *tert*-butylaluminoxane cages with trimethylaluminum gives rise to more active cocatalysts.[84] The data published for these new cocatalysts seem to indicate that these compounds do not achieve the same catalyst activation as MAO, but remain the only, and therefore valuable, model for probing the functioning of MAO cocatalysts.

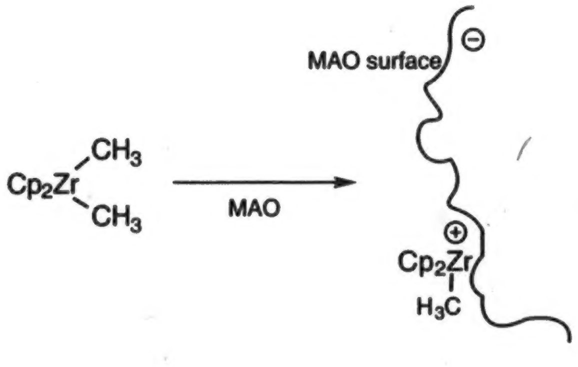
CH3
Cp2Zr
CH3
MAO
MAO surface
⊖
⊕
Cp2Zr
H3C

eq. 1.15

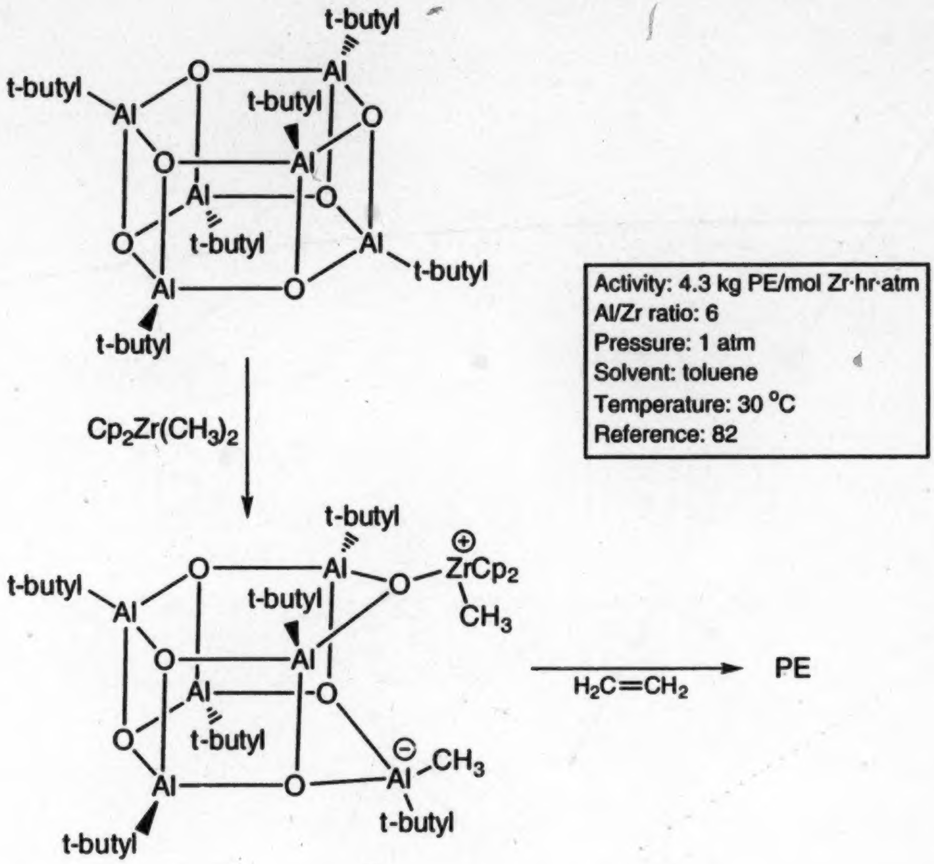

Activity: 4.3 kg PE/mol Zr·hr·atm
Al/Zr ratio: 6
Pressure: 1 atm
Solvent: toluene
Temperature: 30 °C
Reference: 82

eq. 1.16

1.4.3 Weaker coordinating anions: Boron and beyond.

The hypothesis that the unusual low coordinating ability of the MAO anion is essential for the catalyst activity[85] initiated a search for larger and more weakly coordinating counter anions,[86] and led to the discovery of tris(pentafluorophenyl)borane[87] as an efficient alkyl abstractor for generating zirconocene cations.[85] Synthetically two ways are open to achieve low coordinating ability of the counter anion. The first possibility is a further delocalization of the negative charge in the formed counter anion.[55] The second possibility is sterically hindering of the mutual cation/anion approach by increasing the steric bulk of the counter anion.[88] Within this rather restricted framework significant progress has been achieved, as shown in a review with an emphasis on the work of the Marks group.[86] For a review of other approaches towards influencing the cation/anion interactions see reference 89.

1.5 Building an Active Site.

As explained in sections 1.2.1 (page 6) and 1.2.2 (page 9), the combination $MgCl_2/TiCl_4$ gives a highly active catalyst after mixing with a cocatalyst. Although the actual catalytically active species present on the surface of the $MgCl_2$ are unknown, it is likely that these species are kept in place by interacting with the chloride lone pair electrons of neighboring titanium or magnesium atoms. Organometallic Lewis acids have a strong tendency to "plug up" their empty orbitals by aggregation. Such associative behavior can result in the activation of Lewis acids, and may lead in the extreme case to full ionization to generate an ion pair as suggested by Negishi (Fig. 1.3, page 31).[90]

The principle of activation of electrophiles through aggregation could be an important element of heterogeneous Ziegler-Natta catalysis.[90,30] As is well known from the work of Seebach[91] and Noyori,[92] the aggregation of organometallic species through noncovalent bonds to form supramolecules[93] profoundly influences the behavior of the formed species. To study the influence of aggregation on a molecular scale, a reproducible, preferably soluble assembly of Lewis acids is necessary: the aggregation has to be orchestrated. All of the examples cited by Negishi[90] involve bridging halides, which does not allow much influence on the aggregation of participating metals.

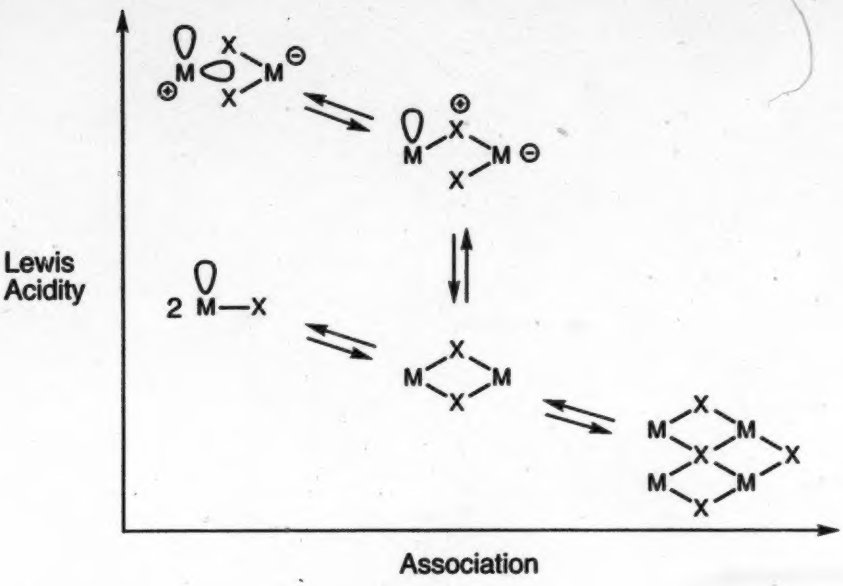

Figure 1.3 Activation of electrophiles through association according to Negishi.[90]

Depending on the required final polymetallic species, the aggregation might in theory be steered in a specific direction by using bridging ligands other than halogens, for instance O, S or N. Unfortunately, designing the ligand having these O, S or N groups placed in such a way that aggregation of the coordinated titanium, magnesium or aluminum takes place to form a structure that might act as a precatalyst site has some inherent difficulties. The actual structure of the catalyst site of a supported Ziegler-Natta catalyst is unknown (see section 1.2.2, page 9) and predicting the aggregation is difficult, if not impossible.[94] Furthermore, by using other bridging ligands a profound and unpredictable influence on the Lewis acidity of the resulting complex is to be expected. To further compound the problem, the aggregation of metals coordinated to the "orchestrating" ligand should not go beyond the ligand, that is, it should stay intramolecular. If intermolecular aggregation were to take place, any control over the final product would be lost, and the so-formed situation would essentially not be different from the existing heterogeneous Ziegler-Natta catalysts.

If however the orchestration of the aggregation of magnesium, titanium and aluminum could be achieved, the resulting species might function as a, possibly soluble, model for heterogeneous Ziegler-Natta catalysts.

In order to select a ligand for such an application, previous approaches towards influencing the aggregation of $TiCl_4$, $MgCl_2$ and Et_3Al in Ziegler-Natta catalysis have to be considered.

1.5.1 Prior Art.

Assembly of well defined Ziegler-Natta catalysts centered in the past on a reproducible crystallization of magnesium and titanium precursors. The major problem encountered in this approach is finding a compatible solvent for both precursors: in general Lewis bases were used.

The synthesis of a chlorobenzene-soluble Mg-Ti species was described in 1980 by Greco, et al.,[95] by dissolving $MgCl_2$ and $TiCl_4$ in Lewis bases (eq. 1.17, page 33). The obtained compounds are magnesium titanates according to conductivity measurements, and are one of the few attempts[96] to assemble magnesium- and titanium-containing molecules to give compounds with a known crystal structure. These compounds show moderate polymerization activities with a decrease in activity over time. The instantaneous activity is therefore higher than the activity averaged over 4 hours (308 kg PE/mol Ti·hr·atm). A polydispersity range of 3.5 - 5.0 was reported.

Using a similar methodology, magnesium titanate structures were obtained from THF (eq. 1.18, page 34) by Sobota, et al., in 1984.[97] Although the crystal structures of these compounds appeared in the literature, no polymerization data were published by this group.

structures of these compounds appeared in the literature, no polymerization data were published by this group.

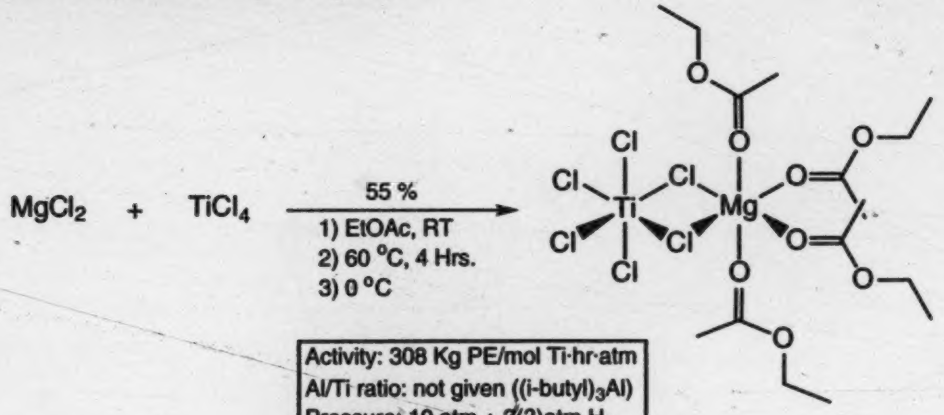

Activity: 308 Kg PE/mol Ti·hr·atm
Al/Ti ratio: not given ((i-butyl)$_3$Al)
Pressure: 10 atm + 3(?)atm H_2
Solvent: heptane
Runtime: 4 Hrs.
Temperature: 90 °C
Reference: 95

eq. 1.17

Using this THF method a whole range of, presumably, magnesium titanates were obtained by Woo, et al., who also reported difficulties in reproducing Sobota's results.[98] The polymerization activities for a set of compounds with a Mg/Ti ratio varying between 11.9 and 3.1 turned out to be in the 11.3 to 3.5 ton polyethylene/mol Ti·hr·atm range. The highest catalyst activity was recorded for the compound with a Mg/Ti ratio of 11.9 (Table 1.1, page 7). No data on the polydispersity of the obtained polyethylene, or on the solubility of the obtained precatalysts were published. Given that the compounds were ball milled before being used, a heterogeneous "semi-supported" Ziegler-Natta catalyst seems to have been created.

In 1991 Zucchini, et al.,[99] published the crystal structure of a bimetallic halide. By dissolving $MgCl_2$ and $Ti(OEt)_4$ in a 1:2 ratio in heptane at 80 °C, crystals were obtained after cooling the solution to 0 °C (eq. 1.19). The so-obtained compound was tested for catalytic activity, and found to display an activity of 3.5 Kg polyethylene/mol Ti·hr·atm in the presence of hydrogen.

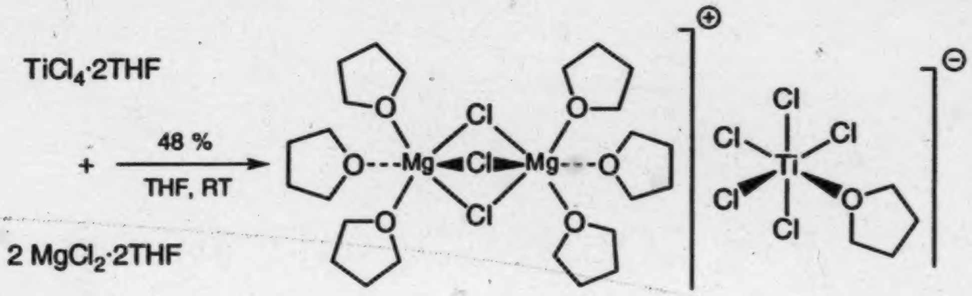

eq. 1.18

The polydispersity of the obtained polyethylene was 5.9. Both the reported activity of this soluble precatalyst as well as the polydispersity of the obtained polyethylene are inferior compared to the ballmilled $MgCl_2/Ti(OEt)_4$ precatalyst combined with 200 equivalents of Et_3Al (activity: 354 Kg PE/mol Ti·hr·atm, polydispersity: 5.5) under otherwise the same polymerization conditions.

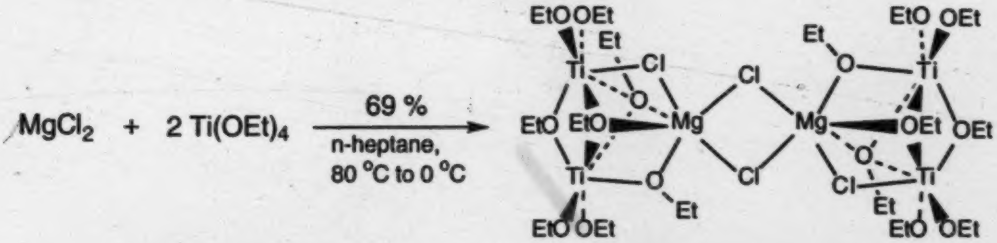

Activity: 370 g PE/mol Ti·hr·atm
Al/Ti ratio: 10 equiv. Et_3Al
Pressure: 6 atm
Solvent: toluene (soluble precat)
Runtime: not given
Temperature: 0 °C
Reference: 99
Polydispersity: not given

Activity: 3.5 Kg PE/mol Ti·hr·atm
Al/Ti ratio: 10 equiv. Et_3Al
Pressure: 6 atm + 4.5 atm H_2
Solvent: hexane (insoluble precat)
Runtime: not given
Temperature: 60 °C
Reference: 99
Polydispersity: 5.9

eq. 1.19

Of all the discussed compounds, the compound of Zucchini et al.[99] is the only one where oxygen-containing ligands are cooperating in the aggregation of the magnesium-titanium compound. The synthesis of this compound is passive, because the ligands used do not geometrically restrict the assembly of the magnesium-titanium compound. An active way of bringing the metals together would be to couple the oxygen ligands - to *preorganize* the oxygen ligands[93] - to bring the titanium, magnesium and/or aluminum atoms together upon coordination to the oxygen. A polydentate ligand is required to achieve such a preorganization of oxygen groups.

1.5.2 Organizing Elements: Polydentate ligands.

Oxygen-containing multidentate ligands can be organized into three classes of compounds - aliphatic polyols, polyphenols, prepared by condensation reactions of aldehydes and phenols (see section 1.5.1, page 32) and polyphenols containing direct *ortho* aryl-aryl bonds, like 2,2'-biphenol and binaphthol derivatives.

One of the requirements of a polydentate ligand is that further modification of the ligand should be possible in case intermolecular aggregation of the formed organometallic species takes place. The use of a ligand based on an aryl ring offers more flexibility[100] in modifying the ligand framework by introducing bulky groups *ortho* to the O, S or N binding site, and is therefore preferred over a polyol multidentate ligand. Although there is no literature on the use of O-,S- or N- containing aryl-based polydentate ligands combining Mg, Ti and Al in one compound, a large amount of literature is available for Ti and Al in combination with bidentate ligands.

The first studies on 2,2'-methylene-bisphenoxide complexes for use in Ziegler-Natta ethene polymerization were reported by Coleman in 1986,[101] after which a steady stream of other authors reported on the same ligand system.[102,103] The polymerization results as reported by Schaverien, et al.,[102] for phenol-based ligands showed moderate to low ethene polymerization activity (Figure 1.4, page 37) except for the sulfide bridged bis(phenolato) ligand.[104] Using MAO as a cocatalyst rather broad polydispersities were obtained for polyethylene, indicating that activation of the chelating phenoxides with MAO does not afford a single well-defined active species according to the authors.[102]

The dynamic behaviour of 1,1'-bis-2-naphtholatetitanium dichloride compounds has been investigated by Heppert, et al.[105] If these bisphenol ligands can be used as a model for 2,2'-methylene-bisphenol ligands, complicated disproportionation and aggregation equilibria with very low activation barriers[105] are possible using these bidentate ligands. This possibility, combined with the extensive investigations into these ligands for use in Ziegler-Natta catalysis, makes this class of ligands less suitable for the intended use of building a discrete catalytic site. Ortho-linked tris- and tetrakisphenols have recently also been developed.[106] Although not enough data are available yet for this new class of multidentate ligands, the *ortho* substituents (phenyl groups) used are sterically not bulky enough to prevent uncontrolled bridging of the formed titanium complexes as witnessed by the published crystal structures.[106]

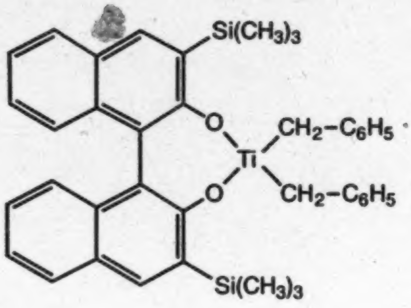
Si(CH3)3
O
Ti
CH2–C6H5
CH2–C6H5
O
Si(CH3)3

Activity: 45 Kg PE/mol Ti·hr·atm
Al/Ti ratio: 500 equiv. MAO
Pressure: 3 atm
Solvent: toluene
Runtime: 25 min.
Temperature: 40 °C
Reference: 102
Polydispersity: 10.5

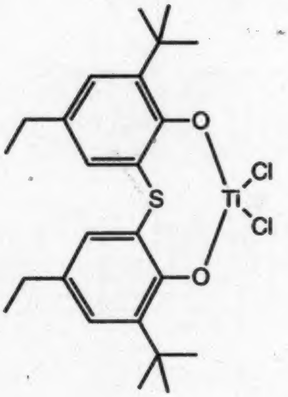

Activity: 1.2 ton PE/mol Ti·hr·atm
Al/Ti ratio: 500 equiv. MAO
Pressure: 3 atm
Solvent: toluene
Runtime: 5 min.
Temperature: 20 °C
Reference: 102
Polydispersity: 11.9

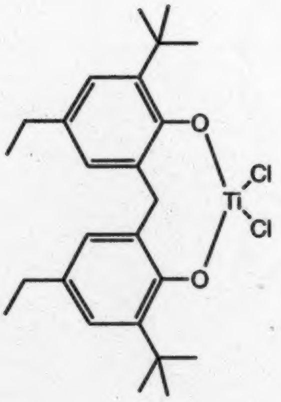

Activity: 98 Kg PE/mol Ti·hr·atm
Al/Ti ratio: 500 equiv. MAO
Pressure: 3 atm
Solvent: toluene
Runtime: 15 min.
Temperature: 20 °C
Reference: 102

Figure 1.4

1.5.3 Calix[4]arenes.

Calixarenes are 1-metacyclophanes (Figure 1.5) that can be obtained by condensation of formaldehyde with *para*-alkylphenols.[107] The tetramer, calix[4]arene, can adopt a "cone" shaped conformation, allowing the formation of inclusion compounds. Because of this property, calix[4]arenes have been used as building blocks to construct receptors and have enjoyed considerable attention.[108] The use of calix[4]arenes as ligands in organometallic chemistry was non-existent until Floriani began to systematically explore the possibilities of this ligand.[109,110]

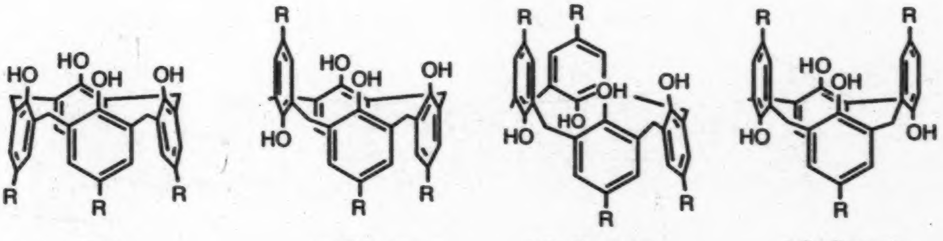

cone partial cone 1,2-alternate 1,3-alternate

Figure 1.5: Calix[4]arene conformations (R= alkyl, H)

Although the metals are anchored to a set of methylene bridged phenoxo groups, the role of the calix[4]arene according to Floriani is different from that of four monomeric phenoxo units. Due to the restricted conformational freedom of the four phenol groups the calix[4]arene acts as an "oxo-surface" and represents a model for heterogeneous supports.[111]

Valuable organometallic chemistry has developed using this oxo-surface analogy but the analogy between this tetradentate ligand and a heterogeneous oxo-surface is actually quite limited.

This model oxo-surface for instance fails to mimic the complete rigidity of a silica surface due to residual conformational mobility of the calix[4]arene frame.[112] Calix[4]arenes can exist in 4 interconverting conformations (cone, partial cone, 1,3-alternate, 1,2-alternate) by rotation about the σ bonds of the methylene bridges (Figure 1.5, page 38). Although in solution the cone conformation dominates presumably due to the formation of a circular set of hydrogen bonds,[113] the rapid inversion of the cone structure at room temperature limits the applicability as a model for a rigid oxo-surface. This problem has been addressed by further modification of the calix[4]arene (for an example see Table 2.3, page 87),[114] but no organometallic derivatives have been reported using these modified calix[4]arenes.

As stated in section 1.5 (page 30), electron deficient metal centers tend to aggregate in solution, forming higher coordinated metal centers.[110,115] According to present heterogeneous catalyst models, it is the presence of geometrically constrained and coordinatively unsaturated metal centers on a rigid oxo surface which causes enhanced or novel catalytic activity.[21] Floriani addressed the uncontrolled intermolecular aggregation problem by partial oxygen alkylation,[111] thereby sterically protecting the reactive metal site. If however a complete set of tetraanionic oxygens in a planar conformation is required with increased steric protection around the oxo-surface, the calix[4]arene frame seems unsuitable.

These limitations of the calix[4]arene oxo-surface are also reflected in the published crystal structures of a limited number of titanium-containing complexes.[117] Because of the described limitations, the unmodified calix[4]arene is not a suitable ligand for the purpose of assembling a controlled-structure Ziegler-Natta catalyst, as stated in section 1.5 (page 30).

1.5.4 Breaking the Ring: Tetraarylethene.

The metacyclophane structure of calix[4]arenes has an inherent limitation as far as steric shielding of the polar pocket is concerned. The cyclophane structure blocks two *ortho* positions around the OH groups by using methylene bridges as an organizing element *and* forces a ring structure, both of which prevent steric shielding of the polar pocket. Even if the modification of the methylene bridges is further developed,[116] the metacyclophane structure of calix[4]arenes prevents the introduction of sterically bulky groups perpendicular to the cone formed by the four phenyl rings.

Another organizing element is necessary to bring four phenoxy groups together, while maintaining the possibility of introducing bulky groups near to the OH groups to hinder, or altogether prevent, the intermolecular aggregation of Lewis acidic metals complexed to these phenoxo groups. A single carbon atom as an organizing element would give rise to a tridentate[118] oxo-surface. Organizing elements beyond ethane or ethene could also be used to bring the phenoxy groups together, but are not considered in this thesis.

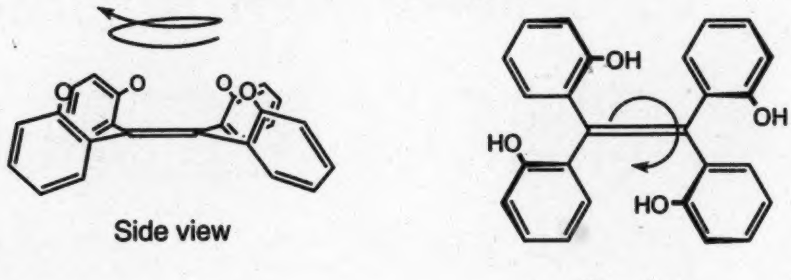

Figure 1.6

Because of the planarity of the organizing element, the tetraphenylethene frame seemed to be a good starting point for building an organizing structure for use in building a Ziegler-Natta catalyst. In addition, a tetraphenylethene frame might give access to a chiral oxo-surface by inducing helicity (Figure 1.6) in these tetraphenylethene molecules,[119] while the deeply buried ethene bond might allow stabilizing interactions with the active catalyst metal. Due to the fact that the calix[4]arene dominates the supramolecular chemistry field, organizing elements other than methylene bridges for bringing four phenoxo groups together do not seem to have been explored. It is therefore not surprising that hardly any use has been made of the tetraphenylethene frame in both supramolecular[120] as well as in organometallic chemistry,[121] although its potential value as a ligand has been recognized.[119]

1.6 Project Goals.

Based on this introduction of Ziegler-Natta chemistry the project goal can now be described as the development of a synthetic route into *tetrakis*-3,5-substituted-2-hydroxyphenylethenes (Figure 1.7) and subsequent use of this new ligand system in the assembly of polymetallic compounds to be tested for the Ziegler-Natta catalysis of polyethylene.

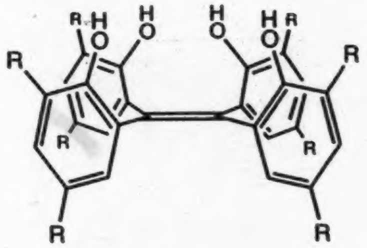

R = alkyl, aryl, halogen

Figure 1.7

1.7 Notes and References.

1. Britovsek, G.J.P.; Gibson, V.C.; Wass, D.F. *Angew. Chem., Int. Ed. Engl.* **1999**, *38*, 428-447.

2. $M_w/M_n = [\delta^2/(M_n)^2] + 1$, with $\delta^2 = \Sigma f_i(M_i - M_n)^2$, $f_i = N_i/\Sigma N_i$ = the probability of finding a discrete polymer molecule i with a molecular weight M_i in a polymer sample, and M_i = molecular weight of a discrete polymer molecule i. For the derivation see: Sheu, W. *J. Chem. Ed.* **2001**, *78*, 554-555.

3. The "failed experiment" story and everything thereafter is unclear, which is reflected in the literature. Compare Gavens: P.D.; Bottrill, M.; Kelland, J.W.; McMeeking, J. in Comprehensive Organometallic Chemistry, G. Wilkinson, F.G.A. Stone, E.W. Abel. Eds.; Pergamon Press: New York, 1982; Chapter 22.5 for example with Ittel, S.D.; Johnson, L.K.; Brookhart, M. *Chem. Rev.* **2000**, *100*, 1169-1203 (ref. 175). The story goes that in an experiment, the "aufbau reaktion" (the formation of alkane oligomers by repeated insertion of ethene in the alkyl-aluminum bond) failed and gave 1-butene instead. This was apparently due to a nickel contamination. It is unclear where the nickel came from, and at what point in the subsequent investigations polyethylene was formed and by what metal in all of the stories. A thorough investigation of the lab notebooks (if still existing) and interviews with former members of the Ziegler group might make an interesting "History of Chemistry" story. To see Ziegler's discovery in the right context: it must be remembered that there was no synthesis was available at that time for HDPE. For a historic introduction from the Ziegler point of view see Wilke, G. in Ziegler Catalysts, G.Fink, R. Mülhaupt, H.H. Brintzinger eds.; Springer: Berlin, Germany, 1995, pages 1-14.

4. For a Natta point of view, see Pino, P.; Mülhaupt, R. *Angew. Chem., Int. Ed. Engl.* **1980**, *19*, 857-875. For the controversy surrounding the Ziegler-Natta catalysts, see Boor, J.; Ziegler-Natta Catalysts and Polymerizations, Academic: New York, 1979 and Comprehensive Organometallic Chemistry, G. Wilkinson, F.G.A. Stone, E.W. Abel. Eds.; Pergamon Press: New York, 1982; Chapter 22.5. To see the discovery of isotactic polypropylene in the right context: Staudinger predicted in 1929 a correlation between physical properties of a polymer and its chain stereochemistry, but no large scale synthetic method for making stereoregular polymers was available until Natta's discovery. Stereoregular polypropylene has a melting point of 165 °C, atactic polypropylene flows at room temperature. See Kaminsky, W. *J. Chem. Soc., Dalton Trans.* **1998**, 1413-1418 and Coates, G.W. *Chem. Rev.* **2000**, *100*, 1223-1252.

5. Soga, K.; Katano, S.; Akimoto, Y. *Polym. J.* **1973**, *5*, 128-134. Chien, J.C.W.; Hsieh, J.T.T. *J. Polymer. Sci., Polym. Chem. Ed.* **1976**, *14*, 1915-1932. Barbé, P.C.; Cecchin, G.; Noristi, L. *Adv. Polym. Sci.* **1987**, *81*, 1-81.

6. Sinn, H.; Kaminsky, W. *Adv. Organomet. Chem.* **1980**, *18*, 99-149. Goodall, B.L. *J. Chem. Ed.* **1986**, *63*, 191-195. Goodall, B.L. in Transition Metal Catalyzed Polymerizations, R.P. Quirk, Hsieh, H.L., G.B. Klingensmith, P.J. Tait Eds.: Harwood Academic / MMI, 1983; page 355-378.

7. Tornqvist, E.G.M.; Langer, A.W. US Pat. 3 032 510 (1962). Wilschinsky, Z.W.; Looney, R.W.; Tornqvist, E.G.M. *J. Catal.* **1973**, *28*, 352. Parsons, I.W.; Caunt, A.D.; Haward, R.N.; Licchelli, J.A.; Al-Hillo, M.R.Y. in Transition Metal Catalyzed Polymerizations, R.P. Quirk, H.L. Hsieh, G.B.

Klingensmith, P.J. Tait Eds.: Harwood Academic / MMI, 1983; page 299-312.

8. Belg. Pat. 650.679 (1963), Solvay

9. Duck, E.W.; Grant, D.; Butcher, A.V.; Timms, D.G. *Eur. Polym. J.* **1974**, *10*, 77-83. Rudham, R.; Keir, D.A.; Eley, D.D. *J. Chem. Soc., Faraday Trans. 1* **1975**, *73*, 1685-1693. Doi, Y.; Soga, K.; Murata, M.; Suzuki, E.; Ono, Y.; Keii, T. *Polym. Commun.* **1983**, *24*, 244-246.

10. Weissermel, K.; Cherdron, H.; Berthold, J.; Diedrich, B.; Keil, K.D.; Rust, K.; Strametz, H.; Toth, T. *J. Polym. Sci., Polym. Symp.* **1975**, *51*, 187-196. Mülhaupt, R.; Klabunde, U.; Ittel, S.D. *J. Chem. Soc., Chem. Commun.* **1985**, 1745-1746. Ittel, S.D.; Mülhaupt, R.; Klabunde, U. *J. Polym. Sci., Polym. Chem. Ed.* **1986**, *24*, 3447-3460.

11. Goodall, B.L. in Transition Metal Catalyzed Polymerizations, R.P. Quirk, Hsieh, H.L., G.B. Klingensmith, P.J. Tait Eds.: Harwood Academic / MMI, 1983; page 355-378. Spitz, R.; Duranel, L.; Guyot, A. *Makromol. Chem.* **1988**, *189*, 549-558.

12. Youchang, X.; Linlin, G.; Wanqi, L.; Naiyu, B.; Youqi, T. *Sci. Sinica* **1979**, *22*, 1045-1055.

13. Price, G.J; in Sonochemistry and Sonoluminescence, L.A.Crum Ed.; Kluwer Academic: The Netherlands, 1999, page 321-343.

14. Murata, M.; Nakano, A.; Kanazawa, S.; Imai, M. in Studies in Surface Science and Catalysis , *89*, Catalyst Design for Tailor-Made Polyolefins, K. Soga, M. Terano Eds.; Elsevier Science: Amsterdam/ Kodansha Ltd., Tokyo, 1989, page 171-178. Kolthammer, B.W.S. in Handbook of Grignard reagents G.S. Silverman, P.E. Rakita eds.; Marcel Dekker: New York, 1996, page 677-683.

15. Böhm, L.L. *Polymer,* **1978**, *19,* 553-566. Jeong, Y.; *Makromol. Chem.* **1990**, *191*, 1487-1496. Jeong, Y.; Lee, D.; Soga, K. *Makromol. Chem., Rapid Comm.* **1991**, *12,* 5-7. Gupta, V.K., Satish, S.; Bhardwaj, I.S. *J. Macromol. Sci., Chem.* **1994**, *A31*, 451-463.

16. Karol, F.J.; Kao, S.C. in Studies in Surface Science and Catalysis , *89,* Catalyst Design for Tailor-Made Polyolefins, K. Soga, M. Terano Eds.; Elsevier Science: Amsterdam/ Kodansha Ltd., Tokyo, (1994), page 389-403. Henrici-Olivé, G.; Olivé, S. *Polym. Lett. Ed.* **1974**, *12*, 39-44. Henrici-Olivé, G.; Olivé, S. *Adv. Polym. Sci.* **1974**, *15*, 1-30. S. Beach, D.L.; Kissin, Y.V. *J. Polym. Sci., Polym. Chem. Ed.* **1984**, *22*, 3027-3042. Kissin, Y.V.; Beach, D.L. *J. Polym. Sci., Polym. Chem. Ed.* **1986**, *24*, 1069-1084. Skupinska, J. *Chem. Rev.* **1991**, *91*, 613-648. Tembe, G.L.; Ravindranathan, M. *React. Kinet. Catal. Lett.* **1994**, *52*, 119-127.

17. Petkov, L.; Kyrtcheva, R.; Radenkov, P.; Dobreva, D. *Polymer* **1978**, *19,* 567-573. Kinkelin, E.; Fink, G.; Bogdanovic, B. *Makromol. Chem., Rapid Commun.* **1986**, *7,* 85-89. Munoz-Escalona, A.; Garcia, H.; Albornoz, A. *J. Appl. Polymer Sci.* **1987**, *34*, 977-988. Yano, T.; Inoue, T.; Ikai, S.; Shimizu, M.; Kai, Y.; Tamura, M. *J. Polymer Sci., Polym. Chem. Ed.* **1988**, *26*, 457-464. Karayannis, N.M.; Johnson, B.V.; Hoppin, C.R.; Kheighatian, H.M. in Transition Metals and Organometallics as Catalysts for Olefin Polymerization, W. Kaminsky, H. Sinn eds.; Springer: Berlin, Germany, 1988, page 231-237.

18. Haward, R.N.; Roper, A.N.; Fletcher, K.L. *Polymer,* **1973**, *14*, 365-372. Gardner, K.; Parsons, I.W.; Haward, R.N. *J. Polym. Sci., Polym. Chem. Ed.* **1978**, *16*, 1683-1696. Caunt, A.D.; Licchelli, J.A.; Parsons, I.W.; Haward, R.N.; Al-Hillo, M.R.Y. *Polymer,* **1983**, *24*, 121-125. Yano, T.; Ikai, S.; Washio, K. *J. Polym. Sci., Polym. Chem. Ed.* **1985**, *23*, 3069.

Makino, K.; Tsuda, K.; Takai, M. *Polymer Bull.* **1991**, *26*, 371-376. Luciani, L.; Milani, F. *Makromol. Chem., Makromol. Symp.* **1993**, *66*, 55-70.

19. Magnesium chloride is unusual in that it can be shaped into uniform spherical particles. Under the right catalyst preparation and polymerization conditions, polymer particles are obtained that retain the original shape of the catalyst particle. This is the replication phenomenon, an industrially highly desirable feature of magnesium chloride supported catalysts. For the replication phenomenon see reference 5 and Dall'Occo, T.; Zucchini, U.; Cuffiani, I. in Transition Metals and Organometallics as Catalysts for Olefin Polymerization, W. Kaminsky, H. Sinn eds.; Springer: Berlin, Germany, 1988; page 209-221. Galli, P. *J. Macromol. Sci. Phys.* **1996**, *B35*, 427-455.

20. Panel Discussion as reported in *Makromol. Chem., Macromol. Symp.* **1993**, *66*, 329-334.

21. Sakai, S. *J. Phys. Chem.* **1994**, *98*, 12053-12058 and references therein. Boero, M.; Parrinello, M.; Terakura, K. *J. Am. Chem. Soc.* **1998**, *120*, 2746-2752. "In contemplating the choice of tools currently at our disposal, it is chastening to recall that, whereas spectroscopic and all other experiments can fail as well as succeed, in practices of computation and simulation the criteria-even the awareness-of failure are less sharply defined." Citation from Thomas, J.M. *Angew. Chem., Int. Ed. Engl.* **1994**, *33*, 913-937.

22. Chien, J.C.W.; Wu, J.C.; Kuo, C. *J. Polymer Sci.* **1983**, *21*, 737-750. Mori, H.; Hasebe, K.; Terano, M. *Polymer* **1999**, *40*, 1389-1394.

23. Rodriguez, L.A.M.; van Looy, H.M.; Gabant, J.A. *J. Polymer Sci. A-1,* **1966**, *4*, 1971-1992. Gerbasi, R.; Marigo, A.; Martorana, A.; Zannetti, R.; Guidetti, G.P.; Baruzzi, G. *Eur. Polym. J.* **1984**, *20*, 967-970.
24. Tait, P. in Transition Metal Catalyzed Polymerizations, R.P. Quirk, H.L. Hsieh, G.B. Klingensmith, P.J. Tait Eds.: Harwood Academic / MMI, 1983; page 115-147. Barbé, P.C.; Noristi, L.; Baruzzi, G.; Marchetti, E. *Makromol. Chem., Rapid Commun.* **1983**, *4*, 249-252.
25. Chien, J.C.W.; Wu, J.C. *J. Polym. Sci., Polym. Chem. Ed.* **1982**, *20*, 2461-2476. Pino, P.; Guastalla, G.; Rotzinger, B.; Mülhaupt, R. in Transition Metal Catalyzed Polymerizations, R.P. Quirk, H.L. Hsieh, G.B. Klingensmith, P.J. Tait Eds.: Harwood Academic / MMI, 1983; page 435-465.
26. Wesslau, H. *Makromol. Chem.* **1958**, *26*, 102-118. Zucchini, U.; Cecchin, G. *Adv. Polym. Sci.* **1983**, *51*, 101-153. Karol, F.J. *Catal. Rev. Sci. Eng.* **1984**, *26*, 557-595.
27. Usami, T.; Gotoh, Y.; Takayama, S.; *Macromolecules* **1986**, *19*, 2722-2726. Schouterden, P.; Groeninckx, G.; Van der Heijden, B.; Jansen, F. *Polymer* **1987**, *28*, 2099-2104. Mirabella, F.M.; Ford, E.A. *J. Polym. Sci., Polym. Phys. Ed.* **1987**, *25*, 777-790. Karoglanian, S.P.; Harrison, I.R. *Polym. Eng. Sci.* **1996**, *36*, 731-736.
28. Keii, T.; Doi, Y.; Suzuki, E.; Tamura, M.; Murata, M.; Soga, K. *Makromol. Chem.* **1984**, *185*, 1537-1557. Spitz, R.; Patin, M.; Robert, P.; Masson, P.; Dupuy, J. in Studies in Surface Science and Catalysis , *89*, Catalyst Design for Tailor-Made Polyolefins, K. Soga, M. Terano Eds.; Elsevier Science: Amsterdam/ Kodansha Ltd., Tokyo, (1994), page 109-118.
29. Podall, H.E.; Foster, W.E. *J. Org. Chem.* **1958**, *23*, 1848-1852. Gibson, V.C.; Segal, J.A.; White, A.J.P.; Williams, D.J. *J. Am. Chem. Soc.* **2000**,

112, 7120-7121. Bailey, P.J.; Coxall, R.A.; Dick, C.M.; Fabre, S.; Parsons, S. *Organometallics* **2001**, *20*, 798-801. Chisholm, M.H.; Huffman, J.C.; Phomphrai, K. *J. Chem. Soc., Dalton Trans.* **2001**, 222-224. Reported results are to be approached with suspicion: magnesium is contaminated with transition metals. A report appearing this year on a polyethylene producing Mg catalyst is likely.

30. An ionic mechanism has been proposed for ethene oligomerization by Al/Ti catalysts, see Langer, A.W. *J. Macromol. Sci. Chem.* **1970**, *A4*, 775-787 and references therein. Ion formation has been measured in THF, see Karol, F.J.; Cann, K.J.; Wagner, B.E. in Transition Metals and Organometallics as Catalysts for Olefin Polymerization, W. Kaminsky, H. Sinn eds.; Springer: Berlin, Germany, 1988; page 149-161.

31. Zakharov, V.A.; Bukatov, G.D.; Yermakov, Y.I. *Adv. Polym. Sci.* **1983**, *51*, 61-100. Pino, P.; Lorenzi, G.P. in Preparation and Properties of Stereoregular Polymers, R.W. Lenz, F. Ciardelli eds.; Reidel Publishing: Dordrecht, Holland, 1980, pages 1-73.

32. Natta, G.; Pino, P.; Mazzanti, G.; Giannini, U. *J. Am. Chem. Soc.* **1957**, *79*, 2975-2976.

33. Breslow, D.S.; Newburg, N.R. *J. Am. Chem. Soc.* **1957**, *79*, 5072-5073. Breslow, D.S.; Newburg, N.R. *J. Am. Chem. Soc.* **1959**, *81*, 81-86.

34. Karl, J.; Erker, G. *J. Mol. Cat. A., Chem.* **1998**, *128*, 85-102. Casey, C.P.; Carpenetti, D.W.; Sakurai, H. *J. Am. Chem. Soc.* **1999**, *121*, 9483-9484. Dahlmann, M.; Erker, G.; Bergander, K. *J. Am. Chem. Soc.* **2000**, *122*, 7986-7998. Casey, C.P.; Carpenetti, D.W. *Organometallics* **2000**, *19*, 3970-3977.

35. Giannini, U.; Zucchini, U.; Albizzati, E. *J. Polym. Sci., Polym. Letters* **1970**, *8*, 405-410. Ballard, D.G.H.; Jones, E.; Medinger, T.; Pioli, A.J.P.

Makromol. Chem. **1971**, *148*, 175-194. See also reference 4 for other attempts.

36. The Cossee-Arlman mechanism is partly based on the mechanism proposed by Breslow (ref. 33), see Chen, E.Y.; Marks, T.J. *Chem. Rev.* **2000**, *100*, 1391-1434 and Brintzinger, H.H.; Fischer, D.; Mülhaupt, R.; Rieger, B.; Waymouth, R.M. *Angew. Chem., Int. Ed. Engl.* **1995**, *34*, 1143-1170. As an illustration of the "hidden experimental facts" in models and the resulting confusion consider the remarks by Bochmann that the Breslow "proposal anticipated several features of the well known Cossee-Arlman polymerization mechanism for heterogeneous catalysts" (M. Bochmann *J. Chem. Soc., Dalton Trans.* **1996**, 255-270, page 256) and by Sinn and Kaminsky that "Henrici-Olivé and Olivé extended the ideas of Cossee for the heterogeneous system to the soluble system" (Sinn, H.; Kaminsky, W. *Adv. Organomet. Chem.* **1980**, *18*, 99-149, page 129).

37. The first use of stereorigid metallocenes for isotactic polypropylene synthesis was published by Ewen, see Ewen, J.A. *J. Am. Chem. Soc.* **1984**, *106*, 6355-6364 and *not* by Brintzinger, et al., (Kaminsky, W.; Külper, K.; Brintzinger, H.H.; Wild, F.R.W.P. *Angew. Chem., Int. Ed. Engl.* **1985**, *24*, 507) as kindly pointed out by Resconi, et al., in reference 60 (reference 3 in that paper). Brintzinger's name is coupled in the literature to the synthesis of chiral *ansa*-metallocenes (Schnutenhaus, H.; Brintzinger, H.H. *Angew. Chem., Int. Ed. Engl.* **1979**, *18*, 777) and the formation of isotactic polypropylene using stereorigid metallocenes, but the last point is not claimed by him in the literature; see Brintzinger, H.H.; Fischer, D.; Mülhaupt, R.; Rieger, B.; Waymouth, R.M. *Angew. Chem., Int. Ed. Engl.* **1995**, *34*, 1151.

38. Both groups were funded by the Deutsche Forschungsgemeinschaft through a special program for research in homogeneous catalysis from 1973 to 1978, see Brintzinger, H.H.; Fischer, D.; Mülhaupt, R.; Rieger, B.; Waymouth, R.M. *Angew. Chem., Int. Ed. Engl.* **1995**, *34*, 1143-1170.

39. Reichert, K.H.; Meyer, K.R. *Makromol. Chem.* **1973**, *169*, 163. Long, W.P.; Breslow, D.S. *Liebigs Ann. Chem.* **1975**, 463-469. Andresen, A.; Cordes, H.; Herwig, J.; Kaminsky, W.; Merck, A.; Mottweiler, R.; Pein, J.; Sinn, H.; Vollmer, H. *Angew. Chem., Int. Ed. Engl.* **1976**, *10*, 630-632. Sinn, H.; Kaminsky, W.; Vollmer, H.J.; Woldt, R. *Angew. Chem., Int Ed. Engl.* **1980**, *19*, 390-392.

40. For the impact on industry see Thayer, A.M. *Chem. Eng. News* September 11, **1995**, 15-20. Tullo, A.H. *Chem. Eng. News* August 7, **2000**, 35-46. It is well possible that the disappearance of $TiCl_3$ from the market has something to do with this. For the impact on science see the 512 page long special issue "Frontiers in Metal-Catalyzed Polymerization" of *Chemical Reviews* April **2000**, *100(4)*.

41. Dyachkovskii, F.S.; Shilova, A.K.; Shilov, A.E. *J. Polym. Sci., Part C* **1967**, *16*, 2333-2339. Zefirova, A.K.; Shilov, A.E. *Dokl. Akad. Nauk. SSSR* **1961**, *136*, 599-602.

42. Reference 4, Sinn and Kaminsky (1980), page 129. "Nevertheless, these experiments proved only that, in an electric field, titanium cations can be observed by their migration, and not that these ions are the actual centers of polymerization."

43. Eisch, J.J.; Piotrowski, A.M.; Brownstein, S.K.; Gabe, E.J.; Lee, F.L. *J. Am. Chem. Soc.* **1985**, *107*, 7219-7221.

44. Jordan, R.F.; Bajgur, C.S.; Willett, R.; Scott, B. *J. Am. Chem. Soc.* **1986**, *108*, 7410-7411. Jordan, R.F. *Adv. Organomet. Chem.* **1991**, *32*, 325-387.

45. Bochmann, M.; Wilson, L.M. *J. Chem. Soc., Chem. Commun.* **1986**, 1610-1611. Yang, X.; Stern, C.L.; Marks, T.J. *J. Am. Chem. Soc.* **1991**, *113*, 3623-3625.

46. Bochmann, M.; Lancaster, S.J. *Angew. Chem., Int. Ed. Engl.* **1994**, *33*, 1634-1637. Bochmann, M.; Lancaster, S.J.; Hursthouse, M.B.; Malik, K.M.A. *Organometallics* **1994**, *13*, 2235-2243. Bochmann, M.; Green, M.L.H.; Powell, A.K.; Saßmannshausen, J.; Triller, M.U.; Wocadlo, S. *J. Chem. Soc., Dalton Trans.* **1999**, 43-49.

47. Haselwander, T.; Beck, S.; Brintzinger, H.H. Ziegler Catalysts, G.Fink, R. Mülhaupt, H.H. Brintzinger eds.; Springer: Berlin, Germany, 1995, page 181-197.

48. Bochmann, M.; Cuenca, T.; Hardy, D.T. *J. Organomet. Chem.* **1994**, *484*, C10-C12. Cuenco, T.; Galakhov, M.; Jiménez, G.; Royo, E.; Royo, P.; Bochmann, M. *J. Organomet. Chem.* **1997**, *543*, 209-215. Royo, E.; Royo, P.; Cuenca, T.; Galakhov, M. *Organometallics* **2000**, *19*, 5559-5567.

49. Green, M.L.H.; Saßmannshausen, J. *J. Chem. Soc., Chem. Commun.* **1999**, 115-116. Chen, E.Y.X.; Kruper, W.J.; Roof, G.; Wilson, D.R. *J. Am. Chem. Soc.* **2001**, *123*, 745-746.

50. Choukroun, R.; Douziech, B.; Donnadieu, B. *Organometallics* **1997**, *16*, 5517-5521.

51. Beck, S.; Geyer, A.; Brintzinger, H.H. *J. Chem. Soc., Chem. Commun.* **1999**, 2477-2478.

52. Beck, S.; Prosenc, M.H.; Brintzinger, H.H. *J. Mol. Cat. A.,Chem.* **1998**, *128*, 41-52. Beck, S.; Lieber, S.; Schaper, F.; Geyer, A.; Brintzinger, H.H. *J. Am. Chem. Soc.* **2001**, *123*, 1483-1489.

53. Möhring, P.C.; Coville, N.J. *J. Organomet. Chem.* **1994**, *479*, 1-29. Everyone seems to have a preference for another system, personal as well as commercial factors may have something to do with this.

54. Siedle, A.R.; Lamanna, W.M.; Newmark, R.A.; Schroepfer, J.N. *J. Mol. Cat. A: Chem.* **1998**, *128*, 257-271.

55. Zhou, J.; Lancaster, S.J.; Walker, D.A.; Beck, S.; Thornton-Pett, M.; Bochmann, M. *J. Am. Chem. Soc.* **2001**, *123*, 223-237.

56. Wu, Z.; Jordan, R.F. *J. Am. Chem. Soc.* **1995**, *117*, 5867-5868.

57. Prosenc, M.H.; Janiak, C.; Brintzinger, H.H. *Organometallics*, **1992**, *11*, 4036-4041.

58. Grubbs, R.H.; Coates, G.W. *Acc. Chem. Res.* **1996**, *29*, 85-93.

59. Piers, W. E.; Irvine, G.J.; Williams, V.C. *Eur. J. Inorg. Chem.* **2000**, 2131-2142. LaPointe, R.E.; Roof, G.R.; Abboud, K.A.; Klosin, J. *J. Am. Chem. Soc.* **2000**, *122*, 9560-9561. Aldridge, S.; Fallis, I.A.; Howard, S.T.; *J. Chem. Soc.., Chem. Commun.* **2001**, 231-232.

60. Siedle, A.R.; Newmark, R.A.; Schroepfer, J.N.; Lyon, P.A. *Organometallics* **1991**, *10*, 400-404. Resconi, L.; Piemontesi, F.; Franciscono, G.; Abis, L.; Fiorani, T. *J. Am. Chem. Soc.* **1992**, *114*, 1025-1032. Brintzinger, H.; Beck, S.; Leclerc, M.; Stehling, U.; Röll, W. in Studies in Surface Science and Catalysis , *89*, Catalyst Design for Tailor-Made Polyolefins, K. Soga, M. Terano Eds.; Elsevier Science: Amsterdam/ Kodansha Ltd., Tokyo, (1994), page 193-200. Stehling, U.; Diebold, J.; Kirsten, R.; Röll, W.; Brintzinger, H.H. *Organometallics* **1994**, *13*, 964-970. Naga, N.; Mizunuma, K. *Polymer* **1998**, *39*, 5059-5067.

61. Kreuder, C.; Jordan, R.F.; Zhang, H. *Organometallics* **1995**, *14*, 2993-3001, page 2999. See also Ziegler, T.; Tschinke, V.; Becke, A. *J. Am. Chem. Soc.* **1987**, *109*, 1351-1358.

62. Burger, B.; Thompson, M.; Cotter, D.; Bercaw, J. *J. Am. Chem. Soc.* **1990**, *112*,1566-1577.

63. Dufaud, V.; Basset, J.M. *Angew. Chem., Int. Ed. Engl.* **1998**, *37*, 806-810. In this work PE is degraded to oligomers under hydrogen pressure using a supported zirconium catalyst. See also: Kaminsky, W.; Hartmann, F. *Angew. Chem., Int. Ed. Engl.* **2000**, *39*, 331- 333.

64. Bochmann, M. *J. Chem. Soc., Dalton Trans.* **1996**, 255-270.

65. Brintzinger, H.H.; Fischer, D.; Mülhaupt, R.; Rieger, B.; Waymouth, R.M. *Angew. Chem., Int. Ed. Engl.* **1995**, *34*, 1157.

66. Scollard, J.D.; McConville, D.H.; Payne, N.C.; Vittal, J.J. *Macromolecules* **1996**, *29*, 5241-5243. Scollard, J.D.; McConville, D.H. *J. Am. Chem. Soc.* **1996**, *118*, 10008-10009.

67. Tinkler, S.; Deeth, R.J.; Duncalf, D.J.; McCamley, A. *J. Chem. Soc., Chem. Commun.* **1996**, 2623-2624. No explanation in the literature has been forthcoming, as far as I am aware, as to why this ligand system has such a low activity for ethene compared to 1-hexene.

68. Coles, M.P.; Jordan, R.F. *J. Am. Chem. Soc.* **1997**, *119*, 8125-8126. Cameron, P.A.; Gibson, V.C.; Redshaw, C.; Segal, J.A.; Bruce, M.D.; White, A.J.P.; Williams, D.J. *J. Chem. Soc., Chem. Commun.* **1999**, 1883-1884.

69. Freemantle, M. *Chem. Eng. News* April 13 **1998**, 11-12.

70. Britovsek, G.J.P.; Gibson, V.C.; Kimberley, B.S.; Maddox, P.J.; McTavish, S.J.; Solan, G.A.; White, A.J.P.; Williams, D.J. *J. Chem. Soc., Chem. Commun.* **1998**, 849-850. Britovsek, G.J.P.; Bruce, M.; Gibson, V.C.;

Kimberley, B.S.; Maddox, P.J.; Mastroianni, S.; McTavish, S.J.; Redshaw, C.; Solan, G.A.; Strömberg, S.; White, A.J.P.; Williams, D.J. J. *J. Am. Chem. Soc.* **1999**, *121*, 8728-8740.

71. Small, B.J.; Brookhart, M.; Bennett, A.M.A. *J. Am. Chem. Soc.* **1998**, *120*, 4049-4050. For the versatility of this system see also Small, B.L.; Brookhart, M. *J. Am. Chem. Soc.* **1998**, *120*, 7143-7144.

72. Younkin, T.R.; Connor, E.F.; Henderson, J.I.; Friederich, S.K.; Grubbs, R.H.; Bansleben, D.A. *Science*, **2000**, *287*, 460-462.

73. See Ittel, S.D.; Johnson, L.K.; Brookhart, M. *Chem. Rev.* **2000**, *100*, 1169-1203, page 1191.

74. Kashiwa, N. *Polymer J.* **1980**, *12*, 603-608.

75. The interest of the chemical industry in MAO at that time (1980) was absent so that H. Sinn was compelled to do the patent application personally while he was senator in Hamburg. Future license fees were convenanted to the Hansische Universitätsstiftung, see Sinn, H. *Macromol. Symp.* **1995**, *97*, 27-52.

76. Pasynkiewicz, S. *Polyhedron* **1990**, *9*, 429-453. Roesky, H.W.; Walawalkar, M.G.; Murugavel, R. *Acc. Chem. Res.* **2001**, *34*, 201-211.

77. Siedle, A.R.; Newmark, R.A.; Lamanna, W.M.; Schroepfer, J.N. *Polyhedron* **1990**, *9*, 301-308. Sishta, C.; Hathorn, R.M.; Marks, T.J. *J. Am. Chem. Soc.* **1992**, *114*, 1112-1114. Tritto, I.; Sacchi, M.C.; Locatelli, P; Li, S.X. *Macromol. Symp.* **1995**, *97*, 101-108. Beck, S.; Brintzinger, H.H. *Inorg. Chim. Acta* **1998**, *270*, 376-381. The role of the byproduct, dimethylaluminum chloride is unclear: could MAO abstract a chloride anion to form a cationic dimethylaluminum species ? What would the role be of such a species ? In relation to these questions see Kim, J.S.; Wojcinski II, L.M.; Liu, S.; Sworen, J.C.; Sen, A. *J. Am. Chem. Soc.* **2000**,

122, 5668-5669. With regard to the huge excess of MAO required: no reports have appeared on the variation of the dielectric constant under these conditions. This increase of the dielectric constant would support ion-pair separation. For a similar case see Rogers, H.R.; Hill, C.L.; Fujiwara, Y.; Rogers, R.J.; Mitchell, H.L.; Whitesides, G.M. *J. Am. Chem. Soc.* **1980**, *102*, 217-226. Rogers, H.R.; Deutch, J.; Whitesides, G.M. *J. Am. Chem. Soc.* **1980**, *102*, 226-231.

78. Ueshima, T.; Fuji, T.; Saegusa, T.; Furukawa, J. *Makromol. Chem.* **1966**, *98*, 58-65. Pasynkiewicz, S.; Sadownik, A.; Kunicki, A. J. *Organomet. Chem.* **1977**, *124*, 265-269. Erker, G.; Albrecht, M.; Werner, S.; Krüger, C. *Z. Naturforsch., B: Anorg. Chem., Org. Chem.* **1990**, *45b*, 1205-1209, see also reference 4 in that paper and reference 18 in Gassman, P.G.; Callstrom, M.R. *J. Am. Chem. Soc.* **1987**, *109*, 7875-7876. Chien, J.C.W.; Wang, B.P *J. Polym. Sci. A* **1990**, *28*, 15-38.

79. Gürtzgen, S.; Rieger, R.; Uzick, W. in proceedings of Metallocenes 95 in Brussels, Belgium 1995, page 429-438.

80. Chen, Y.X.; Rausch, M.D.; Chien, J.C.W.; *J. Polym. Sci., Polym. Chem.* **1995**, *33*, 2093-2108. Karol, F.J.; Kao, S.C.; Wasserman, E.P.; Brady, R.C. *New J. Chem.* **1997**, *21*, 797-805.

81. Müller, C.; Lilge, D.; Kristen, M.O.; Jutzi, P. *Angew. Chem., Int. Ed. Engl.* **2000**, *39*, 789-792.

82. Mason, M.R.; Smith, J.M.; Bott, S.G.; Barron, A.R. *J. Am. Chem. Soc.* **1993**, *115*, 4971-4984. Harlan, C.J.; Mason, M.R.; Barron, A.R. *Organometallics* **1994**, *13*, 2957-2969. Harlan, C.J.; Bott, S.G.; Barron, A.R. *J. Am. Chem. Soc.* **1995**, *117*, 6465-6474. The term "latent Lewis acidity" does not really shed light on the functioning of the aluminoxane cage, or of MAO.

83. Bliemeister, J.; Hagendorf, W.; Harder, A.; Heitmann, B.; Schimmel, I.; Schmedt, E.; Schnuchel, W. Sinn, H.; Tikwe, L.; von Thienen, N.; Urlass, K.; Winter, H.; Zarncke, O. in Ziegler Catalysts, G.Fink, R. Mülhaupt, H.H. Brintzinger eds.; Springer: Berlin, Germany, 1995, page 57-82.

84. Watanabi, M.; McMahon, C.N.; Harlan, C.J.; Barron, A.R. *Organometallics* **2001**, *20*, 460-467.

85. Yang, X.; Stern, C.L.; Marks, T.J. *Organometallics* **1991**, *10*, 840-842. Marks, T.J.; Ahn, H. *J. Am. Chem. Soc.* **1998**, *120*, 13533-13534.

86. Chen, E.Y.; Marks, T.J. *Chem. Rev.* **2000**, *100*, 1391-1434. For an older review see Strauss, S.H. *Chem. Rev.* **1993**, *93*, 927-942.

87. Massey, A.G.; Park, A.J. *J. Organomet. Chem.* **1964**, *2*, 245-250. Massey, A.G.; Park, A.J. *J. Organomet. Chem.* **1966**, *5*, 218-225.

88. Chen, Y.X.; Yang, S.; Stern, C.L.; Marks, T.J. *J. Am. Chem. Soc.* **1996**, *118*, 12451-12452. Li, L.; Marks, T.J. *Organometallics* **1998**, *120*, 6287-6305.

89. Piers, W.E. *Chem. Eur. J.* **1998**, *4*, 13-18.

90. Negishi, E. *Chem. Eur. J.* **1999**, *5*, 411-420.

91. Seebach, D. *Angew. Chem., Int. Ed. Engl.* **1988**, *27*, 1624-1654.

92. Noyori, R.; Kitamura, M. *Angew. Chem., Int. Ed. Engl.* **1991**, *30*, 49-69.

93. Lehn, J.M. *Angew. Chem., Int. Ed. Engl.* **1988**, *27*, 89-112, Lehn, J.M. , Supramolecular Chemistry, Concepts and Perspectives; VCH Weinheim: Germany, 1995. For the preorganization concept, see D.J. Cram *Angew. Chem., Int. Ed. Engl.* **1986**, *25*, 1039. In supramolecular chemistry a host molecule is said to be "preorganized" in case no significant conformational change is necessary for guest binding. The same weak forces that shape the host-guest interaction determine the aggregation/crystallization behavior of organometallic and inorganic

molecules. In this thesis the term "preorganization" is used to describe the minimal conformational change of both ligand and n organometallic groups bound to that ligand necessary to form an "intramolecular aggregate."

94. Veith, M. *Chem. Rev.* **1990**, *90*, 3-16.

95. Greco, A.; Bertolini, G.; Cesca, S. *J. Appl. Polym. Sci.* **1980**, *25*, 2045-2061. Bart, J.C.J.; Bassi, I.W.; Calcaterra, M.; Albizatti, E.; Giannini, U.; Parodi, S. *Z. Anorg. Allg. Chem.* **1981**, *482*, 121-132. Albizzati, E.; Giannetti, E.; Giannini, U. *Makromol. Chem., Rapid Commun.* **1984**, *5*, 673-677.

96. Caulton, K.G.; Hubert-Pfalzgraf, L.G. *Chem. Rev.* **1990**, *90*, 969-995.

97. Sobota, P.; Utko, J.; Lis, T. *J.Chem. Soc., Dalton Trans.* **1984**, 2077-2079. Sobota, P.; Utko, J.; Janas, Z. *J. Organomet. Chem.* **1986**, *316*, 19-23. Sobota, P.; Utko, J.; Sztajnowska, K.; Ejfler, J.; Jerzykiewicz, L.B. *Inorg. Chem.* **2000**, *39*, 235-239.

98. Kim, I.; Woo, S.I. *Polymer Bulletin*, **1989**, *22*, 239-246. Kim, I.; Chung, M.C.; Choi, H.K.; Kim, J.H., Woo, S.I. in Catalytic Olefin Polymerization, K. Soga ed.; Kodansha: Tokyo, 1990, page 323-343. Ko, Y.S.; Han, T.K.; Woo, S.I. in Studies in Surface Science and Catalysis , *89*, Catalyst Design for Tailor-Made Polyolefins, K. Soga, M. Terano Eds.; Elsevier Science: Amsterdam/ Kodansha Ltd., Tokyo, 1989, page 163-169.

99. Malpezzi, L.; Zucchini, U.; Dall'Occo, T. *Inorg. Chim. Acta* **1991**, *180*, 245-249. Abis, L.; Bacchilega, G.; Spera, S.; Zucchini, U.; Dall'Occo, T. *Makromol. Chem.* **1991**, *192*, 981-988. Zucchini, U.; Dall'Occo, T. in Polymer Science, Contemporary Themes, S.Sivaram Ed.; McGraw-Hill: New Delhi, 1991, *1*, 221-228. Dall'Occo, T.; Sartori, F.; Vecellio, G.; Zucchini, U.; Maldotti, A. *Makromol. Chem.* **1993**, *194*, 151-161.

100. Minhas, R.; Duchateau, R.; Gambarotta, S.; Bensimon, C. *Inorg. Chem.* **1992**, *31*, 4933-4938.

101. Coleman III, W.M. *Appl. Catal.* **1986**, *22*, 345-359. This work seems to have gone almost unnoticed, considering the complete absence of any references to this paper (or to the accompanying patents !), see reference 102, 103.

102. van der Linden, A.; Schaverien, C.J.; Meijboom, N.; Ganter, C.; Orpen, A.G. *J. Am. Chem. Soc.* **1995**, *117*, 3008-3021.

103. Floriani, C.; Corazza, F.; Lesueur, W.; Chiesi-Villa, A.; Guastini, C. *Angew. Chem., Int. Ed. Engl.* **1989**, *28*, 66-67.Okuda, J.; Fokken, S.; Kang, H.C.; Massa, W. *Ber. Dtsch. Chem. Ges.* **1995**, *128*, 221-227. Chisholm, M.H.; Huang, J.H.; Huffman, J.C.; Streib, W.E.; Tiedtke, D. *Polyhedron* **1997**, *16*, 2941-2949. Mulford, D.R.; Fanwick, P.E.; Rothwell, I.P. *Polyhedron*, **2000**, *19*, 35-42.

104. Miyatake, T.; Mizunuma, K.; Seki, Y.; Kakugo, M. Makromol. Chem., Rapid Commun. **1989**, *10*, 349. The reason for the increased activity remains unclear. Tellurium and disulfide bridged systems show much lower activity, see: Fokken, S.; Spaniol, T.P.; Kang, H.C.; Massa, W.; Okuda, J. *Organometallics* **1996**, *15*, 5069-5072. Nakayama, Y.; Watanabe, K.; Ueyama, N.; Nakamura, A.; Harada, A. *Organometallics* **2000**, *19*, 2498-2503. Okuda, J.; Fokken, S.; Kleinhenn, T.; Spaniol, T.P. *Eur. J. Inorg. Chem.* **2000**, 1321-1326.

105. Boyle, T.J.; Barnes, D.L.; Heppert, J.A.; Morales, L.; Takusagawa, F. *Organometallics* **1992**, *11*, 1112-1126. Boyle, T.J.; Eilerts, N.W.; Heppert, J.A.; Takusagawa, F. *Organometallics* **1994**, *13*, 2218-2229. Eilerts, N.W.; Heppert, J.A. *Polyhedron* **1995**, *14*, 3255-3271.

106. Kayal, A.; Ducruet, A.F.; Lee, S.C. *Inorg. Chem.* **2000**, *39*, 3696-3704.

107. Gutsche, C.D.; Muthukrishan, R. *J. Org. Chem.* **1978**, *43*, 4905-4906. Gutsche, C.D.; Calixarenes, Royal Society of Chemistry: Cambridge; England, 1989. Calixarenes, A Verstaile Class of Macrocyclic Compounds, J. Vicens, V. Bõhmer eds.: Kluwer, Dordrecht; The Netherlands, 1991.

108. Bõhmer, V. *Angew. Chem., Int. Ed. Engl.* **1995**, *34*, 713-745.

109. Caselli, A.; Solari, E.; Scopelliti, R.; Floriani, C. *J. Am. Chem. Soc.* **2000**, *122*, 538-539. Esposito, V.; Solari, E.; Floriani, C.; Re, N.; Rizzoli, C.; Chiesi-Villa, A. *Inorg. Chem.* **2000**, *39*, 2604-2613 and references in these papers.

110. Roundhill, D.M. *Prog. Inorg. Chem.* **1995**, *43*, 533-591. Wieser, C.; Dieleman, C.B.; Matt, D. *Coord. Chem. Rev.* **1997**, *165*, 93-161.

111. Floriani, C. *Chem. Eur. J.* **1999**, *5*, 19-23.

112. For some examples, see for instance, Gardiner, M.G.; Lawrence, S.M.; Raston, C.L.; Skelton, B.W.; White, A.H. *J. Chem. Soc., Chem. Commun.* **1996**, 2491-2492. Radius, U.; Attner, J. *Eur. J. Inorg. Chem.* **1998**, 299-303. McBurnett, B.G.; Cowley, A.H. *J. Chem. Soc., Chem. Commun.* **1999**, 17-18.

113. Gutsche, C.D.; Dhavan, B.; Levine, J.A.; No, K.H.; Bauer, L.J. *Tetrahedron* **1983**, *39*, 409-426. Gutsche, C.D.; Bauer, L.J. *J. Am. Chem. Soc.* **1985**, *107*, 6052-6059. Araki, K.; Shinkai, S.; Matsuda, T. *Chem. Lett.* **1989**, 581-584. Fischer, S.; Grootenhuis, P.D.J.; Groenen, L.C.; van Hoorn, W.P.; van Veggel, F.C.J.M.; Reinhoudt, D.N.; Karplus, M. *J. Am. Chem. Soc.* **1995**, *117*, 1611-1620. van Loon, J.D.; Groenen, L.C.; Wijmenga, S.S.; Verboom, W.; Reinhoudt, D.N. *J. Am. Chem. Soc.* **1991**, *113*, 2378-2384. Grootenhuis, P.D.J.; Kollman, P.A.; Groenen, L.C.; Reinhoudt, D.N.;

van Hummel, G.J.; Ugozzoli, F.; Andreetti, G.D. *J. Am. Chem. Soc.* **1990**, *112*, 4165-4176.

114. Lhotak, P.; Shinkai, S. *Tet. Lett.* **1996**, *37*, 645-648. Xu, B.; Miao, Y.J.; Swager, T.M. *J. Org. Chem.* **1998**, *63*, 8561-8564. Okada, Y.; Mizutani, M.; Ishii, F.; Kasai, Y.; Nishimura, J. *Tetrahedron* **2001**, *57*, 1219-1227.

115. Anwander, R.; Eppinger, J.; Nagl, I.; Scherer, W.; Tafipolsky, M.; Sirsch, P. *Inorg. Chem.* **2000**, *39*, 4713-4720.

116. Middel, O.; Greff, Z.; Taylor, N.J.; Verboom, W.; Reinhoudt, D.N.; Snieckus, V. *J. Org. Chem.* **2000**, *65*, 667-675 and references therein.

117. Olmstead, M.M.; Sigel, G.; Hope, H.; Xu, X.; Power, P.P. *J. Am. Chem. Soc.* **1985**, *107*, 8087-8091. Ozerov, O.V.; Rath, N.P.; Ladipo, F.T. *J. Organomet. Chem.* **1999**, *586*, 223-233. Ozerov, O.V.; Ladipo, F.T.; Patrick, B.O. *J. Am. Chem. Soc.* **1999**, *121*, 7941-7942. Radius, U.; Friedrich, A. *Z. Anorg. Allg. Chem.* **1999**, *625*, 2154-2159. Ozerov, O.V.; Parkin, S.; Brock, C.P.; Ladipo, F.T. *Organometallics* **2000**, *19*, 4187-4190.

118. A *tetrakis*(2-hydroxyphenyl)methane is a tetradentate ligand, but four OH groups cannot simultaneously be on one side to form an "oxo-surface." For the use of this ligand see Dinger, M.B.; Scott, M.J. *J. Chem. Soc., Chem. Commun.* **1999**, 2525-2526. Dinger, M.B.; Scott, M.J. *Inorg. Chem.* **2000**, *39*, 1238-1254.

119. Rappoport, Z.; Biali, S.E. *Acc. Chem. Res.* **1997**, *30*, 307-314.

120. Ebmeyer, F.; Rebek, J. *Angew. Chem., Int. Ed. Engl.* **1990**, *29*, 1148-1150. Banwell, M.G.; Gable, R.W.; Greenwood, R.J.; Lambert, J.N.; Mackay, M.F.; Walter, J.M. *Synlett* **1997**, 953-955.

121. Roitershtein, D.M.; Ziller, J.W.; Evans, W.J. *J. Am. Chem. Soc.* **1998**, *120*, 11342-11346.

2. The preorganization of four phenol groups

2.1 Introduction.

In Chapter 1 preorganizing four phenol groups possessing sufficient steric hinderance *ortho* to the hydroxy groups was discussed. As stated in Chapter 1, the common approach using *methylene* bridges to force a *meta*-cyclophane organizing structure is of little use because the resulting calix[4]arene (see Figure 2.1) does not allow the introduction of sterically bulky groups perpendicular to the cyclophane ring necessary to preclude *inter*molecular aggregation of organometallic species coordinated to these oxygen groups. Instead an *ethene* group was proposed as an organizing element to bring together four phenoxy groups. Using this approach, four positions *ortho* to the hydroxy groups become available for steric shielding of the preorganized polar pocket (Fig. 2.1).

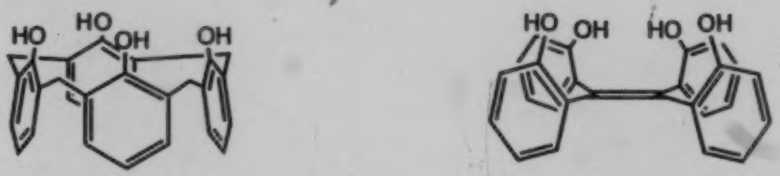

calix[4]arene

tetrakis[2-hydroxyphenyl]ethene

Figure 2.1

A thorough search of both the Beilstein database as well as the Chemical Abstracts database mainly yielded the cyclophane element as the organizing structure for four phenol units. Only one reference was found, to a paper by von Itter and Vögtle,[1] describing the synthesis of a crown ether-bridged *tetrakis*(2-hydroxyphenyl)ethene with an overall yield of 0.74 % starting from *bis*[2-hydroxyphenyl]methane. The key step in this synthesis is a dimerization of a thermally generated carbene, which has a yield of 7 % (eq. 2.1). The use of the carbene dimerization method to obtain the target compound in sufficient quantities was further compromised by literature reports of insertion reactions of carbenes generated from 2,2'-dimethoxyphenylmethanonehydrazone.[2] Unfortunately, both a review on the chemistry of tetraphenylethenes,[3] as well as an often quoted paper on the synthesis of sterically hindered tetraphenylethenes[4] introduce carbene-based synthetic schemes to obtain the desired compounds.

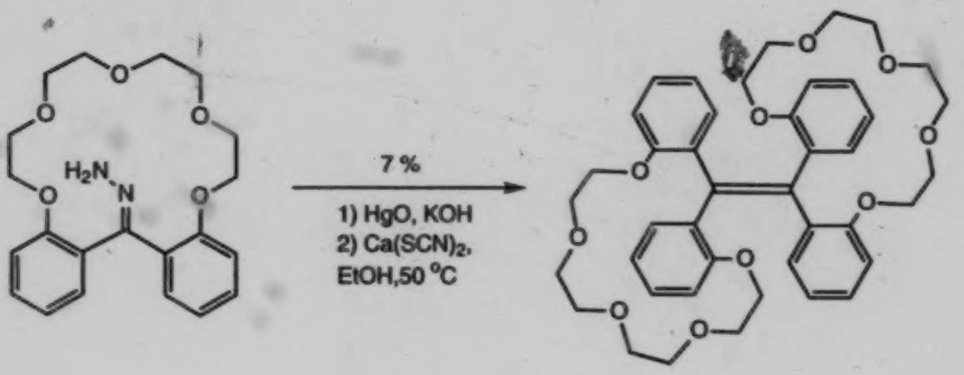

eq. 2.1

In addition to the paper of von Itter and Vögtle[1] the literature search revealed the existence of crownophanes; single crown ether-bridged tetraphenylethenes[5] or stilbenes.[6] These compounds were synthesized making use of a McMurry coupling procedure.[7] Although no *tetrakis*(2-alkoxyaryl)ethenes were reported, the use of a McMurry type coupling of a suitable benzophenone seemed a good starting point for the synthesis of the target compound (see Scheme 2.1a, page 63).

A second potential approach is suggested by an intriguing observation in the literature: when a diarylmethanol is subjected to acidic conditions, tetraarylethene is formed.[8] This procedure was used by Franzen and Joschek[8]

Scheme 2.1: Proposed *tetrakis*[2-alkoxyphenyl]ethene synthesis.

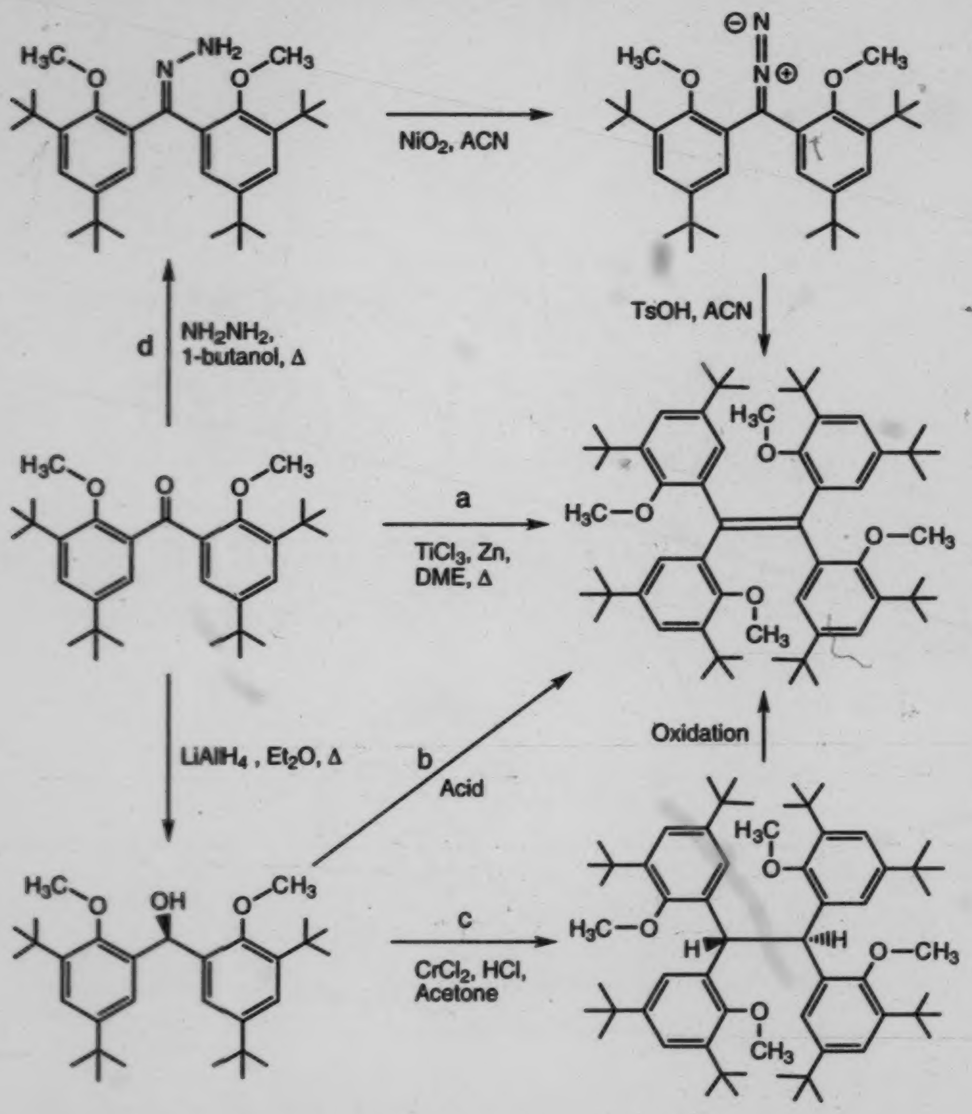
NiO_2, ACN
TsOH, ACN
d
NH_2NH_2, 1-butanol, Δ
a
$TiCl_3$, Zn, DME, Δ
$LiAlH_4$, Et_2O, Δ
b
Acid
c
$CrCl_2$, HCl, Acetone
Oxidation

to synthesize the *tetrakis*-1-naphthylethene, which on heating showed the formation of products characteristic of intermediate carbene formation. No further information on this reaction is available in the literature, suggesting that studying this reaction might yield another simple route into tetraphenylethenes (Scheme 2.1, path b).

Another noncarbene approach to tetraphenylethenes, using the diarylmethanol as a starting material, is the oxidation of tetraphenylethane[9] (Scheme 2.1, path c, page 63). The starting material for all these reactions could be the substituted benzophenone. This is also the starting material for yet another approach: the acid catalyzed decomposition of diaryldiazo compounds (Scheme 2.1, path d, page 63).[10]

2.2 Results.

In order to carry out a McMurry type coupling, the corresponding sterically hindered benzophenone had to be synthesized. A slight modification of the existing oxidative procedure as published by Wuest et al.[11] gave the *bis*[3,5-bis(1,1-dimethylethyl)-2-methoxyphenyl]methanone **1**, which was used in a McMurry type reaction using titanium trichloride and zinc powder as the reducing agent (eq. 2.2, page 65).

Instead of the anticipated olefin, the ethane compound **2** was isolated in varying yields. The characterization of compound **2** was hindered by the absence of a spot on TLC using standard visualization techniques (I_2, UV), and uninformative NMR (in ^{1}H-NMR spectroscopy, the broad benzylic proton at 5.61 ppm is easily missed) and mass spectra (MS(EI) gives extensive fragmentation, electrospray gives a clear M^+). X-ray diffraction on crystals obtained by recrystallization of compound **2** (see appendix page 337 for details) confirmed the assignment.

A structure similar to the product from the McMurry reaction as well as the unexpected over reduction in the McMurry reaction for other ketones have been reported in the literature.[12] Speculations in the literature about why the McMurry coupling fails to give an olefin are centered around the steric effect of the *ortho* placed groups in the starting material.

Therefore, a synthesis based on an *ortho*-directed lithiation was developed which gave the sterically less demanding *bis*[2-methoxyphenyl]methanone **3** in an isolated yield of 77 % (see eq. 2.5, page 69). The McMurry reaction again failed to give the olefin.

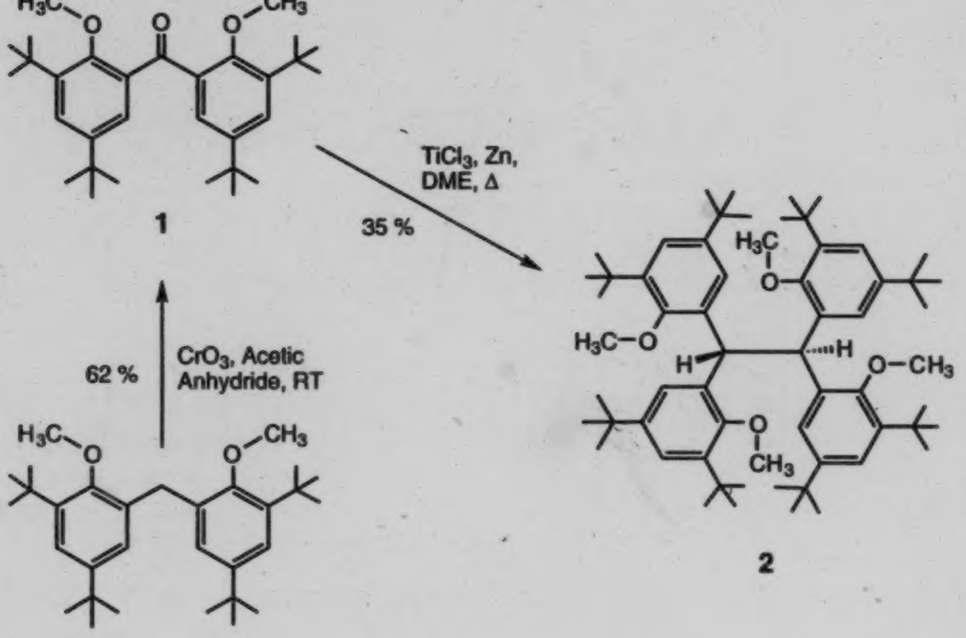
H₃C
O
O
O
CH₃
1
TiCl₃, Zn,
DME, Δ
35 %
62 %
CrO₃, Acetic
Anhydride, RT
H₃C
O
O
CH₃
H₃C
O
H₃C–O
H
H
O–CH₃
O
CH₃
2

eq. 2.2

The reduction of compound **1** affords the carbinol **4**, which under acidic conditions did not give the expected olefin but instead returned an oxepin **5** in reasonable yield (eq. 2.3, page 66), as well as other, uncharacterized products. An approximate structure assignment was aided by the ^{1}H-NMR spectrum of compound **5**, which showed four *tert*-butyl groups at 1.27, 1.34, 1.39 and 1.48 ppm and three aromatic protons at 7.04, 7.15 and 7.28 ppm. A ring-closed product was suggested by the presence of two methylene groups at 4.32 and

5.69 ppm and a single methoxy group at 3.72 ppm, as well as a mass of 450 m/z. For the assignment of the phenyl ring substitution pattern, a T-ROESY experiment was used, which indicated the following connectivity: 5.69↔4.32 and 7.04↔4.32↔3.72 ppm. The observed three-proton connectivity indicated that the methylene bridge had not changed position, and supports the proposed structure. The observed 5.69↔4.32 cross peak indicates the presence of a boat conformation for the proposed seven-membered ring.

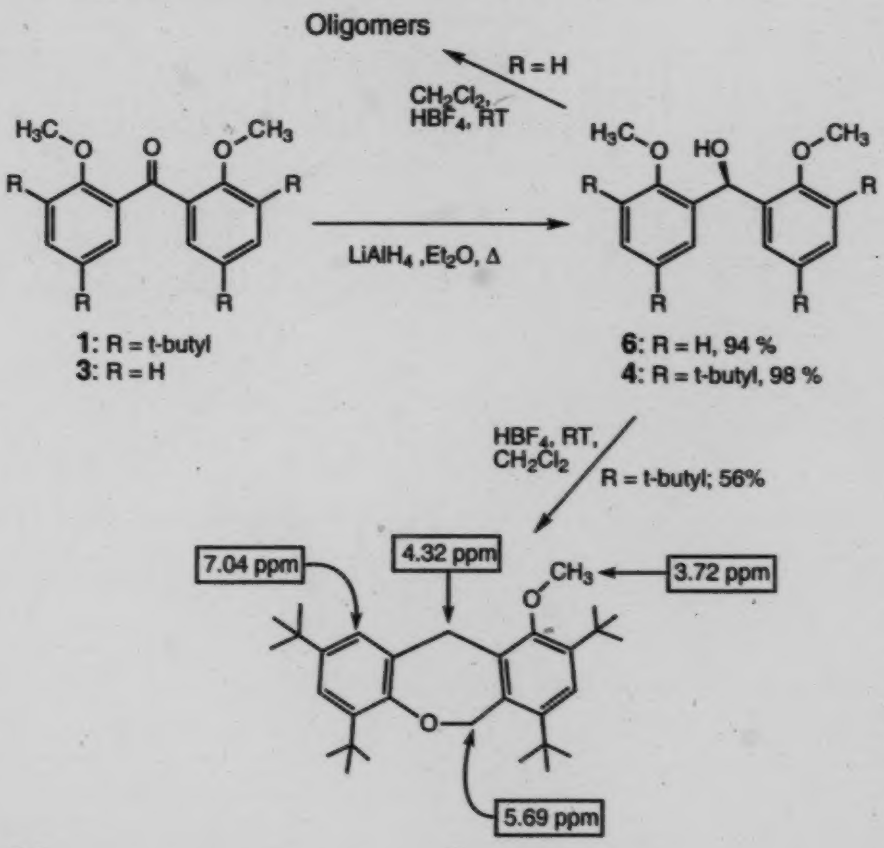
Oligomers
R = H
CH2Cl2,
HBF4, RT
LiAlH4 ,Et2O, Δ
1: R = t-butyl
3: R = H
6: R = H, 94 %
4: R = t-butyl, 98 %
HBF4, RT,
CH2Cl2
R = t-butyl; 56%
7.04 ppm
4.32 ppm
3.72 ppm
5.69 ppm

eq. 2.3 **5**

Reduction of the unsubstituted methanone **3** using lithium aluminum hydride gave the carbinol **6**, which, when subjected to acidic conditions, returned oligomeric products resulting from multiple electrophilic aromatic substitution with a characteristic broad ^{1}H-NMR spectrum.[16] Similar results for bis(2,6-dimethoxyphenyl)methanol and bis(4-methoxyphenyl)methanol were reported in the literature.[16]

The oxidation of the corresponding ethane to form the target compound was also pursued as a practical route into sterically hindered *tetrakis*[2-hydroxyphenyl]ethenes. A general method for the synthesis of tetraarylethanes has been described by Mislow, et al.,[13] using chromium(II)chloride and by Schlögl and Weissensteiner[14] using titanium trichloride.

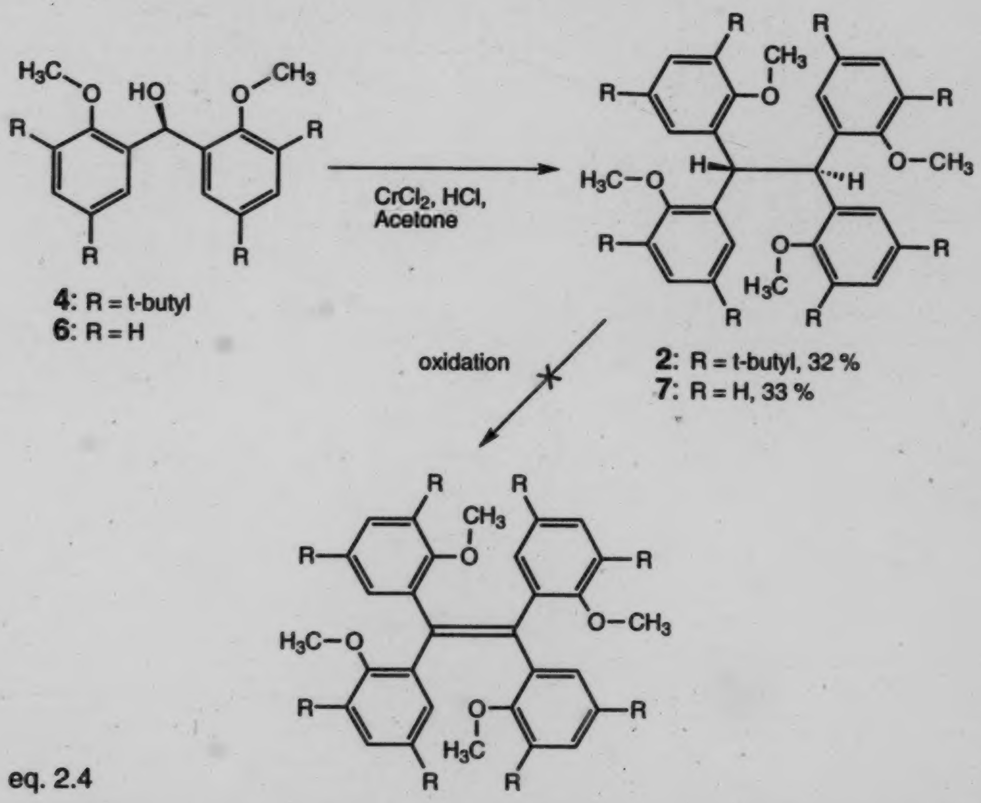

4: R = t-butyl
6: R = H

2: R = t-butyl, 32 %
7: R = H, 33 %

eq. 2.4

Synthesis of the *tetrakis*[3,5-bis(1,1-dimethylethyl)-2-methoxyphenyl]ethane **2** and the *tetrakis*[2-methoxyphenyl]ethane **7** using the Mislow procedure was straightforward, and after repeated recrystallisation from benzene pure products were obtained in low (unoptimized) yields (eq. 2.4, page 67). Both compounds showed a characteristic, but easily missed, singlet of low intensity in the ^{1}H-NMR spectrum around 5.7 ppm for the benzylic proton, as well as the M$^+$ in HRMS at 925.7 (calculated for compound **2**·Na$^+$: 925.7) and 454.2 (calculated for compound **7**: 454.2).

Unfortunately, the products **2** and **7** resisted all oxidation attempts to form the olefin, either by being completely inert or decomposing under the reaction conditions. Attempts to convert these compounds to a set of possibly useful preorganized phenol groups by deprotection also failed. The observed decomposition could be due to the formation of radical cations. According to the literature, radical cations of tetraarylethanes fragment by carbon-carbon bond cleavage.[15] This alternative was therefore abandoned.

Conversion of compound **1** into a hydrazone also turned out to be a problem. No reaction was observed with hydrazine even under forcing conditions for prolonged times, so that the catalytic decomposition route for this compound had to be abandoned.

Instead the hydrazone **8** was made from the methanone **3** in a straightforward way (eq. 2.5, page 69). Oxidation of the hydrazone yielded the *bis*(2-methoxyphenyl)diazomethane (see eq. 2.5, page 69), which was not isolated but treated with anhydrous *para*-toluenesulfonic acid in the absence of light. Addition of a catalytic amount of *para*-toluenesulfonic acid gave immediate release of nitrogen gas accompanied by bleaching of the red solution. In most cases, the product **9** precipitates out as a yellow-white powder, and can be isolated by filtration or removal of the solvent on a rotary evaporator and trituration of the so-obtained solid. The structure of compound **9** was determined by ^{1}H and ^{13}C NMR spectroscopy, elemental analysis and high resolution mass spectroscopy.

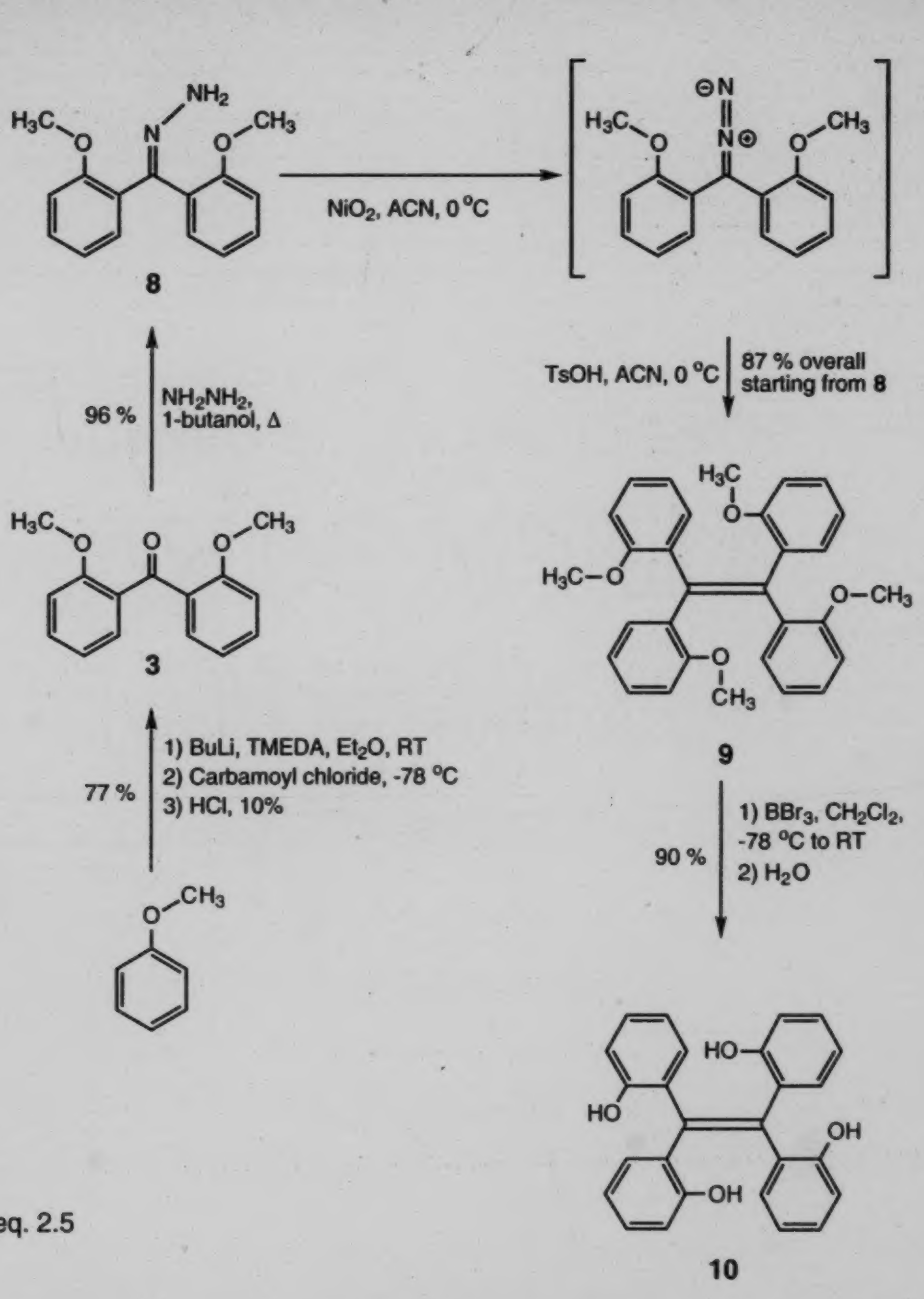
NiO$_2$, ACN, 0 °C
8
96 %
NH$_2$NH$_2$, 1-butanol, Δ
3
77 %
1) BuLi, TMEDA, Et$_2$O, RT
2) Carbamoyl chloride, -78 °C
3) HCl, 10%
TsOH, ACN, 0 °C
87 % overall starting from 8
9
90 %
1) BBr$_3$, CH$_2$Cl$_2$, -78 °C to RT
2) H$_2$O
10

eq. 2.5

At room temperature ^{1}H-NMR spectra (using C_6D_6 as a solvent) show the characteristic methoxy signal at 3.19 ppm, and in the aromatic region of the spectrum a broad doublet and triplet at 7.53 and 6.71 ppm as well as a doublet and multiplet at 6.44 and 6.91 ppm. ^{13}C-NMR is less useful due to the low intensity of the ethene carbon signals at 136.3 ppm (in $CDCl_3$). Another characteristic feature is the blue fluorescence displayed by compounds **9** and **10** (vide infra) in solution as well as on TLC plates. A standard deprotection of the *tetrakis*[2-methoxyphenyl]ethene **9** using boron tribromide gave the *tetrakis*[2-hydroxyphenyl]ethene **10** in good yield, the structure of which was confirmed in an X-ray diffraction experiment, see section 2.3.1 (page 73), and the appendix (page 325).

To modify the obtained tetraarylethenes two routes are possible: modification of the starting material *bis*[2-methoxyphenyl]methanone **3**, or modification of the final product, the tetraarylethene. Both were attempted in order to probe the possibility of further modifying the *tetrakis*[2-methoxyphenyl]ethene frame. For the modification of the tetraarylethenes a *para* substituted analog of the *tetrakis*[2-methoxyphenyl]ethene was used in order to prevent complications caused by multiple electrophilic addition. The *tetrakis*[2-methoxy-4-(1,1-dimethylethyl)phenyl] ethene **11** and the *tetrakis*[2-hydroxy-4-(1,1-dimethylethyl)phenyl]ethene **13** were synthesized by Dr. T. Dzwiniel using the described synthetic methodology.

Conventional bromination procedures[17] cleanly gave the tetrabrominated compounds **12** and **14** in high yield (eq. 2.6, page 71), as indicated by the simple ^{1}H-NMR spectra of the aromatic region and mass spectrometry data. No further modifications of the tetrabrominated compounds **12** and **14** were tried, but the presence of a bromine group on the 3 position should allow introduction of other functional groups using exisiting methodology.

The presence of four methoxy groups centered around the double bond should allow the formation of three geometric isomers when pairwise deprotection is performed. To achieve this, the *bis*[2-methoxyphenyl]methanone was selectively monodeprotected using boron trichloride (eq. 2.7, page 72).[18]

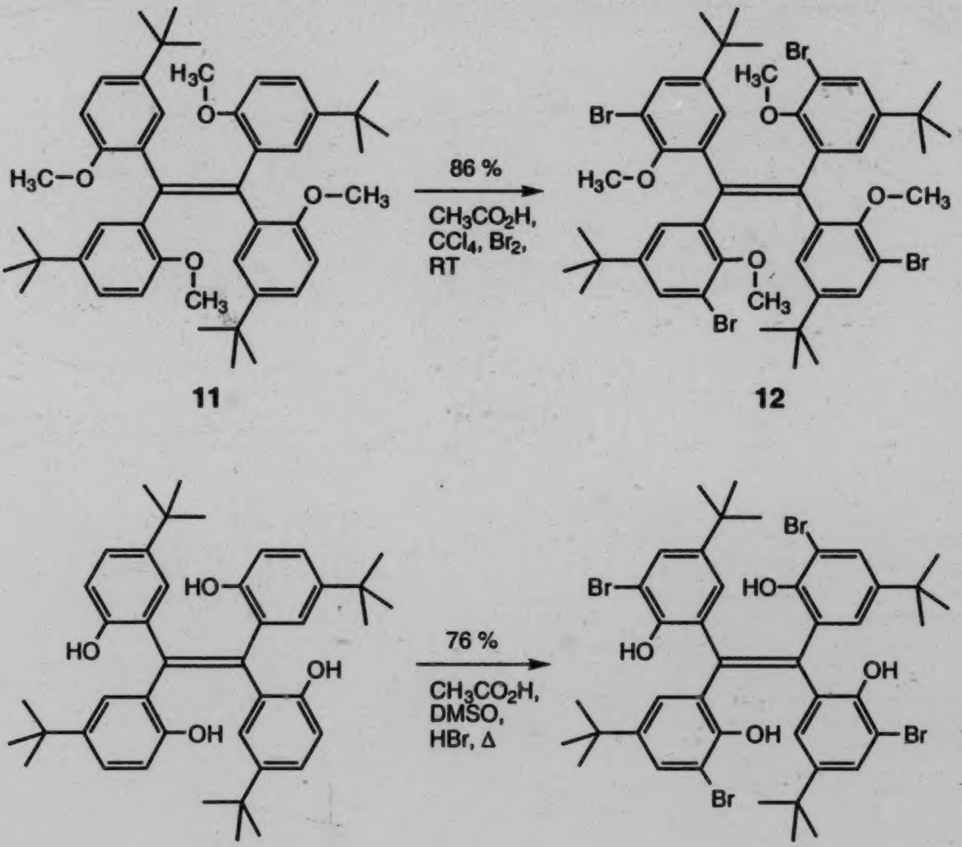
H3C
O
H3C–O
O–CH3
O
CH3
86 %
CH3CO2H,
CCl4, Br2,
RT
Br
Br
H3C
O
H3C-O
O–CH3
O
CH3
Br
Br
HO
HO
OH
OH
76 %
CH3CO2H,
DMSO,
HBr, Δ
Br
Br
HO
HO
OH
OH
Br
Br

11 **12**

13 **14**

eq. 2.6

Reprotection of compound **15** using allyl bromide turned out to be an unfortunate choice (eq. 2.7, page 72).

The formation of the hydrazone from the allyl-protected methanone **16** was accompanied by a side-reaction giving rise to an inseparable mixture of products. A literature search[19] revealed the heat, acid or oxygen promoted intramolecular 1,3-dipolar cycloaddition of hydrazones to a neighbouring allyloxy group. On the basis of these literature reports, the use of an allyl protective group was discontinued. Instead a benzyl group was introduced.

The benzyl group turned out to be stable under the oxidizing conditions employed and did not give problems in the synthesis of the hydrazone: the thesis of Dr. M. Fujita[54] contains the details of the synthesis of the partly protected tetraarylethene.

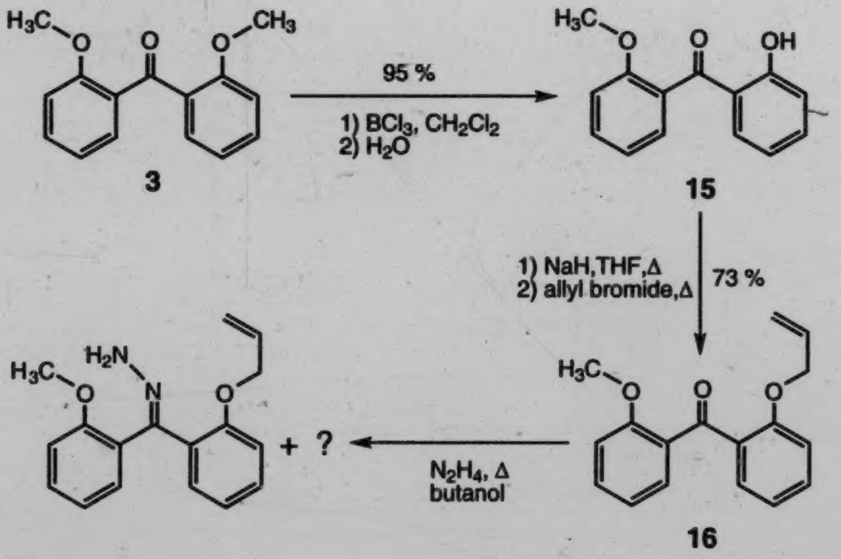

eq. 2.7

2.3 Discussion.

In Chapter 1, section 1.5.3 (page 38), Floriani's calix[4]arene based "oxo-surface" was introduced, and the limitations of calix[4]arenes as a model for heterogenous oxo-surfaces were indicated. Due to the interconverting calix[4]arene conformations, the calix[4]arene can only be a model of limited value for a heterogeneous oxo-surface.

In order to assess the value of the obtained tetraarylethene compounds as an oxo-surface for building organometallic structures it is necessary to determine if the phenyl rings display rapid correlated rotations (for an explanation of "correlated rotations", see reference 5, Chapter 6, page 321) or if rotations are prevented by the steric bulk of the *ortho* substituted phenyl rings.

In case no rotation is taking place in the synthesized compounds, the determination of the kind of isomers obtained becomes important because that would determine the usefulness of these tetraarylethene compounds. Furthermore, theory predicts the possibility of isolating optically active tetraarylethenes in case phenyl ring rotation is sufficiently hindered.[12,25] This would add another dimension to the possible use of these new ligands. If instead a rapid correlated rotation of the phenyl rings is taking place, the oxo-surface analogy is no longer valid and would indicate the necessity of further modifying the phenyl rings in order to stop the internal rotation. In case of high rotational mobility of the phenyl rings it might be possible to stop the internal rotation on lowering the temperature allowing the formation of a calix[4]arene-like circular hydrogen bond array, which would restore the oxo-surface analogy.

Due to the absence of a local C_2 axis in the aryl rings, the stereochemistry of the obtained tetraarylethene compounds becomes quite complicated. In order to clarify the dicussion, the stereochemistry discussion is divided into a static and a dynamic part. The methodology for studying the dynamic behaviour of *ortho*-substituted tetraarylethenes followed by R. Willem, et al., in a paper on *tetrakis*[2-methylphenyl]ethene will be used.[12]

2.3.1 Static stereochemistry of the obtained tetraarylethenes.

Tetraphenylethene in the solid state at -160 °C shows a propeller structure, but the ^{13}C NMR of this compound in solution at room temperature indicates that both edges of the phenyl rings are equivalent under these conditions.[12] This can be explained by any correlated internal rotation of the phenyl rings, assuming the rotation is fast on the NMR time scale.

In case of extreme steric hindrance of the internal rotation the lowest energy conformation would place the four aryl rings perpendicular to the double bond.[20] The number of theoretically possible isomers, when the aryl rings are *ortho* substituted has been derived,[12] and is given in Table 2.1 (page 75). The isomer notation of Willem, et al., will be maintained. Notice that there are 2 sets of enantiomers in this table, I_{2t} and I_3.

If the obtained tetraarylethenes show static stereochemical behaviour, at most a total of eight ^{1}H-NMR signals are expected (in an achiral solvent) for the *ortho* methoxy groups, assuming the aryl rings are perpendicular to the double bond.

If, as an alternative, a propeller like static conformation is assumed, the number of possible methoxy signals doubles to a theoretical maximum of sixteen. At room temperature, the tetraarylethenes **9**, **11** and **12** show a single signal for the methoxy groups in the ^{1}H-NMR spectra.

Tetrakis[2-hydroxyphenyl]ethene **10** can be crystallized from dichloromethane to give crystals suitable for X-ray diffraction: the obtained crystal structure and the crystal structure of *tetrakis*[2-hydroxy-3-bromo-5-(1,1-dimethylethyl)phenyl]ethene **14** (crystallized from *meta*-xylene) are shown in Figures 2.2 (page 76) and 2.3 (page 78), respectively. Crystallographic details are provided in the appendix A, B (page 325 and 331).

In the solid state, the I_{2g} isomer is obtained for both compounds, showing hydrogen bonding between phenol groups bound to the same ethene C, as well as intermolecular hydrogen bonding leading to long stair-like filaments in the crystal structure of compound **10**. No circular array of hydrogen bonds characteristic of calix[4]arenes is observed for compounds **10** and **14**.

Table 1: permutational isomers of *ortho* substituted tetraarylethenes, assuming a static perpendicular conformation[12].

Structure	Abbreviation	Number of heterotopic ortho substituents
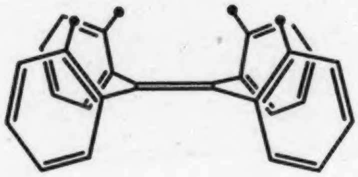	$\mathbf{I}_4$	1
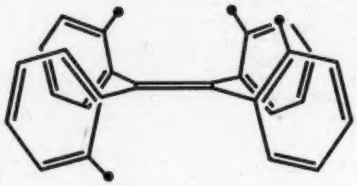	$\mathbf{I}_3$ $\mathbf{I}_{\bar{3}}$	4 4
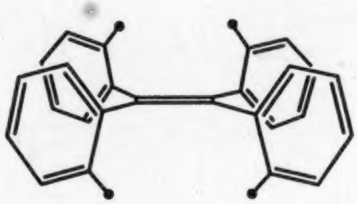	$\mathbf{I}_{2c}$	1
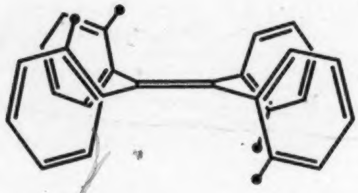	$\mathbf{I}_{2g}$	1
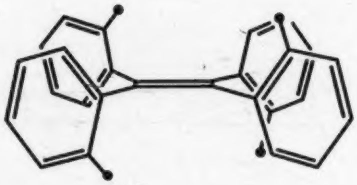	$\mathbf{I}_{2t}$ $\mathbf{I}_{\overline{2t}}$	1 1

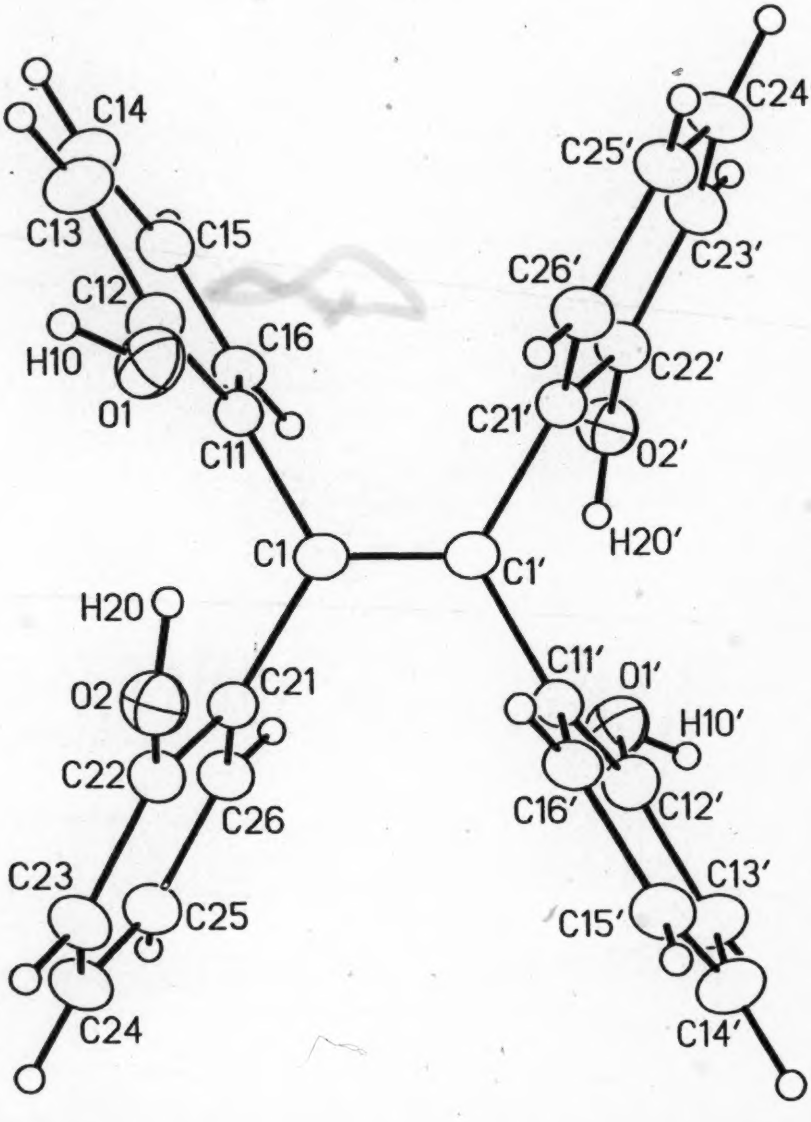
C14
C13
C15
C12
H10
C16
O1
C11
C24′
C25′
C23′
C26′
C22′
C21′
O2′
H20′
C1
C1′
H20
O2
C21
C22
C26
C23
C25
C24
C11′
O1′
H10′
C16′
C12′
C13′
C15′
C14′

Figure 2.2a: Perspective view of one of the two crystallographic independent *tetrakis*[2-hydroxyphenyl]ethene (compound **10**, molecule A in appendix, page 325) molecules. Hydrogen atoms are shown with arbitrarily small thermal parameters.Selected bond distances (Å) and angles(deg): C1-C1'=1.347(9), C1-C11=1.495(6), C1-C21=1.502(6), C12-O1=1.372(6), C22-O2=1.367(6), O1-HO2=1.95 (intra), O2-H01"=1.96 (inter), C11-C1-C21=117.4(4).

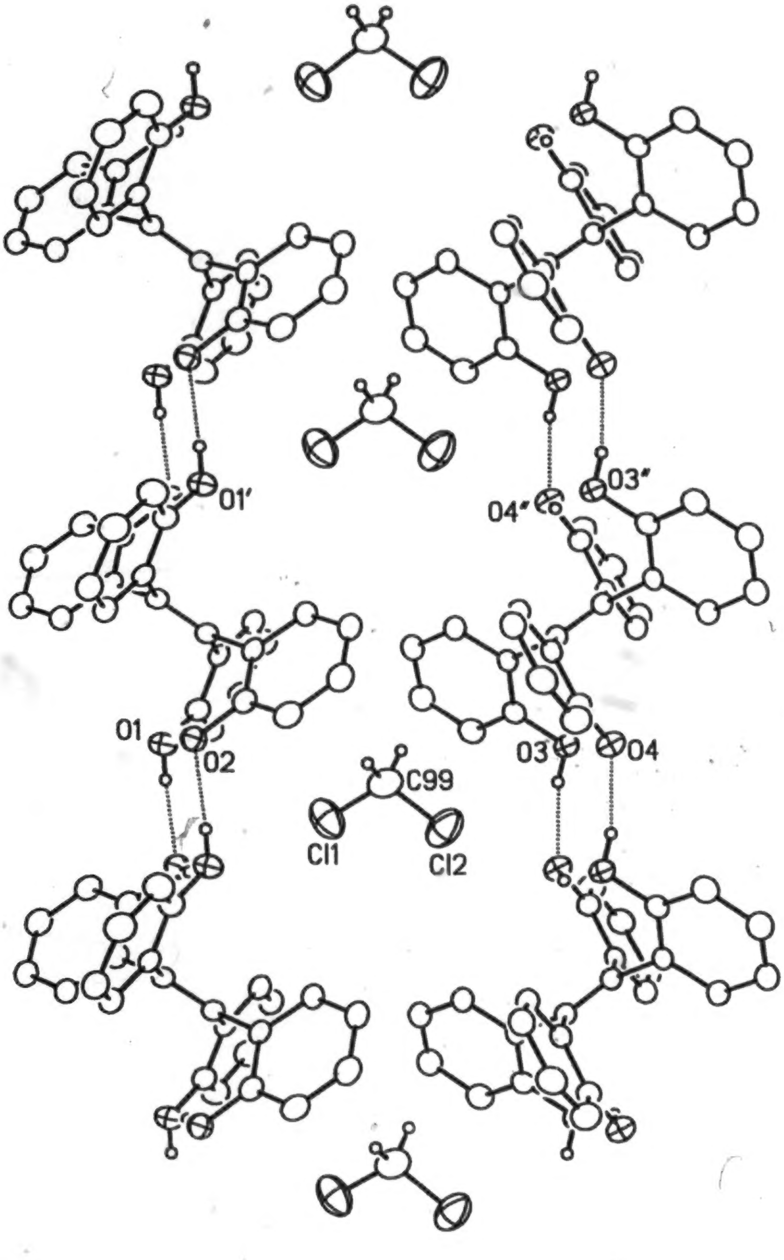
O1'
O4"
O3"
O1
O2
O3
O4
C99
Cl1
Cl2

Figure 2.2b: Illustration of the intermolecular hydrogen bonding within the crystal lattice of compound **10**. Intramolecular interactions are not shown.

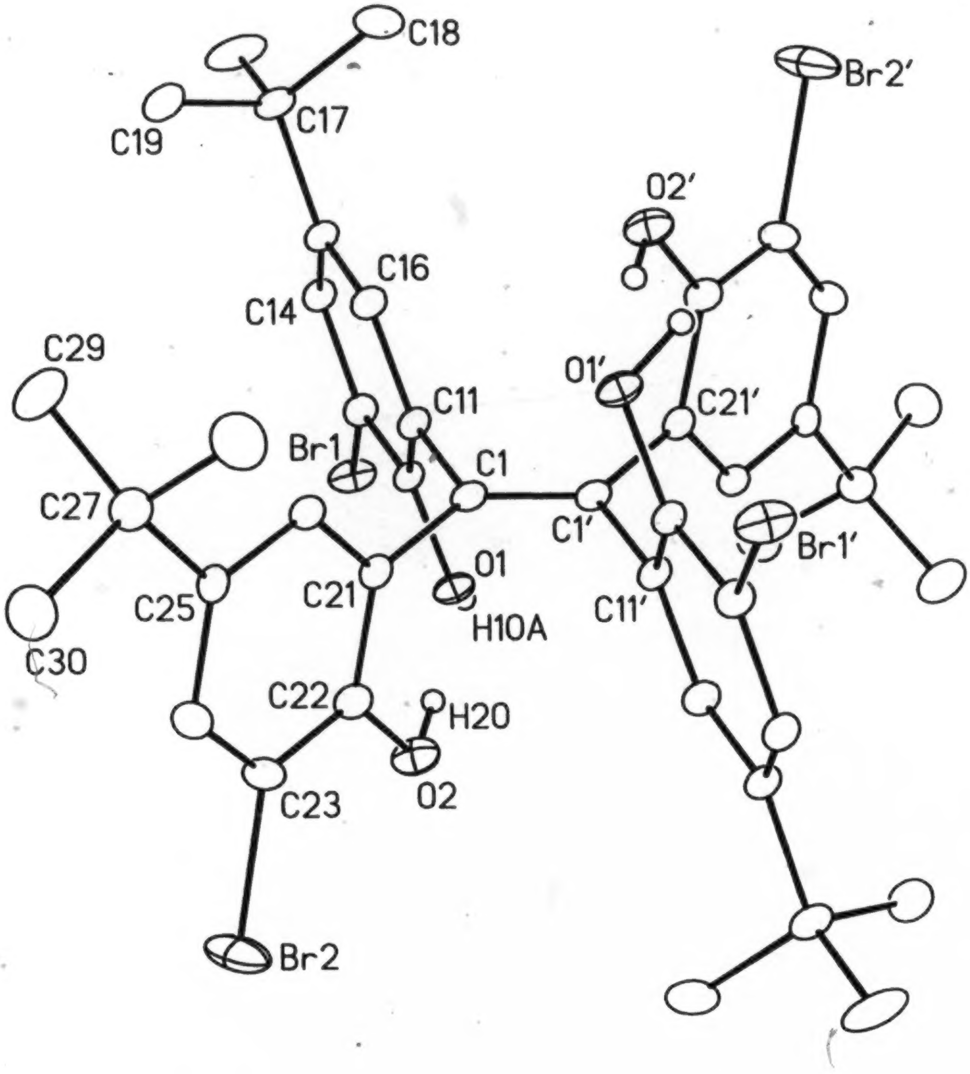
C18
Br2′
C17
C19
O2′
C16
C14
C29
O1′
C21′
C11
Br1
C1
C27
C1′
O1
Br1′
C21
C25
H1OA
C11′
C30
C22
H2O
C23
O2
Br2

Figure 2.3a: Perspective view of the *tetrakis*[2-hydroxy-3-bromo-(1,1-dimethyl ethyl)phenyl]ethene (compound **14**, appendix page 331) molecule. Hydroxyl hydrogens are shown with arbitrarily small thermal parameters; all other hydrogens are not shown. Selected bond distances(Å) and angles (deg): C1-C1'=1.319(7), C1-C21=1.503(5), C1-C11=1.508(4), C12-O1=1.369(4), C13-Br1=1.897(3), C22-O2=1.370(4), C23-Br2=1.902(3), C11-C1-C21=117.3(3), O1-HO1"=2.10, O1-HO2=2.00.

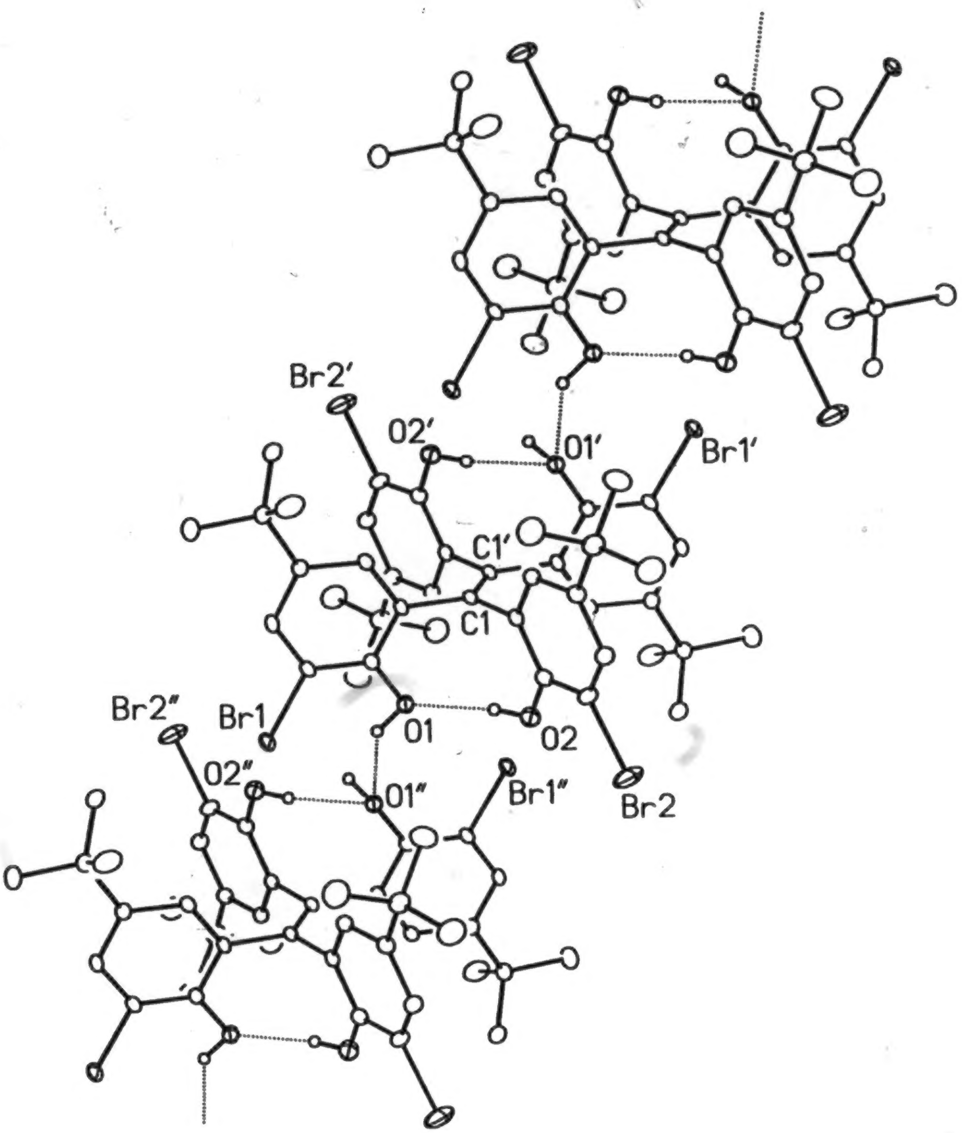
Br2′
O2′
O1′
Br1′
C1′
C1
Br2″
Br1
O1
O2
O2″
O1″
Br1″
Br2

Figure 2.3b: Illustration of intermolecular hydrogen bonding between adjacent compound **14** molecules. Nonbonding distances in Å: O1·····O2=2.836, O1·····O1"=2.947, O2·····Br1"=3.332, O2·····Br2=3.022.

Table 2.2: Selected Crystallographic Data[1] for Tetraarylethenes.

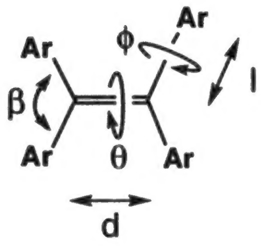

#	Ar:	ref.
T	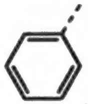	23
10	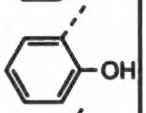	this work
14	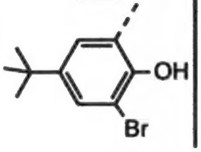	this work

	Angles (degrees)			Bondlength (Å)			
						Hydrogen Bond	
#	θ	β	φ	d	l	Intra	Inter
T	8.4	113.9(3)-115.4(3)	42.9-48.3	1.356(3)	1.491(3)-1.503(3)		
10[2]	1.9(10)	117.4(4)	85.6(7)-93.5(7)	1.347(9)	1.495(6)-1.502(6)	1.95	1.96
10[3]	-0.7(10)	117.2(4)	84.2(7)-95.2(7)	1.328(9)	1.509(6)-1.491(6)	2.01	1.93
14	-0.4(6)	117.3(3)	85.7(5)-94.6(5)	1.319(7)	1.503(5)-1.508(4)	2.00	2.10

1] See appendix and experimental for details. 2] Molecule A in appendix. 3] Molecule B in appendix.

Whereas the *tetrakis*[2-hydroxyphenyl]ethene **10** displays a double hydrogen bond connecting two tetraarylethene units, the brominated compound **14** shows a single hydrogen bond connecting two tetraarylethene units. This also gives rise to chain-like filaments in the crystal structure. The hydroxy group accepting an intermolecular hydrogen bond also seems to accept an intramolecular hydrogen bond.

The torsional angle ϕ (see Table 2.2, page 80) of tetraarylethenes in the Cambridge Database deviates significantly from 90 degrees, giving rise to the so called "tetraarylethene propellers." The hydroxy compounds of this thesis do *not* show the expected propeller conformation: the aryl-ring torsional angle is almost 90 degrees (see Table 2.2, page 80). Maybe the intramolecular hydrogen bonding supplies the force necessary to maintain this conformation in the solid state, but the possibility of additional Coulomb interactions determining the tetraarylethene conformation should also be mentioned.[22] The other structural features shown in the crystal structure of compounds **10** and **14** are less remarkable.

2.3.2 Dynamic Stereochemistry of the obtained tetraarylethenes.

In order to probe if the aryl rings in the synthesized compounds show rotation at room temperature, low temperature ^{1}H-NMR spectroscopy studies were executed. If correlated rotation takes place at room temperature, lower temperatures might slow this process down allowing the observation of the isomers. Increasing the temperature might allow the observation of all possible isomers in case this rotation is absent at room temperature.

To interpret the results of this study the dynamic stereochemistry of *ortho* -substituted tetraarylethenes has to be discussed. The 180° rotation of a

Scheme 2.2: Isomerization scheme for ortho substituted tetraphenyl ethenes, based on a single ring 180° rotation.

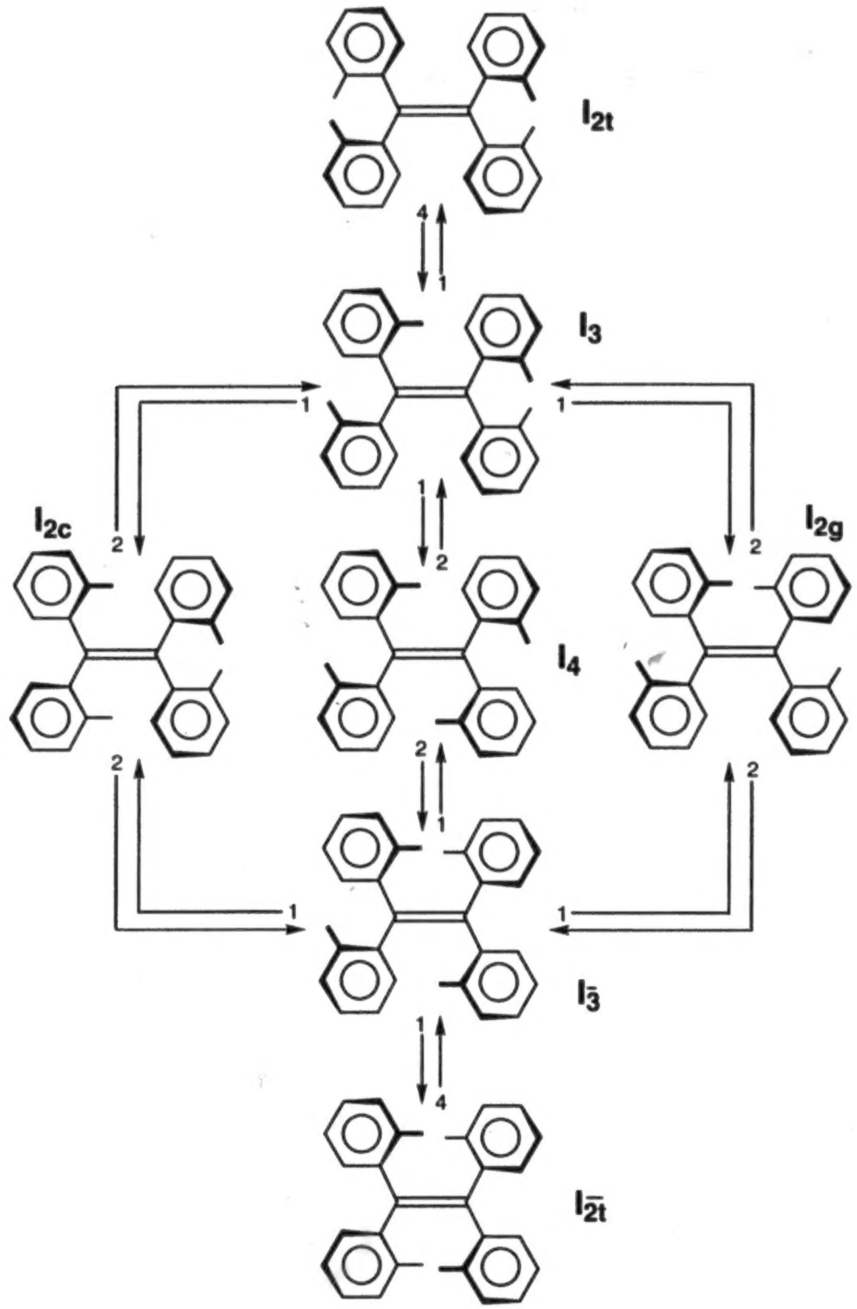
I_{2t}
I_3
I_{2c}
I_4
I_{2g}
$I_{\bar{3}}$
$I_{\overline{2t}}$

single phenyl ring in tetraarylethenes leads to specific isomer interconversions,[12] as shown in isomerization Scheme 2.2 (page 82). Although simultaneous two, three and four ring rotations can be proposed to take place, Force Field calculations predict a much larger activation energy for these rotations.[25] Therefore only the 180° rotation of a *single* aryl ring need to be considered. The numbers at the beginning of the arrows in Scheme 2.2 (page 82) represent the number of different aryl rings that on a 180° rotation lead to the permutational isomer at the end of the arrow. For clarity sake, the isomers in Scheme 2.2 are given with the aryl rings twisted and not in the perpendicular conformation as discussed.

Using this theoretical framework the results of low-temperature ^{1}H-NMR spectroscopy of *ortho*-substituted tetraarylethenes can be analyzed. The NMR spectra of *tetrakis*[2-methoxyphenyl]ethene **9** (page 69) show a gradual broadening of the aromatic and methoxy signals combined with a growing in of signals due to slow isomer interconversion on lowering the temperature. Around -95 °C, the methoxy signal of *tetrakis*[2-methoxyphenyl]ethene **9** has changed into 7 broad singlets one of which has a shoulder indicating the presence of another peak, see Figure 2.4 (page 84). The observed signals might correspond to the presence of all permutational isomers of Scheme 2.2 (page 82).

The intensity of the 8 singlets is different, presumably reflecting the thermodynamic stability of the isomers. At -95 °C the aromatic signals have become complicated, providing additional evidence that the isomer interconversion has slowed down or stopped.

The *tetrakis*[2-methoxy-4-(1,1-dimethylethyl)phenyl]ethene **11** (eq. 2.6, page 71), *tetrakis*[2-hydroxyphenyl]ethene **10** (eq. 2.5, page 69), *tetrakis*[2-hydroxy-3-bromo-5-(1,1-dimethylethyl)-phenyl]ethene **14** (eq. 2.6, page 71) and

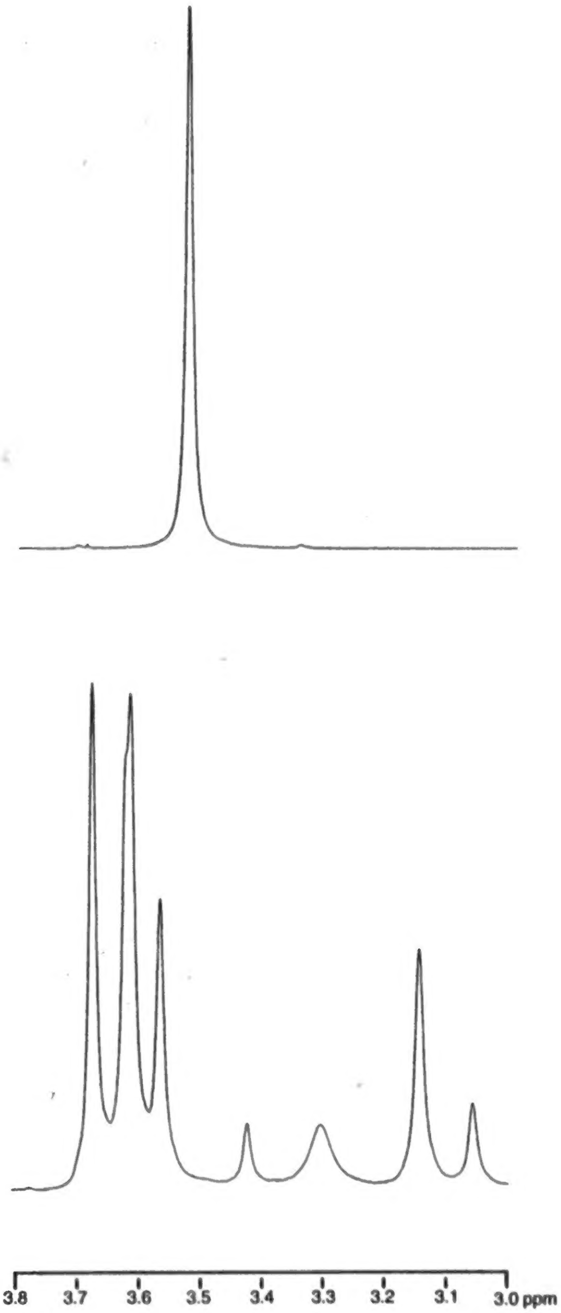

Figure 2.4. ^{1}H-NMR of the methoxy group of *tetrakis*[2-methoxyphenyl]ethene **9** at room temperature (top) and at -95° C (bottom).

tetrakis[2-hydroxy-5-(1,1-dimethylethyl)phenyl]ethene **13** (eq. 2.6, page 71) display similar low temperature behaviour, indicating that the aryl rings of these compounds display rapid correlated rotation at room temperature. In contrast with these observations, the *tetrakis*[2-methoxy-3-bromo-5-(1,1-dimethylethyl) phenyl] ethene **12** (eq. 2.6, page 71) doesn't show any changes in the ^{1}H-NMR spectra on cooling to -95 °C, except for the appearance of some small signals in the baseline, which could be due to impurities or slowing down of fast isomer interconversion.

This last possibility is unlikely, given the fact that the corresponding hydroxy compound **14** (eq. 2.6, page 71), which is sterically less hindered,[26] shows the expected multiple signals indicative of hindered interconversion of isomers on lowering the temperature. The absence of any change in the variable-temperature ^{1}H-NMR spectrum of compound **12** could therefore be due to the absence of isomer interconversion at room temperature. Heating the ^{1}H-NMR sample to 100 °C does not result in changes in the spectrum. The fact that only a single line is observed for both the methoxy and *tert*-butyl signals over the whole temperature range excludes the presence of the I_3 isomers, while steric hinderance arguments would disfavor I_4 (see Scheme 2.2, page 82).

In order to probe if the rotation of the aryl rings actually has stopped, the ^{13}C-T_1 relaxation time of the corresponding hydroxy compound **14** was measured. Theoretically the internal aryl ring rotation should contribute to the overall correlation time of the ^{13}C *ortho* to the double bond, thereby inducing a shorter ^{13}C-T_1 for that specific carbon, when compared to the ^{13}C-T_1 *para* to the ethene bond, which in turn should reflect the overall correlation time of the tumbling molecule.[27] As variable temperature ^{1}H-NMR measurements indicate that the isomer conversion is rapid on the NMR time scale at room temperature, a difference for the measured ^{13}C-T_1 was predicted. The actual measurement on this reference compound failed to show a difference in the *ortho/para* ^{13}C-T_1, indicating that this method might be unsuitable for probing the absence or presence of internal rotation in the corresponding methoxy compound **12**.

Assuming that no diastereomer interconversion is taking place, any I_{2t} isomers present should form a racemic mixture. The presence of such a racemic mixture could be probed using a chiral shift reagent or a chiral NMR solvent.[28]

Both a chiral shift reagent study using Sievers reagent (tris[3-(heptafluoropropyl (+)camphorato]europium(III)), as well as the use of a chiral solvent (α(-)pinene plus a trace of deuterated dichloromethane) failed to give a doubling of the aromatic signals of compound **12** characteristic of the presence of enantiomers in solution. This leaves the question of fast interconversion or no interconversion of isomers at room temperature unresolved for compound **12**.

According to the measured ^1H-NMR chemical shift of the deprotected tetraarylethenes, hydrogen bonding takes place considering that the observed downfield shift of the phenolic hydrogen is comparable in magnitude with the recently introduced cone-fixed calix[4]arene analogs.[29] (see Table 2.3, page 87). For comparison: phenol and *ortho*-methylphenol (5 mM, $CDCl_3$, RT) have a chemical shift of 4.70 ppm and 4.63 ppm, respectively, for the phenolic hydrogen.[29] According to the results of the low temperature ^1H-NMR spectroscopy study, no hindering of the conformational mobility takes place thereby hindering the formation of a calix[4]arene like circular hydrogen bond array. The observed chemical shift of the OH groups also indicate the absence of a significant contribution by a circular hydrogen bond array: such a set of hydrogen bonds would display a characteristic downfield shift (see Table 2.3, page 87).

Table 2.3: ^{1}H-NMR chemical shifts of hydroxy groups of tetradentate ligands.

Compound	**OH Chemical Shift (solvent)**
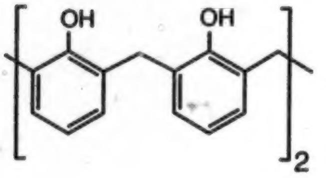	10.34 ppm ($CDCl_3$) [30]
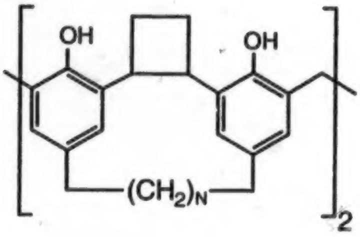	N 5 7.78 ppm ($CDCl_3$) [29] 6 6.71 ppm ($CDCl_3$) [29]
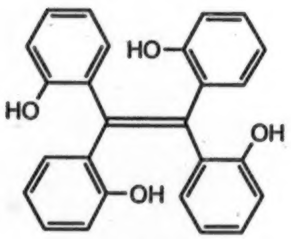 **10**	5.91 ppm (CD_2Cl_2)
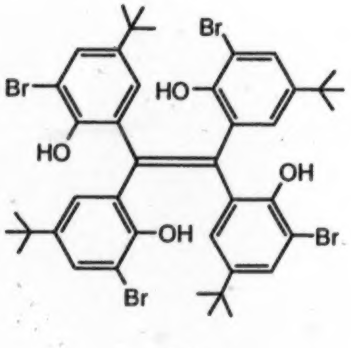 **14**	5.96 ppm (C_6D_6) 5.97 ppm ($CDCl_3$)

2.3.3 On the formation of dihydro-dibenzo[b,e]oxepin.

The inability to isolate the tetraarylethene compounds using the Magidson acid treatment of diarylmethanol was also noted by another group: a publication by Wentrup appeared in 1998 in the literature[31] addressing this observation. The studies of Magidson, Bergmann, as well as Franzen and Joschek[8] are erroneous according to Wentrup. In this latter work, a mass spectrometer coupled to a gas chromatograph was used for the analysis of the product mixtures.[31] At most only traces (0.1 %) of tetraarylethenes were detected in the acid decomposition of bis[1-naphthol]methanol using this sensitive analytical technique.

The unexpected formation of the oxepin when the corresponding carbinol **4** (eq. 2.3, page 66) is treated with acid seems to be related to the combination of a methoxy group bracketed by a methylene or methanone bridge and a *tert*-butyl group. In order to rationalize the results, the conformation of the methoxy group must be considered, as it is nearest to the carbonyl group and the carbocation formed as an intermediate in these reactions.

It is well known from crystallography studies[32] and NMR studies[33] that in sterically unhindered substituted anisoles the methoxy group has a preference for positioning itself in the plane of the phenyl ring, leading to an sp^2 hybridized oxygen, with one lone pair in a p-orbital to maximize the overlap with the aromatic π-orbitals.[33] Some controversy surrounds the estimation of the barrier to internal rotation around the aromatic carbon and the oxygen: values between 11.5 kcal/mol and 1.4 kcal/mol are quoted.[33]

Introduction of two bulky groups *ortho* to the methoxy group forces the methoxy group out of the plane of the phenyl ring, leading to a diminished delocalization of the oxygen lone pair electrons into the benzene π-system.[33] This expresses itself in a characteristic downfield ^{13}C-NMR shift of the methoxy

Table 2.4: ^{13}C-NMR Chemical Shifts of methoxy groups: the buttressing effect.

Compound				^{13}C Chemical Shift OCH_3 group (all in $CDCl_3$)
		Aryl Group:		
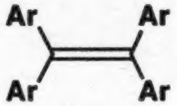	9	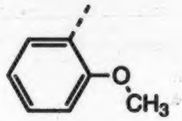		55.3 ppm
	11	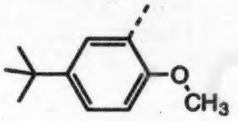		56.0 ppm
	12	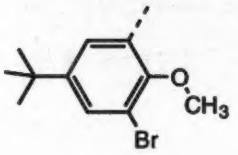		60.1 ppm (in CD_2Cl_2)
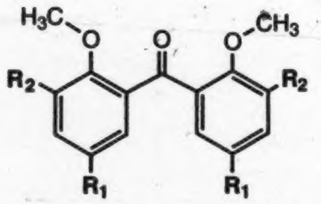		R_1	R_2	
	3	H	H	55.7 ppm
	4	t-butyl	t-butyl	62.8 ppm

group of compounds **4** and **12**, see Table 2.4. Notice that although the electron density on the oxygen *increases*, the ^{13}C NMR shift is downfield, *not* upfield. A clear explanation for this deshielding effect in out-of-plane methoxy groups is absent in the literature, but the observation itself is very consistent.

Using the methoxy ^{13}C-NMR shifts as a marker for the *in* or *out* of plane position of the methoxy group, the *ortho*-substituted compounds in Table 2.4

show evidence for a sterically induced preference for an out-of-plane position of the methoxy groups.

In the following discussion it is assumed that after protonation of the carbinol **4**, the carbocation is formed rapidly, the resulting carbocation is sp^2 hybridized, and the aryl rings at this point are in a propeller conformation. Although the last assumption seems reasonable, it is by no means certain as relief of strain could also be achieved by widening of the phenyl-carbon-phenyl angle instead of by phenyl-carbon rotation.[35]

Under these assumptions the release of steric stress due to the carbon sp^3 to sp^2 conversion would allow the following scenario, see Scheme 2.3 (page 91).

After formation of the carbocation **I**, the steric bulk of the *tert*-butyl group combined with the rotation of the phenyl ring[35] could force the methoxy group into the gap causing an overlap between the empty p orbital[37] of the carbocation and the methyl hydrogens of the methoxy group. Similar buttressing effects are well documented.[2,38] The result of pushing the methoxy group over the carbocation is a hydride abstraction, giving rise to phenoxymethylene cation **II**. Such hydride abstractions are known.[39] Similar acid-catalyzed 1,5-hydride shifts involving an alkoxymethyl cation have been proposed to explain the outcome of rearrangement reactions of steroids (Woodward's "iso reaction"), spiroketals, and large ring systems.[40]

In the proposed mechanism the phenoxymethylene cation **II** has sufficient lifetime to undergo a nucleophilic attack by the electron rich aryl ring neighbour.[41] If an unfavourable seven-membered transition state is assumed, the oxepine could be formed directly (C in Scheme 2.3, page 91). An alternative formation of a six-membered intermediate that undergoes a 1,2-alkyl shift

Scheme 2.3: Proposed mechanism for oxepin formation.

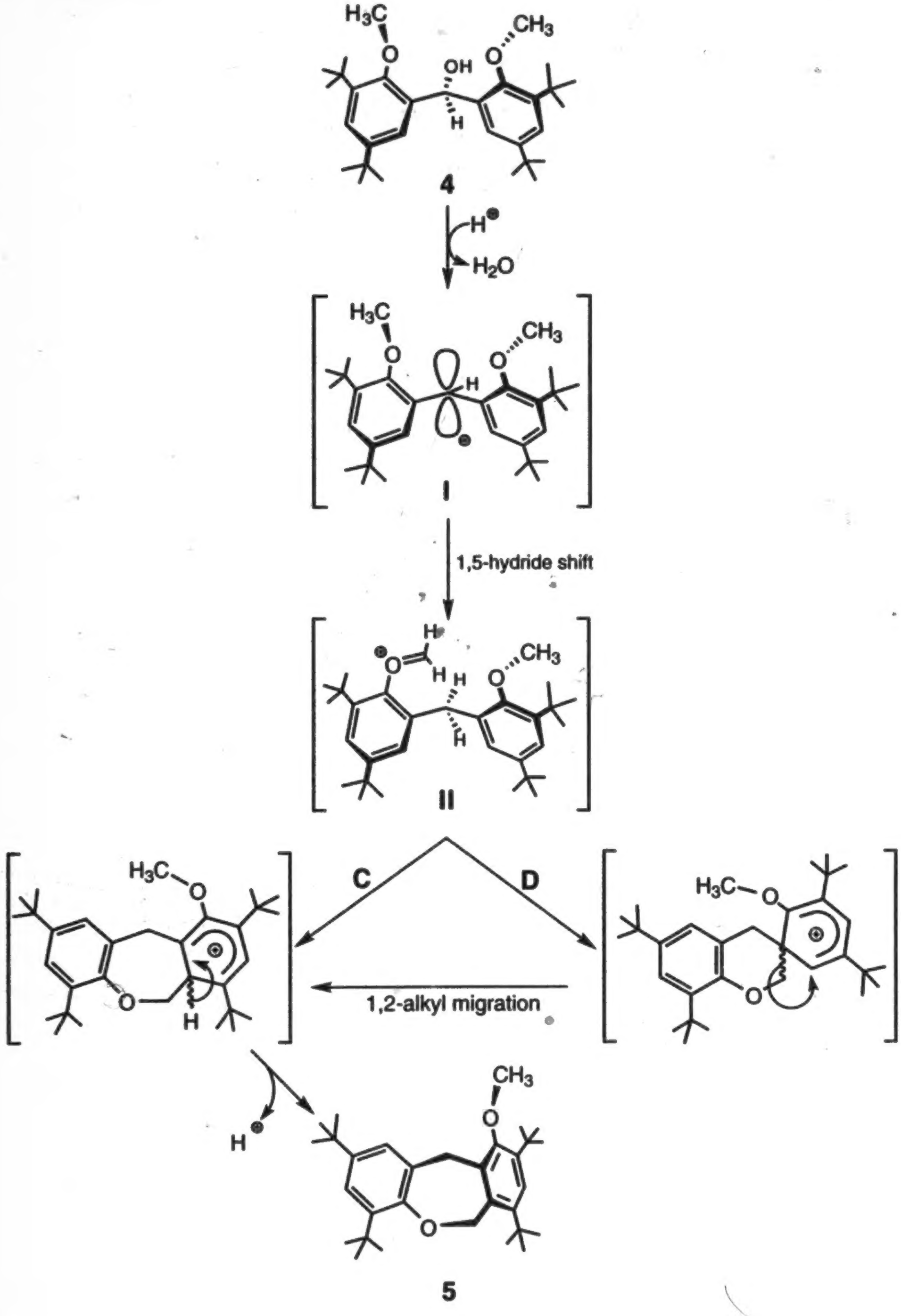
4
H⊕
H2O
I
1,5-hydride shift
II
C
D
1,2-alkyl migration
H⊕
5

followed by proton loss to give the final product is also possible (D in Scheme 2.3, page 91).

In fact, the formation of just such a six-membered intermediate has been proposed to occur in a new double rearrangement observed in mass spectrometry studies of *ortho*-heteroatom substituted alkyldiaryl and triaryl cations (Scheme 2.4, page 93).[42] In the mass spectrometry studies by Ceraulo, et al.,[43] benzyl/tropylium cation formation was observed from *ortho*-substituted diphenylmethyl cations generated by electron impact or chemical ionisation.

The benzyl or tropylium ion formation is proposed to occur through a double rearrangement process consisting of a hydrogen-to-carbon migration, followed by a carbon-to-carbon displacement reaction, followed by fragmentation, as shown in Scheme 2.4 (page 93). This constitutes a new pathway for benzyl/tropylium cation formation not previously reported. More interesting for our discussion is that this new pathway only occurs with *ortho*-alkoxy, mono- or di-alkylamino, or alkylsulfide groups.[42] These observations raise a number of questions.

Using the *tert*-butyl buttressed diphenylmethanol compound, could other *ortho* heteroalkyl groups be induced to form a seven-membered ring ? Another intriguing question is whether the intramolecular rearrangement process can still compete with intermolecular reactions if the positions para to the methoxy group are free: an infinite dilution reaction[43] and accurate product analysis suggest themselves at this point.

Scheme 2.4: Ceraulo's hydrogen-carbon, carbon-carbon double rearrangement leading to benzyl cations as observed under mass spectrometry conditions.[42]

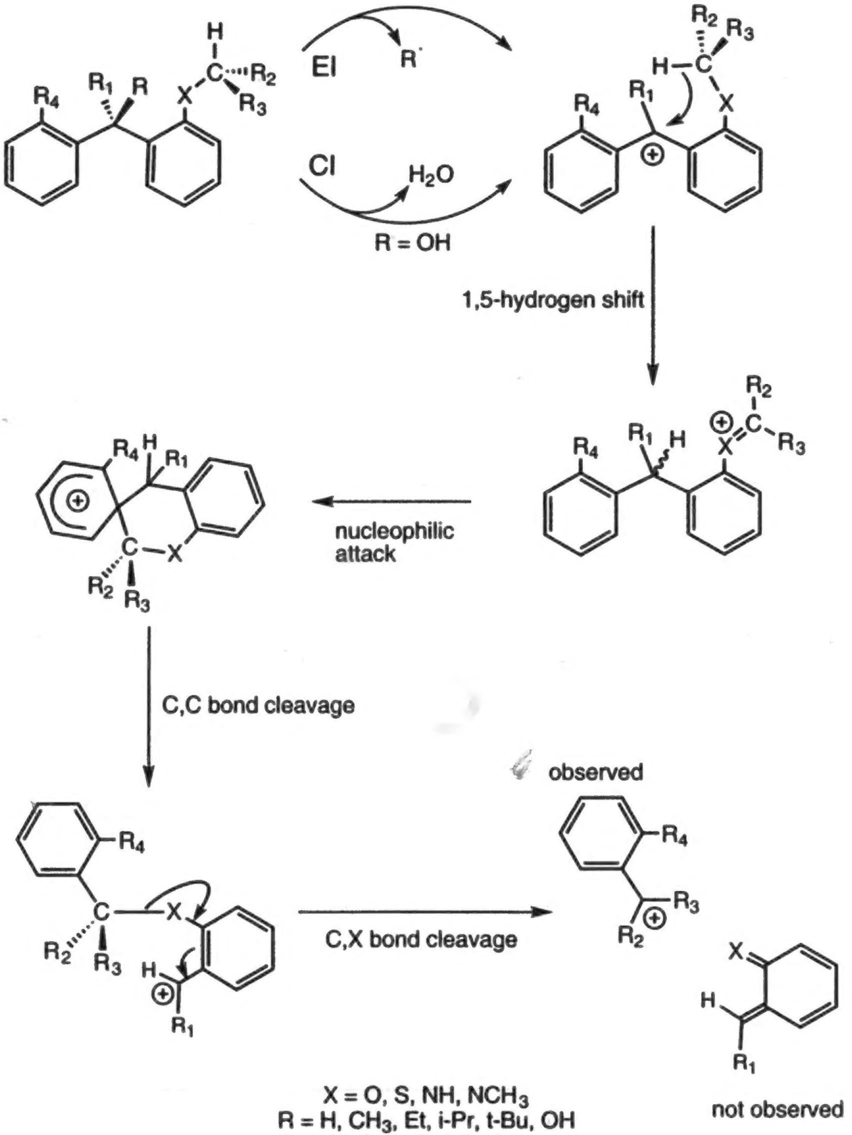
EI
R·
CI
H_2O
R = OH
1,5-hydrogen shift
nucleophilic attack
C,C bond cleavage
observed
C,X bond cleavage
not observed

X = O, S, NH, NCH_3
R = H, CH_3, Et, i-Pr, t-Bu, OH
R_1 = H, CH_3, Et, i-Pr, t-Bu, Ar
R_2, R_2 = H, CH_3
R_4 = H, OCH_3

2.4 Experimental.

General:

All air-sensitive manipulations were conducted under a nitrogen atmosphere using drybox or Schlenk line techniques. Infrared (IR) spectra were recorded on a Nicolet Magna 750 Nic-plan IR microscope, and are reported in reciprocal wave numbers (cm^{-1}) calibrated to the 1601 cm^{-1} absorption of polystyrene. Melting points (mp) were recorded on a Perkin Elmer Pyris 1 DSC differential scanning calorimeter: in case a non-reproducible melting point was obtained for a compound, no melting point is given in the experimental. Elemental analysis (EA) were measured with a Carlo Erba EA1108 elemental analyzer. ^{1}H and ^{13}C nuclear magnetic resonance (NMR) spectra were recorded on a Varian INOVA60 [600 Mhz (^{1}H)], Bruker AM-200 [200 MHz (^{1}H)], Bruker AM-300 [75.5 MHz (^{13}C)], Bruker AM-400 [400 MHz (^{1}H) and 100 MHz (^{13}C)] and Bruker AM-360 [360 MHz (^{1}H)] spectrometers. Chemical shifts are reported in parts per million (ppm, δ) relative to the residual proton signal of the deuterated solvent, which in turn is relative to TMS. Coupling constants are reported in Hertz (Hz). Unless stated otherwise, NMR spectra were obtained at room temperature (23-27 ^{o}C). Coupling constants are reported as J refer to J_{HH} for ^{1}H-NMR spectra, and are reported to 0.2 Hz, although the digital resolution is 0.4 Hz/point. Multiplicities are reported as observed. NMR abbreviations used: T-ROESY (Transmitter Rotating frame Overhauser Enhancement SpectroscopY), NOESY (Nuclear Overhauser Enhancement SpectroscopY).

High resolution mass spectra (HRMS) and low resolution mass spectra (MS) were obtained on a Kratos MS-80RFA spectrometer operating at 70 eV (Electron Impact), positive ion mode, using a heated direct insertion probe. Mass spectrometric analysis using positive mode electrospray (ES) ionization was performed on a Micromass ZabSpec Hybrid Sector-TOF. The liquid carrier, methanol or acetonitrile, was infused into the electrospray source by means of a Harvard syringe pump at a flow rate of 10 μL/minute.

Analytical Thin Layer Chromatography (TLC) was performed on precoated aluminumbacked silica gel plates (E. Merck 60 F_{254}, 0.25 mm) and visualized by irradiation with UV light, iodine or Morstein reagent (20 g ammonium molybdate and 0.4 g cerium(IV)sulfate dissolved in 500 mL 10% sulfuric acid). Celite filtrations were performed using a plug of Hyflo Super Cel (Fisher) on a type C sintered glass funnel under vacuum. Flash column chromatographic separations[45] were performed using silica gel 60 (0.040-0.063 mm, E. Merck).

Cylindrical medium-walled Pyrex vessels equipped with Kontes k-826510 Teflon vacuum stopcocks are referred to as glass bombs. For centrifuging suspensions, an International Equipment Co. Model CL clinical centrifuge was used, with an estimated speed of 2000 rpm. High Vacuum conditions refer to a pressure range of $2 \cdot 10^{-5}$ - $6 \cdot 10^{-6}$ Torr as measured on a oil-diffusion pump-based high vacuum line using a Penning-type vacuum gauge.

Materials: Unless indicated otherwise, solvents and reagents were purchased from commercial vendors, distilled or passed down a plug of neutral alumina, and degassed prior to use by three freeze-pump-thaw cycles on a vacuum line. Benzene, hexanes, pentane, tetrahydrofuran and diethylether were purified by distillation from sodium or potassium benzophenone ketyl. Toluene was purified by distillation over sodium, or by passing through a set of columns containing alumina, copper deoxygenation catalyst and molecular sieves, see Chapter 5 (page 276) of this thesis.

Bis[3,5-bis(1,1-dimethylethyl)-2-methoxyphenyl]methanone 1.

The procedure described by Wuest for the oxidation of bis[3,5-bis(1,1-dimethylethyl)-2-methoxyphenyl]methane using chromium trioxide was slightly modified.[11]

To a suspension of 10 g (23 mmol) of bis[3,5-bis(1,1-dimethylethyl)-2-methoxy phenyl]methane[11] in 200 mL of acetic anhydride was added 3.6 g (36 mmol) of powdered chromium trioxide at once under rapid stirring, followed by slow portion wise addition of another 3.6 g over a period of 30 minutes (note: a 15 to 20 minute delay in the oxidation was observed when good quality, dry, chromium trioxide was used, which is necessary for a good yield. Good stirring was essential; flashes of light could be seen when stirring was inadequate and too much chromium trioxide started to build up at the bottom of the flask. After the reaction mixture reached a temperature of 70 to 80 °C, the amounts of chromium trioxide added were reduced drastically in order to prevent ignition of the reaction mixture). After addition of all the oxidant the reaction was stirred for one hour to let it come to room temperature. To the suspension 40 mL of 2-propanol was added carefully, after which the resulting reaction mixture was passed through a layer of silica gel. The green filtercake was rinsed with acetic anhydride and the solids transferred to a 250 mL Erlenmeyer flask. The filtrate was discarded. To the filtercake 200 mL of dichloromethane and 10 mL of water was added. After mixing the sludge was filtered through a silica gel layer wetted with dichloromethane. This procedure was repeated. The combined, colorless, organic layers were washed with saturated sodium bicarbonate solution, followed by water untill the water tested neutral. The dichloromethane layers were dried over anhydrous magnesium sulfate. After filtration, the solvent was removed under reduced pressure on a rotary evaporator. Yield of pure material: 6.46 g (62 %)

mp: 197 °C; IR (neat):1643, 2959 cm^{-1}; ^{1}H NMR (360 MHz, $CDCl_3$): δ 1.29 (s, 18H), 1.38 (s, 18H), 3.51 (s, 6H), 7.41 (d, J = 4.8 Hz, 2H), 7.49 (d, J = 4.8 Hz, 2H); ^{13}C NMR (75.5 MHz, $CDCl_3$) δ 30.8, 31.5, 34.6, 35.4, 62.8, 126.9, 127.5, 132.3, 142.0, 144.5, 158.0, 198.0(br); HRMS(EI) Calculated for $C_{31}H_{46}O_3$: 466.3447, Found: 466.3445 [100%], 451[87], 57[23]; EA calculated for $C_{31}H_{46}O_3$: C, 79.78; H, 9.93. Found: C, 79.60; H, 10.13.

Attempted synthesis of the bis[3,5-bis(1,1-dimethylethyl)-2-methoxyphenyl]methanone hydrazone.

To a glass bomb containing a small teflon coated stir bar was transferred, using 2 mL of 1-butanol, 0.21 g (0.45 mmol) of bis[3,5-bis(1,1-dimethoxyethyl)-2-methoxyphenyl]methanone **1**. Anhydrous hydrazine (0.5 mL, 16 mol) was added and after flushing with nitrogen the bomb was closed. Behind a polycarbonate safety screen the bomb was heated under stirring for two days at 130 °C, followed by 6 days at 140 °C. Unchanged starting material was recovered.

Attempted synthesis of *tetrakis*[3,5-bis(1,1-dimethylethyl)-2-methoxyphenyl)]ethene by the McMurry coupling.

In a 250 mL three neck round bottom flask equipped with a reflux condenser and nitrogen inlet, 3.15 g (48 mmol) of zinc/copper couple and 2.64 g (7.1 mmol) of $TiCl_3 \cdot 3THF$ in 150 mL dry, oxygen free dimethoxyethane were heated to reflux under nitrogen, and maintained at that temperature overnight. After the suspension had reached room temperature 0.42 g (0.9 mmol) bis[3,5-bis(1,1-dimethylethyl)-2-methoxyphenyl]methanone **1** dissolved in 10 mL of dimethoxyethane was added to the mixture. After 35 hours at reflux, no more changes were visible by TLC. The workup of the reaction consisted of filtering the suspension over Celite and washing the filter cake with hexanes. The combined organic fractions were reduced to dryness on a rotary evaporator. Flash chromatography[45] of the residue dissolved in toluene using toluene as the eluent, gave 0.28 g (35 %) of *tetrakis*[3,5-bis(1,1-dimethylethyl)-2-methoxyphenyl)]ethane. The ethane is impossible to detect on TLC *except* with the Morstein spray reagent. For the product analysis, see the *tetrakis*[3,5-bis(1,1-dimethylethyl)-2-methoxyphenyl)]ethane **2** synthesis.

***Tetrakis*[3,5-bis(1,1-dimethylethyl)-2-methoxyphenyl]ethane 2.**

The Mislow procedure was followed.[13]

In a 25 mL three neck round bottom flask equipped with a nitrogen inlet, 6 mL of acetone and 3 mL of concentrated hydrochloric acid (36-38 %) were combined. Under stirring, nitrogen was passed through for 5 minutes in order to obtain an oxygen-free solution. Bis[3,5-bis(1,1-dimethylethyl)-2-methoxyphenyl]methanol **4** (0.40 g, 0.85 mmol) was added, followed by 0.31 g (2.5 mmol) chromium(II)chloride and another 5 mL of oxygen-free acetone. The green suspension was stirred under a nitrogen atmosphere for 18 hours, at which time a white precipitate had separated out of a deep green solution. The suspension was transferred to 300 mL of water, and extracted three times with 150 mL dichloromethane. The combined organic layers were washed successively with water, pH 7 buffer, and water. The dichloromethane layers were dried over anhydrous magnesium sulfate and filtered. The solvent was removed under reduced pressure using a rotary evaporator. The crude product was obtained with a yield of 0.48 g. After recrystallizing three times from benzene, colorless crystals were obtained that were dried under high vacuum, to give 0.125 g (32 %) of analytically pure material.

IR (neat): 2961,1469,1392,1118,1017 cm^{-1}; ^{1}H NMR (360 MHz, CD_2Cl_2): δ 1.21 (s, 36H), 1.24 (s, 36H), 3.51 (broad s, 12H) 5.61 (broad s, 2H), 7.07 (d, J = 2.3 Hz, 4H), 7.46 (broad d, J = 2.3 Hz, 4H); ^{13}C NMR (125.7 MHz, CD_2Cl_2) δ 31.8, 31.9, 34.8, 35.7, 44.2 (br), 62.2, 127.2, 137.6, 141.6, 144.3, 156.0; ethane ^{13}C-^{1}H coupling constant: 130.0 Hz; HRMS(ES) Calculated for $C_{62}H_{94}O_4Na^+$: 925.7050, Found: 925.7025, MS(EI) 842[20%], 841[60], 840[89], 811[19], 810[29], 451[22], 57[100]; EA calculated for $C_{62}H_{94}O_4$: C, 82.43; H, 10.49. Found: C, 82.17; H, 10.79.

Crystal data for *Tetrakis*[3,5-bis(1,1-dimethylethyl)-2-methoxyphenyl]ethane **2** $C_{62}H_{94}O_4$: crystal dimensions 0.39 x 0.23 x 0.21 mm, monoclinic, space group $P2_1/c$ (No. 14), a = 26.095 (3), b = 10.3280 (13), c = 21.174 (2) (Å), β = 96.492 (9) (°), V = 5670.0 (11), Z = 4, ρ_{calcd} = 1.058 (g cm^{-3}), μ = 0.064 (mm^{-1}). Data collection and refinement conditions: Siemens P4/RA diffractometer using graphite-monochromated Mo Kα radiation (l [Å] = 0.71073), T = 213 (K), scan type θ–2θ, 2θ limit 50.0 (°); 10314 measured reflections, 9987 independent reflections, 2476 included in the refinement ($F_o^2 \geq 2\sigma(F_o^2)$), structure solution by direct methods (*SHELXS–86*), refinement by full-matrix least-squares on F^2 (*SHELXL–93*), absorption correction method: *DIFABS* (transmission max./min. = 1.070/0.788), 595 parameters, R_1 = 0.1256, wR_2 = 0.3081 (based on all data), residual electron density 0.298/–0.268 e Å^{-3}, Details are provided in the appendix, page 337.

Attempted oxidation and deprotection of the *tetrakis*[2-methoxy-3,5-bis(1,1-dimethylethyl)phenyl]ethane 2.

The following reactions were tried, and returned unchanged starting material according to TLC and ^{1}H-NMR spectroscopy: DDQ in THF, diisopropylether and dioxane;[46] TMEDA, n-butyllithium, diethyl ether;[47] DMSO, *tertiary*-butylalcohol, potassium *tertiary*-butoxide, oxygen;[48] *tert*-butyl hypochlorite/ sunlight, carbon tetrachloride.[49] The following reaction showed extensive decomposition of the starting material: neat sulphur or selenium at 350-390 °C (sandbath temperature).[50] A boron tribromide deprotection in dichloromethane gave extensive decomposition while boron trichloride didn't show any deprotection: no further attempts were tried.

Bis[2-methoxyphenyl]methanone 3.

An oven-dried 2L three neck round bottom flask equipped with a nitrogen inlet, dropping funnel and a reflux condenser was charged with 400 mL of n-butyllithium solution in hexanes (titrated, 2.66 M, 1.06 mol)[53] maintaining a nitrogen atmosphere. Approximately 300 mL of hexane was removed *in vacuo* under stirring and the resulting residue redissolved in 1.0 L of diethyl ether (freshly distilled from sodium benzophenone ketyl) and 5 mL (3.85 g, 33 mmol) of *N,N,N',N'*-tetramethylethylenediamine (dried over KOH). The dropping funnel was charged with 116 mL (1.06 mol) of anisole. Under vigorous stirring, 30 mL anisole was added rapidly to the n-butyllithium solution. The solution warmed to reflux under release of butane. The solution can be cooled using a cold water bath in case of a too vigorous reaction. The remaining anisole was added at such a rate that a steady reflux of diethyl ether was maintained. After stirring overnight at room temperature a slightly cloudy yellow solution resulted. The solution was cooled to 0 °C (internal) using an ice bath. The dropping funnel was charged with 49 mL (0.53 mol) of diethylcarbamoyl chloride and 50 mL of dry diethyl ether and the resulting solution was added dropwise (extremely vigorous reaction !) under rapid stirring to the cooled reaction mixture. At the end of the addition, the yellow solution had turned into a white creamy suspension. The cooling bath was removed and the reaction mixture stirred one hour at room temperature. At the end of this period, 10 mL of water was carefully added to quench excess n-butylithium. The resulting sludge was poured onto 2.0 L of ice and the flask rinsed with a small amount of acetone. The suspension was carefully acidified to pH 6 using 12% sulfuric acid solution, and any remaining solvents were removed using a rotary evaporator. The yellow crystal mass was collected by vacuum filtration using a Buchner funnel, washed three times with pentane (to remove anisole), and dried under reduced pressure to give 98 g (0.30 mol) of the pure product (77 %) as a white solid.

mp: 104 °C; IR (neat): 1596, 1248 cm^{-1}; ^{1}H NMR (360 MHz, CDCl$_3$): δ 3.67 (s, 6H), 6.92 (d, J = 8.3 Hz, 2H), 6.99 (td, J = 0.8, 7.5 Hz, 2H), 7.43 (ddd, J = 15.8, 7.5, 1.9 Hz, 2H), 7.51 (dd, J = 1.9, 7.8 Hz, 2H); ^{13}C NMR (75.5 MHz, CDCl$_3$) δ 55.7, 111.5, 120.4, 130.3, 130.4, 132.6, 158.4, 195.4; HRMS(EI) Calculated for $C_{15}H_{14}O_3$: 242.0943, Found: 242.0939 [45%], 135[100], 77[39]; EA calculated for $C_{15}H_{14}O_3$: C, 74.36; H, 5.83. Found: C, 74.27; H, 5.72.

Attempted synthesis of *tetrakis*[2-methoxyphenyl)]ethene by the McMurry coupling.

In a 250 mL three neck round bottom flask equipped with a reflux condenser and nitrogen inlet, a mixture of 1.70 g (4.6 mmol) of $TiCl_3 \cdot 3THF$, 0.20 g (0.9 mmol) bis[2-methoxyphenyl]methanone **3** and 150 mL dry, oxygen-free dimethoxyethane was heated and kept at reflux temperature overnight under nitrogen. Heating was stopped after 13 hours. After the suspension had reached room temperature, 1.51 g zinc/copper couple (23 mmol) was added. The mixture was heated to reflux for another 9 hours until no more changes were detected by TLC. The absence of *tetrakis*[2-methoxyphenyl]ethene **9** and the presence of *tetrakis*[2-methoxyphenyl]ethane **7** (vide infra) was confirmed by TLC (samples of both compounds were available) and ^{1}H-NMR. No product isolation was attempted.

Bis[3,5-bis(1,1-dimethylethyl)-2-methoxyphenyl]methanol 4.

A solution of 5.33 g (11.4 mmol) of bis[3,5-bis(1,1-dimethylethyl)-2-methoxyphenyl]methanone **1** in 300 mL of diethyl ether was cooled to 5 °C (external) under stirring using cold tap water. Portionwise 0.48 g (13 mmol) of lithium aluminum hydride was added. After the addition, a reflux condenser with a nitrogen inlet/oil bubbler was placed, and the suspension brought to reflux for 20 hours. After the reaction mixture reached room temperature, water was added dropwise under rapid stirring until no more hydrogen was released. The grey-white sludge was acidified and the organic layer separated from the water layer. The ether layer was washed with pH 7 buffer followed by water until the water layer tested neutral. After drying the organic layer over anhydrous magnesium sulfate, the solvent was removed on a rotary evaporator after the filtration. Yield of analytically pure material; 5.23 g (98 %).

mp: 137 °C; IR (neat): 3149, 2962, 1229, 1011 cm^{-1}; ^{1}H NMR (360 MHz, CD_2Cl_2): δ 1.24 (s, 18H), 1.42 (s, 18H), 3.11 (d, J = 3.0 Hz, 1H), 3.79 (s, 6H), 6.53 (d, J = 3.0 Hz, 1H), 7.15 (d, J = 2.6 Hz, 2H), 7.31 (d, J = 2.6 Hz, 2H); ^{13}C NMR (75.5 MHz, $CDCl_3$) δ 31.4, 31.5, 34.7, 35.4, 62.4, 66.6, 123.8, 124.4, 136.0, 141.8, 145.7, 155.6; HRMS(EI) Calculated for $C_{31}H_{48}O_3$: 468.3604, Found: 468.3609 [48%], 411[20], 247[45], 191[37], 57[100]; EA calculated for $C_{31}H_{48}O_3$: C, 79.44; H, 10.32. Found: C, 79.39; H, 10.42.

2,4,8,10-tetra(1,1-Dimethylethyl)-6,11-dihydro-5-methoxy-dibenzo[b,e]oxepin 5.

In 40 mL dry dichloromethane was dissolved 0.196 g (0.4 mmol) bis[3,5-bis(1,1-dimethylethyl)-2-methoxyphenyl]methanol **4**. Under stirring, a solution of 43 μL HBF_4, 85% (0.49 mmol, 1.2 equiv.) in diethyl ether was added to give a burgundy red solution. After 5 minutes (for other reaction times see Table 2.5, page 104) the solution was poured into saturated sodium bicarbonate solution, and shaken to obtain a yellow colored dichloromethane layer. Another 35 mL of dichloromethane was added. After separation, the organic layer was washed neutral with water and dried over anhydrous magnesium sulfate. After filtration the solvent was removed using a rotary evaporator. The resulting oily solid was resuspended in absolute ethanol and filtered over a bed of Celite (a Pasteur pipette fitted with a plug of cottonwool and Celite was used).

The remaining white solid on the Celite bed was washed with some ethanol and rinsed off of the filter bed using dichloromethane. The dichloromethane was

Table 2.5: Yield of Oxepin as a function of reactionconditions

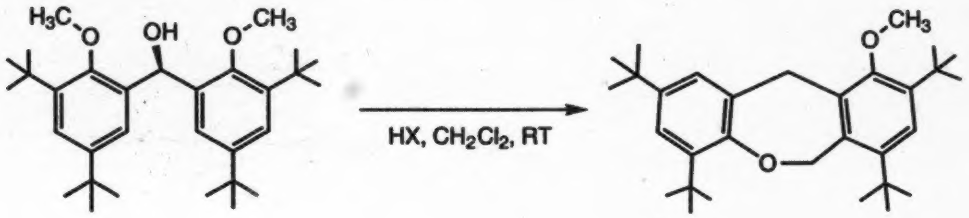

# eq. of Acid	HX	Reaction Time	Oxepin Yield
1	HBF_4	1 min.	48 %
1	Triflic	1 min.	17 %
1	TsOH	30 min.	6 %
1	HBF_4	5 min.	56 %
1	HBF_4	30 min.	51 %
4	HBF_4	30 min.	46 %
1	HBF_4	3 Hrs.	40 %

removed on a rotary evaporator in order to obtain 0.105 g (56 %) of the white, analytically pure, product. The ethanol layer gave a brown oil after removal of the solvent, and according to ^{1}H-NMR spectroscopy and TLC consisted of a mixture of products. Further characterization of the oil was not attempted.

mp: 249 ^{o}C; IR (neat): 2958, 1474, 1231, 1058 cm^{-1}; ^{1}H NMR (360 MHz, CD_2Cl_2): δ 1.27 (s, 9H), 1.34 (s, 9H), 1.39 (s, 9H), 1.48 (s, 9H), 3.72 (s, 3H), 4.32

(s, 2H), 5.69 (s, 2H), 7.04 (d, J = 4.8 Hz, 1H), 7.15 (d, J = 4.8 Hz, 1H), 7.28 (s, 1H); ^{13}C NMR (75.5 MHz, $CDCl_3$) δ 30.3, 31.2, 31.6, 32.6, 33.0, 34.2, 35.4, 35.6, 62.7, 65.3,122.3, 122.8, 123.1, 126.9, 135.4, 136.2, 138.2, 141.3, 141.8, 142.5, 154.3, 155.2, T-ROESY (600 MHz, CD_2Cl_2); 5.69↔4.32, 7.04↔4.32↔3.72 ppm. HRMS(EI) Calculated for $C_{31}H_{46}O_2$: 450.3498, Found: 450.3498 [51%], 394[40], 393[100], 258[27], 243[20], 57[32].

Bis[2-methoxyphenyl]methanol 6.

A solution of 2.27 g (9.4 mmol) of *bis*[2-methoxyphenyl]methanone **3** in 50 mL of diethyl ether and 25 mL of dry tetrahydrofuran was added dropwise to a stirred suspension of 0.38 g (10 mmol) lithium aluminum hydride in 100 mL of dry diethyl ether. After the addition, the suspension was kept 1 hour at reflux under nitrogen. After the suspension had reached room temperature, 0.37 mL of water was added carefully under stirring. The resulting sludge was filtered through a layer of Celite, and the grey filter cake rinsed with ethyl acetate. The combined organic layers were dried over anhydrous magnesium sulfate. After filtration, the solvent was removed under reduced pressure using a rotary evaporator. Yield of analytically pure material: 2.14 g (94 %)

mp: 90 °C; IR (neat): 3502, 1238, 1023 cm^{-1}; ^1H NMR (360 MHz, $CDCl_3$): δ 3.54 (d, J = 4.9 Hz, 1H), 3.83 (s, 6H), 6.36 (d, J = 4.9 Hz, 2H), 6.90 (d, J = 8.4 Hz, 2H), 7.22-7.30 (m, 8H); ^{13}C NMR (75.5 MHz, $CDCl_3$) δ 55.5, 67.5, 110.5, 120.6, 127.9, 128.5, 131.1, 156.9; HRMS(EI) Calculated for $C_{15}H_{16}O_3$: 244.1099, Found: 244.1097 [54%], 226[32], 137[29], 135[100], 109[44], 108[69], 107[37], 91[23], 77[41]; EA calculated for $C_{15}H_{16}O_3$: C, 73.75; H, 6.60. Found: C, 73.69; H, 6.69.

***Tetrakis*[2-methoxyphenyl]ethane 7.**

The synthesis followed the procedure described by Mislow.[13]
Under nitrogen, 6 mL of acetone and 3 mL of concentrated hydrochloric acid were added to a stirred mixture of 0.47 g (1.9 mmol) of bis[2-methoxy phenyl]methanol **6** and 0.66 g (5.4 mmol) of chromium(II)chloride. The resulting green suspension was stirred under nitrogen at room temperature for 16 hours. This suspension was added to 50 mL of water and filtered through a glass frit Buchner funnel (type D) to remove the soluble materials. The almost colorless mass was dissolved in dichloromethane and passed through a bed of silica gel to remove residual chromium salts. The dichloromethane solution was dried over anhydrous magnesium sulfate. After filtration the solvent was removed under reduced pressure using a rotary evaporator. The crude yield before crystallization was 0.33 g. The crude material was dissolved in a small amount of benzene under heating. Colorless crystals were isolated upon cooling and freed from solvent by heating on a high vacuum line[13] to obtain analytically pure material with a yield of 0.15 g (33 %).

mp: 232 °C; IR (neat): 3025, 3001, 2939, 2832, 1495, 1250, 755 cm^{-1}; ^{1}H-NMR (400 MHz, CD_2Cl_2): δ 3.62 (s, 12H), 5.85 (s, 2H) 6.62 (dd, J = 8.2, 1 Hz, 4H), 6.74 (td, J = 7.6, 1.2 Hz, 4H), 6.98 (ddd, J = 8.1, 7.3, 1.8 Hz, 4H), 7.37 (dd, J = 7.8, 1.9 Hz, 4H); HRMS(EI) Calculated for $C_{30}H_{30}O_4$: 454.2144, Found: 454.2141 [6%], 228[49], 227[95], 181[36], 122[29], 121[96], 92[26], 91[100].

Attempted 5-methoxy-6,11-dihydro-dibenzo[b,e]oxepin synthesis.

0.199 g (0.82 mmol) of *bis*[2-methoxyphenyl]methanol **6** was dissolved in 40 mL of dry dichloromethane. Under stirring, 76 µL (0.81 mmol, 1 equiv.) of an 85 % solution of HBF_4 in diethylether was added to give a green color that instantaneously changed to a burgundy red color. After 5 minutes the suspension was poured into saturated sodium bicarbonate solution and shaken to obtain a pink dichloromethane solution. After addition of 35 mL of dichloromethane, the layers were separated and the organic layer washed neutral with water. The dichloromethane layer was dried over anhydrous magnesium sulfate and filtered. The solvent of the resulting solution was removed on a rotary evaporator to obtain 0.11 g of a white solid. ^{1}H-NMR showed broad, unresolved resonances characteristic of oligomer formation.[16] No further characterization was attempted. ^{1}H-NMR (360 MHz, CD_2Cl_2): δ 3.5 (broad m), 5.8 (broad m), 6.6 (broad m), 7.1 (broad m).

Attempted oxidation of *tetrakis*[2-methoxyphenyl]ethane 7.

The following reactions returned unchanged starting material according to TLC and ^{1}H-NMR spectroscopy: DDQ in THF, diisopropyl ether or dioxane;[46] TMEDA, n-butylLithium, diethyl ether;[47] lead(IV)oxide in acetic anhydride. The following reactions gave extensive decomposition according to TLC and ^{1}H-NMR spectroscopy: NBS, AIBN in carbon tetrachloride, nitrosonium tetrafluoroborate in acetonitrile, ferrocenium hexafluorophosphate or trityl hexafluorophosphate in dichloromethane.[15]

Bis[2-methoxyphenyl]methanone hydrazone 8.

In a 250 mL round bottom flask 47.50 g (0.196 mol) 2,2'-dimethoxy benzophenone was mixed with 50 mL (1.0 mol) hydrazine monohydrate and 50 mL of 1-butanol. Under stirring, the suspension was heated to reflux for 16 hours. The resulting reaction mixture consisted of two layers. After cooling, the mixture was poured into 200 mL of water. Crystallization was induced by cooling the container with dry ice. The white crystal mass was isolated by vacuum filtration using a Buchner funnel, washed twice with water, and dried in air. After a single washing with hexanes, pure product was obtained (48.03 g, 95.6 %).

mp: 103 °C; IR (neat): 3397, 1597, 1244, 753 cm^{-1}; ^{1}H NMR (360 MHz, CD_2Cl_2): δ 3.55 (s, 3H), 3.85 (s, 3H), 5.51 (broad s, 2H), 6.84 (dd, J = 14.9, 1.0 Hz, 1H), 6.94 (ddd, J = 13.6, 13.6, 2.0 Hz, 1H), 6.97 (ddd, J = 1.6, 13.2, 13.2 Hz, 1H), 7.01 (broad d, J = 15.0, 3.0 Hz, 1H), 7.08 (dd, J = 13.3, 1.0 Hz, 1H), 7.26 (ddd, J = 14.2, 13.8, 3.2 Hz, 1H), 7.36 (ddd, J = 15.0, 13.0, 3.0 Hz, 1H), 7.44 (dd, J = 13.5, 3.2 Hz, 1H); ^{13}C NMR (75.5 MHz, $CDCl_3$) δ 55.8, 55.9, 111.4, 111.9, 120.6, 121.1, 123.9, 128.8, 129.5, 129.6, 130.0, 130.3, 156.1, 157.6, 185.1; HRMS(EI) Calculated for $C_{15}H_{16}O_2N_2$: 256.1212, Found: 256.1208 [94%], 226[23], 225[100], 210[38], 181[22], 91[59]; EA calculated for $C_{15}H_{16}O_2N_2$: C, 70.29; H, 6.29. Found: C, 70.23; H, 6.35.

Tetrakis[2-methoxyphenyl]ethene 9.

In a 1.0 L Erlenmeyer flask, 62.14 g of nickelperoxide[51] (analyzed by sodium thiosulfate titration of iodine formed by oxidation of sodium iodate using starch as an endpoint indicator: 4.1 mmol/g "active oxygen", 12.7 equiv.) was suspended in 500 mL of dry acetonitrile (stored for several days over 4 Å molecular sieves, or refluxed and collected over calcium hydride). Under stirring in the absence of light and moisture, the reaction mixture was cooled to 10 °C (internal) using an ice bath. In a stoppered Erlenmeyer flask, 20 g (20 mmol) bis[2-methoxyphenyl]methanone hydrazone **8** was dissolved in 200 ml of dry acetonitrile and added in one portion to the stirred and cooled nickel peroxide suspension. After one hour stirring at an internal temperature of 8 °C in the absence of light and moisture, the mixture was quickly filtered under suction through a 5 cm layer of dry aluminum oxide (basic, Brockman I). Flask and filter were rinsed with dry acetonitrile until the solvent was nearly colorless. Under stirring, a solution of anhydrous *p*-toluenesulphonic acid (200 mg in 10 mL of toluene) was added dropwise to the collected, deep red, acetonitrile layers until nitrogen gas started to form. Under vigorous evolution of nitrogen gas, the color of the solution turned light yellow while the solution became warm. After stirring the solution for an additional 30 minutes a white precipitate gradually formed. The volume of the resulting suspension was reduced to 10 % of its original volume using a rotary evaporator, and the precipitate collected by filtration using a glass frit Buchner funnel (type C) and washed with a small amount of acetonitrile to obtain the white product (15.47 g, 87 %).

IR (neat): 1580, 1595, 1241, 747, 745 cm^{-1}; ^{1}H NMR (360 MHz, C_6D_6): δ 3.19 (s, 12H), 6.44 (d, J = 8.1 Hz, 4H), 6.71 (broad t, J = 7.4 Hz, 4H), 6.91 (ddd, J = 8.1, 7.3, 2.0 Hz, 4H), 7.53 (broad d, J = 5.5 Hz, 4H); ^{13}C NMR (75.5 MHz, $CDCl_3$) δ 55.3, 111.2, 119.5, 127.2, 131.9, 132.7, 136.3(br), 157.3; HRMS(EI) Calculated for $C_{30}H_{28}O_4$: 452.1988, Found: 452.1989 [100%], HRMS(ES):

calculated for $C_{30}H_{28}O_4Na^+$: 475.1885, Found: 475.1883; EA Calculated for $C_{30}H_{28}O_4$: C, 79.62; H, 6.24, Found: C, 79.62; H, 6.23.

Tetrakis[2-hydroxyphenyl]ethene 10.

A suspension of 0.47 g (1 mmol) of *tetrakis*[2-methoxyphenyl]ethene **9** in 30 mL of dichloromethane (freshly distilled from calcium hydride) was cooled to -65 °C under nitrogen using a dry ice/acetone cooling bath. To this suspension, 0.7 mL (7 mmol) of boron tribromide was added under stirring. After 10 minutes the cooling bath was removed and the red brown solution left to stir overnight. The next day the mixture was carefully poured into a stirred saturated sodium bicarbonate solution. The resulting white precipitate was isolated by vacuum filtration using a Buchner funnel. The water and dichloromethane layers were separated, and the water layer extracted twice with diethyl ether. The dichloromethane was removed using a rotary evaporator and the resulting solid redissolved in diethyl ether. The combined ether layers were washed neutral with water and dried over anhydrous sodium sulfate. After filtration the diethyl ether was removed under reduced pressure using a rotary evaporator. Recrystallization from diethyl ether followed by drying under vacuum gave 0.38 g pure product (90%).

IR (neat): 3308, 1487, 1447, 752 cm^{-1}; ^1H NMR (200 MHz, CD_2Cl_2) δ 5.91 (broad s, 4H), 6.69 (broad d, J = 8.0 Hz, 4H), 6.77 (td, J = 1.0, 7.4 Hz, 4H), 7.04 (ddd, J = 1.8, 7.4, 8.0 Hz, 4H), 7.14 (dd, J = 1.8, 7.4 Hz, 4H); ^{13}C NMR (75.5 Mz, acetone-d_6) δ 115.9, 120.1, 129.0, 129.9, 130.8, 138.9, 154.1; HRMS (EI) Calculated for $C_{26}H_{20}O_4$: 396.1362. Found: 396.1355 [53%], 242[45], 181[28], 135[100], 121[44], 92[21], 91[29], 77[45], 57[20]; EA Calculated for $C_{26}H_{20}O_4$: C, 78.77; H, 5.09. Found: C, 78.72; H, 4.94.

Crystal data for *tetrakis*[2-hydroxyphenyl]ethene·CH_2Cl_2 ($C_{26}H_{22}Cl_2O_4$): crystal dimensions 0.46 x 0.19 x 0.19 mm, triclinic, space group $P\bar{1}$(No. 2) , a = 8.2310(12), b = 9.6048(12), c = 17.243(2) (Å), α = 75.610(10), β = 78.168(10), γ = 64.983(10) (°), V = 1188.7(3), Z = 2, ρ_{calcd} = 1.345 (g cm^{-3}), μ = 2.715 (mm^{-1}). Data collection and refinement conditions: Siemens P4/RA diffractometer using graphite-monochromated Cu Kα radiation (λ[Å] = 1.54178), T = 213 (K), scan mode θ–2θ, 2θ limit 115.0 (°); 3469 measured reflections, 3200 independent reflections, 2116 included in the refinement ($F_o^2 \geq 2\sigma(F_o^2)$), structure solution by direct methods (*SHELXS–86*), refinement by full-matrix least-squares on F^2 (*SHELXL–93*), data correction by Gaussian integration (face-indexed) (transmission max./min. = 0.6613/0.5072), 302 parameters, H atoms in geometrically calculated positions, R_1 = 0.0831 (based on 2116 observed data), wR_2 = 0.2511 (based on all 3198 data), residual electron density 0.505 / –0.355 e Å^{-3}. See appendix A, page 325, for details of the structure solution.

***Tetrakis*[2-methoxy-5-(1,1-dimethylethyl)phenyl]ethene 11.**

Gift of Dr. T.Dzwiniel. The synthesis was accomplished using the diazo coupling method described above.

IR (neat): 2960, 1604, 1500, 1244, 1038 cm^{-1}; ^{1}H NMR (360 MHz, CD_2Cl_2): δ 1.08 (s, 36H), 3.54 (s, 12H), 6.58 (d, J = 8.7 Hz, 4H), 6.96 (dd, J = 8.3, 2.7 Hz, 4H), 7.12 (d, J = 2.4 Hz, 4H); ^{13}C NMR (75.5 MHz, $CDCl_3$) δ 31.4, 33.7, 56.0, 111.0, 123.2, 130.0, 131.8, 138.79(br), 142.0, 155.5; HRMS(EI) Calculated for $C_{46}H_{60}O_4$: 676.4492, Found: 676.4497 [100%], 338[22], 57[45]

Tetrakis[2-methoxy-3-bromo-5-(1,1-dimethylethyl)phenyl]ethene 12.

In 150 mL glacial acetic acid and 20 mL carbon tetrachloride 1.04 g (1.5 mmol) of *tetrakis*[2-methoxy-5-(1,1-dimethylethylphenyl]ethene **11** was suspended.[17] Under stirring, a carbon tetrachloride solution of 21.5 g (135 mmol) bromine in 30 mL of carbon tetrachloride was added. After 23 hours stirring, in a fume hood the suspension was added slowly to a rapidly stirred solution of 28 g sodium bisulfite in 400 mL of water. The resultant white suspension was transferred to a separatory funnel and extracted three times with 200 mL dichloromethane. The combined organic layers were washed several times with water and a saturated sodium bicarbonate solution. After a final washing with water, the dichloromethane layers were dried over anhydrous magnesium sulfate. After filtration, the solvent was removed on a rotary evaporator to obtain 1.31 g of analytically pure product (86 %).

mp: 331 ^{o}C; IR (neat): 2960, 1551, 1474, 1424, 1246, 1013 cm^{-1}; ^{1}H NMR (360 MHz, CD_2Cl_2): δ 1.06 (s, 36H), 3.39 (broad s, 12H), 7.00 (d, J = 2.8 Hz, 4H), 7.31 (d, J = 2.8 Hz, 4H); ^{13}C NMR (75.5 MHz, $CDCl_3$) δ 31.2, 34.2, 60.1, 116.6, 129.3, 129.9, 136.4, 140.0(br), 147.9, 153.0; HRMS(ES) Calculated for $C_{46}H_{56}O_4Br_4Na^+$: 1015.0777, Found: 1015.0781; EA Calculated for $C_{46}H_{56}O_4Br_4$: C, 55.66; H, 5.69, Found: C, 55.75; H, 5.77.

Chiral Shift Reagent Study: a 7.9 mM solution of the ethene compound in CD_2Cl_2 and a 0.02 M solution of Sievers reagent (*tris*[3-(heptafluoropropyl (+)camphorato]europium(III)) in CD_2Cl_2 were prepared. Aliquots (10, 60, 120, 240 and 500 µL)of the shift reagent were added to the ethene NMR solution: no signal doubling in the aromatic region was observed.

Chiral Solvent Study: The ethene compound was dissolved in a minimum amount of CD_2Cl_2 to create a saturated solution, and diluted with ten times it's volume with α(-)pinene. The aromatic region did not show any signal doubling.

***Tetrakis*[2-hydroxy-5-(1,1-dimethylethyl)phenyl]ethene 13.**

Gift of Dr. T. Dzwiniel. The compound was synthesized using the boron tribromide deprotection method.

mp: 294 °C; IR (neat): 3213, 2961, 1609, 1589, 1500, 1236 cm^{-1}; ^1H NMR (360 MHz, acetone-d_6): δ 1.14 (s, 36H), 6.54 (d, J = 8.6 Hz, 4H), 6.91 (dd, J = 2.5, 8.6 Hz, 4H), 7.29 (d, J = 2.5 Hz, 4H) 8.03 (broad s, OH); ^{13}C NMR (75.5 MHz, acetone-d_6) δ 31.8, 34.3, 115.4, 125.3, 128.2, 129.2, 140.4(br), 142.3, 152.0; HRMS(EI) Calculated for $C_{42}H_{52}O_4$: 620.3865, Found: 620.3858 [100%], 57[93].

***Tetrakis*[2-hydroxy-3-bromo-5-(1,1-dimethylethyl)phenyl]ethene 14.**

In a 100 mL round bottom flask equipped with a reflux cooler, a suspension of 0.30 g (0.48 mmol) *tetrakis*[2-hydroxy-5-(1,1-dimethylethyl)phenyl]ethene **13** in 50 mL of glacial acetic acid, 5 mL of dimethylsulfoxide and 15 mL of 48 % (89 mmol) hydrogen bromide solution, was heated to reflux. After 1.5 hours, the reaction mixture was left to cool to room temperature. After addition of water, acetic acid was removed under reduced pressure using a rotary evaporator. The water layer was neutralized using saturated sodium bicarbonate solution and three times extracted with 50 mL of diethyl ether. The combined organic layers were washed with water until the water layer tested neutral, and dried over anhydrous magnesium sulfate. After filtration, the solvent was removed under reduced pressure on a rotary evaporator. Yield of the analytically pure material: 0.34 g (76 %).

mp: 294 ^oC; IR (neat): 3423, 2960, 1572, 1479, 1287, 1240 cm^{-1}; ^1H NMR (360 MHz, CD_2Cl_2): δ 1.14 (s, 36H), 5.99 (broad s, 4H), 7.10 (d, J = 2.5 Hz, 4H), 7.26 (d,J = 2.5 Hz, 4H); ^{13}C NMR (75.5 MHz, CD_2Cl_2) δ 31.3, 34.1, 109.8, 127.2, 127.5, 128.5, 139.3(br), 144.5, 146.9; HRMS(ES) Calculated for $C_{42}H_{48}O_4Br_4Na^+$: 959.0143, Found: 959.0143; MS(EI): 941[9 %], 940[23], 939[34], 938[81], 937[50], 936[100], 935[36], 934[77], 933[9], 932[21], 257[11], 255[13], 58[51], 57[100]; EA Calculated for $C_{42}H_{48}O_4Br_4$: C, 53.87; H, 5.17; Br, 34.13, Found: C, 53.61; H, 5.17; Br, 33.99.

^{13}C-T_1 measurement: in a glovebox under a nitrogen atmosphere (less than 0.1 ppm oxygen) a saturated $CDCl_3$ solution of the ethene compound was prepared, sealed, and removed from the glovebox and subjected to an inversion recovery experiment[52] (variable delay times used: 0.1, 0.2, 0.4, 0.6, 0.8, 1, 2, 4, 8, 10 and 20 seconds). To achieve thermal equilibrium between each pulse sequence a delay of 10 seconds was incorporated. Spectrometer frequency: 126.7 MHz. Both aromatic ^{13}C *ortho* and *para* to the ethene carbon show the same T_1 (approximately 0.3 sec) at room temperature; the suspiciously short relaxation time may be due to oxygen leaking into the NMR tube during the course of the experiment, and would diminish the validity of this experiment.

Crystal data for *tetrakis*[2-hydroxy-3-bromo-5-(1,1-dimethylethyl)phenyl]ethene m-xylene solvate $C_{42}H_{48}Br_4O_4 \cdot C_8H_{10}$: crystal dimensions 0.27 x 0.12 x 0.09 mm, triclinic, space group *P1* (No. 2) , *a* = 8.7405(6), *b* = 11.8117(7), *c* = 13.4435(9) (Å), α = 99.4880(13), β = 105.7655(12), γ = 107.9714(11) (°), *V* =

1222.75(14), $Z = 1$, $\rho_{calcd} = 1.416$ (g cm^{-3}), $\mu = 3.332$ (mm^{-1}). Data collection and refinement conditions: Bruker P4/RA/SMART 1000 CCD diffractometer using graphite-monochromated Mo Kα radiation (λ[Å] = 0.71073), $T = 193$ (K), scan mode θ–2θ, 2θ limit 52.76 (°); 6529 measured reflections, 4960 independent reflections, 3450 included in the refinement ($F_o^2 \geq 2\sigma(F_o^2)$), structure solution by direct methods (*SHELXS–86*), refinement by full-matrix least-squares on F^2 (*SHELXL–93*), data correction by Gaussian integration (face-indexed) (transmission max./min. = 0.7536/0.4665), 302 parameters, H atoms in geometrically calculated positions, $R_1 = 0.0426$ (based on 3450 observed data), $wR_2 = 0.1112$ (based on all 4960 data), residual electron density 0.970/ –0.894 e Å^{-3}. The hydroxy group hydrogens were located from a difference Fourier map, and refined using an idealized C-O-H geometry as a rotating group. The (idealized) O-H distance was 0.84 Å. Details are provided in the appendix, page 331.

2-Hydroxy-2'-methoxybenzophenone 15.

A literature procedure[18] was followed.

Under nitrogen, 9.80 g (40.5 mmol) 2,2'-dimethoxybenzophenone **3** was dissolved in 200 mL of dry dichloromethane. Under stirring, the solution was cooled to -78 °C using an acetone/dryice cooling bath. A boron trichloride solution (81 mL, 1 M in hexanes) was added to give a burgundy red solution. The cooling bath was removed and the progress of the reaction regularly monitored by TLC. After 5 hours and 40 minutes, ice was added to the solution. The resulting yellow solution was carefully neutralized with saturated sodium bicarbonate solution. After separation the organic layer was washed with water, and dried over anhydrous magnesium sulfate. The solvent was removed under reduced pressure using a rotary evaporator to obtain 9.02 g of the crude product, which was used without further purification. According to the recorded ^{1}H-NMR integration, the material obtained contained approximately 97 % of the mono-deprotected, as well as traces of the bis-deprotected and unreacted 2,2'-dimethoxybenzophenone, giving a net yield of the mono-deprotected material of 95 %.

IR (neat): 3024 (br), 1626, 1608, 1486, 1249, 759 cm^{-1}; ^{1}H NMR (360 MHz, $CDCl_3$) δ 3.78 (s, 3H), 6.80(ddd, J = 1.2, 7.0, 7.2 Hz, 1H), 7.05(m, 3H), 7.30(ddd, J = 1.8, 15.0, 17.6 Hz, 2H), 7.48(m, 2H), 12.17 (s, 1H); ^{13}C NMR ($CDCl_3$) δ 202.2, 162.9, 156.6, 136.5, 133.8, 131.9, 128.9, 120.6, 118.7, 118.0, 111.50, 111.47, 55.7; HRMS (EI) Calculated for $C_{14}H_{12}O_3$: 228.0786. Found: 228.0784 [26%], 213[24], 198[21], 197[100], 135[100], 121[39], 108[43], 92[25], 77[33], 65[26].

2-Allyloxy-2'-methoxybenzophenone 16.

A suspension of 0.76 g (19 mmol) of sodium hydride (60 % dispersion in oil, washed free of oil with dry THF) in 150 mL of dry THF was prepared. A solution of 2.12 g (9.3 mmol) of the 2-hydroxy-2'-methoxybenzophenone **15** in 50 mL of dry THF (distilled over sodium benzophenone ketyl) was added slowly to the suspension under a nitrogen atmosphere. The resulting suspension was heated to reflux for 5 hours. To the deep yellow solution, 1.5 mL allyl bromide, dried over calcium chloride and passed through an aluminum-oxide filled column, was added. After keeping the solution at reflux for another 2 hours, all starting material had reacted according to an ^{1}H-NMR spectrum of the reaction mixture. Some water was added after the solution had reached room temperature and the THF removed under reduced pressure using a rotary evaporator. The product was redissolved in 200 mL of hexanes. The organic layer was washed neutral with water and dried over magnesium sulfate. After filtration, the solvent was removed using a rotary evaporator. The crude product was obtained with a yield of 1.89 g. According to the ^{1}H-NMR spectrum, the crude product consisted of traces of dimethoxybenzophenone, diallyloxybenzophenone, and 96 % of the allyloxymethoxybenzophenone, giving a net yield of 73 % for compound **16**.

IR (neat): 2968, 2895, 1639, 1594, 1485, 1457, 1300, 1253 cm^{-1}; ^{1}H NMR (360 MHz, $CDCl_3$) δ 3.65 (s, 3H), 4.37 (m, 2H), 5.00 (m, 2H), 5.63 (m, 1H), 6.87 (d, J = 0.69 Hz, 1H), 6.89 (d, J = 0.69 Hz, 1H), 6.99 (td, J = 0.9, 7.5 Hz, 1H), 7.02 (td, J = 0.9, 7.5 Hz, 1H), 7.42 (m, 2H), 7.52 (dd, J = 7.8, 1.9 Hz, 1H), 7.58 (dd, J = 7.8, 1.9 Hz, 1H); ^{13}C NMR (acetone-d_6) δ 195.3, 158.7, 157.6, 132.99, 132.89, 132.87, 131.2, 131.0, 130.5, 130.3, 121.0, 120.7, 116.8, 112.9, 112.0, 69.5, 55.9; HRMS (EI) Calculated for $C_{17}H_{16}O_3$: 268.1100. Found: 268.1099 [83%], 253[16], 242[11], 238[27], 237[88], 227[17], 212[19], 197[27], 196[29], 184[19], 168[16], 148[77], 135[100], 121[62], 92[31], 77[45].

Attempted conversion of 2-allyloxy-2'-methoxybenzophenone 16 to the hydrazone.

In a 25 mL round bottom flask equipped with a reflux condenser with calcium chloride guard tube, 1.32 g (4.9 mmol) of 2-allyloxy-2'-methoxybenzophenone **16** and 1 mL (32 mmol) anhydrous hydrazine were dissolved in 2 mL 1-butanol under stirring. After heating the solution to reflux overnight, the solution was poured into 200 mL of water and the water layer three times extracted with 100 mL diethyl ether. The combined ether layers were washed neutral with water, and dried over anhydrous magnesium sulfate. After removal of the solvent on a rotary evaporator a syrup resulted, that according to ^{1}H-NMR spectroscopy did not contain starting material (the O-CH_2 allyl signal at 4.37 ppm and the methoxy signal at 3.65 ppm were absent). Instead four methoxy signals at 3.57, 3.58, 3.85 and 3.87 ppm, and two sets of O-CH_2 allyl signals at 4.23 and 4.55 ppm were present. Instead of the expected signal intensity ratio of 2/3 (OCH_2/OCH_3) a ratio of 1.1/3 was found. A similar reduction of the OCH_2 allyl signal indicating the loss of an allyl group was observed for the aromatic H/OCH_2 allyl signal ratio which should have been 8/2, instead of the found ratio of 8/0.93.

2.5 Notes and References.

1. von Itter, F.A.; Vögtle, F.; Weber, G.; Sheldrick, G.M. *Z. Naturforsch.* **1983**, *38b*, 262-264. von Itter, F.A.; Vögtle, F. *Ber. Dtsch. Chem. Ges.* **1985**, *118*, 2300-2313.
2. Lai, Y.H.; *Aust. J. Chem.* **1991**, *44*, 1151-1155. Tomioka, H.; Nakanishi, K.; Izawa, I. *J. Chem. Soc., Perkin Trans.1* **1991**, 465-470. Tomioka, H.; Kimoto, K.; Murata, H.; Izawa, I.; *J. Chem. Soc., Perkin Trans.1* **1991**, 471-477. Tomioka, H.; Okada, H.; Watanabe, T.; Hirai, K.; *Angew. Chem., Intl. Ed. Engl.* **1994**, *33*, 873-875.
3. Rodd's Chemistry of Carbon Compounds, Coffey, S.; ed. Elsevier Scientific Publishing: New York, 1974, Volume 3 Part F, 301-304.
4. Zimmerman, H.E.; Paskovich D.H. *J. Am. Chem. Soc.* **1964**, *86*, 2149-2160.
5. Fürstner, A.; Seidel, G.; Kopiske, C.; Krüger, C.; Mynott, R. *Liebigs Ann. Chem.* **1996**, 655-662. Barbosa, F.; Peron, V.; Gescheidt, G.; Fürstner, A. *J. Org. Chem.* **1998**, *63*, 8806-8814.
6. Merz, A.; Karl, A.; Futterer, T.; Stacherdinger, N.; Schneider, O.; Lex, J.; Luboch, E.; Biernat, F. *Liebigs Ann. Chem.* **1994**, 1199-1209. Futterer, T.; Merz, A.; Lex, J. *Angew. Chem., Int. Ed. Engl.* **1997**, *36*, 611-613. Merz., A.; Futterer, T.; Lex, J.; Inerowicz, H. *Angew. Chem., Int. Ed. Engl.* **1997**, *36*, 278-280.
7. Tyrlik, S.; Wolochowicz, I. *Bull. Soc. Chim. Fr.* **1973**, 2147. Mukaiyama, T.; Sato, T.; Hanna, J. *Chem. Lett.* **1973** , 1041. McMurry, J.E.; Fleming, M.P. *J. Am. Chem. Soc.* **1974**, *96*, 4708-4709. For the mechanistic aspects of the reaction see: Aleandri, L.E.; Bogdanovic, B.; Gaidies, A.; Jones, D.J.; Liao, S.; Michalowicz, A.; Roziere, J.; Schott, A. *J. Organomet. Chem.* **1993**, *459*, 87-93. Fürstner, A.; Bogdanovic, B.

Angew. Chem., Int. Ed. Engl. **1996**, *35*, 2442-2469. Eisch, J.J.; Shi, X.; Alila, J.R.; Thiele, S. *Chem. Ber./Recueil* **1997**, *130*, 1175-1187. Ephritikhine, M. *J. Chem. Soc., Chem. Commun.* **1998**, 2549-2554.

8. Tschitschibabin, A.E.; Magidson, O.I. *J. Prakt. Chem.* **1914**, *90*, 168-177. Magidson, O.I. *Ber. Dtsch. Chem. Ges.* **1925**, *58*, 433-442. Bergmann, F.; Israelashvili, S. *J. Am. Chem. Soc.* **1946**, *68*, 354-356. Franzen, V.; Joschek, H.I. *Liebigs Ann. Chem.* **1960**, *633*, 7-13.
9. Ali, S.M.; Findlay, J.W.A.; Turner, A.B. *J. Chem. Soc., Perkin Trans.1* **1976**, 407-410.
10. Roberts, J.D.; Watanabe, W. *J. Am. Chem. Soc.* **1950**, *72*, 4869-4871. Whitlock, H.W. *J. Am. Chem. Soc.* **1962**, *84*, 2807-2811. Bethell, D.; Callister, J.D. *J. Chem. Soc.* **1963**, 3801-3815. Bakke, J.M.; Bethell, D.; Parker, V.D. *Acta Chem. Scan.* **1987**, *B 41*, 253-256.
11. Sharma, V.; Bachand, B.; Simard, M.; Wuest, J.D. *J. Org. Chem.* **1994**, *59*, 7785-7792.
12. Newkome, G.R.; Roper, J.M. *J. Org. Chem.* **1979**, *44*, 502-505. Daly, J.J.; Sanz, F.; Sneeden, R.P.A.; Zeiss, H.H. *J. Chem. Soc., Perkin 2* **1972**, 1614-1617. Bottino, F.A.; Finocchiaro, P.; Libertini, E.; Reale A.; Recca, A. *J. Chem. Soc., Perkin 2* **1982**, 77-81. Willem, R.; Pepermans, H.; Hallenga, K.; Gielen, M.; Dams, R.; Geise, H.J. *J. Org. Chem.* **1983**, *48*, 1890-1898.
13. Finnochiaro, P.; Gust, D.; Hounshell, W.D.; Hummel, J.P.; Maravinga, P.; Mislow, K. *J. Am. Chem. Soc.* **1976**, *98*, 4945-4952.
14. Shlögl, K.; Weissensteiner, W. *Synthesis* **1982**, 50-52. Shlögl, K.; Weissensteiner, W.; Widhalm, M. *J. Org. Chem.* **1982**, *47*, 5025-5027.
15. Okamoto, A.; Snow, M.S.; Arnold, D.R. *Tetrahedron* **1986**, *42*, 6175-6187. Popielarz, R.; Arnold, D.R. *J. Am. Chem. Soc.* **1990**, *112*, 3068-

3082. Suzuki, H.; Mori, T. *J. Chem. Soc., Perkin Trans. 2* **1997**, 1265-1273.

16. Balfe, M.P.; Kenyon, J.; Thain, E.M. *J. Chem. Soc.* **1952**, 790-796. Wada, M.; Konishi, H.; Kirishima, K.; Takeuchi, H.; Natsume, S.; Erabi, T. *Bull. Chem. Soc. Jpn.* **1997**, *70*, 2737-2741. Wada, M.; Konishi, H.; Kai, T.; Takeuchi, H.; Natsume, S.; Erabi, T. *Bull. Chem. Soc. Jpn.* **1998**, *71*, 1667-1672.
17. Majetich, G.; Hicks, R.; Reister, S. *J. Org. Chem.* **1997**, *62*, 4321-4326.
18. Dean, F.M.; Goodchild, J.; Houghton, L.E.; Martin, J.A.; Morton, R.B.; Parton, B.; Price, A.W.; Somvichien, N. *Tet. Letters* **1966**, *35*, 4153-4159.
19. Shimizu, T.; Hayashi, Y.; Miki, M.; Teramura, K. *J. Org. Chem.* **1987**, *52*, 2277-2285. Bishop, J.E.; Flaxman, K.A.; Orlek, B.S.; Sammes, P.G., Weller, D.J. *J. Chem. Soc., Perkin Trans. 1* **1995**, 2551-2459.
20. Notice however, that the sterically most hindered *tetrakis*(pentamethylphenyl)ethene prepared to date shows a propeller conformation, see ref. 25.
21. Cairns, T.; Eglinton, G. *Nature* **1962**, *196*, 535-537. Cairns and Eglinton first proposed the circular array of hydrogen bonds for a calix[4]arene, not Gutsche as stated by Rudkevich in ref. 30.
22. Hunter, C.A.; Sanders, J.K.M. *J. Am. Chem. Soc.* **1990**, *112*, 5525-5534.
23. Hoekstra, A.; Vos, A. *Acta Cryst.* **1975**, *B 31*, 1716-1729. Rathore, R.; Lindeman, S.V.; Kumar, A.S.; Kochi, J.K. *J. Am. Chem. Soc.* **1998**, *120*, 6931-6939.
24. Kuchitsu, K.; Fukuyama, T.; Morino, Y. *J. Mol. Struct.* **1967-68**, *1*, 463-479. Smith, W.B. *Org. Magn. Res.* **1981**, *15*, 317-318.
25. Rappoport, Z.; Biali, S.E. *Acc. Chem. Res.* **1997**, *30*, 307-314.

26. The van der Waals volumes for the hydroxy group and methoxy group are 8.04 and 16.87 cm^3/mole, respectively. This does not convey the steric effect accurately because of the mobility of the methyl group. For volume calculations (and the associated inherent difficulties) see Bondi, A. *J. Phys. Chem.* **1964**, *68*, 441-451. Ben-Amotz, D.; Willis, K.G. *J.Phys. Chem.* **1993**, *97*, 7736-7742.

27. Boere, R.T.; Kidd, R.G. *Ann. Rep. NMR Spec.* **1982**, *13*, 319-385. Shaw, D., Fourier Transform NMR Spectroscopy; Elsevier Science: Amsterdam, 1984, Chapter 9.

28. Hayes, K.S.; Hounshell, W.D.; Finocchiaro, P.; Mislow, K. *J. Am. Chem. Soc.* **1977**, *99*, 4152-4153. Offermann, W.; Mannschreck, A. *Tetrahedron Lett.* **1982**, *22*, 3227-3230.

29. Okada, Y.; Nishimura, J. *J. Incl. Phenomena*, **1994**, *19*, 41-53. Yoshimi, Y.; Maeda, H.; Sugimoto, A.; Mizuno, K. *Tet. Letters* **2001**, *42*, 2341-2343.

30. Araki, K.; Iwamoto, K.; Shinkai, S.; Matsuda, T. *Bull. Chem. Soc. Jpn.* **1990**, *63*, 3480-3485. See also: Böhmer, V.; Goldmann, H.; Vogt, W.; Paulus, E.F.; Tobiason, F.L.; Thielman, M.J. *J. Chem. Soc., Perkin Trans. 2*, **1990**, 1769-1775. Grootenhuis, P.D.J.; Kollman, P.A.; Groenen, L.C.; Reinhoudt, D.N.; van Hummel, G.J.; Ugozzoli, F.; Andreetti, G.D. *J. Am. Chem. Soc.* **1990**, *112*, 4165-4176. Rudkevich, D.M. *Chem. Eur. J.* **2000**, *6*, 2679-2686.

31. Regimbald-Krnel, M.; Wentrup, C. *J. Org. Chem.* **1998**, *63*, 8417-8423.

32. Nyburg, S.C.; Faerman, C.H. *J. Mol. Structure* **1986**, *140*, 347-352.

33. Makriyannis, A.; Fesik, S. *J. Am. Chem. Soc.* **1982**, *104*, 6462-6463. Schuster, I.I.; Parvez, M.; Freyer, A.J. *J. Org. Chem.* **1988**, *53*, 5819-5825. Schaefer, T.; Penner, G.H. *Can. J. Chem.* **1988**, *66*, 1635-1640.

Schefer, T.; Sebastian, R.; Lemire, A.; Penner, G.H. *Can. J. Chem.* **1990**, *68*, 1393-1398. Notice that the crystal structure of *tetrakis*[4-methoxy phenyl]ethene shows the methoxy groups in the plane of the phenyl ring, see: Baenziger, N.C.; Buckles, R.E.; Simpson, T.D. *J. Am. Chem. Soc.* **1967**, *89*, 3405-3408. See also appendix page 337

34. Jin, P.; Wildman, T.A. *J. Phys. Chem.* **1991**, *95*, 20-2542.

35. Jost, R.; Sommer, J. *J. Chem. Soc., Perkin Trans. 2* **1983**, 927-932. For a recent investigation on correlated rotations in benzophenones see: Grilli, S.; Lunazzi, I.; Mazzanti, A.; Casarini, D.; Femoni, C. *J. Org. Chem.* **2001**, *66*, 488-495

36. Linker, T.; Schmittel, M. Radikale und Radikalionen in der Organischen Synthese; Wiley-VCH: Weinheim, Germany 1998.

37. As an orbital is defined as the space where there is a certain probability of finding an electron, a noncontradicting description would be to speak of an electron deficient orbital, suggesting a lower, *nonzero*, probability of finding an electron in that orbital.

38. Glyde, E.; Taylor, R. *J. Chem. Soc., Perkin 2* **1977**, 1537-1544.

39. Nenitzescu, C.D.; pages 463-521 in Carbonium Ions, editors G.A. Olah, P. von R. Schleyer; Interscience: New York, 1970, volume 2. Olah, G.A.; Svoboda, J.J. *J. Am. Chem. Soc.* **1973**, *95*, 3794-3796.

40. Woodward, R.B.; Sondheimer, F.; Mazur, Y. *J. Am. Chem. Soc.* **1958**, *80*, 6693. Djerassi, C.; Halpern, O.; Pettit, G.R.; Thomas, G.H. *J. Org. Chem.* **1959**, *24*, 1. Pettit, G.R.; Boyer, W.J. *J. Org. Chem.* **1960**, *25*, 84. Shaw, P.E. *J. Org. Chem.* **1966**, *31*, 2116-2119. Wicha, J.; Caspi, E. *J. Org. Chem.* **1973**, *38*, 1280. Acklin, G.; Graf, W. *Helv. Chim. Acta* **1980**, *63*, 2342-2357. Deslongchamps, P.; Rowan, D.D.; Pothier, N. *Heterocycles* **1981**, *15*, 1093-1096. Deslongchamps, P.; Rowan, D.D.; Pothier, N. *Can.*

J. Chem. **1981**, *59*, 2787-2791. Seo, S.; Uomori, A.; Takeda, K. *J. Org. Chem.* **1986**, *51*, 3823-3827.

41. A similar 1,5-hydride shift, followed by a nucleophilic attack of an aryl ring on the resulting cation has been previously proposed, see: Cohen, T.; Moran, R.M.; Sowinski, G. *J. Org. Chem.* **1961**, *26*, 1-5. In relation to these observations, see also the Menger postulate: Menger, F.M. *Acc. Chem. Res.* **1985**, *18*, 128-134.

42. Ceraulo, L.; Natoli, M.C.; Agozzino, P.; Ferrugia, M.; Lamartina, L. *Org. Mass Spectrom.* **1991**, *26*, 857-861. Natoli, M.C.; Ceraulo, L.; Ferrugia, M.; Lamartina, L. *Eur. Mass Spectrom.* **1999**, *5*, 363-368. Bongiorno, D.; Ceraulo, L.; Lamartina, L.; Natoli, M.C. *Rapid Comm. Mass Spectrom.* **2000**, *14*, 203-206.

43. Russell, D.H.; Freiser, B.S.; McBay, E.H.; Canada, D.C. *Org. Mass Spectrom.* **1983**, *18*, 474-485.

44. In an infinite dilution experiment, the diarylmethanol would be added slowly to an acid solution. As intermolecular reactions are second order in diarylmethanol concentration, while intramolecular reactions are first order in diarylmethanol concentration, the intramolecular reaction is preferred over the intermolecular reaction when the reaction is diluted. This is the so-called Ruggli dilution principle. See: Ruggli, P. *Liebigs Ann. Chem.* **1912**, *392*, 92-100. Rossa, L. Vögtle, F. *Topics in Current Chemistry* **1983**, *113*, 1-86.

45. Still, W.C.; Kahn, M.; Mitra, A. *J. Org. Chem.* **1978**, *43*, 2923-2925.

46. Ali, S.M.; Findlay, J.W.A.; Turner, A.B. *J. Chem. Soc., Perkin 1* **1976**, 407-410.

47. Harvey, R.G.; Nazareno, L.; Cho, H. *J. Am. Chem. Soc.* **1973**, *95*, 2376-2378. Harvey, R.G.; Cho, H. *J. Am. Chem. Soc.* **1974**, *96*, 2434-2441.

48. Rusell, G.A.; Bemis, A.G.; *J. Am. Chem. Soc.* **1966**, *88*, 5491-5497. Pines, H.; Stalick, W.M., Base-Catalyzed Reactions of Hydrocarbons and Related Compounds; Academic Press: New York, 1977, 508-543.

49. Walling, C.; Jacknow, B.B. *J. Am. Chem. Soc.* **1960**, *82*, 6108-6112.

50. Hock, H.; Ernst, F. *Ber. Dtsch. Chem. Ges.* **1959**, *92*, 2716-2723. House, W.T.; Orchin, M. *J. Am. Chem. Soc.* **1960**, *82*, 639-642.

51. Nakagawa, K.; Konaka, R.; Nakata, T. *J. Org. Chem.* **1962**, *27*, 1597-1601.

52. Freeman, R. A Handbook of Nuclear Magnetic Resonance; Wiley: New York, 1988.

53. Suffert, J. *J. Org. Chem.* **1989**, *54*, 509-510.

54. M. Fujita, Ph.D. Thesis, Department of Chemistry, University of Alberta, Edmonton, Fall 2001.

3. Coordination studies of *tetrakis*[2-hydroxyphenyl]ethene with alkylaluminum compounds

3.1 Introduction.

Ligand systems containing multiple Lewis basic sites are widely used in applications ranging from molecular recognition to catalysis.[1] Similar applications could be envisioned for an organized set of Lewis acidic sites.[2]

For instance in metallocene-based Ziegler-Natta chemistry Lewis acidic complexes are used to remove chloride or alkyl groups from the metallocene yielding cationic catalysts for olefin polymerization (see Chapter 1, sections 1.4.2, page 25 and 1.4.3, page 29). Ion-pair separation is one of the elements determining the activity of the catalytic species; the weaker the ion pair interaction the better the catalytic activity.[3] Cocatalysts containing an organized set of multiple Lewis acidic sites might be able to minimize the ion-pair interactions. In spite of the potential of molecules containing multiple Lewis acidic sites suitable for anion and Lewis base complexation, only a few examples of well defined multinuclear Lewis acidic complexes are known.[4]

In Chapter 2 the synthesis of a preorganized tetraphenoxide ligand was described. As phenols react readily with alkylaluminum derivatives to give organoaluminum phenoxides,[5] *tetrakis*[2-hydroxyphenyl]ethene might yield a molecule containing an organized set of multiple Lewis acids, and provide information on the coordination behaviour of the synthesized tetradentate ligand. In addition such a class of compounds might show potential as an active cocatalyst[6] in ethene polymerizations, and therefore attracted our attention.

3.2 Results.

The reaction of *tetrakis*[2-hydroxyphenyl]ethene in a nonpolar solvent with an excess of triethylaluminum yields a white powder after repeated washing of the sparingly soluble solid using pentane (eq. 3.1) to remove excess triethylaluminum.

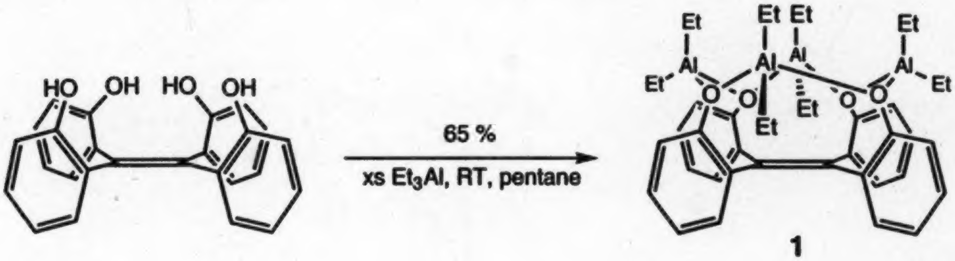
HO
OH
HO
OH
65 %
xs Et_3Al, RT, pentane
Et
Et Et
Et
Al
Al
Al
Al
Et
Et
O
O
Et
Et
O
O

1

eq. 3.1

The so obtained moderately air and water sensitive compound **1** is readily soluble in toluene, benzene, and dichloromethane. The ^{1}H-NMR spectrum of compound **1** in CD_2Cl_2 shows three multiplets in the aromatic region at 7.31 (4H), 7.06 (8H) and 6.94 (4H) ppm. In an NOE experiment, saturation of the aromatic proton at 6.94 ppm shows an NOE effect for the ethyl groups, and is assigned to the proton *ortho* to the phenoxo group (H_1 in Figure 3.1).

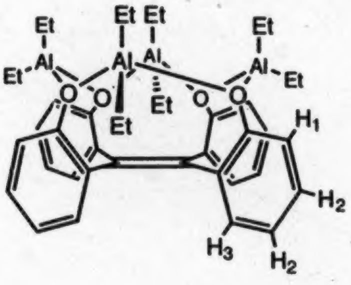
Et
Et Et
Et
Al
Al
Al
Al
Et
Et
O
O
Et
Et
O
O
H_1
H_2
H_3
H_2

H_1 : 6.94 ppm
H_2 : 7.06 ppm
H_3 : 7.31 ppm

Figure 3.1

Saturation of the aromatic protons at 7.31 ppm did not show a substantial NOE effect for the aluminum bound ethyl groups. This aromatic signal is therefore assigned to the proton *ortho* to the double bond (H_3 in Figure 3.1, page 127).

In addition to the aromatic signals, four triplets (each 6H) at 1.22, 1.14, 0.82 and 0.28 ppm as well as four quartets (each 4H) at 0.48, 0.38, -0.76 and -1.37 ppm are present. A homonuclear decoupling experiment established the following connectivity of the aluminum-bound ethyl groups: -1.37 (CH_2) $\leftrightarrow$ 0.28 (CH_3), -0.76 (CH_2) $\leftrightarrow$ 0.82 (CH_3), 0.38 (CH_2) $\leftrightarrow$ 1.14 (CH_3) and 0.48 (CH_2) $\leftrightarrow$ 1.22 (CH_3) ppm. In order to further assign the ^{1}H-NMR spectrum, an NOE experiment was executed, the results of which are shown in Table 3.1 (page 129), and discussed in section 3.3.5 (page 155). According to the integration of aromatic and ethyl signals, one ethene framework combines four diethylaluminum groups. This does not exclude the possibility of intermolecular aggregation, although mass spectrometry indicates the presence of a monomeric species under high vacuum conditions. The ^{1}H-NMR spectrum of compound **1** does not show any change over the temperature range of -80 to + 100 °C, indicating the presence of a highly symmetric and stable species.

Crystals suitable for an X-ray diffraction experiment were obtained by recrystallizing compound **1** from toluene. The crystal structure of compound **1** is shown in Figure 3.3 (page 136). Crystallographic details are provided in the experimental section and in the appendix, page 345. The obvious analogy of compound **1** with a crown ether encouraged experiments to determine its value as a cocatalyst in metallocene based polyethylene synthesis. Several polymerization runs using this compound as a cocatalyst and dichloro[*rac*-ethylenebis(indenyl)]zirconium(IV)[7] as a precatalyst were performed: no catalytic activity was observed.

In order to obtain an indication of the Lewis acidity of compound **1**, both an ^{1}H-NMR titration[8] using THF (Table 3.2, Figure 3.2, page 130, 131) as well as the crotonaldehyde complexation method of Childs[8] were used (Table 3.3, Figure 3.2, page 130, 131).

Table 3.1: Nuclear Overhauser effect (in %) observed on saturating specific ^{1}H-NMR signals of compound **1**.

Observed Signal (ppm)	Saturated Signal (ppm)			
	7.31	6.94	-0.76	-1.37
7.31 (4H,m)	100	-5.4	0.7	1.5
7.06 (8H,m)	-12.9	-88.5	0.6	1.6
6.94 (4H,m)	-7.9	100	11.2	4.4
1.22 (6H,t)	2.1	1.5	1.8	0.9
1.14 (6H,t)	-0.7	1.8	-0.3	2.5
0.82 (6H,t)	0.1	6.4	7.5	0.5
0.28 (6H,t)	-2.0	4.2	-1.9	8.6
0.48 (4H,q)	1.2	0.7	-0.2	0.6
0.38 (4H,q)	0.3	0.9	-0.3	1.3
-0.76 (4H,q)	0.2	4.6	100	-0.7
-1.37 (4H,q)	-0.4	2.4	-2.4	100

Both the absence of any chemical shift difference $\Delta\delta$ (Table 3.3, page 130) for different ligand **1**/crotonaldehyde ratios, and the negligble compound **1** induced chemical shift variation of THF and the crotonaldehyde H_3 are a clear indication that compound **1** has hardly any Lewis acidity.

Table 3.2: THF titration[8] of a 0.02 M solution of compound **1** in toluene-d_8 at room temperature.

THF/ligand ratio	THF Chemical shift δ in ppm (H_a Fig. 3.2)	Δ Chemical Shift (δ complex- δ free THF)
Free THF	3.555	
0.165	3.539	-0.016
0.330	3.546	-0.009
0.417	3.548	-0.007
0.529	3.549	-0.006
0.711	3.550	-0.005
6.98	3.550	-0.005

Table 3.3: Crotonaldehyde complexation[8] of compound **1** compared to other Lewis acids, using the chemical shift difference Δδ of the protons of complexed and free crotonaldehyde.

Observed	Ratio Lewis acid / Crotonaldehyde					
proton	1/0.53[1]	1/1.4[1]	1 / 1[2]			
(Fig. 3.2)	Comp. 1	Comp. 1	$AlCl_3$	$[EtAlCl_2]_2$	$[Et_2AlCl]_2$	$[Et_3Al]_2$
H_1	-0.015	-0.015	-0.20	-0.20	-0.15	-0.34
H_3	0.013	0.013	1.23	1.25	0.91	0.63
H_2	0.010	0.005	0.76	0.77	0.55	0.42
H_4	0.007	0.004	0.47	0.47	0.30	0.23

1] 0.03 M, Room temperature, dichloromethane, 2] literature values, 0.3 M, -60° C, dichloromethane. Δδ = positive for a downfield shift on complexation of crotonaldehyde.

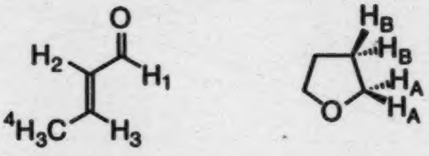

Figure 3.2

This is confirmed by the absence of a reaction between compound **1** and crotonaldehyde at room temperature: ^{1}H-NMR spectroscopy on the aluminum model compounds in Table 3.3 was done at -60 °C because of interfering reactions.[8]

When compound **1** is dissolved in acetonitrile-d_3, a white precipitate forms within minutes, from which crystals of compound **2** start to grow at room temperature (eq. 3.2). The crystals obtained from the acetonitrile-d_3 suspension were of sufficient quality to be used in an X-ray diffraction experiment, allowing the determination of the crystal structure of compound **2**. The structure shows two highly distorted tetraphenylethene ligands encapsulating two pentacoordinated and two tetracoordinated aluminum atoms in between the two ligands (Figure 3.4, page 147).

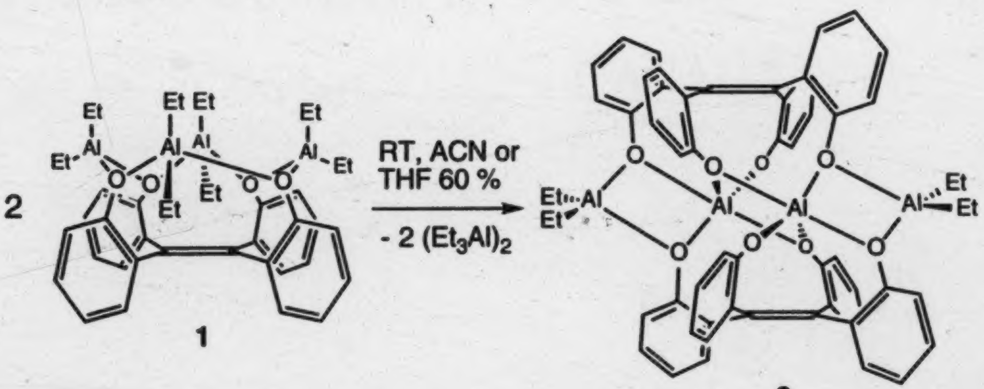

eq. 3.2

The ^{1}H-NMR spectrum of the supernatant contains weak broad aromatic signals and strong signals characteristic for triethylaluminum at -0.32 ppm (2H, q) and 0.96 ppm (3H, t). A similar reaction takes place using THF-d_8 as a solvent, except for the absence of a precipitate. By keeping the initial temperature of the solution low, signal changes can be slowed down sufficiently to follow the reaction.

The crown compound **1**, at -50 °C in THF-d_8, shows a ^{1}H-NMR spectrum that contains a broad quartet at -0.14 ppm (16 H), and a triplet at 0.99 ppm (24 H). The aromatic region is characteristic of a tetraarylethene compound consisting of two broad triplets (6.61, 6.22 ppm) and two broad doublets (7.13, 6.34 ppm).

In this spectrum, the disproportionation products are already visible, presumably formed during the time between mixing, transfer out of the glovebox, and cooling of the solution. New signals are present in the aromatic region and at 0.12 ppm (quartet). The signal for the triethylaluminum methylene is visible as a small quartet at -0.21 ppm.

When this sample is brought to room temperature these signals increase at the expense of the signals at -0.14 and 0.99 ppm. At the same time small broad signals are present at 7.6, 6.5, 1.1 and 0.1 ppm, and become more clearly visible when a sample of a fresh acetonitrile-d_3 reaction mixture of compound **1** is dissolved in THF-d_8.

After 1 hour 30 minutes at room temperature the disproportionation in THF-d_8 is complete: the small broad signals have disappeared and no starting material remains. A precipitate is absent. The final ^{1}H-NMR spectrum consists of a mixture of triethylaluminum, as identified by spiking the solution with triethylaluminum and a new compound with an ethyl group/aryl group ratio of 1/2 according to the integral: a total of 6 ethyl groups have been lost, which appear in the triethylaluminum integral. The aromatic region has become very complicated, showing at least 11 signals in a range from 7.49 to 6.24 ppm.

The new compound that is formed is identical with the crystals isolated from the acetonitrile-d_3 suspension. This is proven by dissolving in THF-d_8 a sample of the crystals obtained from the disproportionation in acetonitrile-d_3. The resulting ^{1}H-NMR spectrum is identical with the spectrum obtained from the disproportionation of compound **1** in THF-d_8, except for the absence of triethylaluminum signals. In addition, placing a sample of the disproportionation product in THF under high vacuum conditions for 5 days before dissolving the sample in CD_2Cl_2 results in a ^{1}H-NMR spectrum that is identical with the spectrum of the compound obtained from the disproportionation in acetonitrile-d_3.

However, the ^{1}H-NMR spectra obtained for compound **2** are solvent dependent: the spectra recorded using THF-d_8 are different from the spectra obtained using CD_2Cl_2 as a solvent. Whereas the THF spectra only show a triplet and a quartet for the aluminum bound ethyl groups, the use of noncoordinating CD_2Cl_2 gives rise to second order multiplets at 0.32 (4H), -1.14 (2H) and -1.34 (2H) ppm and two triplets at 0.97 (6H) and -0.02 (6H) ppm. A homonuclear decoupling experiment established the following connectivity: -1.14 (2H) ↔ -0.02 (6H) ppm, -1.34 (2H) ↔ -0.02 (6H) ppm and 0.32 (4H) ↔ 0.97 (6H) ppm. The presence of an ABX_3 spin system formed by two diastereotopic CH_2 protons at -1.14 and -1.34 ppm and the methyl group at -0.02 ppm, and the presence of an $AA'X_3$ spin system for the other aluminum bound ethyl group (AA' at 0.32 ppm, X_3 at 0.97 ppm) indicates the presence of a nonsymmetric environment for both aluminum bound ethyl groups. This is confirmed by the crystal structure of compound **2** (vide infra).

With the expectation of finding other crown-like compounds, the reactions of *tetrakis*[2-hydroxyphenyl]ethene with trimethylaluminum (eq. 3.3) and diethylaluminum chloride (eq. 3.4) were also briefly studied.

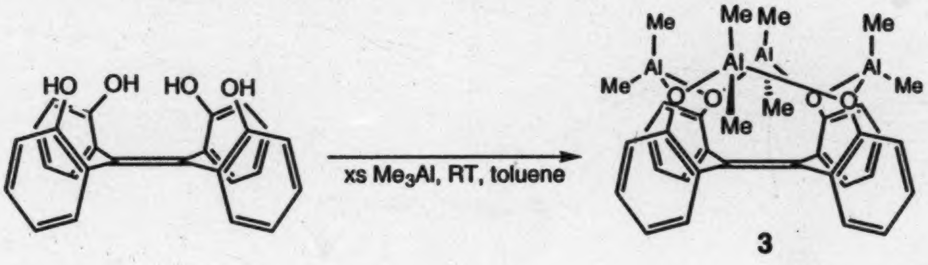

eq. 3.3

Although the analytical data for the compound obtained from the reaction of *tetrakis*[2-hydroxyphenyl]ethene with trimethylaluminum were unsatisfactory because of the low solubility of the obtained material, there are indications that a crown-like compound is formed. Compound **3** shows four methyl groups in the ^{1}H-NMR spectrum at -1.94, -1.32, -0.40 and -0.26 ppm, reminiscent of the four methylene groups at -1.37, -0.76, 0.38 and 0.48 ppm observed for compound **1**.

In addition, although the M^+ ion at m/z 620 is not observed, the $M^+ - CH_3$ [605], $M^+ - CH_3 - AlMe_3$ [533], and $M^+ - CH_3 - 2AlMe_3$ [461] are observed, providing further indirect evidence for the presence of Compound **3**.

The reaction of *tetrakis*[2-hydroxyphenyl]ethene with an excess of diethylaluminum chloride gave product(s) that resisted all initial attempts to recrystallize the obtained material. Crystals suitable for an X-ray diffraction experiment were finally obtained by adding THF to a toluene solution of the reaction products (eq. 3.4 page 135). The crystal structure of the product, compound **4**, is shown in Figure 3.5, page 152.

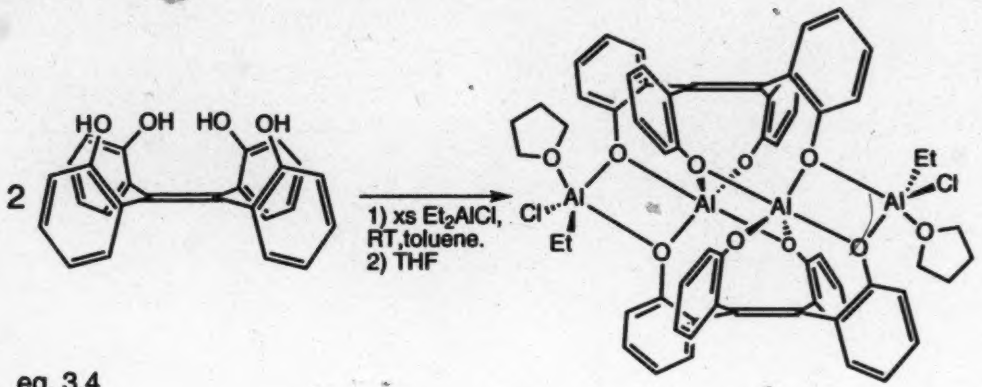

eq. 3.4

4

3.3 Discussion.

3.3.1 The crystal structure of compound 1.

Compound **1** shows in the crystal structure two crystallographically independent molecules of a crown-like eight-membered heterocyclic structure of alternating three coordinate oxygen and four coordinate aluminum atoms on top of the I_4 isomer of the ionized *tetrakis*[2-hydroxyphenyl]ethene (Figure 3.3, page 136).[9] A summary of bond distances and bond angles of the two crystallographically independent molecules in the asymmetric unit is given in the appendix on page 345.

The observed Al-O bond lengths, 1.883(4)-1.891(4) Å are within the range of bond lengths found for other aluminum alkoxides and phenoxides [1.736-2.02 Å].[10,11] The C-O bond distance 1.417(6)-1.433(7) Å is unexceptional [1.403-1.443 Å], as is the Al-C bond length 1.934(7)-1.963(6) Å, which is within the range expected for terminal Al-C bonds [1.946-1.994 Å].[11]

The sum of the angles at each of the oxygen-atoms is 360°, corresponding to a trigonal planar environment at oxygen.

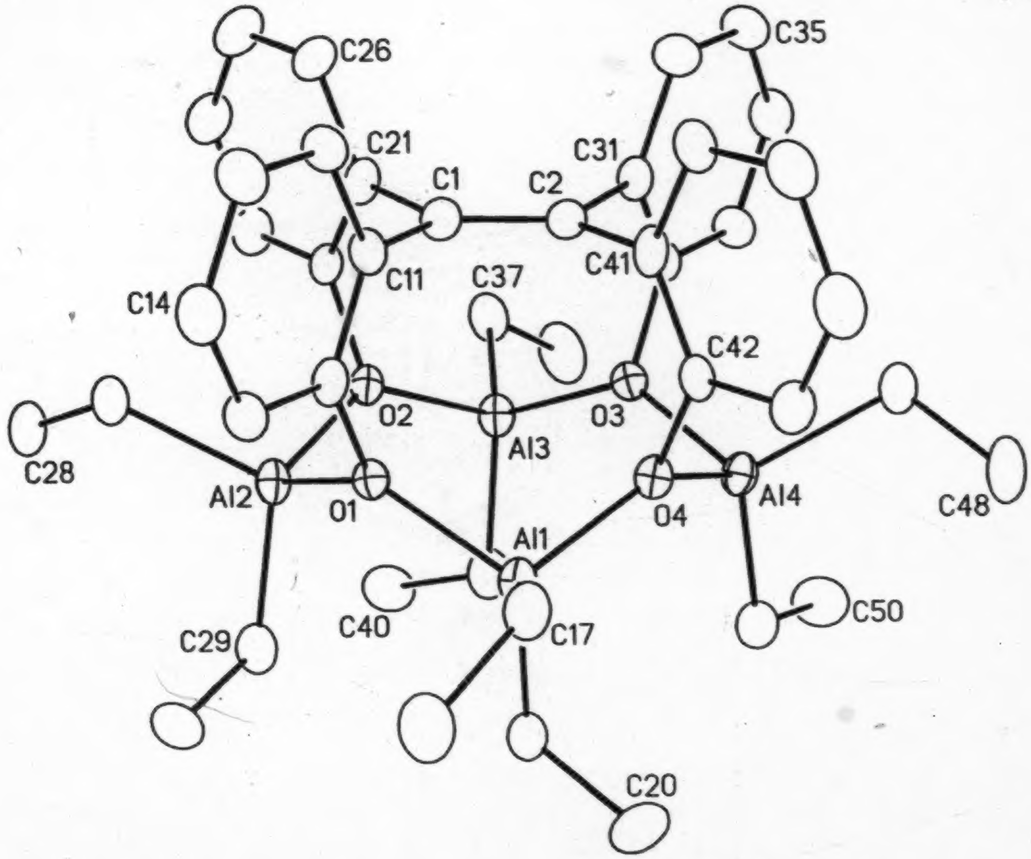
C26
C35
C21
C31
C1
C2
C41
C11
C37
C14
C42
O2
O3
Al3
C28
Al2
O1
O4
Al4
C48
Al1
C40
C17
C50
C29
C20

Figure 3.3a: perspective view of one of the two crystallographically independent compound **1** molecules (A in appendix, page 345) showing the atom labelling scheme. Non-hydrogen atoms are represented by Gaussian ellipsoids at the 20 % probability level. Hydrogen atoms are not shown. Selected bond distances (Å) and bond angles (deg): C1-C2=1.312(8), C1-C21=1.513(8), C1-C11=1.498(8), O1-Al1=1.882(4), O1-Al2=1.871(4),O2-Al2=1.881(4), O4-Al4=1.881(4), O4-Al1=1.873(4), Al1-C17=1.954(6), Al1-C19=1.944(6), Al2-C27=1.963(6), Al2-C29=1.934(7), C11-C1-C21=116.7(5), C41-C2-C31=116.0(5), Al1-O1-Al2=131.9(2), Al4-O4-Al1=133.1(2), O1-Al1-O4=101.5(2), O1-Al2-O2=100.9(2), Al1-O1-C12=114.9(3), Al2-O1-C12=113.2(3), Al2-O2-C22=111.9(3), Al3-O2-C22=114.6(3).

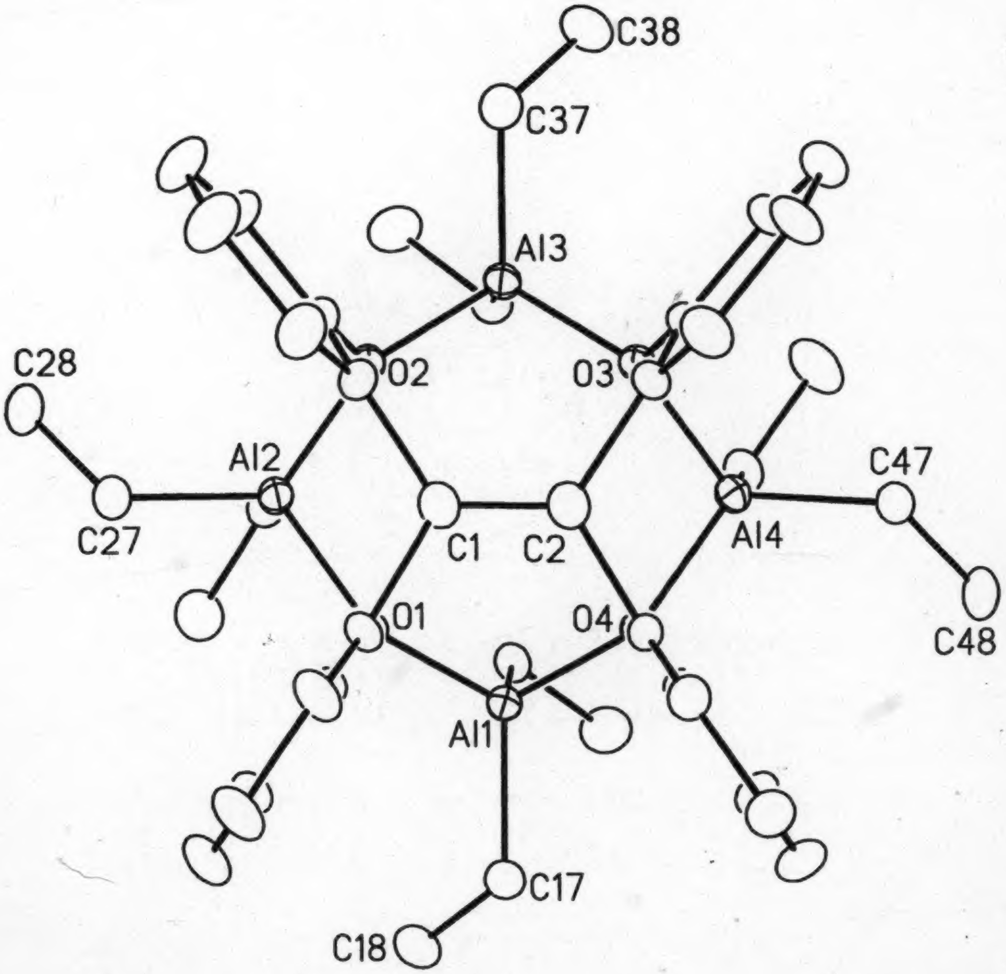
C38
C37
Al3
C28
O2
O3
Al2
C47
C27
C1
C2
Al4
O1
O4
C48
Al1
C17
C18

Figure 3.3b: View of molecule **1** (A in appendix, page 345) with the tetraphenylethene unit above the Al_4O_4 ring, showing the atom labelling of equatorial ethyl groups.

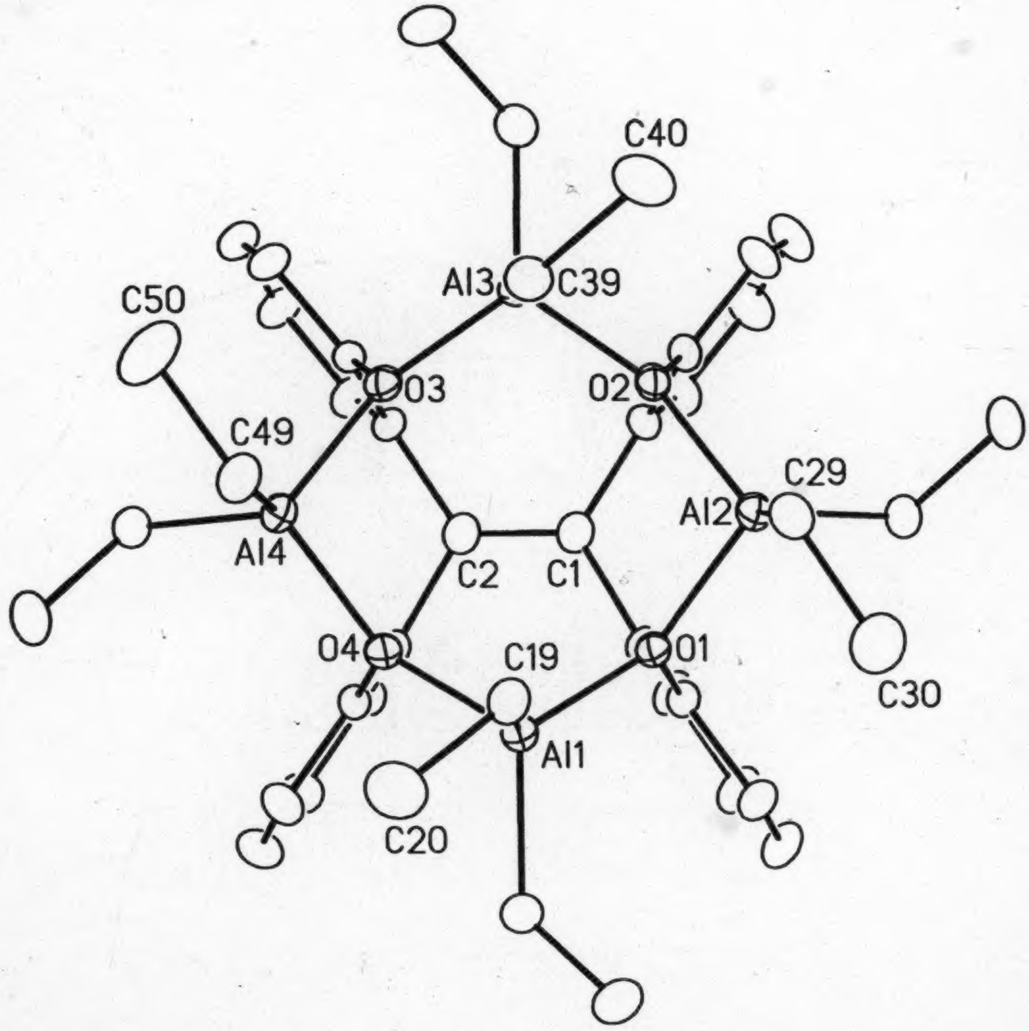
C40
Al3
C39
C50
O3
O2
C49
C29
Al2
Al4
C2
C1
O4
C19
O1
C30
Al1
C20

Figure 3.3c: View of molecule **1** (A in appendix, page 345) with the Al_4O_4 ring above the tetraphenylethene unit, showing the atom labelling for axial ethyl groups.

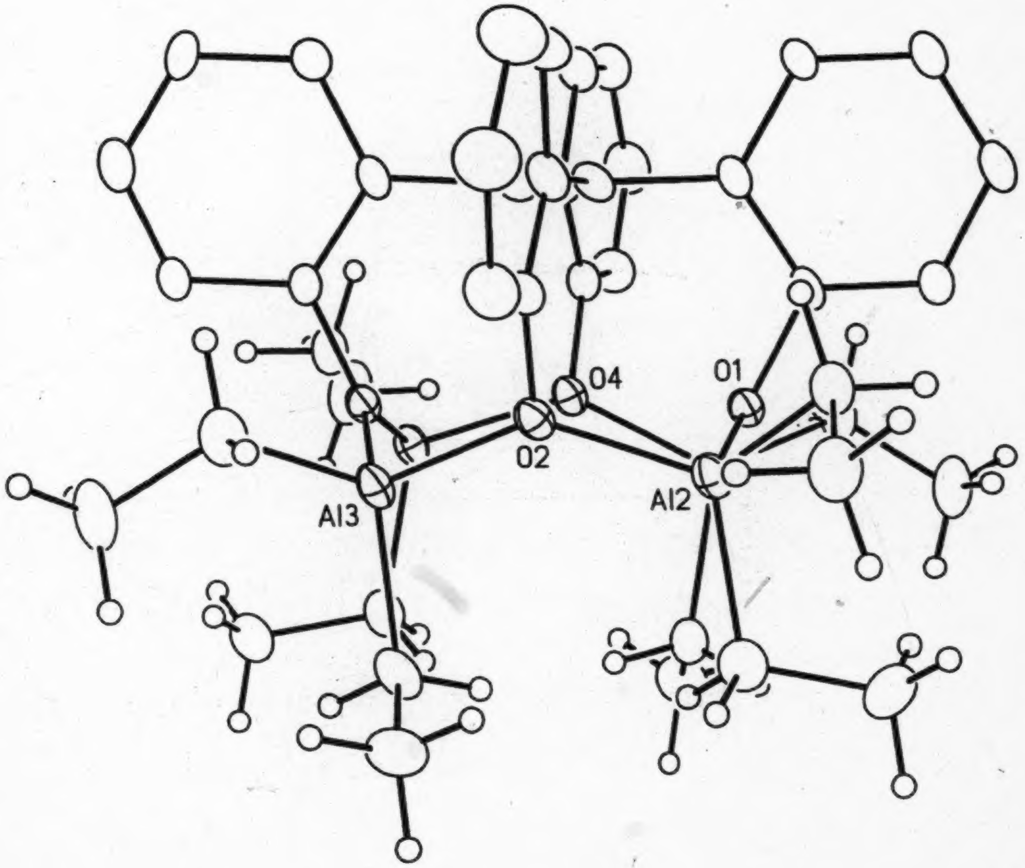

Figure 3.3d: Perspective view of molecule **1** (A in appendix, page 345) across the ethene bond showing the position of the equatorial ethyl groups in relation to the phenyl rings.

The plane formed by the carbon and two Al atoms, containing the oxygen, is placed nearly perpendicular (86.4° av) to the plane formed by the phenoxide ring. Both features are also found in dimeric aluminum phenoxides,[10,11] and trimeric oxygen bridged compounds.[12]

If Pauling's covalent atomic radii are used, an Al-O bond length of 1.30 + 0.73 = 2.03 Å is predicted,[13] while the actual observed bond length is 1.878 Å (av). The combination of a trigonal planar coordination of oxygen bound to aluminum and the perceived shortening of the oxygen aluminum bond has induced some authors to propose O-Al π-interactions.[12,14] At this moment the resulting debate seems to have settled on electrostatic interactions[15] as the explanation for the short bond length: the electronegativity difference in Al-O bonds is 1.83 units, which according to Pauling leads to a partial ionic character of 65 %. When the calculated Al-O bond length is corrected for the ionic contribution,[16,17] the perceived bond shortening is reduced to 0.04 Å.

The discussion on the amount and significance of π-bonding is still ongoing in the literature: ab initio calculations seem to indicate a negligible[19] or substantial[14] presence of π-bonding.

Another reason why the oxygen environment might be trigonal planar is steric crowding.[16] Bartell and Glidewell[20] introduced a set of radii which describe and define the minimum distance of approach of two atoms X and Y in a fragment XMY. The "geminal repulsion radius" refers to the X atom radius in the direction of the Y atom and can be used to rationalize the detailed geometry of molecules.[16,17] Haaland modified the aluminum radius of Bartell to a slightly smaller value of 1.75 Å. Using the geminal repulsion radii of Bartell and Glidewell[20] [Al = 1.85 Å] or Haaland[16,17] [Al = 1.75 Å] the *calculated* sum of the radii for Al-Al and Al-C around the oxygen is always larger then the actual *observed* distance, see Table 3.4, page 141. This steric repulsion might also

Table 3.4: Non-bonding distances around the oxygen atoms in compound 1 in Ångstrom.

Atom/Atom non-bonding distances around oxygen atoms.					
O1	Al1-Al2	3.426	O3	Al3-Al4	3.455
	Al1-C12	2.792		Al3-C32	2.783
	Al2-C12	2.756		Al4-C32	2.734
O2	Al2-Al3	3.453	O4	Al1-Al4	3.444
	Al2-C22	2.758		Al1-C42	2.775
	Al3-C22	2.797		Al4-C42	2.777

Using geminal repulsion radii of Bartell and Glidewell,[20] and in brackets [] using Haaland's repulsion radii[16,17] the following distances are calculated: Al-Al = 3.70 Å [3.50 Å] Al-C = 3.10 Å [3.00 Å]

explain the observed bond angles for Al-O-Al (131.9(2)-133.9(2) degrees) and Al-O-C (110.7(3)-116.3(3) degrees) given that the geminal repulsion radius of Al [1.75 to 1.85 Å] is larger than the radius of C [1.25 Å].

The tetrahedral coordination environment at the Al atoms is irregular with C-Al-C angles of 114.4(3)-111.6(3) degrees, O-Al-O angles of 100.2(2)-102.7(2) degrees and C-Al-O angles varying between 107 and 117 degrees. The small values for the O-Al-O angle have been interpreted as a manifestation of Bent's rule.[21] Values smaller than 100 degrees have been observed for other aluminum phenoxides.[11]

The observed Al-O-Al angles (131.9(2)-133.9(2)) degrees also show a marked deviation from the normal range for the Al-O-Al angle in dimers that range from 92.6-101.5° or trimers, with values in the 120-125° range.[11,12] The observed angles, however, fit nicely in the range of the known bond angles for similar eight membered heterocyclic compounds, see Table 3.5, page 142.

Table 3.5: Comparison of solid state structural features of In, Ga, Al containing eight membered rings.[12]

Compound	M-E (av in Å)	E-M-E (av in deg.)	M-E-M (av in deg.)	C-M-C (av in deg.)
$[Me_2In(\mu\text{-}SAr)]_4$	2.59	91.4	126.9	133.1
$[Me_2Al(\mu\text{-}SAr)]_4$	2.36	97.1	128.8	123.2
$[Me_2Ga(\mu\text{-}SAr)]_4$	2.40	94.9	128.0	126.9
$[Me_2Ga(\mu\text{-}OH)]_4$	1.96	98.8	133.1	129.2
Compound **1**	1.88	101.3	130.1	113.0

SAr = S-2,6-$Me_2C_6H_3$, M = metal, E = O,S

Only one compound in Table 3.5 is aluminum based: the tetrameric organoaluminum thiolate for which an extended chair conformation is found. If the Haaland normal and dative bond distances are used,[16] Al-S (for the thiolate) and Al-O (for compound **1**) distances of 2.43 and 1.85 Å are predicted for a 1:1 normal/dative bond in four-coordinate aluminum atoms, which is close to the observed values of 2.36 Å (Al-S av, Table 3.3)[12] and 1.88 Å (Al-O av). In the aluminum thiolate,[12] a significant difference in the equatorial and axial Al-C bond length is noted, with the equatorial bond length approximately 0.015 Å longer than the axial bond lengths. The average equatorial and axial bond length of compound **1** are 1.954 and 1.942 Å; unfortunately the standard deviation is too large to permit a distinction.

The tetrameric organoaluminum thiolate is, as far as I am aware, the only eight-membered ring based on a phenol or thiophenol ligand containing four aluminum groups. However, this compound does not maintain the solid state ring structure in solution.[12] Other examples of eight-membered rings containing four aluminum groups are the aluminoxanes $(Me_2AlOLi)_4 \cdot 7THF \cdot LiCl$ of

Araki/Roesky,[22] and the (mesitylAlO)$_4$ of Power.[23] In addition, Haaland[24] has reported the gas-phase electron diffraction structure of the dimethylaluminum fluoride tetramer. For examples of eight-membered rings containing a single aluminum group, see reference 27.

The tetraarylethene frame displays an ethene bond distance of 1.301(9)-1.312(8) Å and the four aryl rings are located perpendicular to the ethene bond with a dihedral angle of 89.8(8)-97.8(8) degrees. Another structural element also found in the parent *tetrakis*[2-hydroxyphenyl]ethenes discussed in Chapter 2 is the aryl-C-aryl angle of 116.7(5)/116.8(5) degrees.

3.3.2 Comparison with other aluminum complexes of phenol-based tetradentate ligands.

In order to judge the influence of the preorganization of the four phenol groups using an ethene bridge, the product of the reaction of *tetrakis*[2-hydroxyphenyl]ethene with triethylaluminum should be compared with the products obtained in reactions of other phenol-based tetradentate ligands with trialkylaluminum.

Atwood[25] has published the crystal structure of the product of the reaction between excess trimethylaluminum and *p-tert*-butylcalix[4]arene in toluene (eq. 3.5, page 144). This reaction yields a monomeric compound with two bridging four coordinate aluminum atoms.

The calix[4]arene adopts a severly distorted partial-cone conformation in the crystal structure. Two of the oxygen atoms coordinate to two exo-located trimethylaluminum groups (eq. 3.5, page 144); no yield is given in the original paper.

Although no explanation is given, presumably the intramolecular O-O distances results in a rapid formation of a bridging aluminum group. In addition the limited conformational mobility of the calix[4]arene might play an important role in determining the outcome of the reaction.

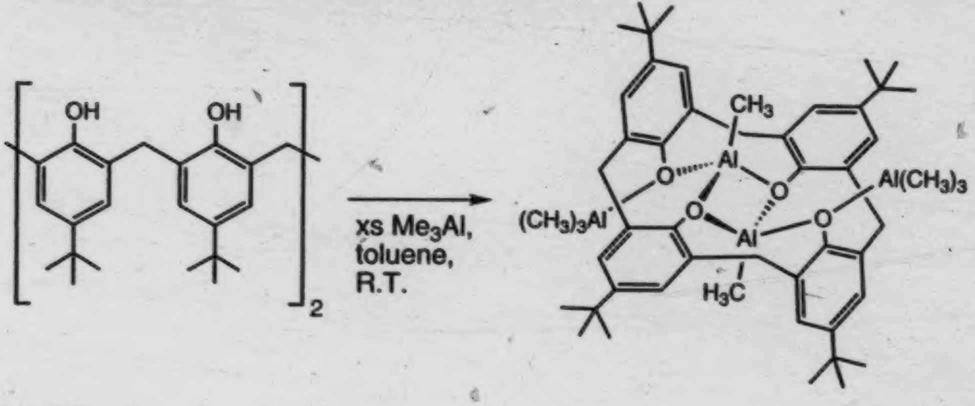

eq. 3.5

The calix[4]arene is presumed to be mainly present in the cone conformation (see section 1.5.3, page 38) at the start of the reaction. Such a cone conformation would maintain a high "local" concentration of OH groups that would become highly activated[26] as the formation of dimethylaluminum phenoxide proceeds. In contrast, due to the presence of all rotational isomers of the *tetrakis*[2-hydroxyphenyl]ethene (see section 2.3.2, page 82), fewer "locally activated" OH groups would be able to make an intramolecular reaction compete with a intermolecular reaction in the presence of excess triethylaluminum.

Another intriguing possibility is the initial formation of an eight-membered ring as observed for compound **1** with the calix[4]arene, that subsequently disproportionates (vide infra) to give the product isolated by Atwood et al. In the absence of any further data, this remains a highly speculative discussion.

Scott has published a bifunctional Lewis acid assembly based on two methylenebisphenol groups linked to the 1 and 8 positions of an anthracene spacer.[27] The reaction of this compound with trimethylaluminum affords a

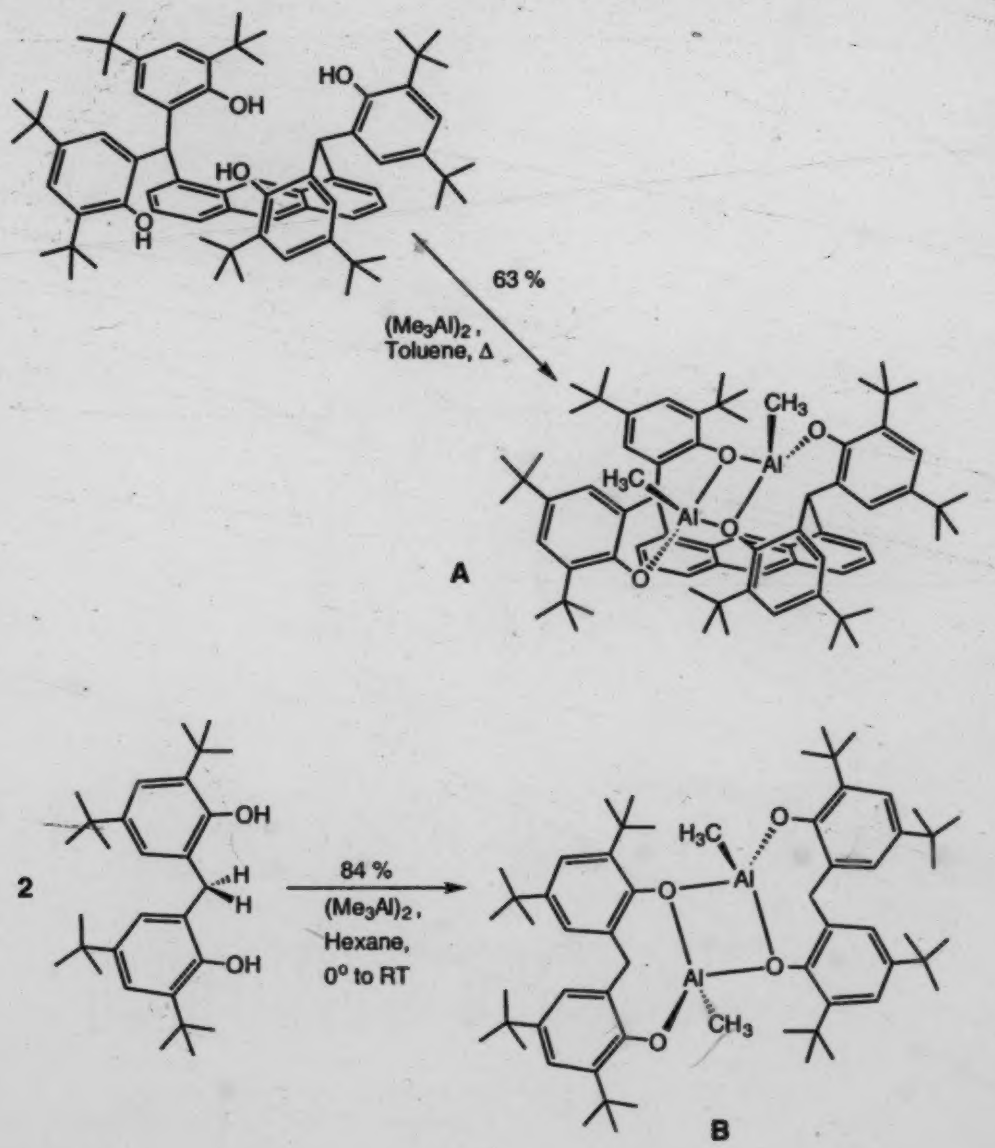
HO
OH
HO
O
H
63 %
(Me3Al)2 ,
Toluene, Δ
CH3
O
Al
O
H3C
Al
O
O
A
2
OH
H
H
OH
84 %
(Me3Al)2 ,
Hexane,
0° to RT
H3C
O
Al
O
Al
O
CH3
O
B

eq. 3.6

species containing a dinuclear aluminum structure (eq. 3.6, A), similar to the dinuclear structure obtained from free methylenebisphenol (eq. 3.6, B). A direct comparison of the products obtained from the calix[4]arene and the *tetrakis*[2-hydroxyphenyl]ethene compounds is less useful here considering the difference in the steric hinderance around the OH groups.

Moreover it is clear that the use of an anthracene linker does not result in a binding situation fundamentally different from the free methylbisphenol ligand in this specific reaction.

The ligand structure of the discussed phenol based tetradentate ligands does have an influence on the aggregation state of the bound aluminum groups. By comparison, dimethylaluminumphenoxide forms in solution a dimer-trimer equilibrium: no tetramer is detected.[5]

3.3.3 The crystal structure of compound 2.

Compound **2** shows in the crystal structure two highly distorted tetraphenylethene ligands encapsulating two pentacoordinated and two tetracoordinated aluminum atoms in between the two ligands (Figure 3.4, page 147). A summary of bond distances and bond angles is given in the appendix E, page 357.

The observed Al-O bond lengths (1.857/1.891 Å) in the tetracoordinate fragment Al2, Al2' are within the range for known aluminum phenoxides [1.79-1.895 Å][10,11] and qualify according to Haaland as a normal/dative hybrid [1.85 Å].[15,16] The Al-C bonds (1.946(5)-1.952(4) Å) [1.946-1.994 Å][11] and C-O bonds (1.355(5)-1.406(5) Å) are within the expected range.[10,11,12] The sum of the angles around the oxygen atoms O2 and O3 is 356 and 360 degrees.The Al-O bond lengths in the pentacoordinate fragment around Al1, Al1' are irregular.[16,17] The sum of the angles of the equatorial Al-O bonds is 350 degrees, which, when combined with the observed range of the O_{ax}-Al-O_{eq} angles (77.8 to 105.8 degrees, av 91.3) is indicative of a distorted trigonal bipyramidal geometry as is the O1'-Al-O22 angle of 168.6 degrees.

The *tetrakis*[2-hydroxyphenyl]ethene frame is highly distorted in this crystal structure (Figure 3.4b, page 148).

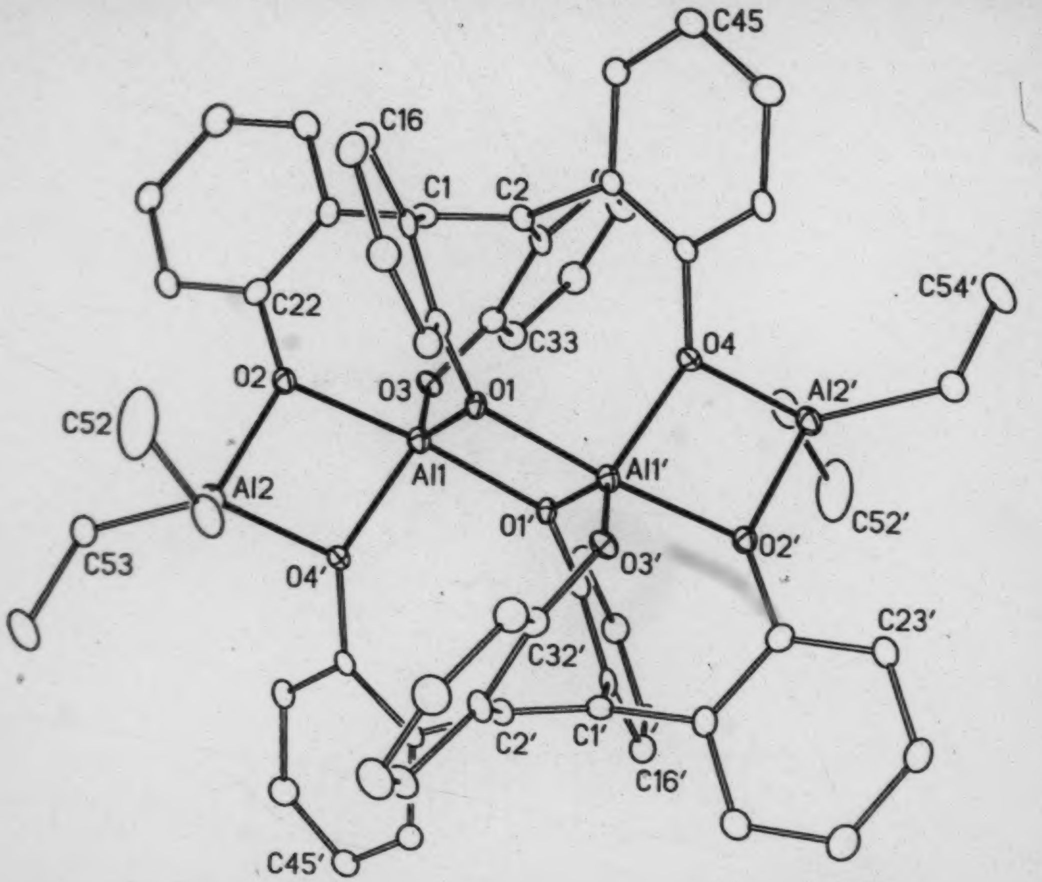
C45
C16
C1
C2
C22
C33
C54′
O4
Al2′
O2
O3
O1
C52
Al2
Al1
Al1′
C52′
O1′
C53
O4′
O3′
O2′
C23′
C32′
C2′
C1′
C16′
C45′

Figure 3.4a. Perspective view of compound **2**, showing the atom labelling scheme. Non-hydrogen atoms are represented by Gaussian ellipsoids at the 20 % probability level. Hydrogen atoms are not shown. Primed atoms are related to unprimed ones via the crystallographic inversion center at (0,0,0). Selected bond distances (Å) and bond angles (deg.): C1-C2=1.346(5), C12-O1=1.406(5), C22-O2=1.375(5), C32-O3=1.355(5), C42-O4=1.397(5), O1'-Al1=1.881(3), O2-Al1=1.924(3), O3-Al1=1.733(3), O4'-Al1=1.846(3), O1-Al1=1.843(3), O2-Al2=1.857(3), O4'-Al2=1.891(3), Al2-C51=1.946(5), Al2-C53=1.952(4), C53-Al2-C51=116.5(2), C11-C1-C21=115.4(4), C41-C2-C31=120.4(4), O1-Al1-O2=94.75(13), O2-Al1-O3=93.50(14), O2-Al2-O4'=78.66(13), O1-Al1-O1'=77.84(13), O1'-Al1-O3=97.87(13), O1'-Al1-O4'=105.81(13), O2-Al1-O1'=168.63(14), O1-Al1-O3=131.58(14), O4'-Al1-O3=122.58(14), O1-Al1-O4'=95.49(13), Al1-O1'-Al1'=102.16(13).

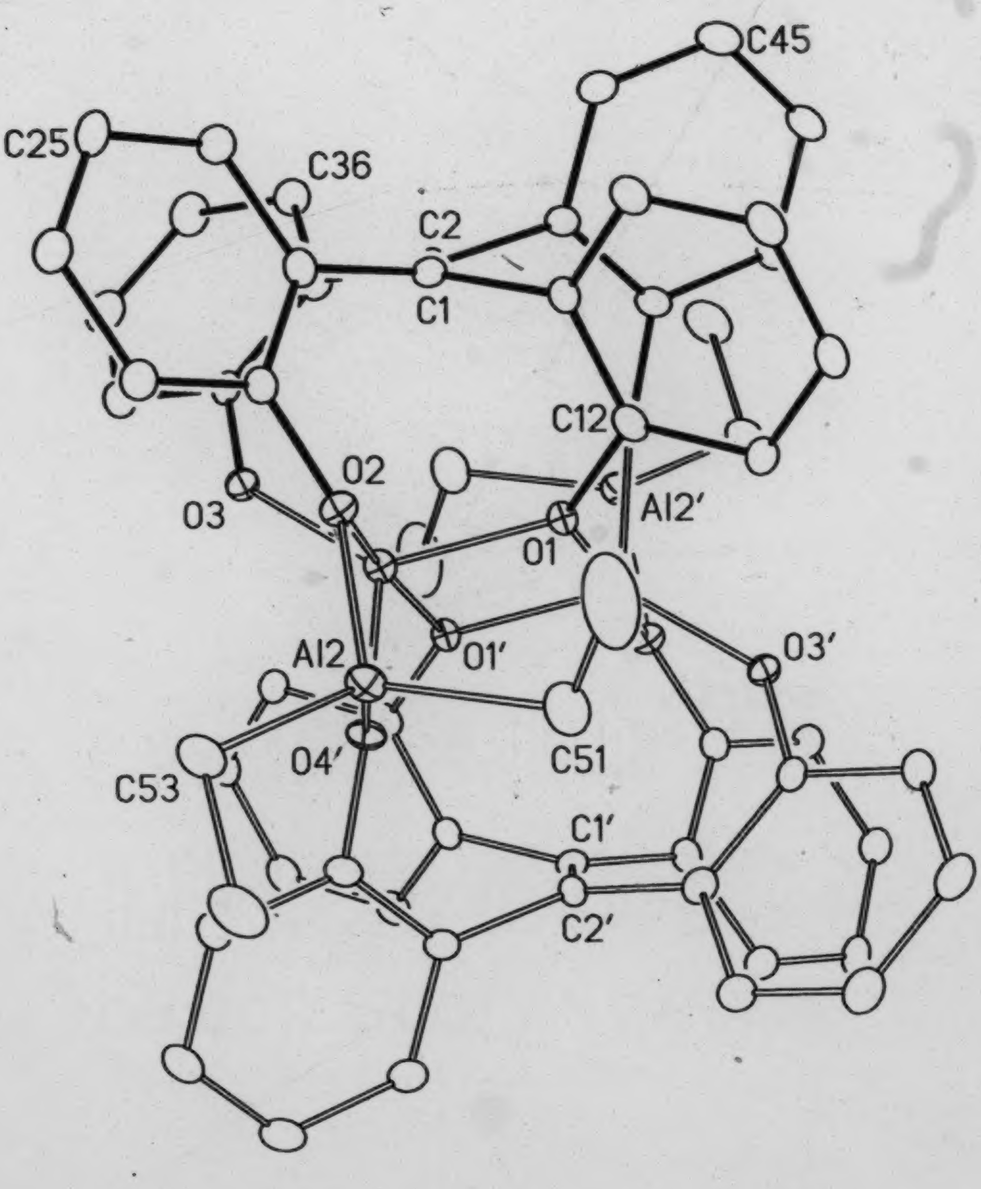
C45
C25
C36
C2
C1
C12
O2
O3
Al2'
O1
O3'
Al2
O1'
O4'
C51
C53
C1'
C2'

Figure 3.4b. Alternate view of compound **2** approximately along the C1-C2 bond, illustrating the twisting of the ethene unit.

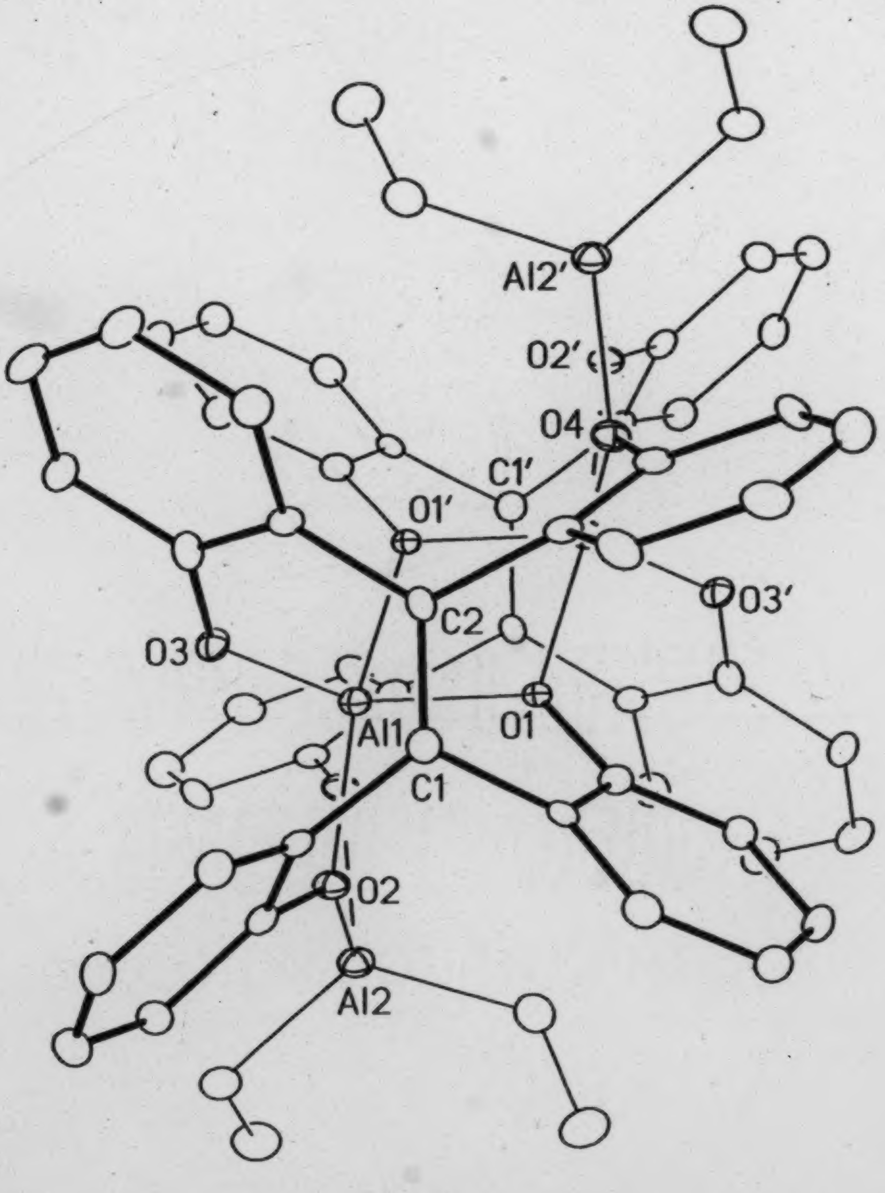
Al2'
02'
04
C1'
01'
C2
03
03'
Al1
01
C1
02
Al2

Figure 3.4c. View of compound **2** from above the ethene unit, showing the twisting of the phenyl rings with respect to the ethene and to each other creating an asymmetric environment for the aluminum-bound ethyl groups.

Not only is the ethene bond twisted (Fig. 3.4b, page 148), as observed in the dihedral angle of 25 to 15 degrees across the double bond, but the phenyl rings are pulled towards the Al_2O_2 frame, leading to an increase of the $O\text{-}C_{phenyl}\text{-}C_{phenyl}$ angle from 120 degrees to 122.7 degrees. The inherent strain is also observed for the $C_{ethene}\text{-}C_{phenyl'}\text{-}C_{phenyl'}$ angle (from 120 to 125.9 degrees). This distortion is located on only one side of the ethene frame, leading to the ethene bond torsion; the other side is less distorted.

This is also expressed in the different phenyl-C_{ethene}-phenyl angles of 115.4 and 120.4 degrees (*tetrakis*[2-hydroxyphenyl]ethene: 116.4°). The ethene bond of 1.346(5) Å has the length of the *tetrakis*[2-hydroxyphenyl]ethene bond (1.347(9) Å). A similar Al_2O_2 four-membered ring system has been reported for calix[4]arenes[28] by Atwood and Raston (eq. 3.7).

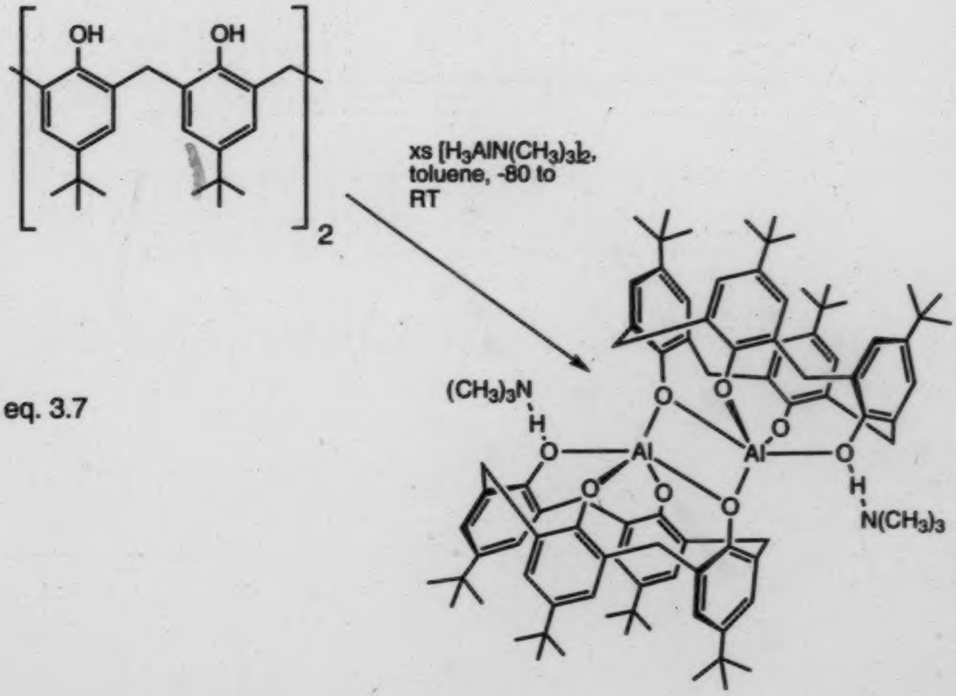

eq. 3.7

Thus, while the crown complex is unique to this ligand system the collapsed structure is more typical.

3.3.4 The crystal structure of compound 4.

The "collapsed" structure as observed in the crystal structure of compound **2** is repeated in the crystal structure of compound **4** (for crystallographic details see the experimental section and the appendix F, page 363). In addition to two highly distorted tetraphenylethene ligands encapsulating two pentacoordinated aluminum atoms in between the two ligands, (Figure 3.5, page 152) the periphery now contains two pentacoordinated ethylaluminum chloride fragments coordinated to THF, presumably because of the higher Lewis acidity of these fragments compared to the diethylaluminum groups in compound **2**.

The Al-C bond (1.957(6) Å) [1.946-1.994 Å][11] is within the expected range,[10,11,12] as is the Al-Cl bond (2.167(2) Å) [2.104-2.199 Å].[10]

The Al-O bond lengths in the pentacoordinate fragment around Al1, Al2 range from 2.082 to 1.740 Å, with the longest Al-O bond lengths axially located. The sum of the angles of the equatorial Al-O bonds is 360 degrees for both Al1 and Al2. The observed range of the O_{ax}-Al-O_{eq} angles (73.4 to 100.0 degrees, av 89.9) and the O_{ax}-Al-$O_{ax'}$ angles of 160.7 and 169.1 degrees are indicative of a distorted trigonal bipyramidal geometry.

As in compound **2**, the *tetrakis*[2-hydroxyphenyl]ethene frame is highly distorted in this crystal structure (Figure 3.5b, page 153). The ethene bond is severly twisted with a dihedral angle across the double bond of 25 to 15 degrees. One of the phenyl rings is twisted away from the position perpendicular to the double bond by 43 degrees: the other rings with dihedral angles across the double bond between 65.9 and 74.7 degrees show smaller deviations from the perpendicular position.

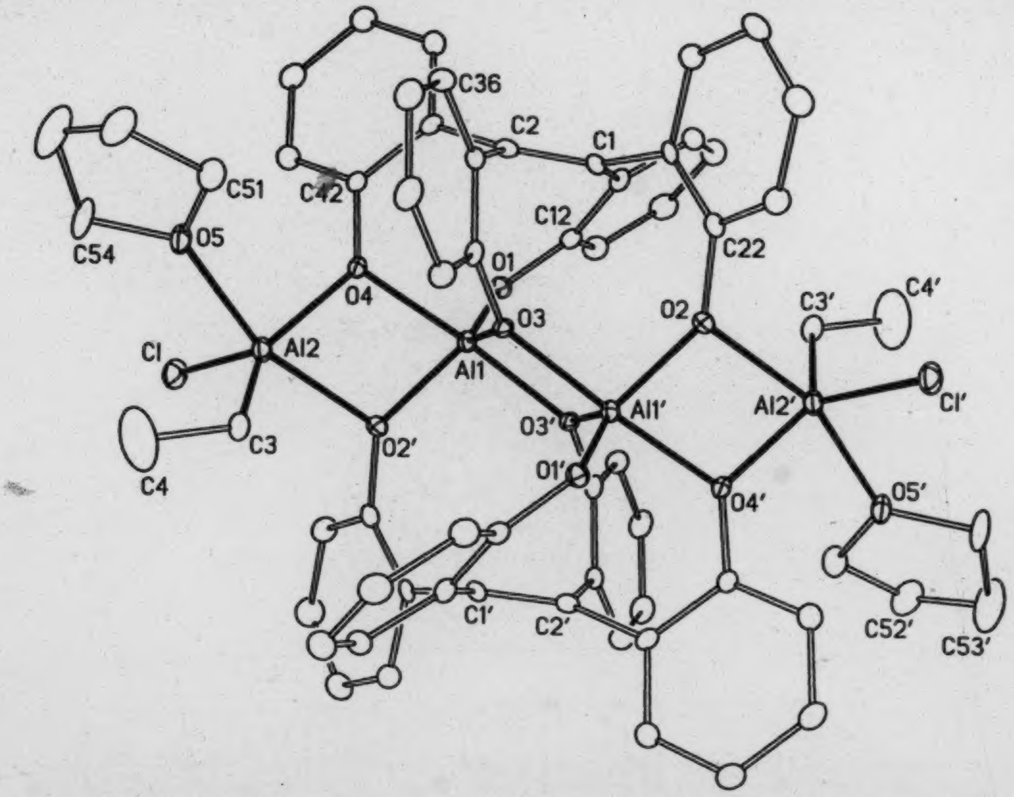

Figure 3.5a. Perspective view of compound **4**, showing the atom labelling scheme. Non-hydrogen atoms are represented by Gaussian ellipsoids at the 20 % probability level. Hydrogen atoms are not shown. Primed atoms are related to unprimed ones via the crystallographic inversion center at (0,0,1/2). Selected bond distances (Å) and bond angles (deg.): C1-C2=1.349(8), C12-O1=1.361(7), C22-O2=1.394(7), C32-O3=1.399(6), C42-O4=1.390(6), O4-Al1=1.923(4), Al1-O3'=1.894(4), Al1-O1=1.740(4), Al1-O2'=1.803(4), Al1-O3=1.859(4), Al2-O4=1.842(4), Al2-O2'=2.082(4), Al2-C3=1.957(6), Al2-C1=2.167(2), Al2-O5=2.009(4), O1-Al1-O4=93.5(2), O2'-Al1-O4=78.3(2), O3-Al1-O4=93.7(2), O1-Al1-O3'=97.1(2), O2'-Al1-O3'=98.3(2), O3-Al1-O3'=77.3(2), O3'-Al1-O4=169.1(2), O1-Al1-O2'=121.0(2), O2'-Al1-O3=107.3(2), O1-Al1-O3=131.6(2), Cl-Al2-O5=91.54(14), O4-Al2-O5=87.7(2), C3-Al2-O5=95.5(2), Cl-Al2-O2'=99.95(13), O4-Al2-O2'=73.4(2), C3-Al2-O2'=92.9(2), O2'-Al2-O5=160.7(2), Cl-Al2-O4=114.7(2), O4-Al2-C3=127.6(2), Cl-Al2-C3=117.5(2), Al1-O3-Al1'=102.7(2), Al1-O4-Al2=104.9(2), Al1-O2'-Al2=100.2(2).

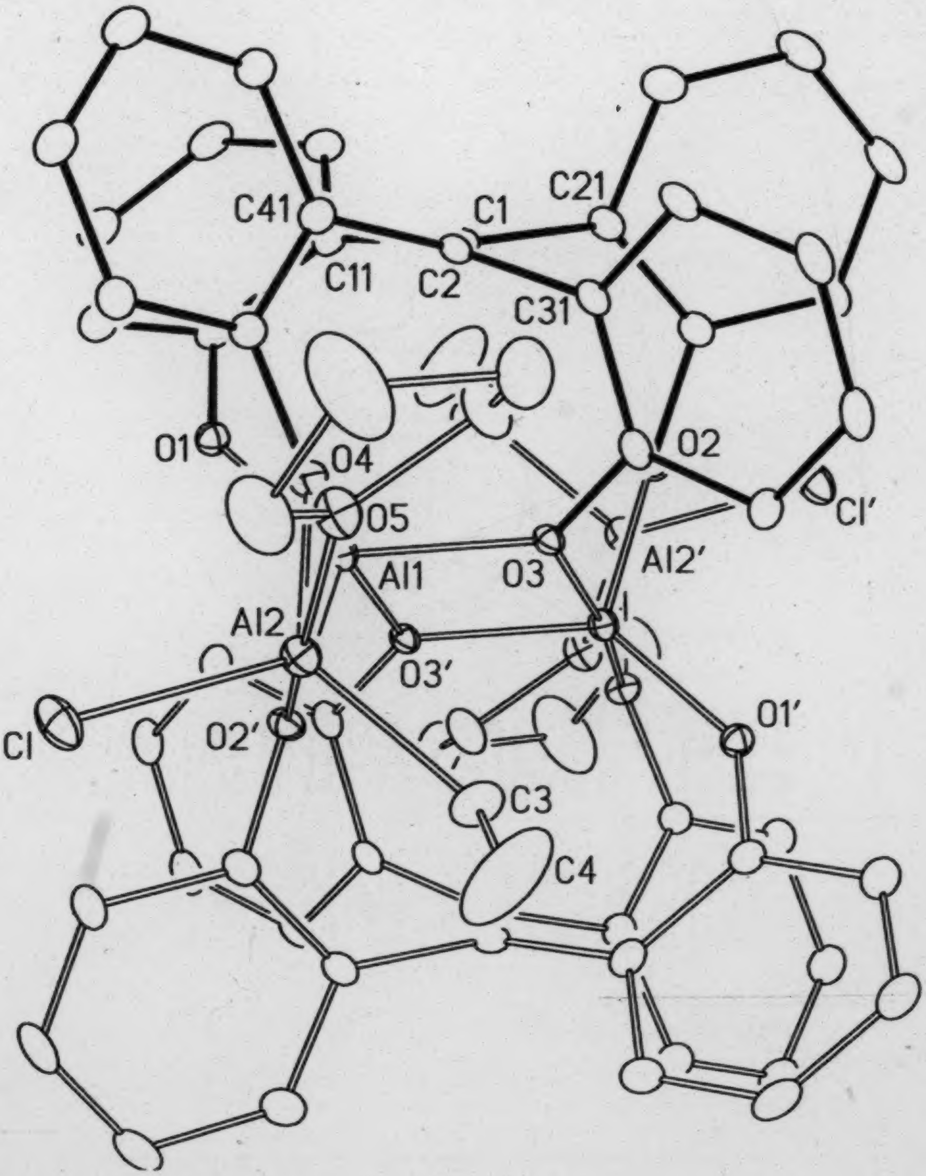
C41
C1
C21
C11
C2
C31
O1
O4
O2
O5
Cl'
Al1
O3
Al2'
Al2
O3'
Cl
O2'
O1'
C3
C4

Figure 3.5b. Alternate view of compound 4 approximately along the C1-C2 bond, illustrating the twisting of the ethene unit.

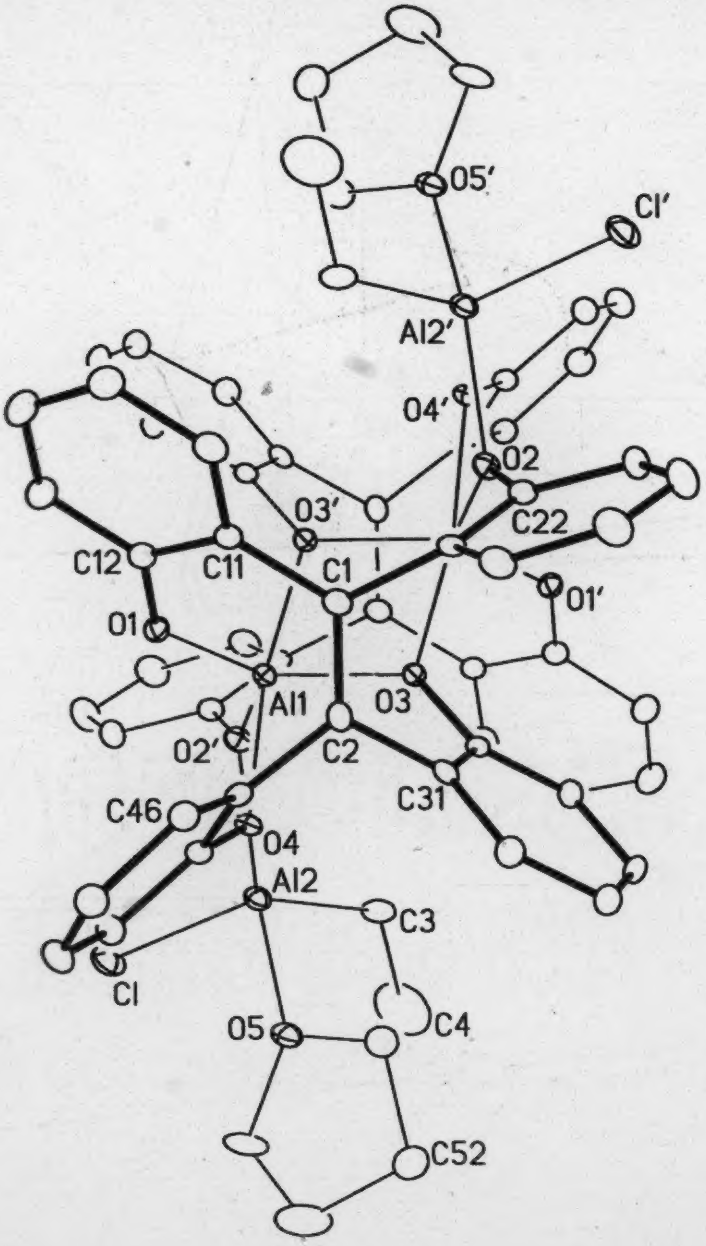
O5'
Cl'
Al2'
O4'
O2
O3'
C22
C12
C11
C1
O1'
O1
Al1
O3
O2'
C2
C46
C31
O4
Al2
C3
Cl
C4
O5
C52

Figure 3.5c. View of compound **4** from above the ethene unit, showing the twisting of the phenyl rings with respect to the ethene and to each other.

The phenyl-C_{ethene}-phenyl angles of 114.8 and 121.3 degrees (*tetrakis*[2-hydroxyphenyl]ethene: 116.4°), as well as the ethene bond length of 1.349(8) Å are similar to the angles and ethene bond length found in compound **2**.

3.3.5 The structure of compound 1 in solution.

There are four magnetically different ethyl groups in the crystal structure of compound **1** (Figure 3.3a, page 136) that might well correspond to the four observed ethyl groups signals in the recorded ^{1}H-NMR spectrum. This observation is of interest because a rigid Lewis acidic crown compound in solution might display an optimum binding situation for anion complexation as the four aluminum groups might be able to interact simultaneously with a complexed anion. If the crystal structure mirrors the structure of compound **1** in solution, it might also be possible to assign the ^{1}H-NMR resonances of the aluminum-bound ethyl groups. In order to probe the structure of compound **1** in solution, NMR spectroscopic techniques were used.

According to the crystal structure four "axial" ethyl groups (see Figure 3.3c, page 138) are standing perpendicular on the surface formed by the four oxygen atoms and pointing away from the phenyl rings. The other four "equatorial" ethyl groups (see Figure 3.3d, page 139) are placed in between the phenyl rings. These ethyl groups therefore experience the shielding effect due to the ring current of the phenyl rings. Based on the observed chemical shift difference of the methylene protons (see Table 3.1 under header "observed signal", page 129) the "equatorial" methylene protons are assigned to the signals at -1.37 and -0.76 ppm, while the "axial" methylene protons are assigned to the signals at 0.38 and 0.48 ppm (see Figure 3.6, page 156), assuming the crystal structure reflects the solution structure.

The observed differences in the chemical shift of the "equatorial" methylene protons is likely due to a difference in the position of the methylene groups in between the phenyl rings (see Figure 3.3d, page 139) and the distance to these phenyl rings. Using the published ring current shielding tables[29] combined with the distances between the methylene groups and the phenyl ring centroids in compound **1**, as obtained from the crystal structure, the difference in the shielding contribution due to the aryl ring current can be calculated for the aluminum bound "equatorial" methylene groups.

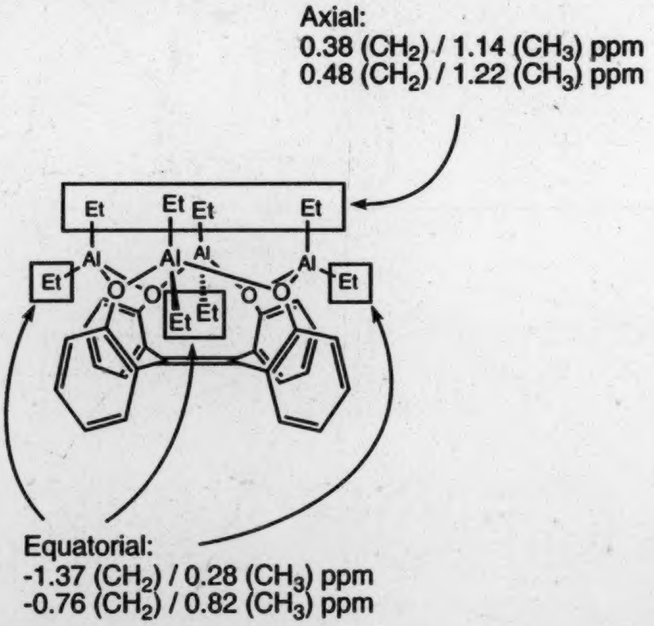

Axial:
0.38 (CH_2) / 1.14 (CH_3) ppm
0.48 (CH_2) / 1.22 (CH_3) ppm

Equatorial:
-1.37 (CH_2) / 0.28 (CH_3) ppm
-0.76 (CH_2) / 0.82 (CH_3) ppm

Figure 3.6 Proposed assignment of compound 1 ^{1}H-NMR signals assuming the crystal structure mirrors the solution structure.

This would allow the assignment of the individual "equatorial" methylene group ^{1}H-NMR signals on the basis of the observed chemical shift difference (-1.37 and -0.76 ppm, Figure 3.6). The assumptions made in this approach are: (1) The ring current shielding of the phenoxide groups of the *tetrakis*[2-

hydroxyphenyl]ethene can be treated as the ring current shielding of benzene groups, and (2) the position of the methylene carbon groups (C_{17}, C_{27}, C_{37}, C_{47}, see Figure 3.7) represent the averaged methylene hydrogen atom position at room temperature. The last assumption is doubtfull, but necessary to account for the possible movement of these methylene carbons in solution. In order to calculate the ring current shielding $\Delta\sigma$ contribution to the chemical shift of the aluminum bound "equatorial" methylene groups ($H_2C[17]$, $H_2C[27]$, $H_2C[37]$, $H_2C[47]$) the values for R, Z and ϕ (see Table 3.6, page 158, and Figure 3.7) were obtained from the crystal structure using molecule A. The computed values of **Z** and ρ (expressed in benzene carbon-carbon bond length units of 1.390 Å) are given in Table 3.6, which in combination with the angle ϕ allows the determination of $\Delta\sigma$.[29]

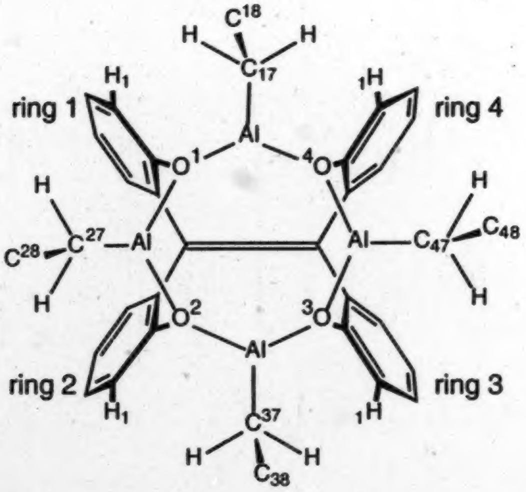

Figure 3.7. Ring numbering and position of equatorial CH_2: topview of compound 1. The aryl rings have been twisted slightly and axial ethyl groups have been removed for clarity.

Table 3.6: Calculated ring shielding contribution $\Delta\sigma$ arising from one benzenering for the equatorial methylene groups based on the cylindrical coordinates ρ, **Z** (in benzene CC bondlength units) and ϕ (in degrees) of C_{17}, C_{27}, C_{37} and C_{47}, in compound **1**.

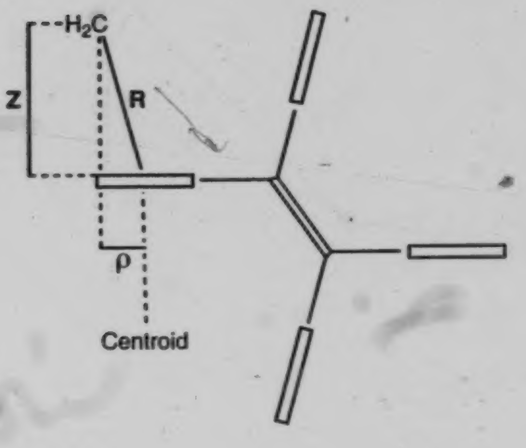

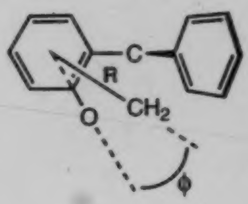

Topview

Sideview

	ρ	**Z**	ϕ	$\Delta\sigma$[1]
C_{17}-Ring[2] 1	2.046	2.007	31.3	0.092
C_{17}-Ring 4	2.024	2.009	30.9	0.111
C_{37}-Ring 2	2.056	2.004	26.9	0.092
C_{37}-Ring 3	2.036	2.031	27.7	0.111
C_{27}-Ring 1	1.603	2.206	3.5	0.196
C_{27}-Ring 2	1.444	2.212	7.5	0.196
C_{47}-Ring 3	1.441	2.216	6.4	0.196
C_{47}-Ring 4	1.593	2.171	4.1	0.196

1) positive means upfield shift. 2) For ring labeling see Figure 3.7

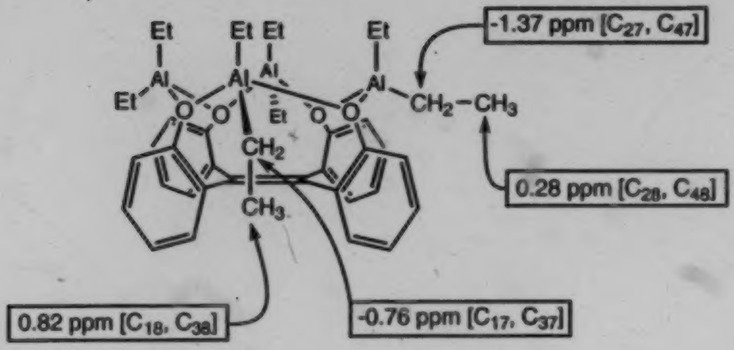

Figure 3.8. Proposed assignment of compound **1** ^{1}H-NMR signals of equatorial ethyl groups. In [] brackets corresponding crystal structure carbon number

On the basis of these calculations the equatorial methylene group *along* the ethene bond (C27, C47 see Figure 3.7, page 157, and Figure 3.8) should be more upfield shifted as $\Sigma\{\Delta\sigma\ (C_{27}, C_{47})\} \approx 0.4$ compared to the equatorial methylene group *perpendicular* to the ethene bond (C_{17}, C_{37} see Figure 3.7, page 157 and Figure 3.8) with a calculated $\Sigma\{\Delta\sigma\ (C_{17}, C_{37})\} \approx 0.2$, see Table 3.6 (page 158).

The signal at -1.37 ppm is therefore assigned to the methylene protons of C_{27} and C_{47}, while the signal at -0.76 ppm is assigned to the methylene protons of C_{17} and C_{37}. Because of the doubtful assumption that the C_{17}, C_{27}, C_{37}, C_{47} positions in the crystal structure represent an average methylene proton position, further confirmation of the proposed assignment is necessary.

According to the crystal structure of compound **1**, the intramolecular distance of the "equatorial" methylene group to the nearest aromatic hydrogen is smaller for the aluminum located perpendicular to the ethene bond compared to the aluminum located along the double bond (Figure 3.9, page 160). This difference in distance might show up in an NOE experiment, thereby confirming or refuting both the assignment of the "equatorial" methylene groups as well as any proposed relation between the solid state structure and the structure of compound **1** in solution.

Before continuing, some assumptions and corresponding limitations of NOE experiments should be mentioned. In the NOE experiment, the following[30] are *assumed:* (1) The experiment is taking place in the extreme narrowing limit. Because of the low molecular weight (732 g/mol) and compact size of compound **1**, combined with the use of a low viscosity solvent, this does not seem an unreasonable assumption. (2) Isotropic tumbling is assumed: compound **1** is approximately spherical. (3) Intramolecular dipolar relaxation dominates the relaxation process, and (4) the leakage term incorporating alternative relaxation mechanisms is the same for the observed aromatic hydrogen NOE for *both* saturated equatorial CH_2 groups.

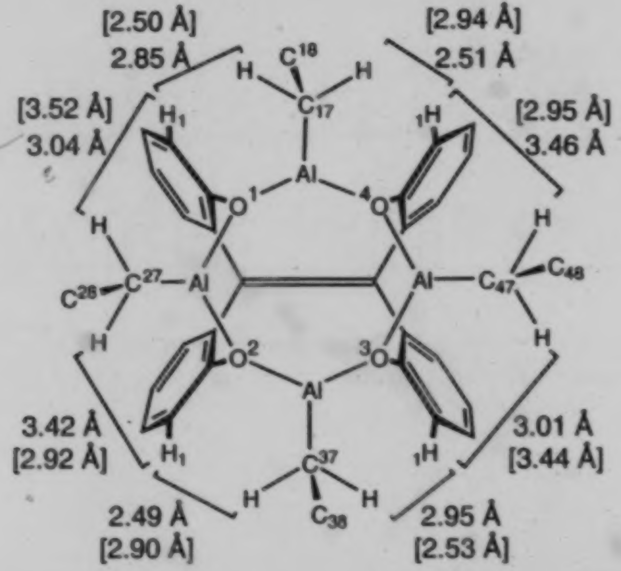
[2.50 Å]
2.85 Å
[2.94 Å]
2.51 Å
[3.52 Å]
3.04 Å
[2.95 Å]
3.46 Å
C18
C17
H
H
H1
1H
Al
O1
4O
H
C28
C27
Al
Al
C47
C48
H
O2
3O
Al
3.42 Å
[2.92 Å]
3.01 Å
[3.44 Å]
H1
1H
C37
H
H
C38
2.49 Å
[2.90 Å]
2.95 Å
[2.53 Å]

Figure 3.9. Non-bonding H-H distances between Aromatic H and equatorial CH_2: topview of compound **1**, molecule A [in brackets molecule B]. The aryl rings have been twisted slightly and axial ethyl groups have been removed for clarity.

(4, continued) The leakage term is the same for *both* observed equatorial CH_2 group NOE's when the aromatic hydrogen is saturated.

Only under these severe restrictions is the inverse distance to the sixth power relation valid.[30] Assumptions (3) and (4) are the weak points in this line of reasoning. Although an increased dilution of the intramolecular dipole-dipole relaxation would reduce the observed NOE enhancement, it is by no means certain (in spite of the geometry of the molecule) that the dilution is the same for all protons under scrutiny. This would lead to unsymmetrical NOE enhancements not related to distance variations.

As the magnitude of the NOE is, under these restrictive conditions, related to the distance between interacting protons by a factor of $1/r^6$, the strongest NOE effect is predicted for the interaction of the C_{17},C_{37} ("perpendicular") methylene protons at -0.76 ppm with the aromatic protons at 6.94 ppm when the distances are used as observed in the crystal structure (Figure 3.9, page 160). The interaction between the C_{27},C_{47} ("along") methylene protons at -1.37 ppm and the aromatic protons at 6.94 ppm is predicted to have a weaker NOE effect. In order to remove the contribution of cross relaxation phenomena in the comparison, the ratio of the magnitude of two measured NOE effects, which should reflect the inverse to the power sixth ratio under the restrictions stated, will be used: the calculated ratio $[1/r^6_{(\text{along})}] / [1/r^6_{(\text{perpendicular})}]$ is given in Table 3.7 (page 162).

Because the distance of the methylene protons of C_{27},C_{47} ("along") to the aromatic protons H_1 in general is larger compared to the distance of the methylene protons of C_{17},C_{37} ("perpendicular") to the same aromatic protons, the calculated NOE ratio is smaller than 1. It should be realized that the calculated ratio as given in Table 3.7, page 162 is for a discrete solid state species not reflecting the ethyl group motion.

Table 3.7: Calculated ratio of the NOE effect between aromatic hydrogens and equatorial CH_2 groups (C_{27}, C_{47}) along the ethene bond and the NOE effect between aromatic hydrogens and equatorial CH_2 groups (C_{17}, C_{37}) perpendicular to the ethene bond based on crystallographically determined shortest intramolecular distances (see Figure 3.9, page 160) in compound 1 using molecule A [in brackets: molecule B in the crystal structure].

CH_2 (perp) to Ar-H (Å)	CH_2 (along) to Ar-H (Å)	
	3.01 [2.92]	3.04 [2.95]
2.49 [2.50]	0.32 [0.39]	0.30 [0.37]
2.51 [2.53]	0.34 [0.42]	0.32 [0.40]

Furthermore, because of the $1/r^6$ factor, the shorter distances have a larger effect on the measured NOE compared to longer distances. In the literature the NOE enhancement intensity has been calculated for rapid unhindered internal rotation of the methyl group of toluene. The calculated "apparent distance" is slightly greater (0-3 %) than the distance of closest approach.[31] Unfortunately, these results are not directly applicable to CH_2R groups without further assumptions with regard to various energy minima in the internal rotation profile of the CH_2R group.[31]

In the absence of a simple method for predicting the NOE ratio, it is *assumed* that only the shortest distances as shown in Table 3.7 contribute significantly to the observed NOE: an NOE ratio of 0.36 (the average of all NOE ratios shown in Table 3.7) is predicted.

When the aromatic proton at 6.94 ppm is saturated the methylene protons at -1.37 ppm experience a 2.4 % NOE, while the methylene protons at -0.76 ppm experience a 4.6 % NOE; the observed ratio is 2.4/4.6 = 0.52 (Figure 3.10, page 163).

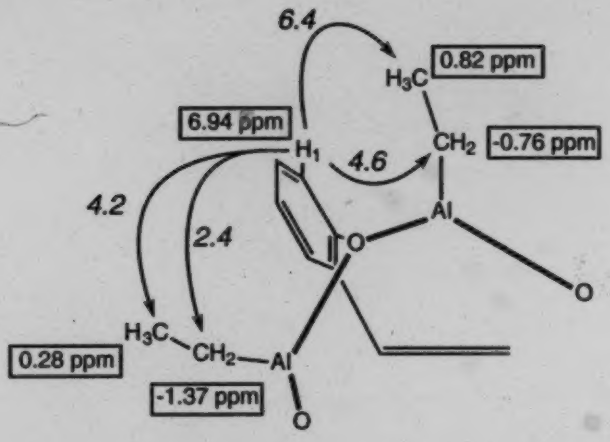

Figure 3.10. Measured NOE effects for equatorial ethyl groups (*in* %) of compound **1** (topview). Axial ethyl groups and other phenoxy- and aluminum-groups omitted for clarity.

Furthermore on saturation of the aromatic proton at 6.94 ppm, the proposed "equatorial" methyl groups reflect a similar effect; the CH_3 at 0.28 ppm (connected to the CH_2 at -1.37 ppm) shows an 4.2 % NOE, while the CH_3 at 0.82 ppm (connected to the CH_2 at -0.76 ppm) has a 6.4 % NOE.

Saturation of the CH_2 at -0.76 ppm results in a 11.2 % NOE at the aromatic proton at 6.94 ppm. When the CH_2 at -1.37 ppm is saturated, the aromatic proton at 6.94 ppm displays a NOE of 4.4 %; the observed ratio is 4.4/11.2 = 0.39 (Figure 3.11, page 164). The observed trend for the magnitude of the NOE, as expressed in the NOE ratio is the same: the *larger* NOE is observed for the equatorial methylene protons at -0.76 ppm assigned to C_{17} and C_{37}, while the equatorial methylene protons at -1.37 ppm assigned to C_{27} and C_{47} shows the *smaller* NOE as predicted. The calculated NOE ratio of 0.36 matches the observed ratio of 0.39 and 0.52 reasonably well considering the number of assumptions.

The remaining NOE observations are more difficult to interpret. On saturation of the -0.76 ppm equatorial methylene protons, the neighboring equatorial ethyl group experiences a negative NOE effect (see Figure 3.12,) through a relay proton, presumably the H_1 aromatic proton which shows a 11.2 % NOE effect (Figure 3.11). This "relay effect" is not observed on saturation of the -1.37 ppm equatorial methylene protons, presumably because the NOE of the aromatic "relay proton" (4.4 %) is weaker.

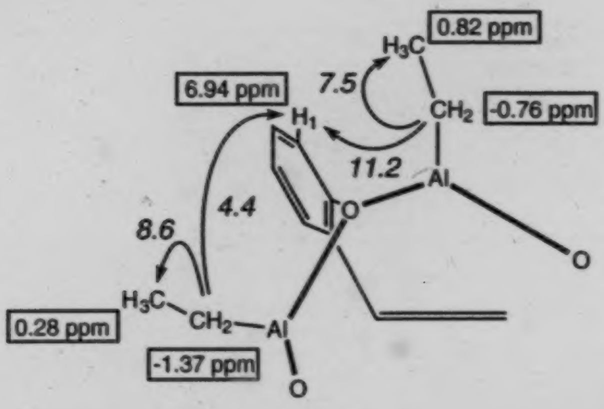
0.82 ppm
H3C
7.5
6.94 ppm
H1
CH2
-0.76 ppm
11.2
Al
4.4
O
8.6
O
H3C
CH2
Al
0.28 ppm
-1.37 ppm
O

Figure 3.11. Measured NOE effects for aromatic H and equatorial methyl groups (*in* %) of compound **1** (topview). Axial ethyl groups and other phenoxy- and aluminum-groups omitted for clarity.

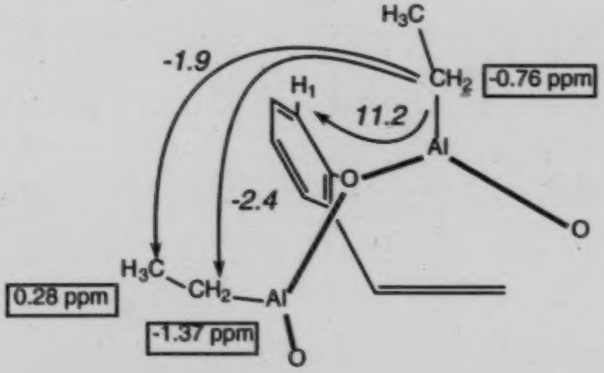
H3C
-1.9
CH2
-0.76 ppm
H1
11.2
Al
O
-2.4
O
H3C
CH2
Al
0.28 ppm
-1.37 ppm
O

Figure 3.12. Measured NOE effects on saturation of equatorial ethyl groups (*in* %) of compound **1** (topview). Axial ethyl groups and other phenoxy- and aluminum-groups omitted for clarity.

The assignment of the axial ethyl groups is possible using the present set of NOE data if the assumption that NOE effects can only be observed between axial and equatorial ethyl groups *bound to the same aluminum atom* holds. Although this seems reasonable based on the 1 / r^6 relation, this assumption makes the assignment less reliable in absence of further NOE data. Unfortunately the proton signals at 0.38, 0.48 and 1.14, 1.22 ppm are too close to each other to allow for selective saturation without influencing the nearest neighbour. When the -1.37 ppm equatorial methylene groups is saturated, the axial methylene group at 1.14 ppm and the corresponding methyl group at 0.38 ppm show an NOE effect (Fig. 3.13).

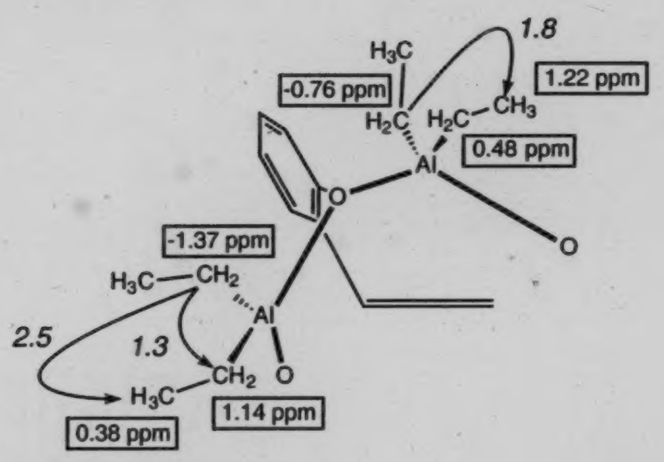

Figure 3.13. Measured NOE effects for axial ethyl groups (*in %*) of compound **1** (topview). Other phenoxy- and aluminum-groups omitted for clarity.

This axial ethyl group is therefore located along the double bond. When the -0.76 ppm equatorial methylene group is saturated, the axial methyl group at 1.22 ppm experiences a 1.8 % NOE. A tentative assignment of the ethyl ^{1}H-NMR chemical shifts of compound **1** is given in Figure 3.14 (page 166).

Keeping the restrictive assumptions in mind, it is possible that the NOE results are being overinterpreted: however, the observed match between theoretical prediction and experimental observation is both good and internally consistent. The NOE data thus do not contradict the proposal that the solution structure in non-Lewis basic solvents is similar to the solid state structure.

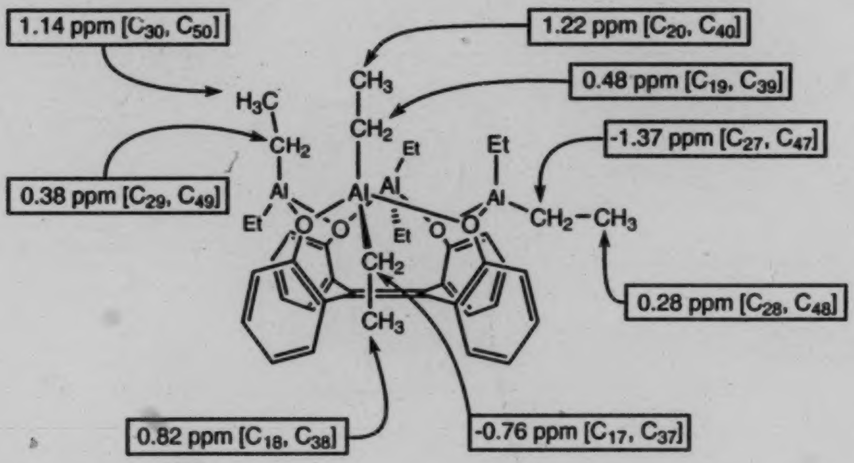
1.14 ppm [C_{30}, C_{50}]
1.22 ppm [C_{20}, C_{40}]
0.48 ppm [C_{19}, C_{39}]
-1.37 ppm [C_{27}, C_{47}]
0.38 ppm [C_{29}, C_{49}]
0.28 ppm [C_{28}, C_{48}]
0.82 ppm [C_{18}, C_{38}]
-0.76 ppm [C_{17}, C_{37}]
H_3C
CH_2
CH_3
CH_2
Et
Al
O
CH_2-CH_3

Figure 3.14. Tentative assignment of compound **1** ^{1}H-NMR signals of axial and equatorial ethyl groups. In [] brackets corresponding crystal structure carbon number

3.3.6 The disproportionation of compound 1.

In spite of the large number of publications on aluminum phenoxides and alkoxides, this type of disproportionation is not often reported. Furthermore compound **1** shows disproportionation, although no disproportionation has been reported for simple dialkylaluminum phenoxides.[5]

The first related disproportionation was reported by Mole[32] in 1966 for dimethylaluminum methoxide (eq. 3.8), which gave in THF or pyridine the insoluble methylaluminum dimethoxide. No disproportionation products of the more soluble dimethylaluminum iso-propoxide were observed in these ^{1}H-NMR spectroscopic studies. Apparently dimethylaluminum iso-propoxide does not undergo disproportionation in these solvents.

The limited solubility of the product was proposed to be the driving force for the reaction. Similar conclusions were reached by Nõth and Suchy who reported the disproportionation of alanes.[33]

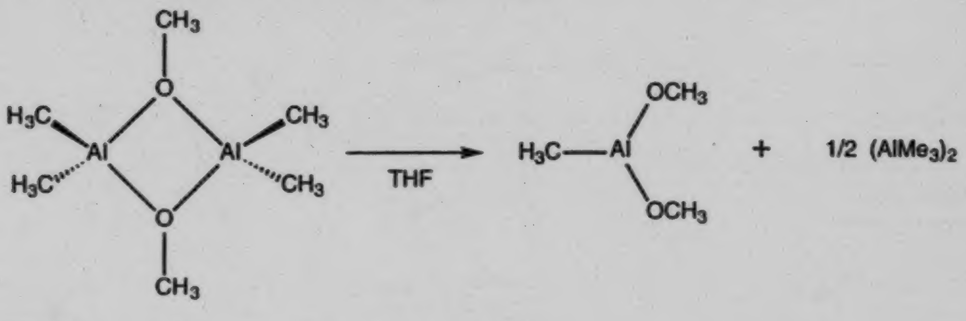

eq. 3.8

Pasynkiewicz reported[34] in 1978 the disproportionation of a diethylaluminum phenoxide in benzene (eq. 3.9) at room temperature. Because this reaction gave soluble products the formation of the triethylaluminum dimer was suggested as the actual driving force. A reinvestigation of this reaction by Ittel et al.[35] (eq. 3.9, page 168) showed that the disproportionation is actually an equilibrium, and not driven by the formation of the triethylaluminum dimer. They furthermore noticed that the aluminum bisphenoxide seems to form a more stable crystalline phase compared to the monophenoxide, thereby shifting the disproportionation in the direction of the aluminum bisphenoxide. The diethylaluminum phenoxides, as investigated by Ittel, et al.,[35] can be trapped as THF and Et_2O adducts in high yield (96 %), without any reported disproportionation simply by adding excess THF or Et_2O to the equilibrating reaction mixture.[36]

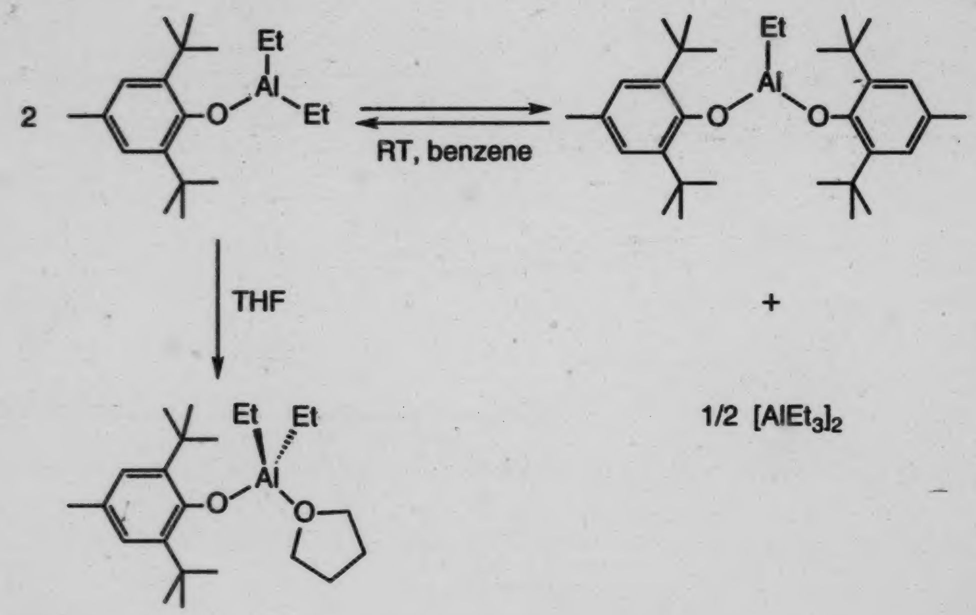

eq. 3.9

An alane disproportionation reaction was reported by Barron et al.[37] in 1993, using the same sterically hindered phenoxo ligand. Although the monophenoxide **A** (eq. 3.10, page 169) seemed stable, addition of *tert*-butylamine gave disproportionation products. Repeated crystallisation from diethyl ether also resulted in disproportionation. No further information on other products formed in the reaction was given.[37]

Unfortunately, these reports do not describe the mechanism of disproportionation. In order to observe a disproportionation a four-center transition state must be reached with an oxygen and an alkyl group bridging two aluminum atoms in compound **1**, if it is assumed that both alkyl exchange and disproportionation operate through the same mechanism.[38] However the mechanism operating for alkyl group exchange in the presence of Lewis bases, which could act as a model for the mechanism of the disproportionation, is *also* unclear.

Kinetic investigations on aluminum alkyl group exchange in the presence of diethyl ether and pyridine by Jeffery and Mole[39] suggest two possible scenarios: a reaction between two four-coordinate aluminum atoms, or a reaction between a three-coordinate aluminum, formed by a prior solvent dissociation, and a tetracoordinate aluminum. Brown and Murell reported[40] kinetic investigations of the alkyl-group exchange between trimethylaluminum·THF and dimethyl sulfide adducts, and did not find a rate-limiting dissociation. Instead a "base-assisted" exchange was proposed. In the "base-assisted" exchange, participation of the second unshared electron pair of the oxygen or sulphur was proposed to bring two aluminum atoms together prior to alkyl group exchange. Examples of alkyl group transfer between a four-coordinate and a three-coordinate aluminum group bound to the same alkoxy/aryloxy group are known.[41]

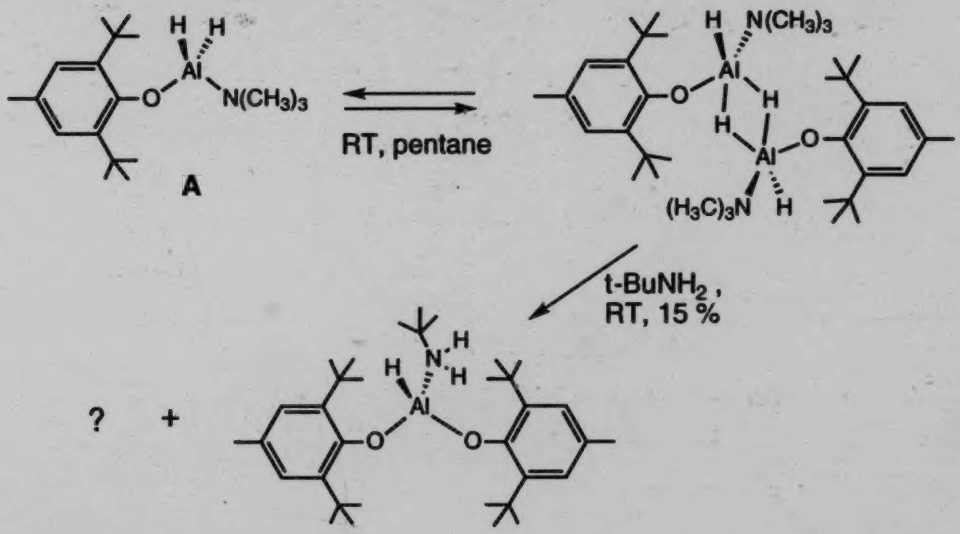

eq. 3.10

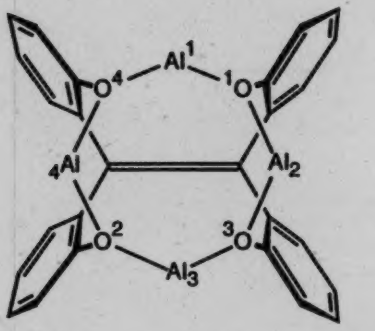

Al_1-Al_3 = 4.70 Å
Al_2-Al_4 = 5.03 Å
Al-C = 1.95 Å (av)
Al-O = 1.69 Å (av)

O_1-O_3 = 2.89 Å
O_2-O_4 = 2.89 Å
O_1-O_4 = 2.91 Å
O_2-O_3 = 2.92 Å

Figure 3.15. Non-bonding distances in compound **1** (topview) compared with covalent Al-C and Al-O bond distances . The aryl rings have been twisted slightly and ethyl groups have been removed for clarity.

In order to achieve a disproportionation transition state without the help of a Lewis basic solvent, the Al-O frame must become more flexible in order to bring the exchanging aluminum and alkyl group near to each other. The observed distances in the crystal structure (see Figure 3.15) combined with the rigidity of the tetradentate frame do not allow the formation of such a transition state, as indicated by the absence of a disproportionation reaction at higher temperatures in the absence of a Lewis basic solvent.

The ^{1}H-NMR spectrum of compound **1** recorded in THF-d_8 at low temperatures no longer shows the four distinct ethyl groups, instead a single ethyl group is observed. This is in contrast with the observations at low concentrations of THF. According to the measured chemical shifts no interaction takes place between the THF and the crown compound **1**.

In order to account for the huge excess of THF necessary to induce the disproportionation, a slow step is proposed (Scheme 3.1, page 172) to lead to a freely rotating aluminum group. Because of the geometry of this intermediate, at least 5 different ethyl group signals are expected in the ^{1}H-NMR spectrum, which is not observed at -50 ^{o}C. If this would be the result of a rapid equilibrium with the crown compound **1**, the axial and equatorial ethyl groups would average (Scheme 3.1, page 172) but not the position of the aluminum groups along the double bond and perpendicular to the double bond (Figure 3.7 and 3.14 page 157, 166). As a result a collapse of the *four* ethyl group signals would occur to give *two* ethyl group signals.

In order to account for the observed single ethyl group resonance at -50 ^{o}C at least two, but preferably more, freely rotating aluminum groups must be present. However, as *two* (three) freely rotating aluminum groups can only exchange *two* (three) positions the rapid averaging of all aluminum groups at -50 ^{o}C is severely compromised. If instead, a set of four freely rotating diethylaluminum groups is proposed as an intermediate in equilibrium with the crown compound **1**, all positions of the crown compound **1** could average, leading to a calculated chemical shift of -0.93 ppm for the quartet and a triplet at 0.87 ppm (average of four triplets and four quartets, see Figure 3.14, page 166).

The observed chemical shift for the intermediate in THF-d_8 is a quartet at -0.14 ppm and a triplet at 0.99 ppm. Although this observation can be made to fit the rapid equilibrium with the crown compound **1** by assuming a solvent/temperature-induced chemical shift for the quartet (-0.93 ppm calculated using data of an ^{1}H-NMR spectrum in CD_2Cl_2 at room temperature, -0.14 ppm recorded in THF-d_8 at -50 ^{o}C), a set of four freely rotating aluminum groups (Scheme 3.1, page 172) could accommodate the observed intermediate at

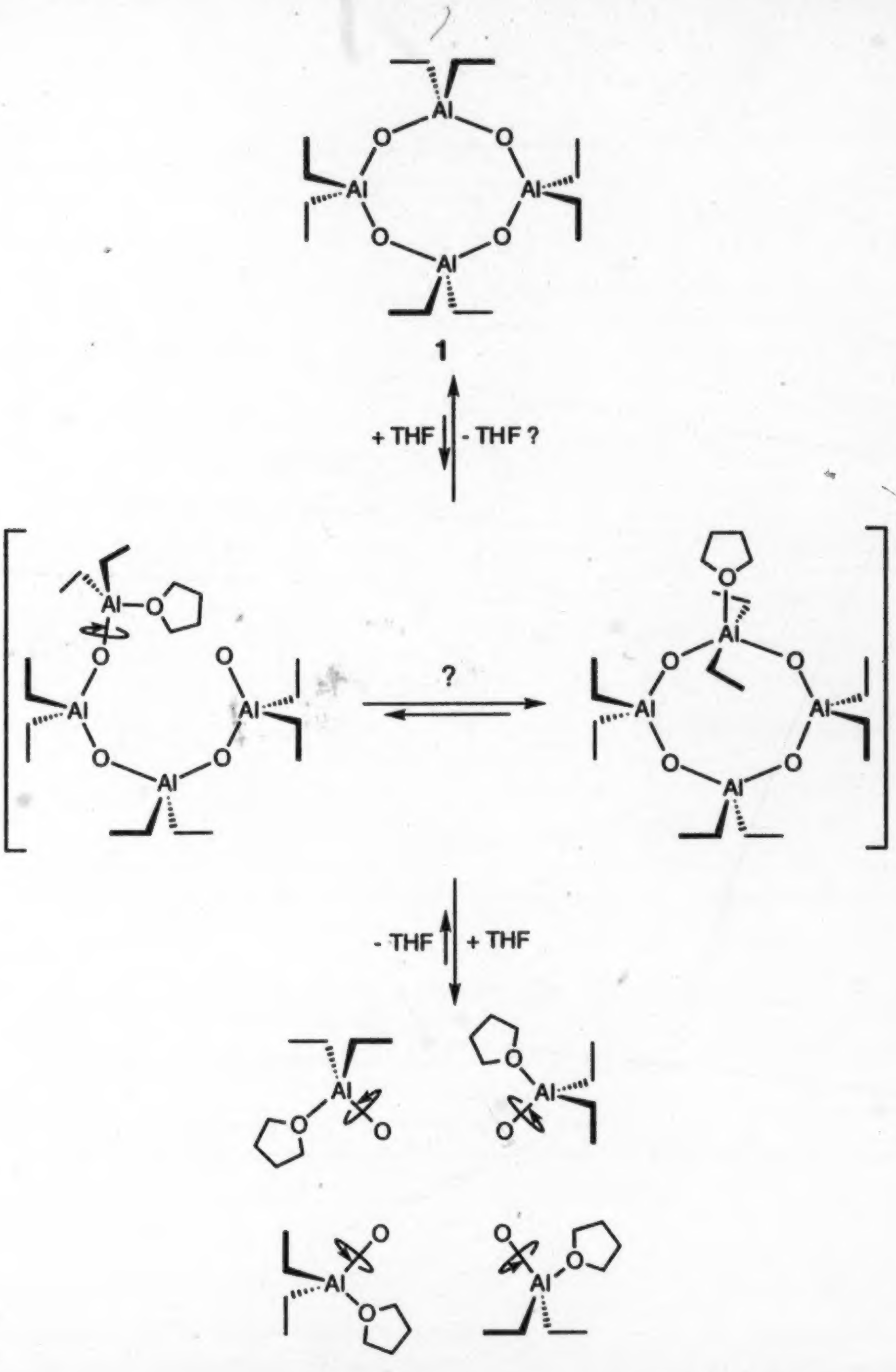

Scheme 3.1: Proposed averaging proces of ethyl groups in compound **1** in THF at low temperatures. Only the aluminum groups and the oxo-surface of compound **1** are shown for clarity.

-50 °C just as well. Such an intermediate would achieve the necessary flexibility for the aluminum and ethyl groups to form a disproportionation transition state[10,31,42] but on the basis of the information available no choice can be made between the two proposed possibilities. In the following discussion four freely rotating aluminum groups are assumed to be present.

The reason why the conversion of the crown compound **1** to the THF-coordinated compound **1** seems to be a "single step" at low temperatures could be the presence of a cooperative effect, whereby the first addition of THF is slow due to the unfavorable entropy change combined with the possible low enthalpy yield for ring opening as reflected by the negligible Lewis acidity[43] of compound **1**. After the first slow THF addition next additions could be much faster, rapidly leading to four THF-coordinated aluminum groups. Under these conditions, rotation around the aryl-ethene bond is unlikely to take place due to the size of the THF coordinated aluminum groups. This would limit the discussion of the disproportionation of compound **1** to aluminum redistribution reactions on the oxo-surface of the I_4 isomer (see section 2.3.1, page 74) of the tetraarylethene frame.

Because in THF-d_8 at -50 °C no additional intermediates are observed, rearrangements following after the formation of the freely rotating intermediate are proposed to be rapid.

Before continuing, a fundamental stereochemical difference between calix[4]arenes and *tetrakis*[2-hydroxyphenyl]ethenes must be pointed out. Whereas the calix[4]arene oxo-surface forms a square array of oxygen groups, the *tetrakis*[2-hydroxyphenyl]ethenes form a rectangular array of oxygen groups. As a result of these geometries a calix[4]arene acting as a bidentate ligand can form 2 diastereomers binding to a single metal, while a *tetrakis*[2-hydroxyphenyl]ethene ligand can form 3 diastereomers, one of which exists as an enantiomer pair (Scheme 3.2, page 175). If the calix[4]arene oxo-surface acts as a tridentate ligand binding a single metal atom only one isomer is possible, but the *tetrakis*[2-hydroxyphenyl]ethene ligand will form an enantiomer pair (Scheme 3.2, page 175). According to Figure 3.15 (page 170) the deviations from a square geometry are small, but small changes in the steric interactions of neighboring aryl rings and positioning of metal groups outside the rectangular array would enforce the stereochemical differences of the bound metals.

Because the energy differences between the possible diastereomers are expected to be small, in reaction schemes a distinction between possible intermediates is arbitrary and use can be made of a permutational approach (vide infra).[44] Such an approach will become necessary when the oxo-surface of the *tetrakis*[2-hydroxyaryl]ethene class of compounds is extended by modification beyond the O_4-surface in order to approach an O_n-surface.[45]

In the proposed mechanism (see Schemes 3.3 to 3.7) a set of intramolecular rearrangements and disproportionations, following the Jeffery and Mole[40] mechanistic proposal, is assumed to take place before a final dimerization of the end product to form compound **2**.

Based on the "local concentration" of aluminum groups, it is likely that an intramolecular reaction mechanism would compete effectively with any intermolecular dimerization. Another point that could be brought against a first step consisting of an intermolecular dimerization is that in the resulting dimer the double tetraarylethene frame imposes even more restrictions on the movement and closest approach of diethylaluminum groups. This would slow down, if not altogether prevent the disproportionation to the observed product.

Scheme 3.2: Stereoisomers for different coordination modes of calix[4]arenes and *tetrakis*[2-hydroxyphenyl]ethenes

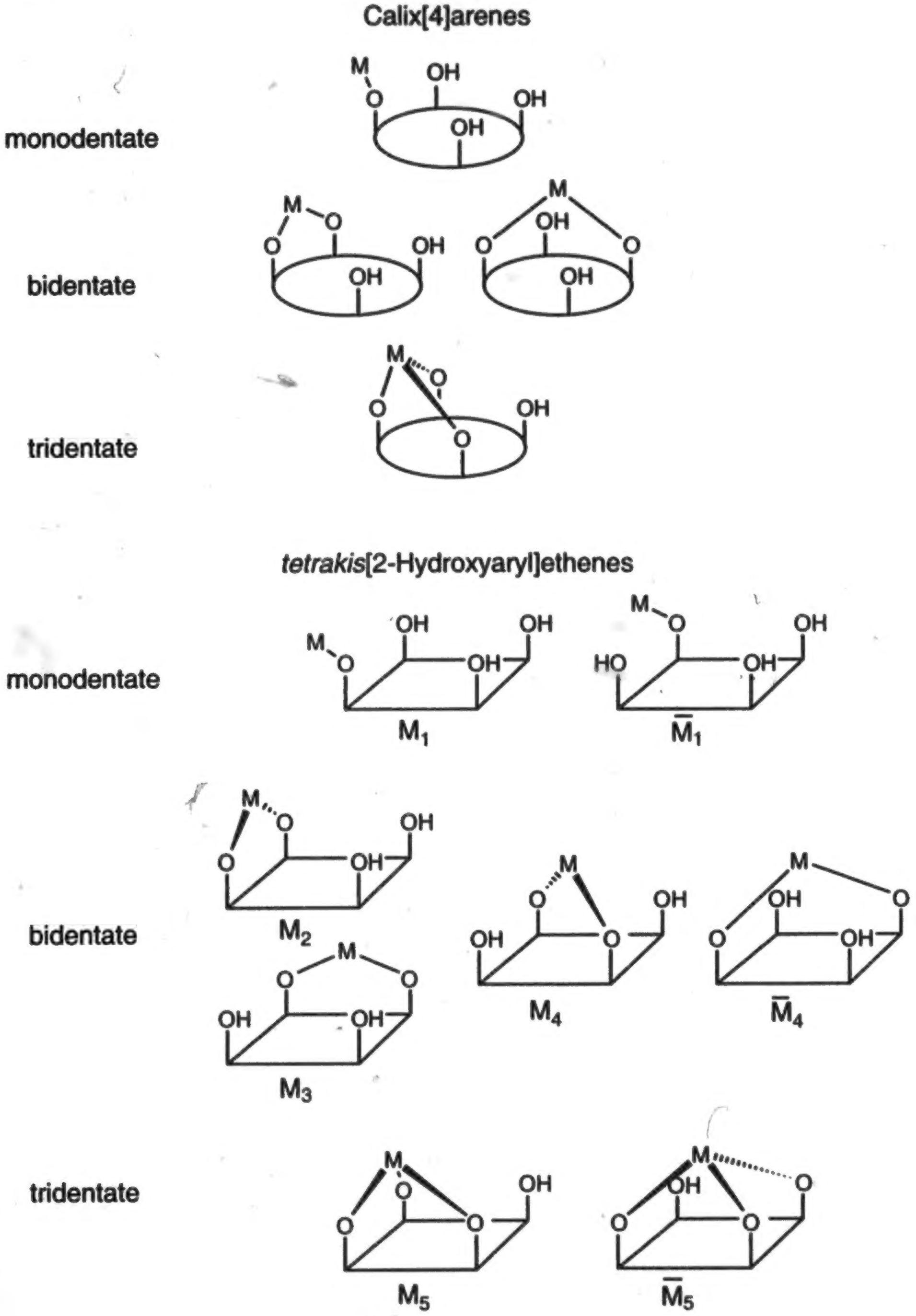

Calix[4]arenes

tetrakis[2-Hydroxyaryl]ethenes

monodentate
bidentate
tridentate
monodentate
bidentate
tridentate
M
O
OH
HO
M_1
$\overline{M}_1$
M_2
M_3
M_4
$\overline{M}_4$
M_5
$\overline{M}_5$

The first stage in the mechanism for the disproportionation of compound **1** starts (Scheme 3.3, page 177) from the proposed THF-coordinated ring opened compound. A four-center transition state is reached whereby two penta-coordinate aluminum centers bridge one ligand oxygen and an ethyl group. After expulsion of $Et_3Al{\cdot}THF$ an intermediate A or C is formed, depending on where the ethyl-donating group is located (*along* the double bond: 2 in Scheme 3.3, *perpendicular* on the double bond: 1 in Scheme 3.3).

The two possible intermediates A and C are proposed to undergo THF-mediated scrambling (Scheme 3.4, pages 178, 179) through a four-center transition state of tetra- and penta-coordinated aluminum atoms. Unlike the intermediates A and C the formed intermediate B exists as a pair of enantiomers and has two "dative" bonds to the central aluminum (not shown in Scheme 3.4, pages 178, 179). As a result of this, intermediate B is likely to be a thermodynamic sink considering the enthalpy of formation for a "dative" bond to be in the order of -19 to -36 kcal/mole.[9,13] Intermediate B might be able to undergo further rearrangements to form the intermediates A and C back, in which case the central aluminum accepts an ethyl group. If all possible rearrangement scenarios for B are followed, a second disproportionation by transfer of an ethyl group from the central aluminum can be envisioned. Through a four coordinate transition state containing two pentacoordinate aluminum atoms an enantiomeric intermediate D is formed after expulsion of $Et_3Al{\cdot}THF$ (Scheme 3.5, page 180).

The final step in the proposed reaction mechanism is the dimerisation of the D enantiomer pair (Scheme 3.6, page 181) to give the centrosymmetric compound **2**. The proposed overall reaction scheme is given in Scheme 3.7, page 182. (continued on page 183)

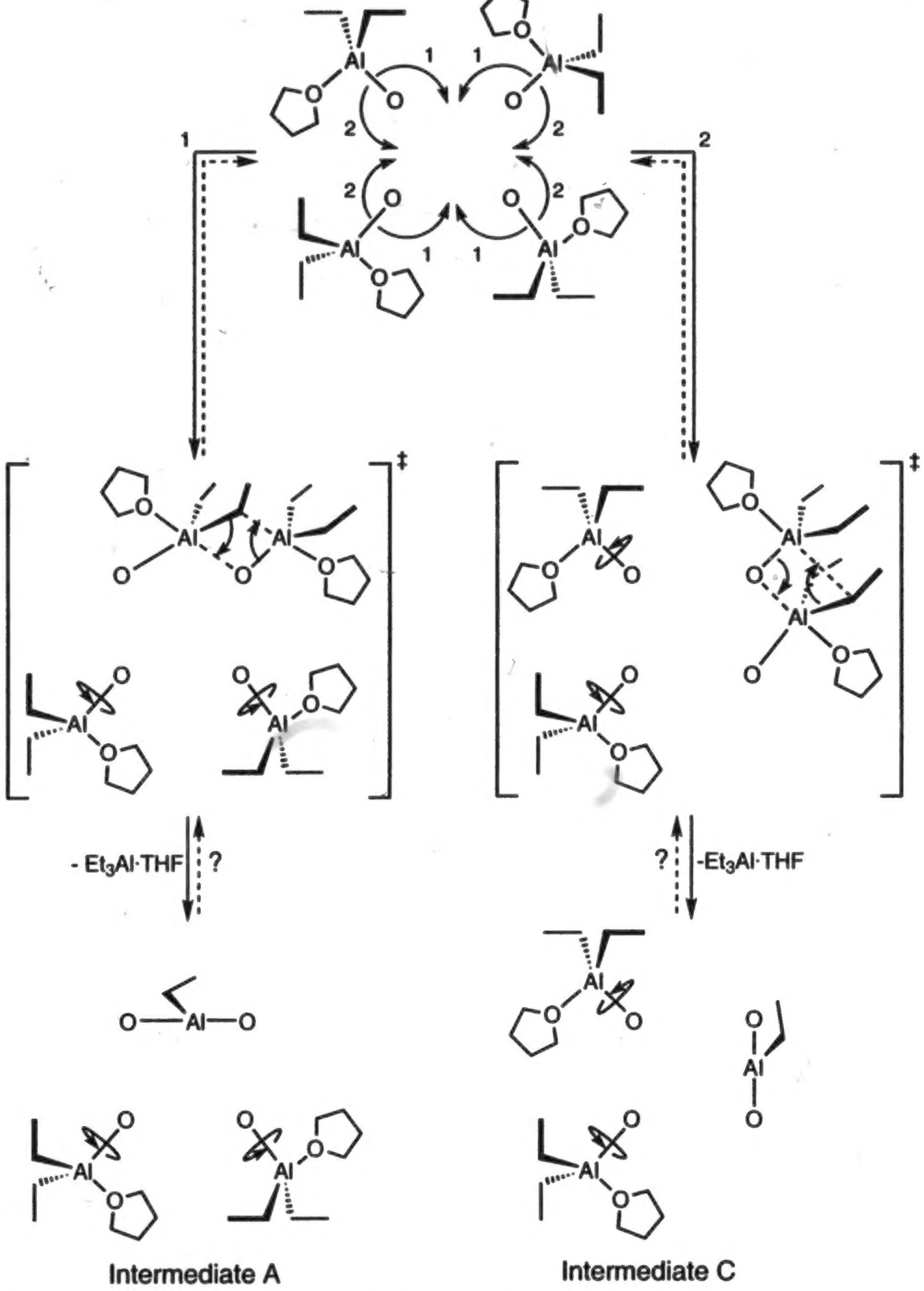
1
1
1
2
2
2
2
1
1
1
2
‡
‡
- Et3Al·THF
?
?
-Et3Al·THF
Intermediate A
Intermediate C

Scheme 3.3: Proposed disproportionation mechanism of compound **1** in THF, first stage. Only the oxo-surface and the aluminum groups located *above* the ethene bond are shown for clarity.

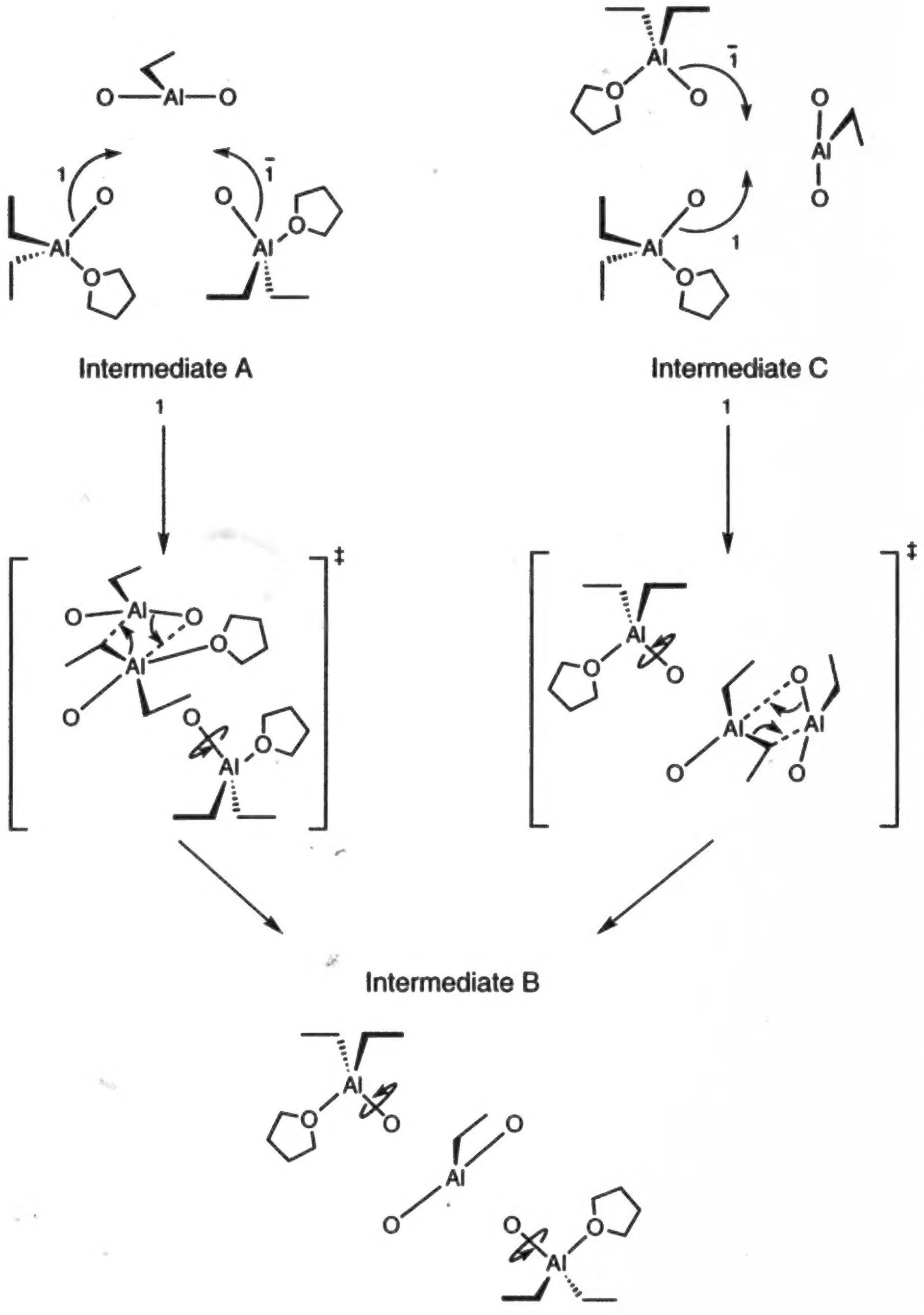
Intermediate A
Intermediate C
1
1̄
‡
Intermediate B
Al
O

Scheme 3.4: Proposed disproportionation mechanism of compound **1** in THF, intermediate interconversion. The formation of only a single enantiomer B of a pair is shown.

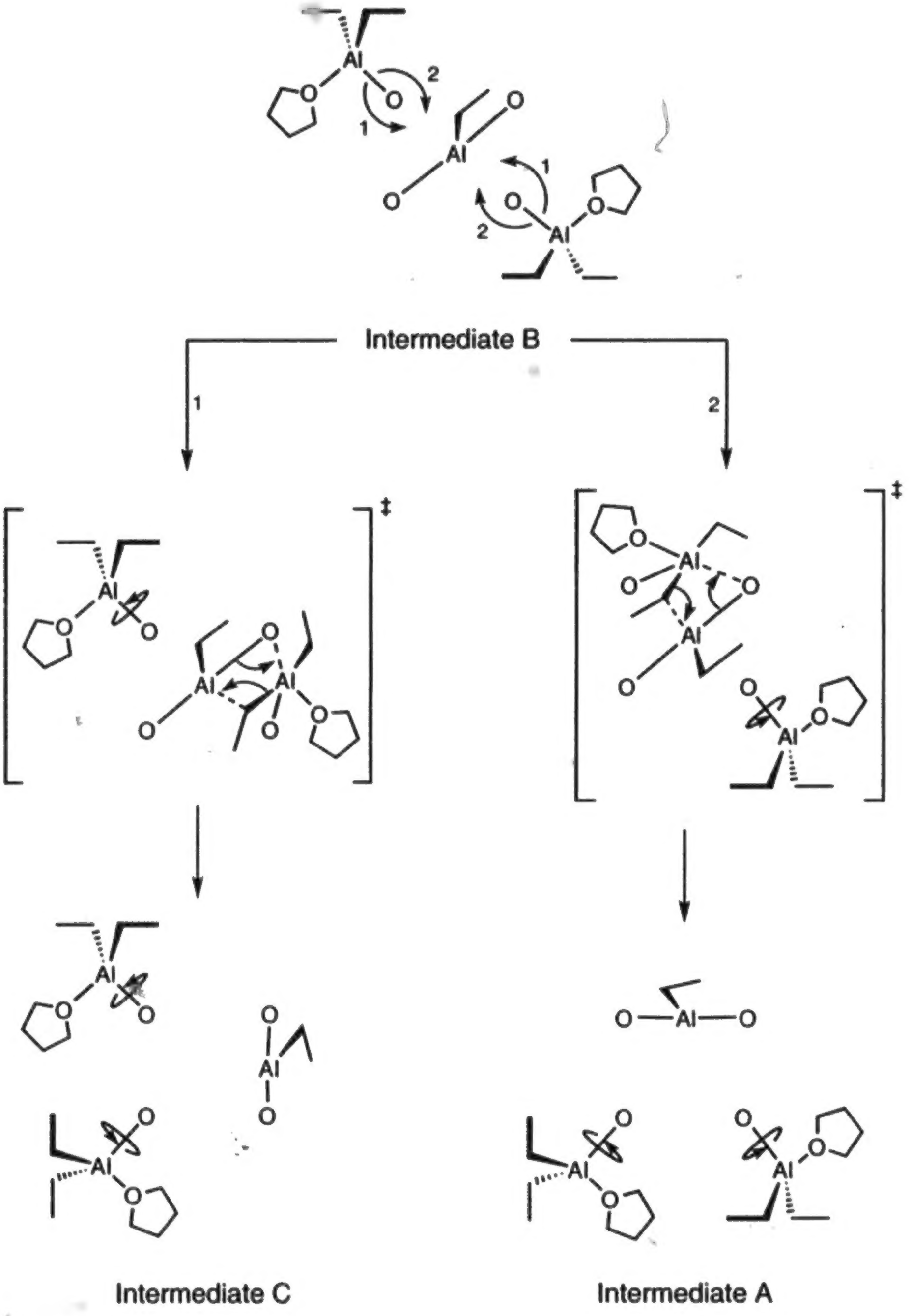
Al
O
1
2
Intermediate B
‡
Intermediate C
Intermediate A

Scheme 3.4 continued: Proposed disproportionation mechanism of compound **1** in THF, intermediate interconversion. Transfer of an ethyl group to the central aluminum atom. Only enantiomer B is shown.

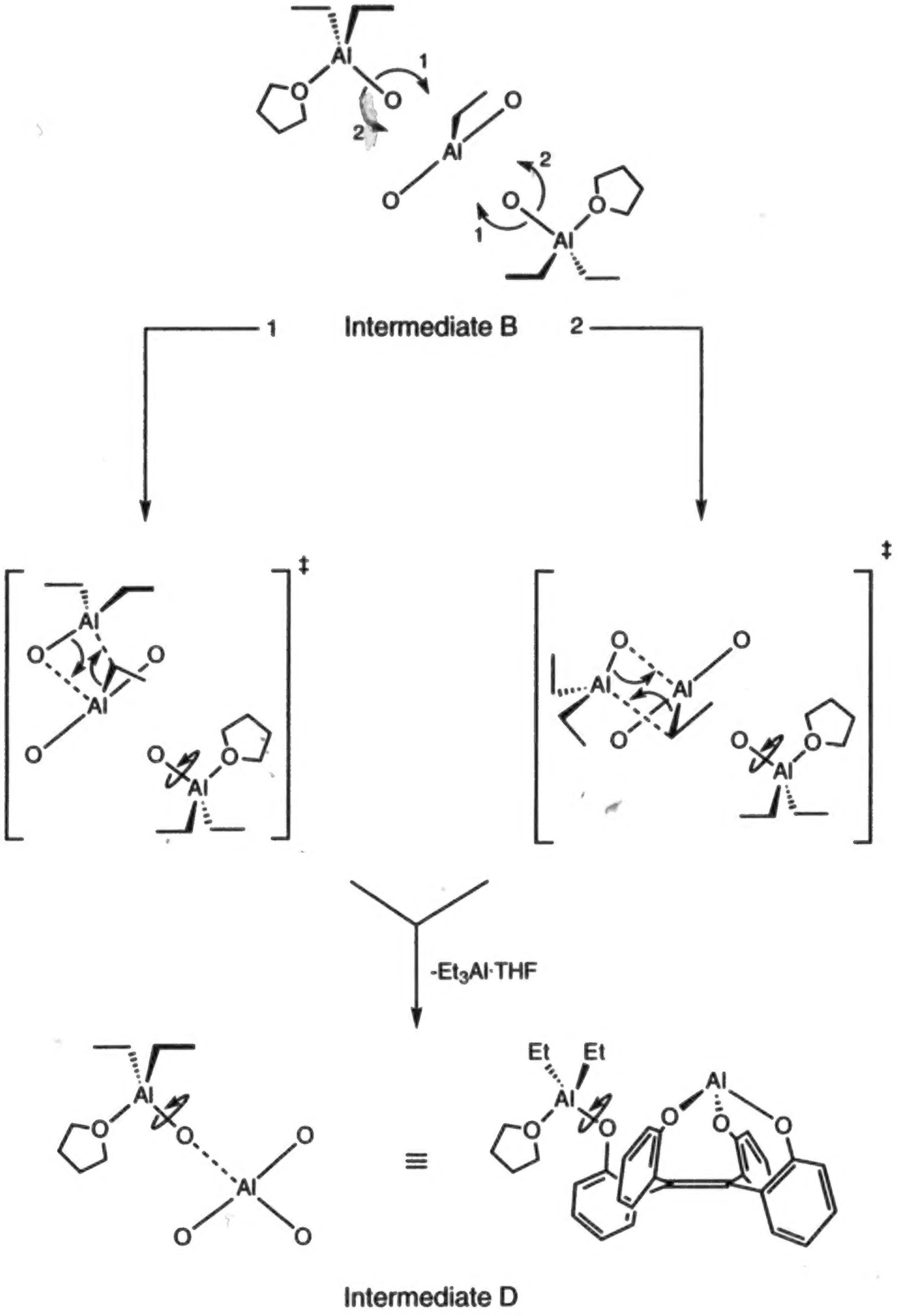
Al
O
1
2
Intermediate B
‡
-Et$_3$Al·THF
Et
Et
≡
Intermediate D

Scheme 3.5: Proposed disproportionation mechanism of compound **1** in THF, transfer of ethyl group from central aluminum.

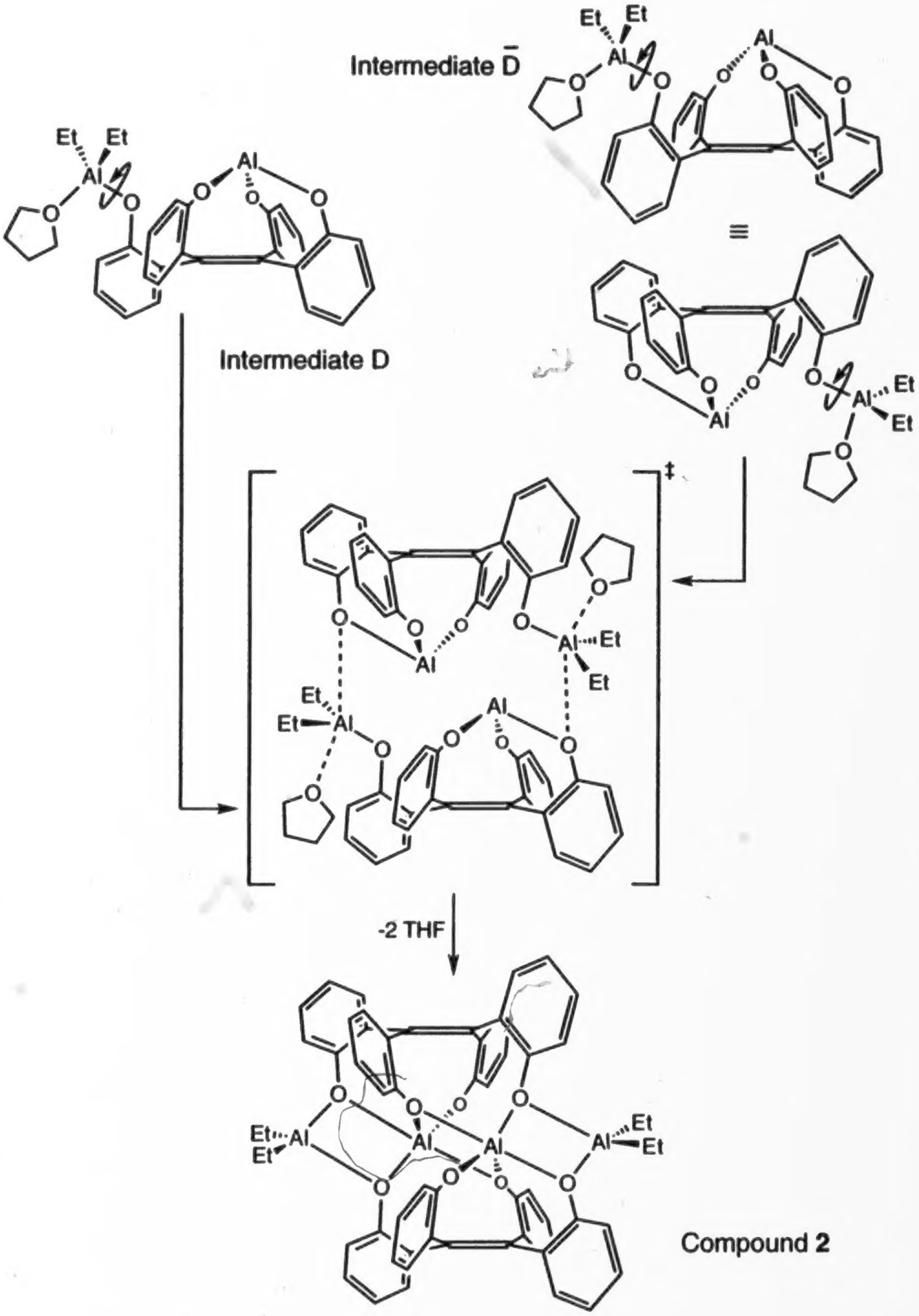
Intermediate D̄
Et
Et
Al
O
Al
O
O
O
≡
Intermediate D
‡
-2 THF
Compound **2**

Scheme 3.6: Proposed dimerisation of intermediate D, D̄, to form compound **2**

Scheme 3.7: Proposed disproportionation mechanism: overall reaction.

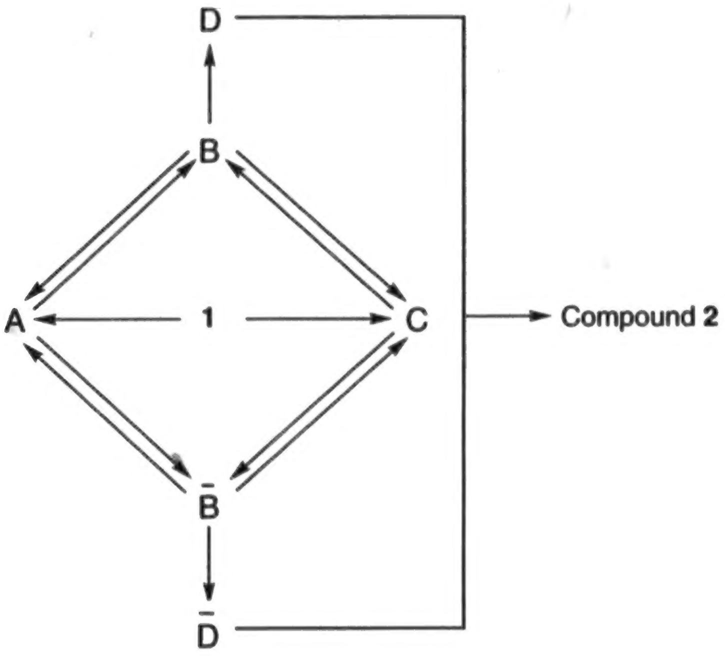
D
B
A
1
C
Compound **2**
$\bar{B}$
$\bar{D}$

(continued from page 176) Using the *ortho* propyl derivative of *tetrakis*[2-hydroxyphenyl]ethene the crystal structures of compounds related to the proposed intermediates A/C and D have been described in the thesis of Dr. M. Fujita[46] together with an alternative disproportionation mechanism. It is tempting to ascribe the formation of the chloroaluminum product **4** to a disproportionation of a corresponding crown-like compound. Unfortunately, the incomplete characterisation of the initial products does not allow such a conclusion. Such crown-like products consisting of four ethylaluminum chloride groups could, assuming rigidity, in theory form up to 20 methylene quartets in the ^{1}H-NMR spectrum corresponding to 8 possible isomers the assignment of which would be a major undertaking.

3.4 Experimental

General.

See General in Experimental section of Chapter 2, page 94.

Tetrakis[2-diethylaluminoxyphenyl]ethene 1.

In the glovebox, 0.42 g (1.1 mmol) of *tetrakis*[2-hydroxyphenyl]ethene was suspended in 20 ml of pentane. Slowly a solution of 0.70 g Et_3Al (6.1 mmol, 5.6 eq.) in 10 mL of pentane was added under rapid stirring. An instantaneous vigorous reaction accompanied by a release of ethane resulted. After 10 minutes the vessel was stoppered and stirred overnight at room temperature. When stirring was stopped at the end of the reaction period, the resulting suspension settled. The top layer was removed and the sludge resuspended in pentane. This procedure was repeated twice. The so obtained material was dried under vacuum to give 0.51 g (65% yield) of a white, moderately air and water sensitive solid.

IR (neat): 2932, 2902, 2864, 1482, 1443, 1196, 829, 766, 689, 666 cm^{-1}; ^1H NMR (400 MHz, CD_2Cl_2): δ 7.31 (m,4H, Ar-H), 7.06 (m,8H, Ar-H), 6.94 (m, 4H, Ar-H), 1.22 (t, J = 8.0 Hz, 6H, Al-CH_2-CH_3), 1.14 (t, J = 8.0 Hz, 6H, Al-CH_2-CH_3), 0.82 (t, J = 8.0 Hz, 6H, Al-CH_2-CH_3), 0.28 (t, J = 8.0 Hz, 6H, Al-CH_2-CH_3), 0.48 (q, J = 8.0 Hz, 4H, Al-CH_2-CH_3), 0.38 (q, J = 8.0 Hz, 4H, Al-CH_2-CH_3), -0.76 (q, J = 8.0 Hz, 4H, Al-CH_2-CH_3), -1.37 (q, J = 8.0 Hz, 4H, Al-CH_2-CH_3). ^1H NMR (400 MHz, THF-d_8, -50 °C): δ 7.13 (bd, J = 7.0 Hz, 4H, Ar-H), 6.61 (bt, J = 7.0 Hz, 4H, Ar-H), 6.34 (bd, J = 8.0 Hz, 4H, Ar-H), 6.22 (bt, J = 7.0 Hz, 4H, Ar-H), 0.99 (bt, J = 8.2 Hz, 24H, Al-CH_2-CH_3), -0.14 (bq, J = 8.2 Hz, 16H, Al-CH_2-

CH_3).^{13}C NMR (75.5 MHz, $CDCl_3$): δ -0.32 (Al-*CH_2*-CH_3, br), 0.51 (Al-*CH_2*-CH_3, br), 0.93 (Al-*CH_2*-CH_3, br), 1.45 (Al-*CH_2*-CH_3, br), 7.6 (Al-CH_2-*CH_3*), 8.3 (Al-CH_2-*CH_3*), 9.1 (Al-CH_2-*CH_3*), 9.3 (Al-CH_2-*CH_3*), 125.5 (Ar), 126.0 (Ar), 128.6 (Ar), 129.5 (Ar), 133.5 (Ar), 149.6 (Ar), 139.3 (ethene C); MS(EI) 731.2[13, M^+-1], 704.4[21], 703.4[49], 621.2[11], 617.3[14], 605.2[16], 590.3[39], 589.3[100]. EA Calculated for $C_{42}H_{56}Al_4O_4$: C, 68.84; H, 7.70, Found: C, 68.59; H, 8.02.

X-ray quality crystals were obtained by recrystallization from toluene at -30 °C. Crystal data (see appendix D page 345 for details) for *tetrakis*[diethylaluminum-2-phenoxo]ethene·0.5 toluene ($C_{45.5}H_{60}Al_4O_4$): crystal dimensions 0.74 x 0.33 x 0.19 mm, triclinic, space group P1(No. 2), a = 12.7113(5), b = 17.9077(7), c = 20.9008(9) (Å), α = 78.881(3), β = 74.132(3), γ = 83.404(3) (°), V = 4480.7(3), Z = 4, ρ_{calcd} = 1.155 (g cm^{-3}), μ = 1.270 (mm^{-1}). Data collection and refinement conditions: Siemens P4/RA diffractometer using graphite-monochromated Cu Kα radiation (λ[Å] = 1.54178), T = 213 (K), scan mode θ–2θ, 2θ limit 115.0 (°); 12078 measured reflections, 11424 independent reflections, 8507 included in the refinement ($F_o^2 \geq 2\sigma(F_o^2)$), structure solution by direct methods (*SHELXS–86*), refinement by full-matrix least-squares on F^2 (*SHELXL–93*), data correction by Gaussian integration (face-indexed) (transmission max./min. = 0.9269/0.4395), 966 parameters, H atoms in geometrically calculated positions, R_1 = 0.0858 (based on 8507 observed data), wR_2 = 0.2546 (based on all 11418 data), residual electron density 0.791 / –0.588 e $Å^{-3}$.

THF titration of *tetrakis*[2-diethylaluminoxyphenyl]ethene 1.

A 18 mM solution of compound **1** in toluene-d_8 was prepared by dissolving 13.4 mg compound **1** in 1.0 mL dry, oxygen free toluene-d_8. A microliter syringe was used for the titration. After each addition of 0.5 µL THF, the solution was mixed, and an ^{1}H-NMR spectrum was recorded. Results are described in the chapter text.

Crotonaldehyde complexation of *tetrakis*[2-diethylaluminoxyphenyl] ethene 1.

A 31 mM solution of compound **1** in CD_2Cl_2 was prepared by dissolving 22.7 mg compound **1** in 1.0 ml dry oxygen-free CD_2Cl_2. A crotonaldehyde solution was made by dissolving 0.1340 g oxygen-free crotonaldehyde (dried over anhydrous calcium chloride, and deoxygenated by three freeze-pump-thaw cycles) in 0.92 g dry oxygen-free CD_2Cl_2 (d: 1.362 g/mL). Of this solution 10 µL (1 eq.) was added to the NMR solution of compound **1** at -78 ^{o}C; crotonaldehyde-induced disproportionation has been previously reported with a reaction with ethylaluminum chlorides.[42] Due to limited solubility of compound **1** at low temperatures, the ^{1}H-NMR spectrum showed broad signals. When the suspension was brought to room temperature, the signals turned sharp, but the ratio of compound **1**/crotonaldehyde according to the integral remained 1/1.4. After removal of the NMR tube from the magnet, the suspension was shaken, and all of the separated material went back into solution to give a compound **1**/crotonaldehyde ratio of 1/0.53. Results are described in the Chapter text. ^{1}H-NMR spectrum of free crotonaldehyde (98 % trans, 400 MHz, room temperature, CD_2Cl_2): δ 9.476 (d, J = 7.9 Hz, 1H, H_1 in figure 8), 6.872 (dq, J = 7.0, 15.4 Hz, 1H, H_3), 6.103 (ddq, J = 1.8, 7.9, 15.4 Hz, 1H, H_2), 2.007 (dd, J = 1.8, 7.0 Hz, 3H, H_4).

Polymerization trials using *tetrakis*[2-diethylaluminoxyphenyl] ethene 1.

a) In a glovebox 4.3 mg (10 µmol) dichloro[*rac*-ethylenebis(indenyl)]-zirconium(IV),[7] and 11.7 mg (12 µmol) compound **1** were dissolved in 10 mL dry, oxygen-free toluene, and stirred for 35 min. After transfer to a crown-cap bottle, the solution was pressurized with 30 psig ethene. After 10 minutes the reaction was quenched using 3 mL of an ethanol/HCl solution. No polyethylene was formed. A similar run using 6 equivalents of compound **1** returned the same result.

b) In a glovebox 5.1 mg (12 µmol) dichloro[*rac*-ethylenebis(indenyl)]-zirconium(IV)[7] and 11.1 mg (97 µmol) Et_3Al were dissolved in 10 ml dry, oxygen-free toluene.[7] After 40 minutes, 12.6 mg (13 µmol) compound **1** was added. After another 40 minutes, the solution was transferred to a crown-cap bottle and pressurized with 30 psig ethene. After 10 minutes the reaction was quenched with 3 mL of an ethanol/HCl solution. No polyethylene was formed.

Disproportionation of *tetrakis*[2-diethylaluminoxyphenyl]ethene 1 in THF: synthesis of compound 2.

Compound **1** (0.205 g) was dissolved in 20 mL dry, oxygen-free THF in a glovebox. After stirring the solution for 14 hours, the solvent was removed under vacuum and the resulting sludge stirred up with 20 mL of pentane. After removal of the pentane, the solid was kept under high vacuum while being heated with an infrared lamp for 5 days. 84 mg (60 %) compound **2** containing a trace of THF was obtained.

IR(solv. cast): 2861, 1597 ,1472, 1449, 754, 693, 651 cm^{-1}. Mass(EI, DIP at 400 ^{o}C): 1006.2 [M^{+}-3], 866.4 [62], 474.8 [23]. ^{1}H-NMR (400 MHz, THF-d_8): δ 7.49 (dd, J = 1.0, 8.0 Hz, 2H), 7.29 (dd, J = 1.8, 7.6 Hz, 2H), 7.18 (dd, J = 1.8, 7.6 Hz, 2H), 7.07 (dd, J = 2.0, 7.4 Hz, 2H), 6.97 (m, 6H), 6.86 (m, 4H), 6.74 (m, 2H), 6.67 (m, 2H), 6.62 (m, 2H) 6.42 (m, 6H), 6.24 (td, J = 7.2, 1.0 Hz, 2H), 1.17 (t, J = 9.6 Hz, 12H), 0.12 (q, J = 9.6 Hz, 8H). ^{1}H-NMR (400 MHz, CD_2Cl_2): δ 7.34 (m, 2H), 7.29 (dd, J=1.8, 8.0 Hz, 2H), 7.20 (m, 6H), 7.12 (m, 6H), 7.05 (m, 4H), 6.94 (td, J = 7.4, 1.0 Hz, 2H) 6.88 (m, 2H), 6.84 (dd, J = 1.0, 8.0 Hz, 2H), 6.76 (td, J = 7.4, 1.0 Hz, 2H), 6.68 (td, J = 7.2, 1.0 Hz, 2H), 6.58 (dd, J = 7.5, 1.8, 2H), 0.97 (X part AA'X_3, t, $J_{apparent}$ = 8.0 Hz, 6H, Al-CH_2-$\mathit{CH_3}$), 0.32 (AA' part AA'X_3 m, 4H, Al-$\mathit{CH_2}$-CH_3), -0.02 (X part ABX_3, t, $J_{apparent}$ = 8.2 Hz, 6H, Al-CH_2-$\mathit{CH_3}$), -1.14 (A part ABX_3, m, 2H, Al-$\mathit{CH_2}$-CH_3), -1.34 (B part ABX_3, m, 2H, Al-$\mathit{CH_2}$-CH_3)

Disproportionation of *tetrakis*[2-diethylaluminoxyphenyl]ethene 1 in acetonitrile.

When compound **1** was dissolved in dry, oxygen-free acetonitrile-d_3 within minutes a white suspension formed, from which X-Ray quality crystals of compound **2** started to grow at room temperature. The ^{1}H-NMR spectrum of these crystals, using THF-d_8 as solvent, was identical with the ^{1}H-NMR spectrum of the compound obtained from the disproportionation of compound **1** in THF. Crystal data (see also appendix E, page 357) for compound **2** ($C_{60}H_{52}Al_4O_8$): monoclinic, space group $P2_1$(a nonstandard setting of $P2_1/c$ [No. 14]) , a = 13.5609(16), b = 10.6880(13), c = 17.991(2) (Å), β = 94.644(3) (°), V = 2599.0(5), Z = 2, ρ_{calcd} = 1.289 (g cm^{-3}), μ = 0.146 (mm^{-1}). Data Collection and Refinement Conditions: Bruker P4/RA/SMART 1000 CCD diffractometer using graphite-monochromated Mo Kα radiation (λ[Å] = 0.71073), T = 193 (K), scan type: ϕ rotations(0.3°)/ω scans(0.3°)(30 s exposures) limit 51.50 (°); 13696 measured reflections, 4937 independent reflections, 1831 included in the refinement ($F_o^2 \geq 2\sigma(F_o^2)$), structure solution by direct methods (*SHELXS–86*), refinement by full-matrix least-squares on F^2 (*SHELXL–93*), data correction by

Gaussian integration (face-indexed) (transmission max./min. = 0.9280/0.6890), 325 parameters, H atoms in geometrically calculated positions, R_1 = 0.0556 (based on 1831 observed data), wR_2 = 0.1154 (based on all 4937 data), residual electron density 0.301 / –0.267 e Å^{-3}.

Tetrakis[2-dimethylaluminoxyphenyl]ethene 3.

In the glovebox, 32 mg (81 μmol) of *tetrakis*[2-hydroxyphenyl]ethene was suspended in 5 ml of toluene. Slowly a solution of 31 mg Me_3Al (0.43 mmol, 5.3 eq.) in 5 mL of toluene was added under rapid stirring. Slowly the ligand dissolved, to form a yellow solution. No gas evolution was observed. After 30 minutes stirring, solvent and excess Me_3Al were removed under vacuum.

IR (neat): 2926, 1483, 1443, 1205, 1171, 886, 788, 767, 686, 615 cm^{-1}; ^1H NMR (400 MHz, CD_2Cl_2): δ 7.30 (m,4H, Ar-H), 7.04 (m,8H, Ar-H), 6.78 (m, 4H, Ar-H), -0.26 (s, 6H), -0.40 (s, 6H), -1.32 (s, 6H), -1.94 (s, 6H). MS(EI) 606.1[20], 605[52], 534[37], 533[100], 517[23], 503[31], 462[13], 461[42], 445[9], 57[25]. EA Calculated for $C_{34}H_{40}Al_4O_4$: C, 68.84; H, 7.70, Found: C, 68.59; H, 8.02.

The reaction of *tetrakis*[2-hydroxyphenyl]ethene with diethylaluminum chloride: compound 4.

In the glovebox to a suspension of 37 mg (93 μmol) *tetrakis*[2-hydroxyphenyl]ethene in 10 ml pentane was added under stirring 245 mg (0.5 mmol) Et_2AlCl as a 25 wt % solution in toluene dissolved in 5 ml pentane. A bright yellow suspension formed. No ethane formation was observed. After stirring overnight the solvent was removed under vacuum and the remaining residue resuspended in pentane. After removal of the pentane, the solid was dissolved in a minimum amount of toluene and placed in a -30 °C freezer inside the glovebox. After addition of a small amount of THF to the solution crystals were obtained of sufficient quality for an X-ray diffraction experiment. Crystal data (see appendix F, page 363 for details) for Compound 4·2 toluene ($C_{64}H_{58}Al_4Cl_2O_{10}\cdot 2\ C_7H_8$): crystal dimensions 0.27 x 0.23 x 0.21 mm, triclinic, space group P_1(No. 2), $a = 12.1840(13)$, $b = 12.891(2)$, $c = 13.5568(13)$ (Å), $\alpha = 66.485(9)$, $\beta = 87.343(8)$, $\gamma = 62.822(9)$ (°), $V = 1712.6(3)$, $Z = 1$, $\rho_{calcd} = 1.309$ (g cm^{-3}), $\mu = 0.270$ (mm^{-1}). Data collection and refinement conditions: Siemens P4/RA diffractometer using graphite-monochromated Mo Kα radiation (λ[Å] = 0.71073), $T = 213$ (K), scan mode θ–2θ, 2θ limit 50.0 (°); 5815 measured reflections, 5519 independent reflections, 3334 included in the refinement ($F_o^2 \geq 2\sigma(F_o^2)$), structure solution by direct methods (*DIRDIF-96*), refinement by full-matrix least-squares on F^2 (*SHELXL–93*), data correction by Gaussian integration (face-indexed) (transmission max./min. = 0.9930/0.9478), 422 parameters, H atoms in geometrically calculated positions, $R_1 = 0.0783$ (based on 3334 observed data), $wR_2 = 0.2168$ (based on all 5518 data), residual electron density 1.202 / –0.503 e Å^{-3}.

3.5 Notes and References.

1. Lehn, J.M. Supramolecular Chemistry, VCH: Weinheim, Germany, **1995**.
2. Bachand, B.; Wuest, J.D. *Organometallics* **1991**, *10*, 2015-2025. Vaugeois, J.; Simard, M.; Wuest, J.D. *Organometallics* **1998**, *17*, 1215-1219. Wuest, J.D.; *Acc. Chem. Res.* **1999**. *32*, 81-89.
3. Zhou, J.; Lancaster, S.J.; Walker, D.A.; Beck, S.; Thornton-Pett, M.; Bochmann, M. *J. Am. Chem. Soc.* **2001**, *123*, 223-237.
4. Piers, W.E.; Irvine, G.J.; Williams, V.C. *Eur. J. Inorg. Chem.* **2000**, 2131-2142. Li, L.; Stern, C.L.; Marks, T.J. *Organometallics* **2000**, *19*, 3332-3337.
5. Jeffery, E.A.; Mole, T. *Aust. J. Chem.* **1968**, *21*, 2683-2696. Starowieyski, K.B.; Pasynkiewicz, S.; Skowronska, M.D. *J. Organomet. Chem.* **1971**, *31*, 149-155.
6. Shreve, A.P.; Mulhaupt, R.; Fultz, W.; Calabrese, J.; Robbins, W.; Ittel, S.D. *Organometallics* **1988**, *7*, 409-416. Siedle, A.R.; Newmark, R.A.; Lamanna, W.M.; Schroepfer, J.N.; *Polyhedron* **1990**, *9*, 301-308.
7. Samuel,E.; Rausch, M.D. *J. Am. Chem. Soc.*, **1973**, *95*, 6263-6267. Chien, J.C.W.; Xu, B. *Makromol. Chem., Rapid Commun.* **1993**, *14*, 109-114.
8. Childs, R.F.; Mulholland, D.L.; Nixon, A. *Can. J. Chem.* **1982**, *60*, 801-808. Stecher, H.A.; Sen, A.; Rheingold, A.L. *Inorg. Chem.* **1988**, *27*, 1132-1133. See also Laszlo, P.; Teston, M. *J. Am. Chem. Soc.* **1990**, *112*, 8750-8754.
9. Similar crown structures have been observed for eight-membered hetero- and carbocyclic rings, see: Glass, R.S. (ed.) Conformational analysis of medium sized heterocycles; VCH Publishers: New York, 1988.

10. Healy, M.D.; Wierda, D.A.; Barron, A.R. *Organometallics* **1988**, *7*, 2543-2548. Cetinkaya,B.; Hitchcock, P.B.; Jasim, H.A.; Lappert, M.F.; Williams, H.D. *Polyhedron* **1990**, *9*, 239-243. Healy, M.D.; Ziller, J.W.; Barron, A.R. *Organometallics* **1992**, *11*, 3041-3049.

11. Kumar, R.; Sierra, M.L.; de Mel, V.S.; Oliver, J.P. *Organometallics* **1990**, *9*, 484-489. Mehrotra, R.C.; Rai, A.K. *Polyhedron* **1991**, *10*, 1967-1994.

12. Oliver, J.P.; Kumar, R. *Polyhedron* **1990**, *9*, 409-427. Taghiof, M.; Heeg, M.J.; Bailey, M.; Dick, D.G.; Kumar, R.; Hendershot, D.G.; Rahbarnoohi, H.; Oliver, J.P. *Organometallics* **1995**, *14*, 2903-2917. Yearwood, B.; Ul Ghazi, S.; Heeg, M.J.; Richardson, N.; Oliver, J.P. *Organometallics* **2000**, *19,* 865-871.

13. Huheey, J.E. *Inorganic Chemistry*, Third Edition, Harper & Row Publishers, New York, **1983**, p. 258.

14. Healy, M.D.; Ziller, J.W.; Barron, A.R. *J. Am. Chem. Soc.* **1990**, *112*, 2949-2954. Barron, A.R.; Dobbs, K.D.; Francl, M.M. *J. Am. Chem. Soc.* **1991**, *113*, 39-43. Barron, A.R. *Polyhedron* **1995**, *14*, 3197-3207.

15. Petrie, M.A.; Olmstead, M.M.; Power, P.P. *J. Am. Chem. Soc.* **1991**, *113*, 8704-8708.

16. Robinson, G.H. (ed.) Coordination Chemistry of Aluminum, VCH Weinheim, Germany, **1993**; Chapter 1.

17. Haaland, A. *Angew. Chem., Int. Ed. Engl.* **1989**, *28*, 992-1007.

18. Blom, R.; Haaland, A. *J. Mol. Struct.* **1985**, *129*, 21-27.

19. Fink, W.H.; Power, P.P.; Allen, T.L. *Inorg. Chem.* **1997**, *36*, 1431-1436. Boiteau, L.; Demachy, I.; Volatron, F. *Chem. Eur. J.* **1997**, *3*, 1860-1865.

20. Glidewell, C. *Inorg. Chim. Acta* **1975**, *12*, 219-227.

21. Jegier, J.A.; Atwood, D.A. *Bull. Soc. Chim. Fr.* **1996**, *133*, 965-971.

22. Ueyama, N.; Araki, T.; Tani, H. *Inorg. Chem.* **1973**, *12*, 2218-2225. Storre, J.; Schnitter, C.; Roesky, H.W.; Schmidt, H.G.; Noltemeyer, M.; Fleischer, R.; Stalke, D. *J. Am. Chem. Soc.* **1997**, *119*, 7505-7513.

23. Wehmschulte, R.J.; Power, P.P. *J. Am. Chem. Soc.* **1997**, *119*, 8387-8388.

24. Gundersen, G.; Haugen, T.; Haaland, A. *J. Organomet. Chem.* **1973**, *54*, 77-86.

25. Atwood, J.L.; Gardiner, M.G.; Jones, C.; Raston, C.L.; Skelton, B.W.; White, A.H. *J. Chem. Soc., Chem. Commun.* **1996**, 2487-2488.

26. McMahon, C.N.; Bott, S.G.; Barron, A.R. *J. Chem. Soc., Dalton Trans.* **1997**, 3129-3137.

27. Cottone, A.; Scott, M.J. *Organometallics* **2000**, *19*, 5254-5256. Ko, B.T.; Chao, Y.C.; Lin, C.C. *Inorg. Chem.* **2000**, *39*, 1463-1469.

28. Atwood, J.L.; Bott, S.G., Jones, C., Raston, C.L. *J. Chem. Soc., Chem. Commun.* **1992**, 1349-1351.

29. Haigh, C.W.; Mallion, R.B. *Org. Magn. Reson.* **1972**, *4*, 203-228. The Haigh and Mallion tables seriously underestimate the shifts above the plane of the benzene ring. For an estimate of the chemical shift *difference* between "along" and "perpendicular" equatorial methylene groups these tables can be used, although the absolute value of the chemical shift difference may change using a more rigorous approach. For this see: Abraham, J.R.; Fell, S.C.M.; Smith, K.M. Org. Magn. Res. 1977, 9, 367-373.

30. Derome, A.E. Modern NMR Techniques for Chemistry Research; Pergamon Press: Oxford, 1988, Chapter 5. Neuhaus, D.; Williamson, M. The Nuclear Overhauser Effect in structural and conformational analysis; VCH Inc.: New York, 1989. Shaw, D. Fourier Transform NMR

Spectroscopy; Elsevier Science Publishers: New York, 1984, Chapter 9. Boere, R.T.; Kidd, G.S. *Ann. Rep. NMR Spectr.* **1982**, 13, 320-385.

31. Tropp, J. *J. Chem. Phys.* **1980**, *72*, 6035. Pegg, D.T.; Bendall, M.R.; Doddrell, D.M. *Aust. J. Chem.* **1980**, *33*, 1167. Keepers, J.W.; James, T.L. *J. Magn. Res.* **1984**, *57*, 404.
32. Mole, T. *Aust. J. Chem.* **1966**, *19*, 373-386.
33. Nöth, H.; Suchy, H. *Zeit. Anorg. Allg. Chem.* **1968**, *358*, 44-66. Nöth, H.; Schlegel, A.; Knizek, J.; Schwenk, H. *Angew. Chem., Int. Ed. Engl.* **1997**, *36*, 2640-2643.
34. Skowrónska-Ptasinska, M.; Starowieyski, K.B.; Pasynkiewicz, S; Carewska, M. *J. Organomet. Chem.* **1978**, *160*, 403-409.
35. Shreve, A.P.; Mulhaupt, R.; Fultz, W.; Calabrese, J.; Robbins, W.; Ittel, S.D. *Organometallics* **1988**, *7*, 409-416.
36. Healy, M.D.; Power, M.B.; Barron, A.R. *J. Coord. Chem.* **1990**, *21*, 363-366.
37. Healy, M.D.; Mason, M.R.; Gravelle, P.W.; Bott, S.G.; Barron, A.R. *J. Chem. Soc., Dalton Trans.* **1993**, 441-454.
38. The polarity of the Lewis basic solvents would also support an ionic mechanism, see Coordination Chemistry of Aluminum; Robinson, G.H. (ed.) VCH: Weinheim, Germany, 1993, Chapter 6.
39. Jeffery, E.A.; Mole, T. *Aust. J. Chem.* **1968**, *21*, 1497-1503. Ham, S.; Jeffery, E.A.; Mole, T.; Saunders, J.K. *Aust. J. Chem.* **1968**, *21*, 659-670.
40. Brown, T.L.; Murrell, L.L. *J. Am. Chem. Soc.* **1972**, *94*, 378-384.
41. Jeffery, J.A.; Mole, T. *Aust. J. Chem.* **1970**, *23*, 715.Benn, R.; Janssen, E.; Lehmkuhl, H.; Rufinska, A. *J. Organomet. Chem.* **1987**, *333*, 169-180.
42. Nixon, A.; Childs, R.F. *J. Polymer Sci.* **1980**, *18*, 1499-1509.

43. Siedle, A.R.; Newmark, R.A.; Lamanna, W.M.; Schroepfer, J.N. *Polyhedron* **1990**, *9*, 301-308.

44. Brocas, J.; Gielen, M.; Willem, R. The Permutational Approach to Dynamic Stereochemistry; McGraw-Hill: New York, 1983.

45. To get an idea of the increasing stereochemical complexity when the oxo-surface is extended beyond O_4: what is the number of possible isomers for bidentate behavior of the surface assuming the presence of a single metal and a planar rectangular array of 8 oxygen groups ? The accompanying chemistry is not expected to become easier (or less interesting) while extending the oxo-surface concept !

46. M. Fujita, Ph.D. Thesis, Department of Chemistry, University of Alberta, Edmonton, Fall 2001

4. The use of the *tetrakis*[2-hydroxyphenyl]ethene oxo-surface in Ziegler-Natta catalysis

4.1 Introduction.

The results of the complexation of alkylaluminum compounds with *tetrakis*[2-hydroxyphenyl]ethene as reported in the previous chapter seem to indicate that the developed preorganization of four phenol groups will lead to an oxo-surface analog in spite of the rotational mobility (see section 2.3.2, page 81 in Chapter 2) of the phenoxy groups. The reported crystal structures (Figures 3.3, 3.4 and 3.5, pages 136,147 and 152 in Chapter 3) all show an "all up" I_4 isomer (Table 2.1, page 75). If these observations can be extrapolated, complexation of transition metals with the *tetrakis*[2-hydroxyphenyl]ethene ligand might yield interesting "crown-like" bridging modes in compounds that could be tested for polymerization activity.

In addition the oxo-surface concept could be tested. As stated in the introduction (section 1.2.1, page 6) the Grignard reagent used for making heterogeneous supported catalysts can also be deposited on silica gel, alumina or other carriers. If the *tetrakis*[2-hydroxyphenyl]ethene acts like an oxo-surface it should be possible to deposit the Grignard reagent on the ligand to form a, possibly soluble, carrier model. Although the relation between this proposed model and the carrier surface is only based on the presence of four OH groups near to each other and therefore tenuous at best, combined with titanium tetrachloride such a discrete magnesium precursor might yield information about the heterogeneous counterpart as well as deliver a highly active catalyst that could be further modified by ligand tuning. In addition, the effect of preorganizing four phenol ligands on the catalyst behavior could be tested by comparing the catalysis results with other phenoxy ligands.

4.2 Results.

4.2.0 Caveat.

The results as reported in this section were obtained while developing both chemistry as well as technology, during which several problems became apparent. Originally, it was assumed that the magnesium chloride salts, as obtained, were soluble. Consequently, extensive use was made of toluene stock solutions in order to accurately measure out the tiny amounts of magnesium salts used in the polymerization experiments. Because of the small amounts, solubility problems only became apparent after the first centrifuge experiments when the stock solutions using toluene turned out to give a precipitate after a centrifuge run. The polymerization results of runs, where use was made of stock solutions and in which the ligand/titanium ratio is important, are therefore not reported. Limited solubility in toluene is assumed for all of the magnesium salts used.

During experiments stock solutions of $TiCl_4$ in toluene turned cloudy in capped polymerization bombs after several hours. In spite of wrapping the gasket with Teflon tape, plasticizer leached out of the gasket and reacted with the $TiCl_4$. The plasticizer can be detected by GCMS. The results obtained of reaction suspensions that have been stored for more then 30 minutes in capped polymerization bombs are therefore more likely to reflect contamination. Instead, solutions were kept in the glovebox after mixing and brought out when needed. Although in large-scale polymerization reactions no use was made of these gaskets, the reactions still failed for no apparent reason. With regard to the small-scale polymerization reactions it was found that stirring of the suspension is crucial; any change in the stirring efficiency is reflected in the yield of PE. Therefore only the highest activities obtained in a set of reactions are reported.

Only Me_3Al and Et_3Al were used in the catalysis experiments in order to approach supported catalyst conditions as much as possible.

Finally it should be pointed out that although the balance inside the glovebox was tested using calibrated weights and was found to be accurate and reproducible under the testing conditions *at that moment*, actual daily use indicated that static electricity could change the readout considerably. While this is no problem for 0.5 g amounts, for 6 mg quantities it is.

Because these "problems" turned up at different times during the research the reported observations should be considered as trends within one and the same data set, while comparison between different experiment sets are to be approached with caution.

4.2.1 Attempts to synthesize discrete group 4 transition metal-containing compounds.

The reaction of *tetrakis*[2-hydroxyphenyl]ethene with different group 4 metal derivatives like $TiCl_4$, $TiCl_3{\cdot}(NMe_3)_2$, $TiCl_3{\cdot}3THF$, $Ti(NMe_2)_4$, $Zr(NMe_2)_4$, $ZrCl_4$ gave powders that resisted repeated attempts to obtain crystals suitable for an X-ray diffraction experiment. In order to determine the potential value of these materials for Ziegler-Natta catalysis, the so-obtained uncharacterized materials were treated with triethylaluminum or trimethylaluminum under an ethene atmosphere. No polymerization activity was observed.

4.2.2 Synthesis of *tetrakis*[2-hydroxyphenyl]ethene supported magnesium salts.

In order to assess the value of *tetrakis*[2-hydroxyphenyl]ethene as an oxo-surface, the compound was treated with 4 equivalents of MeMgCl followed by 4 equivalents of $TiCl_4$. The so obtained precatalyst did show polymerization activity when mixed with Et_3Al as a cocatalyst under ethene pressure. A similar polymerization on a large scale using the magnesium chloride salt of *tetrakis*[2-hydroxyphenyl]ethene combined with 1 equivalent of $TiCl_4$/ligand showed a polymerization activity of 550 Kg/mol Ti·hr·atm and a polydispersity of 5 combined with a high M_w ($1038\cdot10^3$) and M_n ($206\cdot10^3$). For comparison, a large scale polymerization using the magnesium chloride salt of 2,2'-methylenebis[4,6-bis(1,1-dimethylethyl)]phenol and 1.5 equivalent of $TiCl_4$/ligand was executed. The polymerization activity was 248 kg PE/mol Ti·hr·atm, with a polydispersity of 3.8, M_w of $1047\cdot10^3$, and an M_n of $278\cdot10^3$.

Initial attempts to probe the materials obtained from the reaction of a Grignard reagent with *tetrakis*[2-hydroxyphenyl]ethene were hampered by the inability to obtain crystals of suitable quality, which in turn was related to the limited solubility in non-Lewis basic solvents. Finally, a crystal suitable for an X-ray diffraction experiment was obtained using THF as a crystallization solvent (eq. 4.1 and Figure 4.6, page 211).

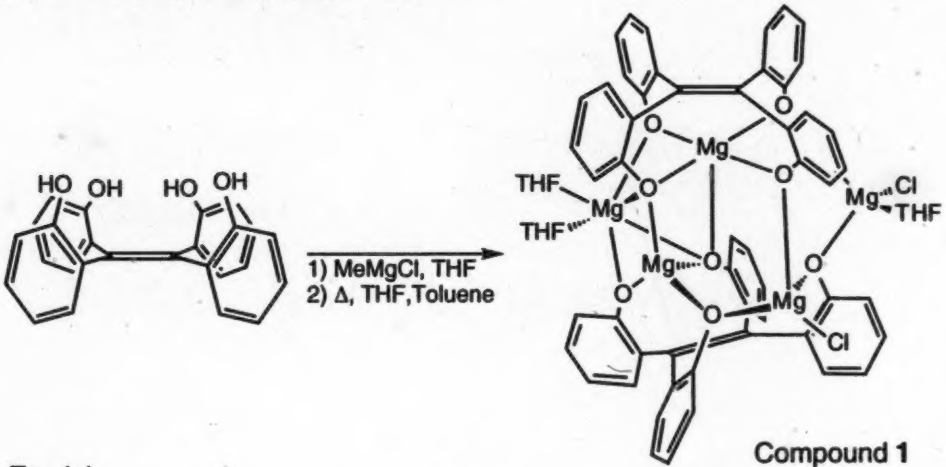

Compound **1**

Eq. 4.1

The crystal structure shows a complicated structure of five magnesium atoms of varying coordination and geometry in between two tetraarylethene ligands. In an attempt to improve the solubility of the obtained magnesium chloride salts, a *tert*-butyl substituted *tetrakis*[5-(1,1-dimethylethyl)-2-hydroxyphenyl]ethene was also used, but this did not improve the solubility or the results of crystallization attempts using the corresponding magnesium chloride salt.

Analysis of these products proved as challenging as obtaining well-defined organometallic compounds. Attempts to characterize the obtained materials using ^{1}H-NMR spectroscopy failed due to the low solubility of the salts in toluene-d_8; when signals were obtained at all, no fine structure was present. An internal standard combined with ^{1}H-NMR spectroscopy was used to determine the amount of the ligand salt that did dissolve in toluene-d_8. Due to the low solubility this method had too low an accuracy to be useful. Other solvents like acetonitrile-d_3 and THF-d_8 gave suspensions at useful concentrations of the magnesium salts, but were not exhaustively investigated.

^{25}Mg-NMR spectroscopy[1] was tried as a possibly useful technique for probing both magnesium salts as well as precatalyst species. To get a reasonable signal-to-noise ratio rather high concentrations of compounds were necessary, requiring at least 0.5 g of dissolved compound/measurement. At the time of measurement only the magnesium chloride salt of 4-*tert*-butylphenol was available in such quantities. A THF-d_8 solution of this salt displayed a signal at 12 ppm relative to 0.18 M magnesium sulfate in D_2O (0 ppm). The signal shifted to 11 ppm on addition of $MgCl_2$. A solution of $MgCl_2$ in THF-d_8 displayed a signal at 11 ppm .

Because the amount of THF remaining after the reaction of the ligands with the Grignard reagent was expected to have a negative influence on the catalytic activity while improving the solubility of the obtained salts in toluene, several attempts at quantifying the amount of THF remaining after the reaction with Grignard reagents were made, but without success. Acidic decomposition of the magnesium salts in combination with ^{1}H-NMR spectroscopy gave insoluble magnesium salts or supersaturated solutions that formed precipitates at unpredictable moments resulting in large variations in the measured THF/ligand ratio and were therefore not further persued. A GC method was tried in order to measure the amount of adhering THF but suffered from low sensitivity to THF as well as incompatibility with the required salt-decomposition technique.

If the obtained magnesium salts consist of a mixture of aryloxymagnesium chlorides and diaryloxymagnesium compounds it might be possible to obtain an idea of the distribution of these groups by probing a possible reactivity difference (see section 4.3.3, page 219) through derivatization with a suitable reagent. For example, the product mixture obtained from the reaction of the magnesium chloride salts with methyl iodide might reflect the distribution of phenoxymagnesium chloride and diphenoxymagnesium groups in the original sample since the methyl iodide would react selectively with the phenoxymagnesium chloride groups in the sample. The observed methoxy group distribution in the isolated product would in that case reflect the distribution of the ROMgCl groups. An experiment using methyl iodide and THF as a solvent failed to return any product containing methyl ether groups according to ^{1}H-NMR spectroscopy; unchanged starting material was obtained instead.

To get some indication of the composition of the magnesium salts, elemental analysis data for C, H, and Cl were used to calculate the ratio of ligand to THF, Mg and Cl. While useful for calculating the ratio of Ti to ligand, no information on the structure of magnesium salts can be derived from such information, except that the observed variation of the elemental analysis data for several samples of the same batch of a magnesium salt can be interpreted as evidence for the heterogeneous nature of the obtained materials.

In an attempt to isolate a discrete polymetallic species for Ziegler-Natta catalysis the magnesium salt of *tetrakis*[5-(1,1-dimethylethyl)-2-hydroxyphenyl]ethene was treated with one equivalent of $TiCl_4$. After repeated attempts a crystal suitable for an X-ray diffraction experiment was obtained. The crystal structure shows a sandwich of two tetraarylethene units with two pentacoordinated titanium atoms in between (eq. 4.2 and Figure 4.7, page 217). No magnesium dichloride remained in the crystal.

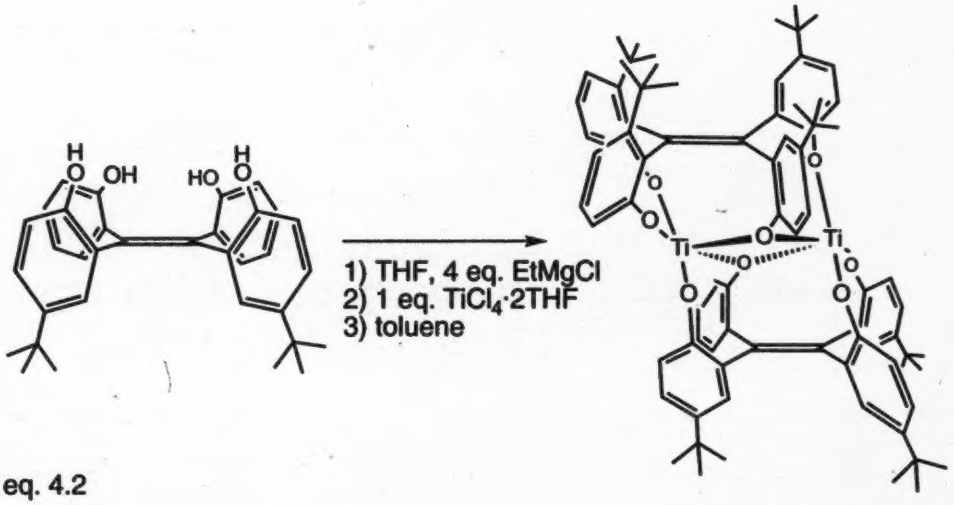

eq. 4.2

4.2.3 Probing the precatalyst homogeneity

If one equivalent of $TiCl_4$ ejected all magnesium as $MgCl_2$ in the starting material, an in-situ generation of a potential support for a catalyst (see page 6, section 1.2.1) would result. It was therefore of interest to determine if the catalytic activity was taking place in a homogeneous or heterogeneous system. Several magnesium salts were tested by making use of a centrifuge technique for separating soluble and insoluble materials, resulting from the reaction between the magnesium chloride salt and $TiCl_4$. By mixing the magnesium chloride salt with $TiCl_4$ inside the glovebox, contamination problems were avoided during regular sampling of the stirred red-brown mixture. Each sample was centrifuged and the precipitate and supernatant carefully separated to test each individually for polymerization activity. All magnesium salts tested gave, after 5 to 7 minute centrifugation at maximum speed, a transparent red-brown gel as a precipitate in addition to clear a red-brown supernatant, independent of the sampling time after mixing and inspite of the apparent formation of an often clear red-brown "solution" upon mixing the magnesium salt and $TiCl_4$. The formed gel is rather voluminous compared to the volume of the white powdery starting material. Because the sample size was known, the amount of Ti in the total sample could be calculated assuming homogeneity.

In the absence of an analytical tool[2] to determine the small amounts of titanium in both precipitate and supernatant the activities were calculated using the total amount of Ti in the sample for *both* precipitate *and* supernatant. The calculated activities are thus always *too low* compared to the activity based on the (unkown) actual amount of Ti present in each phase. The equal distribution of Ti over both precipitate and supernatant for instance would result in doubling of the activities reported, while any deviation from this scenario could yield even higher activities for one of the phases.

The results of the crude *tetrakis*[2-hydroxyphenyl]ethene magnesium salt and 1 equivalent $TiCl_4$ using 70 equivalents of Et_3Al/Ti as a cocatalyst are shown in Figure 4.1 (page 204). In the graph the sample time is given in minutes after mixing the $TiCl_4$ solution and the magnesium salt suspension. The actual reaction time before testing the activity of the so formed precatalyst is less well defined because each heterogeneous reaction mixture is centrifuged for 5 minutes during which physical separation of the formed precipitate and supernatant takes place. The initial activity observed directly after mixing the

Figure 4.1: Variation of the polymerization activity of precipitate and supernatant of samples of the reaction of *tetrakis*[2-hydroxyphenyl]ethenemagnesium chloride salt in toluene with 1 equivalent of $TiCl_4$ in time.

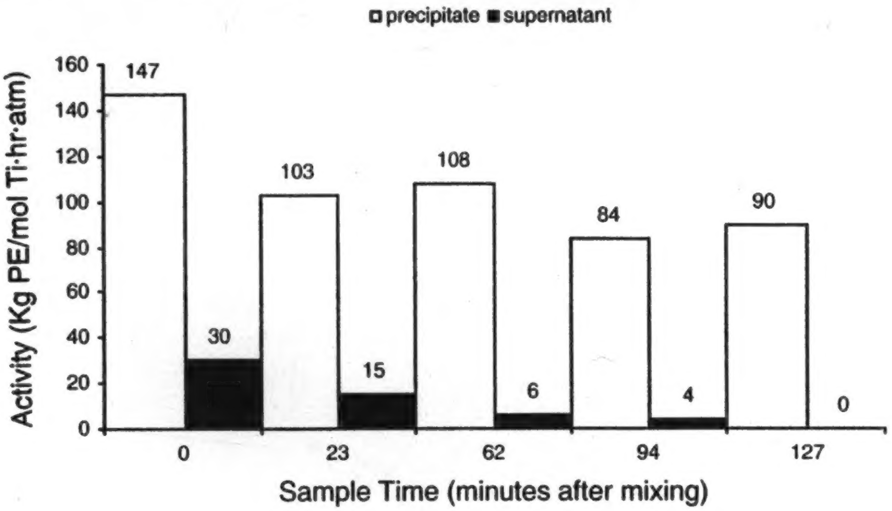

Activity based on assumed [Ti]=$6.6\cdot10^{-6}$ mol/ sample, 70 eq. Et_3Al/Ti, precipitate activity at 127 minutes: after washing 5 times with toluene.

Figure 4.2: Variation of the polymerization activity of precipitate and supernatant of samples of the reaction of *tetrakis*[5-(1,1-dimethylethyl)-2-hydroxyphenyl]ethenemagnesium chloride salt in toluene with 1 equivalent of $TiCl_4$ in time.

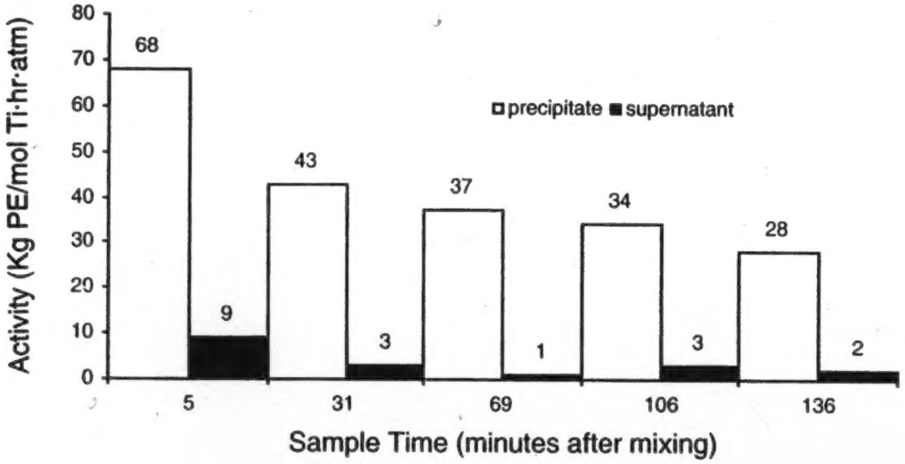

Activity based on assumed [Ti] = $4\cdot10^{-6}$ mol/ sample, 75 eq Et_3Al / Ti

$TiCl_4$ and magnesium chloride salt is 147 Kg/mol Ti·hr·atm for the heterogeneous precatalyst layer and 30 Kg/mol Ti·hr·atm for the homogeneous layer. Both activities decrease in time, but the homogeneous precatalyst layer has hardly any activity left while the heterogeneous layer (after washing the isolated precipitate five times to remove soluble products) still shows an activity of 90 Kg/mol Ti·hr·atm. If instead a more lipohilic tetraarylethene derivative is used (Figure 4.2, page 204) similar effects are observed: the activity of the heterogeneous precatalyst layer is a factor 10-15 times higher compared to the homogeneous layer. The activity using 1 equivalent of $TiCl_4$ drops in time for both homogeneous and heterogeneous layer, the activity of the heterogeneous layer always being larger than the homogeneous layer. This effect is also observed for the structurally "unorganized" crude magnesium chloride salts of 4-*tert*-butylphenol (see Figure 4.3).

The influence of the ligand on the observed catalytic activity is unclear given

Figure 4.3: Variation of the polymerization activity of precipitate and supernatant of samples of the reaction of 4-*tert*-butylphenol magnesium chloride salt in toluene with 1 equivalent of $TiCl_4$ in time.

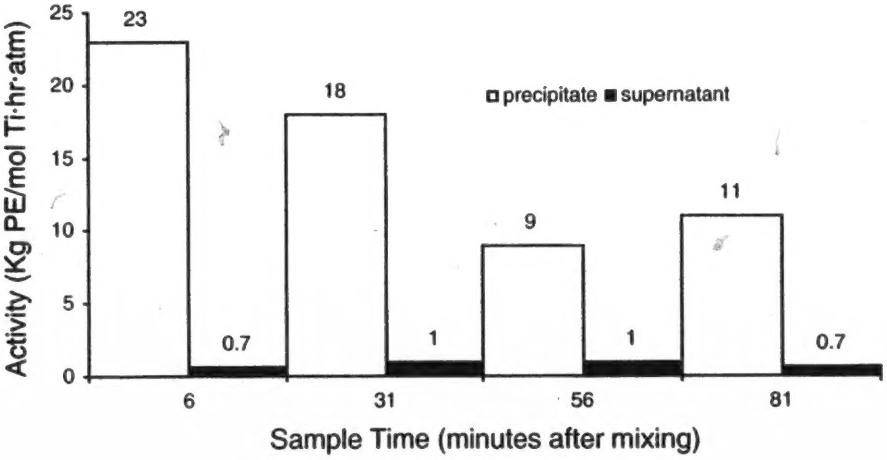

Activity based on assumed [Ti] = $4.4 \cdot 10^{-6}$ mol/ sample, 88 eq Et_3Al / Ti that structurally different ligand systems give similar results.

In order to determine the ligand distribution of 4-*tert*-butylphenol and *tetrakis*[5-(1,1-dimethylethyl)-2-hydroxyphenyl]ethene over the inactive homogeneous layer and the active heterogeneous layer, in a separate experiment both layers were reduced to dryness after separation and dissolved[3] in acetone-d_6 containing a known amount of internal standard. In order to encourage the formation of a ligand titanium complex an excess $TiCl_4$ and a 2 hour reaction time were used. By comparing the integral of the internal standard of known amount with the integral of the ligand using ^{1}H-NMR spectroscopy, the amount of ligand in each layer could be determined.

According to the distribution measured (Table 4.1), under these conditions (excess $TiCl_4$, 2 hours reaction time) most of the ligand is present in the homogeneous phase.

Table 4.1: ligand distribution over the precipitate and supernatant layer using excess $TiCl_4$ and the magnesium chloride salt of 4-*tert*-butylphenol **A** or the magnesium chloride salt of *tetrakis*[5-(1,1-dimethylethyl)-2-hydroxyphenyl] ethene **B**.

Ligand	Eq. $TiCl_4$	Layer Tested[1]	Calculated amount of ligand[2]	Yield PE (g)[3]
A	120	ppt	$2.8 \cdot 10^{-7}$ mol (3 %)	0.44
		super	$8.8 \cdot 10^{-6}$ mol (97 %)	-
B	500	ppt	$1.6 \cdot 10^{-7}$ mol (12 %)	0.39
		super	$1.2 \cdot 10^{-6}$ mol (88 %)	-

1] After separation of the soluble and insoluble part of the $TiCl_4$/magnesium chloride salt, using centrifugation: see experimental. super = supernatant, ppt = precipitate 2] Using 1,3,5-trimethoxybenzene as internal standard in an ^{1}H-NMR experiment; acetone-d_6 as solvent. 3] Separate polymerization experiment using the same suspension as used for determining the ligand distribution.

The isolated heterogeneous phase of the same reaction mixture used for determining the ligand distribution shows appreciable polymerization activity while containing between 3-12 % of the used ligand according to the measured ligand distribution. If polymerization activities are calculated relative to the number of moles of ligand (the number of moles of Ti is unknown) activities of 6645 and 5352 kg PE/*mol ligand*·hr·atm are calculated for the crude magnesium chloride salts of *tetrakis*[5-(1,1-dimethylethyl)-2-hydroxyphenyl] ethene and 4-*tert*-butylphenol respectively.

4.2.4 Optimization of the Ti/ligand magnesium salt ratio.

In order to find out if there is a ideal ratio between the amount of $TiCl_4$ and magnesium chloride salt used, several polymerization runs using the crude magnesium salts of *tetrakis*[5-(1,1-dimethylethyl)-2-hydroxyphenyl]ethene (Figure 4.4, page 208) and 2,2'-thiobis[4,6-(1,1-dimethylethyl)]phenol[27,37] were executed (Figure 4.5, page 208) without separating the formed precatalyst suspension. The decrease in activity in time for the formed catalyst was again observed, while a maximum activity seemed to be obtained for 2 equivalents of $TiCl_4$ for both, structurally unrelated, ligands.

4.2.5 The effect of added hydrogen.

Using 2 equivalents of $TiCl_4$, the magnesium salt of 2,2'-thiobis[4,6-(1,1-dimethylethyl)]phenol[27,37] was also used to investigate the effect of added hydrogen on the molecular weight. As shown in Table 4.2 (page 209) a drastic reduction of both catalyst activity and of the molecular weight of the formed PE takes place when polymerizations are done in the presence of hydrogen. Interestingly, the PE formed by the catalyst based on this ligand system shows

Figure 4.4: Variation of the polymerization activity as a function of the number of $TiCl_4$ equivalents and reagent mixing time for the reaction of $TiCl_4$ with the magnesium chloride salt of *tetrakis*[5-(1,1-dimethylethyl)-2-hydroxyphenyl] ethene.

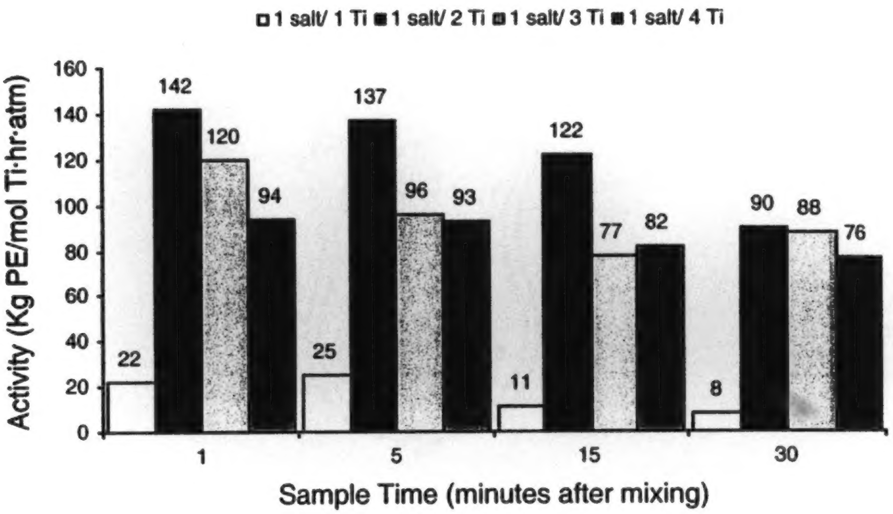

Figure 4.5: Variation of the polymerization activity as a function of the number of $TiCl_4$ equivalents and reagent mixing time for the reaction of $TiCl_4$ with the magnesium chloride salt of 2,2'-thiobis[4,6-bis(dimethylethyl)]phenol.

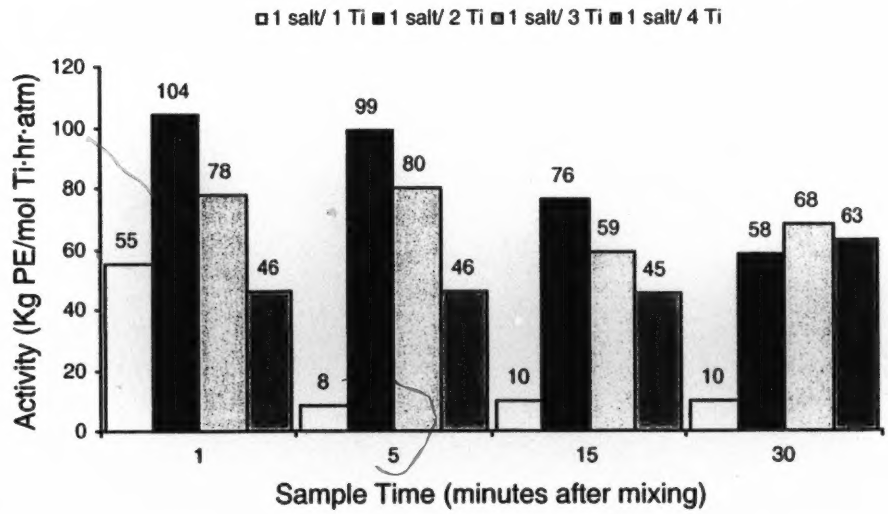

Table 4.2: The efffect of hydrogen on the catalytic behavior of 2 equivalents of $TiCl_4$ combined with the magnesium salt of 2,2'-thiobis[4,6-(1,1-dimethylethyl)]phenol.

gascap H_2	Activity[1]	Weight % Oligomers[3]	M_w[4]	M_n[4]	M_w/M_n[4]
none	104	11	232555	17481	16.5
atm[2]	55	23	145089	6638	22
2.5 psig	24	24	117382	4386	27
5 psig	20	10	106077	5466	19.5

1] highest value of a set of two runs in kg PE/mol Ti·hr·atm. 2] atmospheric pressure H_2 3] Highest value of a duplo, $C_{10}H_{22}$ - $C_{28}H_{58}$ determined using GCMS: see text and experimental. 4] Average of a duplo.

both a broad molecular weight distribution (polydispersity varying between 17 and 27) as well as the formation of an appreciable amount of saturated oligomers (10-24 weight %) in the presence or absence of hydrogen. For the determination of the amount of oligomers, the combined washings and solvent after filtration of the PE were thoroughly cleaned by water extraction under basic and acidic conditions to remove traces of the ligand and inorganic salts. According to GCMS of the so treated dried solvent layers, the oligomers formed are *even* C_{10}-C_{28} alkanes, with a maximum for C_{22}.

4.3 Discussion.

4.3.1 The crystal structure of compound 1.

The solid state structure of compound **1** shows a complicated sandwich of five magnesium atoms with a coordination number ranging from four to six in between two *tetrakis*[2-hydroxyphenyl]ethene molecules (Figure 4.6a page 211, see appendix G, page 371, for details). Unfortunately, the obtained data set is weak, as indicated by the low number of observations (4463) compared to the number of independent reflections (15313). The low number of published crystal structures of phenoxymagnesium compounds[4] further hinders the analysis of the crystal structure.[6]

In the crystal structure Mg4 and Mg5 (Figure 4.6b page 212) are four-coordinate with Mg-O bond lengths in the range of 1.932(13)-1.993(13) Å. This is a range comparable with the observed range for Mg-O bond lengths of published four-coordinate magnesium phenoxide structures [1.931(2)-2.042(6) Å].[7,8] The Mg-Cl bond lengths, of 2.266(7) and 2.281(7) Å, are similar to the Mg-Cl bond lengths in four-coordinate Mg [2.269-2.276(4) Å].[6,8] The geometry of the four coordinate magnesium ions is distorted tetrahedral as expressed by the wide range of O-Mg-Cl and O-Mg-O angles (97.0(5)-123.0(4)°).

Pentacoordinated Mg2 (Figure 4.6c, page 213) is trigonal bipyramidal with the longest Mg-O bond lengths formed to the axial located O11 (Mg2-O11: 2.069(13) Å) of the THF molecule, and O8 of the phenol group of the tetraphenylethene unit (Mg2-O8: 2.241(12) Å). Literature values for Mg-O(axial) bonds aree in the range of 1.879(2)-2.226(3) Å.[7,9] The Mg-O(equatorial) bond lengths range from 1.994(11)-2.020(12) Å, and fall within the reported range [1.954(4)-2.145(2) Å].[7,9] The coordination geometry of Mg2 is distorted as indicated by the wide range of O(axial)-Mg-O(equatorial) bond angles (73.6(4)-102.5(5)°) and O(equatorial)-Mg-O(equatorial) bond angles (90.6(5)-143.1(5)).[9] The observed O(axial)-Mg-O(axial) angle is 168.1(5).

In the crystal structure, Mg3 is hexacoordinate (Figure 4.6d, page 214) and distorted according to the wide range of observed bond

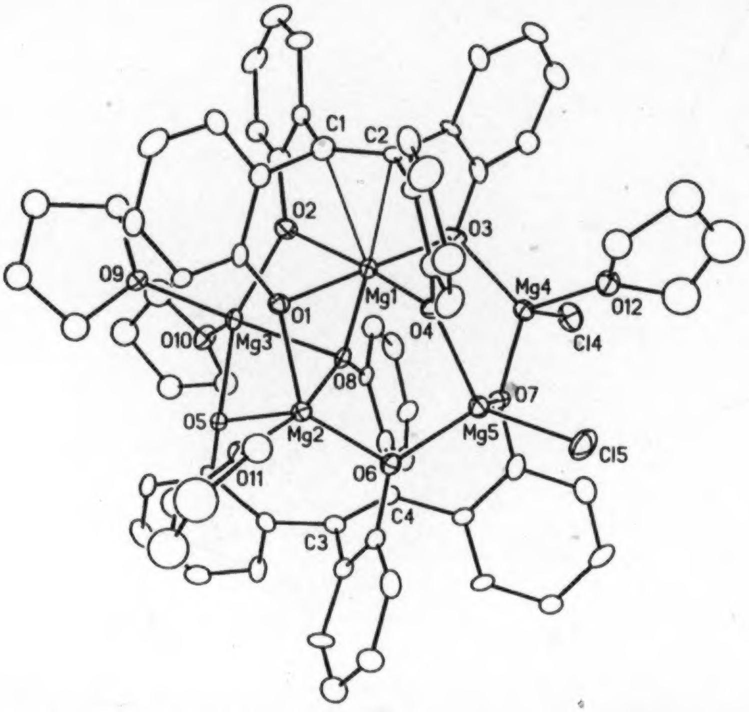

Figure 4.6a: Perspective view of compound **1** showing the atom labeling scheme. Non-hydrogen atoms are represented by Gaussian ellipsoids at the 20% probability level. Hydrogen atoms are not shown. Selected bond distances (Å) and bond angles (deg): Mg1-O1=2.090(12), Mg1-O2=2.120(11), Mg1-O3=1.973(12), Mg1-O4=2.109(11), Mg1-O8=1.989(12), Mg1-C1=2.530(17), Mg1-C2=2.514(17), Mg2-O8=2.241(12), Mg2-O11=2.069(13), Mg2-O1=2.020(12), Mg2-O5=1.994(11), Mg2-O6=1.994(11), Mg3-O9=2.039(11), Mg3-O8=2.205(11), Mg3-O5=2.087(12), Mg3-O2=2.025(13), Mg3-O10=2.070(11), Mg3-O1=2.317(11), Mg4-O3=1.993(13), Mg4-O7=1.952(13), Mg4-O12=2.031(13), Mg4-Cl4=2.266(7), Mg5-O4=1.980(12), Mg5-O6=1.932(13), Mg5-O7=1.982(12), Mg5-Cl5=2.281(7), O1-Mg1-O2=80.9(4), O1-Mg1-O4=85.2(5), O3-Mg1-O4=88.0(5), O2-Mg1-O3=105.5(5), O1-Mg1-O8=77.6(5), O8-Mg2-O11=168.1(5), O5-Mg2-O6=143.1(5), O1-Mg2-O5=90.6(5), O1-Mg2-O6=125.8(5), O8-Mg3-O9=161.2(5), O2-Mg3-O5=153.6(5), O1-Mg3-O10=175.1(5), O3-Mg4-O7=110.5(5), Cl4-Mg4-O12=101.6(5), O4-Mg5-O6=97.4(5), O4-Mg5-O7=97.0(5), O6-Mg5-O7=106.9(5), O4-Mg5-Cl5=123.0(4).

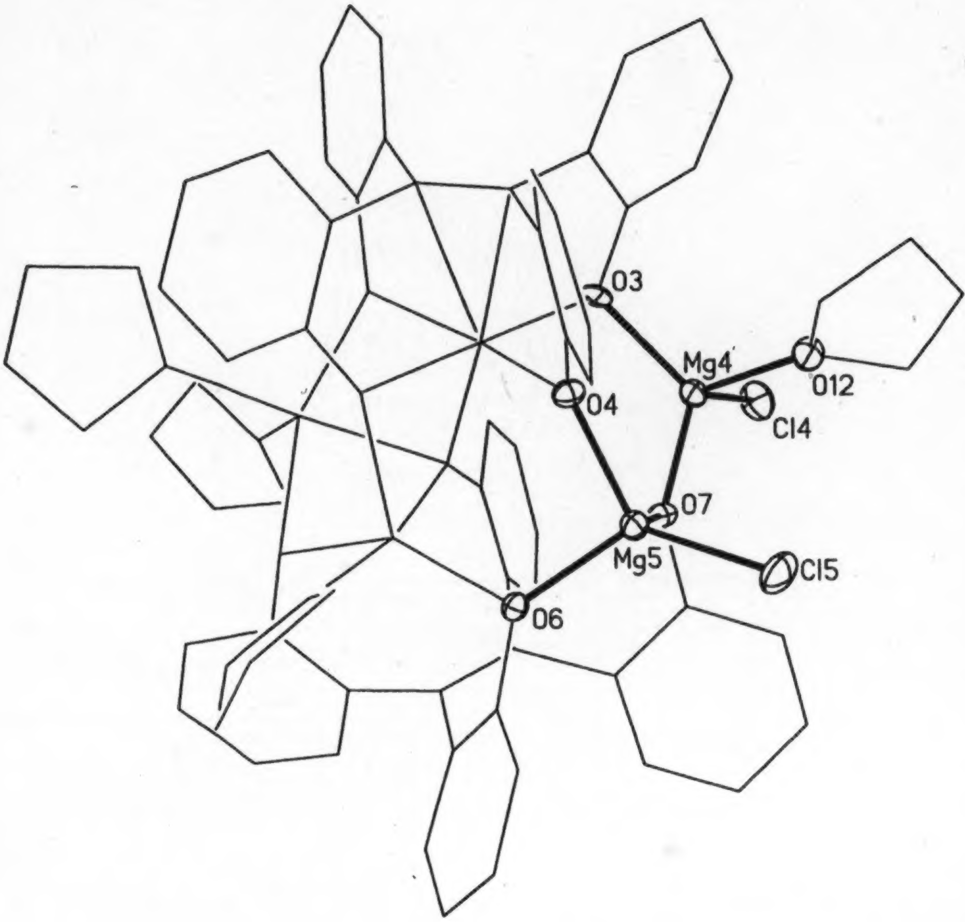
O3
Mg4
O12
O4
Cl4
O7
Mg5
Cl5
O6

Figure 4.6b: Alternate "skeletal" view of the molecule omitting the thermal ellipsoids for the carbon atoms, showing the tetracoordinate Mg4 and Mg5.

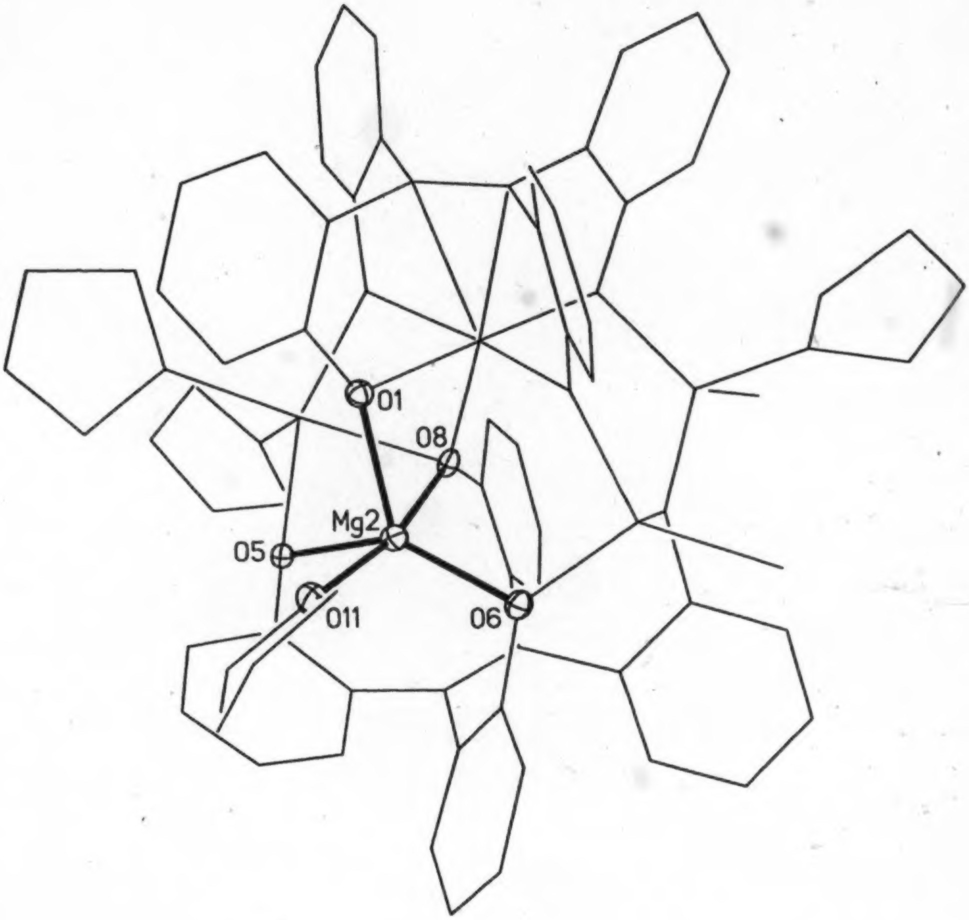
O1
O8
Mg2
O5
O11
O6

Figure 4.6c: Alternate "skeletal" view of the molecule omitting the thermal ellipsoids for the carbon atoms, showing the pentacoordinate Mg2.

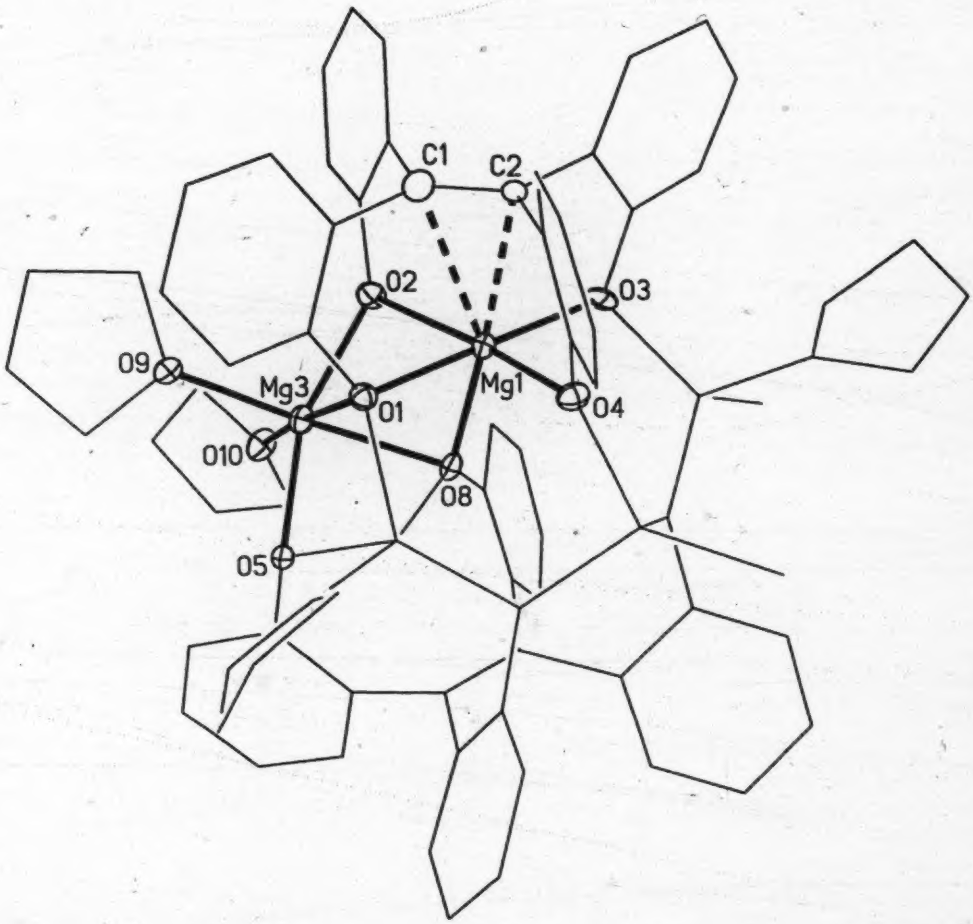
C1
C2
O2
O3
O9
Mg3
O1
Mg1
O4
O10
O8
O5

Figure 4.6d: Alternate "skeletal" view of the molecule omitting the thermal ellipsoids for the carbon atoms, showing the hexacoordinate Mg1 and Mg3.

lengths (Mg-O: 1.973(12)-2.317(11) Å [1.998(3)-2.162(3) Å][9] and bond angles (O-Mg-O(cis): 77.6(4)-106.7(5)°, O-Mg-O(trans): 153.6(5)-172.9(6)°).

No π-complexes of an olefin with Mg are known and only one π complex of an alkyne with magnesium has been reported,[8,10] with Mg-C bond lengths between 2.269(8)-2.468(9) Å. Although it is tempting to assume a bonding interaction between Mg1 and the ethene bond, the shortest Mg-C distance (Mg1-C1: 2.530(17) Å, Mg1-C2: 2.514 (17) Å) is well beyond the observed Mg-C π bond distance of the alkyne complex. In addition to a rather long Mg-C1 Mg-C2 bond lengths, the position of the Mg relative to a plane defined by O1-O2-O3-O4 is -0.1 Å *away* from the ethene bond (position of C1: 2.32 Å, position of C2: 2.35 Å when position of plane is 0). In favor of a Mg-ethene π bond is the wide range of known Mg-(π-C) bond lengths varying from 2.26(1) ((η^5 indenyl)$_2$Mg) to 2.55 Å (CpMgBr·TMEDA).[11] Due to the quality of the data, firm conclusions are not allowed. The data, however, do not seem to support a definitive Mg-ethene interaction, making Mg1 square pyramidal in coordination geometry.

The tetraarylethene frame displays an ethene bond distance of 1.34(2) Å (C1-C2) and 1.33(2) Å (C3-C4). Judged by the dihedral angles the distortion of the C1-C2 bond is minimal (dihedral angle: 1(3)°) while the C3-C4 ethene bond seems to show considerable distortion (dihedral angle: 18(3)-21(3)°). The position of the phenoxy rings in this crystal structure is nearly perpendicular for the groups bound to the C1-C2 ethene bond (dihedral angle range: 76(2)-83(2)°), and more propeller-like for the second ethene bond (dihedral angle range: 58(2)-82(2)°). The observed C-O bond lengths are in the 1.34(2)-1.352(17) Å range and fall within the reported range [1.330(4)-1.386(5) Å].[12] The O2-7 oxygens are tricoordinate, with O-Mg bond lengths of 1.989(12)-

2.317(11) Å. The sum of the bond angles for the atoms surrounding O2-4 and O6,7 fall within a range of 351-359°, indicating a trigonal planar geometry of the atoms surrounding the O atoms. The sum of the angles centered around O5 (337°) indicates a more distorted geometry.

Within this crystal structure, O1 and O8 are tetracoordinate. A similar μ_3-coordination has been observed for $[CpMgOEt]_4$, which forms a tetrameric cluster with a cubane skeleton (eq. 4.3), the corners of which are occupied by Mg and O.[12] The observed O-Mg bond lengths in the crystal structure of compound **1** show a wider range (1.989(12)-2.317(11)) compared with the reported O-Mg bond lengths of the tetrameric $CpMgOEt]_4$ cluster [2.059(2)-2.083(2)].[12] The geometry is however similar: in both compounds small Mg-O-Mg angles (81.0(4)-96.5(5)°, [93.4(1)-98.6(1)][12] and wide C-O-Mg angles (113.1(9)-140.3(11)°, [119.2(1)-122.8(1)][12] are found.

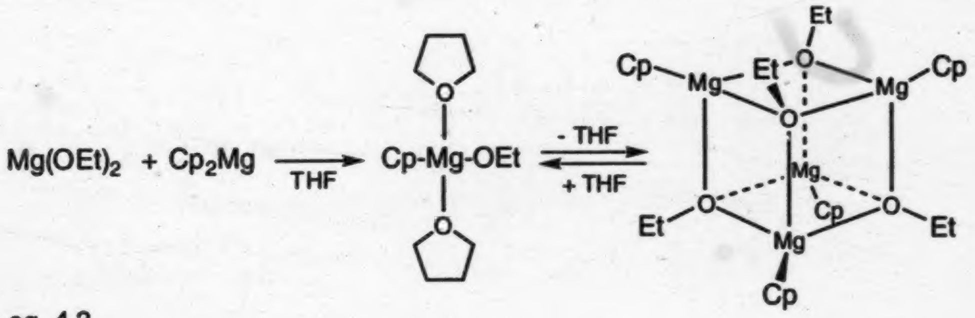

eq. 4.3

4.3.2 The crystal structure of compound 2.

The crystal structure of compound **2** (Figure 4.7a,b page 217, 218 for details see appendix H, page 385) is reminiscent of the collapsed aluminum compounds (section 3.3.3/3.3.4 page 146, 151) and the magnesium compound **1** in this chapter. Trapped in-between two tetraarylethene units are two pentacoordinated titanium atoms giving rise to a centrosymmetric arrangement.

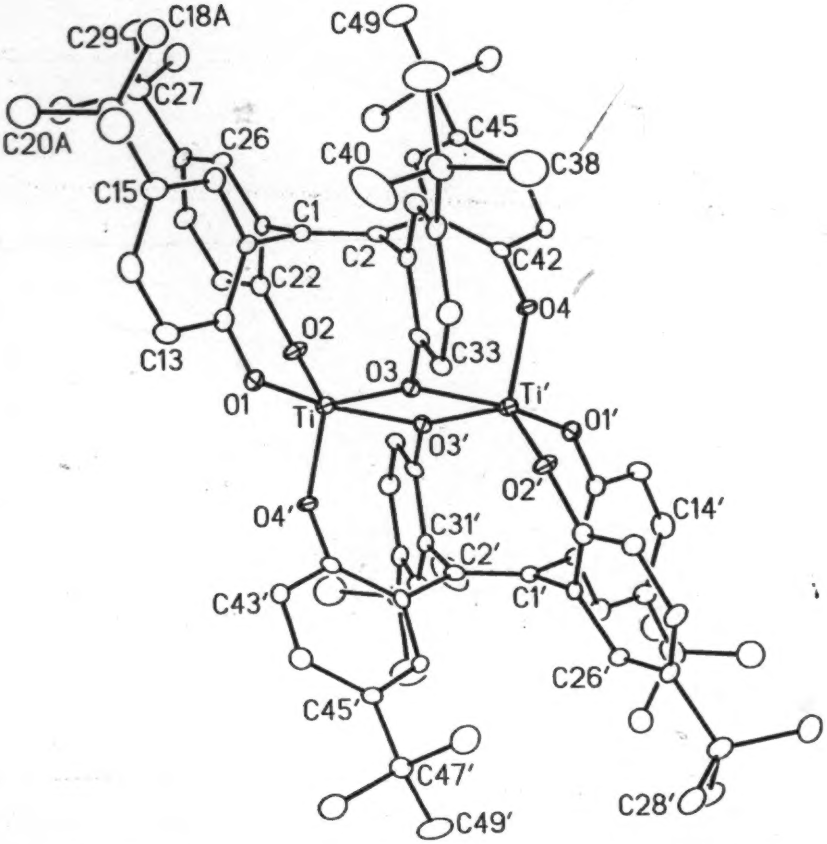
C29
C18A
C49
C27
C20A
C26
C45
C40
C38
C15
C1
C2
C42
C22
O4
O2
C13
C33
O3
O1
Ti
Ti'
O1'
O3'
O2'
C14'
O4'
C31'
C2'
C43'
C1'
C26'
C45'
C47'
C49'
C28'

Figure 4.7a: Perspective view of compound **2** showing the atom labeling scheme. Non-hydrogen atoms are represented by Gaussian ellipsoids at the 20% probability level. Hydrogen atoms are not shown. Primed atoms are related to unprimed ones via the crystallographic inversion center (0, 0, 0) at the center of the molecule. Selected bond distances (Å) and bond angles (deg): Ti-O1=1.812(4), Ti-O2=1.806(4), Ti-O3=1.934(4), Ti-O4'=1.813(4), Ti-O3'=2.122(4), C1-C2=1.356(8), O1-C12=1.357(7), O2-C22=1.379(7), O3-C32=1.385(7), O4-C42=1.372(7), O1-Ti-O3'=166.14(19), O2-Ti-O3=128.11(18), O2-Ti-O4'=112.12(19), O3-Ti-O4'=112.53(18), O3-Ti-O3'=72.3(2), O1-Ti-O2=101.0(2), O1-Ti-O4'=102.43(19), O1-Ti-O3=93.93(19), O2-Ti-O3'=86.50(18), O3'-Ti-O4'=85.16(17).

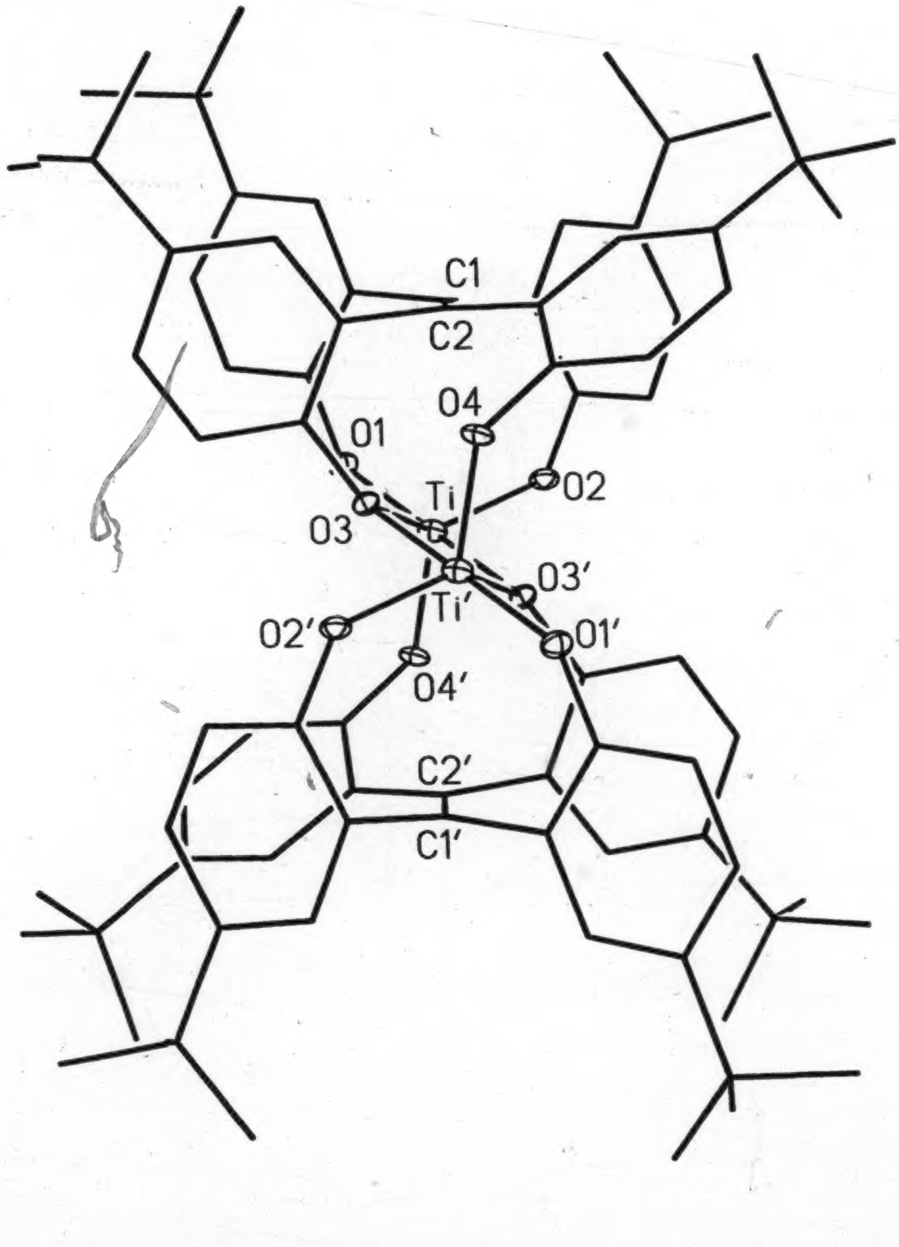
C1
C2
O4
O1
O2
Ti
O3
O3′
Ti′
O2′
O1′
O4′
C2′
C1′

Figure 4.7b: View of the molecule approximately along the C1–C2 bond axis.

No coordinating solvent or magnesium chloride molecules are present. The observed Ti-O distances, (1.806(4)-1.813(4) Å, are within the normal range [1.809-1.937 Å],[13] except for the Ti-O3' bond length which is significantly longer (2.122(4) Å). The Ti atom is pentacoordinated with a trigonal bipyramidal geometry. The sum of the observed equatorial bond angles for the oxygen atoms surrounding the Ti atom (353°) seems to indicate a slight distortion from planarity for the equatorial oxygens. The remaining details do not seem to fit the trigonal bipyramidal assignment that well. For instance the variation in the axial Ti-O bond length is large, Ti-O1 = 1.812(4), Ti-O3' = 2.122(4) with the smaller bond length not significantly different from the remaining equatorial Ti-O bond lengths. Furthermore the O1-Ti-O3' bond angle of 166.14(19) deviates from the expected 180°. Further distortion is indicated by the range of O(axial)-Ti-O(equatorial) angles of 72.3(2)-102.43(19).

The tetraarylethene frame displays both a twist of a single aryl ring (dihedral angle: 36.8(8) for ring containing C41, rest of aryl rings: 76.2(8)-95.1(7)) as well as a distortion of 7.6(8)-10.7(10)° of the ethene bond to accommodate the two metal atoms. This has also been observed in previously characterized compounds. The angle between the aryl rings is 113.6(5)° for the rings perpendicular to the double bond and 113.6(5)° for the twisted rings, similar to the collapsed aluminum compound (115.4 and 120.4 respectively).

4.3.3 On the formation of compound 1 and 2.

The addition of a Grignard reagent "RMgCl" to a carbonyl group is a standard organic reaction. The intermediate formed is postulated to be an alkoxy- or aryloxymagnesium chloride. Inspite of the importance of the formed intermediates (that could have been used as reaction product models) it seems as if there is no structural proof on the existence of alkoxy or phenoxy magnesium chlorides. Isolated reaction products for which crystal structures are available invariably are bromides.[4] Reactions of dialkylmagnesium Grignard reagents with alcohols and phenols have been studied, but only a single reference is available on the reaction mechanism.[14] The reaction of alkylmagnesium halides and dialkylmagnesium with benzophenone has been studied only to reveal an extremely complex reaction system.[15] In order to understand the complexity surrounding the formation of compound **1** the following relevant points need to be discussed.

1) An alkylmagnesium chloride Grignard reagent consists in solution of different components taking part in a Schlenk equilibrium (eq. 4.4).[16]

$$R_2Mg \quad + \quad MgCl_2 \rightleftharpoons 2\ RMgCl$$

$$K = \frac{[RMgCl]^2}{[R_2Mg][MgCl_2]} = 5$$

$$\text{in THF and } R = \text{Me, Et}$$

eq. 4.4

As a result *at least* two species are present in solution that both will react with a phenolic OH group to give different products. It is known that the reactivity of the R_2Mg towards electrophiles is higher than that of RMgCl.[15] This reactivity is however modified by the Schlenk equilibrium. For MeMgCl and EtMgCl in THF the equilibrium constant is 5,[15] possibly compensating for the reactivity difference between the dialkylmagnesium and the alkylmagnesium chloride by increasing the amount of the less reactive alkylmagnesium chloride at the cost of the dialkylmagnesium. Unfortunately, the rate constants (k_1 and k_2 in eq. 4.5) for the reaction of ROH with the individual species are unknown so that the ratio of the two reaction products (I and II) cannot be predicted.[17]

2) Although no studies of the reaction of phenols with Grignard reagents are known, on the basis of the reaction of benzophenone with dimethylmagnesium

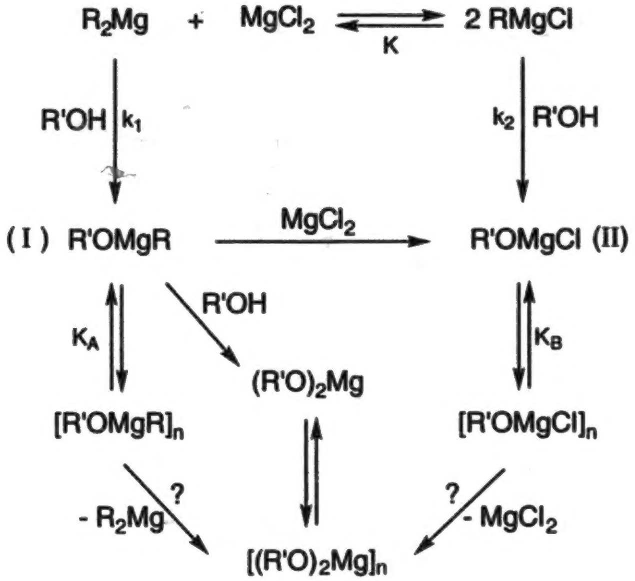

eq. 4.5

and methylmagnesium chloride[14,15] complications are expected to occur *after* the formation of ROMgCl and ROMgR. Grignard reagents in general associate (K_A and K_B in eq. 4.5), although aggregates can be broken down depending on the solvent used. The bridging strength varies according to RO bridging > THF coordination > Cl bridging > Br bridging > I bridging > alkyl bridging.[16] In THF the initially formed aryloxymagnesium compounds will therefore associate with any magnesium species available (*not* shown in eq. 4.5), modifying the reactivity of the complexed Grignard reagent and presumably altering the Schlenk equilibrium as well. In addition the association of the initially formed product can lead to alkyl or halogen exchange (eq. 4.5). Such a process can convert formed ROMgR into ROMgCl.[15]

3) Magnesium aryloxides show intermolecular ligand transfer (eq. 4.6, page 222).[9] Although disproportionation has not been documented, based on the ease with which magnesium-bound aryloxy ligands exchange, any sufficiently

large solubility or stability difference between products on the left and right side of the equilibrium should result in an equilibrium shift.[18] The influence of dissolved $MgCl_2$ on such an equilibrium awaits investigation, nor is it known if aryloxymagnesium chlorides indeed undergo similar processes.[4]

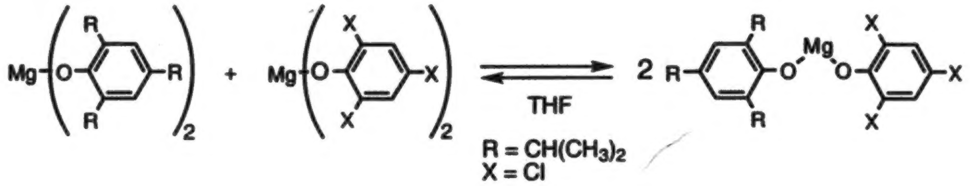

eq. 4.6

The ^{25}Mg-NMR spectroscopy results of the magnesium chloride salt of 4-*tert*-butylphenol in THF seem to indicate the presence of $MgCl_2$. This $MgCl_2$ may have been introduced in the actual reaction of the phenol with the Grignard (see point 1) or could have formed in a disproportionation as described in point 3.

Based on these reported observations a proposed mechanism for the formation of compound **1** is a hazardous speculation, especially since it is unclear if the single crystals obtained from an amorphous mass represent the bulk properties of the obtained material.[19] Because the starting magnesium chloride salt is undefined, any proposed reaction mechanism between the salt and $TiCl_4$ is subjected to the same objection. The formed molecule **2** is, however, relevant from another point of view. Exactly the same geometric coordination pattern is displayed by the titanium complex of p-*tert*-butylcalix[4]arene (eq. 4.7, page 223),[20] confirming the relation between the *tetrakis*[2-hydroxyphenyl]ethene ligands and the calix[4]arene class of ligands.

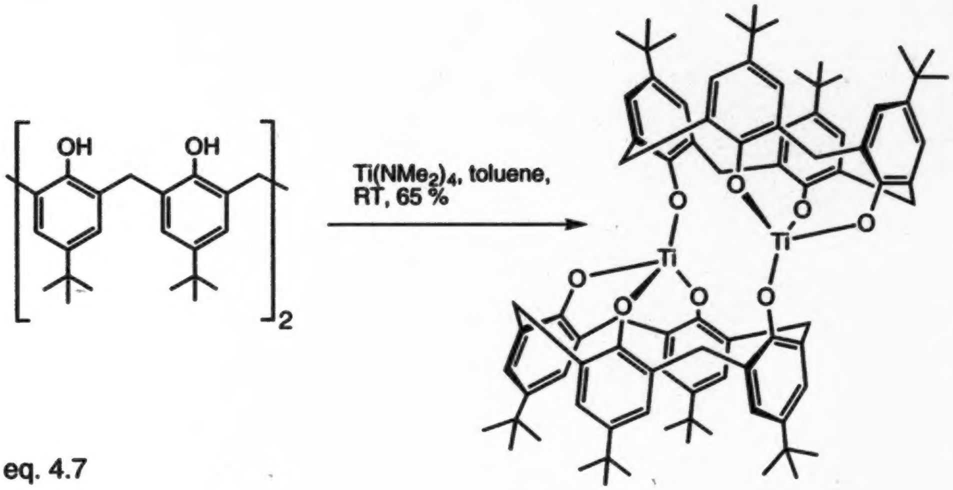

eq. 4.7

4.4 The Ziegler-Natta catalysis results.

In order to interpret the obtained results, while keeping the limitations of the obtained data in mind, the following working hypothesis will be used. Immediately after mixing the heterogeneous magnesium salts with $TiCl_4$ in toluene, complex aggregates of $MgCl_2$, possibly unreacted ROMgCl/(RO)$_2$Mg, and titanium phenoxide compounds are formed.[21] Each of the possible titanium phenoxides will be activated by the formed $MgCl_2$. For another interpretation, see the thesis of Dr. M. Fujita.[39]

The insoluble aggregates are the result of the absence of coordinating solvents (the reaction occurs in toluene) that would keep the magnesium salts in solution,[4,37] and represents the "activated" $MgCl_2$ as discussed in section 1.2.1, page 6. With regard to the formed titanium phenoxides, sufficient literature (and patent) precedent is available on the activation of "non-classical" titanium compounds by $MgCl_2$.[22] It is likely that a range of products will be present as a result of the heterogeneous reaction conditions used. The increased reaction temperatures reported for the synthesis of "activated" $MgCl_2$ by the chemical route (see section 1.2.1, page 6) might well be required to assure the formation of "byproduct free" $MgCl_2$.[38]

The first investigations into the use of $Ti(OR)_4/MgCl_2$ combinations were published in the patent literature; both high activity[22] as well as a lower polydispersity (2.9/3.4) were claimed.[22,23] The first article in the open literature seems to have been that of Soga, et al.,[24] showing an increase in propene polymerization activity of Ti(O-n-Butyl)$_4$ as a function of the amount of $MgCl_2$. No increase in catalyst activity was observed beyond a Mg/Ti ratio of 6.

In a review article, Zucchini and Cecchin[23] claimed that, for $MgCl_2$-supported titanium catalysts, the polydispersity increased with the electronegativity of the titanium substituents. In the published literature, no data were provided to support this claim.[25] Zucchini did, however, publish a study[26] on $MgCl_2$ supported "non-classical" catalysts, showing that the replacement of chloride atoms on the titanium by n-butoxy groups lowered the activity of the catalyst, while replacement by phenoxy groups showed little effect on the activity of the obtained catalysts (Table 4.3, page 225).

The only polydispersity data with regard to the claimed narrow polydispersity of $MgCl_2$ supported $Ti(OR)_4$ seems to have been published by Yano, et al.,[28] for Ti(O-n-Butyl)$_4$ and for $Ti(OEt)_4$ by Zucchini and Dall'Occo.[29]

Yano, et al., investigated the use of solubilized $MgCl_2$ using 2-ethylhexanol as well as in-situ-generated $MgCl_2$ from n-butylethylmagnesium, 2-ethylhexanol and diethylaluminumchloride. In combination with Ti(O-n-Butyl)$_4$, high-temperature ethene-polymerization catalysts were investigated. Although the activities of the so-created catalysts are not impressive at 200 °C, the data do show a decrease in the polydispersity as well as an increase in the activity of the catalyst when the $MgCl_2$/Ti ratio was increased (Table 4.4, page 226).[28]

Table 4.3: The influence of the supported titanium compound on the catalyst activity [reference 26].

$$\mathrm{MgCl_2} \xrightarrow[\mathrm{Ti(OR)_{4\text{-}n}Cl_n}]{\text{Ballmill,}} \mathrm{[MgCl_2]_x\,[Ti(OR)_{4\text{-}n}Cl_n]_y} \xrightarrow[\text{Ethene}]{\mathrm{R_3Al,}} \mathrm{PE}$$

$Ti(OR)_{4-n}Cl_n$[a]	Activity[b]
$TiCl_4$	$1.5 \cdot 10^3$
$Ti(OPh)_4$	$1.3 \cdot 10^3$
$Cl_3Ti(OR)$[c]	760
$Cl_2Ti(OR)_2$	790
$ClTi(OR)_3$	570
$Ti(OR)_4$	640

[a] 2 Wt % on comilled $MgCl_2$

[b] in Kg PE/mol Ti·hr·atm, 3 hour run, 75° C, Hexane, 1800 eq. $((CH_3)_2CHCH_2)_3Al$

[c] R = n-Butyl

Table 4.4: The influence of $MgCl_2$ on the PE polydispersity of $Ti(O\text{-}n\text{-}Butyl)_4$ based Ziegler-Natta catalysts [reference 28].

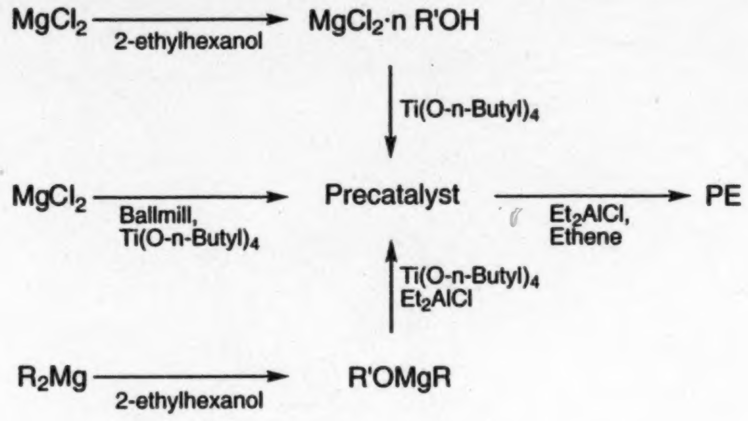
$MgCl_2$
2-ethylhexanol
$MgCl_2 \cdot n\ R'OH$
$Ti(O\text{-}n\text{-}Butyl)_4$
$MgCl_2$
Ballmill,
$Ti(O\text{-}n\text{-}Butyl)_4$
Precatalyst
Et_2AlCl,
Ethene
PE
$Ti(O\text{-}n\text{-}Butyl)_4$
Et_2AlCl
R_2Mg
2-ethylhexanol
R'OMgR

Precatalyst	Mg/Ti Ratio	Ti/Et_2AlCl Ratio	Activity[a]	M_w/M_n
$Ti(O\text{-}n\text{-}Butyl)_4$	-	100	10	10.5
Ballmilled $MgCl_2$ / $Ti(O\text{-}Bu)_4$	7.1	100	51	-
Dissolved[b] $MgCl_2$ / $Ti(O\text{-}Bu)_4$	7.1	100	100	-
R'OMgR[c]/ $Ti(O\text{-}Bu)_4$	14	100	359	5.7
R'OMgR[c]/ $Ti(O\text{-}Bu)_4$	28	180	407	3.8

a] in Kg PE/mol Ti·hr·atm, 20 minute run, 200 °C, Shell-Sol-71

b] 2-ethylhexanol as $MgCl_2$ dissolving agent.

c] generated in situ from butylethylmagnesium and 2-ethylhexanol.

More moderate polymerization temperatures were employed by Zucchini and Dall'Occo.[29] Using a co-milled $MgCl_2/Ti(OEt)_4$ catalyst a polymerization activity of 354 Kg/mol Ti·hr·atm was reported, with a polydispersity of 5.5 (Figure 4.8, see also section 1.5.1, page 32).[29]

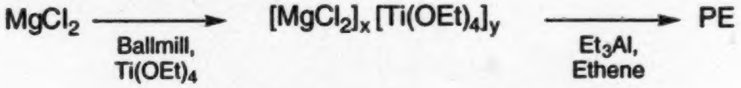
$MgCl_2$
Ballmill,
$Ti(OEt)_4$
$[MgCl_2]_x[Ti(OEt)_4]_y$
Et_3Al,
Ethene
PE

1 Wt % Ti on ballmilled $MgCl_2$, 60 °C, Hexane,
200 eq. Et_3Al. Activity: 354 Kg/mol Ti·hr·atm,
Polydispersity: 5.5, reference 29

Figure 4.8

The use of $MgCl_2$ as an activating support has recently been revived by Sobota, et al., to obtain high activity ethene polymerization catalysts using dichlordialkoxytitanium and diethoxydialkoxytitanium compounds (Figure 4.9).[30] Unfortunately polydispersity data were not reported.

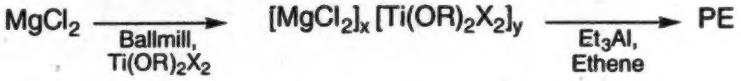
$MgCl_2$
Ballmill,
$Ti(OR)_2X_2$
$[MgCl_2]_x[Ti(OR)_2X_2]_y$
Et_3Al,
Ethene
PE

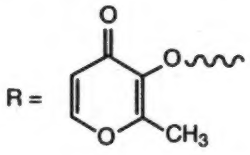

X	Activity[a]
Cl	$2.8 \cdot 10^3$
OEt	$1.7 \cdot 10^3$

a] in Kg PE/mol Ti·hr·atm, 500 eq. Et_3Al/Et_2AlCl (1:1), 50 °C, Hexane, Mg/Ti = 10, runtime: not given. Reference 30.

Figure 4.9

On the basis of the proposed working hypothesis, following the addition of 1 equivalent of $TiCl_4$ rapid initial formation of insoluble $MgCl_2$ takes place under formation of a presumably wide range of titanium phenoxides differing in the amount of chloride groups present on the titanium (Scheme 4.1, page 229).

The formed $MgCl_2$ will have no solubility in the absence of donor solvents[37] and will form amorphous $MgCl_2$ aggregates trapping both soluble and insoluble compounds. Because of the heterogeneous reaction conditions there is a possibility that unreacted starting material is also trapped. As a result of the proposed solubility of the formed titanium phenoxides, the Mg/Ti ratio will change in time as titanium phenoxides are removed from the $MgCl_2$ aggregates. This would result in a complex (and without further data unpredictable) variation of the catalyst activity[24] and possibly the polydispersity[28] of the formed PE as a function of the $TiCl_4$/magnesium salt mixing time. The partitioning of the formed titanium phenoxides due to adsorption on $MgCl_2$, trapping by $MgCl_2$ aggregates and dissolving in toluene is represented by $K_{1,2,3,4}$ in Scheme 4.1.

On activation with Et_3Al *both* phases will contain titanium phenoxides. Assuming that the behavior of the tetraarylethene ligand is not fundamentally different from that of a phenoxy ligand, the insoluble, $MgCl_2$-supported part should show high polymerization catalysis while the soluble part should show low polymerization activity (vide infra, Figure 4.10, page 231) using trialkylaluminum as a cocatalyst. This would imply that ligand systems that give titanium phenoxides of limited solubility could exhibit higher activity, and yield well defined PE compared to soluble titanium phenoxides. Indeed the initial activity of the isolated precipitates seems to decrease going from *tetrakis*[2-hydroxyphenyl]ethene via the more lipohilic *tetrakis*[5-(1,1-dimethylethyl)-2-hydroxyphenyl]ethene to 4-*tert*-butylphenol (see Figure 4.1, 4.2 and 4.3, page 204 and 205) when one equivalent of $TiCl_4$ is used.

Scheme 4.1: proposed reaction mechanism leading to active Ziegler-Natta catalysts.

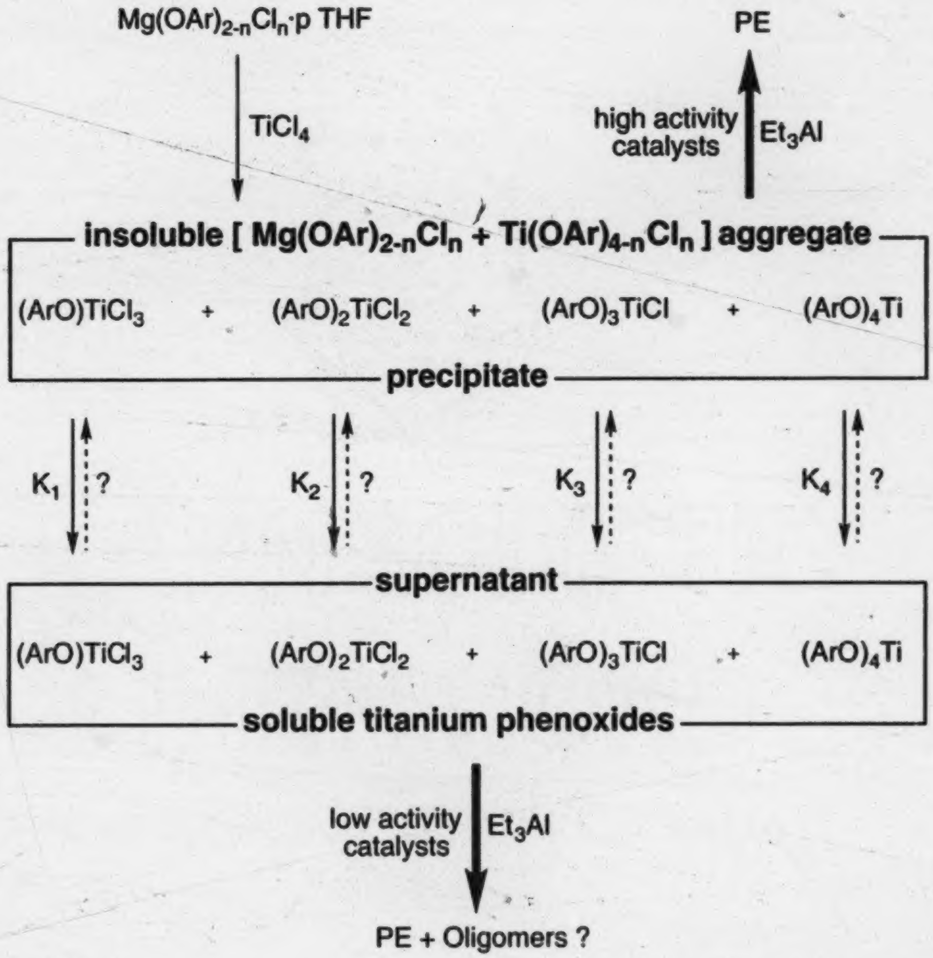
$Mg(OAr)_{2-n}Cl_n \cdot p$ THF
$TiCl_4$
PE
high activity catalysts
Et_3Al
insoluble [$Mg(OAr)_{2-n}Cl_n$ + $Ti(OAr)_{4-n}Cl_n$] aggregate
$(ArO)TiCl_3$ + $(ArO)_2TiCl_2$ + $(ArO)_3TiCl$ + $(ArO)_4Ti$
precipitate
K_1 ?
K_2 ?
K_3 ?
K_4 ?
supernatant
$(ArO)TiCl_3$ + $(ArO)_2TiCl_2$ + $(ArO)_3TiCl$ + $(ArO)_4Ti$
soluble titanium phenoxides
low activity catalysts
Et_3Al
PE + Oligomers ?

In all cases the supernatant shows hardly any activity in spite of the red color indicating the presence of titanium containing compounds in that phase, when trialkylaluminum cocatalysts are used. When an excess $TiCl_4$ is used to favor the formation of potential precatalysts in the form of titanium phenoxides according to Table 4.1 (page 206) between 80-90% of the ligand is present in the supernatant, presumably as titanium phenoxides, indicating that under these conditions the formed titanium phenoxide species are well soluble.

Although neither the oligomer content nor the sidechain branching of the obtained PE was determined in the centrifuge experiments, valuable information with regard to the active catalytic center(s) could have been obtained. According to literature reports $Ti(OAr)_4$ compounds are used as oligomerization catalysts that give a high yield of 1-butene and hardly any PE (Figure 4.10).[31] If a Ziegler-Natta catalyst would also be present, the formed 1-butene would be incorporated in the growing PE chain.

By mixing a *soluble* catalyst for the oligomerization of ethene to form 1-butene with an *insoluble* $MgCl_2$-supported $TiCl_4$ catalyst, a dual function

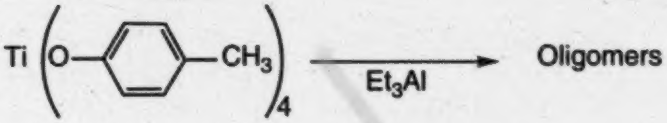

	Weigth %				
Et_3Al/Ti	C_4	C_6	C_8	C_{10}	PE
6[a]	68	22	1	1.2	7.8
20[a]	71	28	1.1	0.4	-

a] 1Hour run, 25 °C, Solvent: not given, reference 31. Catalyst activity for $Et_3Al/Ti = 3.7$, 90 °C, n-heptane, 2 hours, 10 Kg 1-butene/mol Ti·hr·atm, reference 32.

Figure 4.10

catalyst was created by Beach and Kissin to form branched polyethylene.[32] The soluble oligomerization precatalyst was Ti(OR)$_4$ (R = alkyl, aryl, Figure 4.10, page 230) that apparently does not adsorb on the available MgCl$_2$ surface once activated. It was noticed by the authors that Ti(OR)$_4$ compounds were only effective oligomerization catalysts in solution (insoluble Ti(OR)$_4$ did not display oligomerization catalysis) and in the absence of hydrogen.[32] Furthermore, at high concentrations, Ti(OR)$_4$ lowered the activity of the supported catalyst by both poisoning the supported catalyst as well as increasing the copolymerization with 1-butene according to Beach and Kissin.[32]

In the absence of a synthetic route into tetraarylethene-based titanium compounds (see however the thesis of Dr. M. Fujita[39] for titanium compounds of the sterically more hindered *ortho* propylated *tetrakis*[2-hydroxyphenyl]ethene), as well as data on the formation of oligomers in the supernatant or side-chain branching in the formed PE, any relation between these observations and the experimental data remains unproven.

Although the proposed "leaching" of titanium phenoxides out of the formed MgCl$_2$ clusters seems reasonable, it is unclear why the precipitate, as formed from the magnesium chloride salt of *tetrakis*[2-hydroxyphenyl]ethene, remains active after washing the precipitate 5 times with toluene. The remaining titanium must be strongly attached to, or entrapped in, the magnesium clusters. The alternative, the formation of a classic TiCl$_4$·n MgCl$_2$ compound cannot be ruled out given the heterogeneous nature of the starting reactants and should express itself in a characteristic broad polydispersity of the formed PE. An additional source of TiCl$_4$ could be formed by disproportionation of titanium phenoxides.[18]

The actual measured polydispersity of a large scale reaction was 5.5 and could be interpreted as indicating the involvement of phenoxy groups in the active catalyst center. Unfortunately, no polydispersity data for a Ti(OAr)$_4$ derived catalyst are available for comparison, but the polydispersity obtained for the catalyst derived from the magnesium chloride salt of 2,2'-methylenebis[4,6-bis(1,1-dimethylethyl)]phenol (3.8) and the polydispersities obtained from titaniumtetraalkoxides (5.5 and 3.8, Figure 4.8, page 227 and Table 4.4, page 226) seem to indicate that the ligand structure has little to contribute to the polydispersity except supplying oxygen(s) to the catalytically active center.

The results obtained for the magnesium chloride salts of *tetrakis*[5-(1,1-dimethylethyl)-2-hydroxyphenyl]ethene and 2,2'-thiobis[4,6-bis(1,1-dimethylethyl)]phenol show a decrease of catalyst activity with increasing mixing time, and a decrease of catalyst activity with an increase of the number of equivalents of $TiCl_4$ added. Both could be interpreted as a leaching of titanium phenoxides out of the formed $MgCl_2$ clusters.

The remaining observations are not easily explained using the working hypothesis. It is, for instance, unclear why the highest activity is observed for both ligand systems using 2 equivalents of $TiCl_4$. The ratio of available $MgCl_2$/Ti may have something to do with this. Nor does the low activity of the 1 equivalent $TiCl_4$/magnesium chloride salt of *tetrakis*[5-(1,1-dimethylethyl)-2-hydroxyphenyl] ethene fit the observed higher activity of the precipitate obtained in the centrifuge experiment (compare Figures 4.2 and 4.4, page 204 and 208). Without further analytical data on the polydispersity and polymer structure of the obtained PE, oligomerization activity of the catalyst mix and the titanium/ligand content of both heterogeneous and homogeneous phase, no conclusions can be drawn.

Results more amenable to interpretation were obtained on detailed analysis of the products formed by the catalyst made from the magnesium chloride salt of 2,2'-thiobis[4,6-(1,1-dimethylethyl)]phenol and 2 equivalents of $TiCl_4$ in the presence of hydrogen and ethene. Not only was the polydispersity in the range of classic Ziegler-Natta supported catalysts (see Table 4.2, page 209), the weight percentage of oligomers was unexpectedly high. The last observation would indicate the presence of an oligomerization catalyst, which would fit the working hypothesis. However, it is well known that the presence of sulphur (as a thioether)[33] in classic supported Ziegler-Natta catalysts induces the formation of oligomers. The presence of oligomers can therefore not be used as supporting evidence for the working hypothesis. In addition, the isolated oligomers are alkanes, not 1-alkenes, presumably explaining their presence in solution instead of being incorporated in the growing polymer chain. Without further information an explanation is rather difficult to give, especially as Beach and Kissin[32] specifically state that no oligomerization activity is observed in the presence of hydrogen. If the formed PE would contain a lot of sidechain branching, the presence of both a hydrogenation catalyst and an oligomerization catalyst (in addition to a polymerization catalyst) could be proposed, except that according to Table 4.2 (page 209) in the absence of hydrogen alkanes are *also* formed. This is likely due to traces of hydrogen still present in the polymerization setup, in spite of a thorough flushing with ethene (the order of the experiment was atmospheric H_2, 5 psig H_2, "no" H_2, 2.5 psig H_2) before the runs without hydrogen were started. The observed variation in the weight % oligomers reflects the loss of oligomer during the cleaning of the organic layers. An internal standard (like tridecane) added *before* the cleanup would have given more internally consistent results.

4.5 Experimental

General (see also the General section in the Experimental for Chapter 2, page 94).

Gas chromatography was performed on a Hewlett Packard 5890 GC coupled to a 5970 mass selective detector and an 7673 GC SFC auto injector. A HP5 (25 m, 0.32 mm id, 0.52 μ coating of 5% diphenylpolysiloxane/ 95% dimethylpolysiloxane) capillary column was used, at a flowrate of 1 ml/min. helium. By starting the analysis at a column temperature of 50 °C and increasing the temperature by 10 °C/min. to a final temperature of 290 °C a gas chromatogram of all oligomers present was obtained.

Size-exclusion chromatography was performed in the Department of Chemical Engineering and Materials, University of Alberta, Wanke group, on an Alliance GPCV 2000 using a refractive index detector, and at NOVA, Calgary, using an unspecified system and 1,2,4-trichlorobenzene as a solvent. Relevant data for the Alliance GPCV - Columns: 3 Styragel HT-6E (mixed bed) columns in series. Solvent: 1,2,4-trichlorobenzene, at a flowrate of 1 ml/min. and 140 °C. Calibration: narrow polydispersity polystyrene samples. Polyethylene samples were dissolved in trichlorobenzene at 160 °C before injection.

For centrifuging suspensions, an International Equipment Co., Model CL clinical centrifuge was used, with an estimated speed of 2000 rpm.

Small scale polymerizations were performed using syringe techniques at 30 psig ethene (Praxair CP grade) pressure, using Lab Glass 20 mL pressure reaction bottles LG-3921-100, and crown caps/Neoprene gaskets LG-3922-100. All PE syringes (Aldrich Z23,072-3) free of contaminating lubricants were used in all polymerization runs. These syringes were filled inside the glovebox and transferred out of the glovebox maintaining a nitrogen atmosphere by drawing in a nitrogen blanket over the solution in the syringe and inserting the needle in a rubber stopper. This prevents contamination of the solution by toluene soluble compounds in the rubber stopper as well as by atmospheric oxygen. In order to minimize contamination of the precatalyst mixture, the gasket was wrapped in Teflon tape (Aldrich Teflon sealing tape 1 inch wide, Z22188-0), but the exposure of the precatalyst to the so treated gasket should be kept at a minimum as plasticizers can be detected in the toluene solution by GCMS after a polymerization run. In order to improve the reproducibility of polymerization runs, it is advisable to use a suitable magnetic stirrer like the Ikamag IKA RCT Basic, and selected Teflon coated stir bars that give a consistent deep and stable vortex at maximum stirring speed. Glassware and stirrer bars were air dried at 120 °C overnight, and rinsed with tributylaluminum and polymerization quality toluene before use. All catalytic activity calculations are based on an absolute pressure of ethene.

Larger scale polymerizations were performed using a modified Parr 4841 controller assembly for stirring and monitoring the reaction temperature combined with a Andrews Glass Co. reactor. The reactor consisted of a Lab Crest 110-900-0012 multiported stirring assembly with an in-house constructed collar to mount the assembly in the Parr setup. On the stirring assembly was mounted a type J thermocouple, injection port, vacuum/gas release port combined with a safety valve (75 psig), pressure gauge (0-100 psig) and a gas/liquid inlet port on which an in-house manufactured pressure burette could be mounted using a Swagelok quick-connect fitting. A 12 ounce (300 mL) glass vessel was mounted on the stirring assembly using a Neoprene gasket/stainless steel collar combination. It is advisable to replace the gasket regularly in order to maintain a good seal: the effect of the gasket plasticizer on catalyst activity has not been tested. Before use, the assembled apparatus was put under vacuum and heated to 120 °C overnight using the Parr heating mantle and an external type J thermocouple securely mounted in the gap between the glass vessel and the heating mantle. Both stirrer and glass vessel were rinsed with tributylaluminum and polymerization-quality toluene before use. The ethene was passed through a column containing copper deoxygenation catalyst, Engelhard Cu-0226S, followed by a column containing a mixture of 13X and 3A molecular sieves. Hydrogen was treated in the same way. The flow of ethene was measured using an uncalibrated Teledyne-Hastings-Raydist mass flowmeter with a range of 0-9.99 slpm, connected to a Fisher Recordall series 5000 recorder. Attempts to maintain the reaction temperature at a specific value using a Neslab RTE-211 cooling bath were not successful: all polymerization reactions were therefore initiated at room temperature without further temperature control.

Ether-free ethylmagnesium chloride.

The procedure described by Ziegler and Holzkamp was used.[34]

A setup consisting of a reflux condenser connected to an oil bubbler, three neck round bottom flask with stir bar, nitrogen inlet and dropping funnel was charged with 200 ml dry, oxygen-free toluene. The dropping funnel was charged with 100 ml 2M ethylmagnesium chloride in diethyl ether. Under a brisk reflux of toluene, the Grignard solution was added slowly to the toluene. At the end of the addition the volume of the resulting suspension was reduced to 150 ml under rapid stirring by passing a flow of nitrogen over the boiling suspension into the atmosphere through an oil bubbler. The remaining oil was further reduced under an oil pump vacuum to obtain a white solid. To remove traces of remaining solvent the solid was pulverized in the glovebox and kept under high

vacuum at a temperature of 90 °C for 4 days. The obtained solid Grignard contained less then 1% diethyl ether according to ^{1}H-NMR spectroscopy.
^{1}H-NMR (360 MHz, THF-d_8/C_6D_6 = 1/1): δ -0.24 (q, J = 8.0 Hz, 2H), 1.66 (t, J = 8.0 Hz, 3H).

Preparation of Ziegler-Natta catalysts using *tetrakis*[2-hydroxyphenyl]ethene.

a) To a suspension of 53 mg ($1.3 \cdot 10^{-4}$ mol) *tetrakis*[2-hydroxyphenyl]ethene (see page 101 for synthesis) in 10 mL dry, oxygen-free hexane was added while stirring under nitrogen 54 mg ($2.9 \cdot 10^{-4}$ mol, 2.2 eq.) $TiCl_4$. The color of the suspension turned dark brown. The suspension was stirred overnight at room temperature. The next day solvent was removed under vacuum and the solids transferred to a glovebox. The solid was extracted with 10 mL toluene, and the resulting dark brown solution filtered over Celite to remove any solids remaining. The solution was reduced to dryness under vacuum to obtain 70 mg of solid. A solution was prepared from 2.3 mg of this solid in 6 mL toluene and placed in a glass bomb equipped with stir bar. After placement of a gasket and crown cap, the solution was transferred out of the glovebox. After purging the content of the bomb with ethene while stirring, the bomb was pressurized with 30 psig ethene. After injection of 1.4 mL 2M Me_3Al no PE formation was observed within 10 minutes. The experiment was stopped by venting the ethene gas and injecting 3 mL of a 2.4% HCl in EtOH solution.

b) To a stirred suspension of 49 mg (1.2 mmol, 4 eq.) KH in 20 mL Et_2O in a glovebox was added 0.12 g (0.31 mmol) *tetrakis*[2-hydroxyphenyl]ethene. After release of hydrogen, the solution was stoppered and stirred overnight at room temperature. The next day a solution of 118 mg (0.6 mmol, 2 eq.) $TiCl_4$ in 1 mL pentane was added. Immediately a dark brown precipitate formed. After stirring overnight, the clear top layer was carefully removed from the precipitate and the remaining solid extracted with Et_2O. Both the remaining precipitate as well as the solid obtained by evaporating the Et_2O were dried under vacuum. Neither solid (4 mg in 6 mL toluene, 30 psig ethene) showed any sign of polymerization activity when treated with Et_3Al in the presence of ethene.

c) Other ratios and reaction conditions for treatment of *tetrakis*[2-hydroxyphenyl]ethene with $TiCl_3{\cdot}(NMe_3)_2$, $TiCl_3{\cdot}3$ THF, $Ti(NMe_2)_4$, $Zr(NMe_2)_4$ or $ZrCl_4$ were also conducted. None of the so-obtained materials gave crystals of suitable quality, in spite of numerous attempts using different solvents, nor did the so-obtained crude reaction products show any catalytic activity when suspended in toluene and exposed to trialkylaluminum in the presence of ethene.

d) In the glovebox, to a stirred solution of 0.11 g ($2.8{\cdot}10^{-4}$ mol) *tetrakis*[2-hydroxyphenyl]ethene in 6 ml THF was added 0.38 mL (1.1 mmol, 4 eq.) of a 3 M solution of MeMgCl in Et_2O. After 1 hour a solution of 55 mg (1.2 mmol, 4.1 eq.) $TiCl_4$ in 1 mL pentane was added to the solution, changing the color of the solution to a deep red brown within 5 minutes. After 30 minutes the red brown solution was reduced to dryness under vacuum and the solid washed with pentane to remove excess $TiCl_4$. A solution of 1.2 mg of the so obtained material in 6 ml toluene was prepared in a glass bomb equipped with a stir bar. After placement of a gasket and crown cap, the solution was transferred out of the glovebox. While stirring the contents, the bomb was purged with ethene and pressurized to 30 psig ethene. After the injection of 1 mL 1M Et_3Al, rapid PE formation was observed during a 10 minute polymerization run, after which the experiment was stopped by venting the ethene gas and injecting 3 mL of a 2.4% HCl in EtOH solution. The PE formed was not isolated.

Analyses of the magnesium salts.

a) By ^{1}H-NMR spectroscopy: In the glovebox, 10 mg samples of the magnesium chloride salts were suspended in 1 mL of a solution consisting of 15 g toluene-d_8 (d: 0.943 g/mL) and 9.7 mg 1-hexene as a chemically inert internal standard ($7.3 \cdot 10^{-6}$ mol 1-hexene/ml toluene-d_8). All magnesium salts tested gave cloudy solutions except the 4-*tert*butylphenol derived magnesium chloride salt. The suspensions were filtered through a plug of Celite into an NMR tube, after which an ^{1}H-NMR spectrum was taken. Overlap problems between toluene signals and ligand signals, as well as the low intensity of both ligand and internal standard signals did not allow a calculation of the amount of material dissolved in toluene. For the results see the individual magnesium chloride salts (vide infra).

b) By ^{25}Mg-NMR spectroscopy: 0.58 g of 4-*tert*butylphenoxymagnesium chloride salt was suspended in 0.5 mL THF-d_8, and filtered through a plug of cottonwool into a 5 mm NMR tube. On a Bruker WH400 using an acquisition time of 0.41 seconds and a 90° pulse of 39.5 μs, a ^{25}Mg signal was obtained with 58177 scans (RG = 200) at 12 ppm ($W_{1/2}$ = 588 Hz, 24 ppm) relative to an external 0.18 M $MgSO_4$ solution in D_2O (24.49 MHz = 0 ppm). No magnetic susceptibility corrections were applied, while baseline distortions were removed by zerofilling the first points of the FID and manual baseline correction. Addition of $MgCl_2$ to the 4-*tert*butylphenoxymagnesium chloride THF-d_8 solution caused a shift of the signal to 11 ppm ($W_{1/2}$ = 539 Hz, 22 ppm) as well as an increase in signal intensity (RG = 200, NS = 15629). A similar chemical shift (11 ppm, $W_{1/2}$

= 343 Hz, 14 ppm) was observed for 8 mg $MgCl_2$ in 0.5 mL THF-d_8. No other magnesium chloride salts were tested.

c) By quantitative GC: Several aryloxymagnesium chloride samples were dissolved in 1.5 mL EtOH each to give a concentration of 0.4 to 4.5 mg salt/ mL EtOH. THF in the so obtained samples was adsorbed on a Supelco solid microphase micro extraction fiber, that subsequently was inserted in the injection port of the GC. The GC detection limit was found to be in the order of 1 mg ($1.4 \cdot 10^{-5}$ mol) THF/ ml EtOH. Other decomposition techniques were also tried. Using a solvent consisting of 95% EtOH/ 5% HCl or 95% Acetone/ 5% HCl, no improvement of the detection limit could be achieved. The GC column was damaged during use due to HCl incompatibility.

d) By quantitative ^{1}H-NMR spectroscopy, THF content: Several aryloxymagnesium chloride samples were dissolved in the following solvent combinations: D_2O followed by acetone-d_6, acetone-d_6 followed by D_2O/D_2SO_4, D_2O/D_2SO_4 followed by acetone-d_6, and acetonitrile-d_3 followed by D_2O/D_2SO_4. Limited solubility of the salts as well as supersaturation resulting in the delayed formation of precipitates in the NMR solution, led to large differences (30-200% depending on ligand) in the calculated number of THF molecules/ ligand between solvent combinations.

e) By derivatization: In THF 66 mg of a magnesium chloride salt of *tetrakis*[2-hydroxyphenyl]ethene was stirred with 42 μL methyl iodide overnight. The next day the solution was diluted with saturated $NaHCO_3$ solution, and extracted with 100 mL ethyl acetate. The water layer was acidified with 10% HCl, and extracted with 100 mL ethyl acetate. The combined organic layers were washed neutral with water, dried over anhydrous magnesium sulfate, and after filtration reduced to dryness using a rotatory evaporator. ^{1}H-NMR spectroscopy of the resulting solid only showed the presence of *tetrakis*[2-hydroxyphenyl]ethene.

f) By elemental analysis. Under the following assumptions, elemental analysis data might be used to obtain an indication of the composition of the magnesium salts: (1) the solvents and ligands used do not decompose under the reaction conditions, (2) the solid only consists of Mg, Cl, THF and ligand molecules, and (3) no matrix effects occur that would change the C,H,X analysis in the elemental analysis procedure. For example, the 4-*tert*-butylphenoxymagnesium chloride salt can be described as consisting of one 4-*tert*-butylphenoxy group, n magnesium atoms, o chloride atoms and p THF molecules. The solid can be analyzed for C, H and Cl. Because the C and H contribution of THF to the total %C and %H is different, by making use of [100 x (10+4p) x 12.0107]/MW = % C measured and [100 x (13+8p) x 1.00794]/MW = % H measured, p (the number of THF molecules per ligand) and MW can be calculated. The number of Cl atoms can be calculated from the mass % Cl and subsequently o (the number of magnesium atoms per ligand) can be calculated. The obtained values of n,o and p represent *only* the ratios of the number of magnesium atoms, chloride atoms and THF molecules versus the ligand. The calculated molecular weight *only* represents an "artificial" molecule consisting of a single ligand and additional Mg and Cl atoms together with THF molecules to obtain a solution of the elemental analysis, but it does provide a formula from which the amount of $TiCl_4$ to be used can be determined.

Tetrakis[2-hydroxyphenyl]ethene magnesium chloride salt.

a) Polymerization study.

In the glovebox, a solution of 0.47 g (1.2 mmol) *tetrakis*[2-hydroxyphenyl]ethene (see page 110 for synthesis) in 20 mL THF was slowly added under stirring to a solution of 0.43 g (4.8 mmol, 4 eq.) EtMgCl in 20 mL THF. After transfer out of the glovebox, the solution was heated to reflux overnight under nitrogen. The next day the volume of the solution was reduced under vacuum to 25 mL at which point a dense white precipitate formed, which was isolated by centrifuging the suspension and discarding the supernatant. The so-obtained solid was washed twice with a small amount of THF, and dried under vacuum. EA range for % C = 62.8735 to 63.2354 (n=3), % H = 5.1369 to 5.2442 (n=3), % Cl = 7.12, 6.91 (n=2). Calculated MW based on average % H,C,Cl = 675, Ligand$\cdot$$Mg_{2.7}Cl_{1.3}$$\cdot$2.4 THF. ^{1}H-NMR (toluene-d_8/1-hexene, 200 MHz): in addition to the standard, the following signals were observed δ 7.2 (broad, overlap with residual H signal of toluene-d_8), 3.59 (broad, THF), 1.4 (broad, THF, overlap with alkyl part of 1-hexene at 1.24 ppm).

To a suspension of 21.4 mg of the magnesium salt ($3.2\cdot10^{-5}$ mol ligand according to calculated MW) and 23 g (27 mL) toluene was added under rapid stirring 0.28 g ($3.2\cdot10^{-5}$ mol, 1 eq. $TiCl_4$) of a solution consisting of 0.14 g $TiCl_4$ in 6.3 g toluene. Directly after mixing, and 23, 62, 94 and 127 minutes after mixing 4.8 g samples of the stirred dark brown suspension were taken by filling up a centrifuge tube to a fixed, marked, height and centrifuged for 5 minutes at 2000 rpm. The supernatant and the red brown transparent precipitate were carefully separated, and the precipitate resuspended in 4.8 g toluene using the same fixed, marked, height. The suspension and supernatant were transferred to 10 mL glass polymerization bombs and capped with a gasket and crown cap. Outside the glovebox, the content of the bombs were flushed and pressurized with 32 psig ethene. Polymerization was started by injection of 1 mL ($4.7 \cdot 10^{-4}$ mol, 70 eq./Ti) Et_3Al stock solution consisting of 0.8758 g Et_3Al in 16 mL toluene. The reaction was stopped after a run of 10 minutes by venting the ethene and injecting 3 mL of a 2.4% HCl in EtOH solution into the bomb. Workup consisted of filtering and washing (with EtOH/HCl solution) the PE, and drying the so obtained material under vacuum at 50 °C overnight. See text chapter and Figure 4.1, page 203 and Table 4.5 (page 243), for results. The last sample was treated in the same way, except the precipitate was suspended in toluene and centrifuged/washed 5 times. The supernatant of the first washing didn't show polymerization activity, while the precipitate remained active after 5 washings, see text chapter and Table 4.5 (page 243).

b) Large scale polymerization.

In the glovebox, to a solution of 0.41 g (1 mmol) *tetrakis*[2-hydroxyphenyl] ethene dissolved in 15 mL THF was added under rapid stirring 1.4 mL 3M (4.3 mmol, 4.1 eq.) methylmagnesium chloride solution in Et_2O. The solution was stirred at room temperature overnight. The next day half of the solvent was removed under vacuum, and 9 mL of pentane was added. After the precipitate had settled the pentane was carefully removed using a Pasteur pipette. The so-obtained material was dried under vacuum to give a white powder. EA range for %C = 59.7745 to 60.0053 (n=3), %H = 5.2457 to 5.2917 (n=3), %Cl = 9.9 to 10.2 (n=3). Calculated MW = 759, $Ligand \cdot Mg_{3.2} \cdot Cl_{2.2} \cdot 3.0\ THF$. Of the so-obtained magnesium salt, 11.8 mg ($1.6 \cdot 10^{-5}$ mol based on MW calculated from EA data) was suspended in 50 mL toluene together with 3.3 mg ($1.8 \cdot 10^{-5}$ mol) $TiCl_4$ inside a pressure addition funnel. This suspension was added to a rapidly stirred solution of 0.12 g (1.7 mmol, 93 eq./Ti) Me_3Al in 250 mL toluene under 30 psig ethene. An exotherm of 46 °C (22 to 68 °C) was observed over a period

Table 4.5: Polymerization study: homogeneity of the reaction using the *tetrakis*[2-hydroxyphenyl]ethene magnesium chloride salt and 1 equivalent $TiCl_4$.

Sample Time (minutes)[1]	Polym. Time (minutes, seconds)	PE Yield (g)	Activity[2] (kg PE/mol Ti·hr·atm)	Delay[3] (minutes)
0 ppt	10min18sec	0.5061	147	17
0 sup	10min18sec	0.1033	30	17
23 ppt	10min15sec	0.3538	103	24
23 sup	10min15sec	0.0529	15	24
62 ppt	10min8sec	0.3686	108	19
62 sup	10min8sec	0.0196	6	19
94 ppt	8min45sec	0.2469	84	11
94 sup	10min9sec	0.0142	4	11
127 ppt	10min13sec	0.3084	90	86
127 sup1	20min30sec	0.0163	2	31
127 sup2	13min36sec	-	-	51

1] ppt = precipitate, sup = supernatant, sup1,2 = supernatant after first and second washing. 5 minute centrifuge run 2] based on assumed [Ti] = $6.6 \cdot 10^{-6}$ mol for each sample, sample size 4.8 g. 3] Delay between separation of supernatant and precipitate after centrifuging, and the polymerization experiment.

of 39 minutes, with the maximum ethene uptake 21 minutes after injecting the precatalyst. The reaction was stopped by venting the ethene and injecting 10 mL of a 2.4% HCl in EtOH solution. The so obtained PE suspension was cast into 400 mL EtOH/HCl solution, placed in an ultrasonic bath for 10 minutes and filtered over a type C glassfrit. The PE was dried overnight under vacuum at 50 °C. Yield of white powder: 19.47 g. Calculated activity: 550 kg PE/mol Ti·atm·hr. Polydispersity: 5, $M_n = 206 \cdot 10^3$, $M_w = 1038 \cdot 10^3$.

Compound 1: The magnesium complex of *tetrakis*[2-hydroxyphenyl] ethene.

In the glovebox, a solution of 0.12 g (0.3 mmol) of *tetrakis*[2-hydroxyphenyl]ethene dissolved in 12 mL THF was added to 0.5 mL (1.2 mmol, 4 eq.) rapidly stirred 3 M Et_2O solution of methylmagnesium chloride. The solution was stirred overnight at room temperature. The next day the solvent was removed under vacuum and the solid resuspended in a small amount of THF. After settling of the solids, the clear top layer was carefully removed using a Pasteur pipette and the remaining precipitate was dissolved in a small amount of boiling THF. After addition of toluene to form a supersaturated solution a crystal of sufficient quality for a X-ray diffraction study was obtained by leaving the solution undisturbed at room temperature for several days.

Crystal data (see appendix G, page 371 for details) for compound 1 ($C_{77}H_{76}Cl_2Mg_5O_{12.5}$): crystal dimensions 0.19 × 0.10 × 0.09 mm, orthorhombic, space group $Pna2_1$ (No. 33), a = 24.7812 (16), b = 20.7209 (16), c = 14.8495 (11) (Å), V (Å^3) = 7625.1 (10), $Z = 4$, ρ_{calcd} = 1.214 (g cm^{-3}), μ = 0.185 (mm^{-1}). Data collection and refinement conditions: Bruker P4/RA/SMART 1000 CCD diffractometer using graphite-monochromated MoKα radiation (λ [Å] = 0.71073), T = 193 (K), scan type ϕ rotations (0.3°) / ω scans (0.3°) (30 s exposures), 42345 measured reflections, 15313 independent reflections, 4463 included in the refinement ($F_o^2 \geq 2\sigma(F_o^2)$), structure solution by direct methods/fragment search (*DIRDIF–96*), refinement by full-matrix least-squares on F^2 (*SHELXL–93*), absorption correction method *SADABS,* transmission max./min. = 0.9803/0.7620, 784 parameters, R_1 = 0.0864 (based on 4463 observed data), wR_2 = 0.2828 (based on all 15313 data), residual electron density 0.811/-0.382 e Å^{-3}.

2,2'-Methylenebis[4,6-bis(1,1-dimethylethyl)]phenoxymagnesium chloride salt.

a) Large scale polymerization.

In a glovebox to a stirred solution of 0.13 g ($3.2 \cdot 10^{-4}$ mol) 2,2'-methylenebis[4,6-bis(1,1-dimethylethyl)]phenol[35] in 5 mL Et_2O a solution of 0.21 mL ($6.3 \cdot 10^{-4}$, 2 eq.) 3M MeMgCl (in Et_2O) in 10 mL THF was added dropwise. The solution was stirred at room temperature. The next day 2/3 of the solution was removed under reduced pressure, and the same volume of hexane was added to form a white precipitate. After centrifuging the suspension, the supernatant was carefully removed using a Pasteur pipette and the hexane washing procedure repeated. The resulting sludge was dried under vacuum to obtain a white powder that was kept overnight on a high vacuum line. EA %C = 61.5444, %H = 8.4291, %Cl = 12.16. Calculated MW = 849, Ligand·$Mg_{2.5}Cl_{2.9}$·3.6 THF.

Of the so obtained magnesium salt, 10.2 mg ($1.2 \cdot 10^{-5}$ mol based on MW calculated from EA data) was suspended in 50 mL toluene together with 3.6 mg ($1.9 \cdot 10^{-5}$ mol) $TiCl_4$ inside a pressure addition funnel. This suspension was added to a rapidly stirred solution of 0.19 g (2.7 mmol, 145 eq./Ti) Me_3Al in 250 mL toluene under 30 psig ethene. An exotherm of 29 °C (23 to 52 °C) was observed over a period of 78 minutes, with the maximum ethene uptake 41 minutes after injecting the precatalyst. The reaction was stopped by venting the ethene and injecting 10 mL of a 2.4% HCl in EtOH solution. The so obtained PE suspension was cast into 500 mL EtOH/HCl solution, placed in an ultrasonic bath for 10 minutes and filtered over a type C glassfrit. The PE was dried overnight under vacuum at 50 °C. Yield of white powder: 18.15 g. Calculated activity: 248 kg PE/mol Ti·atm·hr. Polydispersity: 3.8, $M_n = 278 \cdot 10^3$, $M_w = 1047 \cdot 10^3$.

***tetrakis*[5-(1,1Dimethylethyl)-2-hydroxyphenyl]ethene magnesium chloride salt.**

In a glovebox, a solution of 1.1 g (1.7 mmol) *tetrakis*[5-(1,1dimethylethyl)-2-hydroxyphenyl]ethene (gift of Dr. T. Dzwiniel) in 20 mL THF was slowly added under stirring to a solution of 0.62 g (6.9 mmol, 4.1 eq.) EtMgCl in 80 mL THF. The solution was stirred overnight at room temperature. The next day the solution was reduced to dryness. EA range for % C = 60.3799 to 60.4836 (n=3), % H = 7.1185 to 7.2591 (n=3), % Cl = 11.66 to 11.79 (n=3). Calculated MW based on average % C,H,Cl = 1234, Ligand·$Mg_{4.6}Cl_{4.2}\cdot$5.0 THF. ^{1}H-NMR (toluene-d_8/1-hexene, 200 MHz): superimposed on the signals of the standard (see attempts to analyze the magnesium salts, part a) were the following signals δ 7.7 - 6.1 (broad s, overlap with residual signal of toluene-d_8), 3.57 (broad s, THF). The other THF signal was present around 1.37-1.0 ppm and overlapping with both 1-hexene and *tert*-butyl signals leading to a broad single peak. The starting material displayed the following ^{1}H-NMR spectrum (toluene-d_8/1-hexene, 200 MHz) δ 7.34 (d, J = 4.2 Hz, 4H), 6.88 (dd, J = 4.2, 14.6 Hz, 4H), 6.47 (d, J = 14.6 Hz, 4H). Because of the presence of 1-hexene as an internal standard and the very low concentration of the starting material, due to the low solubility of the compound, the OH and *tert*-butyl signals could not be assigned.

a) Polymerization study: influence of Ti/ligand ratio.

General procedure: in the glovebox, a suspension of 6 mg of the magnesium phenoxide salt in 4.8 g toluene was prepared in a 10 mL glass polymerization bomb. After placing a gasket and crown cap the bomb was transferred out of the glovebox. Solutions of $TiCl_4$ (varying ratios Ti/ligand, see chapter text, Figure 4.4, page 207 and Tables 4.6 A to D pages 248 to 251) and Et_3Al were prepared, and stored in 1 mL syringes (see general experimental part). After

Table 4.6 A:Polymerization study using the *tetrakis*[5-(1,1dimethylethyl)-2-hydroxyphenyl]ethene magnesium chloride salt.: influence of Ti/ligand ratio, Ti/ligand ratio = 1/1.

1 equivalent Ti / Ligand					
Mixing Time (minutes, seconds)	Amount of Mg salt (mg)	Ti/Al Stock solution[1] (mL)	Polym. Time (minutes, seconds)	PE yield (g)	Activity[2] (kg PE/ mol Ti·hr·atm)
23 sec	6.3	0.92	10min4sec	0.0886	34
36 sec	6.2	0.91	10min9sec	0.0321	12
60 sec	6.2	0.91	10min8sec	0.1554	22*
60 sec	6.8	1.00	10min5sec	0.0623	9
4 min	6.4	0.94	10min2sec	0.0661	25*
4 min	6.9	1.00	10min5sec	0.0259	9
15 min	6.5	0.95	10min14sec	0.0305	11*
30 min	6.0	0.88	10min5sec	0.0207	8*

1] $TiCl_4$ stock solution used: of a solution of 0.1360 g $TiCl_4$ diluted to a total weight of 6.6119 g using toluene, 0.5120 g was diluted to a volume of 10 mL using toluene to give a concentration of $5.5 \cdot 10^{-6}$ mol $TiCl_4$ / mL. Et_3Al stock solution used: 0.8384 g Et_3Al was diluted to a total weight of 9.9173 g using toluene to give a concentration of $6.4 \cdot 10^{-4}$ mol Et_3Al / mL, or 116 eq. Et_3Al / Ti.

2] activities used in figure are marked *

Table 4.6 B:Polymerization study using the *tetrakis*[5-(1,1dimethylethyl)-2-hydroxyphenyl]ethene magnesium chloride salt.: influence of Ti/ligand ratio, Ti/ligand = 2/1.

2 equivalents Ti / Ligand					
Mixing Time (minutes)	Amount of Mg salt (mg)	Ti/Al Stock solution[1] (mL)	Polym. Time (minutes, seconds)	PE yield (g)	Activity[2] (kg PE/ mol Ti·hr·atm)
1 min	6.8	1.00	5min0sec	0.3305	119
1 min	6.3	0.93	5min18sec	0.3897	142*
5 min	6.3	0.93	4min42sec	0.4037	137*
5 min	6.4	0.96	5min42sec	0.3505	115
15 min	6.4	0.95	8min56sec	0.5772	122*
30 min	6.0	0.89	10min5sec	0.4519	90*

[1] $TiCl_4$ stock solution used: of a solution of 0.1622 g $TiCl_4$ diluted to a total weight of 7.1964 g using toluene, 0.9244 g was diluted to a volume of 10 mL using toluene to give a concentration of $1.1 \cdot 10^{-5}$ mol $TiCl_4$ / mL. Et_3Al stock solution used: 1.5702 g Et_3Al was diluted to a total weight of 10.2562 g using toluene to give a concentration of $1.2 \cdot 10^{-3}$ mol Et_3Al / mL, or 109 eq. Et_3Al / Ti.

[2] activities used in figure are marked *

Table 4.6 C:Polymerization study using the *tetrakis*[5-(1,1dimethylethyl)-2-hydroxyphenyl]ethene magnesium chloride salt.: influence of Ti/ligand ratio, Ti/ligand ratio = 3/1.

3 equivalents Ti / Ligand					
Mixing Time (minutes)	Amount of Mg salt (mg)	Ti/Al Stock solution[1] (mL)	Polym. Time (minutes, seconds)	PE yield (g)	Activity[2] (kg PE/ mol Ti·hr·atm)
1 min	6.2	0.88	5min5sec	0.4651	120*
1 min	6.3	0.90	5min5sec	0.4105	103
5 min	6.9	0.98	5min5sec	0.3402	79
5 min	6.8	0.98	5min8sec	0.4537	96*
15 min	6.1	0.87	7min57sec	0.3617	60
15 min	6.3	0.90	6min3sec	0.5171	77*
30 min	6.3	0.90	8min28sec	0.3692	85
30 min	6.0	0.86	8min39sec	0.5528	88*

1] $TiCl_4$ stock solution used: of a solution of 0.2899 g $TiCl_4$ diluted to a total weight of 7.0093 g using toluene, 0.7837 g was diluted to a volume of 10 mL using toluene to give a concentration of $1.7 \cdot 10^{-5}$ mol $TiCl_4$ / mL. Et_3Al stock solution used: 2.2335 g Et_3Al was diluted to a total weight of 10.2171 g using toluene to give a concentration of $1.7 \cdot 10^{-3}$ mol Et_3Al / mL, or 100 eq. Et_3Al / Ti.
2] activities used in figure are marked *

Table 4.6 D:Polymerization study using the *tetrakis*[5-(1,1dimethylethyl)-2-hydroxyphenyl]ethene magnesium chloride salt.: influence of Ti/ligand ratio, Ti/Ligand ratio = 4/1.

4 equivalents Ti / Ligand					
Mixing Time (minutes)	Amount of Mg salt (mg)	Ti/Al Stock solution[1] (mL)	Polym. Time (minutes, seconds)	PE yield (g)	Activity[2] (kg PE/ mol Ti·hr·atm)
1 min	6.5	0.96	5min10sec	0.4784	86
1 min	6.2	0.96	5min11sec	0.4969	94*
5 min	6.1	0.90	5min23sec	0.5021	93*
5 min	6.7	0.99	5min37sec	0.3911	63
15 min	6.6	0.97	5min15sec	0.4648	82*
15 min	6.4	0.94	5min27sec	0.4064	71
30 min	6.4	0.94	5min34sec	0.3794	65
30 min	6.1	0.90	5min18sec	0.4056	76*

1] $TiCl_4$ stock solution used: of a solution of 0.0977 g $TiCl_4$ diluted to a total weight of 5.6508 g using toluene, 2.4142 g was diluted to a volume of 10 mL using toluene to give a concentration of $2.2 \cdot 10^{-5}$ mol $TiCl_4$ / mL. Et_3Al stock solution used: 2.7003 g Et_3Al was diluted to a total weight of 11.8262 g using toluene to give a concentration of $1.7 \cdot 10^{-3}$ mol Et_3Al / mL, or 78 eq. Et_3Al / Ti.
2] activities used in figure are marked *

purging and pressurizing the polymerization bomb with 32 psig ethene, the $TiCl_4$ solution was injected under rapid stirring followed by the Et_3Al (approximately 100 eq./Ti, see Tables 4.6 A to D, pages 248 to 251) solution after a measured time interval. After 10 minutes the polymerization was stopped by venting the ethene and injecting 3 mL of a 2.4% HCl in EtOH solution. The PE was isolated by filtration, and dried overnight under vacuum at 50 °C. For results see chapter text, Figure 4.4, page 208 and Tables 4.6 A to D, pages 248 to 251.

b) Polymerization study: homogeneity of the reaction.

In a glovebox, 30 mg ($2.5 \cdot 10^{-5}$ mol based on MW calculated from EA data) of the *tetrakis*[5-(1,1-dimethylethyl)-2-hydroxyphenyl]ethenemagnesium chloride salt was suspended in 24.24 g (28 mL) toluene. Under stirring 0.29 g ($2.8 \cdot 10^{-5}$ mol, 1.1 eq. $TiCl_4$) of a solution consisting of 0.12 g $TiCl_4$ in 6.6 g toluene was added to the suspension. The rapidly stirred red brown suspension was sampled at regular intervals. A 3.5 g sample was centrifuged for 7.5 minutes and the supernatant was carefully transferred to a polymerization bomb without disturbing the red transparent precipitate using a Pasteur pipette. Additional toluene was added to bring the mass to approximately 4.8 g. The precipitate was resuspended in 4.8 g toluene and transferred to a polymerization bomb. Both vessels were capped with a gasket and crown cap and brought out of the glovebox. The polymerization bombs were flushed and pressurized with 32 psig ethene. Polymerizations were initiated by injection of 1 mL Et_3Al ($3 \cdot 10^{-4}$ mol, 75 eq./Ti) as a solution consisting of 0.94 g Et_3Al in 24 g toluene. The reaction was stopped after 10 minutes by venting the ethene and injecting 3 mL of a 2.4% HCl in EtOH solution. The PE was isolated by filtration and dried

Table 4.7: Polymerization study: homogeneity of the reaction using the *tetrakis*[5-(1,1dimethylethyl)-2-hydroxyphenyl]ethene magnesium chloride salt and 1 equivalent $TiCl_4$.

Sample Time (minutes)[1]	Polym. Time (minutes, seconds)	PE Yield (g)	Activity[2] (kg PE/mol Ti·hr·atm)	Delay[3] (minutes)
5 ppt	10min0sec	0.1381	68	28
5 sup	10min0sec	0.0181	9	28
31 ppt	10min12sec	0.0886	43	42
31 sup	10min12sec	0.0055	3	42
69 ppt	10min14sec	0.0767	37	34
69 sup	10min14sec	0.0023	1	34
106 ppt	10min15sec	0.0711	34	31
106 sup	10min15sec	0.0064	3	31
136 ppt	10min48sec	0.0673	28	36
136 sup	10min48sec	0.0037	2	36

1] ppt = precipitate, sup = supernatant, 7.5 minute centrifuge run 2] based on assumed [Ti] = $4 \cdot 10^{-6}$ mol for each sample, sample size 3.5 g. 3] Delay between separation of supernatant and precipitate after centrifuging, and the polymerization experiment.

overnight under vacuum at 50 °C. For time intervals and results see chapter text, Figure 4.2, page 204 and Table 4.7.

c) Ligand distribution study using excess $TiCl_4$.

In the glovebox 9.4 mg ($7.6 \cdot 10^{-6}$ mol based on MW calculated from EA data) of the *tetrakis*[5-(1,1dimethylethyl)-2-hydroxyphenyl]ethene magnesium chloride salt was suspended in 4.8 g toluene. The suspension was added in two hours to a stirred solution of 0.73 g $TiCl_4$ (500 eq. Ti/ligand) in 16 g of toluene using a syringe pump.

1) Polymerization part. Under stirring, a 4.8 g sample was taken of the resulting deep red suspension, and centrifuged for 7 minutes. The supernatant was carefully removed and placed in a glass bomb equipped with stir bar. The isolated red gel was resuspended in toluene, centrifuged, and after careful removal of the slightly colored top layer using a Pasteur pipette resuspended in toluene. After repeating the washing procedure one more time, the red gel was resuspended in 4.8 g toluene and transferred to a glass bomb equipped with a stir bar. Both bombs were sealed with a gasket and a crown cap. After transfer out of the glovebox, the bombs were flushed with ethene while stirring. After pressurizing with 32 psig ethene 1 mL ($5 \cdot 10^{-4}$ mol) of a Et_3Al solution consisting of 0.68 g Et_3Al in 10.3 g toluene was injected under rapid stirring. Polymerization started immediately in the suspension of the precipitate as indicated by a strong temperature increase of the bomb. No significant polymerization activity was observed for the supernatant solution. The polymerizations were terminated by injection of 3 mL of a 2.4% HCl in EtOH solution after 6 minutes. The PE was isolated by vacuum filtration. After overnight drying at 50 °C under vacuum 0.39 g of white PE was obtained. A 4.33 g sample of the red suspension contained $1.6 \cdot 10^{-7}$ mol of the ligand (see part 2), a 4.8 g sample thus contains $1.8 \cdot 10^{-7}$ mol ligand resulting in a calculated activity of 6645 Kg PE/*mol ligand*·atm·hr for the heterogeneous layer.

2) Ligand distribution part. Under stirring a 4.33 g sample was taken of the deep red suspension as used in part *1)*, and centrifuged for 7 minutes. The solution on top of the red gel was carefully removed using a Pasteur pipette, and the gel was resuspended in toluene. The suspension was centrifuged for 7 minutes, and the washing procedure repeated one more time. The precipitate, as well as the collected homogeneous toluene layers, were reduced to dryness under vacuum. Both solids were dissolved in a standard solution consisting of 8.5728 g (9.8 mL) acetone-d_6 (d: 0.872 g/mL) and 4.4 mg ($2.6 \cdot 10$-5 mol) 1,3,5-trimethoxybenzene. ^{1}H-NMR (360 MHz) of the standard solution: δ 6.08 (s, 3H), 3.73 (s, 9H), 2.09 (s). ^{1}H-NMR (200 MHz, toluene-d_8/1-hexene) of *tetrakis*[5-(1,1-dimethylethyl)-2-hydroxyphenyl]ethene: δ 8.03 (broad s, OH), 7.30 (d, J = 2.6 Hz, 4H), 6.94 (dd, J = 2.6, 8.8 Hz, 4H), 6.55 (d, J = 8.8 Hz, 4H), 1.13 (s, 36H).

The resulting solid of the washing layers was mixed with 1.5 mL standard solution. The resulting cloudy suspension might indicate a loss of ligand due to solubility problems: adding THF-d_8 did not remove the cloudiness but did introduce impurities in the form of additional signals in the 0.8-2.0 ppm region. In addition to the signals of the standard solution, the following signals were observed in the aromatic region: δ 7.85 -7.5 (several broad s, integral: 0.04116), 7.15 (residual toluene in sample), 6.8 (broad s, integral: 0.05240). The aromatic hydrogen of trimethoxybenzene at δ 6.08 (s, integral: 0.07722, 3H, $3.99 \cdot 10^{-6}$ mol trimethoxybenzene) together with the signals at 7.85-7.5 and 6.8 ppm were used to calculate the ligand content in the supernatant after correction for the number of observed hydrogen atoms; see text chapter and Table 4.1, page 206.

The solid resulting from drying the precipitate was dissolved[3] in 1.0 mL of the same acetone-d_6 standard solution. In addition to the signals of the standard solution the ^{1}H-NMR spectrum displayed in the aromatic region the following signals: δ 7.29 (d, J = 3.0 Hz, 4H, integral: 0.00821), 6.92 (dd, J = 2.7, 8.3 Hz, 4H, integral: 0.01050) and 6.55 (d, J = 8.3 Hz, 4H, integral: 0.00786). The signal of trimethoxybenzene δ 6.08 ppm (s, integral: 0.11358, 3H, $2.7 \cdot 10^{-6}$ mol trimethoxybenzene) together with the signals at 7.29, 6.92 and 6.55 ppm were used to calculate the ligand content in the precipitate after correction for the number of observed hydrogen atoms, see text chapter and Table 4.1, page

206. The *tert*-butyl signals of the ligand were present at 1.15 ppm as a broad multiplet, while THF seemed to be absent from the sample.

Compound 2: the titanium sandwich of *tetrakis*[4-(1,1-dimethyl ethyl)-2-hydroxyphenyl]ethene.

In a glovebox, a solution of 0.12 g (0.2 mmol) of *tetrakis*[4-(1,1-dimethylethyl)-2-hydroxyphenyl]ethene (gift of Dr. T. Dzwiniel) in 10 mL THF was slowly added to a stirred solution of 70 mg (0.8 mmol, 4 eq.) EtMgCl in 10 mL THF. After 1 hour stirring at room temperature a solution of 65 mg (0.2 mmol, 1 eq.) $TiCl_4 \cdot 2THF$ in 3 mL THF was added. A deep red color developed within 5 minutes. After stirring the solution overnight at room temperature, the solution was reduced to 5 mL under vacuum, and 20 mL of pentane was added. After settling of the formed precipitate, the top layer was carefully removed using a Pasteur pipette, and the precipitate extracted for a second time with 20 mL of pentane. The so obtained sludge was extracted twice with 20 mL of toluene to give a deep red toluene solution. After reducing the volume of the solution to approximately 5 mL, the concentrated solution was placed at -30 ^{o}C inside the glovebox fridge to obtain crystals of X-ray diffractable quality. Attempts to use this procedure for preparing similar compounds from *tetrakis*[2-hydroxyphenyl]ethene as well as scale-up trials using *tetrakis*[5-(1,1-dimethylethyl)-2-hydroxyphenyl]ethene to obtain well defined compounds for further analysis and use in polymerization experiments failed. No significant amount of product could be extracted out of the sludge (after pentane extraction) using toluene in these cases.

Crystal data (see appendix H page 385 for details) for compound **2** ($C_{84}H_{96}O_8Ti_2 \cdot 2C_7H_8$): crystal dimensions 0.20 × 0.08 × 0.06 mm, monoclinic, space group *P*2$_1$/*c* (No. 14), *a* = 12.3256 (16), *b* = 23.396 (3), *c* = 15.2484 (17)

(Å), β = 107.982 (3) (°), V (Å^3) = 4182.4 (9), Z = 2, ρ_{calcd} = 1.202 (g cm^{-3}), μ (mm^{-1}) = 0.248. Data collection and refinement conditions: Bruker P4/RA/SMART 1000 CCD diffractometer using graphite-monochromated Mo$K\alpha$ radiation (λ [Å] = 0.71073), T = 193 (K), scan type ϕ rotations (0.3°) / ω scans (0.3°) (30 s exposures), 23649 measured reflections, 8559 independent reflections, 2426 included in the refinement ($F_o^2 \geq 2\sigma(F_o^2)$), structure solution method by direct methods (*SHELXS–86*), refinement method by full-matrix least-squares on F^2 (*SHELXL–93*), absorption correction method *SADABS*, transmission max./min. = 0.9803/0.7377, 436 parameters, R_1 = 0.0725 (based on 2426 observed data), wR_2 = 0.1805 (based on all 8559 data), residual electron density 0.498/-0.586 e Å^{-3}.

4-*tert*-Butylphenoxymagnesium chloride salt.

In the glovebox a THF solution of 0.51 g (5.8 mmol) EtMgCl in 100 mL THF was prepared. Under stirring, a solution of 0.85 g (5.7 mmol) azeotropically dried 4-*tert*-butylphenol in 30 mL THF was slowly added to the clear Grignard solution. After stirring overnight at room temperature, the top layer was removed from the precipitate and the white precipitate washed twice with pentane to remove traces of THF. After removal of solvent under oil pump vacuum 1.64 g of a white powder was obtained. A THF solution of 0.8 g of the so obtained solid was heated to reflux overnight under nitrogen. The next day 2/3 of the solvent was removed while stirring under oil pump vacuum. The resulting suspension was centrifuged and the clear top layer removed using a Pasteur pipette. The remaining solid was washed with pentane, and dried under oil pump vacuum to yield 0.2 g of a white solid. EA range for % C = 59.7980 to 60.1518 (n=3), % H = 8.0395 to 8.2002 (n=3), % Cl = 9.89 to 10.74 (n=3). Calculated MW = 368, Ligand·$Mg_{1.2}Cl_{1.1}$·2.1 THF. ^{1}H-NMR (toluene-d_8/1-hexene, 200 MHz):

superimposed on the signals of the standard (see attempts to analyze the magnesium salts, part a) were the following signals δ 8.38 (broad d, J = 3.4 Hz), 7.55 (broad d, J = 3.4 Hz), 7.24 (broad d, J = 2.2 Hz), 7.12 (broad s ?, overlap with residual signal of toluene-d_8), 6.80 (broad s), 3.64 (broad s, THF). The other THF signal was present around 1.25-1.22 ppm and overlapping with both 1-hexene and *tert*-butyl signals leading to a broad single peak. 4-*tert*-Butylphenol dispays the following ^{1}H-NMR spectrum (toluene-d_8/1-hexene, 200 MHz): δ 7.07 (2nd order m, overlap with residual toluene-d_8), 6.46 (2nd order m, 2H), 3.85 (s, 1H), 1.20 (s, 9H)

a) Polymerization study.

In the glovebox, 34.2 mg (calculated amount of ligand based on EA: $9.3 \cdot 10^{-5}$ mol) of the 4-*tert*butylphenoxymagnesium chloride salt was suspended in 25.3 g toluene. While stirring 0.29 g ($2.4 \cdot 10^{-5}$ mol) of a $TiCl_4$ solution (0.104 g $TiCl_4$ in 6.4123 g toluene) was added. After 6, 31, 56 and 81 minutes of stirring, a 4.6 g sample was taken of the stirred red-brown suspension and centrifuged at maximum speed for 6 minutes. The red, transparent precipitate was carefully separated from the supernatant and resuspended in 4.8 g toluene. The suspension and supernatant were transferred to 10 mL glass polymerization bombs and capped with a gasket and crown cap. Outside the glovebox the bombs were flushed with ethene and pressurized with 32 psig ethene. Polymerization was started by injection of 1 mL ($3.9 \cdot 10^{-4}$ mol, 88 eq./Ti) Et_3Al stock solution. The reaction was stopped after a run of 10 minutes by venting the ethene and injecting 3 mL of a 2.4% HCl in EtOH solution. Workup consisted of filtering and washing (with EtOH/HCl solution) the PE, and drying the so-obtained material under vacuum at 50 °C overnight. See text chapter, Figure 4.3, page 205 and Table 4.8, page 259, for results.

Table 4.8: Polymerization study: homogeneity of the reaction using the 4-*tert*butylphenoxymagnesium chloride salt and 1 equivalent $TiCl_4$.

Sample Time (minutes)[1]	Polym. Time (minutes, seconds)	PE Yield (g)	Activity[2] (kg PE/mol Ti·hr·atm)	Delay[3] (minutes)
6 ppt	10min28sec	0.0530	23	23
6 sup	10min28sec	0.0015	0.7	23
31 ppt	11min25sec	0.0446	18	17
31 sup	11min25sec	0.0028	1	17
56 ppt	10min29sec	0.0210	9	16
56 sup	10min29sec	0.0020	1	16
81 ppt	10min27sec	0.0252	11	13
81 sup	10min27sec	0.0016	0.7	13

1] ppt = precipitate, sup = supernatant, 6 minute centrifuge run 2] based on assumed [Ti] = $4.4 \cdot 10^{-6}$ mol for each sample, sample size 4.6 g. 3] Delay between separation of supernatant and precipitate after centrifuging, and the polymerization experiment.

b) Ligand distribution study using excess $TiCl_4$.

In the glovebox, 12.4 mg ($3.4 \cdot 10^{-5}$ mol based on MW calculated from EA data) of the 4-*tert*butylphenoxymagnesium chloride salt was suspended in 4.8 g (5.6 mL) toluene. The suspension was added over two hours to a stirred solution of 0.76 g ($4 \cdot 10^{-3}$ mol, 119 eq./ligand)$TiCl_4$ in 16 g of toluene using a syringe pump.

1) Polymerization part. Under stirring, a 4.8 g sample was taken of the resulting deep red suspension and centrifuged for 7 minutes. The supernatant was carefully removed using a Pasteur pipette and placed in a glass bomb equipped with stir bar. The isolated red gel was resuspended in toluene, centrifuged and, after careful removal of the slightly colored top layer, resuspended in toluene. After repeating the washing procedure one more time, the red gel was resuspended in 4.8 g toluene and transferred to a glass bomb equipped with a stir bar. Both bombs were closed with a gasket and crown cap. The bombs were flushed with ethene while stirring after transfer out of the glovebox. After pressurizing with 32 psig ethene, 1 mL ($5 \cdot 10^{-4}$ mol) of a solution of 0.68 g Et_3Al in 12 mL toluene was injected under rapid stirring. Polymerization started immediately in the suspension of the precipitate as indicated by a strong temperature increase of the bomb. No polymerization activity was observed for the supernatant solution. After 5 minutes the polymerization was terminated by injection of 3 mL of a 2.4% HCl in EtOH solution. The formed PE was isolated by vacuum filtration. After overnight drying at 50 °C under vacuum, 0.4380 g of white PE was obtained. A 4.33 g sample of the red suspension contains $2.8 \cdot 10^{-7}$ mol of the ligand (see part 2), thus the 4.8 g sample contains $3.1 \cdot 10^{-7}$ mol ligand, resulting in a calculated activity of 5352 kg PE/*mol ligand*·atm·hr for the heterogeneous layer.

2) Ligand distribution part. Under stirring, a 4.33 g sample was taken of the deep red suspension as used in part *1)*, and centrifuged for 7 minutes. The solution on top of the red gel was carefully removed using a Pasteur pipette, and the gel was resuspended in toluene. The suspension was centrifuged for 7 minutes, and the procedure repeated one more time. The precipitate as well as the collected homogeneous toluene layers were reduced to dryness under vacuum. Both solids were dissolved in a standard solution consisting of 8.5728 g (9.8 mL) acetone-d_6 (d: 0.872 g/mL) and 4.4 mg ($2.6 \cdot 10^{-5}$ mol) 1,3,5-trimethoxybenzene. ^{1}H-NMR (360 MHz) of the standard solution: δ 6.08 (s, 3H), 3.73 (s, 9H), 2.09 (s). ^{1}H-NMR (200 MHz, acetone-d_6) of 4-*tert*-butylphenol: 7.98 (broad s, OH), 7.21 (2nd order m, 2H), 6.74 (2nd order m, 2H), 1.25 (s, 9H). The resulting solid from the washing layers was mixed with 1.5 mL of the same standard solution resulting in a clear solution.[3] In addition to the signals of the standard solution the following signals were observed: δ 7.70 (broad s, integral: 0.00677), 7.2 (2nd order m, overlap with residual toluene in sample), 6.74 (2nd order m, integral: 0.11826, assume 2H), 3.62 (m), 1.25 (s), 1.18 (m). A signal of THF was present at 3.6 ppm. The aromatic hydrogen of trimethoxybenzene at δ 6.08 (s, integral: 0.08065, 3H, $3.99 \cdot 10^{-6}$ mol trimethoxybenzene) together with the signal at 6.74 ppm was used to calculate the ligand content in the supernatant after correction for the number of observed hydrogen nuclei; see text chapter and Table 4.1, page 206.

The solid resulting from drying the precipitate was dissolved in 1.0 mL of the same acetone-d_6 standard solution. In addition to the signals of the standard solution the ^{1}H-NMR spectrum displayed in the aromatic region the following signals: δ 7.21 (2nd order m, overlap with residual toluene in sample), 6.74 (2nd order m, integral: 0.0048, assume 2H), 6.08 (s, integral: 0.06916, 3H, $2.7 \cdot 10^{-6}$ mol trimethoxybenzene). The signals at 6.74 and 6.08 ppm were used to calculate the ligand content in the precipitate after correction for the number of observed hydrogens, see text chapter and Table 4.1, page 206.

2,2'-Thiobis[4,6-bis(1,1-dimethylethyl)]phenoxymagnesium chloride.

In the glovebox, to a solution of 0.49 g EtMgCl in 50 mL THF was added under stirring a solution of 1.1 g 2,2'-thiobis[4,6-bis(1,1-dimethylethyl)]phenol[36] in 60 mL THF. The so obtained solution was stirred overnight at room temperature. The next day, the solution was reduced under vacuum to an oil, at which point 100 mL hexane was added, resulting in the formation of a dense gel. The gelatinous material was centrifuged to obtain a precipitate that was dried under vacuum. EA range for % C = 58.2841 to 58.5238 (n=3), % H = 7.9062 to 8.1043 (n=3), % Cl = 11.47 to 12.52 (n=3). Calculated MW = 900, Ligand·$Mg_{2.5}Cl_{3.1}$·4 THF.

a) Polymerization study: influence of Ti/ligand ratio.

General procedure: in the glovebox, a suspension of 6 mg of the magnesium chloride salt in 4.8 g toluene was prepared in a polymerization bomb and after sealing with a gasket and crown cap, the bomb was transferred out of the glovebox. Solutions of $TiCl_4$ (varying ratios Ti/ligand, see chapter text, Figure 4.5, page 208 and Tables 4.9 A to D, pages 263 to 266) and Et_3Al were prepared, and stored in 1 mL syringes (see general experimental part). After purging and pressurizing the polymerization bomb with 32 psig ethene the $TiCl_4$ solution was injected under rapid stirring followed by the Et_3Al (100 eq./Ti) solution after a measured time interval (see text and Table 4.9 A to D for other times). After 10 minutes, the polymerization was stopped by venting the ethene and injecting 3 mL of a 2.4% HCl in EtOH solution. The PE was isolated by filtration, and dried overnight under vacuum at 50 °C. For the results see chapter text and Tables 4.9 A to D, pages 263 to 266.

b) Polymerization study: molecular weight regulation by hydrogen.

General procedure: in the glovebox, a suspension of 5 mg of the magnesium chloride salt in 4.8 g toluene was prepared in a polymerization bomb and after sealing with a gasket and crown cap, the bomb was transferred out of the glovebox. Solutions of $TiCl_4$ (ratio Ti/ligand = 2) and Et_3Al (ratio Et_3Al/Ti = 100) were prepared and stored in 1 mL syringes, see Table 4.10, page 268. Without stirring the bomb was flushed free of nitrogen using hydrogen and pressurized to the required "gascap" pressure. After closing the hydrogen supply, the volume of the tubing and the volume above the liquid in the glass

Table 4.9 A: Polymerization study using the 2,2'-thiobis[4,6-bis(1,1-dimethylethyl)]phenoxymagnesium chloride salt.: influence of Ti/ligand ratio, Ti/Ligand ratio = 1/1.

1 equivalent Ti / Ligand					
Mixing Time (minutes, seconds)	Amount of Mg salt (mg)	Ti/Al Stock solution[1] (mL)	Polym. Time (minutes, seconds)	PE yield (g)	Activity[2] (kg PE/ mol Ti·hr·atm)
1 min	5.8	0.96	9min56sec	0.0672	21
1 min	5.1	0.84	9min48sec	0.1534	55*
5 min	5.4	0.89	9min56sec	0.0246	8*
5 min	5.5	0.91	9min55sec	0.0209	7
15 min	5.4	0.89	10min35sec	0.0315	10*
15 min	5.3	0.88	10min44sec	0.0188	6
30 min	5.7	0.94	10min12sec	0.0322	10*
30 min	5.5	0.91	9min33sec	0.0151	5

1] $TiCl_4$ stock solution used: of a solution of 0.1977 g $TiCl_4$ diluted to a total weight of 5.2049 g using toluene, 0.3356 g was diluted to a volume of 10 mL using toluene to give a concentration of $6.7\cdot10^{-6}$ mol $TiCl_4$ / mL. Et_3Al stock solution used: 0.7888 g Et_3Al was diluted to a volume of 10 mL using toluene to give a concentration of $6.9\cdot10^{-4}$ mol Et_3Al / mL, or 103 eq. Et_3Al / Ti.
2] activities used in figure are marked *

Table 4.9 B: Polymerization study using the 2,2'-thiobis[4,6-bis(1,1-dimethylethyl)]phenoxymagnesium chloride salt.: influence of Ti/ligand ratio, Ti/Ligand ratio = 2/1.

2 equivalents Ti / Ligand					
Mixing Time (minutes)	Amount of Mg salt (mg)	Ti/Al Stock solution[1] (mL)	Polym. Time (minutes, seconds)	PE yield (g)	Activity[2] (kg PE/ mol Ti·hr·atm)
1 min	5.7	0.64	10min23sec	0.5973	93
1 min	5.6	0.63	10min1sec	0.6596	104*
5 min	5.8	0.65	9min34sec	0.4867	78
5 min	5.7	0.64	10min13sec	0.6495	99*
15 min	5.8	0.65	10min3sec	0.4956	76*
15 min	5.8	0.65	10min18sec	0.4922	73
30 min	5.6	0.63	10min2sec	0.3638	58*
30 min	5.3	0.60	10min8sec	0.3414	56

1] $TiCl_4$ stock solution used: of a solution of 0.2596 g $TiCl_4$ diluted to a total weight of 5.7243 g using toluene, 0.8279 g was diluted to a volume of 10 mL using toluene to give a concentration of $2.0 \cdot 10^{-5}$ mol $TiCl_4$ / mL. Et_3Al stock solution used: 2.2775 g Et_3Al was diluted to a volume of 10 mL using toluene to give a concentration of $2.0 \cdot 10^{-3}$ mol Et_3Al / mL, or 100 eq. Et_3Al / Ti.

2] activities used in figure are marked *

Table 4.9 C: Polymerization study using the 2,2'-thiobis[4,6-bis(1,1-dimethylethyl)]phenoxymagnesium chloride salt.: influence of Ti/ligand ratio, Ti/Ligand ratio = 3/1.

3 equivalents Ti / Ligand					
Mixing Time (minutes)	Amount of Mg salt (mg)	Ti/Al Stock solution[1] (mL)	Polym. Time (minutes, seconds)	PE yield (g)	Activity[2] (kg PE/ mol Ti·hr·atm)
1 min	5.8	0.93	8min19sec	0.5295	65
1 min	5.6	0.90	9min3sec	0.6680	78*
5 min	5.4	0.87	8min13sec	0.5162	69
5 min	5.2	0.84	9min52sec	0.6994	80*
15 min	5.8	0.93	9min59sec	0.5421	56
15 min	5.2	0.84	9min12sec	0.4783	59*
30 min	5.9	0.95	9min51sec	0.6697	68*
30 min	5.2	0.84	9min55sec	0.2969	34

1] $TiCl_4$ stock solution used: of a solution of 0.1698 g $TiCl_4$ diluted to a total weight of 5.2317 g using toluene, 1.2124 g was diluted to a volume of 10 mL using toluene to give a concentration of $2.1\cdot10^{-5}$ mol $TiCl_4$ / mL. Et_3Al stock solution used: 2.2974 g Et_3Al was diluted to a volume of 10 mL using toluene to give a concentration of $2.0\cdot10^{-3}$ mol Et_3Al / mL, or 95 eq. Et_3Al / Ti.

2] activities used in figure are marked *

Table 4.9 D: Polymerization study using the 2,2'-thiobis[4,6-bis(1,1-dimethylethyl)]phenoxymagnesium chloride salt.: influence of Ti/ligand ratio, Ti/Ligand ratio = 4/1.

4 equivalents Ti / Ligand					
Mixing Time (minutes)	Amount of Mg salt (mg)	Ti/Al Stock solution[1] (mL)	Polym. Time (minutes, seconds)	PE yield (g)	Activity[2] (kg PE/ mol Ti·hr·atm)
1 min	5.4	1.00	10min6sec	0.5662	46*
2 min	5.3	1.00	10min7sec	0.4235	35
5 min	5.3	1.00	10min3sec	0.4202	35
5 min	5.2	0.99	10min4sec	0.5442	46*
15 min	5.1	0.97	10min1sec	0.5139	45*
19 min	5.4	1.00	10min4sec	0.6666	54
30 min	5.6	1.10	10min2sec	0.5645	45
30 min	5.6	1.10	10min7sec	0.8083	63*

1] $TiCl_4$ stock solution used: of a solution of 0.1532 g $TiCl_4$ diluted to a total weight of 7.1112 g using toluene, 2.0542 g was diluted to a volume of 10 mL using toluene to give a concentration of $2.3\cdot10^{-5}$ mol $TiCl_4$ / mL. Et_3Al stock solution used: 2.5938 g Et_3Al was diluted to a volume of 10 mL using toluene to give a concentration of $2.3\cdot10^{-3}$ mol Et_3Al / mL, or 100 eq. Et_3Al / Ti.
2] activities used in figure are marked *

polymerization bomb represents the gascap and is filled with hydrogen at a certain pressure. Next the bomb was pressurized to 30 psig using ethene and stirring was started. The $TiCl_4$ solution was injected, followed 1 minute later by the Et_3Al solution: for experimental details and results see Table 4.10, page 268. After 10 minutes, the polymerization was stopped by venting the bomb and injecting 3 ml 2.4% HCl in EtOH solution. The PE was isolated by filtration and dried under vacuum overnight at 50 °C. For the polydispersity data obtained by size-exclusion chromatography see Table 4.11, page 269. The filtrate was washed subsequently with 10% HCl, 10% NaOH, 10% HCl, saturated $NaHCO_3$ solution and water and dried over anhydrous $MgSO_4$. After removal of the volatile fraction under vacuum the mass of the resulting oil was determined, and the oil analyzed using GCMS. The gas chromatograms obtained for each fraction displayed a set of peaks with identical t_{ret} and intensity variation. For the result of the atmospheric H_2 run, see Table 4.12, page 270.

Table 4.10: Polymerization study using the 2,2'-thiobis[4,6-bis(1,1-dimethylethyl)]phenoxymagnesium chloride salt.: the influence of hydrogen on the oligomer content.

gascap H_2	Amount Mg salt (mg)	Ti/Al Stock[1] (mL)	Polym. Time[2]	Yield PE (g)	Yield[3] Oligom. (g)	Wt. % Oligom. (%)	Catalyst Activity[4]
none	4.9	0.94	9min53s	0.4111	0.0508	11	104*
none	5.2	0.99	9min53s	0.5976	0.0528	8	75
atm.	4.9	0.94	9min47s	0.2965	0.0878	23	55*
atm.	5.2	0.99	9min44s	0.2275	0.0244	10	40
2.5 psig	4.5	0.86	9min56s	0.1083	0.0341	24	24*
2.5 psig	5.2	0.99	9min53s	0.1390	0.0180	12	22
5 psig	4.7	0.90	9min48s	0.1054	0.0119	10	20
5 psig	4.8	0.92	9min52s	0.1141	0.0102	8	21*

1] $TiCl_4$ stock solution used: of a solution of 0.2316 g $TiCl_4$ diluted to a total weight of 6.4319 g using toluene, 0.6144 g was diluted to a volume of 10 mL using toluene to give a concentration of $1.2 \cdot 10^{-5}$ mol $TiCl_4$ / mL. Et_3Al stock solution used: 1.3267 g Et_3Al was diluted to a volume of 10 mL using toluene to give a concentration of $1.2 \cdot 10^{-3}$ mol Et_3Al / mL, or 100 eq. Et_3Al / Ti. 2] min = minutes, s = seconds, 3] Oligom. = oligomer, Wt. = weight, 4] Oligomer samples used for GCMS, see Table 4.12, and PE samples used for size exclusion chromatography, see Table 4.11 are marked *, Activity in kg PE/mol Ti·hr·atm

Table 4.11: Polymerization study using the 2,2'-thiobis[4,6-bis(1,1-dimethylethyl)]phenoxymagnesium chloride salt.: molecular weight regulation by hydrogen.

Gascap	M_n	M_w	M_z	M_w / M_n
no H_2	17090	242697	514870	14
	17871	222413	510270	19
atm. H_2	6440	140040	428051	22
	6836	150138	564624	22
2.5 psig H_2	4362	117838	368580	27
	4410	116925	389497	27
5 psig H_2	5468	108611	342108	20
	5464	103542	313113	19

Table 4.12: Polymerization study using the 2,2'-thiobis[4,6-bis(1,1-dimethylethyl)]phenoxymagnesium chloride salt; oligomer analysis using GCMS of the atmospheric hydrogen gas cap.

t_{ret} (minutes)	Area (%)	Mass Spectrum (m/z)	Assignment
5.98	4.5	43, 57, 71, 85, 91, 98	$C_{10}H_{22}$
9.08	5.7	43, 57, 71, 85, 99, 112	$C12H_{26}$
12.01	6.9	43, 57, 71, 85, 98, 113, 127, 140, 155, 198	$C_{14}H_{30}$
14.64	9.5	43, 57, 71, 85, 99, 113, 127, 141, 156	$C_{16}H_{34}$
17.00	10.2	43, 57, 71, 85, 99, 113, 127, 141, 170	$C_{18}H_{38}$
19.15	11.2	43, 57, 71, 85, 99, 126, 141, 155, 169, 197, 211, 282	$C_{20}H_{42}$
21.11	12.9	43, 57, 71, 85, 99, 113, 127, 141, 155, 169, 197, 225, 338	$C_{22}H_{46}$
22.91	13.0	43, 57, 71, 85, 99, 113, 127, 141, 155, 169, 197, 225, 338	$C_{24}H_{50}$
24.59	9.9	43, 57, 71, 85, 99, 113, 127, 141, 155, 182, 211, 224	$C_{26}H_{54}$
26.50	8.2	43, 57, 71, 85, 99, 113, 125, 169, 394	$C_{28}H_{58}$

4.8 Notes and References.

1. Lehmkuhl, H.; Mehler, K.; Benn, R.; Rufinska, A.; Krüger, C. *Ber. Dtsch. Chem. Ges.* **1986**, *119*, 1054.
2. ICP-AES could be used to determine the amount of Ti and Mg in the sample.
3. Homogeneity *cannot* be assumed without experimental proof.
4. The number of X-ray crystallographic studies of magnesium chloride containing compounds is very limited. According to a search of the Cambridge Structural Database no aryloxy/alkoxymagnesium chlorides are present in that database, nor do structures of aryloxymagnesium chlorides seem to have been published. For a disordered alkoxymagnesium chloride, see Sobota, P.; Utko, J.; Janas, Z.; Szafert, S. *J. Chem. Soc., Chem. Commun.* **1996**, 1923-1924
5. Glidewell, C. *Inorg. Chim. Acta* **1975**, *12*, 219-227. Haaland, A. *Angew. Chem., Int. Ed. Engl.* **1989**, *28*, 992-1007.
6. Markies, P.R.; Akkerman, O.S.; Bickelhaupt, F.; Smeets, W.J.J.; Spek, A.L. *Adv. Organomet. Chem.* **1991**, *32*, 147-226. Uhm, H.L. in Handbook of Grignard Reagents Silverman, G.S.; Rakita, P.E. eds.; Marcel Dekker: New York, 1996, pp 117-143. Bickelhaupt, F. in Grignard Reagents: New Developments; Richet, H.G. ed.; Wiley: Chichester, U.K., 2000, pp 299-328.
7. Roesky, H.W.; Scholz, M.; Noltemeyer, M. *Ber. Dtsch. Chem. Ges.* **1990**, *123*, 2303-2309. Zechmann, C.A.; Boyle, T.J.; Rodriguez, M.A.; Kemp, R.A. *Polyhedron* **2000**, *19*, 2557-2564.
8. Troyanov, S.I.; Varga, V.; Mach. K. *Organometallics* **1993**, *12*, 2820-2824.

9. Henderson, K.W.; Mulvey, R.E.; Reinhard, F.B.M.; Clegg, W.; Horsburgh, L. *J. Am. Chem. Soc.* **1994**, *116*, 10777-10778.

10. Jutzi, P. *Adv. Organomet. Chem.* **1986**, *26*, 217-295.

11. Johnson, C.; Toney, J.; Stucky, G.D. *J. Organomet. Chem.* **1975**, *40*, C11-C13. Atwood, J.L.; Smith, K.D. *J. Am. Chem. Soc.* **1974**, *96*, 994-998.

12. Calabrese, J.; Cushing, M.A.; Ittel, S.D. *Inorg. Chem.* **1988**, 27, 867-870.

13. Orpen, A.G.; Brammer, L.; Allen, F.H.; Kennard, O.; Watson, D.G.; Taylor, R. *J. Chem. Soc., Dalton Trans.* **1989**, S1-S83.

14. Ashby, E.C.; Nackashi, J.; Parris, G.E. *J. Am. Chem. Soc.* **1975**, *97*, 3162-3171.

15. Ashby, E.C.; Laemmle, J.; Neumann, H.M. *Acc. Chem. Res.* **1974**, *7*, 272-280. For a more recent set of additional complications (on top of the ones described in the Accounts of Chemical Research review) see: Holm, T.; Crossland, I. in Grignard Reagents: New Developments; Richet, H.G. ed.; Wiley: Chichester, U.K., 2000, pp 1-26.

16. Cannon, K.C.; Krow, G.R. in Handbook of Grignard Reagents, Silverman, G.S.; Rakita, P.E. eds.; Marcel Dekker: New York, 1996, pp 271-289. But see eq. 4.3 on page 216.

17. The combination Me_2Mg/MeMgBr has a k (Me_2Mg) = 10 k (MeMgBr), but due to the Schlenk equilibrium the concentration [MeMgBr] = 10 [Me_2Mg] thereby cancelling the reactivity difference between the two species for the reaction with benzophenone ! See Ashby, E.C.; Laemmle, J.; Neumann, H.M. *Acc. Chem. Res.* **1974**, *7*, 272-280, page 278.

18. Nielson, A.J.; Schwerdtfeger, P.; Waters, J.M. *J. Chem. Soc., Dalton Trans.* **2000**, 529-537.

19. Aakeröy and Seddon have suggested (in relation to the occurrence of polymorphism in a review article on hydrogen bonding) that single-crystal data should *always* be compared with that of the bulk material obtainable from powder diffraction. By simulating the powder pattern from the single-crystal data and comparing the result with the experimentally recorded data an assessment of the agreement between single-crystal and bulk material can be made. See Aakeröy, C.B.; Seddon, K.R. *Chem. Soc. Rev.* **1993**, 397-407, page 404, 405.

20. Olmstead, M.M.; Sigel, G.; Hope, H.; Xu, X.; Power, P.P. *J. Am. Chem. Soc.* **1985**, *107*, 8087-8091.

21. Lee, D.; Jeong, Y.; Soga, K.; Shiono, T. *J. Appl. Polym. Sci.* **1993**, *47*, 1449-1461. Gupta, V.K.; Satish, S.; Bhardwaj, I.S. *J. Macromol. Sci., Pure Appl. Chem.* **1994**, *A31*, 451-463.

22. Gavens, P.D.; Bottrill, M.; Kelland, J.W.; McMeeking, J. in Comprehensive Organometallic Chemistry, G. Wilkinson, F.G.A. Stone, E.W. Abel. Eds.; Pergamon Press: New York, 1982; Chapter 22.5, page 532 and Table 13 on page 533. This effect has also been described for the previous generation ($AlCl_3/TiCl_3/TiCl_4$) Ziegler-Natta catalysts. See: Wesslau, H. *Makromol. Chem.* **1958**, *26*, 102-118.

23. Zucchini, U.; Cecchin, G. *Adv. Polym. Sci.* **1983**, *51*, 101-153.

24. Doi, Y.; Soga, K.; Murata, M.; Suzuki, E.; Ono, Y.; Keii, T. *Polym. Commun.* **1983**, *24*, 244-246.

25. Reference 209 "Zucchini, U.: Unpublished results" in Zucchini, U.; Cecchin, G. *Adv. Polym. Sci.* **1983**, *51*, 101-153. A thorough search revealed that the results are still unpublished by Zucchini. A paper in 1984 (next reference in this list) did contain the results of an investigation on $MgCl_2/Ti(OR)_4$ catalysts but only a single intrinsic viscosity is given for

each polymerization run so that no information is presented on the polydispersity of the obtained PE. For the use of intrinsic viscosities in determining polydispersities see N.C.Billingham, Molar Mass Measurements in Polymer Science; Wiley, New York, 1977, page 185.

26. Zucchini, U.; Cuffiani, I.; Pennini, G. *Makromol. Chem., Rapid Commun.* **1984**, *5*, 567-571. Notice that no evidence was given in the article on the stability or synthesis of the presumed $(RO)_3TiCl$, $(RO)_2TiCl_2$, $(RO)TiCl_3$. It is possible that disproportionation gave rise to mixtures of compounds explaining the unexpected variation in observed activities of the compounds.

27. van der Linden, A.; Schaverien, C.J.; Meijboom, N.; Ganter, C.; Orpen, A.G. *J. Am. Chem. Soc.* **1995**, *117*, 3008-3021.

28. Yano, T.; Ikai, S.; Shimizu, M.; Washio, K. *J. Polym. Sci., Polym. Chem. Ed.* **1985**, *23*, 1455-1467.

29. Zucchini, U.; Dall'Occo, T. in Polymer Science, Contemporary Themes; Ed. Sivaram, S.; McGraw-Hill, New Delhi, 1991, Volume 1, 221-228.

30. Sobota, P.; Przybylak, K.; Utko, J.; Jerzykiewicz, L.B.; Pombeiro, A.J.L.; Guedes da Silva, M.F.C.; Szczegot, K. *Chem. Eur. J.* **2001**, *7*, 951-958. Sobota, P.; Szafert, S. *J. Chem. Soc., Dalton Trans.* **2001**, 1379-1386.

31. Tembe, G.L.; Ravindranthan, M. *React. Kinet. Catal. Lett.* **1994**, *52*, 119-127. See also Karol, F.J.; Kao, S. in Studies in Surface Science and Catalysis , *89*, Catalyst Design for Tailor-Made Polyolefins, K. Soga, M. Terano Eds.; Elsevier Science: Amsterdam/ Kodansha Ltd., Tokyo, 1989, page 389-403.

32. Beach, D.L.; Kissin, Y.V. *J. Polym. Sci., Polym. Chem. Ed.* **1984**, *22*, 3027-3042. Kissin, Y.V.; Beach, D.L. *J. Polym. Sci., Polym. Chem.* **1986**, *24*, 1069-1084.

33. Henrici-Olivé, G.; Olivé, S. *Adv. Polym. Sci.* **1974**, *15*, 1. Skupinska, J. *Chem. Rev.* **1991**, *91*, 613-648.

34. Ziegler, K.; Holzkamp, E. *Ber. Dtsch. Chem. Ges.* **1957**, *605*, 93-97.

35. Casiraghi, G.; Casnati, G.; Pochini, A.; Puglia, G.; Ungaro, R.; Sartori, G. *Synthesis* **1981**, 143-146.

36. Pastor, S.D.; Spivack, J.D.; Steinhuebel, L.P. *J. Heterocyclic Chem.* **1984**, *21*, 1285-1286.

37. Zechmann, C.A.; Boyle, T.J.; Rodriguez, M.A.; Kemp, R.A. *Polyhedron* **2000**, *19*, 2557-2564.

38. See for instance Lee, D.; Jeong, Y.; Soga, K. *Ind. Eng. Chem. Res.* **1992**, *31*, 2642-2647.

39. M. Fujita, Ph.D. Thesis, Department of Chemistry, University of Alberta, Edmonton, Fall 2001.

5. Development of new instrumentation

5.1 Introduction.

The classic development of new polymerization catalysts can be subdivided into four steps. Ligand preparation (Chapter 2, page 61), complex synthesis and screening of these complexes for ethene polymerization activity, followed by polymer analysis (Chapter 4, page 196). Within such a scheme any of the said steps can limit the pace of improvement of the catalyst system under study.

Traditional ligand preparation and complex synthesis depend on the synthetic skills of the individual and are time consuming. The activity screening and polymer analysis are more technical in nature and allow further improvements to increase the throughput speed; the first point is addressed in this chapter.

During the studies described in this thesis it was observed that for large scale polymerization trials one of the rate determining factors seemed to be the supply of toluene free of polymerization inhibiting substances. An improvement of a solution published in the literature for the solvent supply problem is given in section 5.2 of this chapter. Section 5.3 (page 297) of this chapter describes a potential solution for screening a large number of ligand complexes.

5.2 The solvent purification unit.

In the literature a simple adaptation of an existing industrial setup for the purification of solvents is described.[1] In addition several companies[2] offer solvent purification systems based on the same concept. All these systems consist of a large solvent reservoir, which contains the solvent that is "pre" deoxygenated by passing nitrogen through the solvent for a certain amount of time before further processing the solvent.

The pretreated solvent is pushed through a set of columns C1 and C2 (see Fig. 5.1, page 278) containing a deoxygenation catalyst, followed by a drying agent, using pressurized nitrogen as the propellant. At the end of the columns the now oxygen and water free solvent is collected in a dry reservoir in the absence of contaminants.

The basic flow scheme of this setup, as given in the literature, is shown in Figure 5.1 (page 278). In general the system is characterized by a rather liberal use of expensive connectors and valves, some of which are only used one time during the life of the columns. A vacuum pump combined with a nitrogen purge is used for obtaining a contaminant free atmosphere in the collection vessel, while the actual purging of the big solvent storage reservoir has to be done in a fumehood.

An alternative setup, that is more automated and directed towards the end users is given in Figure 5.2 (page 279). Instead of using standard valves, a combination of solenoid valves (V1, V2, V4) and check valves (CV1, CV2) is used, which have to open in specific sequences during the collection of solvents.

Some of the problems inherent to the system described in the literature are also addressed, like the purging of the solvent storage reservoir, the question of what happens when the solvent storage reservoir is empty (which in the original setup is apparently answered when, after checking the nitrogen pressure, on opening the valve V_8 to the collection vessel no solvent shows up) and purging the collection vessel.

Furthermore, in this setup safety issues can be addressed using the same electronics that are necessary for turning specific solenoid valves on and off during operation.

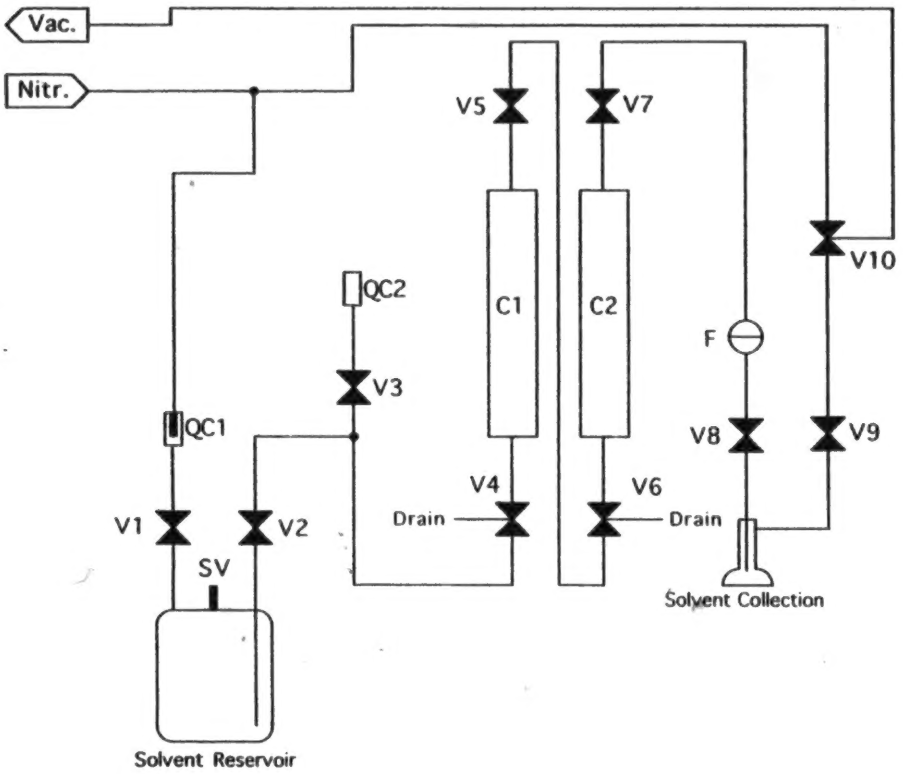
Vac.
Nitr.
V5
V7
V10
QC2
C1
C2
F
V3
QC1
V8
V9
V4
V6
V1
V2
Drain
Drain
SV
Solvent Collection
Solvent Reservoir

Figure 5.1. Solvent purification unit according to reference 1. QC1,2; Quick Connect connectors, SV; safety valve, V1,2,3; twoway valves, V4,6,10; threeway valves, F; filter, C1,2; columns, see text, Vac; vacuum line, Nitr.; nitrogen line.

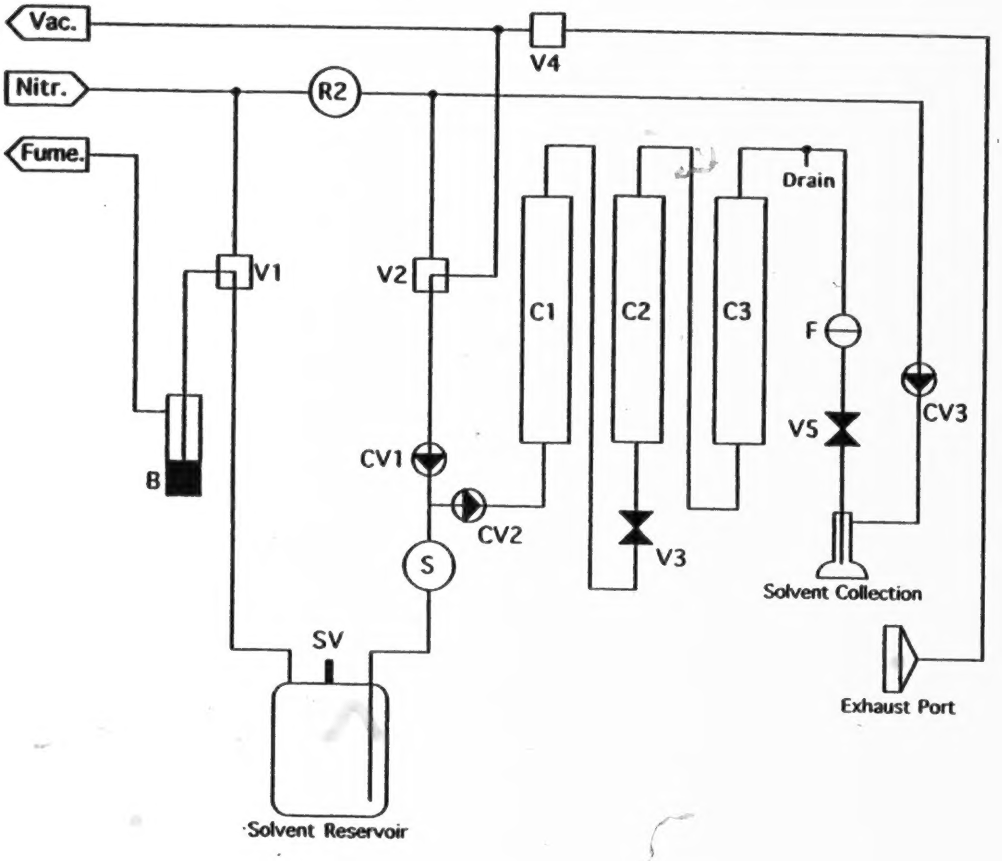
Vac.
Nitr.
Fume.
V4
R2
Drain
V1
V2
C1
C2
C3
F
CV3
V5
B
CV1
CV2
V3
S
Solvent Collection
SV
Exhaust Port
Solvent Reservoir

Figure 5.2. Modified solvent purification unit. V1,2; threeway solenoid valves, V3; bellows valve, V4; twoway solenoid valve, CV1,2,3; check valves, R2; pressure regulator, B; bubbler, SV; safety valve, S; solvent sensor, C1,2,3; columns, see text. F; filter, V5; ball valve, Vac.; vacuum line, Nitr.; nitrogen line, Fume; fumehood line.

5.2.1. Theory of functioning.

In order to assess what functions the electronic part of the system has to address, a table is constructed that shows specific situations during the use of the apparatus. Each of these situations is further split up into states that describe what the apparatus has to do in that specific state. Transitions between states (and situations) occur when specific signals characteristic for a certain situation are recorded.

For instance, when the main switch is turned on (recorded signal), the electronics have to activate the solenoid valve V1 that pressurizes the main solvent storage vessel (action following "on" signal) and have to turn on a light signal inside the on/off button: this is the "actual use of apparatus" situation.

In Table 5.1 (page 281) four basic situations in the use of the apparatus are given: a rest state, the actual use of the apparatus, a situation where the main solvent reservoir is empty, and a problem situation which in theory could include things like solvent spill, fire, nitrogen tank empty, or just electronics malfunctioning. In Table 5.1 (page 281) the necessary signals required to jump from one state to another are not given: these signals are given in a state diagram (vide infra).

The rest state S1 is self explanatory: there is no pressure on the main solvent storage reservoir, and the resevoir is connected to an oil bubbler B to maintain an inert atmosphere. All electronics and solenoid valves are in a rest state (this is actually the state shown in Fig. 5.2, page 279). In order to make the user aware that power is applied to the electronics the display on the front panel is on, and in a hold state.

Notice that this state is inherently "safe": nothing will happen when the power supply fails by accident.

Table 5.1: Situation/State Action Table

	SITUATION:						
	Rest	Solvent Take Off		Reservoir Empty			Problem
Action[1]							
LED							
L5 on/off	0	1	1	0	0	1	0
L6 empty	0	0	0	1	0	0	0
L7 wait	0	0	0	0	1	1	0
L8 error	0	0	0	0	0	0	1
Buzzer	0	0	0	1	0	0	1
Timer	Hold	Hold	Count Down	Reset	Count Down	Reset	Reset
Solenoid Valves							
V1 press.	0	1	1	0	0	0	0
V2 purge	0	0	0	0	1	1	0
V4 vac.	0	1	1	1	1	1	0
	S 1	**S 3**	**S 4**	**S 5**	**S 6**	**S 7**	**S 9**
	STATE						

---

1. Note: 0 = off, 1 = on

For the electronics we have to define a "pre" rest state state S8 that automatically leads to rest state S1. This state S8 is not given in Table 5.1, while during development of the hardware state S2 was eliminated explaining its absence in Table 5.1. When the power supply is turned on, a reset is generated that automatically leads to this rest state S1 via S8. Rest state S1 can also be reached by pressing a reset button.

The signals that actually induce transitions between states are given in a so called State Diagram next to the arrows that connect specific states: see Schemes 5.1, 5.2 and 5.3.

When someone would like to use the setup, a switch on the front panel would have to be turned on. This action would lead to a new state S3 where the solvent storage reservoir is pressurized (by activating V1), and suction is applied near the solvent take off (by activating V4), to remove solvent vapors: see Scheme 5.1. In addition an indicator light comes on in the on/off switch (L5).

The opening of the valve V5, indicating use of the unit, is recorded by the electronics in the form of the *opening* of switch FillSW, whereupon a countdown counter is started.

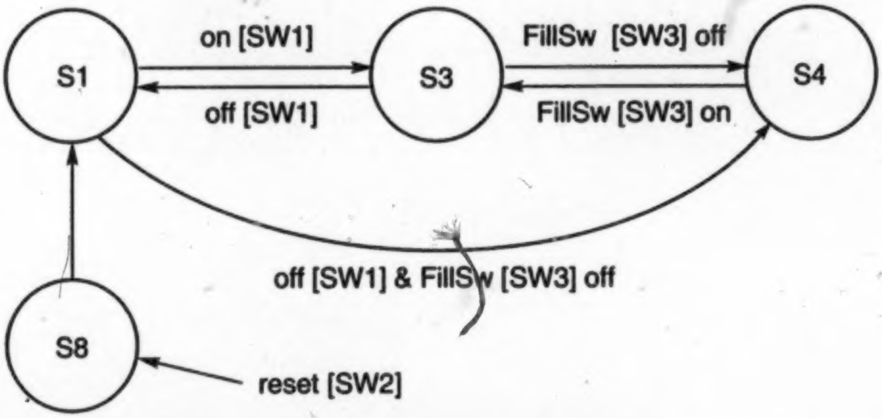

Scheme 5.1. State Diagram of solvent take off situation.

The value of the counter is shown in a display (DIS1) on the front panel. In this way, a rough indicator for the amount of solvent left in the storage reservoir is obtained.

This counting down defines a new state S4, see Table 5.1. Closing the valve on the front panel after solvent has been collected, returns the system to state S3. After purging the contents of the receiving flask for a certain amount of time, the user would close the stopcocks on the flask and remove the flask from the solvent outlet tube. The whole sequence would finish by pressing the on/off button, bringing the system back to the reststate S1 and releasing the pressure in the solvent storage reservoir through the oil bubbler B which should be connected to a fumehood.

It is possible that a hasty user just opens the valve on the front panel, or is interested in dry (not oxygen free) solvent: automatically the system would jump from reststate S1 to the solvent take off state S4, by pressurizing the solvent storage reservoir (V1) and activating the solvent vapor removal (V4). All these actions constitute the "solvent take off" situation, as given in Scheme 5.1 (page 282) and Table 5.1 (page 281).

As the supply of solvent is limited by the solvent reservoir content, at a certain point in one of the states S3 or S4 nitrogen gas instead of solvent will be pushed through the columns. If this event could be detected with a sensor, the electronics could automatically shut down the system. This defines state S5, which is reached when the solvent sensor FL1 records "no solvent" in either state S3 or S4, see scheme 5.2 (page 284). This situation is noticable for the user by a buzzer sounding, and a visual signal "reservoir empty" (L6) turning on (see Table 5.1, page 281). In addition, the timer is reset to 99 and the indicator light in the on/off button (L5) goes off. The vapor suction stays on permanently (solenoid valve V4).

In order to force the prospective user to think about safety, the alarm state S5 can only be left by closing the solvent take off valve V5 (closing the FillSW) on the front panel as well as pressing the RepSW reset button mounted on the solvent storage reservoir *after* refilling this reservoir.

Closing the solvent take off valve on the front panel combined with a reset signal leaves state S5 to reach state S6. In this state a visual signal "wait" (L7) comes on, and the visual (L6) and audio signals (buzzer) are switched off.

At this point low pressure nitrogen is used to purge the recently filled solvent storage reservoir: solenoid valve V2 is turned on. The vapor generated in this process leaves through the oil bubbler B (see Figure 5.2, page 279) to a fumehood. During this time a count down process (99 to 00) is visible on the display: a purge of twenty minutes is programmed.

If during this time the solvent take off valve (V5 and FillSW) on the front panel is opened, the system returns to state S5 sounding an alarm and restarting the whole sequence.

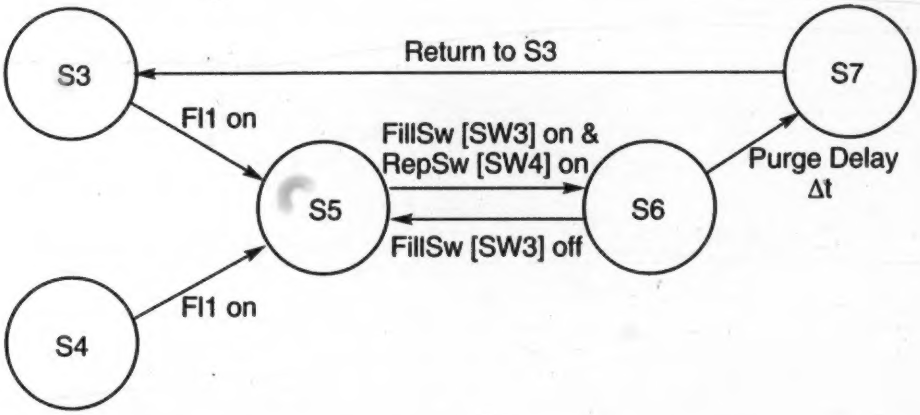

Scheme 5.2. State Diagram of solvent reservoir empty situation.

If no interruption by the user takes place, at the end of twenty minutes the apparatus returns to state S3 via state S7 by pressurizing (V1 activated) the now purged solvent storage reservoir, after switching off V2, see Figure 5.2 (page 279).

Finally a "problem situation" is defined, with its corresponding state S9. This is a state similar to the reststate S1 except that none of the switches or sensors can bring the system out of this state *except* a reset (by pressing the reset switch, or unplugging the mains). In order to make users aware of the problem the buzzer sounds, and a "error" visual signal (L8) is turned on, while all solenoid valves are put in the deactivated state. Its function is to shut down the system completely, until a major electronic or hardware problem has been solved by the user. Any combination of switches that would signal an empty nitrogen cylinder, too high a temperature of the solenoid valves, power supply or surroundings (indicating possible problems), or just the flooding of solvent, could be used to reach this state.

Originally the use of a flood sensor (NoahFld) was anticipated, which could shut the sytem down on the appearance of solvent in the tray of the apparatus due to, for instance, leaks in the combined hardware, or just the opening the valve (V5) on the front panel without a collection reservoir mounted properly. The electronics allows these sensors / switches to be connected, but none of these possibilties has been tested.

The resulting overall State Diagram for the solvent purification unit is given in Scheme 5.3 (page 286), and consists of a combination of Scheme 5.1 and 5.2 with the state S9 corresponding to the "problem situation".

5.2.2 Detailed description: electronic part.

The required actions (outputs) and the different inputs in the State Diagram are defined as "on/off" in the previous section. In that way the whole system as described in section 5.2.1 can be handled by solid state logic elements. In the most advanced form this would mean a microprocessor plus program, and in the least advanced form the use of handsfull of discrete logic components.

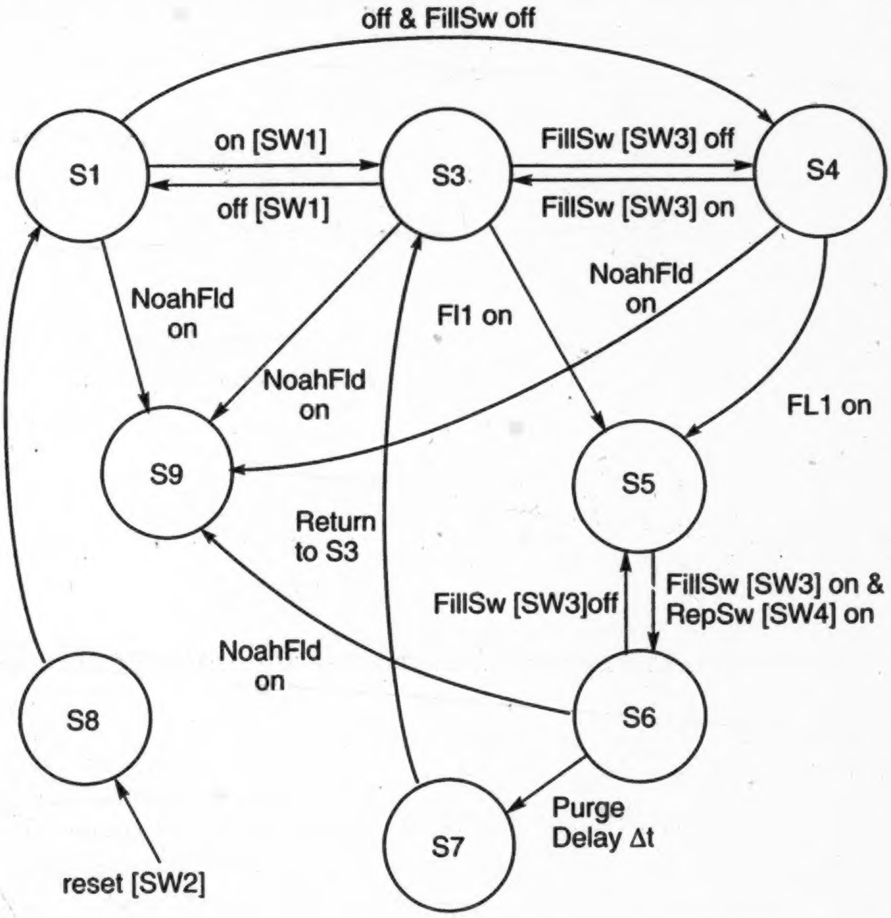
off & FillSw off
S1
on [SW1]
off [SW1]
S3
FillSw [SW3] off
FillSw [SW3] on
S4
NoahFld on
NoahFld on
Fl1 on
NoahFld on
FL1 on
S9
S5
Return to S3
FillSw [SW3]off
FillSw [SW3] on & RepSw [SW4] on
NoahFld on
S8
S6
S7
Purge Delay Δt
reset [SW2]

Scheme 5.3. State Diagram of the solvent purification unit.

Intermediate between flexible programming of an expensive microprocessor to follow the different states S as described above, and the cheap but inflexible discrete logic component approach is the field programmable logic gate array.[3] Simply stated, this is a multipin chip that contains thousands of logic components, that can be connected in specific ways to get the logic functions the user wants by programming the chip (such a programmed gate array is *not* a microprocessor: it does not contain a stored instruction set).

The fact that the chip can be programmed also implies complete flexibility in assigning specific pins to be an input or output. The Xilinx Corporation manufactures gate arrays that can repeatedly be programmed, thereby allowing changes to be made in the electronic scheme. After defining input and output signals the State Diagram (Scheme 5.3, page 286) could be assembled on a 84 pin Xilinx XC 9572,[4] the pin assignment of which is given in the appendix I together with the electric scheme (page 392). The State Diagram of Scheme 5.3 now defines what states will be occupied after the Xilinx chip receives or generates certain signals, exactly giving the output as defined in Table 5.1 (page 281) for each of the states as defined in section 5.2.1.

By itself the programmed XC 9572 is of not much use; it needs to be connected to the necessary switches and sensors, and needs a clock signal in addition to a power supply.

A special Burr Brown IC, the DRV101T, is used for turning the solenoid valves on and off. This IC is a pulse-width modulated solenoid driver and allows a more efficient use of the power supply.[5]

The printed circuit board contains space for mounting a voltage regulator. Such a regulator is not used due to overheating problems of the IC. Unfortunately there is not enough space available for using a larger heat sink so that instead separate power supplies for the electronics and the solenoid valves are used.

The problem of the solvent sensor is solved by assembling a light gate based on a light source (a light emitting diode) combined with a photodiode (a Burr Brown OPT101). This sensor detects the absence of solvent when the light beam falling on the photodiode is blocked by a float made of an NMR tube. By adjusting the length of the sealed glass NMR tube, it will float in the presence of liquid and sink in the absence of liquid. This glass float contains a piece of black paper that will block the light beam when the float is positioned at the bottom of the device, a situation that will occur in the absence of liquid.

Notice that if the float leaks or the electronics fail, a "reservoir empty" signal is generated, that, due to its permanent nature, would reveal the malfunctioning of the sensor.

With this short description a rough outline of the electronic components is given,[6] for which a double layer printed circuitboard with plated through holes was developed;[7] see the appendix, page 392. After thorough testing of the assembled printed circuit board, the electronics are mounted and connected to the power supplies, switches and solenoid valves.

5.2.3. Detailed description: hardware.

In section 5.2.1 no attention was given to the actual solvent take off although this is the part where solvent contamination is most likely to occur.

First of all, the tubing of the solvent take-off must be kept oxygen and water free. Secondly, after the solvent take off, any remain[illegible] in the tubing must be removed or kept under nitrogen.

In the Grubbs setup[1] these problems are solved by putting the solvent take-off junction (and the solvent collection reservoir) under vacuum. This solution requires more valves, and more manipulations during the solvent take-off as well as an additional vacuum pump.

In the solvent purification unit described here, the original benzophenone-ketyl technology is maintained. All of the solvent take-off junction is permanently kept under a positive nitrogen pressure, and when not in use closed with a protective cap.

When actual solvent collection is required the protective cap on the solvent delivery tube is removed, the collection flask (a standard model as used with benzophenone-ketyl stills) placed, and positioned near an exhaust port. Both valves on the collection flask are opened, and any remaining solvent is removed under a flow of nitrogen by heating the flask with a heat gun. In this setup the solvent delivery tube is kept permanently under a slight overpressure of nitrogen delivered by regulator R2 (see Fig. 5.2, page 279). This nitrogen pressure is also the pressure used for purging the solvent collection flask before and after solvent collection. This does require removal of solvent vapors, and this is what the suction on the exhaust port mounted on the front achieves: the in-house laboratory vacuum line is used for this. As the outlet on the collection flask is near the exhaust port, solvent vapors do not contaminate the laboratory space. After cooling, a valve on the front (V5) is opened and solvent flows under a protective nitrogen blanket in the collection flask.

The solvent take off tube requires a good seal in order to maintain an inert atmosphere to keep the collected solvent clean. Originally a stainless steel balljoint was thought to do this properly. This turned out to be a mistake: due to the pressure used, solvent as well as nitrogen are leaking past the balljoint. Instead an O-ring seal with a clamp is used, the combination of which maintains a solvent/nitrogen leak free seal.

In order to make the solvent purification unit more user friendly, the columns C1, C2 and C3 containing aluminum oxide, deoxygenation catalyst, and molsieves, are mounted upright in order to obtain a compact unit. In this way some resemblance to the old benzophenone-ketyl stills is maintained, while allowing several units to be placed next to each other on a laboratory bench. The frame of the solvent purification unit contains in addition to the columns, all solenoid valves, tubing, electronics and a power supply. In order to contain any solvent spills, the whole unit is protected by a removable stainless steel cover and placed in a stainless steel tray.

The unit is grounded, and the original plastic valve handle on the front panel is replaced by a stainless steel one: in this way any static charge on the user of the apparatus is removed before the actual use of the setup. The solvent reservoir is placed next to the solvent purification unit, and electrically connected to it in order to prevent the build up of static charge.

For the connection of the solvent reservoir to the columns, thick, slightly flexible, 0.25 inch Teflon tubing is used. All connections are made using Swagelok fittings.

The columns are made of stainless steel and contain at the top a copper gasket and knife edge seal which gives a more reliable seal at the high temperatures necessary for column regeneration. Before use the columns were helium leak tested at 60 psig.

The internal connections are all made with 0.25 inch stainless steel tubing, and if necessary, supported by a frame. The valve (V5) at the front panel is actually mounted away from the front panel in order to obtain the necessary space for a T-joint connecting the nitrogen purge line, the column outlet , and a solvent take off made of 3/8 inch stainless steel tubing. For the hardware component list see the appendix J, page 399.

In order for the electronics to detect the opening and closing of the valve V5 at the frontpanel, a magnetic switch SW3 is mounted perpendicular to the shaft of the valve, while a magnet (actually the core of a magnetic stir bar) aligned with this switch is glued inside a hole drilled in the shaft. In this way opening of the valve turns the magnet away from the aligned switch/magnet position, and as a result the magnetic switch opens. The opening of the magnetic switch is recorded by the electronics mounted directly behind the stainless steel front panel.

5.2.4 Detailed description: starting the solvent purification unit.

As the described system contains fewer valves compared to the one described in the literature,[1] more care is required in assembly. In practice this is not a problem. The materials with which the columns are filled are dried for 12 hours in an oven at 150 °C, and, while hot, poured into the columns.

The alumina column C1 (see Fig. 5.2, page 279) and the molsieve column C3 are placed in a large glassblowers oven with exhaust, and heated for 8 hours at 350 °C under a stream of approximately 5.3 scfh/2.5 slpm nitrogen (copper tubing with swagelok fittings is sufficiently flexible for use). The oven is brought to room temperature *maintaining* a flow of nitrogen until the columns are at room temperature. At this point the columns are closed using the standard Swagelok endcap.

The deoxygenation catalyst is treated similarly, except that the bellows valve V3 *has* to be connected to the nitrogen/hydrogen line. While maintaining a 7% hydrogen/nitrogen mixture (using needle valves) at a flowrate of 10.6 scfh/5 slpm the column is heated to 250 °C and kept at that temperature for 10 to 12 hours. When oven and column have reached a manageable temperature, the *outlet* of the column is closed after cleaning the seat of the fitting using a standard Swagelok endcap, and after closing the bellows valve V3 the column is removed from the oven. As it is important that the column remains oxygen free, the exact Swagelok procedure for mounting the endcap *must* be followed. The final mounting of the columns is now straightforward: exact following of the Swagelok rules for tightening the connections[8] is recommended at this point.

The *empty* solvent storage reservoir is purged with nitrogen, as well as all the lines leading to the first column (C1, containing alumina) to be mounted. This column is mounted under a flow of nitrogen, and purged before proceeding to the next step. The outlet of column C1 is attached under a vigorous flow of nitrogen to the bellows valve V3 of the deoxygenation column C2.

This valve is opened while maintaining nitrogen pressure, and the endcap at the top of the column is removed. Next, the deoxygenation column C2 is connected to the molsieve containing column C3. As this column must contain traces of oxygen it is purged for a while before connecting it to the filter F and main valve V5 at the front panel. This should be done with the drain (one arm of the T-joint) open.

While maintaining a flow of nitrogen through the columns, the electronics are connected to the mains, and the main valve V5 at the front panel is opened. When the counter reaches 89 the "reservoir empty" signal appears; the main valve at the front panel is closed. Now the T-joint should be closed with a Swagelok endcap.

The solvent storage reservoir is filled with solvent, and after pressing the reset button SW4 on the solvent reservoir, the contents are purged with nitrogen for twenty minutes.

After twenty minutes purging the only things that remain before actual use are adjustment of the regulator on the nitrogen tank, of the low pressure regulator R2, adjustment of the solvent flow rate and removal of fines (that might block the filter) from the columns.

The high pressure regulator on the nitrogen tank is set at 18 psig. Next the solvent outlet cap is removed in order to adjust the low pressure regulator to a gentle flow. Now a collection flask can be attached, carefully adjusting the outlet to bring it near to the exhaust port: both valves on the collection flask should be open. To start filling the columns the on/off switch needs to be turned on. The speed with which solvent fills the columns can be adjusted with the bellows valve V3 on the deoxygenation column. Slow filling is advised as long as the counter[9] on the front panel is above 89.

The progress of the solvent front can be monitored by checking the temperature of the columns: a clear increase in temperature can be recorded when the column materials are wetted with solvent for the first time. Depending on the volume of the solvent storage reservoir a refilling of solvent may be necessary: the "empty" alarm will sound. When the solvent reaches the top of the last column, solvent will start to come out of the drain.

Approximately 2 liters are collected, or as much as necessary to remove fines that might block the filter F. After closing the bellows valve V2, the drain is closed (place the endcap on the T-joint and tighten). Slowly the bellows valve V3 on the deoxygenation column C2 is reopened until a reasonable filling rate of the collection flask is obtained. If necessary, the low pressure regulator R2 is readjusted to maintain a good purge while filling the solvent reservoir. Notice that too high a purge pressure will result in overpressure in the collection bottle, which can give amusing effects when the bottle is opened inside a glovebox. The main valve V5 on the front panel is closed together with the stopcocks on the collection vessel. While maintaining nitrogen pressure on the solvent storage reservoir, the areas around connections are checked for solvent leaks. Offending connectors are tightened.

With these last adjustments, the solvent purification unit is ready for use: the apparatus is returned to the rest state by pressing the switch on the front panel (SW1), the collection flask is removed (discard the contents), and the cap on the solvent outlet tube is mounted.

5.2.5 Discussion.

The appartus as described has been in use for approximately 10 months during which some minor modifications were necessary.

By itself the solvent purification system does what it is supposed to do: give solvent, toluene in this case, of a purity equal to or better than toluene dried/refluxed over potassium under nitrogen gas: The purity of the collected solvent was checked by doing polymerization reactions parallel to polymerization reactions using toluene collected using a potassium/nitrogen still. No difference in activity, under otherwise the same conditions, was noted.

The only mechanical problem that had to be addressed was the failure of the check valves. Although rated for the right pressure range, and having Kalrez seals, the originally used check valves failed to close after a short period of use.

The failure of check valve CV2 did not appear to cause problems. The columns would not maintain the pressure after the solvent storage reservoir was brought to atmospheric pressure, and as a result some fines may have been passed to this reservoir possibly aggrevating the check valve failure.

The failure of check valve CV1 required immediate attention. When pressurized, solvent passed the check valve in the direction of the solenoid valve V2, which might damage it. In order to close this check valve after a solvent purge, the pressure difference over the check valve CV1 was increased by connecting it after purging to a vacuum line, see Figure 5.2, page 278. This did not solve the problem: now the solvent passed into the vacuum line. The only solution left was to replace it with a different kind of check valve: this turned out to function better. The vacuum line connection to the check valve CV1 was maintained. No solvent has been detected in the lines during several months of use.

During 10 months of use some negative aspects in the electronics did turn up. While testing the unit by switching it on and off repeatedly, it was observed that the solenoid power supply randomly would break down resulting in temporary failure of the setup. This would happen approximately one out of a hundred times switching the apparatus on and off and although the internal automatic fuse in the power supply would reset the power after some time, this would limit the reliability of the apparatus. The reason seemed to be unsuitable diodes (1N4004) mounted over the solenoid valves to suppress the inductive kick.[10] Replacing these diodes with Schottky diodes seems to have solved the problem.

Secondly, it turns out that the number of power interruptions in the chemistry department is rather high: the solvent purification unit keeps track of these events by resetting itself (counter 99) or, more annoyingly, locking up (counter left digit 0, right digit off).

In the last case, the power supply of the electronics has to be unplugged, and after 2 minutes plugged in again: a small battery introduced in the electronics power supply might solve this departmental nuisance.

Originally the solvent sensor was found to be very sensitive to nitrogen bubbles, generating a system reset characteristic for a "solvent reservoir empty" during the pressurizing of the solvent storage reservoir. However, this problem seems to have solved itself for unclear reasons, thereby making further electronic modifications unnecessary.

5.2.6 Safety considerations.

In the original proposal, the solvent storage reservoir was to be placed in a solvent storage cabinet with exhaust, while the unit itself was to be placed on top. The tray on which the unit was to be mounted would have had a drain that leads to a waste container. With hindsight this seems like a safety overkill, although a solvent cabinet would prevent the user from inhaling solvent fumes when refilling the storage reservoir and in addition would offer protection in case one of the flexible teflon tubes were to be damaged. Safety is clearly compromised on this point.

The described system has been optimized for toluene, and URL certified components were used when available. However it should be stressed that the solvent compatibilty remains a point of close attention, especially for the solenoid valves: the described system is after all a *toluene* purification unit *prototype*.

As stated in part 1 the developed electronics allow the connection of a flood sensor: from a safety point of view this should be tried.

Yet another improvement would be a pressure switch mounted separately or in series with the reset switch on the solvent reservoir. Although the following has not happened yet, it is conceivable that a hasty person, on observing the alarm signal indicating an empty solvent storage reservoir, closes the main valve V5 on the front panel, and presses the reset switch on the reservoir *before* refilling it. An altogether unhealthy situation, because now the reservoir is being purged during refilling. A pressure switch that closes a contact when atmospheric pressure is reached and placed strategically to monitor the pressure in the solvent reservoir, or better, in the solvent supply lines would solve most of this problem.[11]

5.3 Introduction: the descending well reactor.

As stated in section 5.1, one of the key steps in the development of more active catalysts is the testing of the synthesized complexes. In practice this means a time consuming number of catalytic runs. Classic Ziegler-Natta and metallocene catalysts pose significant problems in the number of slurry phase runs that can be performed parallel or in series.

Both co- and pre-catalyst are often extremely sensitive to impurities like water and oxygen, making working under an inert atmosphere necessary. In practice the problem of the interference of impurities with the polymerization reaction is partly solved by using thick glasswall tubes, filled and capped inside a glovebox, as the reactor. This procedure works, but is tedious and time limited due to the leaching of contaminating components from the Neoprene septum.

Furthermore pre- and co-catalyst have to be mixed under ethene pressure. In practice this is usually done by making use of syringe techniques, which, depending on the dexterity of the user, will introduce varying amounts of contaminants and is not without safety hazards when using trialkylaluminum or MAO solutions. For highly active catalysts the concentration has to be lowered (the tube will fill up with polymer very fast, limiting the observation time window), but this automatically increases the sensitivity of the system under investigation for impurities introduced in the test setup.

To summarize: mixing the catalyst precursors under an ethene atmosphere in a slurry phase run outside the glovebox requires the use of syringe techniques. This limits the number of catalytic runs, the accuracy of small volume runs and can form a safety risk as well due to the pyrophoric nature of some of the reactants.

By restating the problem, a solution suggests itself: discard the syringe technique and replace it with a simple technique for allowing two physically separate solutions (or suspensions) to mix under an ethene atmosphere.

5.3.1 Theory of operation.

Imagine a hollow Teflon plunger that can slide smoothly in a stainless steel barrel. By itself this hollow plunger can act as a reaction vessel, especially when a stir bar is added to the hollow plunger. Because the plunger can slide smoothly in the barrel, only a slight pressure at the top is needed to bring it down from its upper position to a lower position.

If the barrel is straight and smooth, there is no advantage: the hollow plunger filled with a reaction mixture can only be moved up and down within the barrel.

If instead the barrel broadens at the top, a second resevoir is formed when the plunger is in its uppermost position. This second reservoir, when filled with a solution, will empty itself into the hollow plunger when that plunger starts to move downward under the influence of gas pressure applied at the top of the assembly.

A cross section of such a device is shown in Figure 5.3 (page 299), including the stainless steel barrel and hollow Teflon plunger, but with the top and bottom plate removed: notice the gas inlet at the top of the barrel for applying pressure to force the plunger down.

In use, both the Teflon plunger as well as the reservoir formed when this plunger is in the uppermost position can be filled with the precatalyst **2** (and a stir bar, not shown), and cocatalyst **1** in Figure 5.4a (page 300).

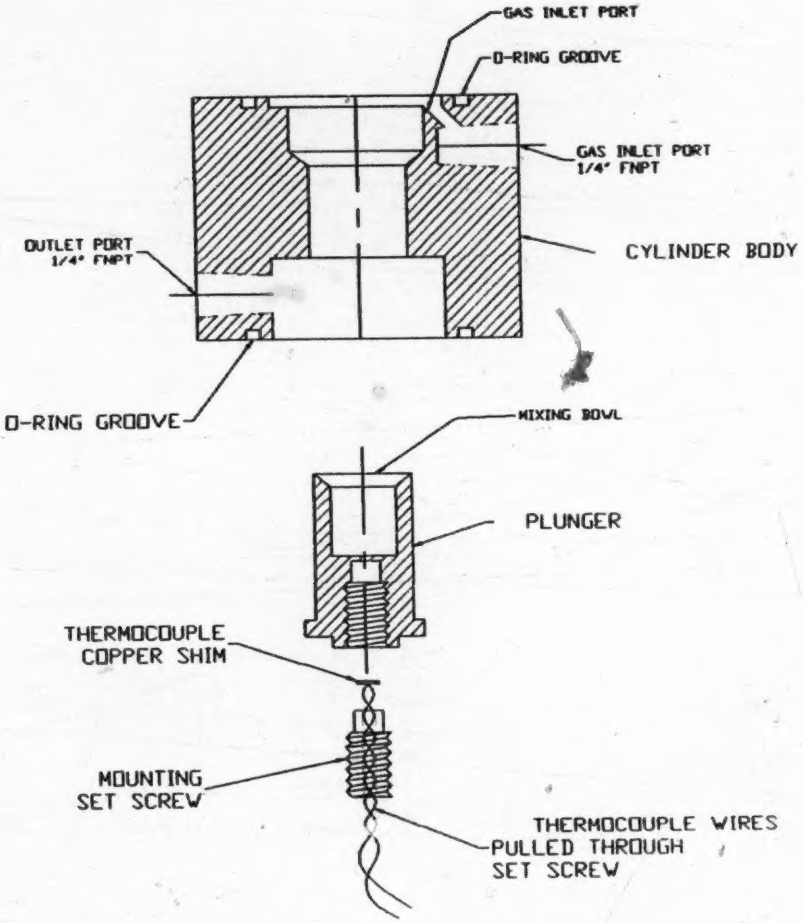
GAS INLET PORT
O-RING GROOVE
GAS INLET PORT 1/4" FNPT
CYLINDER BODY
OUTLET PORT 1/4" FNPT
O-RING GROOVE
MIXING BOWL
PLUNGER
THERMOCOUPLE COPPER SHIM
MOUNTING SET SCREW
THERMOCOUPLE WIRES PULLED THROUGH SET SCREW

Figure 5.3. Full section view of the descending well reactor.

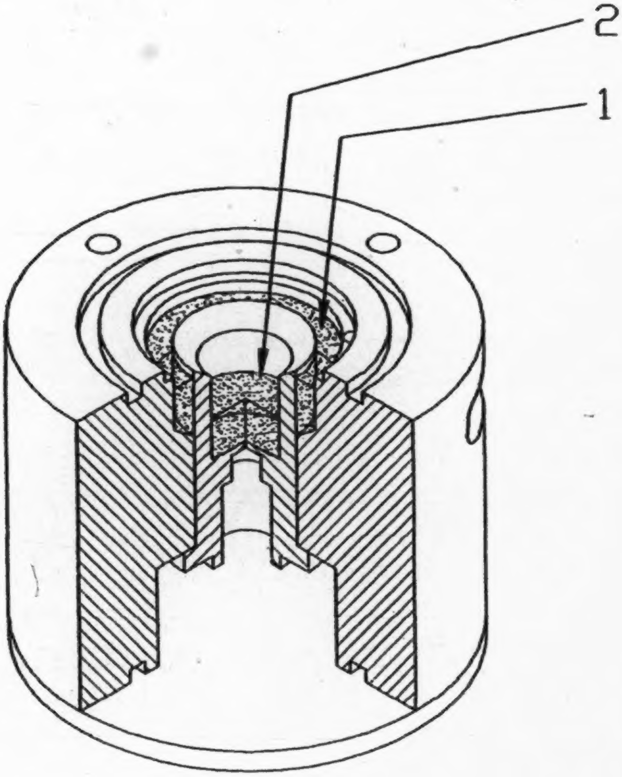

Figure 5.4a. Isometric halfsection of the descending well reactor: **Initial State**. The plunger is in the fully ascended position and both reactor chambers are filled with reactants **1** and **2** (top plate removed for clarity).

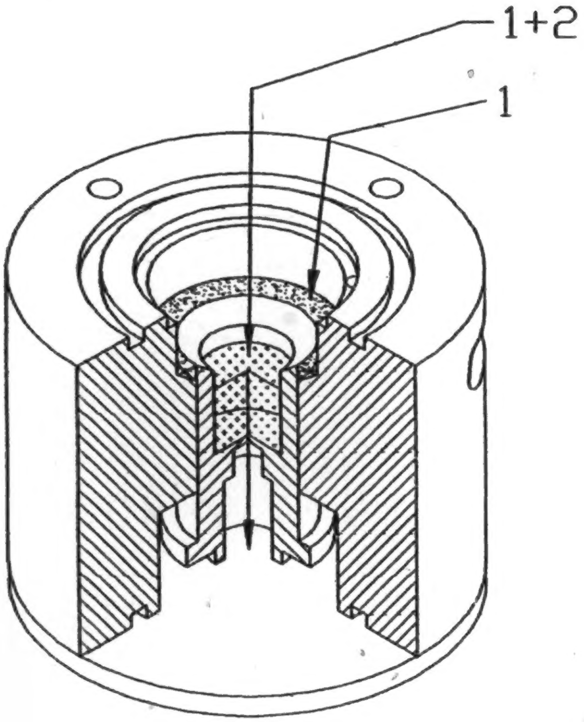

Figure 5.4b. Isometric halfsection of the descending well reactor: **Intermediate State.** Gaspressure in the upper part of the reactor forces the plunger down, starting the mixing of reactants **1** and **2**.

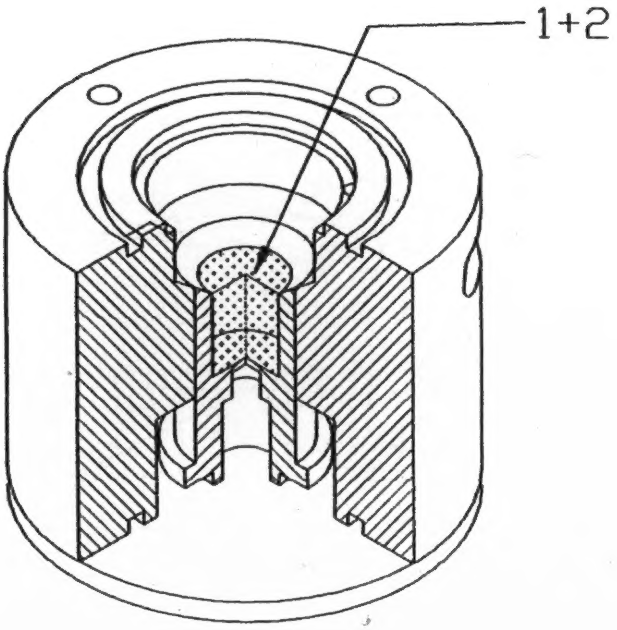

Figure 5.4c. Isometric Halfsection of the descending well reactor: **Final State**. The downward moving plunger has reached the lowest position. The mixing of reactants **1** and **2** is complete.

For sensitive polymerization catalyst precursors this step would have to be done in the glovebox. After securing the top plate which protects the contents from exposure to air, the whole setup is brought out of the glovebox. Outside the glovebox, the reactor is placed on a magnetic stirrer, and flushed with ethene. Pressurizing the upper chamber forces the Teflon plunger down, see Figure 5.4b (page 301), starting the mixing proces of precatalyst **2** and cocatalyst **1** under an ethene atmosphere.

When the Teflon plunger reaches the endplate the mixing of pre and cocatalyst would be complete, Figure 5.4c (page 302).

The polymerization of ethene is an exothermic process, which should result in a measurable increase in the temperature of the reaction mixture. The rate of the temperature increase in the polymerization reaction mixture is a function of the heat loss of the system, the heat capacity of the mixture, and the heat generated in the reaction. The last variable will be a function of the catalyst activity. If we assume the heat loss and heat capacity constant, the activity of the polymerization catalyst expresses itself in the rate of the temperature increase of the reaction mixture. This can be measured using a thermocouple as a temperature probe.

Such a thermocouple is mounted on a copper shim disk, that acts as a "heat integrator", and is pressed tightly against a thin teflon membrane separating the disk from the reaction mixture using a mounting set screw (see Figure 5.3, page 287). The thermocouple wires are brought out of the stainless steel barrel using the outlet port drilled in the bottom part of the barrel.

5.3.2. Assembly and testing of the descending well reactor.

An exploded view of the reactor is given in Figure 5.5 (page 306). In the version as used in testing, the bottom plate **7** and an accompanying Viton o-ring

4 are mounted on the cylinder body **5** with four countersunk flathead screws **8**. The bottom plate can easily be removed for inspection of the Teflon plunger **6** and the thermocouple assembly **9** and **10**. The reactor outlet port acts as the thermocouple wire outlet. The top plate consists of a Plexiglass protective plate **2** and, facing the pre- and co-catalyst solutions, a Pyrex glass plate **3**. These are clamped leak-free on a Viton o-ring using four hex socket cap screws **1**. The advantage of using a transparent top plate is that the reactor contents can be observed during the reaction. Because the plunger is moving down, the coupling with the magnetic stirrer becomes stronger. This also implies that the bottom plate has to be made of stainless steel. The volume of the Teflon plunger in the tested prototype is 1 mL.

For a trial run 0.56 g of a dichloro[*rac*-ethylenebis(indenyl)]zirconium(IV) solution in toluene with a concentration of 761 nmol/g was stored in the outer rim, while 0.42 g of a MAO 10 wt % solution in toluene (1700 eq) was poured in the Teflon plunger containing a stir bar. After sealing and transfer out of the glovebox, the filled reactor was connected to an ethene tank and after temperature equilibration pressurized with 30 psig ethene. The temperature of the reactor was recorded using a Omega thermocouple readout unit (type T), see Table 5.3 (page 305). Polyethylene formed as white flakes giving a crater like structure at the liquid/gas interface at the top of the Teflon plunger. No attempt was made to isolate the polyethylene formed.

These results allow the following conclusions: first, the basic concept seems to work. The catalyst precursors can be mixed outside the glovebox to form an active catalyst without using syringe techniques. In this experiment polyethylene is formed. Secondly, efficient mixing in this small a volume is a problem: the stirrer bar doesn't do its job properly as polyethylene builds up at the interface between gas and liquid phase. Thirdly, the temperature measurement needs substantial improvement, in order to accurately measure small increases in temperature.

As far as the actual measured temperature increase is concerned: it is unclear at this point to what extent this is actually due to a reaction taking place. When the ethene gas supply is switched off after 15 minutes, the temperature of the cell drops by 1.9 °C in 37 minutes. When, after this period, the ethene supply is switched on again, the temperature is measured to increase by 2.0 °C. These observations can be explained by assuming the catalyst stays dormant after consumption of the remaining ethene, causing the observed increase in temperature when the ethene polymerization resumes.

Table 5.3: Testing the descending well reactor.

Time (min.)	Temperature (°C)	Gas supply
start	22.6	off
1	23.4	on
5	25.2	on
10	25.1	on
15	25.4	off
52	23.5	off
57	25.5	on

When the ethene gas supply is switched on again, however, the pressure pushes the Teflon membrane tightly against the copper disk. The resulting good thermal contact between reactor content and thermocouple may now give an "accurate", but artificially increased temperature compared to the previous value.

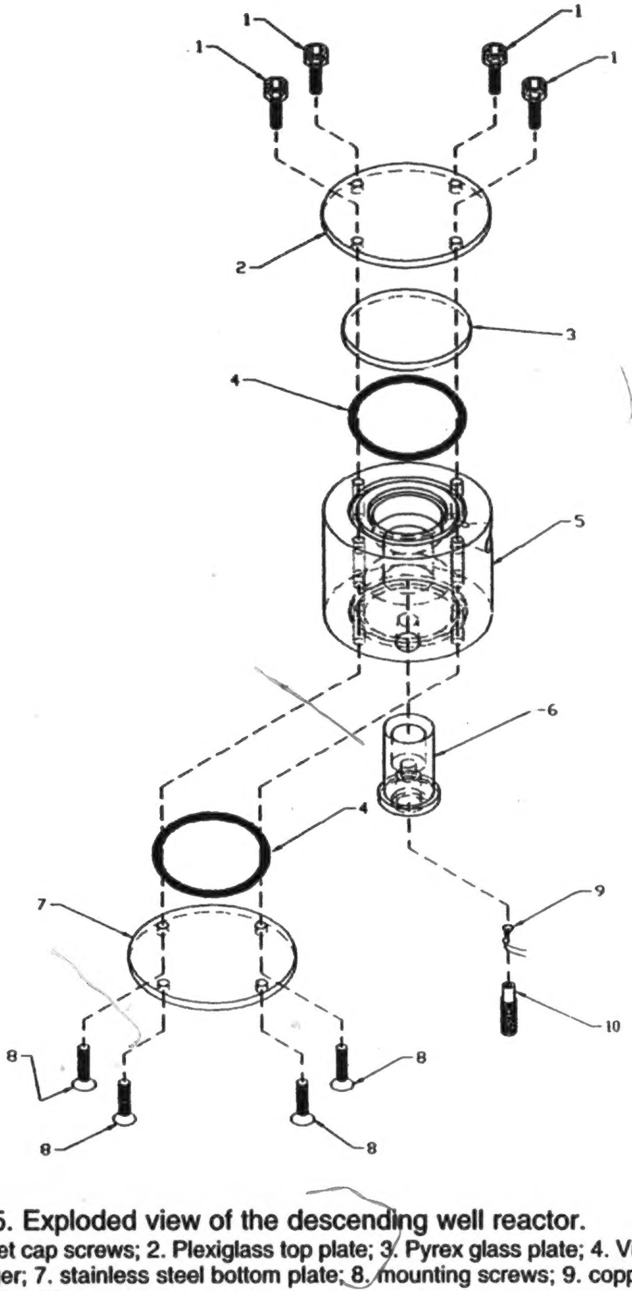

Figure 5.5. Exploded view of the descending well reactor.
1. hex socket cap screws; 2. Plexiglass top plate; 3. Pyrex glass plate; 4. Viton O-ring; 5. barrel; 6. teflon plunger; 7. stainless steel bottom plate; 8. mounting screws; 9. copper shim plate & type T thermocouple; 10. set screw.

The last explanation combined with the observed low absolute value of the measured temperature raises serious doubt about the correct interpretation of the measured values. It could be an increase of the temperature of the reactor content, but a malfunctioning temperature sensor could explain the results just as well. A better design of the temperature sensor, and more experiments are necessary to show beyond doubt the relation "active catalyst" = "increase of reactor temperature" for this descending well reactor type.

Notes and References.

1. Pangborn, A.B.; Giardello, M.A.; Grubbs, R.H.; Rosen, R.K.; Timmers, F.J. *Organometallics* **1996**, *15*, 1518-1520.
2. MBraun, Vacuum Atmospheres, Solv-Tek Inc., and Innovative Technology are some of the companies that are selling, or are in the process of designing, solvent purification units.
3. Bostock, G. *Electronics World* **1997**, *5*, 393-396, Bursky, D. *Electronic Design* **2000**, 97-113, Xilinx Databook (version 1.1) **1996**.
4. Xilinx Student Edition, Prentice Hall, ISBN 0-13-028907-8
5. Duration of 100 % duty cycle was set at 100 msec., after which the duty cycle was adjusted to 60 %: see Burr Brown Datasheet.
6. The freeware used for drawing the schemes in this chapter is McCad Schematics Lite, Vamp Inc.: see www.mccad.com
7. Component placement and routing were done manually using Easytrax freeware: see www.apcircuits.com
8. Swagelok gageable tube fittings catalog MS-01-140 **1996**, page 53.
9. The electronics will not detect an empty solvent reservoir until the display hits 89, in order not to return to state S5 before the lines/solvent sensor are filled with solvent after a refill.
10. Horowitz, P.; Hill, W. The Art of Electronics; Cambridge University: Cambridge, 1990, page 52.
11. Such a modification also opens the possibility of continuously checking the integrity of the solvent supply lines while the system is pressurized.

6. General discussion and conclusions

In this thesis a high-yield synthetic route was developed into *tetrakis*[2-hydroxyphenyl]ethene, the key step of which consists of an acid-catalyzed coupling of two bis(2-methoxyphenyl)diazomethane molecules (section 2.2. page 69). This calix[4]arene analog is based on an ethene bond as an organizing element for four phenol units. Due to the topology change, compared to a calix[4]arene, four positions *ortho* to the OH groups have become available for further modifications near to the polar pocket. Such a modification is necessary in order to prevent intermolecular aggregation of metal complexes coordinating to the oxo-surface.[1]

The so-obtained compound is air-stable, with limited solubility in aliphatic and aromatic solvents but good solubility in polar solvents like acetone and THF. These solutions are characterized by a deep blue fluorescence on excitation (254 nm, TLC UV lamp).

Although assumed on the basis of the geometrical arrangement of four phenol groups, the actual similarity between calix[4]arenes and the *tetrakis*[2-hydroxyphenyl]ethene turned out to be limited. Whereas in a calix[4]arene the circular hydrogen-bond array is partly maintained[2] in solution (as evidenced by the downfield shift of the OH hydrogens in ^{1}H-NMR spectroscopy), such an effect is not observed for the *tetrakis*[2-hydroxyphenyl]ethene (section 2.3.2, page 81). It was hoped that lowering the temperature would result in the formation of a single isomer displaying the sought-for circular hydrogen-bond array thereby indicating that an actual oxo-surface had formed. Instead the *para* substituted *tetrakis*[5-(1,1-dimethylethyl)-2-hydroxyphenyl] ethene shows multiple *tert*-butyl peaks at low temperatures (section 2.3.2, page 81) indicating that several isomers are present at -95 °C. For the sterically more hindered *tetrakis*[2-methoxyphenyl]ethene the number of methoxy signals at low temperatures corresponds to the presence of all possible stereoisomers,[3] indicating that, based on steric interactions, no overruling preference for one isomer is present. The observed variation of the methoxy-signal intensities, as well as the signal assignment, awaits further investigation. The results of the variable temperature ^{1}H-NMR spectroscopy studies shows that at room temperature the aryl rings of these compounds have a high rotational mobility. Hence no *permanent* oxo-surface is available using the synthesized *tetrakis*[2-hydroxyaryl]ethene compounds at room temperature.

The presence or absence of rotation will remain of importance especially with regard to the question if an oxo-surface[4] can be created by hindering the internal rotation and if the individual stereoisomers (some of which should exist as enantiomeric pairs) can be isolated. Such an isolation would not only be the first of it's kind, but also might allow a closer look at the proposed interconversions of the stereoisomers by correlated rotation and the related concept of "non-interdigitation of modes."[5]

According to the data presented in this thesis, further modification of the obtained *tetrakis*[2-methoxyphenyl]ethenes seems possible using conventional aromatic electrophilic substitution reactions (section 2.2, page 71). The ease and high yield with which deprotection can be achieved using BBr_3 as well as the high yield of the bromination of the aromatic rings indicate that a feared side reaction, the formation of a Lewis-acid-induced cation radical (eq. 6.1, page 311), does not readily take place.[6] Although not addressed in this thesis both the electrochemistry as well as the fluorescence of all new (organometallic) compounds await further investigation.

Because four *ortho* positions next to the OH groups have become available, further modification of the steric shielding of the polar pocket can be envisioned.

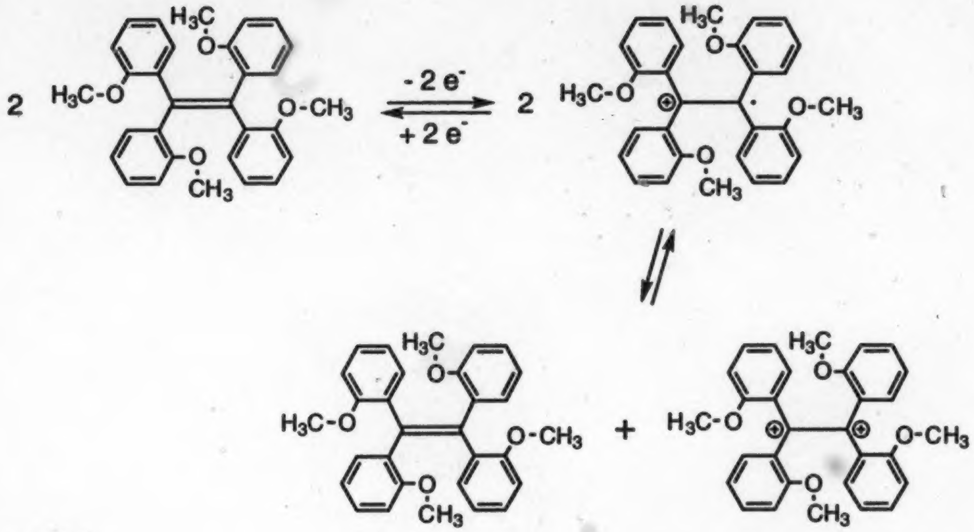

eq. 6.1

There are however certain limitations to the present steric shielding concept to prevent intermolecular aggregation of organometallic species. Introduction of bulky groups *ortho* to the proposed polar pocket can result in unintended effects, one of which is related to the mobility of the aryl rings. It is this mobility that can turn the aryl rings away from each other due to steric interactions of organometallic groups (the large circles in eq. 6.2) buttressed by large R groups, thereby destroying the "oxo-surface" (eq. 6.2).

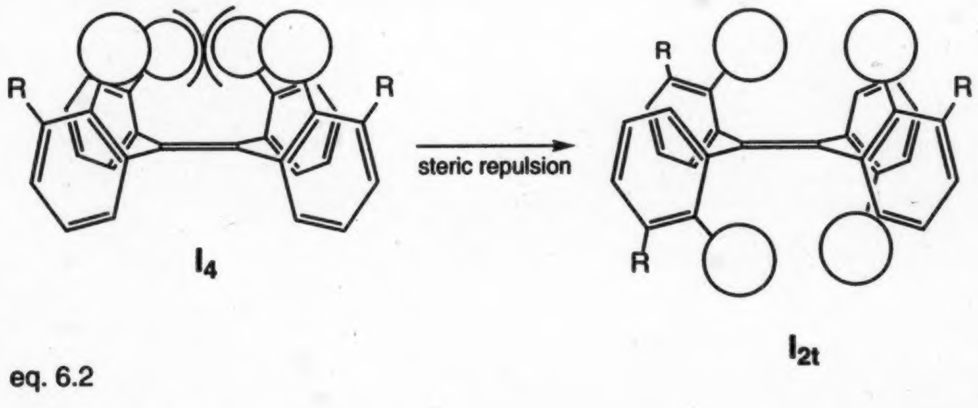

eq. 6.2

This problem could potentially be circumvented by modifying the ligand so as to lock the rings in place.

The other problem is related to the amount of steric shielding that would be necessary to prevent aggregation. If the absence or presence of disproportionation of $Cl_3Ti(OAr)$ complexes is to be used as a model for predicting the amount of steric shielding required,[7] at least a *tert*-butyl group has to be placed *ortho* to the hydroxy groups of the *tetrakis*[2-hydroxyphenyl]ethene. This would, however, increase the inward steric pressure on metals coordinated to the oxygen groups possibly resulting in an *intra*molecular disproportionation. In order to prevent this from happening, a different steric-shielding concept is required for constructing an oxo-surface that prevents intermolecular aggregation while allowing intramolecular aggregation of metals coordinated to the oxygen groups of the ligand.

The original oxo-surface of Floriani[4] was necessarily limited to an O_4 core due to the use of a calix[4]arene, with the present ligand this no longer applies and could, by modification of the ligand, lead to oxo-surfaces beyond the O_4 core creating a new and challenging field.[8] Furthermore, there is no reason why *tetrakis*[2-heteroaryl]ethenes could not be synthesized and used as ligands. In short, the use of the ethene bond as an organizing element in (in)organic supramolecular chemistry cannot be predicted and is only restricted by the creativity of the chemist.

Given that the phenoxy groups of the *tetrakis*[2-hydroxyaryl]ethene compounds show high rotational mobility at room temperature, the reaction of *tetrakis*[2-hydroxyphenyl]ethene with triethylaluminum was expected to give a mixture of products. Instead, an unprecedented "anti-crown" is obtained in non-Lewis basic solvents (section 3.3.1, page 135).[9] Apparently, after reacting with the trialkylaluminum, the individual aryl rings can rotate into a position that allows interaction with the lone pair electrons of the neighboring aryloxy group (a in equation 6.3, page 314). Another explanation, following the Barron proposal[10] for OH activation by trialkylaluminum, could be that after the formation of the first aryloxyaluminum group, the neighboring hydroxy groups continue to rotate, but only hydroxy groups next to the aryloxyaluminum group are activated for further reaction with trialkylaluminum (b in equation 6.3, page 314). This would automatically force the formation of an "all up" isomer, and would lead to the observed "anti-crown" (1 in equation 6.3, page 314).

According to ^{1}H-NMR spectroscopy studies, the so-obtained crown compound is rigid in non-Lewis basic solvents (section 3.3.5, page 155). The anion-complexing ability of the crown compound was not investigated, but interesting dynamic behavior is to be expected. According to a THF titration and a crotonaldehyde complexation study (section 3.2, page 127) the crown compound has a low Lewis acidity, characteristic of dialkylaluminum phenoxides.[11] The low Lewis acidity presumably compromises the use of this compound as an anion abstracting agent. No polymerization activity was observed for mixtures of the crown compound, a zirconocene precatalyst and trialkylaluminum. Strangely enough, the obtained compound did disproportionate when dissolved in THF or acetonitrile, although the THF titration indicated the absence of an interaction between THF and the crown compound. The disproportionation product is an "aluminum-sandwich" between two tetraarylethene ligands. A similar structure is formed by calix[4]arenes, but no isolation of a calix[4]arene crown has been reported, confirming the presence of both a relation between the chemistry of the calix[4]arene mimic (the *tetrakis*[2-hydroxyaryl]ethenes) and calix[4]arene chemistry as well as indicating the differences between the two ligand systems (section 3.3.6, page 166).

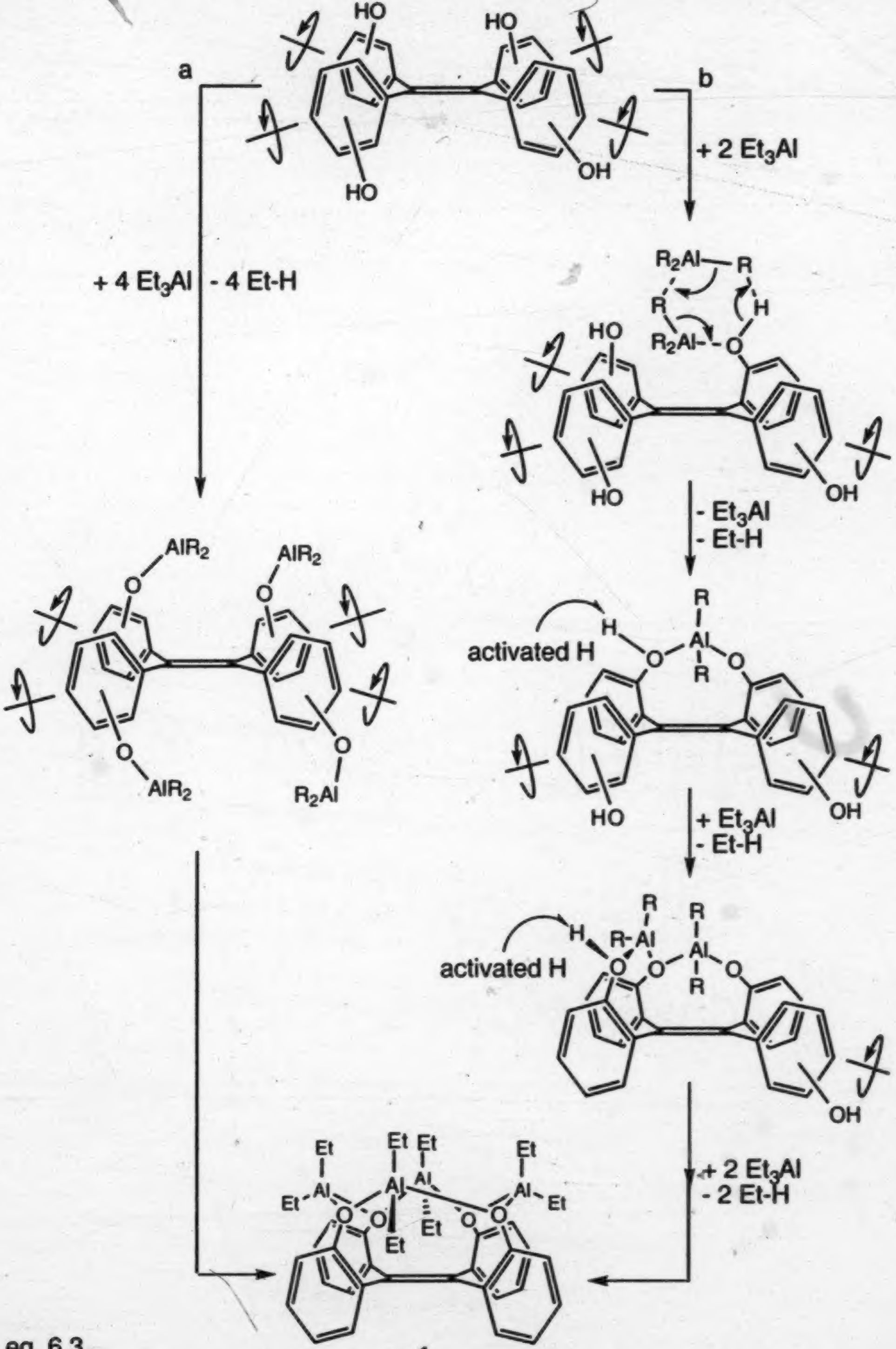
a
b
HO
HO
HO
OH
+ 2 Et3Al
+ 4 Et3Al
- 4 Et-H
R2Al
R
R
H
R2Al
O
AlR2
AlR2
O
O
O
AlR2
R2Al
- Et3Al
- Et-H
activated H
H
R
Al
R
+ Et3Al
- Et-H
activated H
+ 2 Et3Al
- 2 Et-H
Et
Al
Et

eq. 6.3

1

In order to propose a mechanism for the observed disproportionation, a large number of possible isomer interconversions must be taken into consideration due to the presence of a rectangular oxo-surface and the related modification of reaction stereochemistry. Development of a permutational approach[12] may be necessary in the future, especially when the oxo-surface concept[4] is extended beyond the O_4 core. Low temperature ^{1}H-NMR spectroscopy (section 3.2, page 127) indicated that an intermediate is formed in the disproportionation reaction in which the positions of the ethyl groups in the starting material have averaged out to a single triplet and quartet. An intermediate in which the four aluminum groups can freely rotate due to coordination with THF is proposed to account for this behavior. As a result of the acquired mobility, the necessary flexibility is obtained for achieving a transition-state geometry that allows intramolecular disproportionation. If the relative position of the oxygen groups is maintained – that is if the oxo-surface remains intact – during the disproportionation, several intermediates can be proposed to be formed, but only one of these can lead to the observed product. In order to account for the yield of product, interconversions between possible intermediate products are proposed to take place. The final step is proposed to be a dimerisation of two enantiomers to give a centrosymmetric structure (section 3.3.6, page 166). The proposed reaction is unfortunately compromised by the unproven assumption of an oxo-surface. If instead, free aryl-ring rotation is assumed, a multitude of isomer-interconversion paths become possible probably requiring a mathematical approach to find a path leading to the observed product.

The ease with which an aluminum crown compound is formed contrasts strongly with the experienced difficulty in obtaining characterizable compounds using group 4 transition metals. The only compounds isolated, in unknown yield, a "titanium sandwich" (section 4.3.1, page 216) and a "magnesium sandwich" (section 4.3.2, page 209) again show similarities with calix[4]arene chemistry. Presumably the "sandwich" structure has the highest solubility of all possible product structures, thereby allowing isolation of these products. Interestingly, all "sandwich" structures described in this thesis show both a twisting of the ethene bond as well as severe twisting of a single aryl ring, while the other aryl rings seem to maintain a position perpendicular on the ethene bond within the teraarylethene frame. These observations seem to fit the proposed isomer interconversion with the lowest energy barrier (Section 2.3.2, page 81). A detailled study of the crystal structures could yield interesting results when more "twisted" aryl rings are found in organometallic compounds using tetraarylethene ligands.[23]

Although several reasons are possible to explain the inability to obtain other crown-like compounds, most likely the difficulties are related to the solubility of the obtained transition metal compounds, the strength of the internal dative bond and the disproportionation stability.

An additional element of variation is introduced by using Grignard reagents that by their very nature are heterogeneous. Although not investigated, the synthesis of aryloxymagnesium chlorides by making use of dialkylmagnesium followed by a conversion to the aryloxy magnesium chloride might be more fruitful. In that case only the stability of the so obtained compound toward disproportionation remains to be investigated. No literature on this topic has been published.

The, for practical purposes heterogeneous, Ziegler-Natta precatalysts as used in this thesis are prepared by adding $TiCl_4$ to the magnesium chloride salts in toluene. This leads to the in situ formation[13] of "activated" $MgCl_2$, which in turn is proposed to form the isolated precipitate in the described centrifuge experiments (section 4.4, page 223). Stepwise assembly of an active site model (see section 1.6, page 41) was not pursued due to problems obtaining well-characterized starting materials for such an approach. For results of such an approach using a sterically more hindered *ortho* propyl *tetrakis*[2-hydroxyphenyl]ethene, see the thesis of dr. M. Fujita.

Although not widely known, $MgCl_2$ not only activates $TiCl_4$ but also $Cl_nTi(OR)_{4-n}$ compounds.[14] In order to explain the measured time-curve behavior, the formation of $MgCl_2$ clusters is proposed.[15] The so formed clusters can trap both toluene-soluble, as well as toluene-insoluble $Cl_nTi(OR)_{4-n}$ compounds (R = phenoxy based ligand), both of which are activated[16] by $MgCl_2$. As a result of time dependent leaching, the toluene-soluble part is transferred from the insoluble $MgCl_2$ cluster to the homogeneous phase suffering deactivation in the process. Without further information on the ligand distribution and Ti, Mg and Cl content of both phases, no conclusions on the validity of the proposed mechanism can be drawn.

The simplest way of testing this hypothesis would be to form the titanium derivatives of *tetrakis*[2-hydroxyaryl]ethene, and to add the so-obtained material to a THF solution of $MgCl_2$. After removal of THF (and possibly ball milling the material to regain highly dispersed material) similar activity and PE polydispersity would be predicted according to the proposed hypothesis. Furthermore, the precipitate needs to be analyzed for Mg, Ti and Cl because there are at this point only literature reports, but no experimental data to support the working hypothesis. Even with positive results from such an experiment, a lot of essential details remain unclear. For instance, what are the adsorption rates for $TiCl_n(OR)_{4-n}$ species on $MgCl_2$ as a function of n ? Can catalyst activity and PE polydispersity be related to n ?

Based on literature reports[17] and the actual measured polydispersity of the produced PE (which for supported Ziegler-Natta catalysts is surprisingly small), the involvement of oxygen near to the active center is proposed. Given that a range of structurally diverse alkoxy and aryloxy ligands give similar polydispersities (section 4.2, page 197 and reference 17), the actual structure of the ligand which contains the oxygen group seems to have little influence on the measured PE polydispersity. It should also be noted that no information is available on the relation between the precatalyst structure and the structure of the generated catalyst(s): the stability of the formed aryloxy/titanium bond in the presence of trialkyl aluminum cocatalysts needs to be investigated.[18]

Because of the narrowing of the polydispersity due to the general oxygen effect, proving the concept of building an active site becomes more difficult. The observed polydispersity should be in the 2-2.5 range or lower, preferably, before an influence of the ligand structure beyond the mere presence of oxygen atoms can be claimed. Such polydispersities (and lower) have actually been found for highly shielded titaniumphenoxide compounds that, however, show negligible polymerization activity.[19]

Investigations into the actual nature of the active site formed is possibly further complicated by the dualistic catalytic character of $Ti(OR)_4$ (R = aryl, alkyl)[20] if literature reports can be extrapolated to the tetraarylethene ligand system. Both a supported, highly active polymerization catalyst(s)[14] as well as a soluble oligomerization catalyst(s) (with negligible polymerization activity)[20] could be present when a trialkylaluminum reagent is used as a cocatalyst. Experiments determining the presence of sidechain branching or the formation of oligomers might confirm a relation between the experiments described in the literature and in that way support the proposed hypothesis.[13] The measurement of the oligomer formation using GCMS is probably more likely to give answers, given that for the sidechain branching determination the M_w has to be brought down in order to be able to dissolve a PE sample for ^{1}H-NMR spectroscopy or TREF analysis. The usual approach using hydrogen might quench any oligomerization catalytic activity present,[21] if literature reports on $Ti(OR)_4$ (R = alkyl, aryl) are equally valid for the created system. The observed oligomer formation by the magnesium chloride salt of 2,2'-thiobis[4,6-bis(1,1-dimethylethyl)]phenol cannot be considered as evidence for the correctness of the proposed hypothesis: it is known that sulphur containing compounds[22] can induce the formation of oligomers with supported catalysts. Furthermore, the oligomers obtained are alkanes instead of the expected alkenes,[20,22] possibly implying the presence of three different catalysts: a polymerization, oligomerization and hydrogenation catalyst. Further investigations are necessary to determine in which phase what activity is taking place.

It should, however, be emphasized that the experiments as described in this thesis need further investigations as well as duplication in order to confirm both the data obtained as well as the proposed hypothesis. With regard to the measured activities, the analysis of the Mg, Ti, Cl and ligand content of both precipitate as well as supernatant in the centrifuge experiments should yield further information on the true activities of the formed catalysts, which at this moment is unknown because the amount of Ti in both the heterogeneous and in the homogeneous phases are unknown.

In the Chapter 5 of this thesis, some of the technical problems encountered in this research were addressed: the design and fabrication of an automated solvent purification system, as well as a micro-well reactor is described. The solvent purification unit has been in use for several months, proving useful in polymerization experiments. During use some minor problems were solved. Although not all possibilities incorporated in the system have been tested, further development by adding a liquid spill sensor is possible. The microwell reactor, which forms a potential solution to the contamination problems encountered in small scale polymerization runs, was designed, built, and used. According to the results obtained major design modifications are necessary in order to make a usable system. Both the stirring of the reactor contents and the temperature measurement of the reactor solvent showed major shortcomings. These shortcomings will have to be addressed in future modifications.

6.1 Notes and References.

1. Such aggregation behavior is observed with sterically unhindered calix[4]arenes, see : Gardiner, M.G.; Lawrence, S.M.; Raston, C.L.; Skelton, B.W.; White, A.H. *J. Chem. Soc., Chem. Commun.* **1996**, 2491-2492. Radius, U.; Attner, J. *Eur. J. Inorg. Chem.* **1998**, 299-303. McBurnett, B.G.; Cowley, A.H. *J. Chem. Soc., Chem. Commun.* **1999**, 17-18.
2. Cairns, T.; Eglinton, G. *Nature* **1962**, *196*, 535-537. Araki, K.; Iwamoto, K.; Shinkai, S.; Matsuda, T. *Bull. Chem. Soc. Jpn.* **1990**, *63*, 3480-3485. Böhmer, V.; Goldmann, H.; Vogt, W.; Paulus, E.F.; Tobiason, F.L.; Thielman, M.J. *J. Chem. Soc., Perkin Trans. 2*, **1990**, 1769-1775. Grootenhuis, P.D.J.; Kollman, P.A.; Groenen, L.C.; Reinhoudt, D.N.; van Hummel, G.J.; Ugozzoli, F.; Andreetti, G.D. *J. Am. Chem. Soc.* **1990**, *112*, 4165-4176. Rudkevich, D.M. *Chem. Eur. J.* **2000**, *6*, 2679-2686.
3. Willem, R.; Pepermans, H.; Hallenga, K.; Gielen, M.; Dams, R.; Geise, H.J. *J. Org. Chem.* **1983**, *48*, 1890-1898.
4. Floriani, C. *Chem. Eur. J.* **1999**, *5*, 19-23. Caselli, A.; Solari, E.; Scopelliti, R.; Floriani, C. *J. Am. Chem. Soc.* **2000**, *122*, 538-539. Esposito, V.; Solari, E.; Floriani, C.; Re, N.; Rizzoli, C.; Chiesi-Villa, A. *Inorg. Chem.* **2000**, *39*, 2604-2613.
5. It should be stressed that the four aryl rings in tetraarylethenes *do not* "rotate" freely: the rotations are *correlated.* A CPK model of tetraphenylethene does not allow rotation of any of the phenyl rings. For stereochemical consequences of correlated rotation in tetraarylethenes see: Mislow, K. *Acc. Chem. Res.* **1976**, *9*, 26-33. Willem, R.; Pepermans, Hoogzand, C.; Hallenga, K.; Gielen, M. *J. Am. Chem. Soc.* **1981**, *103*, 2297-2306. For permutational analysis see: Klemperer, W.G. *J. Am.*

Chem. Soc. **1972**, *94*, 6940-6944. Gielen, M.; Vanlautem, N. *Bull. Soc. Chim. Belges* **1970**, *79*, 679-688. Klein, D.J.; Cowley, A.H. *J. Am. Chem. Soc.* **1975**, *97*, 1633-1640. Willem, R. *J. Chem. Soc., Dalton Trans.* **1979**, 33-40. For the non interdigitation of modes concept see: Finocchiaro, P.; Gust, D.; Hounshell, W.D.; Hummel, J.P.; Maravigna, P.; Mislow, K. *J. Am. Chem. Soc.* **1976**, *98*, 4945-4952. Finnocchiaro, P.; Hounshell, W.D.; Mislow, K. *J. Am. Chem. Soc.* **1976**, *98*, 4952-4963. For a review of topological stereochemistry see Walba, D.M. *Tetrahedron* **1985**, *41*, 3161-3211. None of these topics have been treated in this thesis but are important for understanding the complexity surrounding the use of tetraarylethenes.

6. Buck, H.M.; Bloemhoff, W.; Oosterhoff, L.J. *Tet. Lett.* **1960**, *9*, 5-11. Lewis, I.C.; Singer, L.S. *J. Chem. Phys.* **1963**, *43*, 2712-2727. Valenzuela, J.A.; Bard, A.J. *J. Chem. Phys.* **1968**, *72*, 286-290. Svanholm, U.; Jensen, B.S.; Parker, V.D. *J. Chem. Soc., Perkin 2* **1974**, 907-911. Bock, H.; Näther, C.; Havlas, Z. *J. Chem. Soc., Chem. Commun.* **1995**, 1111-1112.
7. Nielson, A.J.; Schwerdtfeger, P.; Waters, J.M. *J. Chem. Soc., Dalton Trans.* **2000**, 529-537. In this publication the obtained $Cl_3Ti(OAr)$ compounds are monomeric in benzene according to molecular weight determinations, but display disproportionation in $CHCl_3$ and CH_2Cl_2. Although this is the only publication that reports in detail on disproportionations of Ti compounds, the role of the solvent in these disproportionations is not investigated or discussed.
8. As the extent of the oxo-surface increases by inclusion of additional aryloxy moieties, so would the complexity of the created organometallic complexes using such a surface. Ultimately the information content would grow to such an extent as to be useless. The value of the concept

remains in the possibility of breaking down the complexity by isolating smaller subunits.

9. Crown ethers are Lewis basic, therefore Lewis acidic "crown-like" compounds have been called "anti-crown" because of the opposite complexation behavior.

10. McMahon, C.N.; Bott, S.G.; Barron, A.R. *J. Chem. Soc., Dalton Trans.* **1997**, 3129-3137.

11. Siedle, A.R.; Newmark, R.A.; Lamanna, W.M.; Schroepfer, J.N. *Polyhedron* **1990**, *9*, 301-308.

12. Brocas, J.; Gielen, M.; Willem, R. The Permutational Approach to Dynamic Stereochemistry; McGraw-Hill: New York, 1983.

13. Lee, D.; Jeong, Y.; Soga, K.; Shiono, T. *J. Appl. Polym. Sci.* **1993**, *47*, 1449-1461. Gupta, V.K.; Satish, S.; Bhardwaj, I.S. *J. Macromol. Sci., Pure Appl. Chem.* **1994**, *A31*, 451-463.

14. Gavens, P.D.; Bottrill, M.; Kelland, J.W.; McMeeking, J. in Comprehensive Organometallic Chemistry, G. Wilkinson, F.G.A. Stone, E.W. Abel. Eds.; Pergamon Press: New York, 1982; Chapter 22.5, page 532 and Table 13 on page 533.

15. In absence of a coordinating solvent (the reaction is done in toluene), the Mg salts will aggregate and precipitate. Although the used Mg salts contain THF, the Lewis basicity is probably not strong enough to prevent aggregation. Furthermore the fate of the THF in the presence of $TiCl_4$ is unclear. See: Zechmann, C.A.; Boyle, T.J.; Rodriguez, M.A.; Kemp, R.A. *Polyhedron* **2000**, *19*, 2557-2564.

16. Zucchini, U.; Cuffiani, I.; Pennini, G. *Makromol. Chem., Rapid Commun.* **1984**, *5*, 567-571.

17. Yano, T.; Ikai, S.; Shimizu, M.; Washio, K. *J. Polym. Sci., Polym. Chem. Ed.* **1985**, *23*, 1455-1467. Zucchini, U.; Dall'Occo, T. in Polymer Science, Contemporary Themes; Ed. Sivaram, S.; McGraw-Hill, New Delhi, 1991, Volume 1, 221-228.

18. There are indications in the literature of the possibility that the phenoxy ligand doesn't remain on the titanium in the presence of trialkylaluminum cocatalysts. See: Firth, A.V.; Stewart, J.C.; Hoskin, A.J.; Stephan, D.W. *J. Organomet. Chem.* **1999**, *591*, 185-193.

19. Thorn, M.G.; Etheridge, Z.C.; Fanwick, P.E.; Rothwell, I.P. *Organometallics* **1998**, *17*, 3636-3638. Thorn, M.G.; Etheridge, Z.C.; Fanwick, P.E.; Rothwell, I.P. *J. Organomet. Chem.* **1999**, *591*, 148-162. For a recent high activity Ti based living catalyst see: Saito, J.; Mitani, M.; Mohri, J.; Yoshida, Y.; Matsui, S.; Ishii, S.; Kojoh, S.; Kashiwa, N.; Fujita, T. *Angew. Chem. Int. Ed. Engl.* **2001**, *40*, 2918-2920

20. Beach, D.L.; Kissin, Y.V. *J. Polym. Sci., Polym. Chem. Ed.* **1984**, *22*, 3027-3042. Kissin, Y.V.; Beach, D.L. *J. Polym. Sci., Polym. Chem.* **1986**, *24*, 1069-1084. Tembe, G.L.; Ravindranthan, M. *React. Kinet. Catal. Lett.* **1994**, *52*, 119-127.

21. As an alternative IR could be used to determine sidechain branching in PE, see: Blitz, J.P.; McFaddin, D.C. *J. Appl. Polym. Sci.* **1994**, *51*, 13-20. For ^{13}C-NMR see: Jurkiewicz, A.; Eilerts, N.W.; Hsieh, E.T. *Macromolecules* **1999**, *32*, 5471-5476.

22. Henrici-Olivé, G.; Olivé, S. *Adv. Polym. Sci.* **1974**, *15*, 1. Skupinska, J. *Chem. Rev.* **1991**, *91*, 613-648.

23. Britton, D.; Dunitz, J.D. *J. Am. Chem. Soc.* **1981**, *103*, 2971-2979. In this paper pathways for substitution at Sn(IV) are derived using crystal structures and the structure correlation method.

Appendix A: Chapter 2, Section 2.3.1, page 73

Crystallographic details for compound 10, SDL Code: JMS9801.

Compound 10: *Tetrakis*(2-hydroxyphenyl)ethene dichloromethane solvate

Formula: $C_{27}H_{22}Cl_2O_4$ ($C_{26}H_{20}O_4 \cdot CH_2Cl_2$)

Crystallographic Experimental Details

A. Crystal Data

formula	$C_{27}H_{22}Cl_2O_4$
formula weight	481.35
crystal dimensions (mm)	0.46 × 0.19 × 0.19
crystal system	triclinic
space group	$P\bar{1}$ (No. 2)
unit cell parameters[a]	
a (Å)	8.2310 (12)
b (Å)	9.6048 (12)
c (Å)	17.243 (2)
α (deg)	75.610 (10)
β (deg)	78.168 (10)
γ (deg)	64.983 (10)
V (Å^3)	1188.7 (3)
Z	2
ρ_{calcd} (g cm^{-3})	1.345
μ (mm^{-1})	2.715

B. Data Collection and Refinement Conditions

diffractometer	Siemens P4/RA[b]
radiation (λ [Å])	graphite-monochromated Cu Kα (1.54178)
temperature (°C)	–60
scan type	θ–2θ
data collection 2θ limit (deg)	115.0
total data collected	3469 ($0 \le h \le 8$, $-9 \le k \le 10$, $-18 \le l \le 18$)

Crystallographic Experimental Details (continued)

independent reflections	3200
number of observations (*NO*)	2116 ($F_o^2 \ge 2\sigma(F_o^2)$)
structure solution method	direct methods (*SHELXS–86*[c])
refinement method	full-matrix least-squares on F^2 (*SHELXL–93*[d])
absorption correction method	Gaussian integration (face-indexed)
range of transmission factors	0.6613–0.5072
data/restraints/parameters	3198 [$F_o^2 \ge -3\sigma(F_o^2)$] / 0 / 302
goodness-of-fit (*S*)[e]	1.046 [$F_o^2 \ge -3\sigma(F_o^2)$]
final *R* indices[f]	
$F_o^2 > 2\sigma(F_o^2)$	**R_1 = 0.0831**, wR_2 = 0.2100
all data	R_1 = 0.1162, **wR_2 = 0.2511**
largest difference peak and hole	0.505 and –0.355 e Å^{-3}

[a] Obtained from least-squares refinement of 38 reflections with $53.0° < 2\theta < 57.7°$.

[b] Programs for diffractometer operation, data collection, data reduction and absorption correction were those supplied by Siemens.

[c] Sheldrick, G. M. *Acta Crystallogr.* **1990**, *A46*, 467–473.

[c] Beurskens, P. T.; Beurskens, G.; Bosman, W.P.; de Gelder, R.; Garcia Granda, S.; Gould, R. O.; Israel, R; Smits, J M.M. (1996). The *DIRDIF-96* program system. Crystallography Laboratory, University of Nijmegen, The Netherlands.

[d] Sheldrick, G. M. *SHELXL-93*. Program for crystal structure determination. University of Göttingen, Germany, 1993. Refinement on F_o^2 for all reflections except for 2 having $F_o^2 < -3\sigma(F_o^2)$. Weighted *R*-factors wR_2 and all goodnesses of fit *S* are based on F_o^2; conventional *R*-factors R_1 are based on F_o, with F_o set to zero for negative F_o^2. The observed criterion of $F_o^2 > 2\sigma(F_o^2)$ is used only for calculating R_1, and is not relevant to the choice of reflections for refinement. *R*-factors based on F_o^2 are statistically about twice as large as those based on F_o, and *R*-factors based on ALL data will be even larger.

[e] $S = [\Sigma w(F_o^2 - F_c^2)^2/(n - p)]^{1/2}$ (n = number of data; p = number of parameters varied; $w = [\sigma^2(F_o^2) + (0.1268P)^2 + 1.1841P]^{-1}$ where $P = [\mathrm{Max}(F_o^2, 0) + 2F_c^2]/3$).

[f] $R_1 = \Sigma||F_o| - |F_c||/\Sigma|F_o|$; $wR_2 = [\Sigma w(F_o^2 - F_c^2)^2/\Sigma w(F_o^4)]^{1/2}$.

Selected Interatomic Distances (Å)

(a) bond distances

Molecule A			*Molecule B*		
Atom1	Atom2	Distance	Atom1	Atom2	Distance
O1	C12	1.372(6)	O3	C32	1.391(6)
O2	C22	1.367(6)	O4	C42	1.380(6)
C1	C1'	1.347(9)	C2	C2"	1.328(9)
C1	C11	1.495(6)	C2	C31	1.509(6)
C1	C21	1.502(6)	C2	C41	1.491(6)
C11	C12	1.376(7)	C31	C32	1.370(7)
C11	C16	1.398(7)	C31	C36	1.403(7)
C12	C13	1.393(7)	C32	C33	1.398(7)
C13	C14	1.374(8)	C33	C34	1.378(8)
C14	C15	1.375(8)	C34	C35	1.369(8)
C15	C16	1.385(7)	C35	C36	1.379(7)
C21	C22	1.392(7)	C41	C42	1.386(7)
C21	C26	1.379(7)	C41	C46	1.391(7)
C22	C23	1.389(7)	C42	C43	1.386(7)
C23	C24	1.369(8)	C43	C44	1.383(8)
C24	C25	1.374(8)	C44	C45	1.380(8)
C25	C26	1.387(7)	C45	C46	1.380(7)

Primed atoms are related to unprimed ones via the crystallographic inversion center at (0, 0, $^1/2$).
Double-primed atoms are related to unprimed ones via the inversion center at (0, $^1/2$, 0).

(b) nonbonded distances

Molecule A			*Molecule B*		
Atom1	Atom2	Distance	Atom1	Atom2	Distance
O1	H2O	1.95	O3	H4O	2.01
O2	H1O†	1.96	O4	H3O‡	1.93

†At $1-x, \bar{y}, 1-z$.

‡At $1-x, 1-y, \bar{z}$.

(c) bond distances within the solvent dichloromethane molecule

Atom1	Atom2	Distance	Atom1	Atom2	Distance
Cl1	C99	1.737(8)	Cl2	C99	1.709(8)

Selected Interatomic Angles (deg)

(a) Molecule A				*(b) Molecule B*			
Atom1	Atom2	Atom3	Angle	Atom1	Atom2	Atom3	Angle
C1'	C1	C11	121.9(5)	C2"	C2	C31	120.8(5)
C1'	C1	C21	120.7(5)	C2"	C2	C41	122.0(5)
C11	C1	C21	117.4(4)	C31	C2	C41	117.2(4)
C1	C11	C12	121.0(4)	C2	C31	C32	122.0(4)
C1	C11	C16	121.2(4)	C2	C31	C36	119.4(4)
C12	C11	C16	117.8(4)	C32	C31	C36	118.6(4)
O1	C12	C11	118.8(5)	O3	C32	C31	119.4(4)
O1	C12	C13	119.6(5)	O3	C32	C33	119.3(5)
C11	C12	C13	121.6(5)	C31	C32	C33	121.2(5)
C12	C13	C14	118.9(6)	C32	C33	C34	118.5(5)
C13	C14	C15	121.4(5)	C33	C34	C35	121.6(5)
C14	C15	C16	118.8(5)	C34	C35	C36	119.4(5)
C11	C16	C15	121.5(5)	C31	C36	C35	120.7(5)
C1	C21	C22	121.2(4)	C2	C41	C42	120.5(5)
C1	C21	C26	120.6(5)	C2	C41	C46	121.3(4)
C22	C21	C26	118.3(4)	C42	C41	C46	118.1(5)
O2	C22	C21	120.3(4)	O4	C42	C41	120.3(5)
O2	C22	C23	119.3(5)	O4	C42	C43	118.5(5)
C21	C22	C23	120.4(5)	C41	C42	C43	121.1(5)
C22	C23	C24	120.0(5)	C42	C43	C44	119.3(5)
C23	C24	C25	120.5(5)	C43	C44	C45	120.8(5)
C24	C25	C26	119.3(5)	C44	C45	C46	119.1(5)
C21	C26	C25	121.4(5)	C41	C46	C45	121.6(5)

Primed atoms are related to unprimed ones via the crystallographic inversion center at (0, 0, $^1/2$).

Double-primed atoms are related to unprimed ones via the inversion center at (0, $^1/2$, 0).

(c) within the solvent dichloromethane molecule

Atom1	Atom2	Atom3	Angle
Cl1	C99	Cl2	117.1(5)

Torsional Angles (deg)

(a) Molecule A					*(b) Molecule B*				
Atom1	Atom2	Atom3	Atom4	Angle	Atom1	Atom2	Atom3	Atom4	Angle
C11	C1	C1'	C21'	1.9(10)	C31	C2	C2"	C41"	-0.7(10)
C1'	C1	C11	C12	-91.8(7)	C2"	C2	C31	C32	84.2(7)
C1'	C1	C11	C16	90.3(7)	C2"	C2	C31	C36	-95.2(7)
C21	C1	C11	C12	90.0(6)	C41	C2	C31	C32	-96.5(6)
C21	C1	C11	C16	-87.8(5)	C41	C2	C31	C36	84.2(6)
C1'	C1	C21	C22	85.6(7)	C2"	C2	C41	C42	-90.6(7)
C1'	C1	C21	C26	-93.5(7)	C2"	C2	C41	C46	90.4(7)
C11	C1	C21	C22	-96.2(6)	C31	C2	C41	C42	90.1(6)
C11	C1	C21	C26	84.6(6)	C31	C2	C41	C46	-88.9(6)
C1	C11	C12	O1	2.3(7)	C2	C31	C32	O3	1.8(7)
C1	C11	C12	C13	179.8(5)	C2	C31	C32	C33	-176.4(5)
C16	C11	C12	O1	-179.8(4)	C36	C31	C32	O3	-178.8(4)
C16	C11	C12	C13	-2.2(7)	C36	C31	C32	C33	3.0(7)
C1	C11	C16	C15	178.5(4)	C2	C31	C36	C35	177.6(4)
C12	C11	C16	C15	0.6(7)	C32	C31	C36	C35	-1.7(7)
O1	C12	C13	C14	-179.8(5)	O3	C32	C33	C34	179.9(5)
C11	C12	C13	C14	2.6(9)	C31	C32	C33	C34	-1.9(8)
C12	C13	C14	C15	-1.3(9)	C32	C33	C34	C35	-0.5(9)
C13	C14	C15	C16	-0.3(9)	C33	C34	C35	C36	1.7(9)
C14	C15	C16	C11	0.7(8)	C34	C35	C36	C31	-0.6(8)
C1	C21	C22	O2	2.4(7)	C2	C41	C42	O4	0.2(7)
C1	C21	C22	C23	-176.8(5)	C2	C41	C42	C43	178.8(5)
C26	C21	C22	O2	-178.4(4)	C46	C41	C42	O4	179.2(4)
C26	C21	C22	C23	2.4(7)	C46	C41	C42	C43	-2.1(7)
C1	C21	C26	C25	178.6(5)	C2	C41	C46	C45	179.7(4)
C22	C21	C26	C25	-0.6(7)	C42	C41	C46	C45	0.7(7)
O2	C22	C23	C24	178.5(5)	O4	C42	C43	C44	-179.0(5)
C21	C22	C23	C24	-2.3(8)	C41	C42	C43	C44	2.3(8)

Torsional Angles (continued)

(a) Molecule A					*(b) Molecule B*				
Atom1	Atom2	Atom3	Atom4	Angle	Atom1	Atom2	Atom3	Atom4	Angle
C22	C23	C24	C25	0.3(9)	C42	C43	C44	C45	-1.1(9)
C23	C24	C25	C26	1.5(9)	C43	C44	C45	C46	-0.3(9)
C24	C25	C26	C21	-1.4(8)	C44	C45	C46	C41	0.5(8)

Primed atoms are related to unprimed ones via the crystallographic inversion center at (0, 0, $^1/2$).
Double-primed atoms are related to unprimed ones via the inversion center at (0, $^1/2$, 0).

Appendix B: Chapter 2, Section 2.3.1, page 73.

crystallographic details for compound 14, XCL Code: JMS0016.

Compound 14: *Tetrakis(*3-bromo-5-*t*-butyl-2-hydroxyphenyl)ethylene, *m*-xylene solvate

Formula: $C_{50}H_{58}Br_4O_4$ ($C_{42}H_{48}Br_4O_4 \cdot C_8H_{10}$)

Crystallographic Experimental Details

A. Crystal Data

formula	$C_{50}H_{58}Br_4O_4$
formula weight	1042.60
crystal dimensions (mm)	0.27 × 0.12 × 0.09
crystal system	triclinic
space group	*P*1 (No. 2)
unit cell parameters[a]	
a (Å)	8.7405 (6)
b (Å)	11.8117 (7)
c (Å)	13.4435 (9)
α (deg)	99.4880 (13)
β (deg)	105.7655 (12)
γ (deg)	107.9714 (11)
V (Å^3)	1222.75 (14)
Z	1
ρ_{calcd} (g cm^{-3})	1.416
μ (mm^{-1})	3.332

B. Data Collection and Refinement Conditions

diffractometer	Bruker P4/RA/SMART 1000 CCD[b]
radiation (λ [Å])	graphite-monochromated Mo Kα (0.71073)
temperature (°C)	–80
scan type	ϕ rotations (0.3°) / ω scans (0.3°) (30 s exposures)
data collection 2θ limit (deg)	52.76
total data collected	6520 ($-10 \le h \le 10$, $-14 \le k \le 14$, $-16 \le l \le 16$)
independent reflections	4960
number of observed reflections (*NO*)	3450 [$F_o^2 \ge 2\sigma(F_o^2)$]
structure solution method	direct methods (*SHELXS–86*[c])
refinement method	full-matrix least-squares on F^2 (*SHELXL–93*[d])

Crystallographic Experimental Details (continued)

absorption correction method	Gaussian integration (face-indexed)
range of transmission factors	0.7536–0.4665
data/restraints/parameters	4960 [$F_o^2 \geq -3\sigma(F_o^2)$] / 0 / 302
goodness-of-fit (S)[e]	0.999 [$F_o^2 \geq -3\sigma(F_o^2)$]
final R indices[f]	
R_1 [$F_o^2 \geq 2\sigma(F_o^2)$]	0.0426
wR_2 [$F_o^2 \geq -3\sigma(F_o^2)$]	0.1112
largest difference peak and hole	0.970 and –0.894 e Å^{-3}

[b] Programs for diffractometer operation, data collection, data reduction and absorption correction were those supplied by Bruker.

[c] Sheldrick, G. M. *Acta Crystallogr.* **1990**, *A46*, 467–473.

[d] Sheldrick, G. M. *SHELXL-93*. Program for crystal structure determination. University of Göttingen, Germany, 1993. Refinement on F_o^2 for all reflections (all of these having $F_o^2 \geq -3\sigma(F_o^2)$). Weighted R-factors wR_2 and all goodnesses of fit S are based on F_o^2; conventional R-factors R_1 are based on F_o, with F_o set to zero for negative F_o^2. The observed criterion of $F_o^2 > 2\sigma(F_o^2)$ is used only for calculating R_1, and is not relevant to the choice of reflections for refinement. R-factors based on F_o^2 are statistically about twice as large as those based on F_o, and R-factors based on ALL data will be even larger.

[e] $S = [\Sigma w(F_o^2 - F_c^2)^2/(n - p)]^{1/2}$ (n = number of data; p = number of parameters varied; $w = [\sigma^2(F_o^2) + (0.0605P)^2]^{-1}$ where $P = [\mathrm{Max}(F_o^2, 0) + 2F_c^2]/3$).

[f] $R_1 = \Sigma||F_o| - |F_c||/\Sigma|F_o|$; $wR_2 = [\Sigma w(F_o^2 - F_c^2)^2/\Sigma w(F_o^4)]^{1/2}$.

Selected Interatomic Distances (Å)

(a) within tetrakis(3-bromo-5-t-butyl-2-hydroxyphenyl)ethylene

Atom1	Atom2	Distance	Atom1	Atom2	Distance
Br1	C13	1.897(3)	C15	C17	1.539(4)
Br2	C23	1.902(3)	C17	C18	1.538(5)
O1	C12	1.369(4)	C17	C19	1.528(6)
O1	H1OA"	2.10†	C17	C20	1.537(5)
O1	H2O	2.00†	C21	C22	1.396(4)
O2	C22	1.370(4)	C21	C26	1.396(4)
C1	C1'	1.319(7)	C22	C23	1.390(5)
C1	C11	1.508(4)	C23	C24	1.381(5)
C1	C21	1.503(5)	C24	C25	1.393(5)
C11	C12	1.404(4)	C25	C26	1.398(5)
C11	C16	1.387(4)	C25	C27	1.540(5)
C12	C13	1.386(4)	C27	C28	1.533(6)
C13	C14	1.390(4)	C27	C29	1.533(6)
C14	C15	1.386(4)	C27	C30	1.522(6)
C15	C16	1.398(4)			

Primed atoms are related to unprimed ones via the crystallographic inversion center (0, 0, 0).
Double-primed atoms are related to unprimed ones via the inversion center (1/2, 0, 0).
†Nonbonded distance.

(b) within the solvent m-xylene molecule

Atom1	Atom2	Distance	Atom1	Atom2	Distance
C1S	C2S	1.375(18)	C3S	C4S	1.349(15)
C1S	C6S	1.39(2)	C3S	C8S	1.542(15)
C1S	C7S	1.514(14)	C4S	C5S	1.377(13)
C2S	C3S	1.379(19)	C5S	C6S	1.402(18)

Selected Interatomic Angles (deg)

(a) within tetrakis(3-bromo-5-t-butyl-2-hydroxyphenyl)ethylene

Atom1	Atom2	Atom3	Angle	Atom1	Atom2	Atom3	Angle
C1'	C1	C11	120.7(4)	C19	C17	C20	110.1(4)
C1'	C1	C21	122.0(3)	C1	C21	C22	120.1(3)
C11	C1	C21	117.3(3)	C1	C21	C26	120.9(3)
C1	C11	C12	120.2(3)	C22	C21	C26	119.0(3)
C1	C11	C16	120.4(3)	O2	C22	C21	121.0(3)
C12	C11	C16	119.4(3)	O2	C22	C23	120.7(3)
O1	C12	C11	119.7(2)	C21	C22	C23	118.3(3)
O1	C12	C13	122.4(3)	Br2	C23	C22	117.9(3)
C11	C12	C13	117.9(3)	Br2	C23	C24	119.7(3)
Br1	C13	C12	119.2(2)	C22	C23	C24	122.3(3)
Br1	C13	C14	118.8(2)	C23	C24	C25	120.4(3)
C12	C13	C14	121.9(3]	C24	C25	C26	117.3(3)
C13	C14	C15	121.0(3)	C24	C25	C27	122.4(3)
C14	C15	C16	116.9(3)	C26	C25	C27	120.3(3)
C14	C15	C17	123.4(3)	C21	C26	C25	122.7(3)
C16	C15	C17	119.7(3)	C25	C27	C28	109.0(3)
C11	C16	C15	122.9(3)	C25	C27	C29	109.4(3)
C15	C17	C18	109.4(3)	C25	C27	C30	112.4(3)
C15	C17	C19	108.4(3)	C28	C27	C29	109.4(4)
C15	C17	C20	111.5(3)	C28	C27	C30	107.3(3)
C18	C17	C19	109.3(3)	C29	C27	C30	109.3(4)
C18	C17	C20	108.1(3)				

Primed atoms are related to unprimed ones via the crystallographic inversion center (0, 0, 0).

Selected Interatomic Angles (continued)

(b) within the solvent m-xylene molecule

Atom1	Atom2	Atom3	Angle	Atom1	Atom2	Atom3	Angle
C2S	C1S	C6S	117.7(12)	C2S	C3S	C8S	118.0(12)
C2S	C1S	C7S	124.3(15)	C4S	C3S	C8S	120.5(12)
C6S	C1S	C7S	118.0(16)	C3S	C4S	C5S	120.4(11)
C1S	C2S	C3S	120.8(12)	C4S	C5S	C6S	118.5(10)
C2S	C3S	C4S	121.1(12)	C1S	C6S	C5S	121.3(12)

Torsional Angles (deg)

Atom1	Atom2	Atom3	Atom4	Angle	Atom1	Atom2	Atom3	Atom4	Angle
C11	C1	C1'	C21'	-0.4(6)	C1	C21	C22	C23	179.5(3)
C1'	C1	C11	C12	86.5(5)	C26	C21	C22	O2	-179.5(3)
C1'	C1	C11	C16	-94.3(5)	C26	C21	C22	C23	-0.9(5)
C21	C1	C11	C12	-93.9(4)	C1	C21	C26	C25	-179.3(3)
C21	C1	C11	C16	85.3(4)	C22	C21	C26	C25	1.0(5)
C1'	C1	C21	C22	-85.7(5)	O2	C22	C23	Br2	0.5(5)
C1'	C1	C21	C26	94.6(5)	O2	C22	C23	C24	179.2(3)
C11	C1	C21	C22	94.6(3)	C21	C22	C23	Br2	-178.1(2)
C11	C1	C21	C26	-85.0(4)	C21	C22	C23	C24	0.5(5)
C1	C11	C12	O1	-1.9(5)	Br2	C23	C24	C25	178.4(3)
C1	C11	C12	C13	179.1(3)	C22	C23	C24	C25	-0.2(6)
C16	C11	C12	O1	178.9(3)	C23	C24	C25	C26	0.3(5)
C16	C11	C12	C13	-0.1(5)	C23	C24	C25	C27	179.8(3)
C1	C11	C16	C15	179.3(3)	C24	C25	C26	C21	-0.7(5)
C12	C11	C16	C15	-1.5(5)	C27	C25	C26	C21	179.8(3)
O1	C12	C13	Br1	2.1(5)	C24	C25	C27	C28	124.6(4)
O1	C12	C13	C14	-177.7(3)	C24	C25	C27	C29	-115.9(4)
C11	C12	C13	Br1	-179.0(3)	C24	C25	C27	C30	5.7(5)
C11	C12	C13	C14	1.2(5)	C26	C25	C27	C28	-56.0(4)
Br1	C13	C14	C15	179.3(3)	C26	C25	C27	C29	63.6(5)
C12	C13	C14	C15	-0.9(6)	C26	C25	C27	C30	-174.8(3)

Torsional Angles (continued)

Atom1	Atom2	Atom3	Atom4	Angle	Atom1	Atom2	Atom3	Atom4	Angle
C13	C14	C15	C16	-0.7(5)	C6S	C1S	C2S	C3S	-6(2)
C13	C14	C15	C17	-179.5(3)	C7S	C1S	C2S	C3S	175.1(12)
C14	C15	C16	C11	1.9(5)	C2S	C1S	C6S	C5S	4(2)
C17	C15	C16	C11	-179.2(3)	C7S	C1S	C6S	C5S	-176.2(13)
C14	C15	C17	C18	-123.2(4)	C1S	C2S	C3S	C4S	5(2)
C14	C15	C17	C19	117.7(4)	C1S	C2S	C3S	C8S	178.3(11)
C14	C15	C17	C20	-3.6(5)	C2S	C3S	C4S	C5S	-2.7(17)
C16	C15	C17	C18	58.0(4)	C8S	C3S	C4S	C5S	-176.0(10)
C16	C15	C17	C19	-61.1(5)	C3S	C4S	C5S	C6S	1.5(16)
C16	C15	C17	C20	177.6(4)	C4S	C5S	C6S	C1S	-2(2)
C1	C21	C22	O2	0.8(5)					

Primed atoms are related to unprimed ones via the crystallographic inversion center (0, 0, 0).

Appendix C: Chapter 2, Section 2.2, page 64.

Crystallographic details for compound 2, SDL Code: JMS9713.

Compound 2: 1,1,2,2-tetra(3,5-di-*t*-butyl-2-methoxyphenyl)ethane

Formula: $C_{62}H_{94}O_4$

Crystallographic Experimental Details

A. Crystal Data	
formula	$C_{62}H_{94}O_4$
formula weight	903.37
crystal dimensions (mm)	0.39 × 0.23 × 0.21
crystal system	monoclinic
space group	$P2_1/c$ (No. 14)
unit cell parameters[a]	
a (Å)	26.095 (3)
b (Å)	10.3280 (13)
c (Å)	21.174 (2)
β (deg)	96.492 (9)
V (Å^3)	5670.0 (11)
Z	4
ρ_{calcd} (g cm^{-3})	1.058
μ (mm^{-1})	0.064
B. Data Collection and Refinement Conditions	
diffractometer	Siemens P4/RA[b]
radiation (λ [Å])	graphite-monochromated Mo Kα (0.71073)
temperature (°C)	–60
scan type	θ–2θ
data collection 2θ limit (deg)	50.0

Crystallographic Experimental Details (continued)

total data collected	10314 ($-31 \le h \le 30, 0 \le k \le 12, 0 \le l \le 25$)
independent reflections	9987
number of observations (*NO*)	2476 ($F_o^2 \ge 2\sigma(F_o^2)$)
structure solution method	direct methods (*SHELXS–86*[c])
refinement method	full-matrix least-squares on F^2 (*SHELXL–93*[d])
absorption correction method	*DIFABS*[e]
range of absorption correction factors	1.070–0.788
data/restraints/parameters	9986 [$F_o^2 \ge -3\sigma(F_o^2)$]/0/595
goodness-of-fit (S)[f]	1.014 [$F_o^2 \ge -3\sigma(F_o^2)$]
final R indices[g]	
$F_o^2 > 2\sigma(F_o^2)$	**R_1 = 0.1256**, wR_2 = 0.1969
all data	R_1 = 0.3765, **wR_2 = 0.3081**
largest difference peak and hole	0.298 and -0.268 e Å^{-3}

[a] Obtained from least-squares refinement of 48 reflections with $17.0° < 2\theta < 24.6°$.

[b] Programs for diffractometer operation and data collection were those of the XSCANS system supplied by Siemens.

[c] Sheldrick, G. M. *Acta Crystallogr.* **1990**, *A46*, 467–473.

[d] Sheldrick, G. M. *SHELXL-93*. Program for crystal structure determination. University of Göttingen, Germany, 1993. Refinement on F_o^2 for all reflections except for 1 having $F_o^2 < -3\sigma(F_o^2)$. Weighted R-factors wR_2 and all goodnesses of fit S are based on F_o^2; conventional R-factors R_1 are based on F_o, with F_o set to zero for negative F_o^2. The observed criterion of $F_o^2 > 2\sigma(F_o^2)$ is used only for calculating R_1, and is not relevant to the choice of reflections for refinement. R-factors based on F_o^2 are statistically about twice as large as those based on F_o, and R-factors based on ALL data will be even larger.

[e] Walker, N.; Stuart, D. *Acta Crystallogr.* **1983**, *A39*, 158–166.

[f] $S = [\Sigma w(F_o^2 - F_c^2)^2/(n-p)]^{1/2}$ (n = number of data; p = number of parameters varied; $w = [\sigma^2(F_o^2) + (0.0627P)^2 + 1.2974P]^{-1}$ where $P = [\mathrm{Max}(F_o^2, 0) + 2F_c^2]/3$).

[g] $R_1 = \Sigma||F_o| - |F_c||/\Sigma|F_o|$; $wR_2 = [\Sigma w(F_o^2 - F_c^2)^2/\Sigma w(F_o^4)]^{1/2}$.

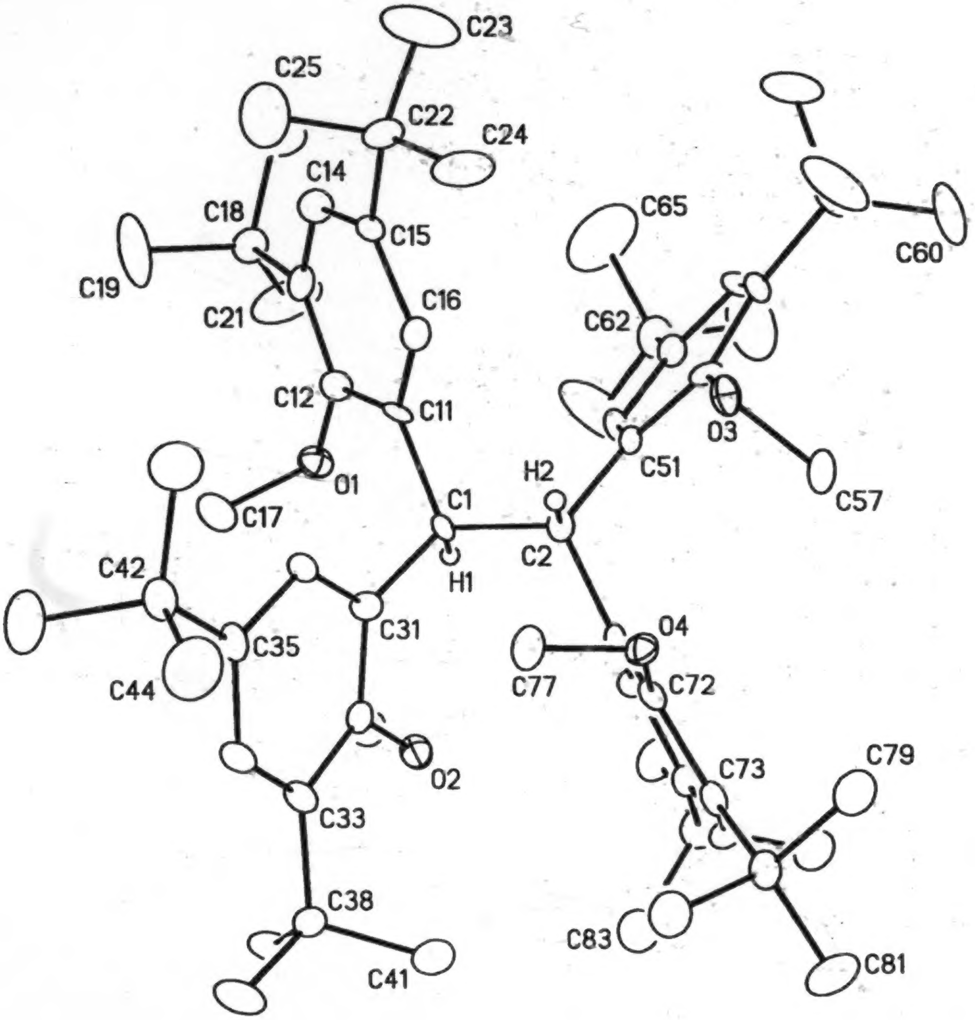
C23
C25
C22
C24
C14
C18
C15
C65
C60
C19
C21
C16
C62
C12
C11
O3
H2
C51
O1
C57
C1
C17
C42
C2
H1
O4
C31
C35
C77
C72
C44
C73
C79
O2
C33
C38
C83
C81
C41

Figure 1: Perspective view of the 1,1,2,2-tetra(3,5-di-*t*-butyl-2-methoxyphenyl)ethane molecule showing the atom labelling scheme. Non-hydrogen atoms are represented by Gaussian ellipsoids at the 20% probability level. The hydrogen atoms H1 and H2 are shown with arbitrarily small thermal parameters; all other hydrogens are not shown.

Selected Interatomic Distances (Å)

Atom1	Atom2	Distance	Atom1	Atom2	Distance
O1	C12	1.390(10)	C38	C39	1.514(12)
O1	C17	1.437(10)	C38	C40	1.549(12)
O2	C32	1.393(10)	C38	C41	1.545(12)
O2	C37	1.431(9)	C42	C43	1.517(12)
O3	C52	1.407(10)	C42	C44	1.496(13)
O3	C57	1.437(9)	C42	C45	1.554(13)
O4	C72	1.394(10)	C51	C52	1.403(11)
O4	C77	1.433(9)	C51	C56	1.382(11)
C1	C2	1.581(10)	C52	C53	1.405(12)
C1	C11	1.533(11)	C53	C54	1.385(11)
C1	C31	1.525(11)	C53	C58	1.536(12)
C2	C51	1.556(11)	C54	C55	1.387(12)
C2	C71	1.539(11)	C55	C56	1.393(11)
C11	C12	1.397(12)	C55	C62	1.527(13)
C11	C16	1.377(11)	C58	C59	1.526(13)
C12	C13	1.397(12)	C58	C60	1.485(13)
C13	C14	1.409(12)	C58	C61	1.525(14)
C13	C18	1.530(13)	C62	C63	1.420(15)
C14	C15	1.391(12)	C62	C64	1.493(14)
C15	C16	1.385(11)	C62	C65	1.53(2)
C15	C22	1.538(12)	C71	C72	1.377(11)
C18	C19	1.507(13)	C71	C76	1.390(11)
C18	C20	1.518(13)	C72	C73	1.430(12)
C18	C21	1.507(14)	C73	C74	1.409(12)
C22	C23	1.476(13)	C73	C78	1.530(12)
C22	C24	1.504(13)	C74	C75	1.375(11)
C22	C25	1.527(14)	C75	C76	1.403(11)
C31	C32	1.417(11)	C75	C82	1.524(12)
C31	C36	1.390(11)	C78	C79	1.540(12)
C32	C33	1.425(11)	C78	C80	1.528(11)
C33	C34	1.383(12)	C78	C81	1.517(12)
C33	C38	1.535(12)	C82	C83	1.548(13)
C34	C35	1.388(12)	C82	C84	1.522(13)
C35	C36	1.397(11)	C82	C85	1.550(13)
C35	C42	1.534(12)			

Selected Interatomic Angles (deg)

Atom1	Atom2	Atom3	Angle	Atom1	Atom2	Atom3	Angle
C12	O1	C17	112.5(7)	C32	C31	C36	118.7(8)
C32	O2	C37	115.7(7)	O2	C32	C31	119.9(8)
C52	O3	C57	111.1(7)	O2	C32	C33	119.2(9)
C72	O4	C77	117.8(7)	C31	C32	C33	120.6(9)
C2	C1	C11	110.5(7)	C32	C33	C34	116.9(9)
C2	C1	C31	111.9(7)	C32	C33	C38	120.5(9)
C11	C1	C31	112.6(7)	C34	C33	C38	122.4(9)
C1	C2	C51	111.1(7)	C33	C34	C35	123.8(9)
C1	C2	C71	113.5(7)	C34	C35	C36	118.0(9)
C51	C2	C71	111.2(7)	C34	C35	C42	120.4(9)
C1	C11	C12	120.9(8)	C36	C35	C42	121.5(9)
C1	C11	C16	120.6(9)	C31	C36	C35	121.6(9)
C12	C11	C16	118.4(9)	C33	C38	C39	113.8(8)
O1	C12	C11	118.2(9)	C33	C38	C40	109.9(8)
O1	C12	C13	119.9(9)	C33	C38	C41	108.2(8)
C11	C12	C13	121.8(9)	C39	C38	C40	108.4(9)
C12	C13	C14	116.4(10)	C39	C38	C41	109.8(9)
C12	C13	C18	126.3(10)	C40	C38	C41	106.5(9)
C14	C13	C18	117.4(10)	C35	C42	C43	113.5(8)
C13	C14	C15	123.0(10)	C35	C42	C44	109.7(9)
C14	C15	C16	117.2(9)	C35	C42	C45	109.9(9)
C14	C15	C22	119.5(9)	C43	C42	C44	107.8(9)
C16	C15	C22	123.3(10)	C43	C42	C45	107.9(9)
C11	C16	C15	122.6(10)	C44	C42	C45	107.8(9)
C13	C18	C19	113.0(9)	C2	C51	C52	120.0(8)
C13	C18	C20	111.8(9)	C2	C51	C56	120.7(8)
C13	C18	C21	114.4(10)	C52	C51	C56	119.2(8)
C19	C18	C20	105.4(10)	O3	C52	C51	117.0(8)
C19	C18	C21	107.9(11)	O3	C52	C53	121.2(9)
C20	C18	C21	103.5(10)	C51	C52	C53	121.8(9)
C15	C22	C23	112.8(10)	C52	C53	C54	115.8(9)
C15	C22	C24	111.6(9)	C52	C53	C58	125.4(9)
C15	C22	C25	107.6(9)	C54	C53	C58	118.8(9)
C23	C22	C24	110.7(10)	C53	C54	C55	124.0(9)

Selected Interatomic Angles (continued)

Atom1	Atom2	Atom3	Angle	Atom1	Atom2	Atom3	Angle
C23	C22	C25	109.3(10)	C54	C55	C56	118.2(9)
C24	C22	C25	104.6(10)	C54	C55	C62	120.8(9)
C1	C31	C32	122.0(8)	C56	C55	C62	120.9(10)
C1	C31	C36	119.2(8)	C51	C56	C55	120.6(9)
C53	C58	C59	117.6(9)	C72	C73	C78	124.4(9)
C53	C58	C60	110.6(9)	C74	C73	C78	120.9(9)
C53	C58	C61	107.7(9)	C73	C74	C75	125.2(10)
C59	C58	C60	107.1(10)	C74	C75	C76	116.5(9)
C59	C58	C61	105.1(10)	C74	C75	C82	120.2(10)
C60	C58	C61	108.3(10)	C76	C75	C82	123.3(9)
C55	C62	C63	115.2(10)	C71	C76	C75	122.2(9)
C55	C62	C64	110.7(10)	C73	C78	C79	109.1(8)
C55	C62	C65	107.6(10)	C73	C78	C80	112.2(8)
C63	C62	C64	110.3(12)	C73	C78	C81	112.7(8)
C63	C62	C65	108.2(12)	C79	C78	C80	107.8(8)
C64	C62	C65	104.2(11)	C79	C78	C81	106.8(8)
C2	C71	C72	123.4(8)	C80	C78	C81	108.0(8)
C2	C71	C76	117.6(8)	C75	C82	C83	108.5(8)
C72	C71	C76	118.9(9)	C75	C82	C84	112.1(9)
O4	C72	C71	121.4(9)	C75	C82	C85	110.9(9)
O4	C72	C73	116.0(9)	C83	C82	C84	106.8(9)
C71	C72	C73	122.3(9)	C83	C82	C85	109.2(9)
C72	C73	C74	114.7(9)	C84	C82	C85	109.2(9)

Torsional Angles (deg)

Atom1	Atom2	Atom3	Atom4	Angle	Atom1	Atom2	Atom3	Atom4	Angle
C17	O1	C12	C11	95.1(10)	C12	C13	C14	C15	3.8(15)
C17	O1	C12	C13	-87.7(10)	C18	C13	C14	C15	-176.1(9)
C37	O2	C32	C31	-79.7(10)	C12	C13	C18	C19	92.8(14)
C37	O2	C32	C33	105.5(10)	C12	C13	C18	C20	-148.5(10)

Torsional Angles (continued)

Atom1	Atom2	Atom3	Atom4	Angle	Atom1	Atom2	Atom3	Atom4	Angle
C57	O3	C52	C51	93.0(9)	C12	C13	C18	C21	-31.3(15)
C57	O3	C52	C53	-88.6(10)	C14	C13	C18	C19	-87.3(13)
C77	O4	C72	C71	74.1(11)	C14	C13	C18	C20	31.4(13)
C77	O4	C72	C73	-111.9(9)	C14	C13	C18	C21	148.6(11)
C11	C1	C2	C51	-49.2(10)	C13	C14	C15	C16	3.2(14)
C11	C1	C2	C71	-175.4(7)	C13	C14	C15	C22	-178.7(9)
C31	C1	C2	C51	-175.5(7)	C14	C15	C16	C11	-5.9(14)
C31	C1	C2	C71	58.3(10)	C22	C15	C16	C11	176.1(9)
C2	C1	C11	C12	143.6(8)	C14	C15	C22	C23	-47.1(14)
C2	C1	C11	C16	-38.6(11)	C14	C15	C22	C24	-172.4(9)
C31	C1	C11	C12	-90.6(10)	C14	C15	C22	C25	73.5(12)
C31	C1	C11	C16	87.3(10)	C16	C15	C22	C23	130.8(11)
C2	C1	C31	C32	-87.4(10)	C16	C15	C22	C24	5.5(14)
C2	C1	C31	C36	88.7(10)	C16	C15	C22	C25	-108.6(11)
C11	C1	C31	C32	147.5(9)	C1	C31	C32	O2	-6.2(13)
C11	C1	C31	C36	-36.4(12)	C1	C31	C32	C33	168.6(8)
C1	C2	C51	C52	139.6(8)	C36	C31	C32	O2	177.7(8)
C1	C2	C51	C56	-36.8(11)	C36	C31	C32	C33	-7.6(14)
C71	C2	C51	C52	-92.9(10)	C1	C31	C36	C35	-172.8(8)
C71	C2	C51	C56	90.6(10)	C32	C31	C36	C35	3.5(14)
C1	C2	C71	C72	-118.2(9)	O2	C32	C33	C34	-178.9(8)
C1	C2	C71	C76	65.0(10)	O2	C32	C33	C38	4.8(13)
C51	C2	C71	C72	115.7(9)	C31	C32	C33	C34	6.3(14)
C51	C2	C71	C76	-61.1(10)	C31	C32	C33	C38	-170.0(9)
C1	C11	C12	O1	1.4(12)	C32	C33	C34	C35	-1.0(14)
C1	C11	C12	C13	-175.7(8)	C38	C33	C34	C35	175.2(9)
C16	C11	C12	O1	-176.4(8)	C32	C33	C38	C39	-61.4(12)
C16	C11	C12	C13	6.4(14)	C32	C33	C38	C40	176.8(9)
C1	C11	C16	C15	-176.6(8)	C32	C33	C38	C41	60.9(12)
C12	C11	C16	C15	1.3(14)	C34	C33	C38	C39	122.5(10)
O1	C12	C13	C14	174.2(8)	C34	C33	C38	C40	0.8(13)
O1	C12	C13	C18	-5.9(15)	C34	C33	C38	C41	-115.2(11)
C11	C12	C13	C14	-8.7(14)	C33	C34	C35	C36	-3.0(14)

Torsional Angles (continued)

Atom1	Atom2	Atom3	Atom4	Angle	Atom1	Atom2	Atom3	Atom4	Angle
C11	C12	C13	C18	171.2(9)	C33	C34	C35	C42	-179.0(9)
C34	C35	C36	C31	1.7(14)	C54	C55	C62	C65	-66.7(14)
C42	C35	C36	C31	177.7(9)	C56	C55	C62	C63	-11.3(17)
C34	C35	C42	C43	173.8(9)	C56	C55	C62	C64	-137.3(11)
C34	C35	C42	C44	53.2(12)	C56	C55	C62	C65	109.5(12)
C34	C35	C42	C45	-65.2(12)	C2	C71	C72	O4	-0.8(13)
C36	C35	C42	C43	-2.1(14)	C2	C71	C72	C73	-174.4(8)
C36	C35	C42	C44	-122.7(10)	C76	C71	C72	O4	176.0(8)
C36	C35	C42	C45	118.9(10)	C76	C71	C72	C73	2.4(13)
C2	C51	C52	O3	7.6(12)	C2	C71	C76	C75	178.2(8)
C2	C51	C52	C53	-170.7(8)	C72	C71	C76	C75	1.2(14)
C56	C51	C52	O3	-175.9(8)	O4	C72	C73	C74	-176.6(8)
C56	C51	C52	C53	5.8(13)	O4	C72	C73	C78	3.7(13)
C2	C51	C56	C55	176.4(8)	C71	C72	C73	C74	-2.7(13)
C52	C51	C56	C55	-0.1(13)	C71	C72	C73	C78	177.6(8)
O3	C52	C53	C54	174.0(8)	C72	C73	C74	C75	-0.5(14)
O3	C52	C53	C58	-6.8(15)	C78	C73	C74	C75	179.2(9)
C51	C52	C53	C54	-7.7(13)	C72	C73	C78	C79	-58.7(12)
C51	C52	C53	C58	171.5(9)	C72	C73	C78	C80	60.7(12)
C52	C53	C54	C55	4.3(14)	C72	C73	C78	C81	-177.2(9)
C58	C53	C54	C55	-174.9(9)	C74	C73	C78	C79	121.6(10)
C52	C53	C58	C59	-12.6(16)	C74	C73	C78	C80	-119.1(10)
C52	C53	C58	C60	110.9(12)	C74	C73	C78	C81	3.1(13)
C52	C53	C58	C61	-131.0(11)	C73	C74	C75	C76	3.8(14)
C54	C53	C58	C59	166.6(10)	C73	C74	C75	C82	-177.2(9)
C54	C53	C58	C60	-70.0(13)	C74	C75	C76	C71	-4.1(14)
C54	C53	C58	C61	48.2(13)	C82	C75	C76	C71	176.9(9)
C53	C54	C55	C56	1.0(15)	C74	C75	C82	C83	64.9(12)
C53	C54	C55	C62	177.3(10)	C74	C75	C82	C84	-177.3(9)
C54	C55	C56	C51	-3.2(14)	C74	C75	C82	C85	-55.0(13)
C62	C55	C56	C51	-179.5(9)	C76	C75	C82	C83	-116.1(10)
C54	C55	C62	C63	172.6(12)	C76	C75	C82	C84	1.7(14)
C54	C55	C62	C64	46.6(15)	C76	C75	C82	C85	124.0(10)

Appendix D: Chapter 3, Section 3.3.1, page 135.

Crystallographic details for compound 1, SDL Code: JMS9808.

Compound 1: Tetrakis(2-{diethylaluminoxy}phenyl)ethylene hemitoluene solvate

Formula: $C_{45.5}H_{60}Al_4O_4$ ($C_{42}H_{56}Al_4O_4 \cdot 0.5C_7H_8$)

Crystallographic Experimental Details

A. Crystal Data	
formula	$C_{45.5}H_{60}Al_4O_4$
formula weight	778.85
crystal dimensions (mm)	0.74 × 0.33 × 0.19
crystal system	triclinic
space group	$P\bar{1}$ (No. 2)
unit cell parameters[a]	
a (Å)	12.7113 (5)
b (Å)	17.9077 (7)
c (Å)	20.9008 (9)
α (deg)	78.881 (3)
β (deg)	74.132 (3)
γ (deg)	83.404 (3)
V (Å^3)	4480.7 (3)
Z	4
ρ_{calcd} (g cm^{-3})	1.155
μ (mm^{-1})	1.270
B. Data Collection and Refinement Conditions	
diffractometer	Siemens P4/RA[b]
radiation (λ [Å])	graphite-monochromated Cu Kα (1.54178)
temperature (°C)	–60
scan type	θ–2θ
data collection 2θ limit (deg)	115.0
total data collected	12078 ($0 \le h \le 11$, $-19 \le k \le 19$, $-21 \le l \le 22$)
independent reflections	11424
number of observations (*NO*)	8507 ($F_o^2 \ge 2\sigma(F_o^2)$)
structure solution method	direct methods/fragment search (*DIRDIF–96*[c])
refinement method	full-matrix least-squares on F^2 (*SHELXL–93*[d])
absorption correction method	semiempirical (ψ scans)
range of transmission factors	0.9269–0.4395
data/restraints/parameters	11418 [$F_o^2 \ge -3\sigma(F_o^2)$] / 42[e] / 966

goodness-of-fit (S)[f]	1.049 [$F_o^2 \geq -3\sigma(F_o^2)$]
final R indices[g]	
$F_o^2 > 2\sigma(F_o^2)$	$R_1 = 0.0858$, $wR_2 = 0.2150$
all data	$R_1 = 0.1129$, $wR_2 = 0.2456$
largest difference peak and hole	0.791 and –0.588 e Å^{-3}

Crystallographic Experimental Details (continued)

[a] Obtained from least-squares refinement of 42 reflections with 54.9° < 2θ < 57.7°.

[b] Programs for diffractometer operation, data collection, data reduction and absorption correction were those supplied by Siemens.

[c] Beurskens, P. T.; Beurskens, G.; Bosman, W.P.; de Gelder, R.; Garcia Granda, S.; Gould, R. O.; Israel, R; Smits, J M.M. (1996). The *DIRDIF-96* program system. Crystallography Laboratory, University of Nijmegen, The Netherlands.

[d] Sheldrick, G. M. *SHELXL-93*. Program for crystal structure determination. University of Göttingen, Germany, 1993. Refinement on F_o^2 for all reflections except for 6 having $F_o^2 < -3\sigma(F_o^2)$. Weighted R-factors wR_2 and all goodnesses of fit S are based on F_o^2; conventional R-factors R_1 are based on F_o, with F_o set to zero for negative F_o^2. The observed criterion of $F_o^2 > 2\sigma(F_o^2)$ is used only for calculating R_1, and is not relevant to the choice of reflections for refinement. R-factors based on F_o^2 are statistically about twice as large as those based on F_o, and R-factors based on ALL data will be even larger.

[e] All carbon-carbon bond distances within the inversion-disordered solvent toluene molecules were constrained to be equal (within 0.01 Å), i.e. d(C90–C91) = d(C91–C92) = d(C91–C92') = d(C92–C93) = d(C93–C90') = d(C90'–C94) = d(C94–C92') and d(C95–C96) = d(C96–C97) = d(C96–C97") = d(C97–C98) = d(C98–C95") = d(C95"–C99) = d(C99–C97"). Primed atoms are related to unprimed ones via the crystallographic inversion center at (0, 0, 0) while double-primed atoms are related to unprimed ones via the crystallographic inversion center at ($^1/2$, $^1/2$, 0). See Fiure 7 for an illustration of the disorder mode.

[f] $S = [\Sigma w(F_o^2 - F_c^2)^2/(n - p)]^{1/2}$ (n = number of data; p = number of parameters varied; $w = [\sigma^2(F_o^2) + (0.1110P)^2 + 13.2939P]^{-1}$ where $P = [\mathrm{Max}(F_o^2, 0) + 2F_c^2]/3$).

[g] $R_1 = \Sigma||F_o| - |F_c||/\Sigma|F_o|$; $wR_2 = [\Sigma w(F_o^2 - F_c^2)^2/\Sigma w(F_o^4)]^{1/2}$.

Selected Interatomic Distances (Å)

(a) molecule A

Atom1	Atom2	Distance
Al1	O1	1.882(4)
Al1	O4	1.873(4)
Al1	C17	1.954(6)
Al1	C19	1.944(6)
Al2	O1	1.871(4)
Al2	O2	1.881(4)
Al2	C27	1.963(6)
Al2	C29	1.934(7)
Al3	O2	1.878(4)
Al3	O3	1.863(4)
Al3	C37	1.949(7)
Al3	C39	1.947(7)
Al4	O3	1.891(4)
Al4	O4	1.881(4)
Al4	C47	1.951(7)
Al4	C49	1.942(7)
O1	C12	1.417(6)
O2	C22	1.433(7)
O3	C32	1.417(7)
O4	C42	1.430(7)
C1	C2	1.312(8)
C1	C11	1.498(8)
C1	C21	1.513(8)
C2	C31	1.522(8)
C2	C41	1.501(8)
C11	C12	1.401(8)
C11	C16	1.387(8)
C12	C13	1.382(8)
C13	C14	1.385(8)
C14	C15	1.375(10)
C15	C16	1.383(9)
C17	C18	1.540(10)
C19	C20	1.538(9)
C21	C22	1.379(8)
C21	C26	1.412(8)
C22	C23	1.375(8)
C23	C24	1.375(9)
C24	C25	1.374(10)

(b) molecule B

Atom1	Atom2	Distance
Al1	O1	1.880(4)
Al1	O4	1.865(4)
Al1	C17	1.957(6)
Al1	C19	1.944(7)
Al2	O1	1.875(4)
Al2	O2	1.875(4)
Al2	C27	1.959(6)
Al2	C29	1.940(7)
Al3	O2	1.876(4)
Al3	O3	1.869(4)
Al3	C37	1.968(6)
Al3	C39	1.941(7)
Al4	O3	1.877(4)
Al4	O4	1.887(4)
Al4	C47	1.930(7)
Al4	C49	1.945(7)
O1	C12	1.430(6)
O2	C22	1.424(6)
O3	C32	1.444(7)
O4	C42	1.430(7)
C1	C2	1.301(9)
C1	C11	1.507(8)
C1	C21	1.509(8)
C2	C31	1.508(8)
C2	C41	1.522(8)
C11	C12	1.393(8)
C11	C16	1.390(8)
C12	C13	1.384(8)
C13	C14	1.394(9)
C14	C15	1.372(10)
C15	C16	1.383(9)
C17	C18	1.537(9)
C19	C20	1.541(9)
C21	C22	1.392(8)
C21	C26	1.393(8)
C22	C23	1.381(8)
C23	C24	1.385(9)
C24	C25	1.373(10)

Selected Interatomic Distances (continued)

(a) molecule A

Atom1	Atom2	Distance
C25	C26	1.356(9)
C27	C28	1.540(9)
C29	C30	1.553(10)
C31	C32	1.372(7)
C31	C36	1.405(9)
C32	C33	1.402(8)
C33	C34	1.363(9)
C34	C35	1.364(9)
C35	C36	1.381(9)
C37	C38	1.536(10)
C39	C40	1.553(9)
C41	C42	1.371(8)
C41	C46	1.399(9)
C42	C43	1.399(8
C43	C44	1.378(10)
C44	C45	1.358(10)
C45	C46	1.389(9)
C47	C48	1.542(9)
C49	C50	1.544(9)

(b) molecule B

Atom1	Atom2	Distance
C25	C26	1.390(9)
C27	C28	1.532(9)
C29	C30	1.544(10)
C31	C32	1.381(8)
C31	C36	1.394(8)
C32	C33	1.387(8)
C33	C34	1.377(10)
C34	C35	1.378(10)
C35	C36	1.368(9)
C37	C38	1.529(10)
C39	C40	1.542(9)
C41	C42	1.391(8)
C41	C46	1.400(8)
C42	C43	1.376(8)
C43	C44	1.371(9)
C44	C45	1.376(10)
C45	C46	1.371(9)
C47	C48	1.531(9)
C49	C50	1.534(9)

(c) within the solvent toluene molecules
Selected Interatomic Distances (Å)

(a) molecule A

Atom1	Atom2	Distance
C90	C91	1.425(5)
C91	C92	1.425(5)
C91	C92'	1.425(5)
C92	C93	1.425(5)
C93	C90'	1.425(5)
C94	C90'	1.425(5)
C94	C92'	1.425(5)

(b) molecule B

Atom1	Atom2	Distance
C95	C96	1.369(6)
C96	C97	1.370(6)
C96	C97"	1.370(6)
C97	C98	1.369(6)
C98	C95"	1.369(6)
C99	C95"	1.369(6)
C99	C97"	1.369(6)

Primed atoms are related to unprimed ones via the crystallographic inversion center at (0, 0, 0).

Double-primed atoms are related to unprimed ones via the inversion center at ($^1/2$, $^1/2$, 0).

Selected Interatomic Angles (deg)

(a) molecule A				*(b) molecule B*			
Atom1	Atom2	Atom3	Angle	Atom1	Atom2	Atom3	Angle
O1	Al1	O4	101.5(2)	O1	Al1	O4	102.2(2)
O1	Al1	C17	110.2(2)	O1	Al1	C17	110.4(2)
O1	Al1	C19	113.0(2)	O1	Al1	C19	107.7(2)
O4	Al1	C17	110.8(2)	O4	Al1	C17	110.5(3)
O4	Al1	C19	107.2(2)	O4	Al1	C19	112.1(2)
C17	Al1	C19	113.4(3)	C17	Al1	C19	113.3(3)
O1	Al2	O2	100.9(2)	O1	Al2	O2	101.1(2)
O1	Al2	C27	110.2(2)	O1	Al2	C27	108.9(2)
O1	Al2	C29	107.1(2)	O1	Al2	C29	115.9(2)
O2	Al2	C27	108.6(2)	O2	Al2	C27	108.6(2)
O2	Al2	C29	116.9(2)	O2	Al2	C29	110.1(2)
C27	Al2	C29	112.4(3)	C27	Al2	C29	111.6(3)
O2	Al3	O3	102.7(2)	O2	Al3	O3	101.9(2)
O2	Al3	C37	110.2(2)	O2	Al3	C37	110.3(2)
O2	Al3	C39	107.0(2)	O2	Al3	C39	111.0(2)
O3	Al3	C37	110.6(3)	O3	Al3	C37	110.6(3)
O3	Al3	C39	112.8(2)	O3	Al3	C39	107.9(2)
C37	Al3	C39	113.0(3)	C37	Al3	C39	114.4(3)
O3	Al4	O4	100.2(2)	O3	Al4	O4	101.1(2)
O3	Al4	C47	110.6(2)	O3	Al4	C47	108.9(3)
O3	Al4	C49	107.5(2)	O3	Al4	C49	115.8(2)
O4	Al4	C47	107.9(2)	O4	Al4	C47	109.6(2)
O4	Al4	C49	116.5(2)	O4	Al4	C49	109.1(3)
C47	Al4	C49	113.3(3)	C47	Al4	C49	111.8(3)
Al1	O1	Al2	131.9(2)	Al1	O1	Al2	133.1(2)
Al1	O1	C12	114.9(3)	Al1	O1	C12	113.6(3)
Al2	O1	C12	113.2(3)	Al2	O1	C12	113.2(3)
Al2	O2	Al3	133.4(2)	Al2	O2	Al3	133.2(2)
Al2	O2	C22	111.9(3)	Al2	O2	C22	111.1(3)
Al3	O2	C22	114.6(3)	Al3	O2	C22	115.6(3)
Al3	O3	Al4	133.9(2)	Al3	O3	Al4	132.5(2)
Al3	O3	C32	115.4(3)	Al3	O3	C32	114.4(3)
Al4	O3	C32	110.7(3)	Al4	O3	C32	113.0(3)
Al1	O4	Al4	133.1(2)	Al1	O4	Al4	132.9(2)
Al1	O4	C42	113.6(3)	Al1	O4	C42	116.3(3)
Al4	O4	C42	110.8(3)	Al4	O4	C42	113.3(3)
C2	C1	C11	120.6(6)	C2	C1	C11	122.0(6)

Selected Interatomic Angles (continued)

(a) molecule A

Atom1	Atom2	Atom3	Angle
C2	C1	C21	122.6(6)
C11	C1	C21	116.7(5)
C1	C2	C31	122.8(6)
C1	C2	C41	120.9(6)
C31	C2	C41	116.0(5)
C1	C11	C12	121.2(5)
C1	C11	C16	120.7(6)
C12	C11	C16	118.0(5)
O1	C12	C11	120.0(5)
O1	C12	C13	119.0(5)
C11	C12	C13	121.0(5)
C12	C13	C14	119.7(6)
C13	C14	C15	119.9(6)
C14	C15	C16	120.4(6)
C11	C16	C15	120.9(6)
Al1	C17	C18	114.5(5)
Al1	C19	C20	111.6(5)
C1	C21	C22	122.4(5)
C1	C21	C26	119.8(5)
C22	C21	C26	117.4(5)
O2	C22	C21	119.3(5)
O2	C22	C23	118.9(5)
C21	C22	C23	121.7(6)
C22	C23	C24	119.4(6)
C23	C24	C25	120.2(6)
C24	C25	C26	120.5(7)
C21	C26	C25	120.8(6)
Al2	C27	C28	111.5(4)
Al2	C29	C30	109.7(5)
C2	C31	C32	120.9(5)
C2	C31	C36	120.2(5)
C32	C31	C36	118.7(5)
O3	C32	C31	120.9(5)
O3	C32	C33	118.4(5)
C31	C32	C33	120.7(6)
C32	C33	C34	119.5(6)
C33	C34	C35	120.8(6)

(b) molecule B

Atom1	Atom2	Atom3	Angle
C2	C1	C21	121.1(6)
C11	C1	C21	116.8(5)
C1	C2	C31	122.2(6)
C1	C2	C41	121.9(6)
C31	C2	C41	115.6(5)
C1	C11	C12	121.9(5)
C1	C11	C16	119.7(6)
C12	C11	C16	118.1(5)
O1	C12	C11	119.9(5)
O1	C12	C13	118.1(5)
C11	C12	C13	122.0(5)
C12	C13	C14	118.3(6)
C13	C14	C15	120.7(6)
C14	C15	C16	120.3(6)
C11	C16	C15	120.7(6)
Al1	C17	C18	113.6(5)
Al1	C19	C20	110.3(5)
C1	C21	C22	122.0(5)
C1	C21	C26	119.8(6)
C22	C21	C26	117.8(6)
O2	C22	C21	119.9(5)
O2	C22	C23	118.4(5)
C21	C22	C23	121.7(5)
C22	C23	C24	119.2(6)
C23	C24	C25	120.5(6)
C24	C25	C26	119.8(6)
C21	C26	C25	120.9(7)
Al2	C27	C28	112.3(4)
Al2	C29	C30	111.4(5)
C2	C31	C32	121.9(5)
C2	C31	C36	121.1(6)
C32	C31	C36	116.7(5)
O3	C32	C31	119.7(5)
O3	C32	C33	118.3(5)
C31	C32	C33	122.0(6)
C32	C33	C34	119.9(6)
C33	C34	C35	119.0(7)

Selected Interatomic Angles (continued)

(a) molecule A				*(b) molecule B*			
Atom1	Atom2	Atom3	Angle	Atom1	Atom2	Atom3	Angle
C34	C35	C36	120.5(7)	C34	C35	C36	120.6(7)
C31	C36	C35	119.9(6)	C31	C36	C35	121.8(7)
Al3	C37	C38	114.2(5)	Al3	C37	C38	113.5(5)
Al3	C39	C40	110.0(5)	Al3	C39	C40	111.8(5)
C2	C41	C42	122.2(5)	C2	C41	C42	121.2(5)
C2	C41	C46	119.9(6)	C2	C41	C46	120.2(6)
C42	C41	C46	117.8(5)	C42	C41	C46	118.3(6)
O4	C42	C41	119.6(5)	O4	C42	C41	120.6(5)
O4	C42	C43	119.9(5)	O4	C42	C43	118.3(5)
C41	C42	C43	120.5(6)	C41	C42	C43	121.1(6)
C42	C43	C44	120.5(7)	C42	C43	C44	119.4(7)
C43	C44	C45	120.2(6)	C43	C44	C45	120.5(7)
C44	C45	C46	119.7(7)	C44	C45	C46	120.2(7)
C41	C46	C45	121.3(6)	C41	C46	C45	120.5(7)
Al4	C47	C48	112.6(5)	Al4	C47	C48	113.0(5)
Al4	C49	C50	109.7(5)	Al4	C49	C50	109.5(5)

(c) within the solvent toluene molecules

C90	C91	C92	118.5(9)	C95	C96	C97	118.7(10)
C90	C91	C92'	124.3(8)	C95	C96	C97"	125.5(10)
C92	C91	C92'	116.7(8)	C97	C96	C97"	114.0(11)
C91	C92	C93	118.0(9)	C96	C97	C98	119.6(9)
C90'	C93	C92	124.3(8)	C95"	C98	C97	125.5(10)
C90'	C94	C92'	118.5(9)	C95"	C99	C97"	118.7(10)

Primed atoms are related to unprimed ones via the crystallographic inversion center at (0, 0, 0). Double-primed atoms are related to unprimed ones via the inversion center at ($^1/2$, $^1/2$, 0).

Torsional Angles (deg)

(a) molecule A					*(b) molecule B*				
Atom1	Atom2	Atom3	Atom4	Angle	Atom1	Atom2	Atom3	Atom4	Angle
O4	Al1	O1	Al2	95.4(3)	O4	Al1	O1	Al2	-91.7(3)
O4	Al1	O1	C12	-85.3(4)	O4	Al1	O1	C12	86.0(4)
C17	Al1	O1	Al2	-147.2(3)	C17	Al1	O1	Al2	150.7(3)
C17	Al1	O1	C12	32.2(4)	C17	Al1	O1	C12	-31.6(4)
C19	Al1	O1	Al2	-19.1(4)	C19	Al1	O1	Al2	26.6(4)
C19	Al1	O1	C12	160.2(4)	C19	Al1	O1	C12	-155.7(4)
O1	Al1	O4	Al4	-94.8(3)	O1	Al1	O4	Al4	93.7(3)
O1	Al1	O4	C42	84.3(3)	O1	Al1	O4	C42	-86.5(4)
C17	Al1	O4	Al4	148.1(3)	C17	Al1	O4	Al4	-148.8(3)
C17	Al1	O4	C42	-32.7(4)	C17	Al1	O4	C42	31.1(4)
C19	Al1	O4	Al4	23.9(4)	C19	Al1	O4	Al4	-21.4(4)
C19	Al1	O4	C42	-156.9(4)	C19	Al1	O4	C42	158.4(4)
O1	Al1	C17	C18	79.9(6)	O1	Al1	C17	C18	-168.9(5)
O4	Al1	C17	C18	-168.5(5)	O4	Al1	C17	C18	78.8(6)
C19	Al1	C17	C18	-47.9(6)	C19	Al1	C17	C18	-48.0(7)
O1	Al1	C19	C20	-173.7(4)	O1	Al1	C19	C20	74.5(5)
O4	Al1	C19	C20	75.3(5)	O4	Al1	C19	C20	-173.8(5)
C17	Al1	C19	C20	-47.3(6)	C17	Al1	C19	C20	-47.9(6)
O2	Al2	O1	Al1	-85.9(3)	O2	Al2	O1	Al1	83.5(3)
O2	Al2	O1	C12	94.7(4)	O2	Al2	O1	C12	-94.2(4)
C27	Al2	O1	Al1	159.4(3)	C27	Al2	O1	Al1	-162.3(3)
C27	Al2	O1	C12	-20.0(4)	C27	Al2	O1	C12	20.0(4)
C29	Al2	O1	Al1	36.9(4)	C29	Al2	O1	Al1	-35.5(4)
C29	Al2	O1	C12	-142.5(4)	C29	Al2	O1	C12	146.8(4)
O1	Al2	O2	Al3	83.7(3)	O1	Al2	O2	Al3	-85.8(3)
O1	Al2	O2	C22	-94.8(3)	O1	Al2	O2	C22	95.0(3)
C27	Al2	O2	Al3	-160.5(3)	C27	Al2	O2	Al3	159.8(3)
C27	Al2	O2	C22	21.0(4)	C27	Al2	O2	C22	-19.5(4)
C29	Al2	O2	Al3	-32.0(4)	C29	Al2	O2	Al3	37.3(4)
C29	Al2	O2	C22	149.4(4)	C29	Al2	O2	C22	-142.0(4)
O1	Al2	C27	C28	-166.8(5)	O1	Al2	C27	C28	82.3(5)
O2	Al2	C27	C28	83.6(5)	O2	Al2	C27	C28	-168.4(4)
C29	Al2	C27	C28	-47.4(6)	C29	Al2	C27	C28	-46.9(5)
O1	Al2	C29	C30	65.1(5)	O1	Al2	C29	C30	-175.7(4)
O2	Al2	C29	C30	177.3(4)	O2	Al2	C29	C30	70.4(5)
C27	Al2	C29	C30	-56.1(5)	C27	Al2	C29	C30	-50.2(6)

Torsional Angles (continued)

(a) molecule A					*(b) molecule B*				
Atom1	Atom2	Atom3	Atom4	Angle	Atom1	Atom2	Atom3	Atom4	Angle
O3	Al3	O2	Al2	-91.6(3)	O3	Al3	O2	Al2	94.3(3)
O3	Al3	O2	C22	86.9(3)	O3	Al3	O2	C22	-86.5(4)
C37	Al3	O2	Al2	150.6(3)	C37	Al3	O2	Al2	-148.2(3)
C37	Al3	O2	C22	-30.9(4)	C37	Al3	O2	C22	31.0(4)
C39	Al3	O2	Al2	27.4(4)	C39	Al3	O2	Al2	-20.4(4)
C39	Al3	O2	C22	-154.1(4)	C39	Al3	O2	C22	158.8(4)
O2	Al3	O3	Al4	93.2(3)	O2	Al3	O3	Al4	-92.4(3)
O2	Al3	O3	C32	-86.6(3)	O2	Al3	O3	C32	85.6(3)
C37	Al3	O3	Al4	-149.3(3)	C37	Al3	O3	Al4	150.3(3)
C37	Al3	O3	C32	30.9(4)	C37	Al3	O3	C32	-31.7(4)
C39	Al3	O3	Al4	-21.6(4)	C39	Al3	O3	Al4	24.5(4)
C39	Al3	O3	C32	158.5(4)	C39	Al3	O3	C32	-157.5(4)
O2	Al3	C37	C38	-166.1(5)	O2	Al3	C37	C38	80.6(6)
O3	Al3	C37	C38	81.1(6)	O3	Al3	C37	C38	-167.4(5)
C39	Al3	C37	C38	-46.4(6)	C39	Al3	C37	C38	-45.3(6)
O2	Al3	C39	C40	72.8(5)	O2	Al3	C39	C40	-173.3(5)
O3	Al3	C39	C40	-175.0(4)	O3	Al3	C39	C40	75.8(5)
C37	Al3	C39	C40	-48.6(6)	C37	Al3	C39	C40	-47.7(6)
O4	Al4	O3	Al3	-84.3(3)	O4	Al4	O3	Al3	84.5(3)
O4	Al4	O3	C32	95.6(3)	O4	Al4	O3	C32	-93.6(3)
C47	Al4	O3	Al3	162.1(3)	C47	Al4	O3	Al3	-160.1(3)
C47	Al4	O3	C32	-18.1(4)	C47	Al4	O3	C32	21.8(4)
C49	Al4	O3	Al3	37.9(4)	C49	Al4	O3	Al3	-33.2(4)
C49	Al4	O3	C32	-142.2(4)	C49	Al4	O3	C32	148.7(4)
O3	Al4	O4	Al1	84.4(3)	O3	Al4	O4	Al1	-86.0(3)
O3	Al4	O4	C42	-94.8(3)	O3	Al4	O4	C42	94.2(3)
C47	Al4	O4	Al1	-159.9(3)	C47	Al4	O4	Al1	159.1(3)
C47	Al4	O4	C42	21.0(4)	C47	Al4	O4	C42	-20.7(4)
C49	Al4	O4	Al1	-31.2(4)	C49	Al4	O4	Al1	36.5(4)
C49	Al4	O4	C42	149.6(4)	C49	Al4	O4	C42	-143.3(4)
O3	Al4	C47	C48	-171.2(5)	O3	Al4	C47	C48	82.4(6)
O4	Al4	C47	C48	80.1(5)	O4	Al4	C47	C48	-167.8(5)
C49	Al4	C47	C48	-50.4(6)	C49	Al4	C47	C48	-46.8(6)
O3	Al4	C49	C50	68.2(6)	O3	Al4	C49	C50	-178.6(5)
O4	Al4	C49	C50	179.6(5)	O4	Al4	C49	C50	68.2(6)
C47	Al4	C49	C50	-54.4(6)	C47	Al4	C49	C50	-53.1(6)

Torsional Angles (continued)

(a) molecule A					*(b) molecule B*				
Atom1	Atom2	Atom3	Atom4	Angle	Atom1	Atom2	Atom3	Atom4	Angle
Al1	O1	C12	C11	100.4(5)	Al1	O1	C12	C11	-97.2(5)
Al1	O1	C12	C13	-81.6(5)	Al1	O1	C12	C13	83.1(5)
Al2	O1	C12	C11	-80.1(5)	Al2	O1	C12	C11	81.0(6)
Al2	O1	C12	C13	97.9(5)	Al2	O1	C12	C13	-98.7(5)
Al2	O2	C22	C21	81.0(5)	Al2	O2	C22	C21	-81.6(5)
Al2	O2	C22	C23	-97.1(5)	Al2	O2	C22	C23	95.8(5)
Al3	O2	C22	C21	-97.9(5)	Al3	O2	C22	C21	99.0(5)
Al3	O2	C22	C23	84.0(6)	Al3	O2	C22	C23	-83.6(6)
Al3	O3	C32	C31	98.2(5)	Al3	O3	C32	C31	-97.0(5)
Al3	O3	C32	C33	-84.9(5)	Al3	O3	C32	C33	83.2(6)
Al4	O3	C32	C31	-81.7(5)	Al4	O3	C32	C31	81.4(5)
Al4	O3	C32	C33	95.2(5)	Al4	O3	C32	C33	-98.4(5)
Al1	O4	C42	C41	-100.0(5)	Al1	O4	C42	C41	98.6(5)
Al1	O4	C42	C43	82.1(6)	Al1	O4	C42	C43	-82.9(6)
Al4	O4	C42	C41	79.4(5)	Al4	O4	C42	C41	-81.5(5)
Al4	O4	C42	C43	-98.6(5)	Al4	O4	C42	C43	97.0(5)
C11	C1	C2	C31	-174.4(5)	C11	C1	C2	C31	174.9(5)
C11	C1	C2	C41	-0.3(9)	C11	C1	C2	C41	1.5(10)
C21	C1	C2	C31	1.4(9)	C21	C1	C2	C31	-1.8(10)
C21	C1	C2	C41	175.5(5)	C21	C1	C2	C41	-175.2(5)
C2	C1	C11	C12	-91.1(7)	C2	C1	C11	C12	93.0(8)
C2	C1	C11	C16	92.9(7)	C2	C1	C11	C16	-94.5(8)
C21	C1	C11	C12	92.8(7)	C21	C1	C11	C12	-90.2(7)
C21	C1	C11	C16	-83.2(7)	C21	C1	C11	C16	82.3(8)
C2	C1	C21	C22	90.7(8)	C2	C1	C21	C22	-89.8(8)
C2	C1	C21	C26	-97.2(7)	C2	C1	C21	C26	97.8(8)
C11	C1	C21	C22	-93.3(7)	C11	C1	C21	C22	93.4(7)
C11	C1	C21	C26	78.8(8)	C11	C1	C21	C26	-79.0(8)
C1	C2	C31	C32	-91.5(7)	C1	C2	C31	C32	95.1(8)
C1	C2	C31	C36	94.6(7)	C1	C2	C31	C36	-91.4(8)
C41	C2	C31	C32	94.2(6)	C41	C2	C31	C32	-91.0(7)
C41	C2	C31	C36	-79.8(7)	C41	C2	C31	C36	82.5(7)
C1	C2	C41	C42	92.9(7)	C1	C2	C41	C42	-91.2(8)
C1	C2	C41	C46	-90.0(7)	C1	C2	C41	C46	95.1(8)
C31	C2	C41	C42	-92.7(7)	C31	C2	C41	C42	94.9(7)
C31	C2	C41	C46	84.5(6)	C31	C2	C41	C46	-78.8(7)

C1	C11	C12	O1	4.0(8)	C1	C11	C12	O1	-6.7(8)
C1	C11	C12	C13	-174.0(5)	C1	C11	C12	C13	173.0(6)
C16	C11	C12	O1	-179.9(5)	C16	C11	C12	O1	-179.3(5)
C16	C11	C12	C13	2.1(9)	C16	C11	C12	C13	0.4(9)
C1	C11	C16	C15	176.3(6)	C1	C11	C16	C15	-173.5(6)
C12	C11	C16	C15	0.2(9)	C12	C11	C16	C15	-0.7(10)
O1	C12	C13	C14	178.7(5)	O1	C12	C13	C14	179.1(5)
C11	C12	C13	C14	-3.3(9)	C11	C12	C13	C14	-0.6(9)
C12	C13	C14	C15	2.2(10)	C12	C13	C14	C15	1.1(10)
C13	C14	C15	C16	0.1(11)	C13	C14	C15	C16	-1.4(10)
C14	C15	C16	C11	-1.2(11)	C14	C15	C16	C11	1.3(10)
C1	C21	C22	O2	-5.0(8)	C1	C21	C22	O2	4.7(8)
C1	C21	C22	C23	173.1(6)	C1	C21	C22	C23	-172.6(6)
C26	C21	C22	O2	-177.2(5)	C26	C21	C22	O2	177.3(5)
C26	C21	C22	C23	0.8(9)	C26	C21	C22	C23	0.0(9)
C1	C21	C26	C25	-172.5(7)	C1	C21	C26	C25	173.8(6)
C22	C21	C26	C25	0.0(10)	C22	C21	C26	C25	1.1(10)
O2	C22	C23	C24	176.7(6)	O2	C22	C23	C24	-177.6(5)
C21	C22	C23	C24	-1.4(10)	C21	C22	C23	C24	-0.3(9)
C22	C23	C24	C25	1.1(12)	C22	C23	C24	C25	-0.5(10)
C23	C24	C25	C26	-0.3(13)	C23	C24	C25	C26	1.6(11)
C24	C25	C26	C21	-0.2(12)	C24	C25	C26	C21	-1.8(11)
C2	C31	C32	O3	4.2(8)	C2	C31	C32	O3	-7.0(8)
C2	C31	C32	C33	-172.6(5)	C2	C31	C32	C33	172.8(6)
C36	C31	C32	O3	178.2(5)	C36	C31	C32	O3	179.2(5)
C36	C31	C32	C33	1.4(8)	C36	C31	C32	C33	-1.0(9)
C2	C31	C36	C35	173.7(6)	C2	C31	C36	C35	-173.1(6)
C32	C31	C36	C35	-0.4(9)	C32	C31	C36	C35	0.7(10)
O3	C32	C33	C34	-178.7(5)	O3	C32	C33	C34	-179.6(6)
C31	C32	C33	C34	-1.8(9)	C31	C32	C33	C34	0.6(10)
C32	C33	C34	C35	1.2(10)	C32	C33	C34	C35	0.2(11)
C33	C34	C35	C36	-0.2(11)	C33	C34	C35	C36	-0.4(12)
C34	C35	C36	C31	-0.2(11)	C34	C35	C36	C31	0.0(12)
C2	C41	C42	O4	-3.6(8)	C2	C41	C42	O4	4.3(8)
C2	C41	C42	C43	174.3(5)	C2	C41	C42	C43	-174.2(6)
C46	C41	C42	O4	179.2(5)	C46	C41	C42	O4	178.2(5)
C46	C41	C42	C43	-2.9(8)	C46	C41	C42	C43	-0.3(9)
C2	C41	C46	C45	-175.3(6)	C2	C41	C46	C45	175.3(6)
C42	C41	C46	C45	2.0(9)	C42	C41	C46	C45	1.4(9)
O4	C42	C43	C44	-178.9(6)	O4	C42	C43	C44	-179.3(6)
C41	C42	C43	C44	3.2(9)	C41	C42	C43	C44	-0.8(10)
C42	C43	C44	C45	-2.5(11)	C42	C43	C44	C45	0.9(11)
C43	C44	C45	C46	1.7(11)	C43	C44	C45	C46	0.2(12)

Torsional Angles (continued)

(a) molecule A					*(b) molecule B*				
Atom1	Atom2	Atom3	Atom4	Angle	Atom1	Atom2	Atom3	Atom4	Angle
C44	C45	C46	C41	-1.4(10)	C44	C45	C46	C41	-1.4(11)
C90	C91	C92	C93	-177.3(14)	C95	C96	C97	C98	-172.3(19)
C92'	C91	C92	C93	10.3(19)	C97"	C96	C97	C98	-6.5(24)
C91	C92	C93	C90'	-14.1(24)	C96	C97	C98	C95"	-1.0(35)

Primed atoms are related to unprimed ones via the crystallographic inversion center at (0, 0, 0). Double-primed atoms are related to unprimed ones via the inversion center at ($^{1}/2$, $^{1}/2$, 0).

Appendix E: Chapter 3, Section 3.3.3, page 146

Crystallographic details for compound 2, SDL Code: JMS9912

Compound 2: [{tetra(2-phenoxy)ethene}(Al)(AlEt$_2$)]$_2$

Formula: $C_{60}H_{52}Al_4O_8$

Crystallographic Experimental Details

A. Crystal Data

formula	$C_{60}H_{52}Al_4O_8$
formula weight	1008.94
crystal dimensions (mm)	L × W × H
crystal system	monoclinic
space group	$P2_1/n$ (a nonstandard setting of $P2_1/c$ [No. 14])
unit cell parameters[a]	
a (Å)	13.5609 (16)
b (Å)	10.6880 (13)
c (Å)	17.991 (2)
β (deg)	94.644 (3)
V (Å^3)	2599.0 (5)
Z	2
ρ_{calcd} (g cm^{-3})	1.289
μ (mm^{-1})	0.146

B. Data Collection and Refinement Conditions

diffractometer	Bruker P4/RA/SMART 1000 CCD[b]
radiation (λ [Å])	graphite-monochromated Mo Kα (0.71073)
temperature (°C)	–80
scan type	ϕ rotations (0.3°) / ω scans (0.3°) (30 s exposures)
data collection 2θ limit (deg)	51.50
total data collected	13696 ($-16 \le h \le 16$, $-13 \le k \le 13$, $-21 \le l \le 21$)
independent reflections	4937
number of observations (*NO*)	1831 [$F_o^2 \ge 2\sigma(F_o^2)$]
structure solution method	direct methods (*SHELXS–86*[c])
refinement method	full-matrix least-squares on F^2 (*SHELXL–93*[d])
absorption correction method	*SADABS*
range of transmission factors	0.9280 0.6890
data/restraints/parameters	4937 [$F_o^2 \ge -3\sigma(F_o^2)$] / 0 / 325
goodness-of-fit (S)[e]	0.770 [$F_o^2 \ge -3\sigma(F_o^2)$]

Crystallographic Experimental Details (continued)

final *R* indices[f]	
R_1 $[F_o^2 \geq 2\sigma(F_o^2)]$	0.0556
wR_2 $[F_o^2 \geq -3\sigma(F_o^2)]$	0.1154
largest difference peak and hole	0.301 and –0.267 e Å^{-3}

[a] Obtained from least-squares refinement of 2065 centered reflections.

[b] Programs for diffractometer operation, data collection, data reduction and absorption correction were those supplied by Bruker.

[c] Sheldrick, G. M. *Acta Crystallogr.* **1990**, *A46*, 467–473.

[d] Sheldrick, G. M. *SHELXL-93*. Program for crystal structure determination. University of Göttingen, Germany, 1993. Refinement on F_o^2 for all reflections (all of these having $F_o^2 \geq -3\sigma(F_o^2)$). Weighted *R*-factors wR_2 and all goodnesses of fit *S* are based on F_o^2; conventional *R*-factors R_1 are based on F_o, with F_o set to zero for negative F_o^2. The observed criterion of $F_o^2 > 2\sigma(F_o^2)$ is used only for calculating R_1, and is not relevant to the choice of reflections for refinement. *R*-factors based on F_o^2 are statistically about twice as large as those based on F_o, and *R*-factors based on ALL data will be even larger.

[e] $S = [\Sigma w(F_o^2 - F_c^2)^2/(n - p)]^{1/2}$ (n = number of data; p = number of parameters varied; $w = [\sigma^2(F_o^2) + (0.0235P)^2]^{-1}$ where $P = [\mathrm{Max}(F_o^2, 0) + 2F_c^2]/3$).

[f] $R_1 = \Sigma||F_o| - |F_c||/\Sigma|F_o|$; $wR_2 = [\Sigma w(F_o^2 - F_c^2)^2/\Sigma w(F_o^4)]^{1/2}$.

Selected Interatomic Distances (Å)

Atom1	Atom2	Distance	Atom1	Atom2	Distance
Al1	O1	1.843(3)	Al1	O1'	1.881(3)
Al1	O2	1.924(3)	Al1	O3	1.733(3)
Al1	O4'	1.846(3)	Al2	O2	1.857(3)
Al2	O4'	1.891(3)	Al2	C51	1.946(5)
Al2	C53	1.952(4)	O1	Al1	1.881(3)
O1	C12	1.406(5)	O2	C22	1.375(5)
O3	C32	1.355(5)	O4	Al1	1.846(3)
O4	Al2	1.891(3)	O4	C42	1.397(5)
C1	C2	1.346(5)	C1	C11	1.497(6)
C1	C21	1.484(6)	C2	C31	1.476(5)
C2	C41	1.510(5)	C11	C12	1.393(6)
C11	C16	1.388(5)	C12	C13	1.379(5)
C13	C14	1.391(5)	C14	C15	1.373(6)
C15	C16	1.375(6)	C21	C22	1.391(6)
C21	C26	1.404(6)	C22	C23	1.376(5)
C23	C24	1.387(6)	C24	C25	1.375(6)
C25	C26	1.390(5)	C31	C32	1.419(6)
C31	C36	1.410(5)	C32	C33	1.412(5)
C33	C34	1.377(5)	C34	C35	1.373(6)
C35	C36	1.382(5)	C41	C42	1.396(5)
C41	C46	1.389(5)	C42	C43	1.392(5)
C43	C44	1.371(6)	C44	C45	1.376(6)
C45	C46	1.387(6)	C51	C52	1.517(6)
C53	C54	1.543(5)			

Primed atoms are related to unprimed ones via the crystallographic inversion center at (0, 0, 0).

Selected Interatomic Angles (deg)

Atom1	Atom2	Atom3	Angle	Atom1	Atom2	Atom3	Angle
O1	Al1	O1'	77.84(13)	O1	Al1	O2	94.75(13)
O1	Al1	O3	131.58(14)	O1	Al1	O4'	95.49(13)
O1'	Al1	O2	168.63(14)	O1'	Al1	O3	97.87(13)
O1'	Al1	O4'	105.81(13)	O2	Al1	O3	93.50(14)
O2	Al1	O4'	78.09(12)	O3	Al1	O4'	122.58(15)

Selected Interatomic Angles (continued)

Atom1	Atom2	Atom3	Angle	Atom1	Atom2	Atom3	Angle
O2	Al2	O4'	78.66(13)	O2	Al2	C51	113.25(18)
O2	Al2	C53	116.44(18]	O4'	Al2	C51	107.96(18]
O4'	Al2	C53	118.24(16]	C51	Al2	C53	116.5(2)
Al1	O1	Al1'	102.16(13)	Al1	O1	C12	127.3(3)
Al1'	O1	C12	129.3(2)	Al1	O2	Al2	99.54(14
Al1	O2	C22	120.5(2)	Al2	O2	C22	135.6(3)
Al1	O3	C32	135.5(3)	Al1'	O4	Al2'	101.20(14)
Al1'	O4	C42	137.1(2)	Al2'	O4	C42	121.2(2)
C2	C1	C11	118.6(4)	C2	C1	C21	125.9(4)
C11	C1	C21	115.4(4)	C1	C2	C31	122.4(4)
C1	C2	C41	116.8(4)	C31	C2	C41	120.4(4)
C1	C11	C12	117.1(4)	C1	C11	C16	124.5(4)
C12	C11	C16	118.4(4)	O1	C12	C11	118.4(4)
O1	C12	C13	120.1(4)	C11	C12	C13	121.4(4)
C12	C13	C14	118.6(4)	C13	C14	C15	120.8(5)
C14	C15	C16	120.1(4)	C11	C16	C15	120.7(5)
C1	C21	C22	120.4(4)	C1	C21	C26	120.9(4)
C22	C21	C26	118.5(4)	O2	C22	C21	117.1(4)
O2	C22	C23	121.9(4)	C21	C22	C23	120.8(4)
C22	C23	C24	119.8(5)	C23	C24	C25	121.0(5)
C24	C25	C26	119.2(5)	C21	C26	C25	120.7(5)
C2	C31	C32	120.9(4)	C2	C31	C36	121.4(4)
C32	C31	C36	117.7(4)	O3	C32	C31	122.7(4)
O3	C32	C33	117.9(4)	C31	C32	C33	119.4(4)
C32	C33	C34	120.3(5)	C33	C34	C35	121.2(5)
C34	C35	C36	119.5(5)	C31	C36	C35	121.8(5)
C2	C41	C42	126.7(4)	C2	C41	C46	115.8(4)
C42	C41	C46	117.1(4)	O4	C42	C41	122.7(4)
O4	C42	C43	117.2(4)	C41	C42	C43	120.1(4)
C42	C43	C44	121.7(4)	C43	C44	C45	119.1(5)
C44	C45	C46	119.4(5)	C41	C46	C45	122.6(5)
Al2	C51	C52	112.7(4)	Al2	C53	C54	112.4(3)

Primed atoms are related to unprimed ones via the crystallographic inversion center at (0, 0, 0).

Torsional Angles (deg)

Atom1	Atom2	Atom3	Atom4	Angle	Atom1	Atom2	Atom3	Atom4	Angle
O1'	Al1	O1	C12	168.0(4)	O2	Al1	O1	Al1'	171.28(15)
O2	Al1	O1	C12	-20.7(3)	O3	Al1	O1	Al1'	-89.8(2)
O3	Al1	O1	C12	78.2(3)	O4'	Al1	O1	Al1'	92.33(15)
O4'	Al1	O1	C12	-99.7(3)	O1	Al1	O1'	C12'	167.7(4)
O2	Al1	O1'	Al1'	-50.0(8)	O2	Al1	O1'	C12'	117.6(7)
O3	Al1	O1'	Al1'	130.96(15)	O3	Al1	O1'	C12'	-61.4(4)
O1	Al1	O2	Al2	-93.07(14)	O1	Al1	O2	C22	106.8(3)
O1'	Al1	O2	Al2	-44.3(8)	O1'	Al1	O2	C22	155.5(7)
O3	Al1	O2	Al2	134.69(15)	O3	Al1	O2	C22	-25.5(3)
O4'	Al1	O2	Al2	12.11(13)	O4'	Al1	O2	C22	-148.0(3)
O1	Al1	O3	C32	19.4(5)	O1	Al1	O3	C32	-61.3(4)
O2	Al1	O3	C32	118.9(4)	O4'	Al1	O3	C32	-163.0(3)
O4'	Al2	O2	Al1	-11.80(13)	O4'	Al2	O2	C22	143.5(4)
C51	Al2	O2	Al1	93.1(2)	C51	Al2	O2	C22	-111.7(4)
C53	Al2	O2	Al1	-127.86(17)	C53	Al2	O2	C22	27.4(4)
O2	Al2	C51	C52	66.0(4)	O4'	Al2	C51	C52	151.1(3)
C53	Al2	C51	C52	-73.0(4)	O2	Al2	C53	C54	-176.5(3)
O4'	Al2	C53	C54	92.5(3)	C51	Al2	C53	C54	-38.7(4)
Al1	O1	C12	C11	-43.3(5)	Al1	O1	C12	C13	134.8(3)
Al1'	O1	C12	C11	121.5(4)	Al1'	O1	C12	C13	-60.4(5)
Al1	O2	C22	C21	-45.4(5)	Al1	O2	C22	C23	130.6(3)
Al2	O2	C22	C21	163.2(3)	Al2	O2	C22	C23	-20.8(6)
Al1	O3	C32	C31	-33.8(6)	Al1	O3	C32	C33	143.8(3)
Al1'	O4	C42	C41	-72.5(5)	Al1'	O4	C42	C43	106.9(4)
Al2'	O4	C42	C41	116.7(4)	Al2'	O4	C42	C43	-63.9(4)
C11	C1	C2	C31	162.0(4)	C11	C1	C2	C41	-24.8(6)
C21	C1	C2	C31	-14.7(7)	C21	C1	C2	C41	158.6(4)
C2	C1	C11	C12	-66.1(6)	C2	C1	C11	C16	114.0(5)
C21	C1	C11	C12	110.9(5)	C21	C1	C11	C16	-69.0(6)
C2	C1	C21	C22	118.7(5)	C2	C1	C21	C26	-66.0(6)
C11	C1	C21	C22	-58.1(5)	C11	C1	C21	C26	117.2(4)
C1	C2	C31	C32	-46.1(6)	C1	C2	C31	C36	135.1(5)
C41	C2	C31	C32	140.9(4)	C41	C2	C31	C36	-37.9(6)
C1	C2	C41	C42	101.7(5)	C1	C2	C41	C46	-71.1(5)
C31	C2	C41	C42	-84.9(6)	C31	C2	C41	C46	102.3(5)
C1	C11	C12	O1	-2.8(6)	C1	C11	C12	C13	179.1(4)
C16	C11	C12	O1	177.1(3)	C16	C11	C12	C13	-0.9(6)
C1	C11	C16	C15	-178.7(4)	C12	C11	C16	C15	1.3(6)

Torsional Angles (continued)

Atom1	Atom2	Atom3	Atom4	Angle	Atom1	Atom2	Atom3	Atom4	Angle
O1	C12	C13	C14	-178.0(3)	C11	C12	C13	C14	0.0(6)
C12	C13	C14	C15	0.6(6)	C14	C15	C16	C11	-0.7(7)
C1	C21	C22	O2	-9.7(6)	C1	C21	C22	C23	174.2(4)
C26	C21	C22	O2	174.9(4)	C26	C21	C22	C23	-1.2(6)
C1	C21	C26	C25	-174.6(4)	C22	C21	C26	C25	0.8(6)
O2	C22	C23	C24	-175.6(4)	C21	C22	C23	C24	0.2(6)
C22	C23	C24	C25	1.2(7)	C23	C24	C25	C26	-1.5(7)
C24	C25	C26	C21	0.5(6)	C2	C31	C32	O3	-2.0(7)
C2	C31	C32	C33	-179.6(4)	C36	C31	C32	O3	176.8(3)
C36	C31	C32	C33	-0.8(6)	C2	C31	C36	C35	179.5(4)
C32	C31	C36	C35	0.6(7)	O3	C32	C33	C34	-177.8(4)
C31	C32	C33	C34	-0.1(6)	C32	C33	C34	C35	1.2(7)
C33	C34	C35	C36	-1.4(8)	C34	C35	C36	C31	0.4(7)
C2	C41	C42	O4	8.2(6)	C2	C41	C42	C43	-171.1(4)
C46	C41	C42	O4	-179.1(3)	C46	C41	C42	C43	1.6(6)
C2	C41	C46	C45	172.6(4)	C42	C41	C46	C45	-0.9(6)
O4	C42	C43	C44	179.5(4)	C41	C42	C43	C44	-1.1(6)
C42	C43	C44	C45	-0.1(6)	C43	C44	C45	C46	0.7(7)
C44	C45	C46	C41	-0.2(7)					

Primed atoms are related to unprimed ones via the crystallographic inversion center at (0, 0, 0).

Appendix F: Chapter 3, Section 3.3.4, page 151.

Crystallographic details for compound 4, SDL Code: JMS9811.

Compound 4: $[\{C_2(C_6H_4O)_4\}(Al)(AlClEt\{OC_4H_8\})]_2 \cdot 2PhMe$

Formula: $C_{78}H_{74}Al_4Cl_2O_{10}$ ($C_{64}H_{58}Al_4Cl_2O_{10} \cdot 2C_7H_8$)

Crystallographic Experimental Details

A. Crystal Data

formula	$C_{78}H_{74}Al_4Cl_2O_{10}$
formula weight	1350.19
crystal dimensions (mm)	0.27 × 0.23 × 0.21
crystal system	triclinic
space group	$P\bar{1}$ (No. 2)
unit cell parameters[a]	
a (Å)	12.1840 (13)
b (Å)	12.891 (2)
c (Å)	13.5568 (13)
α (deg)	66.485 (9)
β (deg)	87.343 (8)
γ (deg)	62.822 (9)
V (Å^3)	1712.6 (3)
Z	1
ρ_{calcd} (g cm^{-3})	1.309
μ (mm^{-1})	0.207

B. Data Collection and Refinement Conditions

diffractometer	Siemens P4/RA[b]
radiation (λ [Å])	graphite-monochromated Mo Kα (0.71073)
temperature (°C)	–60
scan type	θ–2θ
data collection 2θ limit (deg)	50.0
total data collected	5815 ($-14 \le h \le 0$, $-13 \le k \le 12$, $-16 \le l \le 16$)
independent reflections	5519
number of observations (*NO*)	3334 ($F_o^2 \ge 2\sigma(F_o^2)$)
structure solution method	direct methods/fragment search (*DIRDIF–96*[c])
refinement method	full-matrix least-squares on F^2 (*SHELXL–93*[d])
absorption correction method	semiempirical (ψ scans)
range of transmission factors	0.9930–0.9478

Crystallographic Experimental Details (continued)

data/restraints/parameters	5518 [$F_o^2 \geq -3\sigma(F_o^2)$] / 7[e] / 422
goodness-of-fit (S)[f]	1.028 [$F_o^2 \geq -3\sigma(F_o^2)$]
final R indices[g]	
$F_o^2 > 2\sigma(F_o^2)$	$R_1 = 0.0783$, $wR_2 = 0.1770$
all data	$R_1 = 0.1385$, $wR_2 = 0.2168$
largest difference peak and hole	1.202 and –0.503 e Å^{-3}

[a] Obtained from least-squares refinement of 44 reflections with 22.0° < 2θ < 24.8°.

[b] Programs for diffractometer operation, data collection, data reduction and absorption correction were those supplied by Siemens.

[c] Beurskens, P. T.; Beurskens, G.; Bosman, W.P.; de Gelder, R.; Garcia Granda, S.; Gould, R. O.; Israel, R; Smits, J M.M. (1996). The *DIRDIF-96* program system. Crystallography Laboratory, University of Nijmegen, The Netherlands.

[d] Sheldrick, G. M. *SHELXL-93*. Program for crystal structure determination. University of Göttingen, Germany, 1993. Refinement on F_o^2 for all reflections except for 1 having $F_o^2 < -3\sigma(F_o^2)$. Weighted R-factors wR_2 and all goodnesses of fit S are based on F_o^2; conventional R-factors R_1 are based on F_o, with F_o set to zero for negative F_o^2. The observed criterion of $F_o^2 > 2\sigma(F_o^2)$ is used only for calculating R_1, and is not relevant to the choice of reflections for refinement. R-factors based on F_o^2 are statistically about twice as large as those based on F_o, and R-factors based on ALL data will be even larger.

[e] All carbon-carbon bond distances within one of the disordered solvent toluene molecules were fixed at 1.40 Å.

[f] $S = [\Sigma w(F_o^2 - F_c^2)^2/(n - p)]^{1/2}$ (n = number of data; p = number of parameters varied; $w = [\sigma^2(F_o^2) + (0.0817P)^2 + 5.0698P]^{-1}$ where $P = [\mathrm{Max}(F_o^2, 0) + 2F_c^2]/3$).

[g] $R_1 = \Sigma||F_o| - |F_c||/\Sigma|F_o|$; $wR_2 = [\Sigma w(F_o^2 - F_c^2)^2/\Sigma w(F_o^4)]^{1/2}$.

Selected Interatomic Distances (Å)

(a) within $[\{C_2(C_6H_4O)_4\}(Al)(AlClEt\{OC_4H_8\})]_2$

Atom1	Atom2	Distance
Cl	Al2	2.167(2)
Al1	O1	1.740(4)
Al1	O2'	1.803(4)
Al1	O3	1.859(4)
Al1	O3'	1.894(4)
Al1	O4	1.923(4)
Al2	O2'	2.082(4)
Al2	O4	1.842(4)
Al2	O5	2.009(4)
Al2	C3	1.957(6)
O1	C12	1.361(7)
O2	C22	1.394(7)
O3	C32	1.399(6)
O4	C42	1.390(6)
O5	C51	1.459(7)
O5	C54	1.443(7)
C1	C2	1.349(8)
C1	C11	1.479(8)
C1	C21	1.500(7)
C2	C31	1.493(8)
C2	C41	1.491(7)
C3	C4	1.455(11)
C11	C12	1.417(8)
C11	C16	1.397(8)
C12	C13	1.387(8)
C13	C14	1.378(9)
C14	C15	1.386(9)
C15	C16	1.379(9)
C21	C22	1.407(8)
C21	C26	1.391(8)
C22	C23	1.392(8)
C23	C24	1.372(9)
C24	C25	1.377(9)
C25	C26	1.380(9)
C31	C32	1.394(8)
C31	C36	1.385(8)
C32	C33	1.391(8)
C33	C34	1.390(8)
C34	C35	1.374(9)
C35	C36	1.393(9)
C41	C42	1.393(8)
C41	C46	1.386(8)
C42	C43	1.380(8)
C43	C44	1.386(8)
C44	C45	1.377(9)
C45	C46	1.401(8)
C51	C52	1.487(9)
C52	C53	1.500(12)
C53	C54	1.448(11)

Primed atoms are related to unprimed ones via the inversion center at (0, 0, $^{1}/2$).

Selected Interatomic Distances (continued)

(b) within the solvent toluene molecules

Atom1	Atom2	Distance	Atom1	Atom2	Distance
C90	C91	1.39(2)	C91	C92"	1.32(2)
C90"	C93	1.38(3)	C92	C93	1.36(3)
C90"	C94	1.55(2)	C92"	C94	1.33(2)
C91	C92	1.57(2)			

Double-primed atoms are related to unprimed ones via the inversion center at ($^1/2$, 0, 0).

Selected Interatomic Angles (deg)

(a) within $[\{C_2(C_6H_4O)_4\}(Al)(AlClEt\{OC_4H_8\})]_2$

Atom1	Atom2	Atom3	Angle	Atom1	Atom2	Atom3	Angle
O1	Al1	O2'	121.0(2)	Al2	C3	C4	120.9(6)
O1	Al1	O3	131.6(2)	C1	C11	C12	120.9(5)
O1	Al1	O3'	97.1(2)	C1	C11	C16	120.6(5)
O1	Al1	O4	93.5(2)	C12	C11	C16	118.4(5)
O2'	Al1	O3	107.3(2)	O1	C12	C11	122.4(5)
O2'	Al1	O3'	98.3(2)	O1	C12	C13	118.7(5)
O2'	Al1	O4	78.3(2)	C11	C12	C13	118.8(6)
O3	Al1	O3'	77.3(2)	C12	C13	C14	121.2(6)
O3	Al1	O4	93.7(2)	C13	C14	C15	120.7(6)
O3'	Al1	O4	169.1(2)	C14	C15	C16	118.7(6)
Cl	Al2	O2'	99.95(13)	C11	C16	C15	122.0(6)
Cl	Al2	O4	114.7(2)	C1	C21	C22	128.0(5)
Cl	Al2	O5	91.54(14)	C1	C21	C26	114.7(5)
Cl	Al2	C3	117.5(2)	C22	C21	C26	116.8(5)
O2'	Al2	O4	73.4(2)	O2	C22	C21	122.9(5)
O2'	Al2	O5	160.7(2)	O2	C22	C23	117.0(5)
O2'	Al2	C3	92.9(2)	C21	C22	C23	120.1(5)
O4	Al2	O5	87.7(2)	C22	C23	C24	120.8(6)
O4	Al2	C3	127.6(2)	C23	C24	C25	120.3(6)

Selected Interatomic Angles (continued)

(a) within $[\{C_2(C_6H_4O)_4\}(Al)(AlClEt\{OC_4H_8\})]_2$

Atom1	Atom2	Atom3	Angle	Atom1	Atom2	Atom3	Angle
O5	Al2	C3	95.5(2)	C24	C25	C26	118.7(6)
Al1	O1	C12	137.0(4)	C21	C26	C25	123.1(6)
Al1'	O2	Al2'	100.2(2)	C2	C31	C32	116.9(5)
Al1'	O2	C22	137.1(3)	C2	C31	C36	124.3(5)
Al2'	O2	C22	122.7(3)	C32	C31	C36	118.8(6)
Al1	O3	Al1'	102.7(2)	O3	C32	C31	119.0(5)
Al1	O3	C32	126.7(3)	O3	C32	C33	120.2(5)
Al1'	O3	C32	128.6(3)	C31	C32	C33	120.8(5)
Al1	O4	Al2	104.9(2)	C32	C33	C34	119.4(6)
Al1	O4	C42	119.3(3)	C33	C34	C35	120.3(6)
Al2	O4	C42	131.8(3)	C34	C35	C36	120.1(6)
Al2	O5	C51	119.5(3)	C31	C36	C35	120.6(6)
Al2	O5	C54	129.9(4)	C2	C41	C42	120.8(5)
C51	O5	C54	109.0(5)	C2	C41	C46	120.4(5)
C2	C1	C11	122.3(5)	C42	C41	C46	118.7(5)
C2	C1	C21	115.9(5)	O4	C42	C41	117.2(5)
C11	C1	C21	121.3(5)	O4	C42	C43	121.8(5)
C1	C2	C31	120.2(5)	C41	C42	C43	121.0(5)
C1	C2	C41	124.9(5)	C42	C43	C44	119.4(6)
C43	C44	C45	121.1(6)	C31	C2	C41	114.8(5)
C44	C45	C46	118.9(6)	C51	C52	C53	103.7(6)
C41	C46	C45	120.9(6)	C52	C53	C54	105.0(7)
O5	C51	C52	105.3(5)	O5	C54	C53	107.0(6)

Primed atoms are related to unprimed ones via the inversion center at (0, 0, $^{1}/2$).

Selected Interatomic Angles (continued)

(b) within the solvent toluene molecules

Atom1	Atom2	Atom3	Angle	Atom1	Atom2	Atom3	Angle
C90	C91	C92	113.6(14)	C95	C96	C97	140.6(11)
C90	C91	C92"	133.2(19)	C95	C96	C97*	92.2(14)
C92	C91	C92"	113.0(15)	C97	C96	C97*	126.5(6)
C91	C92	C93	115.7(14)	C96	C97	C98	127.7(13)
C90"	C93	C92	130.4(19)	C95*	C98	C97	104.8(12)
C90"	C94	C92"	118.4(13)	C95*	C99	C97*	140.7(11)

Double-primed atoms are related to unprimed ones via the inversion center at (^{1}/2, 0, 0). Starred atoms are related to unprimed ones via the inversion center at (^{1}/2, ^{1}/2, 0).

Torsional Angles (deg)

Atom1	Atom2	Atom3	Atom4	Angle	Atom1	Atom2	Atom3	Atom4	Angle
O2'	Al1	O1	C12	-163.5(5)	Al1	O1	C12	C11	-33.0(8)
O3	Al1	O1	C12	19.9(6)	Al1	O1	C12	C13	145.5(5)
O3'	Al1	O1	C12	-59.3(5)	Al1'	O2	C22	C21	-70.8(7)
O4	Al1	O1	C12	118.1(5)	Al1'	O2	C22	C23	110.3(6)
O1	Al1	O3	Al1'	-88.2(3)	Al2'	O2	C22	C21	110.2(5)
O1	Al1	O3	C32	76.9(5)	Al2'	O2	C22	C23	-68.6(6)
O2'	Al1	O3	Al1	94.9(2)	Al1	O3	C32	C31	-45.5(6)
O2'	Al1	O3	C32	-100.0(4)	Al1	O3	C32	C33	133.7(4)
O3'	Al1	O3	Al1'	-0.002(1)	Al1'	O3	C32	C31	115.8(5)
O3'	Al1	O3	C32	165.1(5)	Al1'	O3	C32	C33	-65.0(6)
O4	Al1	O3	C32	-21.2(4)	Al1	O4	C42	C41	-48.0(6)
O4	Al1	O3	Al1'	173.7(2)	Al1	O4	C42	C43	129.3(5)
O1	Al1	O4	Al2	135.9(2)	Al2	O4	C42	C41	158.1(4)
O1	Al1	O4	C42	-24.3(4)	Al2	O4	C42	C43	-24.6(8)
O2'	Al1	O4	Al2	15.0(2)	Al2	O5	C51	C52	-154.9(5)
O2'	Al1	O4	C42	-145.2(4)	C54	O5	C51	C52	11.8(8)
O3	Al1	O4	Al2	-91.9(2)	Al2	O5	C54	C53	173.5(7)

Torsional Angles (continued)

Atom1	Atom2	Atom3	Atom4	Angle	Atom1	Atom2	Atom3	Atom4	Angle
O3	Al1	O4	C42	107.9(4)	C51	O5	C54	C53	8.5(10)
O3'	Al1	O4	Al2	-57.7(10)	C11	C1	C2	C31	163.0(5)
O3'	Al1	O4	C42	142.1(9)	C11	C1	C2	C41	-14.4(9)
Cl	Al2	O4	Al1	-106.7(2)	C21	C1	C2	C31	-24.5(8)
Cl	Al2	O4	C42	49.9(5)	C21	C1	C2	C41	158.0(5)
O2'	Al2	O4	Al1	-13.2(2)	C2	C1	C11	C12	-47.0(8)
O2'	Al2	O4	C42	143.5(5)	C2	C1	C11	C16	136.0(6)
O5	Al2	O4	Al1	162.6(2)	C21	C1	C11	C12	140.9(5)
O5	Al2	O4	C42	-40.7(5)	C21	C1	C11	C16	-36.0(8)
C3	Al2	O4	Al1	67.4(3)	C2	C1	C21	C22	96.8(7)
C3	Al2	O4	C42	-136.0(5)	C2	C1	C21	C26	-74.7(7)
Cl	Al2	O5	C51	-172.9(4)	C11	C1	C21	C22	-90.7(7)
Cl	Al2	O5	C54	23.6(6)	C11	C1	C21	C26	97.9(7)
O2'	Al2	O5	C51	-46.1(8)	C1	C2	C31	C32	-68.6(7)
O2'	Al2	O5	C54	150.4(7)	C1	C2	C31	C36	113.9(6)
O4	Al2	O5	C51	-58.3(5)	C41	C2	C31	C32	109.1(6)
O4	Al2	O5	C54	138.2(6)	C41	C2	C31	C36	-68.4(7)
C3	Al2	O5	C51	69.3(5)	C1	C2	C41	C42	117.5(6)
C3	Al2	O5	C54	-94.2(6)	C1	C2	C41	C46	-65.9(8)
Cl	Al2	C3	C4	-48.7(9)	C31	C2	C41	C42	-60.1(7)
O2'	Al2	C3	C4	-151.5(8)	C31	C2	C41	C46	116.6(6)
O4	Al2	C3	C4	137.4(8)	C1	C11	C12	O1	-1.7(8)
O5	Al2	C3	C4	46.0(9)	C1	C11	C12	C13	179.9(5)
C16	C11	C12	O1	175.3(5)	O3	C32	C33	C34	-178.8(5)
C16	C11	C12	C13	-3.1(8)	C31	C32	C33	C34	0.3(8)
C1	C11	C16	C15	179.8(5)	C32	C33	C34	C35	0.0(9)
C12	C11	C16	C15	2.8(8)	C33	C34	C35	C36	0.7(9)
O1	C12	C13	C14	-176.5(5)	C34	C35	C36	C31	-1.8(9)
C11	C12	C13	C14	2.0(9)	C2	C41	C42	O4	-6.8(8)
C12	C13	C14	C15	-0.4(10)	C2	C41	C42	C43	175.8(5)
C13	C14	C15	C16	0.0(9)	C46	C41	C42	O4	176.5(5)
C14	C15	C16	C11	-1.2(9)	C46	C41	C42	C43	-0.9(8)
C1	C21	C22	O2	13.0(9)	C2	C41	C46	C45	-174.1(5)
C1	C21	C22	C23	-168.2(6)	C42	C41	C46	C45	2.6(9)
C26	C21	C22	O2	-175.8(5)	O4	C42	C43	C44	-178.6(5)
C26	C21	C22	C23	3.1(8)	C41	C42	C43	C44	-1.4(9)
C1	C21	C26	C25	172.6(6)	C42	C43	C44	C45	2.0(10)

Torsional Angles (continued)

Atom1	Atom2	Atom3	Atom4	Angle	Atom1	Atom2	Atom3	Atom4	Angle
C22	C21	C26	C25	0.2(9)	C43	C44	C45	C46	-0.3(10)
O2	C22	C23	C24	175.6(6)	C44	C45	C46	C41	-2.1(9)
C21	C22	C23	C24	-3.3(9)	O5	C51	C52	C53	-26.6(9)
C22	C23	C24	C25	0.2(11)	C51	C52	C53	C54	32.1(11)
C23	C24	C25	C26	3.0(11)	C52	C53	C54	O5	-25.2(12)
C24	C25	C26	C21	-3.2(11)	C90	C91	C92	C93	-179.1(13)
C2	C31	C32	O3	0.1(7)	C92"	C91	C92	C93	5.3(16)
C2	C31	C32	C33	-179.0(5)	C91	C92	C93	C90"	-7.2(25)
C36	C31	C32	O3	177.7(5)	C95	C96	C97	C98	-172.9(32)
C36	C31	C32	C33	-1.4(8)	C97*	C96	C97	C98	18.6(38)
C2	C31	C36	C35	179.6(5)	C96	C97	C98	C95*	-8.1(21)
C32	C31	C36	C35	2.1(8)					

Primed atoms are related to unprimed ones via the inversion center at (0, 0, $^{1}/2$).

Double-primed atoms are related to unprimed ones via the inversion center at ($^{1}/2$, 0, 0).

Starred atoms are related to unprimed ones via the inversion center at ($^{1}/2$, $^{1}/2$, 0).

Appendix G: Chapter 4, Section 4.3.1, page 209

Crystallographic details for compound 1, XCL Code: JMS9926.

Compound: $[Mg_5Cl_2(THF)_4\{C_2(C_6H_4\text{-}2\text{-}O\text{-})_4\}_2]\cdot PhMe\cdot 0.5THF$

Formula: $C_{77}H_{76}Cl_2Mg_5O_{12.5}$ ($C_{68}H_{64}Cl_2Mg_5O_{12}\cdot C_7H_8\cdot 0.5C_4H_8O$)

Crystallographic Experimental Details

A. Crystal Data

formula	$C_{77}H_{76}Cl_2Mg_5O_{12.5}$
formula weight	1393.83
crystal dimensions (mm)	0.19 × 0.10 × 0.09
crystal system	orthorhombic
space group	$Pna2_1$ (No. 33)
unit cell parameters[a]	
a (Å)	24.7812 (16)
b (Å)	20.7209 (16)
c (Å)	14.8495 (11)
V (Å^3)	7625.1 (10)
Z	4
ρ_{calcd} (g cm^{-3})	1.214
μ (mm^{-1})	0.185

B. Data Collection and Refinement Conditions

diffractometer	Bruker P4/RA/SMART 1000 CCD[b]
radiation (λ [Å])	graphite-monochromated Mo Kα (0.71073)
temperature (°C)	–80
scan type	ϕ rotations (0.3°) / ω scans (0.3°) (30 s exposures)
data collection 2θ limit (deg)	52.80
total data collected	42345 ($-27 \le h \le 31$, $-25 \le k \le 25$, $-17 \le l \le 18$)
independent reflections	15313
number of observations (*NO*)	4463 [$F_o^2 \ge 2\sigma(F_o^2)$]
structure solution method	direct methods/fragment search (*DIRDIF–96*[c])
refinement method	full-matrix least-squares on F^2 (*SHELXL–93*[d])
absorption correction method	*SADABS*
range of transmission factors	0.9803–0.7620
data/restraints/parameters	15313 [$F_o^2 \ge -3\sigma(F_o^2)$] / 10[e] / 784

Crystallographic Experimental Details (continued)

Flack absolute structure parameter[f]	0.1 (3)
goodness-of-fit (*S*)[g]	0.887 [$F_o^2 \ge -3\sigma(F_o^2)$]
final *R* indices[h]	
R_1 [$F_o^2 \ge 2\sigma(F_o^2)$]	0.0864
wR_2 [$F_o^2 \ge -3\sigma(F_o^2)$]	0.2828
largest difference peak and hole	0.811 and –0.382 e Å^{-3}

[a] Obtained from least-squares refinement of 5270 centered reflections.

[b] Programs for diffractometer operation, data collection, data reduction and absorption correction were those supplied by Bruker.

[c] Beurskens, P. T.; Beurskens, G.; Bosman, W. P.; de Gelder, R.; Garcia Granda, S.; Gould, R. O.; Israel, R.; Smits, J. M. M. (1996). The *DIRDIF-96* program system. Crystallography Laboratory, University of Nijmegen, The Netherlands.

[d] Sheldrick, G. M. *SHELXL-93*. Program for crystal structure determination. University of Göttingen, Germany, 1993. Refinement on F_o^2 for all reflections (all of these having $F_o^2 \ge -3\sigma(F_o^2)$). Weighted *R*-factors wR_2 and all goodnesses of fit *S* are based on F_o^2; conventional *R*-factors R_1 are based on F_o, with F_o set to zero for negative F_o^2. The observed criterion of $F_o^2 > 2\sigma(F_o^2)$ is used only for calculating R_1, and is not relevant to the choice of reflections for refinement. *R*-factors based on F_o^2 are statistically about twice as large as those based on F_o, and *R*-factors based on ALL data will be even larger.

[e] An idealized geometry was imposed upon the solvent THF molecule by applying the following constraints: d(O20S–C21S) = d(O20S–C24S) = 1.45 Å; d(C21S–C22S) = d(C22S–C23S) = d(C23S–C24S) = 1.50 Å; d(O20S···C22S) = d(O20S···C23S) = 2.42 Å; d(C21S···C24S) = 2.35 Å; d(C21S···C23S) = d(C22S···C24S) = 2.46 Å.

[f] Flack, H. D. *Acta Crystallogr.* **1983**, *A39*, 876–881. The Flack parameter will refine to a value near zero if the structure is in the correct configuration and will refine to a value near one for the inverted configuration.

[g] $S = [\Sigma w(F_o^2 - F_c^2)^2/(n-p)]^{1/2}$ (n = number of data; p = number of parameters varied; $w = [\sigma^2(F_o^2) + (0.1069P)^2]^{-1}$ where $P = [\mathrm{Max}(F_o^2, 0) + 2F_c^2]/3$).

[h] $R_1 = \Sigma||F_o| - |F_c||/\Sigma|F_o|$; $wR_2 = [\Sigma w(F_o^2 - F_c^2)^2/\Sigma w(F_o^4)]^{1/2}$.

Selected Interatomic Distances (Å)

(a) within $[Mg_5Cl_2(THF)_4\{C_2(C_6H_4\text{-}2\text{-}O\text{-})_4\}_2]$

Atom1	Atom2	Distance	Atom1	Atom2	Distance
Cl4	Mg4	2.266(7)	Cl5	Mg5	2.281(7)
Mg1	O1	2.090(12)	Mg1	O2	2.120(11)
Mg1	O3	1.973(12)	Mg1	O4	2.109(11)
Mg1	O8	1.989(12)	Mg1	C1	2.530(17)
Mg1	C2	2.514(17)	Mg2	O1	2.020(12)
Mg2	O5	1.994(11)	Mg2	O6	1.994(11)
Mg2	O8	2.241(12)	Mg2	O11	2.069(13)
Mg3	O1	2.317(11)	Mg3	O2	2.025(13)
Mg3	O5	2.087(12)	Mg3	O8	2.205(11)
Mg3	O9	2.039(11)	Mg3	O10	2.070(11)
Mg4	O3	1.993(13)	Mg4	O7	1.952(13)
Mg4	O12	2.031(13)	Mg5	O4	1.980(12)
Mg5	O6	1.932(13)	Mg5	O7	1.982(12)
O1	C12	1.351(17)	O2	C22	1.346(19)
O3	C32	1.34(2)	O4	C42	1.371(19)
O5	C52	1.36(2)	O6	C62	1.392(19)
O7	C72	1.38(2)	O8	C82	1.352(17)
O9	C91	1.424(19)	O9	C94	1.48(2)
O10	C101	1.42(2)	O10	C104	1.44(2)
O11	C111	1.43(2)	O11	C114	1.44(2)
O12	C121	1.46(2)	O12	C124	1.46(3)
C1	C2	1.34(2)	C1	C11	1.49(2)
C1	C21	1.46(2)	C2	C31	1.45(2)
C2	C41	1.49(2)	C3	C4	1.33(2)
C3	C51	1.49(2)	C3	C61	1.47(2)
C4	C71	1.50(2)	C4	C81	1.50(2)
C11	C12	1.46(2)	C11	C16	1.38(2)
C12	C13	1.34(2)	C13	C14	1.43(2)
C14	C15	1.40(2)	C15	C16	1.37(3)
C21	C22	1.38(2)	C21	C26	1.40(2)
C22	C23	1.41(2)	C23	C24	1.40(3)
C24	C25	1.34(3)	C25	C26	1.40(3)
C31	C32	1.45(2)	C31	C36	1.40(2)
C32	C33	1.36(2)	C33	C34	1.39(3)
C34	C35	1.39(3)	C35	C36	1.43(3)

Selected Interatomic Distances (continued)

Atom1	Atom2	Distance	Atom1	Atom2	Distance
C41	C42	1.38(2)	C41	C46	1.42(2)
C42	C43	1.44(2)	C43	C44	1.38(2)
C44	C45	1.45(3)	C45	C46	1.39(3)
C51	C52	1.42(2)	C51	C56	1.35(2)
C52	C53	1.42(2)	C53	C54	1.34(2)
C54	C55	1.42(2)	C55	C56	1.38(2)
C61	C62	1.42(2)	C61	C66	1.39(2)
C62	C63	1.41(2)	C63	C64	1.37(2)
C64	C65	1.39(2)	C65	C66	1.44(2)
C71	C72	1.43(2)	C71	C76	1.37(2)
C72	C73	1.40(2)	C73	C74	1.35(2)
C74	C75	1.37(2)	C75	C76	1.39(2)
C81	C82	1.41(2)	C81	C86	1.38(2)
C82	C83	1.38(2)	C83	C84	1.43(2)
C84	C85	1.42(2)	C85	C86	1.39(2)
C91	C92	1.52(2)	C92	C93	1.56(2)
C93	C94	1.51(2)	C101	C102	1.56(2)
C102	C103	1.51(2)	C103	C104	1.43(3)
C111	C112	1.50(3)	C112	C113	1.40(3)
C113	C114	1.46(3)	C121	C122	1.48(3)
C122	C123	1.53(3)	C123	C124	1.34(4)

(b) within the solvent toluene molecule

Atom1	Atom2	Distance	Atom1	Atom2	Distance
C10S	C11S	1.56(3)	C11S	C12S	1.38(3)
C11S	C16S	1.41(3)	C12S	C13S	1.42(3)
C13S	C14S	1.30(3)	C14S	C15S	1.34(3)
C15S	C16S	1.49(3)			

Selected Interatomic Angles (deg)

(a) within $[Mg_5Cl_2(THF)_4\{C_2(C_6H_4\text{-}2\text{-}O\text{-})_4\}_2]$

Atom1	Atom2	Atom3	Angle	Atom1	Atom2	Atom3	Angle
O1	Mg1	O2	80.9(4)	O1	Mg1	O3	172.6(5)
O1	Mg1	O4	85.2(5)	O1	Mg1	O8	77.6(5)
O1	Mg1	C1	78.5(6)	O1	Mg1	C2	95.6(5)
O2	Mg1	O3	105.5(5)	O2	Mg1	O4	164.5(5)
O2	Mg1	O8	82.3(5)	O2	Mg1	C1	71.1(5)
O2	Mg1	C2	98.9(5)	O3	Mg1	O4	88.0(5)
O3	Mg1	O8	106.7(5)	O3	Mg1	C1	99.8(6)
O3	Mg1	C2	79.8(5)	O4	Mg1	O8	101.4(5)
O4	Mg1	C1	99.5(5)	O4	Mg1	C2	75.6(5)
O8	Mg1	C1	146.6(6)	O8	Mg1	C2	172.9(6)
C1	Mg1	C2	30.8(5)	O1	Mg2	O5	90.6(5)
O1	Mg2	O6	125.8(5)	O1	Mg2	O8	73.6(4)
O1	Mg2	O11	99.3(5)	O5	Mg2	O6	143.1(5)
O5	Mg2	O8	80.1(5)	O5	Mg2	O11	90.7(5)
O6	Mg2	O8	102.5(5)	O6	Mg2	O11	89.3(5)
O8	Mg2	O11	168.1(5)	O1	Mg3	O2	77.6(4)
O1	Mg3	O5	80.6(4)	O1	Mg3	O8	68.9(4)
O1	Mg3	O9	92.5(5)	O1	Mg3	O10	175.1(5)
O2	Mg3	O5	153.6(5)	O2	Mg3	O8	79.4(5)
O2	Mg3	O9	99.3(5)	O2	Mg3	O10	102.8(5)
O5	Mg3	O8	79.0(4)	O5	Mg3	O9	96.3(5)
O5	Mg3	O10	97.8(5)	O8	Mg3	O9	161.2(5)
O8	Mg3	O10	106.3(5)	O9	Mg3	O10	92.3(5)
Cl4	Mg4	O3	122.1(4)	Cl4	Mg4	O7	116.2(5)
Cl4	Mg4	O12	102.9(4)	O3	Mg4	O7	110.5(5)
O3	Mg4	O12	101.6(5)	O7	Mg4	O12	99.0(5)
Cl5	Mg5	O4	123.0(4)	Cl5	Mg5	O6	117.9(4)
Cl5	Mg5	O7	111.7(4)	O4	Mg5	O6	97.4(5)
O4	Mg5	O7	97.0(5)	O6	Mg5	O7	106.9(5)
Mg1	O1	Mg2	96.6(5)	Mg1	O1	Mg3	82.8(4)
Mg1	O1	C12	119.9(11)	Mg2	O1	Mg3	83.2(4)
Mg2	O1	C12	140.3(11)	Mg3	O1	C12	114.4(9)
Mg1	O2	Mg3	89.5(5)	Mg1	O2	C22	117.3(10)
Mg3	O2	C22	144.2(11)	Mg1	O3	Mg4	115.4(6)

Selected Interatomic Angles (continued)

Atom1	Atom2	Atom3	Angle	Atom1	Atom2	Atom3	Angle
Mg1	O3	C32	118.4(11)	Mg4	O3	C32	117.5(11)
Mg1	O4	Mg5	121.0(6)	Mg1	O4	C42	115.3(10)
Mg5	O4	C42	122.9(10)	Mg2	O5	Mg3	90.0(5)
Mg2	O5	C52	122.9(10)	Mg3	O5	C52	124.0(10)
Mg2	O6	Mg5	114.1(6)	Mg2	O6	C62	108.0(9)
Mg5	O6	C62	134.8(9)	Mg4	O7	Mg5	119.4(6)
Mg4	O7	C72	131.8(10)	Mg5	O7	C72	104.1(9)
Mg1	O8	Mg2	92.8(5)	Mg1	O8	Mg3	88.0(4)
Mg1	O8	C82	125.1(10)	Mg2	O8	Mg3	81.0(4)
Mg2	O8	C82	138.5(10)	Mg3	O8	C82	113.1(9)
Mg3	O9	C91	125.9(10)	Mg3	O9	C94	122.9(10)
C91	O9	C94	111.1(12)	Mg3	O10	C101	132.3(10)
Mg3	O10	C104	119.5(11)	C101	O10	C104	107.9(13)
Mg2	O11	C111	125.3(11)	Mg2	O11	C114	123.2(12)
C111	O11	C114	111.0(15)	Mg4	O12	C121	134.0(11)
Mg4	O12	C124	121.8(13)	C121	O12	C124	104.1(15)
Mg1	C1	C2	74.0(10)	Mg1	C1	C11	98.9(12)
Mg1	C1	C21	99.6(11)	C2	C1	C11	121.2(15)
C2	C1	C21	124.3(17)	C11	C1	C21	114.5(15)
Mg1	C2	C1	75.3(11)	Mg1	C2	C31	97.1(11)
Mg1	C2	C41	99.3(11)	C1	C2	C31	121.4(16)
C1	C2	C41	121.0(16)	C31	C2	C41	117.6(15)
C4	C3	C51	120.8(16)	C4	C3	C61	119.5(16)
C51	C3	C61	119.3(15)	C3	C4	C71	124.4(16)
C3	C4	C81	124.7(15)	C71	C4	C81	110.8(14)
C1	C11	C12	124.2(16)	C1	C11	C16	118.2(17)
C12	C11	C16	117.6(17)	O1	C12	C11	118.2(15)
O1	C12	C13	121.0(16)	C11	C12	C13	120.7(15)
C12	C13	C14	120.1(17)	C13	C14	C15	119.0(17)
C14	C15	C16	120.6(18)	C11	C16	C15	121.9(19)
C1	C21	C22	118.6(16)	C1	C21	C26	121.8(18)
C22	C21	C26	119.5(17)	O2	C22	C21	118.4(15)
O2	C22	C23	119.8(17)	C21	C22	C23	121.5(17)
C22	C23	C24	117.5(18)	C23	C24	C25	121.4(18)
C24	C25	C26	122(2)	C21	C26	C25	118(2)
C2	C31	C32	123.2(16)	C2	C31	C36	118.0(19)
C32	C31	C36	118.7(18)	O3	C32	C31	119.7(15)

Selected Interatomic Angles (continued)

Atom1	Atom2	Atom3	Angle	Atom1	Atom2	Atom3	Angle
O3	C32	C33	120.2(18)	C31	C32	C33	120.0(19)
C32	C33	C34	121(2)	C33	C34	C35	120(2)
C34	C35	C36	120(2)	C31	C36	C35	120(2)
C2	C41	C42	121.9(16)	C2	C41	C46	118.8(17)
C42	C41	C46	119.1(18)	O4	C42	C41	120.2(16)
O4	C42	C43	119.3(16)	C41	C42	C43	120.4(17)
C42	C43	C44	122(2)	C43	C44	C45	117(2)
C44	C45	C46	122(2)	C41	C46	C45	120(2)
C3	C51	C52	122.2(15)	C3	C51	C56	115.9(16)
C52	C51	C56	121.7(16)	O5	C52	C51	123.7(15)
O5	C52	C53	119.0(16)	C51	C52	C53	117.2(16)
C52	C53	C54	121.0(17)	C53	C54	C55	120.3(17)
C54	C55	C56	120.0(17)	C51	C56	C55	119.7(17)
C3	C61	C62	120.7(16)	C3	C61	C66	122.8(16)
C62	C61	C66	116.4(17)	O6	C62	C61	119.0(15)
O6	C62	C63	118.9(16)	C61	C62	C63	122.0(17)
C62	C63	C64	118.9(17)	C63	C64	C65	122.3(18)
C64	C65	C66	117.5(19)	C61	C66	C65	122.6(18)
C4	C71	C72	122.0(15)	C4	C71	C76	119.4(17)
C72	C71	C76	117.8(16)	O7	C72	C71	121.0(14)
O7	C72	C73	121.8(18)	C71	C72	C73	117.2(18)
C72	C73	C74	123(2)	C73	C74	C75	121.1(18)
C74	C75	C76	117.5(17)	C71	C76	C75	123.8(18)
C4	C81	C82	118.7(15)	C4	C81	C86	119.4(16)
C82	C81	C86	121.6(16)	O8	C82	C81	121.5(15)
O8	C82	C83	118.8(15)	C81	C82	C83	119.7(16)
C82	C83	C84	119.0(17)	C83	C84	C85	120.5(17)
C84	C85	C86	119.2(17)	C81	C86	C85	119.9(18)
O9	C91	C92	106.4(15)	C91	C92	C93	102.7(14)
C92	C93	C94	102.8(16)	O9	C94	C93	104.7(16)
O10	C101	C102	105.1(14)	C101	C102	C103	103.3(16)
C102	C103	C104	107.3(17)	O10	C104	C103	106.0(17)
O11	C111	C112	102.1(18)	C111	C112	C113	108(3)
C112	C113	C114	105(3)	O11	C114	C113	104.4(19)
O12	C121	C122	105.0(18)	C121	C122	C123	102(2)
C122	C123	C124	109(3)	O12	C124	C123	108(3)

Selected Interatomic Angles (deg)

(b) within the solvent toluene molecule

Atom1	Atom2	Atom3	Angle	Atom1	Atom2	Atom3	Angle
C10S	C11S	C12S	124(3)	C10S	C11S	C16S	117(3)
C12S	C11S	C16S	119(3)	C11S	C12S	C13S	118(3)
C12S	C13S	C14S	122(3)	C13S	C14S	C15S	127(3)
C14S	C15S	C16S	114(3)	C11S	C16S	C15S	121(2)

Torsional Angles (deg)

Atom1	Atom2	Atom3	Atom4	Angle	Atom1	Atom2	Atom3	Atom4	Angle
O2	Mg1	O1	Mg2	119.1(5)	O2	Mg1	O1	Mg3	36.9(4)
O2	Mg1	O1	C12	-77.2(10)	O3	Mg1	O1	Mg2	-91(4)
O3	Mg1	O1	Mg3	-173(4)	O3	Mg1	O1	C12	73(4)
O4	Mg1	O1	Mg2	-67.7(5)	O4	Mg1	O1	Mg3	-149.9(4)
O4	Mg1	O1	C12	96.0(10)	O8	Mg1	O1	Mg2	35.1(4)
O8	Mg1	O1	Mg3	-47.1(4)	O8	Mg1	O1	C12	-161.2(11)
C1	Mg1	O1	Mg2	-168.4(5)	C1	Mg1	O1	Mg3	109.4(5)
C1	Mg1	O1	C12	-4.7(10)	C2	Mg1	O1	Mg2	-142.7(5)
C2	Mg1	O1	Mg3	135.1(5)	C2	Mg1	O1	C12	21.0(11)
O1	Mg1	O2	Mg3	-42.9(5)	O1	Mg1	O2	C22	112.3(12)
O3	Mg1	O2	Mg3	140.9(5)	O3	Mg1	O2	C22	-63.8(12)
O4	Mg1	O2	Mg3	-69(2)	O4	Mg1	O2	C22	86(2)
O8	Mg1	O2	Mg3	35.7(5)	O8	Mg1	O2	C22	-169.1(12)
C1	Mg1	O2	Mg3	-123.8(6)	C1	Mg1	O2	C22	31.4(12)
C2	Mg1	O2	Mg3	-137.2(5)	C2	Mg1	O2	C22	18.0(12)
O1	Mg1	O3	Mg4	83(4)	O1	Mg1	O3	C32	-64(4)
O2	Mg1	O3	Mg4	-128.6(6)	O2	Mg1	O3	C32	84.5(12)
O4	Mg1	O3	Mg4	59.1(6)	O4	Mg1	O3	C32	-87.7(11)
O8	Mg1	O3	Mg4	-42.1(7)	O8	Mg1	O3	C32	171.0(10)
C1	Mg1	O3	Mg4	158.4(6)	C1	Mg1	O3	C32	11.6(12)
C2	Mg1	O3	Mg4	134.9(7)	C2	Mg1	O3	C32	-12.0(11)
O1	Mg1	O4	Mg5	97.5(7)	O1	Mg1	O4	C42	-72.6(12)
O2	Mg1	O4	Mg5	123.4(19)	O2	Mg1	O4	C42	-47(3)
O3	Mg1	O4	Mg5	-85.5(7)	O3	Mg1	O4	C42	104.5(12)

Torsional Angles (continued)

Atom1	Atom2	Atom3	Atom4	Angle	Atom1	Atom2	Atom3	Atom4	Angle
O8	Mg1	O4	Mg5	21.1(8)	O8	Mg1	O4	C42	-148.9(11)
C1	Mg1	O4	Mg5	174.9(7)	C1	Mg1	O4	C42	4.9(13)
C2	Mg1	O4	Mg5	-165.5(8)	C2	Mg1	O4	C42	24.5(12)
O1	Mg1	O8	Mg2	-31.0(4)	O1	Mg1	O8	Mg3	49.8(4)
O1	Mg1	O8	C82	166.9(11)	O2	Mg1	O8	Mg2	-113.3(5)
O2	Mg1	O8	Mg3	-32.4(4)	O2	Mg1	O8	C82	84.6(11)
O3	Mg1	O8	Mg2	142.7(4)	O3	Mg1	O8	Mg3	-136.4(4)
O3	Mg1	O8	C82	-19.3(12)	O4	Mg1	O8	Mg2	51.4(5)
O4	Mg1	O8	Mg3	132.3(5)	O4	Mg1	O8	C82	-110.7(11)
C1	Mg1	O8	Mg2	-76.3(10)	C1	Mg1	O8	Mg3	4.6(11)
C1	Mg1	O8	C82	121.6(13)	C2	Mg1	O8	Mg2	-13(4)
C2	Mg1	O8	Mg3	68(4)	C2	Mg1	O8	C82	-175(4)
O1	Mg1	C1	C2	122.4(11)	O1	Mg1	C1	C11	2.4(9)
O1	Mg1	C1	C21	-114.5(11)	O2	Mg1	C1	C2	-153.4(12)
O2	Mg1	C1	C11	86.5(10)	O2	Mg1	C1	C21	-30.3(10)
O3	Mg1	C1	C2	-50.2(11)	O3	Mg1	C1	C11	-170.3(10)
O3	Mg1	C1	C21	72.8(12)	O4	Mg1	C1	C2	39.4(11)
O4	Mg1	C1	C11	-80.7(10)	O4	Mg1	C1	C21	162.5(11)
O8	Mg1	C1	C2	167.5(11)	O8	Mg1	C1	C11	47.5(15)
O8	Mg1	C1	C21	-69.4(16)	C2	Mg1	C1	C11	-120.1(15)
C2	Mg1	C1	C21	123.1(17)	O1	Mg1	C2	C1	-56.2(11)
O1	Mg1	C2	C31	-176.8(10)	O1	Mg1	C2	C41	63.6(10)
O2	Mg1	C2	C1	25.4(11)	O2	Mg1	C2	C31	-95.2(10)
O2	Mg1	C2	C41	145.1(10)	O3	Mg1	C2	C1	129.7(11)
O3	Mg1	C2	C31	9.1(10)	O3	Mg1	C2	C41	-110.5(10)
O4	Mg1	C2	C1	-139.7(11)	O4	Mg1	C2	C31	99.6(11)
O4	Mg1	C2	C41	-20.0(10)	O8	Mg1	C2	C1	-74(4)
O8	Mg1	C2	C31	166(4)	O8	Mg1	C2	C41	46(5)
C1	Mg1	C2	C31	-120.6(16)	C1	Mg1	C2	C41	119.7(16)
O5	Mg2	O1	Mg1	-110.8(5)	O5	Mg2	O1	Mg3	-29.0(4)
O5	Mg2	O1	C12	91.5(15)	O6	Mg2	O1	Mg1	62.5(7)
O6	Mg2	O1	Mg3	144.4(5)	O6	Mg2	O1	C12	-95.1(16)
O8	Mg2	O1	Mg1	-31.3(4)	O8	Mg2	O1	Mg3	50.5(4)
O8	Mg2	O1	C12	171.0(16)	O11	Mg2	O1	Mg1	158.4(5)
O11	Mg2	O1	Mg3	-119.7(5)	O11	Mg2	O1	C12	0.8(16)
O1	Mg2	O5	Mg3	32.3(5)	O1	Mg2	O5	C52	164.0(12)
O6	Mg2	O5	Mg3	-138.7(8)	O6	Mg2	O5	C52	-7.0(16)
O8	Mg2	O5	Mg3	-41.0(4)	O8	Mg2	O5	C52	90.7(12)
O11	Mg2	O5	Mg3	131.5(5)	O11	Mg2	O5	C52	-96.8(12)

Torsional Angles (continued)

Atom1	Atom2	Atom3	Atom4	Angle	Atom1	Atom2	Atom3	Atom4	Angle
O1	Mg2	O6	Mg5	-36.2(8)	O1	Mg2	O6	C62	160.7(9)
O5	Mg2	O6	Mg5	132.7(8)	O5	Mg2	O6	C62	-30.5(14)
O8	Mg2	O6	Mg5	42.5(7)	O8	Mg2	O6	C62	-120.7(10)
O11	Mg2	O6	Mg5	-137.1(6)	O11	Mg2	O6	C62	59.7(10)
O1	Mg2	O8	Mg1	32.9(4)	O1	Mg2	O8	Mg3	-54.6(4)
O1	Mg2	O8	C82	-169.4(14)	O5	Mg2	O8	Mg1	126.4(5)
O5	Mg2	O8	Mg3	38.9(4)	O5	Mg2	O8	C82	-75.9(14)
O6	Mg2	O8	Mg1	-91.1(5)	O6	Mg2	O8	Mg3	-178.6(5)
O6	Mg2	O8	C82	66.6(14)	O11	Mg2	O8	Mg1	87(3)
O11	Mg2	O8	Mg3	0(3)	O11	Mg2	O8	C82	-115(3)
O1	Mg2	O11	C111	-72.7(13)	O1	Mg2	O11	C114	116.0(13)
O5	Mg2	O11	C111	-163.4(13)	O5	Mg2	O11	C114	25.3(14)
O6	Mg2	O11	C111	53.5(13)	O6	Mg2	O11	C114	-117.8(13)
O8	Mg2	O11	C111	-125(3)	O8	Mg2	O11	C114	64(3)
O2	Mg3	O1	Mg1	-39.4(4)	O2	Mg3	O1	Mg2	-137.0(5)
O2	Mg3	O1	C12	80.2(11	O5	Mg3	O1	Mg1	125.6(4)
O5	Mg3	O1	Mg2	28.0(4)	O5	Mg3	O1	C12	-114.8(12)
O8	Mg3	O1	Mg1	43.8(4)	O8	Mg3	O1	Mg2	-53.8(4)
O8	Mg3	O1	C12	163.4(12)	O9	Mg3	O1	Mg1	-138.4(5)
O9	Mg3	O1	Mg2	124.0(5)	O9	Mg3	O1	C12	-18.8(12)
O10	Mg3	O1	Mg1	55(6)	O10	Mg3	O1	Mg2	-42(6)
O10	Mg3	O1	C12	175(6)	O1	Mg3	O2	Mg1	38.4(4)
O1	Mg3	O2	C22	-102.1(18)	O5	Mg3	O2	Mg1	3.5(13)
O5	Mg3	O2	C22	-137.0(18)	O8	Mg3	O2	Mg1	-32.1(4)
O8	Mg3	O2	C22	-172.6(19)	O9	Mg3	O2	Mg1	128.9(5)
O9	Mg3	O2	C22	-11.6(19)	O10	Mg3	O2	Mg1	-136.6(5)
O10	Mg3	O2	C22	82.9(19)	O1	Mg3	O5	Mg2	-28.1(4)
O1	Mg3	O5	C52	-159.0(12)	O2	Mg3	O5	Mg2	6.4(13)
O2	Mg3	O5	C52	-124.5(15)	O8	Mg3	O5	Mg2	42.0(4)
O8	Mg3	O5	C52	-88.9(12)	O9	Mg3	O5	Mg2	-119.6(5)
O9	Mg3	O5	C52	109.5(12)	O10	Mg3	O5	Mg2	147.2(5)
O10	Mg3	O5	C52	16.3(13)	O1	Mg3	O8	Mg1	-46.2(4)
O1	Mg3	O8	Mg2	47.0(4)	O1	Mg3	O8	C82	-173.8(12)
O2	Mg3	O8	Mg1	34.5(4)	O2	Mg3	O8	Mg2	127.7(5)
O2	Mg3	O8	C82	-93.1(11)	O5	Mg3	O8	Mg1	-130.3(5)
O5	Mg3	O8	Mg2	-37.1(4)	O5	Mg3	O8	C82	102.1(11)
O9	Mg3	O8	Mg1	-53.2(18)	O9	Mg3	O8	Mg2	40.0(18)
O9	Mg3	O8	C82	179.2(16)	O10	Mg3	O8	Mg1	134.8(5)
O10	Mg3	O8	Mg2	-132.0(5)	O10	Mg3	O8	C82	7.2(12)

Torsional Angles (continued)

Atom1	Atom2	Atom3	Atom4	Angle	Atom1	Atom2	Atom3	Atom4	Angle
O1	Mg3	O9	C91	82.2(12)	O1	Mg3	O9	C94	-95.1(12)
O2	Mg3	O9	C91	4.4(13)	O2	Mg3	O9	C94	-173.0(12)
O5	Mg3	O9	C91	163.0(12)	O5	Mg3	O9	C94	-14.4(13)
O8	Mg3	O9	C91	89(2)	O8	Mg3	O9	C94	-89(2)
O10	Mg3	O9	C91	-98.9(12)	O10	Mg3	O9	C94	83.7(12)
O1	Mg3	O10	C101	14(7)	O1	Mg3	O10	C104	-160(6)
O2	Mg3	O10	C101	108.0(15)	O2	Mg3	O10	C104	-66.1(14)
O5	Mg3	O10	C101	-55.3(16)	O5	Mg3	O10	C104	130.7(13)
O8	Mg3	O10	C101	25.5(17)	O8	Mg3	O10	C104	-148.5(13)
O9	Mg3	O10	C101	-151.9(15)	O9	Mg3	O10	C104	34.0(14)
Cl4	Mg4	O3	Mg1	133.5(5)	Cl4	Mg4	O3	C32	-79.3(12)
O7	Mg4	O3	Mg1	-8.7(8)	O7	Mg4	O3	C32	138.5(11)
O12	Mg4	O3	Mg1	-113.0(7)	O12	Mg4	O3	C32	34.2(12)
Cl4	Mg4	O7	Mg5	163.5(5)	Cl4	Mg4	O7	C72	11.9(15)
O3	Mg4	O7	Mg5	-51.8(8)	O3	Mg4	O7	C72	156.5(13)
O12	Mg4	O7	Mg5	54.3(7)	O12	Mg4	O7	C72	-97.4(14)
Cl4	Mg4	O12	C121	154.7(16)	Cl4	Mg4	O12	C124	-20.6(17)
O3	Mg4	O12	C121	27.6(17)	O3	Mg4	O12	C124	-147.8(16)
O7	Mg4	O12	C121	-85.6(16)	O7	Mg4	O12	C124	99.0(16)
Cl5	Mg5	O4	Mg1	159.6(5)	Cl5	Mg5	O4	C42	-31.1(14)
O6	Mg5	O4	Mg1	-70.1(7)	O6	Mg5	O4	C42	99.2(13)
O7	Mg5	O4	Mg1	38.1(7)	O7	Mg5	O4	C42	-152.7(12)
Cl5	Mg5	O6	Mg2	161.0(4)	Cl5	Mg5	O6	C62	-41.8(15)
O4	Mg5	O6	Mg2	27.4(6)	O4	Mg5	O6	C62	-175.4(14)
O7	Mg5	O6	Mg2	-72.3(7)	O7	Mg5	O6	C62	84.9(14)
Cl5	Mg5	O7	Mg4	-95.2(6)	Cl5	Mg5	O7	C72	63.4(10)
O4	Mg5	O7	Mg4	34.5(7)	O4	Mg5	O7	C72	-166.9(10)
O6	Mg5	O7	Mg4	134.5(6)	O6	Mg5	O7	C72	-66.9(11)
Mg1	O1	C12	C11	6.1(17)	Mg1	O1	C12	C13	-176.2(11)
Mg2	O1	C12	C11	160.3(11)	Mg2	O1	C12	C13	-22(2)
Mg3	O1	C12	C11	-89.7(14)	Mg3	O1	C12	C13	88.0(15)
Mg1	O2	C22	C21	-26(2)	Mg1	O2	C22	C23	147.6(13)
Mg3	O2	C22	C21	108.0(9)	Mg3	O2	C22	C23	-78(2)
Mg1	O3	C32	C31	13(2)	Mg1	O3	C32	C33	-167.7(13)
Mg4	O3	C32	C31	-133.5(14)	Mg4	O3	C32	C33	46.1(19)
Mg1	O4	C42	C41	-25(2)	Mg1	O4	C42	C43	154.2(13)
Mg5	O4	C42	C41	165.0(12)	Mg5	O4	C42	C43	-16(2)
Mg2	O5	C52	C51	-17(2)	Mg2	O5	C52	C53	167.2(11)
Mg3	O5	C52	C51	98.5(17)	Mg3	O5	C52	C53	-77.0(17)

Torsional Angles (continued)

Atom1	Atom2	Atom3	Atom4	Angle	Atom1	Atom2	Atom3	Atom4	Angle
Mg2	O6	C62	C61	49.1(16)	Mg2	O6	C62	C63	-128.6(13)
Mg5	O6	C62	C61	-109.1(16)	Mg5	O6	C62	C63	73.2(19)
Mg4	O7	C72	C71	-125.2(15)	Mg4	O7	C72	C73	58(2)
Mg5	O7	C72	C71	80.1(15)	Mg5	O7	C72	C73	-96.6(15)
Mg1	O8	C82	C81	138.7(13)	Mg1	O8	C82	C83	-39.1(19)
Mg2	O8	C82	C81	-14(2)	Mg2	O8	C82	C83	168.5(11)
Mg3	O8	C82	C81	-116.7(13)	Mg3	O8	C82	C83	65.5(17)
Mg3	O9	C91	C92	172.8(10)	C94	O9	C91	C92	-9.5(18)
Mg3	O9	C94	C93	164.6(11)	C91	O9	C94	C93	-13.1(19)
Mg3	O10	C101	C102	158.3(12)	C104	O10	C101	C102	-27(2)
Mg3	O10	C104	C103	-150.5(14)	C101	O10	C104	C103	34(2)
Mg2	O11	C111	C112	-173.4(15)	C114	O11	C111	C112	-1(2)
Mg2	O11	C114	C113	155.5(14)	C111	O11	C114	C113	-17(2)
Mg4	O12	C121	C122	-142.0(15)	C124	O12	C121	C122	34(2)
Mg4	O12	C124	C123	144(2)	C121	O12	C124	C123	-32(3)
Mg1	C1	C2	C31	89.4(16)	Mg1	C1	C2	C41	-92.1(15)
C11	C1	C2	Mg1	90.9(16)	C11	C1	C2	C31	-179.8(16)
C11	C1	C2	C41	-1(3)	C21	C1	C2	Mg1	-90.8(17)
C21	C1	C2	C31	-1(3)	C21	C1	C2	C41	177.0(16)
Mg1	C1	C11	C12	-0.3(17)	Mg1	C1	C11	C16	180.0(12)
C2	C1	C11	C12	-77(2)	C2	C1	C11	C16	103.3(19)
C21	C1	C11	C12	104.6(18)	C21	C1	C11	C16	-75(2)
Mg1	C1	C21	C22	30.0(17)	Mg1	C1	C21	C26	-153.5(15)
C2	C1	C21	C22	107(2)	C2	C1	C21	C26	-76(2)
C11	C1	C21	C22	-74(2)	C11	C1	C21	C26	102(2)
Mg1	C2	C31	C32	-6.2(18)	Mg1	C2	C31	C36	173.9(14)
C1	C2	C31	C32	-83(2)	C1	C2	C31	C36	97(2)
C41	C2	C31	C32	98(2)	C41	C2	C31	C36	-82(2)
Mg1	C2	C41	C42	15.6(18)	Mg1	C2	C41	C46	-158.6(15)
C1	C2	C41	C42	94(2)	C1	C2	C41	C46	-80(2)
C31	C2	C41	C42	-88(2)	C31	C2	C41	C46	98(2)
C51	C3	C4	C71	-154.6(16)	C51	C3	C4	C81	21(3)
C61	C3	C4	C71	18(3)	C61	C3	C4	C81	-166.6(16)
C4	C3	C51	C52	-103(2)	C4	C3	C51	C56	82(2)
C61	C3	C51	C52	84(2)	C61	C3	C51	C56	-91(2)
C4	C3	C61	C62	58(2)	C4	C3	C61	C66	-123.9(19)
C51	C3	C61	C62	-129.8(17)	C51	C3	C61	C66	49(2)
C3	C4	C71	C72	-129.5(19)	C3	C4	C71	C76	61(2)
C81	C4	C71	C72	55(2)	C81	C4	C71	C76	-115.4(17)

Torsional Angles (continued)

Atom1	Atom2	Atom3	Atom4	Angle	Atom1	Atom2	Atom3	Atom4	Angle
C3	C4	C81	C82	74(2)	C3	C4	C81	C86	-112.3(19)
C71	C4	C81	C82	-110.4(17)	C71	C4	C81	C86	64(2)
C1	C11	C12	O1	-3(2)	C1	C11	C12	C13	178.8(15)
C16	C11	C12	O1	176.3(13)	C16	C11	C12	C13	-1(2)
C1	C11	C16	C15	-179.7(16)	C12	C11	C16	C15	1(2)
O1	C12	C13	C14	-176.2(13)	C11	C12	C13	C14	1(2)
C12	C13	C14	C15	-1(2)	C13	C14	C15	C16	0(3)
C14	C15	C16	C11	0(3)	C1	C21	C22	O2	-9(2)
C1	C21	C22	C23	177.7(16)	C26	C21	C22	O2	174.9(16)
C26	C21	C22	C23	1(3)	C1	C21	C26	C25	-177.6(18)
C22	C21	C26	C25	-1(3)	O2	C22	C23	C24	-176.1(16)
C21	C22	C23	C24	-2(3)	C22	C23	C24	C25	4(3)
C23	C24	C25	C26	-4(3)	C24	C25	C26	C21	3(3)
C2	C31	C32	O3	-2(3)	C2	C31	C32	C33	178.2(16)
C36	C31	C32	O3	177.7(15)	C36	C31	C32	C33	-2(3)
C2	C31	C36	C35	178.7(17)	C32	C31	C36	C35	-1(3)
O3	C32	C33	C34	-177.0(16)	C31	C32	C33	C34	3(3)
C32	C33	C34	C35	0(3)	C33	C34	C35	C36	-3(3)
C34	C35	C36	C31	4(3)	C2	C41	C42	O4	3(3)
C2	C41	C42	C43	-176.5(16)	C46	C41	C42	O4	177.1(16)
C46	C41	C42	C43	-2(3)	C2	C41	C46	C45	176.3(17)
C42	C41	C46	C45	2(3)	O4	C42	C43	C44	-178.9(18)
C41	C42	C43	C44	0(3)	C42	C43	C44	C45	2(3)
C43	C44	C45	C46	-2(3)	C44	C45	C46	C41	0(3)
C3	C51	C52	O5	12(3)	C3	C51	C52	C53	-172.3(15)
C56	C51	C52	O5	-173.3(16)	C56	C51	C52	C53	2(2)
C3	C51	C56	C55	173.8(16)	C52	C51	C56	C55	-1(3)
O5	C52	C53	C54	174.8(16)	C51	C52	C53	C54	-1(2)
C52	C53	C54	C55	-1(3)	C53	C54	C55	C56	3(3)
C54	C55	C56	C51	-1(3)	C3	C61	C62	O6	7(2)
C3	C61	C62	C63	-175.7(15)	C66	C61	C62	O6	-172.0(14)
C66	C61	C62	C63	6(2)	C3	C61	C66	C65	175.9(17)
C62	C61	C66	C65	-6(3)	O6	C62	C63	C64	175.7(15)
C61	C62	C63	C64	-2(2)	C62	C63	C64	C65	-2(3)
C63	C64	C65	C66	2(3)	C64	C65	C66	C61	2(3)
C4	C71	C72	O7	15(2)	C4	C71	C72	C73	-167.9(14)
C76	C71	C72	O7	-174.6(14)	C76	C71	C72	C73	2(2)
C4	C71	C76	C75	168.6(16)	C72	C71	C76	C75	-2(3)
O7	C72	C73	C74	175.9(15)	C71	C72	C73	C74	-1(2)

Torsional Angles (continued)

Atom1	Atom2	Atom3	Atom4	Angle	Atom1	Atom2	Atom3	Atom4	Angle
C72	C73	C74	C75	-1(3)	C73	C74	C75	C76	2(3)
C74	C75	C76	C71	0(3)	C4	C81	C82	O8	-8(2)
C4	C81	C82	C83	169.5(15)	C86	C81	C82	O8	177.7(14)
C86	C81	C82	C83	-5(2)	C4	C81	C86	C85	-173.4(15)
C82	C81	C86	C85	1(2)	O8	C82	C83	C84	-177.1(14)
C81	C82	C83	C84	5(2)	C82	C83	C84	C85	-2(3)
C83	C84	C85	C86	-2(3)	C84	C85	C86	C81	3(3)
O9	C91	C92	C93	27.4(18)	C91	C92	C93	C94	-34.7(19)
C92	C93	C94	O9	29.3(19)	O10	C101	C102	C103	11(2)
C101	C102	C103	C104	10(2)	C102	C103	C104	O10	-26(2)
O11	C111	C112	C113	20(3)	C111	C112	C113	C114	-31(3)
C112	C113	C114	O11	29(3)	O12	C121	C122	C123	-23(3)
C121	C122	C123	C124	4(3)	C122	C123	C124	O12	17(3)
C10S	C11S	C12S	C13S	176(2)	C16S	C11S	C12S	C13S	1(3)
C10S	C11S	C16S	C15S	-178(2)	C12S	C11S	C16S	C15S	-3(3)
C11S	C12S	C13S	C14S	0(4)	C12S	C13S	C14S	C15S	2(5)
C13S	C14S	C15S	C16S	-4(5)	C14S	C15S	C16S	C11S	5(4)

Appendix H: Chapter 4, Section 4.3.2, page 216.

Crystallographic details for compound 2, SDL Code: JMS9927.

Compound 2: $[\{C_2(C_6H_3{}^tBu\{O\text{-}\})_4\}_2Ti_2]\cdot 2PhMe$

Formula: $C_{98}H_{112}O_8Ti_2$ ($C_{84}H_{96}O_8Ti_2\cdot 2C_7H_8$)

Crystallographic Experimental Details

A. Crystal Data	
formula	$C_{98}H_{112}O_8Ti_2$
formula weight	1513.68
crystal dimensions (mm)	0.20 × 0.08 × 0.06
crystal system	monoclinic
space group	$P2_1/c$ (No. 14)
unit cell parameters[a]	
a (Å)	12.3256 (16)
b (Å)	23.396 (3)
c (Å)	15.2484 (17)
β (deg)	107.982 (3)
V (Å^3)	4182.4 (9)
Z	2
ρ_{calcd} (g cm^{-3})	1.202
μ (mm^{-1})	0.248
B. Data Collection and Refinement Conditions	
diffractometer	Bruker P4/RA/SMART 1000 CCD[b]
radiation (λ [Å])	graphite-monochromated Mo Kα (0.71073)
temperature (°C)	–80
scan type	ϕ rotations (0.3°) / ω scans (0.3°) (30 s exposures)
data collection 2θ limit (deg)	52.88
total data collected	23649 ($-15 \leq h \leq 15$, $-29 \leq k \leq 29$, $-15 \leq l \leq 19$)
independent reflections	8559
number of observed reflections (*NO*)	2426 [$F_o^2 \geq 2\sigma(F_o^2)$]
structure solution method	direct methods (*SHELXS–86*[c])
refinement method	full-matrix least-squares on F^2 (*SHELXL–93*[d])
absorption correction method	*SADABS*
range of transmission factors	0.9803–0.7377

Crystallographic Experimental Details (continued)

data/restraints/parameters	8559 [$F_o^2 \geq -3\sigma(F_o^2)$] / 6[e] / 436
goodness-of-fit (S)[f]	0.812 [$F_o^2 \geq -3\sigma(F_o^2)$]
final R indices[g]	
R_1 [$F_o^2 \geq 2\sigma(F_o^2)$]	0.0725
wR_2 [$F_o^2 \geq -3\sigma(F_o^2)$]	0.1805
largest difference peak and hole	0.498 and –0.586 e Å^{-3}

[a] Obtained from least-squares refinement of 3028 centered reflections.

[b] Programs for diffractometer operation, data collection, data reduction and absorption correction were those supplied by Bruker.

[c] Sheldrick, G. M. *Acta Crystallogr.* **1990**, *A46*, 467–473.

[d] Sheldrick, G. M. *SHELXL-93*. Program for crystal structure determination. University of Göttingen, Germany, 1993. Refinement on F_o^2 for all reflections (all of these having $F_o^2 \geq -3\sigma(F_o^2)$). Weighted R-factors wR_2 and all goodnesses of fit S are based on F_o^2; conventional R-factors R_1 are based on F_o, with F_o set to zero for negative F_o^2. The observed criterion of $F_o^2 > 2\sigma(F_o^2)$ is used only for calculating R_1, and is not relevant to the choice of reflections for refinement. R-factors based on F_o^2 are statistically about twice as large as those based on F_o, and R-factors based on ALL data will be even larger.

[e] The methyl carbon positions of the disordered solvent toluene molecule were refined in idealized positions by fixing d(C_{methyl}–C_{ipso})) = 1.54 Å and d($C_{methyl} \cdots C_{ortho}$)) = 2.54 Å. The toluene ring carbons were refined as idealized hexagons with d(C–C) = 1.39 Å.

[f] $S = [\Sigma w(F_o^2 - F_c^2)^2/(n - p)]^{1/2}$ (n = number of data; p = number of parameters varied; $w = [\sigma^2(F_o^2) + (0.0504P)^2]^{-1}$ where $P = [\mathrm{Max}(F_o^2, 0) + 2F_c^2]/3$).

[g] $R_1 = \Sigma||F_o| - |F_c||/\Sigma|F_o|$; $wR_2 = [\Sigma w(F_o^2 - F_c^2)^2/\Sigma w(F_o^4)]^{1/2}$.

Selected Interatomic Distances (Å)

Atom1	Atom2	Distance	Atom1	Atom2	Distance
Ti	O1	1.812(4)	Ti	O2	1.806(4)
Ti	O3	1.934(4)	Ti	O3'	2.122(4)
Ti	O4'	1.813(4)	O1	C12	1.357(7)
O2	C22	1.379(7)	O3	C32	1.385(7)
O4	C42	1.372(7)	C1	C2	1.356(8)
C1	C11	1.491(8)	C1	C21	1.493(8)
C2	C31	1.515(8)	C2	C41	1.489(8)
C11	C12	1.386(8)	C11	C16	1.386(8)
C12	C13	1.379(9)	C13	C14	1.395(9)
C14	C15	1.387(9)	C15	C16	1.401(9)
C15	C17	1.549(10)	C17	C18A	1.495(14)
C17	C19A	1.616(15)	C17	C20A	1.472(13)
C17	C18B	1.50(2)	C17	C19B	1.45(2)
C17	C20B	1.72(2)	C21	C22	1.396(8)
C21	C26	1.404(8)	C22	C23	1.390(8)
C23	C24	1.392(8)	C24	C25	1.386(9)
C25	C26	1.411(8)	C25	C27	1.533(9)
C27	C28	1.542(9)	C27	C29	1.528(10)
C27	C30	1.526(9)	C31	C32	1.393(8)
C31	C36	1.389(8)	C32	C33	1.391(8)
C33	C34	1.371(8)	C34	C35	1.403(8)
C35	C36	1.383(8)	C35	C37	1.524(9)
C37	C38	1.526(9)	C37	C39	1.521(9)
C37	C40	1.483(10)	C41	C42	1.417(8)
C41	C46	1.411(8)	C42	C43	1.395(8)
C43	C44	1.385(8)	C44	C45	1.383(8)
C45	C46	1.394(8)	C45	C47	1.532(8)
C47	C48	1.527(8)	C47	C49	1.523(9)
C47	C50	1.519(8)			

Primed atoms are related to unprimed ones via the crystallographic inversion center (0, 0, 0).

Selected Interatomic Angles (deg)

Atom1	Atom2	Atom3	Angle	Atom1	Atom2	Atom3	Angle
O1	Ti	O2	101.0(2)	O1	Ti	O3	93.93(19)
O1	Ti	O3'	166.14(19)	O1	Ti	O4'	102.43(19)
O2	Ti	O3	128.11(18)	O2	Ti	O3'	86.50(18)
O2	Ti	O4'	112.12(19)	O3	Ti	O3'	72.3(2)
O3	Ti	O4'	112.53(18)	O3'	Ti	O4'	85.16(17)
Ti	O1	C12	144.3(4)	Ti	O2	C22	139.2(4)
Ti	O3	Ti'	107.7(2)	Ti	O3	C32	130.2(4)
Ti'	O3	C32	116.2(3)	Ti'	O4	C42	128.0(4)
C2	C1	C11	121.1(6)	C2	C1	C21	125.2(6)
C11	C1	C21	113.6(5)	C1	C2	C31	115.3(6)
C1	C2	C41	124.7(6)	C31	C2	C41	120.0(6)
C1	C11	C12	119.2(6)	C1	C11	C16	120.9(6)
C12	C11	C16	119.6(7)	O1	C12	C11	119.8(6)
O1	C12	C13	120.4(6)	C11	C12	C13	119.7(7)
C12	C13	C14	120.4(6)	C13	C14	C15	120.9(7)
C14	C15	C16	117.7(7)	C14	C15	C17	120.7(7)
C16	C15	C17	121.6(6)	C11	C16	C15	121.6(6)
C15	C17	C18A	114.3(8)	C15	C17	C19A	106.9(8)
C15	C17	C20A	109.0(8)	C15	C17	C18B	112.0(10)
C15	C17	C19B	115.9(11)	C15	C17	C20B	103.6(10)
C18A	C17	C19A	107.6(9)	C18A	C17	C20A	112.5(10)
C19A	C17	C20A	106.0(9)	C18B	C17	C19B	117.3(15)
C18B	C17	C20B	104.5(13)	C19B	C17	C20B	101.1(15)
C1	C21	C22	119.8(6)	C1	C21	C26	120.9(6)
C22	C21	C26	118.7(6)	O2	C22	C21	120.6(6)
O2	C22	C23	118.5(6)	C21	C22	C23	120.9(6)
C22	C23	C24	118.9(7)	C23	C24	C25	122.6(7)
C24	C25	C26	117.3(6)	C24	C25	C27	121.2(7)
C26	C25	C27	121.5(6)	C21	C26	C25	121.4(6)
C25	C27	C28	108.3(6)	C25	C27	C29	112.2(6)
C25	C27	C30	109.9(6)	C28	C27	C29	107.1(6)
C28	C27	C30	110.6(6)	C29	C27	C30	108.6(7)
C2	C31	C32	117.5(6)	C2	C31	C36	123.2(6)
C32	C31	C36	119.0(6)	O3	C32	C31	119.6(6)
O3	C32	C33	120.9(6)	C31	C32	C33	119.5(6)
C32	C33	C34	120.1(6)	C33	C34	C35	122.1(7)
C34	C35	C36	116.5(6)	C34	C35	C37	119.7(7)

Selected Interatomic Angles (continued)

Atom1	Atom2	Atom3	Angle	Atom1	Atom2	Atom3	Angle
C36	C35	C37	123.6(6)	C31	C36	C35	122.8(6)
C35	C37	C38	110.5(6)	C35	C37	C39	111.3(6)
C35	C37	C40	110.7(6)	C38	C37	C39	105.7(6)
C38	C37	C40	109.5(7)	C39	C37	C40	109.0(7)
C2	C41	C42	123.4(6)	C2	C41	C46	119.7(6)
C42	C41	C46	116.8(6)	O4	C42	C41	122.6(6)
O4	C42	C43	117.3(6)	C41	C42	C43	120.0(6)
C42	C43	C44	120.2(6)	C43	C44	C45	122.3(6)
C44	C45	C46	116.8(6)	C44	C45	C47	124.3(6)
C46	C45	C47	118.9(6)	C41	C46	C45	123.8(6)
C45	C47	C48	111.3(5)	C45	C47	C49	110.9(6)
C45	C47	C50	108.1(5)	C48	C47	C49	108.3(5)
C48	C47	C50	108.1(6)	C49	C47	C50	110.1(6)

Primed atoms are related to unprimed ones via the crystallographic inversion center (0, 0, 0).

Torsional Angles (deg)

Atom1	Atom2	Atom3	Atom4	Angle	Atom1	Atom2	Atom3	Atom4	Angle
O2	Ti	O1	C12	-62.0(7)	O3	Ti	O1	C12	68.0(7)
O3'	Ti	O1	C12	59.9(11)	O4'	Ti	O1	C12	-177.9(7)
O1	Ti	O2	C22	30.5(6)	O3	Ti	O2	C22	-73.5(6)
O3'	Ti	O2	C22	-137.8(6)	O4'	Ti	O2	C22	138.9(6)
O1	Ti	O3	Ti'	-178.0(2)	O1	Ti	O3	C32	-26.9(5)
O2	Ti	O3	Ti'	-70.7(3)	O2	Ti	O3	C32	80.4(5)
O3'	Ti	O3	Ti'	0.0	O3'	Ti	O3	C32	151.1(5)
O4'	Ti	O3	Ti'	76.8(2)	O4'	Ti	O3	C32	-132.1(5)
O1	Ti	O3'	C32'	164.2(7)	O2	Ti	O3'	C32'	-72.4(4)
O3	Ti	O3'	C32'	155.7(5)	O1	Ti	O4'	C42'	-80.3(5)
O2	Ti	O4'	C42'	172.2(5)	O3	Ti	O4'	C42'	19.4(5)
Ti	O1	C12	C11	7.1(11)	Ti	O1	C12	C13	-172.0(5)
Ti	O2	C22	C21	26.4(9)	Ti	O2	C22	C23	-151.6(5)
Ti	O3	Ti'	O1'	-8.5(8)	Ti	O3	Ti'	O2'	-131.9(2)
Ti	O3	Ti'	O4	115.5(2)	Ti	O3	C32	C31	-59.2(7)
Ti	O3	C32	C33	121.2(6)	Ti'	O3	C32	C31	89.9(6)
Ti'	O3	C32	C33	-89.7(6)	Ti'	O4	C42	C41	86.0(7)
Ti'	O4	C42	C43	-93.4(6)	C11	C1	C2	C31	7.6(8)
C11	C1	C2	C41	-172.5(5)	C21	C1	C2	C31	-169.3(6)

Torsional Angles (continued)

Atom1	Atom2	Atom3	Atom4	Angle	Atom1	Atom2	Atom3	Atom4	Angle
C21	C1	C2	C41	10.6(10)	C2	C1	C11	C12	-90.8(8)
C2	C1	C11	C16	95.1(7)	C21	C1	C11	C12	86.4(7)
C21	C1	C11	C16	-87.7(7)	C2	C1	C21	C22	76.2(8)
C2	C1	C21	C26	-112.2(7)	C11	C1	C21	C22	-100.9(7)
C11	C1	C21	C26	70.7(7)	C1	C2	C31	C32	88.1(7)
C1	C2	C31	C36	-85.1(7)	C41	C2	C31	C32	-91.9(7)
C41	C2	C31	C36	94.9(7)	C1	C2	C41	C42	-145.3(6)
C1	C2	C41	C46	36.8(8)	C31	C2	C41	C42	34.7(8)
C31	C2	C41	C46	-143.3(6)	C1	C11	C12	O1	5.0(9)
C1	C11	C12	C13	-176.0(6)	C16	C11	C12	O1	179.1(6)
C16	C11	C12	C13	-1.8(10)	C1	C11	C16	C15	174.7(6)
C12	C11	C16	C15	0.6(10)	O1	C12	C13	C14	-179.0(6)
C11	C12	C13	C14	1.9(10)	C12	C13	C14	C15	-0.8(11)
C13	C14	C15	C16	-0.4(11)	C13	C14	C15	C17	178.3(7)
C14	C15	C16	C11	0.5(10)	C17	C15	C16	C11	-178.2(7)
C14	C15	C17	C18A	171.4(9)	C14	C15	C17	C19A	52.4(10)
C14	C15	C17	C20A	-61.9(11)	C14	C15	C17	C18B	140.1(12)
C14	C15	C17	C19B	1.9(17)	C14	C15	C17	C20B	-107.9(12)
C16	C15	C17	C18A	-10.0(12)	C16	C15	C17	C19A	-128.9(8)
C16	C15	C17	C20A	116.8(9)	C16	C15	C17	C18B	-41.2(13)
C16	C15	C17	C19B	-179.5(15)	C16	C15	C17	C20B	70.8(12)
C1	C21	C22	O2	-3.3(9)	C1	C21	C22	C23	174.7(6)
C26	C21	C22	O2	-175.0(5)	C26	C21	C22	C23	2.9(9)
C1	C21	C26	C25	-174.7(6)	C22	C21	C26	C25	-3.0(9)
O2	C22	C23	C24	177.2(5)	C21	C22	C23	C24	-0.8(10)
C22	C23	C24	C25	-1.4(10)	C23	C24	C25	C26	1.3(10)
C23	C24	C25	C27	-178.2(6)	C24	C25	C26	C21	0.9(9)
C27	C25	C26	C21	-179.6(6)	C24	C25	C27	C28	-67.5(8)
C24	C25	C27	C29	174.5(7)	C24	C25	C27	C30	53.5(9)
C26	C25	C27	C28	113.1(7)	C26	C25	C27	C29	-4.9(9)
C26	C25	C27	C30	-126.0(7)	C2	C31	C32	O3	6.4(8)
C2	C31	C32	C33	-174.0(6)	C36	C31	C32	O3	179.9(5)
C36	C31	C32	C33	-0.5(9)	C2	C31	C36	C35	172.6(6)
C32	C31	C36	C35	-0.5(9)	O3	C32	C33	C34	-179.4(6)
C31	C32	C33	C34	1.0(9)	C32	C33	C34	C35	-0.6(10)
C33	C34	C35	C36	-0.4(9)	C33	C34	C35	C37	174.9(6)
C34	C35	C36	C31	0.9(9)	C37	C35	C36	C31	-174.2(6)
C34	C35	C37	C38	61.3(8)	C34	C35	C37	C39	178.5(6)

Torsional Angles (continued)

Atom1	Atom2	Atom3	Atom4	Angle	Atom1	Atom2	Atom3	Atom4	Angle
C34	C35	C37	C40	-60.2(9)	C36	C35	C37	C38	-123.7(7)
C36	C35	C37	C39	-6.6(10)	C36	C35	C37	C40	114.8(8)
C2	C41	C42	O4	1.4(9)	C2	C41	C42	C43	-179.2(5)
C46	C41	C42	O4	179.4(5)	C46	C41	C42	C43	-1.2(9)
C2	C41	C46	C45	179.9(5)	C42	C41	C46	C45	1.9(9)
O4	C42	C43	C44	179.7(6)	C41	C42	C43	C44	0.3(9)
C42	C43	C44	C45	0.0(10)	C43	C44	C45	C46	0.6(10)
C43	C44	C45	C47	-176.5(6)	C44	C45	C46	C41	-1.6(9)
C47	C45	C46	C41	175.7(6)	C44	C45	C47	C48	-13.9(9)
C44	C45	C47	C49	-134.6(7)	C44	C45	C47	C50	104.6(7)
C46	C45	C47	C48	168.9(6)	C46	C45	C47	C49	48.3(8)
C46	C45	C47	C50	-72.5(7)					

Primed atoms are related to unprimed ones via the crystallographic inversion center (0, 0, 0).

Appendix I: Chapter 5, Section 5.2.2, Page 286.

a) Pin Assignment Xilinx XC 9572

Pin # 8,16,23-27,31,33-37,39,40,42,44,46,48-50,52-57,60,81,82 GND

Pin# 10,14,17,18,21,32,43,63,65,67,72,75,79 Not Connected

Pin# 22,38,58,61,64,73,78 Vcc

Pin#	1	seg GL, TendownR	45	[FL1], Sens.
	2	[EMPTY], L6	47	[RESET], SW2
	3	seg DL, TendownR	51	[BUZZER]
	4	[ON], L5	59	TDO, JTAG
	5	seg EL, TendownR	62	[V4], DRV4
	6	[OFFSW], SW1	66	[V2], DRV3
	7	seg EM, TendownL	68	seg AL, TendownR
	9	seg CM, TendownL	69	seg BL, TendownR
	11	seg DM, TendownL	70	seg FL, TendownR
	12	[CLK], Osc. input	71	seg FM, TendownL
	13	[FILLSW], SW3	74	[V1], DRV2
	15	[REPSW], SW4	76	seg BM, TendownL
	19	[ERROR], L8	77	seg AM, TendownL
	28	TDI, JTAG	80	seg GM, TendownL
	29	TMS, JTAG	83	seg CL, TendownR
	30	TCK, JTAG	84	[WAIT], L7
	41	[NOAHFLD]		

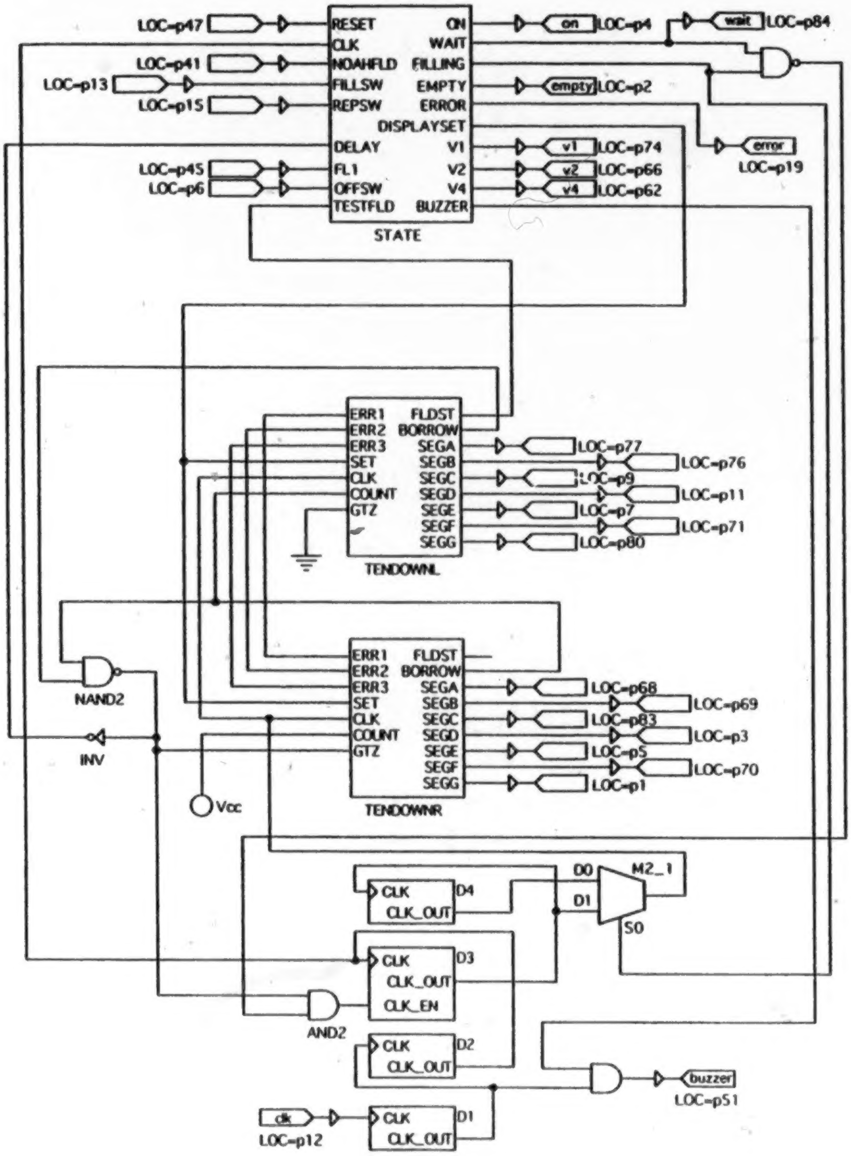
LOC=p47
LOC=p41
LOC=p13
LOC=p15
LOC=p45
LOC=p6
RESET
CLK
NOAHFLD
FILLSW
REPSW
DELAY
FL1
OFFSW
TESTFLD
ON
WAIT
FILLING
EMPTY
ERROR
DISPLAYSET
V1
V2
V4
BUZZER
STATE
on
LOC=p4
wait
LOC=p84
empty
LOC=p2
error
LOC=p19
v1
LOC=p74
v2
LOC=p66
v4
LOC=p62
ERR1
ERR2
ERR3
SET
CLK
COUNT
GTZ
FLDST
BORROW
SEGA
SEGB
SEGC
SEGD
SEGE
SEGF
SEGG
LOC=p77
LOC=p76
LOC=p9
LOC=p11
LOC=p7
LOC=p71
LOC=p80
TENDOWNL
NAND2
INV
ERR1
ERR2
ERR3
SET
CLK
COUNT
GTZ
FLDST
BORROW
SEGA
SEGB
SEGC
SEGD
SEGE
SEGF
SEGG
LOC=p68
LOC=p69
LOC=p83
LOC=p3
LOC=p5
LOC=p70
LOC=p1
Vcc
TENDOWNR
D0
M2_1
D1
S0
CLK
CLK_OUT
D4
CLK
CLK_OUT
CLK_EN
D3
AND2
CLK
CLK_OUT
D2
buzzer
LOC=p51
clk
LOC=p12
CLK
CLK_OUT
D1

Figure 1. Electrical scheme of the Xilinx 9572 (U1).

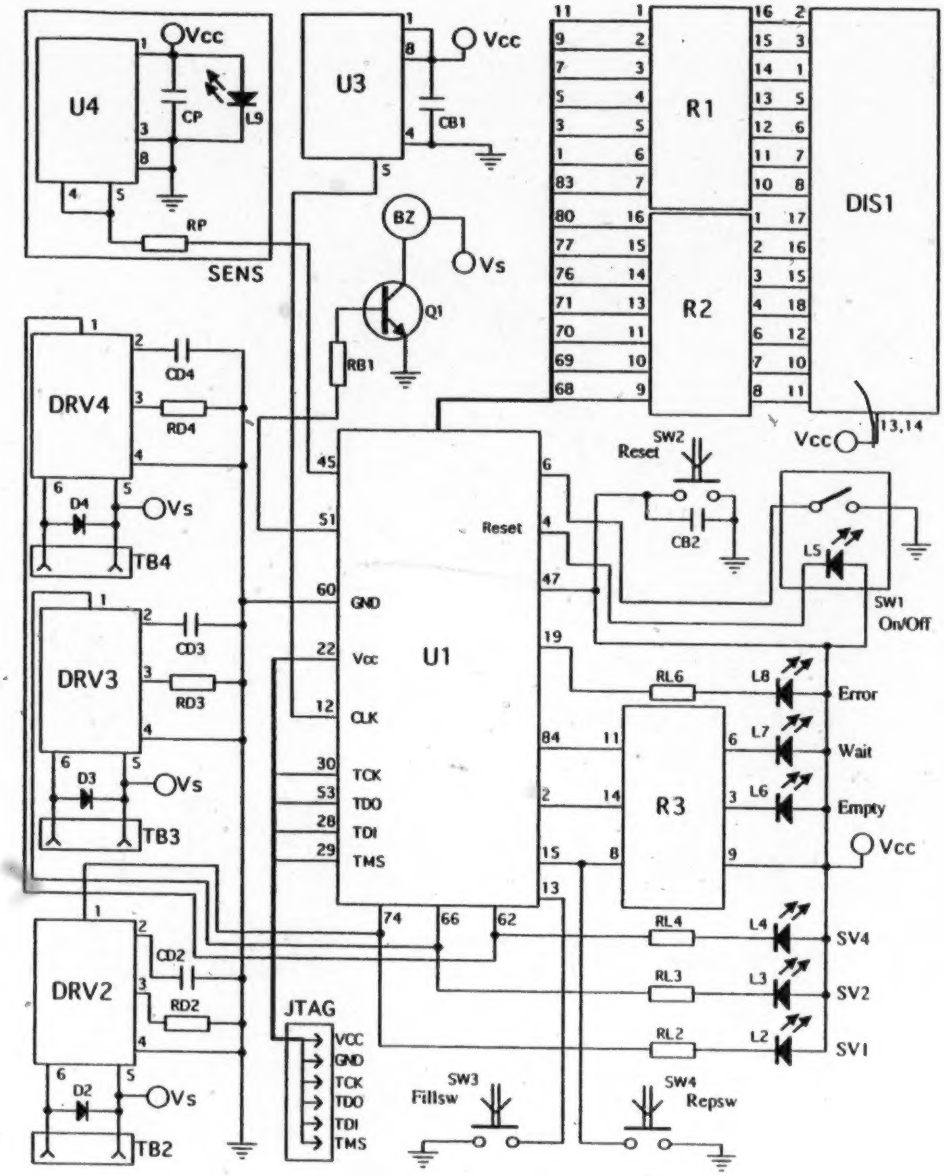
U4
Vcc
CP
L9
RP
SENS
U3
Vcc
CB1
BZ
Vs
Q1
RB1
R1
R2
DIS1
Vcc
13,14
DRV4
CD4
RD4
D4
Vs
TB4
DRV3
CD3
RD3
D3
Vs
TB3
DRV2
CD2
RD2
D2
Vs
TB2
U1
Reset
GND
Vcc
CLK
TCK
TDO
TDI
TMS
SW2
Reset
CB2
L5
SW1
On/Off
RL6
L8
Error
L7
Wait
R3
L6
Empty
Vcc
RL4
L4
SV4
RL3
L3
SV2
RL2
L2
SV1
JTAG
VCC
GND
TCK
TDO
TDI
TMS
SW3
Fillsw
SW4
Repsw

Figure 2. Electrical scheme of solvent purification unit.

b) Component list electronics.

Resistors

R1,2,3	470 Ω isolated resistor network, Bourns 4116R-001
RD2,3,4	18 KΩ, 5 % metal, 1/4 W
RL2,3,4	1.5 KΩ, 1 % metal, 0.6 W
RB1	1.5 KΩ, 1 % metal, 0.6 W
RP	150 Ω, 1 %, 1/4 W

Capacitors

CD2,3,4	0.1 μF/50 V ,10 % Ceramic
CB1, CP	0.1 μF/50 V ,10 % Ceramic
CB2	6.8 μF/16 V , Tantalum

Semiconductors

Q1	2N4401
D2,3,4	Schottky 90V/1.1 A, DO-41 (IR)
L2-8	LED
L9	High Intensity LED
DIS1	Lumex LDD-A516 RT (c.a.)
U1	XC9572, 84 pins PLCC (Xilinx)
U3	2.048 CMOS, TTL Osc. (Epson)
U4	OPT101 (Burr Brown)

Miscellaneous

SW1	Alt. Switch (n.o.), Omron A3BJ-500R, Case: A3GJ-6021-3, Socket: A3G-4011, LED: A3B-005R [on/off]
SW2	Mom. Switch (n.o., Panasonic) [reset]
SW3	Magnetic Position Sensor (n.o., spst, Hamlin), 59065-010-ND, [fillsw]
SW4	Mom. Switch (n.o., C&K) [repsw]
Socket	84 pins PLCC (Amphenol)
TB2,3,4	2 pole Terminal Block (OST)
JTAG	6 pins header (Molex)
BZ	Piezoelectric Ceramic Buzzer, 86 dB, 15 V pp, Panasonic EFB-AA40D102
Sensor	ELS-1100, GEMS optical level sensor [noahfld], optional
Heatsinks	Vertical mount with tabs, TO-220
PwrSupply	24 V, 1.2 A, single output, Power One, HB24-1.2-A 5 V, 300 mA, single output, Cui Stack wall transformer

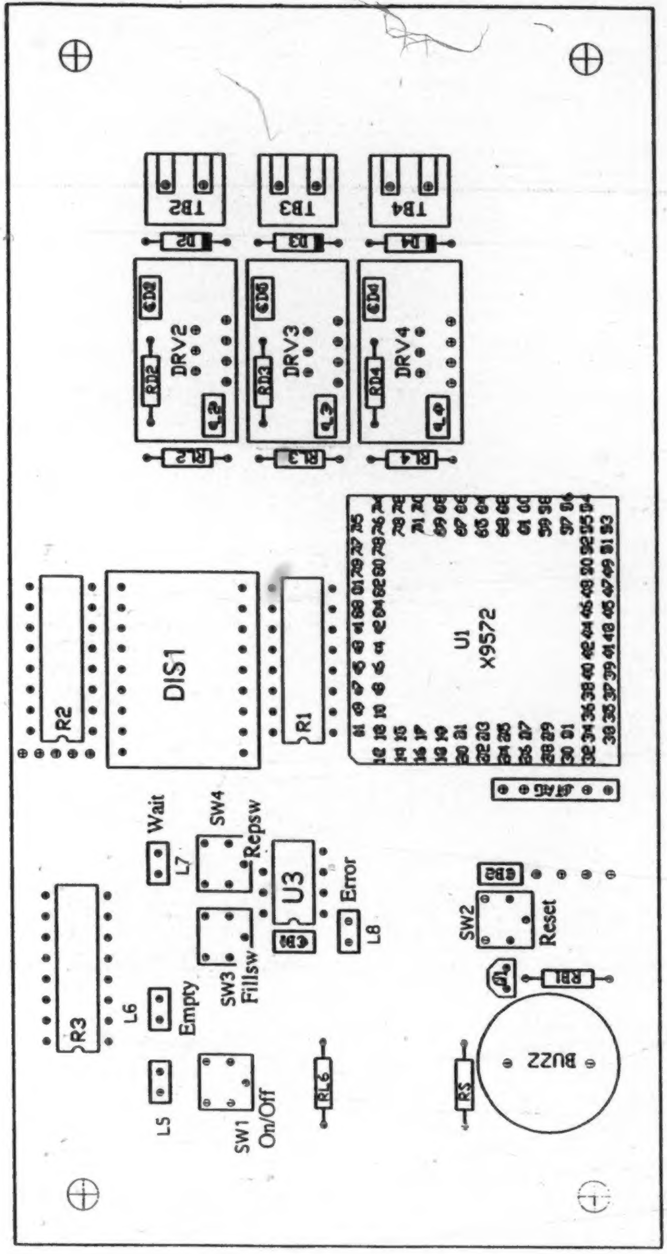
TB2
TB3
TB4
D2
D3
D4
DRV2
DRV3
DRV4
RD2
RD3
RD4
RL2
RL3
RL4
DIS1
R1
R2
R3
U1
X9572
JTAG
Wait
SW4
Repsw
L7
U3
Error
L8
SW3
Fillsw
L6
Empty
L5
SW1
On/Off
RL6
SW2
Reset
RB1
RS
BUZZ

Figure 3. Component placement on the printed circuit board of the solvent purification unit.

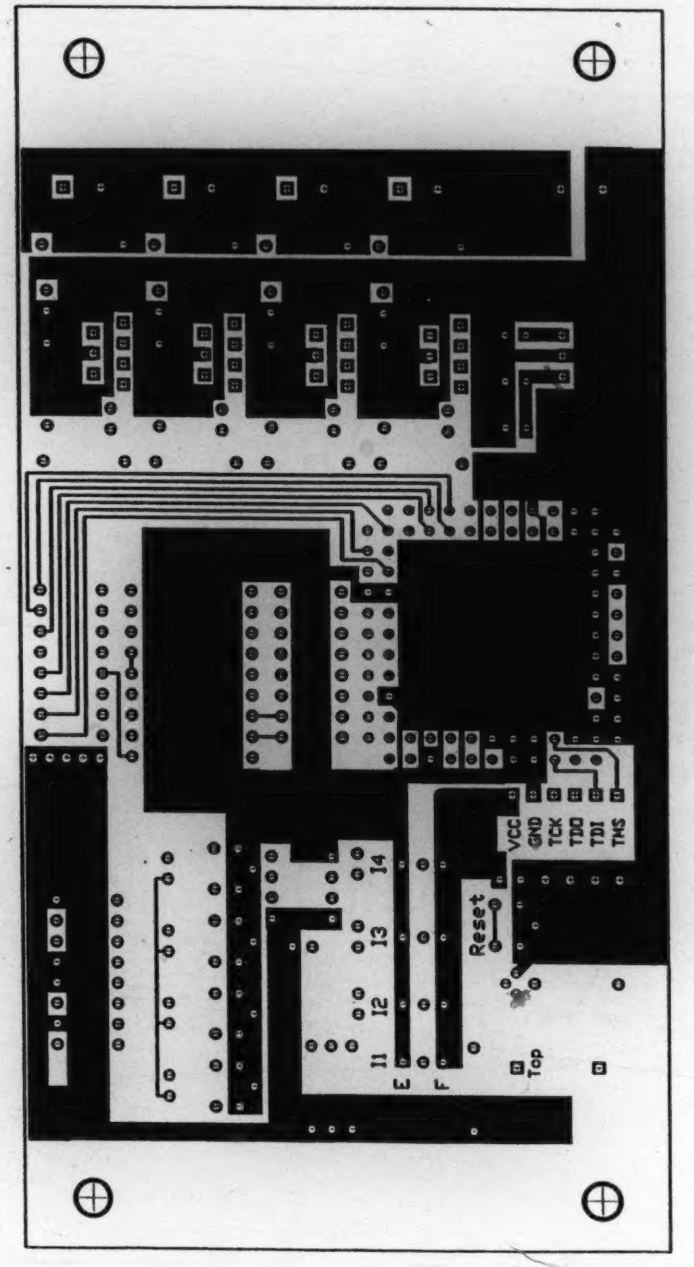
VCC
GND
TCK
TDO
TDI
TMS
Reset
I4
I3
I2
I1
E
F
Top

Figure 4. Printed circuit board for the solvent purification unit, front.

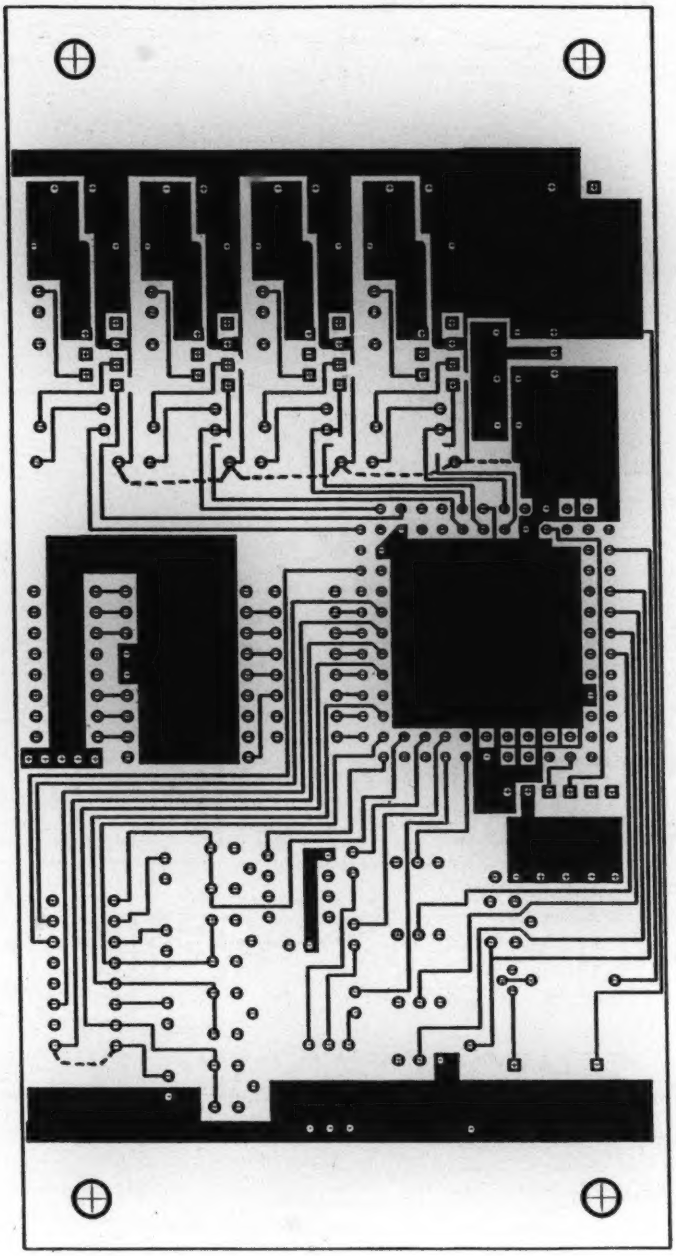

Figure 5. Printed circuit board of the solvent purification unit, back. Dotted lines are bridging wires.

Appendix J: Chapter 5, Section 5.2.3, Page 288.

a) Hardware component list.

Unless noted otherwise all connectors are Swagelok connectors. All connections are made with 1/4 inch stainless steel tubing, except the solvent take off tube, which is 3/8 inch SS.

The following connections which are made with 1/4 inch PFA tubing (wall thickness 0.062 inch, Swagelok PFA-T4-062): Connection between oilbubbler B and V1, connection between the Solvent Reservoir and V1, connection between CV1 and V2, connection between the Solvent Reservoir and sensor S and all the vacuum line and nitrogen line connections.

The connections to the vacuum line, the nitrogen tank and the fumehood were made using SS-6-HC-1-400 (hose connector) and SS-5-HC-A-401 (tube adapter) connectors.

The columns were mounted hanging in a painted steel frame made of 1 inch tubing with size 20x9x23 inch (d x w x h), and can be easily removed for (re)generation. In addition to the three columns, the solenoid valves V1, V2 and V4, as well as the sensor S, bubbler B, regulator R2, electronics and one power supply (Vs, 24 V, 1.2 A) are mounted in this steel frame.

The front panel is made of stainless steel, and shows behind a glass plate the display DIS1 and three LEDs L6, 7 and 8. Valve V5, switch SW1, the exhaust port and solvent take off are also mounted on the front panel. The whole setup is protected by a thin stainless steel case mounted on the frame.

In the following hardware list the main items are listed first, followed by the Swagelok connectors necessary to interconnect these items using 1/4 inch tubing.

Components

V1, V2	Bürkert threeway solenoid valve, Type 6014, 24 V DC, S.S., two Bürkert adapters (1/4 inch female to the solenoid valve thread), four SS-400-1-4 (male connector), two SS-400-8-4 (female elbow)
V3	Bellows valve, SS-4H2, and one SS-400-7-4 (female connector)
V4	Burkert two-way solenoid valve, Type 6013, 24 V DC, SS., and two SS-400-1-4 (male connector)
V5	Ball valve, SS-43S4-RD-1466
F	15 μFilter, SS-4FW-15
CV1, CV2	Check valve SS-4C-KZ-1/3
CV3	Check valve SS-4C-KZ-1/3
R2	Regulator, low pressure, Norgren, and two SS-400-1-4 (male connector)

Bubbler	
B	Bubbler, constructed from a 1L Nalgene bottle 2104-0032, two bulkhead unions SS-400-61 and piece of Teflon tubing (the bubbler is filled with mineral oil).
Reservoir	
	Solvent Reservoir, SS., 3 Gallons, EPDM O-ring, complete with safety valve, set at 125 psig. Alloy Products pressure vessel 72-03: borrowed from Prof. N.Branda. On this reservoir a pressure gauge 0-80 psig and switch SW4 are mounted.
Exhaust Port	
	Constructed from SS. tubing, silver soldered on a SS. plate, on which a male connector SS-400-1-4W is silver soldered.
Columns	
C1,C2,C3	Columns, constructed from 20 inch SS. tubing, diameter 3 inch, wall thickness 1/16 inch, 3 3/8 SS. High Vacuum flanges with knife edges and copper gasket. Connectors: SS-400-2-4W (male elbow, weld), six SS-400-P (plug) and for C2 one SS-400-7-4 (female connector). Column volume: 2 L. Retaining sieves: 60 Mesh SS.
Column Fillings	
C1	Alumina La Roche A2 (12x32)
C2	Deoxygenation Catalyst, Engelhard Cu-0226S
C3	Molecular sieves, 50/50 mix of 13X and 3A
Sensor	
S	The sensor is constructed from Teflon tubing 1 inch in diameter, two SS-1610-3-16-6 (Union Tee), two SS-1610-P (plug), two SS-400-R-6 (reducer) and an NMR tube. Around the transparent Teflon tubing a black Delrin collar is mounted containing a hole perpendicular to the direction of the solvent flow. In this hole the LED and (on the opposite side) the photo diode are mounted. On top of the photo diode additional electronic components (U4, CP, L9 and RP) are mounted.
Solvent Take Off	
	Constructed from a reducer SS-400-R-6BT, a reducing union tee SS-600-3-6-4 and a SS O-ring joint (in which was mounted a 60 Mesh SS. gauze), 674850-0009, Kontes. In addition the valve V5, filter F and the drain SS-400-3 (union tee) and plug SS-400-P are mounted in a steel support behind the front panel together with the magnetic switch SW3.